ÉCOLE NATIONALE DES PONTS ET CHAUSSÉES

IP PARIS

THÈSE DE DOCTORAT

de l'École nationale des ponts et chaussées

Analyse et échantillonnage de dynamiques stochastiques métastables et hors d'équilibre

École doctorale N°531, MSTIC

Mathématiques

Thèse préparée au CERMICS,
au sein de l'équipe MATHERIALS d'Inria de Paris

Thèse soutenue le 19 décembre 2025, par

Noé BLASSEL

Composition du jury:

Nils BERGLUND Professeur, Université d'Orléans	*Président du jury*
Emma HORTON Professeure adjointe, University of Warwick	*Examinatrice*
Sylvie MÉLÉARD Professeure, École Polytechnique	*Examinatrice*
Yannick PRIVAT Professeur, Université de Lorraine	*Examinateur*
Josselin GARNIER Professeur, École Polytechnique	*Rapporteur*
Laurent MICHEL Professeur, Institut de Mathématiques de Bordeaux	*Rapporteur*
Gabriel STOLTZ Professeur, École nationale des ponts et chaussées	*Directeur de thèse*
Tony LELIÈVRE Professeur, École nationale des ponts et chaussées	*Directeur de thèse*

Analysis and sampling of metastable and nonequilibrium stochastic dynamics

Noé Blassel

Thèse de doctorat en
Mathématiques Appliquées

Préparée au sein du laboratoire CERMICS
de l'École Nationale des Ponts et Chaussées, IP Paris

Septembre 2025

Directeurs de thèse: Gabriel Stoltz & Tony Lelièvre

À André Espi.

Abstract

This thesis explores mathematical and algorithmic questions at the intersection of computational physics and probability theory, specifically focusing on Molecular Dynamics (MD). MD simulations are essential for understanding the macroscopic properties of matter based on an atomistic description, yet they face persistent and significant hurdles. The primary challenge addressed in this work is the "timescale problem" caused by metastability: molecular systems often remain trapped in local ensembles of atomic configurations (or *metastable states*) for extended periods of time, making the simulation of rare transition events computationally prohibitive, even though these events are crucial to the understanding of the macroscopic behavior of the system. This thesis contributes to the analysis and sampling of these molecular dynamics through three complementary axes: the spectral analysis and optimization of metastable states, the computation of nonequilibrium transport coefficients, and the rigorous derivation of overdamped limits for degenerate stochastic differential equations.

The first main contribution addresses the definition and optimization of metastable states to improve accelerated sampling algorithms, specifically the Parallel Replica (ParRep) method. The efficiency of such algorithms relies on a large separation of timescales within a defined metastable region: the system must relax to a local equilibrium (the *quasi-stationary distribution*) much faster than it exits the state. We first provide a theoretical foundation for analyzing these timescales by deriving *quantitative spectral asymptotics* for the infinitesimal generator of the overdamped Langevin dynamics. A key novelty of this work is the analysis of Dirichlet eigenvalues on domains with temperature-dependent boundaries. In the low-temperature limit, we rigorously derive precise asymptotic estimates for the principal eigenvalue (related to the mean exit time) and the spectral gap (related to the relaxation time). We establish a modified Eyring-–Kramers formula that accounts for the specific geometry of the domain boundary near saddle points, demonstrating that the pre-exponential factor of the exit rate is highly sensitive to the shape of the domain, in a way that can be computed explicitly.

We also propose a novel numerical method to optimize the definition of metastable states. Standard definitions based on basins of attraction of the potential energy are often sub-optimal, particularly when entropic effects are significant. We formulate the definition of a metastable state as an eigenvalue *shape optimization* problem, aiming to maximize the separation of timescales, understood as the ratio of the exit time to the local relaxation time. We derive analytic shape derivatives for the Dirichlet eigenvalues of reversible diffusions and

construct a robust local ascent algorithm to deform the domain boundary. To handle the high dimensionality of realistic molecular systems, we propose a strategy based on dynamical coarse-graining using collective variables. We validate this methodology on a biomolecular system, demonstrating empirically that optimized domains can yield significant improvements in the separation of timescales compared to standard definitions.

The second axis of the thesis shifts focus to *nonequilibrium molecular dynamics* (NEMD) and the computation of transport coefficients, such as mobility and shear viscosity. Standard NEMD methods impose a fixed external force and measure the resulting average flux. We introduce a dual approach based on constrained stochastic dynamics. In this framework, the flux is constrained to a fixed value, and the average force required to sustain this flux is measured. We derive the stochastic differential equation governing these dynamics in a general setting, and focus on underdamped Langevin systems, typically used in practice to compute transport coefficients. Through numerical experiments on Lennard–Jones fluids, we demonstrate empirically that the constant-flux method yields consistent linear response estimates in the thermodynamic limit, and that the corresponding estimators exhibit lower asymptotic variance than standard NEMD estimators, making them a computationally efficient alternative for calculating transport properties.

A final contribution addresses the rigorous link between two models of molecular dynamics. We study the high-friction limit of the kinetic or underdamped Langevin equation with a position-dependent friction coefficient. By deriving new functional-analytic—so-called *hypocoercive*—estimates, we provide a new proof of the convergence of the position process to the overdamped Langevin dynamics with anisotropic and position-dependent fluctuation-dissipation coefficients. This approach avoids the complexities of some previous methods, and clearly elucidates the origin of the noise-induced drift term in the limiting equation.

Résumé de la thèse

Cette thèse traite de questions mathématiques et algorithmiques à l'interface de la physique statistique computationnelle et de la théorie des probabilités, et plus spécifiquement de certaines méthodes numériques issues de la dynamique moléculaire (MD). Les simulations de MD sont cruciales pour comprendre les propriétés macroscopiques de la matière en se fondant sur la description atomique, mais se heurtent néanmoins à des obstacles persistants et importants. Le principal défi abordé dans ce travail est le "problème des échelles de temps" induit par la métastabilité des systèmes considérés. Les systèmes moléculaires restent souvent piégés dans des ensembles locaux de configurations atomiques (ou *états métastables*) pendant de longues périodes, rendant la simulation des événements rares de transition très coûteuse en termes de calcul, alors même que ces événements sont cruciaux pour la compréhension du comportement macroscopique du système. Cette thèse contribue à l'analyse et à l'échantillonnage de ces dynamiques à travers trois axes : l'analyse spectrale et l'optimisation des états métastables, le calcul des coefficients de transport hors équilibre, et la dérivation de limites sur-amorties pour certaines équations différentielles stochastiques dégénérées.

La première contribution principale porte sur la définition et l'optimisation des états métastables afin d'améliorer une famille d'algorithmes d'échantillonnage dynamique accéléré, de type "Parallel Replica" (ParRep). L'efficacité de tels algorithmes repose sur une grande séparation des échelles de temps au sein d'une région métastable définie : le système doit converger vers un équilibre local (la *distribution quasi-stationnaire*) beaucoup plus vite qu'il ne quitte l'état. Nous fournissons d'abord un fondement théorique pour l'analyse de ces échelles de temps en établissant des *asymptotiques spectrales quantitatives* pour le générateur infinitésimal de la dynamique de Langevin sur-amortie. Une nouveauté clé de ce travail réside dans l'analyse des valeurs propres de Dirichlet sur des domaines dont la frontière dépend de la température. Dans la limite de basse température, nous dérivons rigoureusement des estimations asymptotiques précises pour la valeur propre principale (liée au temps de sortie moyen) et le trou spectral (lié au temps de relaxation). Nous établissons une formule d'Eyring–Kramers modifiée qui prend en compte la géométrie spécifique de la frontière du domaine près des points-selles, démontrant que le préfacteur du taux de sortie est très sensible à la forme du domaine, d'une manière qui peut être calculée explicitement.

Nous proposons également une nouvelle méthode numérique pour optimiser la définition des états métastables. Les définitions standard basées sur les bassins d'attraction de l'énergie

potentielle sont souvent sous-optimales, particulièrement lorsque les effets entropiques sont importants. Nous formulons la définition d'un état métastable comme un problème d'*optimisation de forme* pour un objectif dépendant des valeurs propres, visant à maximiser la séparation des échelles de temps, comprise comme le rapport entre le temps de sortie et le temps de relaxation local. Nous dérivons des dérivées de forme analytiques pour les valeurs propres de Dirichlet de diffusions réversibles et construisons un algorithme robuste d'ascension locale pour déformer la frontière du domaine. Pour gérer les difficultés liées à la grande dimension des systèmes moléculaires, nous proposons une stratégie basée sur un "coarse-graining" dynamique utilisant des variables collectives. Nous validons cette méthodologie sur un système biologique, démontrant empiriquement que les domaines optimisés peuvent apporter des améliorations notables dans la séparation des échelles de temps par rapport aux définitions standard.

Le deuxième axe de la thèse se concentre sur la *dynamique moléculaire hors équilibre* (NEMD) et le calcul des coefficients de transport, tels que la mobilité et la viscosité de cisaillement. Les méthodes NEMD standard imposent une force externe fixe et mesurent le flux moyen résultant. Nous introduisons une approche duale basée sur une dynamique stochastique contrainte. Dans ce cadre, le flux est contraint à une valeur fixe, et la force moyenne requise pour maintenir ce flux est mesurée. Nous dérivons l'équation différentielle stochastique régissant ces dynamiques dans un cadre général, et nous nous concentrons sur les systèmes de Langevin sous-amortis, typiquement utilisés en pratique pour calculer ces coefficients de transport. À travers des expériences numériques sur des fluides de Lennard–Jones, nous démontrons empiriquement que la méthode à flux constant produit des estimateurs de réponse linéaire équivalents dans la limite thermodynamique, et que ces estimateurs présentent souvent une variance asymptotique plus faible que les estimateurs NEMD standard, ce qui fait de la méthode duale une alternative efficace numériquement pour le calcul de propriétés de transport.

Enfin, une dernière contribution aborde le lien rigoureux entre deux modèles de dynamique moléculaire. Nous étudions la limite de l'équation de Langevin dite cinétique ou sous-amortie dans le régime grande friction, avec un coefficient de friction anisotrope dépendant de la variable de position. En dérivant de nouvelles estimées d'analyse fonctionnelle dites *hypocoercives*, nous fournissons une nouvelle preuve de la convergence du processus de position vers la dynamique de Langevin sur-amortie avec des coefficients de diffusion anisotropes. Cette approche évite les complexités de certaines méthodes précédentes et élucide clairement l'origine du terme de dérive induit par le bruit dans l'équation limite.

Remerciements

Il est facile de s'imaginer qu'une thèse en mathématiques est le fruit d'un travail solitaire. C'est complètement faux, et il faut commencer ce manuscrit par quelques mots pour les nombreuses personnes qui ont rendu ce travail possible et qui ont enrichi les trois dernières années de ma vie.

Mes premiers mots vont à Gabriel, qui m'a fait confiance en premier en me proposant un stage de M2, et m'a à cette occasion fait découvrir cet univers scientifique passionnant qu'est la dynamique moléculaire. À toi et à Tony, pour votre encadrement d'une bienveillance et d'une rigueur totale, pour les nombreuses opportunités humaines et scientifiques que vous m'avez offertes, et pour votre délicatesse quand il s'agissait de me faire atterrir, je vous témoigne ma reconnaissance non-bornée. C'est également grâce à Gabriel que je possède ma meilleure (et à vrai dire mon unique) poêle à frire.

Je voudrais profondément remercier Josselin Garnier et Laurent Michel, qui ont accepté de rapporter cette thèse malgré la longueur de ce manuscrit. Merci pour leurs remarques précieuses. Merci également à Nils Berglund, Emma Horton, Sylvie Méléard et Yannick Privat d'avoir participé à mon jury de thèse.

À Danny Perez, pour avoir posé en premier la question qui m'a occupé pendant deux ans, et pour les nombreux échanges scientifiques très intéressants que nous avons pu avoir à Chicago et ailleurs, merci. Merci également à Joe Greener, d'avoir créé Molly.jl, qui m'a beaucoup facilité la tâche, et de m'avoir invité à Cambridge pour y travailler, je garderai un excellent souvenir de cette semaine au LMB.

Outre les personnes que j'ai déjà citées, je remercie tous les autres qui m'ont permis de présenter mes travaux et d'échanger en dehors de mon entourage immédiat. Je pense notamment à Éric Cancès, à qui je dois également mon financement de thèse, Alessandra Bianchi, Matteo Quattropani, Feliks Nüske, Wei Zhang, Sebastian Matera, Laurent Michel, Francis Nier, Boris Nectoux, Dorian Le Peutrec, Julien Reygner, Mouad Ramil, Thomas Swinburne, Xiaocheng Shang, Alessandra Iacobucci, Rachel Kurchin et Michael Herbst, avec qui je continue en postdoc. Ces conférences, écoles d'été et groupes de travail ont aussi été l'occasion de m'ouvrir à un très large champ de points de vue sur mon domaine de recherche et tant d'autres, et ont contribué pour beaucoup à rendre ce travail possible et motivant. Je pense en particulier aux discussions du groupe de travail sur les méthodes d'échantillonnage dynamique à Jussieu,

dont je remercie les habitués pour les nombreuses discussions très stimulantes: Olivier Adjoua, Nicolaï Gouraud, Jérôme Hénin, Louis Lagardère, Pierre Monmarché et Thomas Plé.

Merci à Aurélien Alfonsi et Urbain Vaes pour m'avoir donné l'opportunité d'enseigner à l'École des Ponts. Merci en particulier à Urbain de m'avoir associé à l'élaboration du cours de calcul scientifique en Julia, ce fut une expérience très agréable et formatrice. Merci bien sûr aux étudiantes et aux étudiants, et particulièrement à Alfonso Mateos Vicente et Jack Prezerowitz, que j'ai pu encadrer pendant leur projet ou leur stage respectivement.

Merci à Isabelle, Stéphanie et Julien G. pour leur soutien légendaire en toutes circonstances, et pour leur indulgence face à mes nombreux faux pas administratifs. Merci en particulier d'avoir permis l'organisation de ces journées mémorables à Provins et à Parent.

La qualité de la recherche au CERMICS doit beaucoup à l'excellente ambiance qui règne parmi ses membres non-permanents. Je dis merci du fond du coeur à tous ceux que j'ai croisés durant ces trois dernières années, pour avoir rendu meilleure chaque journée que j'ai passée au labo. Merci à Albéric, Amélie, Anh-Dung, Annamaria, Antonin D., Antoine, Bahaa, Camila, Clément, Cyrille, Elise, Emanuele, Épiphane, Étienne, Fabian, François C., François, Gabriele, Gaspard, Germain, Giulia, Grégoire E., Grégoire O., Guillaume C., Guillaume S., Hadrien, Hélène, Héloïse, Henri, Hervé, Jean, Jonathan, Julien W., Kacem, Kexin, Laura, Laurent, Léo B., Léo R., Louis-Pierre, Lu, Luis-Enrique, Maël, Martin, Mathias, Mathis A., Mathis B., Matteo, Nail, Owen, Paul, Pierre, Rekha, Rémy, Roberta, Rose, Rutger, Seta, Simon, Sofiane, Solène, Thibault, Thomas B., Vincent, Vitor, Yann, Yubo, Yukuan et Zuodong. Merci en particulier à Alfred, Alicia, Edoardo, Éloise, Régis, Solal, Théo et Zoé, pour les sorties course à pied à Noisiel ou ailleurs. Merci à la team phys-stat: Charlotte, Antonin C., Inass, Jean-Baptiste, Louis, Raphaël, Pierre M., Renato, Shiva et Thomas P., pour les nombreuses discussions et les moments conviviaux que nous avons pu vivre à Dresde, Chicago, Bilbao, Magdeburg, Birmingham ou l'Aquila. Je souhaite du courage et de la réussite à Charlotte et Raphaël pour leur troisième année de thèse, et de même à ceux qui suivront.

Je remercie les dieux du hasard et leurs exécutants. Steve, par ta grâce, je m'en sors au bout de trois années avec un log-ratio café offert/café payé sensiblement positif, merci également pour ta propre positivité. Merci au RER A de m'avoir, pour l'essentiel, épargné ses aléas.[1]

Merci à Samuel, Sarah et Joaquim pour les heures à grimper ou à soulever de la fonte, à Ali et à Clovis d'avoir partagé avec moi cet appartement à Aubervilliers, et à vous tous pour votre humour, vos engagements politiques, et votre sens de la fête. Votre amitié embellit ma vie.

Merci à mes parents, qui m'ont apporté leur amour et leur soutien depuis tant d'années, et à mes frères Luc et Thomas, qui me ressemblent si peu, mais que j'aime tellement. Merci à mes grands-parents, biologiques et adoptifs, qui ont toujours été des boussoles. Merci en particulier à André pour ton exemple – ce manuscrit t'est dédié.

Emma, merci pour ta patience, ces derniers mois à m'attendre, alors que tu venais toi-même de rentrer d'un si long voyage. Merci pour notre amour et toutes les choses que nous partageons.

[1] Mes sentiments à l'égard de la Deutsche Bahn sont plus mitigés.

Contents

Chapter 1

Introduction

This thesis addresses some theoretical and algorithmic questions in computational physics from the mathematical point of view. Our contributions are motivated by persistent challenges in the computation of dynamical properties in molecular systems, both in the equilibrium and nonequilibrium settings, using stochastic models of molecular motion. Computing dynamical properties requires sampling informative microscopic trajectories of the molecular system of interest. The main obstruction is *metastability*, a central phenomenon in this thesis, which implies that such trajectories are necessarily long relative to the timescales of thermal atomic motion. For many systems, the timescale gap is such that sampling sufficiently long trajectories is simply infeasible with standard methods, and requires the conception, analysis and implementation of dedicated numerical strategies.

In Section 1.1, we present a (necessarily incomplete) overview of the field of molecular dynamics, with a particular emphasis on the mathematical framework which will be used throughout this thesis. In Section 1.2, we present in more detail the problem of measuring dynamical properties, as well as one class of algorithmic solutions designed to address the sampling of long trajectories, the so-called *accelerated molecular dynamics* (AMD) methods of Arthur Voter and collaborators, see [332, 333, 334, 312]. For the purpose of introducing these methods clearly and identifying the main algorithmic questions, this discussion is partly formal. We review in Section 1.3 some of the main mathematical approaches to study metastability in molecular systems, and introduce useful mathematical formalism in view of analyzing and optimizing the efficiency of AMD algorithms. We finally present the contributions of this thesis in Section 1.4.

1.1 An overview of molecular dynamics

Molecular dynamics (MD) is a set of techniques aimed at extracting properties of atomistic systems from carefully designed computer simulations. For details on the associated algorithms and additional background on MD from an applied perspective, we refer the interested reader to [7, 133, 324]. Due to the development of flexible and efficient methodologies, as well as the steady increase in available computational power over the last seventy years, MD has

become a mainstay of computational physics, and is now routinely used in a variety of scientific applications from computational thermodynamics and material science to drug discovery and cell biology. We refer to [26] for a historical perspective. Fundamentally, MD simulates the time-evolution of systems at the atomic scale, by treating atoms as classical point particles, whose trajectories are governed by a defined set of dynamical laws. From the simulation and recording of these trajectories, several important scientific needs can be covered. Indeed, MD is simultaneously:

- *A means to compute properties of matter*: MD provides numerical estimators for thermodynamic, structural and dynamical quantities that may be difficult or impossible to measure experimentally, due to extreme conditions or prohibitive costs. This includes materials which have not been synthesized yet, so that MD is a crucial tool in new materials discovery. Typical outputs include radial distribution functions, free-energy differences, pressure and enthalpy, defect formation energies, reaction rates, and transport coefficients. With sufficiently long sampling, MD yields statistically converged values that can be used to parametrize coarser models. The computation of dynamical properties, and the associated need for long-time microscopic sampling, are the core motivation for the contributions of this thesis.

- *A numerical microscope*: MD simulations allow to resolve molecular trajectories at a level of detail which is far beyond the reach of physical experiments. The analysis of MD trajectories can help to visualize reaction pathways, identify transition states, observe collective rearrangements (such as nucleation, defect propagation or protein folding), and extract mechanistic hypotheses that guide theoretical developments and experiments. These insights are especially valuable for understanding rare events and conformational changes, where a single trajectory can reveal the sequence of microscopic steps behind an observed macroscopic transition. MD simulations can be understood as *in silico* experiments, which have become an important tool of modern materials and biological research.

- *A benchmark for new methods*: an important use case of MD simulations is the development and testing of novel numerical and modelling tools for MD itself, which in turn often have implications for computational science at large. Because realistic atomistic simulations combine the challenges of high dimensionality, multimodality, anisotropy, time-dependent signals and multiscale behavior, they make a perfect testbed to prototype and benchmark numerical methods.

- *A hurdle for theory*: high-fidelity MD simulations have themselves become a source of "ground truth" data. Notably, long trajectories produced on bespoke hardware [300] are routinely used to test biophysical hypotheses and to train data-driven models. At the same time, algorithms used in MD simulations are sources of inspiration for many interesting mathematical questions, which are still a fruitful area of research, and some of which we address in this thesis.

Appreciating the vast discrepancies between the atomic, macroscopic and computational realms is key to understanding the scope of molecular dynamics simulations. It is therefore

instructive to review some of the characteristic scales at play. Some typical atomistic orders of magnitude are given below.

- Macroscopic amounts of matter are counted in moles of molecules, which are multiples of Avogadro's number $N_\mathrm{A} = 6.022 \times 10^{23}$. A tablespoon of liquid water at room temperature contains about 0.8 moles of H_2O molecules.
- Length is measured in units of Ångströms ($1\ \text{Å} = 10^{-10}\,\mathrm{m}$). For example, the Bohr radius of hydrogen is 0.529 Å, while the helix of B-DNA has a diameter of 20 Å.
- Time is measured in units of femtoseconds ($1\,\mathrm{fs} = 10^{-15}\,\mathrm{s}$), which is also the typical timestep for MD simulations. The fastest molecular motions, such as the period of hydrogen bond stretching vibrational modes, are of the order of 10 fs.

For comparison, we list some orders of magnitude related to the scale of achievable computations.

- A 2018 projection [278] estimates the size of the global "datasphere" (the total amount of digital information on Earth) to reach 175 zettabytes by 2025, which corresponds to $0.29\,N_\mathrm{A}$ bytes.
- Typical consumer machines provide on the order of 10^{12} bytes of persistent storage capacity, whereas data centers and high-performance computing facilities operate at the 10^{15}–10^{18} bytes scale.
- Personal CPUs and GPUs deliver on the order of 10^{9}–10^{12} floating-point operations per second (FLOPS), while modern exascale machines target sustained performance at around 10^{18} FLOPS [297].

This profound disparity between available computational resources and atomic scales implies that MD will fall short of fully resolving the microscopic trajectories of macroscopic systems (say, a second-long evolution of a millimeter-sized sample) for a foreseeable future.

The floating-point operation cost of advancing the simulation by a single timestep typically scales linearly with the number of atoms in the system: this fact imposes a hard limit on the (length × system size) of a feasible simulation given available computational resources at any fixed time. Critically, it also reveals a present bottleneck for observing phenomena of scientific interest: with timesteps on the order of 1fs, simulating a single μs of a system's evolution requires executing on the order of a billion sequential steps. Yet, many important processes are known to take place over timescales of milliseconds to seconds, or even longer.

Nevertheless, landmark MD simulations have consistently scaled up to larger numbers of atoms (and also to longer simulation times, but for rather different reasons). Scaling in the spatial domain (i.e. increasing the number of atoms in the system) can be achieved by exploiting a common property of molecular systems, namely the *locality* of interactions. This property allows to distribute the cost of advancing the simulation by one timestep, leveraging parallel computing architectures and domain decomposition algorithms. This locality is the structural property which allows the linear scaling of the cost of MD simulations with system

size. The link between locality and scalability is as ancient as MD itself, and underpins some of the earliest algorithmic innovations in the field, such as neighbor lists [328].

The situation is seemingly bleaker in the time domain. The sequential nature of trajectories forbids distributing the computational cost of a single long simulation across parallel simulations of shorter segments. At first glance, the only way to extend the achievable computational timescales is by hardware-level or low-level software optimizations of the simulation procedure. This challenge is known as the *timescale problem* of MD. While progress has been made using this brute-force approach, today still, for a typical solvated protein, a full day of computation on one high-performance GPU yields, at best, a few hundred ns of trajectory time [170], and still much less for the large systems of interest to materials science.

To enable the simulation of long trajectories for relevant systems (without requiring access to highly specialized hardware) sophisticated algorithms have to be developed to go beyond sequential MD. A class of such methods are the so-called *accelerated MD* methods pioneered by Arthur Voter [332, 334, 312], which play a crucial role in this thesis, and are discussed in further detail in Section 1.2 below. Similarly to the algorithms allowing to scale in space, these methods rely on a structural property of many molecular systems, namely their *metastability*. Loosely speaking, a metastable system spends the majority of its time in long-lived, quasi-stationary states, punctuated by rare and abrupt transitions between them. Metastable systems have become an object of study in their own right in mathematical physics, for which many mathematical results have been obtained, some of which we review in Section 1.3, derive in Chapter 2, and apply in Chapter 3.

Some historical milestones. Despite the challenges discussed above, full-atom "brute-force" MD simulations have been successfully applied to various problems. Here we list some simulations, notable for their historical importance and/or their novel magnitude, both in the spatial and time domains.

- *1953*: Metropolis et al. [247] compute the equation of state for a hard-sphere model using a Monte Carlo method, spawning the field of computational statistical physics. This early work is followed in *1957* by the first simulation [4] of the molecular dynamics of a hard sphere model.
- *1964*: Rahman [273] measures properties of liquid Argon using a MD simulation of interacting Lennard–Jones particles. Results are consistent with experimental measurements. This is followed in *1971* by the more challenging case of liquid water [274] by Rahman and Stillinger.
- *1975*: Levitt and Warshel [237] simulate a protein folding using a coarse-grained energy minimization procedure.
- *1988*: Levitt and Sharon [236] perform the first simulation of a protein in explicit water solvent, a 0.2 nanosecond-long trajectory.
- *1998*: Duan and Kollman [109] publish the first microsecond-long simulation of a fast-folding protein in explicit solvent, the villin headpiece, exposing the intricate mechanisms underlying protein folding.

- *2002*: Abraham et al. [1] carry out the first MD simulation involving more than a billion atoms, a short trajectory of a flawed FCC crystal undergoing ductile failure.
- *2008*: Germann and Kadau [135] report the first MD simulation involving a trillion atoms, 40 timesteps of a Lennard–Jones crystal.
- *2010*: Shaw et al. [301] perform the first millisecond-long simulation of a protein in explicit solvent, using a dedicated machine design [300], and at great financial cost.
- *2017*: Perilla and Schulten [269] publish a full-atom simulation of the HIV-1 viral capsid in water (64 million atoms for 1.2 μs).

Long MD trajectories provide valuable insight into the thermodynamic and kinetic properties of molecular systems, by revealing their microscopic states and how they change in time. The framework of statistical mechanics, which we now introduce, connects the microscopic state of a physical system to its macroscopic properties, and in so doing provides the basis for the measurement of physical properties from simulation data.

1.1.1 Elements of statistical mechanics

Statistical mechanics is the rigorous attempt to reconcile the microscopic point of view, in which a system's many microscopic degrees of freedom evolve according to fundamental physical laws, and the macroscopic point of view, according to which only a handful of variables are relevant to describe the system's state and evolution. Here, we present the necessary formalism to treat the molecular systems of interest in MD. In particular, we restrict our scope to classical systems. We note however that a similar Gibbsian formalism also exists for quantum systems (see [126, 20]) and has been more generally used to great effect in the study of a variety of disordered systems, such as spin glasses [113], Hopfield networks [265] and their quantum counterparts [282, 287].

Microscopic states, their energy and classical dynamics. In this thesis, we consider systems of $N \geqslant 1$ point particles, representing classical atomic nuclei. The system's microscopic configuration, or *microstate*, is described by the positions and momenta (masses times velocities) of each one of these nuclei. The microstate therefore corresponds to a point in *phase space*,

$$(q, p) \in \mathcal{E} := \mathcal{Q} \times \mathcal{P}, \tag{1.1}$$

where $\mathcal{Q}$ is a configurational domain, and for a configuration $(q, p) \in \mathcal{E}$, $q \in \mathcal{Q}$ is the position variable, and $p \in \mathcal{P}$ is the associated momentum variable in the momentum space $\mathcal{P}$.

To each microstate $(q, p) \in \mathcal{E}$, we associate its energy $H(q, p)$. The function H is called the *Hamiltonian*. In most situations, $\mathcal{Q} \subset \mathbb{R}^{3N}$, $\mathcal{P} = \mathbb{R}^{3N}$, and the Hamiltonian takes the

separable form

$$H(q,p) = V(q) + \frac{1}{2}p^\top M^{-1}p, \qquad M = \begin{pmatrix} m_1\mathbb{I}_3 & 0 & \cdots & 0 \\ 0 & m_2\mathbb{I}_3 & \cdots & 0 \\ \vdots & \ddots & \ddots & \vdots \\ 0 & \cdots & 0 & m_N\mathbb{I}_3 \end{pmatrix} \tag{1.2}$$

where $V : \mathcal{Q} \to \mathbb{R}$ is a potential energy function, the term $K(p) = \frac{1}{2}p^\top M^{-1}p$ is the kinetic energy, and M is a diagonal matrix encoding the atomic masses in the system, with $m_i > 0$ giving the mass of the i-th particle for $1 \leqslant i \leqslant N$. For $1 \leqslant i \leqslant N$, we will also denote by $q_i \in \mathbb{R}^3$ and $p_i \in \mathbb{R}^3$ respectively the position and momentum of the i-th nucleus.

The classical equations of motion, as described by Newton's second law, can be written compactly using the Hamiltonian (1.2). They are equivalently expressed by the following ordinary differential equation in $\mathcal{E}$:

$$\frac{\mathrm{d}}{\mathrm{d}t} X_t = J\nabla H(X_t), \qquad X_t = (q_t, p_t) \in \mathcal{E}, \tag{1.3}$$

where J is the *symplectic matrix*

$$J = \begin{pmatrix} 0 & \mathbb{I}_{3N} \\ -\mathbb{I}_{3N} & 0 \end{pmatrix}. \tag{1.4}$$

In this form, the equation (1.3) is known as *Hamiltonian dynamics*, and its trajectories in phase space describe the time-evolution of an isolated system of classical particles.

On the choice of the interaction potential V. The potential is the crucial physical ingredient, as it encodes the interactions between nuclei, and thus deeply influence their dynamics. Ideally, it is defined by the ground-state energy $V_{\mathrm{BO}}(q)$ of the electronic Hamiltonian associated to a given position $q \in \mathcal{Q}$ of classical nuclei, in the Born–Oppenheimer approximation [56]. For systems of interest in MD, computing V_{BO} requires solving a very high-dimensional partial differential equation (PDE) eigenvalue problem, which is computationally prohibitive. Instead, one resorts to a variety of approximations to estimate V_{BO}, or rather its gradient ∇V_{BO} with respect to q, since the dynamics (1.3) only depends on the force $-\nabla V$. These classes of approximations are also known as *force fields*, of which we distinguish three main families.

- *Ab initio methods* leverage the considerable work in electronic structure theory over the last 100 years. Many numerical methods have been developed to address the problem of approximating the ground-state V_{BO}: with no claim of exhaustivity, popular schemes include the Hartree–Fock method, the more precise (and costly) post–Hartree–Fock methods, as well as methods rooted in density functional theory (DFT), see [188, 65] for comprehensive introductions. While such methods can be very accurate, as they incorporate quantum effects of the electronic structure in the classical nuclear dynamics, their poor scaling with respect to system size and their high cost of evaluation limit their applications to small systems and short simulation times. They are nevertheless essential to capture some phenomena, such as bond-breaking in chemical reactions.

- *Empirical force fields*, which constitute the most important class of methods historically, proceed by first selecting a set of prototypical systems $\mathcal{S}$, and for each $s \in \mathcal{S}$, introducing a parametric ansatz $V_\theta^s(q)$ for V_{BO}. The functional form of V_θ^s is hand-crafted to find a balance between physical principles and computational efficiency. To allow the functional form to be transferable to systems with varying number of atoms and molecular topologies, V_θ^s is usually expressed as a sum of local energy contributions from each atom in s, which are themselves functions of the corresponding *atomic environment*, given by the relative positions of neighboring atoms, their species, and their adjacency relationship in the covalent bond structure. A regression can then be performed to select an optimal parameter θ^*, in order to replicate a set of targeted thermodynamic or structural properties over $\mathcal{S}$, measured either experimentally or using ab initio computations. The empirical potential $V_{\theta^*}^{s'}$ can then be used to probe systems $s' \notin \mathcal{S}$. The oldest and simplest example of empirical potential is the Lennard–Jones pair-potential (Equation (1.6) below), which only uses two parameters. Many families of force-fields of this type are still widely used, such as CHARMM [63], AMBER [264] and GROMOS [299] for biomolecules, EAM [92] and MEAM [25] for metallic systems, or Tersoff-type potentials [316] for multi-species solids.

- *Machine-learned interatomic potentials* (MLIPs) can be understood as the application of modern machine-learning architectures to the empirical approach described above. While they are conceptually the same, the two approaches nevertheless differ in that the parameter θ no longer has any clear physical meaning. MLIPs have recently gathered interest, due to the hope of nearly matching the accuracy of ab-initio methods at a fraction of their computational cost. This promise has gained some credence in recent years, due to the demonstrated flexibility of various machine-learning architectures, and to the rapid increase in the availability of ab-initio training data. We refer to [28, 184] for recent overviews. This class of models typically defines the potential in two steps, by first computing for each atom a feature vector of so-called *descriptors* encoding its atomic environment, and designed to enforce some physical priors, such as the locality of interactions and various symmetries. Common choices include radial symmetry functions [29], SOAP [23] and ACE [108] descriptors. In a second step, the descriptor is used as input to a machine-learning model, typically a linear model [319], neural network [29] or Gaussian process [24], giving the energy contribution for a single atom. Summing over atoms gives the final functional form. Crucially, forces on each atom, which are required for dynamics (and training the model), can usually be computed efficiently using reverse-mode automatic differentiation [27].

To give a concrete example–which will be used in Chapter 3– we consider the simplest variant of the AMBER [264] force-field. It decomposes the potential energy into contributions associated with bond stretching, bond bending, torsional energy, and pairwise interactions, modelling Van der Waals and electrostatic interactions between nuclei. More precisely, the

interatomic potential is given by

$$\begin{aligned} V(q) = &\sum_{\text{bonds }\{i,j\}} \frac{k_{\mathrm{b}}^{ij}}{2}(r_{ij} - r_0^{ij})^2 + \sum_{\text{angles }\{i,j,k\}} \frac{k_{\mathrm{a}}^{ij}}{2}(\alpha_{ijk} - \alpha_0^{ijk})^2 \\ &+ \sum_{\text{dihedrals }\{i,j,k,\ell\}} E^{ijk\ell}\left(1 + \cos\left(n^{ijk\ell}\phi_{ijk\ell} - \gamma^{ijk\ell}\right)\right) \\ &+ \sum_{1\leqslant i<j\leqslant N} \left(4\varepsilon_{ij}\left[\left(\frac{\sigma^{ij}}{r_{ij}}\right)^{12} - \left(\frac{\sigma^{ij}}{r_{ij}}\right)^{6}\right] + \frac{C^{ij}}{r_{ij}}\right), \end{aligned} \tag{1.5}$$

where the first three sums give the so-called *bonded* energy contributions, and run over covalent bond chains of increasing length involving atom i: 2-chains defining a bond length $r_{ij} = |q_i - q_j|$, 3-chains defining a bond angle α_{ijk}, and 4-chains defining a dihedral (or torsional) angle $\phi_{ijk\ell}$. The final two sums give the *non-bonded* contributions, respectively a Lennard–Jones type term, and a Coulombic interaction term. The various parameters $\theta^{ijk\ell} = \left(k_{\mathrm{b}}^{ij}, r_0^{ij}, k_{\mathrm{a}}^{ijk}, \alpha_0^{ijk}, E^{ijk\ell}, n^{ijk\ell}, \gamma^{ijk\ell}, \varepsilon^{ij}, \sigma^{ij}, C^{ij}\right)$ are determined by the atomic species of atoms i, j, k and ℓ, as well as their ordering in the covalent chain for bonded interaction terms. This functional form can be decomposed into a sum $V(q) = \sum_{i=1}^{N} V_i(q)$, where V_i is the contribution of atom i to the total energy. A schematic representation of the different types of bonded interaction terms is given in Figure 1.2.

For simpler systems, such as monoatomic noble-gas fluids, this general form reduces to the Lennard–Jones potential

$$V(q) = \sum_{1\leqslant i<j\leqslant N} V_{\mathrm{LJ}}\left(|q_i - q_j|\right), \qquad V_{\mathrm{LJ}}(r) = 4\varepsilon\left[\left(\frac{\sigma}{r}\right)^{12} - \left(\frac{\sigma}{r}\right)^{6}\right], \tag{1.6}$$

which now depends only on two parameters, an energy ε and a length σ, and which we will use in Chapter 4. It is represented for reference in Figure 1.1.

In the case where the position domain $\mathcal{Q} = (L\mathbb{T})^d$ is periodic (see the next paragraph), some modifications to the non-bonded interaction terms in (1.5) are generally performed for the sake of efficiency. Namely, the short-range Lennard–Jones-type energy is truncated in such a way that all atomic pairs (i, j) with $r_{ij} > r_{\mathrm{c}}$ do not contribute, where $0 < r_{\mathrm{c}} < L/2$ is a fixed cutoff-radius, see [7, Section 1.6.3], and the choice $r_{\mathrm{c}} < L/2$ ensures that no atom interacts with one of its periodic images. A finite cutoff radius implies that forces need only be computed for pairs of neighboring atoms, which represents a substantial efficiency gain in large systems. Various cutoff strategies ensure the regularity of the resulting potential (see [7, Section 5.2.3]). The cutoff radius should be chosen sufficiently large in order for the modified potential to be a small perturbation of the original one. For this reason, this simple strategy cannot be applied to Coulombic interaction terms which decay too slowly with respect to interatomic distance, except in prohibitively large systems. To treat these Coulombic long-range terms, a number of strategies have been proposed, most notably those based on the Ewald summation trick, see [133, Chapter 12] and [7, Chapter 6]. This family of methods relies on a preliminary approximation of the system's charge density, and on the fact that the electrostatic energy of a periodic charge density can be evaluated efficiently, by considering the electrostatic Poisson equation in the Fourier representation.

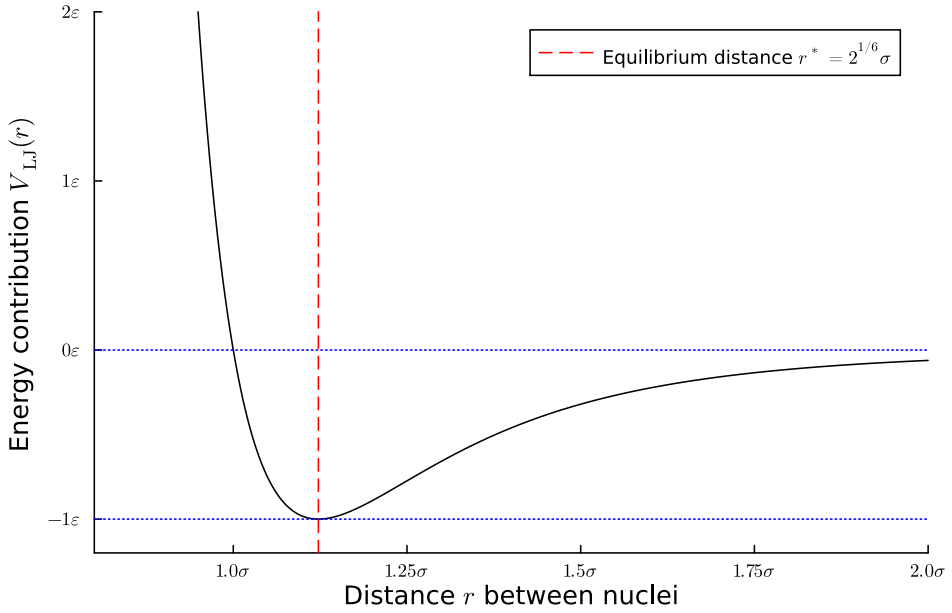

Figure 1.1: The pairwise Lennard–Jones potential defined in (1.6). The functional form imposes a Van der Waals-like attraction between nuclei further apart than the equilibrium distance $r^* = 2^{1/6}\sigma$, and a very strong repulsion between nuclei closer than r^*.

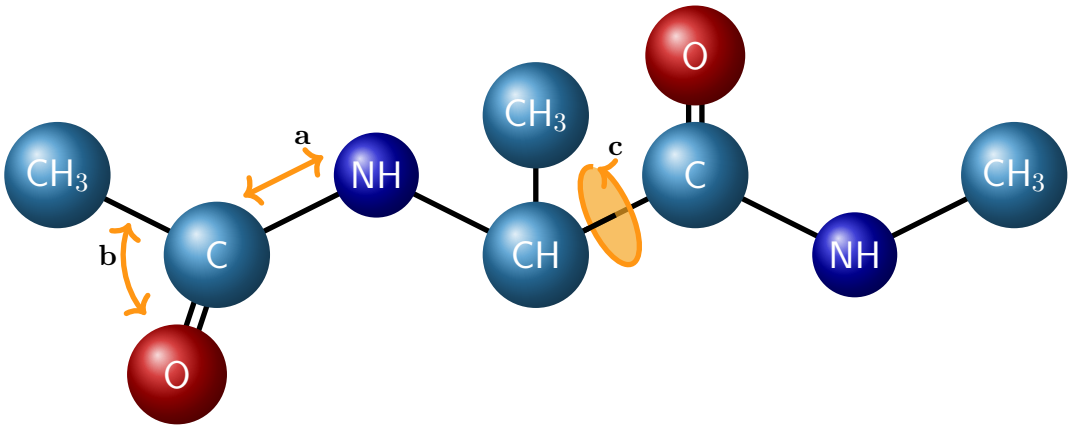

Figure 1.2: Bond topology of alanine dipeptide, a toy model for a protein, often used as a benchmark biophysical system, including in Chapter 3. Orange arrows give examples of contributing modes to the AMBER energy (1.5). **a**: Stretching of the (C–N) bond. **b**: Angle bending associated to the (C–C=O) 3-chain. **c** Torsion of the backbone dihedral angle Ψ, defined by the (N–C–C–N) 4-chain. Hydrogen bonds are not represented for the sake of readability.

Boundary conditions. The specific definition of the phase space $\mathcal{E}$ depends on the physical model and properties of interest. We distinguish several common choices.

- *Periodic boundary conditions*: this common choice corresponds to setting $\mathcal{Q} = (L\mathbb{T})^d$ and $\mathcal{P} = \mathbb{R}^d$, where $\mathbb{T} = \mathbb{R}/\mathbb{Z}$ is the unit one-dimensional torus, $d = 3N$ is the number of position degrees of freedom in the system, and $L > 0$ is a length parameter fixing the size of the domain. This setup is essential for studying the bulk properties of matter, as the periodic unit cell models a small portion of the molecular medium while its images represent the surrounding environment, reducing surface effects.

- *Unbounded domains*: setting $\mathcal{Q}$ and $\mathcal{P}$ equal to $\mathbb{R}^d$ is appropriate for studying isolated molecular systems, such as small atomic clusters or single molecules in vacuum.

- *Non-flat position manifolds*: for certain applications, it is useful to restrict the particle positions to a non-flat manifold $\mathcal{Q}$. This can be useful for enforcing geometric constraints, such as fixed bond length or angles, or for expressing the equations of motion in non-Cartesian coordinates [326]. Such constraints can improve the stability of numerical schemes [293, 10, 22], allowing for larger time steps, and can be used for computing free energy differences [308, 230]. In this geometric setting, the momentum associated to a given position $q \in \mathcal{Q}$ is a cotangent vector $p \in T^*_q\mathcal{Q}$, and the phase space $\mathcal{E}$ is the cotangent bundle: $\mathcal{E} = T^*\mathcal{Q}$, which no longer has the simple product form (1.1).

- *Exotic boundary conditions*: for the purpose of some specialized simulations, one can consider a variety of additional boundary conditions. For instance, one can consider walls at the boundary of a domain $\partial\mathcal{Q}$, on which particles are subject to specular and diffusive reflections, or absorption. Absorbing boundary conditions play a crucial role in the local approach to metastability, see Section 1.3 below and Chapters 2 and 3 of this thesis. Mixed conditions, which are periodic with respect to a subset of coordinates, can be used to study interfaces such as cell membranes, see for example [53]. One can even consider time-dependent definitions, such as Lees–Edwards boundary conditions [215], which allow to study shear flows.

The choice of boundary conditions fixes the geometry of the phase space. The next step is to relate this collection of microstates to the macroscopic state of the system.

Statistical ensembles. The basic postulate of statistical mechanics, as formalized by Gibbs in [136], is that the system's macroscopic configuration is a probability distribution $\pi \in \mathcal{P}(\mathcal{E})$ over the set of possible microstates. The distribution π is also known as a statistical or *thermodynamic ensemble*. In this statistical description, the ensemble π assigns to each microstate a likelihood of being the microscopic realization of an observed macrostate, and the choice of ensemble is a basic modelling assumption.

Given a physical observable $\varphi : \mathcal{E} \to \mathbb{R}$, we can define the macroscopic value of φ as the *ensemble average*:

$$\mathbb{E}_\pi[\varphi] = \int_{\mathcal{E}} \varphi \, \mathrm{d}\pi. \tag{1.7}$$

For example, the pressure P of an isotropic fluid in a periodic box, described by pairwise interactions such as (1.6), can be expressed as an ensemble average (1.7) of the instantaneous bulk pressure:

$$\varphi_P(q,p) = \frac{1}{3L^3}\left(p^\top M^{-1} p - q^\top \nabla V(q)\right).$$

To make this notion of macroscopic configuration operational, one should have a principled way to assign a specific ensemble to a specific set of physical conditions. We distinguish two approaches.

- *Dynamical definitions.* In these constructions, the ensemble π is identified with an invariant probability measure or *steady state* of the system's underlying dynamics. Whether the dynamics are deterministic or stochastic, whenever the system is ergodic with respect to π, time averages of observables along a single, long trajectory will converge to the ensemble average (1.7). This approach provides a physical justification for the ensemble by connecting it directly to the microscopic time-evolution of the system, in the case a model of the microscopic dynamics is available. It also the viewpoint which underpins theoretically the computation of macroscopic properties using equilibrium and nonequilibrium molecular dynamics.

- Variational definitions based on the *principle of maximal entropy*, as described in [185, 186], offer a fairly general alternative. This approach frames the problem of determining the thermodynamic ensemble from the sole knowledge of macroscopic data as one of statistical inference. Namely, the ensemble π is defined as the probability distribution which maximizes the information entropy, given by the ensemble average $S[\pi] = -\langle \log \pi \rangle_\pi$ (with some abuse of notation), subject to a set of constraints fixed by observing the values of a finite number of macroscopic variables. Informally, this principle selects the most uninformative distribution compatible with the available information, and draws a connection between statistical mechanics and information theory. Solving for π generally leads to explicit expressions, without the need for any reference to a microscopic dynamics.

Examples of statistical ensembles. We now give some examples, the first two of which were introduced by Gibbs in [136], and are of primary interest for MD.

- *The microcanonical ensemble* (NVE) describes an isolated system with a fixed number of particles (N), volume (V), and total energy (E). It is given by the probability measure π_{NVE}, where

$$\forall\, A \in \mathcal{B}(\mathcal{E}), \qquad \pi_{NVE}(A) = \frac{1}{Z_{NVE}} \int_{A \cap H^{-1}(E)} |\nabla H|^{-1} \mathrm{d}\mathcal{H}_{H^{-1}(E)},$$

  where H is the Hamiltonian (1.2), $\mathcal{H}_{H^{-1}(E)}$ is the $(d-1)$-dimensional Hausdorff measure on the constant-energy surface $H^{-1}(E)$ and

$$Z_{NVE} = \int_{H^{-1}(E)} |\nabla H|^{-1} \mathrm{d}\mathcal{H}_{H^{-1}(E)}$$

is a normalizing constant known as the *microcanonical partition function*. Dynamically, it is an invariant measure of Hamiltonian dynamics (1.3) started at a point $X_0 \in H^{-1}(E)$. The choice of the microcanonical ensemble can also be motivated by postulating equiprobability for microstates of equal energy; the measure π_{NVE} can then be defined (see [229, Section 1.2.3.1]) as the limit as $\delta \to 0$ of uniform probability distributions on the energy shells $\mathcal{S}(E,\delta) := H^{-1}(E-\delta, E+\delta)$, which are known to maximize the information entropy in $\mathcal{P}(\mathcal{S}(E,\delta))$ (whenever $\mathcal{S}(E,\delta)$ is compact).

- *The canonical ensemble* (NVT) describes a system with fixed number of particles and volume, in thermal equilibrium with a heat bath at a constant temperature T. It is given by the *Boltzmann–Gibbs distribution*

$$\forall\, A \in \mathcal{B}(\mathcal{E}), \qquad \mu(A) = \frac{1}{Z_\mu(\beta)} \int_A \mathrm{e}^{-\beta H(q,p)}\, \mathrm{d}q\, \mathrm{d}p, \tag{1.8}$$

  where μ is parametrized by

$$\beta = (k_{\mathrm{B}} T)^{-1},$$

  k_{B} is Boltzmann's constant and

$$Z_\mu(\beta) = \int_{\mathcal{E}} \mathrm{e}^{-\beta H(q,p)}\, \mathrm{d}q\, \mathrm{d}p$$

  is the *canonical partition function*. It is an invariant probability measure for a system evolving under various dynamics (often stochastic, some of which are discussed in Section 1.1.2 below) which model the interaction with the heat bath. From the point of view of the maximum entropy principle, it is derived by maximizing the information entropy subject to the constraint of a fixed *average* energy, which is related to the temperature T by the formula $\langle H \rangle_\mu = -\frac{\partial}{\partial \beta} \log\, Z_\mu(\beta)$.

- Other equilibrium ensembles can be constructed to model more general physical conditions. The *isothermal-isobaric ensemble* (NPT) describes systems at constant temperature and pressure P, which are often relevant for biological applications, and is derived from the maximal entropy principle by fixing the average energy and average volume of the system (related to the pressure P). The *grand-canonical ensemble* ($\boldsymbol{\mu}$VT) describes systems that can exchange both heat and particles with a bath, and is defined by fixing the average energy and average particle number (related to the chemical potential $\boldsymbol{\mu}$).

- *Nonequilibrium ensembles*, describe systems driven away from thermal equilibrium by the application of non-conservative forces or thermal gradients. These systems are characterized by the presence of irreversible fluxes and entropy production. Most often, these ensembles are defined dynamically, as the invariant measure of some nonequilibrium process, in which case the ensemble is also known as a nonequilibrium steady-state (NESS). The question of finding variational constructions for nonequilibrium ensembles has been investigated in the physical literature (see [187]), but does not appear to be fully settled at this time. We elaborate on this type of ensemble in Section 1.2.2 below.

Finally, let us mention that *equivalence of ensembles* results allow to relate averages in one ensemble to averages in another. For instance, it has been shown that, for homogeneous

systems with short-range interactions, the NVE and NVT ensembles are equivalent (in several ways, and under technical conditions, see [323] for a detailed discussion) in the thermodynamic limit $N, V \to +\infty$ keeping the particle density $\rho = N/V$ fixed. In particular, so called *macrostate equivalence* results imply that, for intensive observables φ, the canonical averages $\mu(\varphi)$ and corresponding microcanonical averages $\pi_{NVE}(\varphi)$ converge to a common limit when $N \to +\infty$, where T and $E = Nu$ are chosen so that the canonical specific energy $\mu\left(H/N\right)$ converges to the microcanonical one u. Equivalence results for nonequilibrium ensembles is also a current topic of interest, see [76] for an example.

Collective variables and canonical free-energies. An important quantity associated with the canonical ensemble is the Helmholtz free-energy

$$A(\beta) = -\frac{1}{\beta} \log Z_\mu(\beta), \tag{1.9}$$

from which a variety of thermodynamic properties may be deduced as a function of the parameter β. For instance, a simple formal computation shows that the Helmholtz free-energy, information entropy $S(\beta) := -\langle \log\Big(\mathrm{e}^{-\beta H}/Z_\mu(\beta)\Big)\rangle_\mu$ and internal energy $U(\beta) := \langle H \rangle_\mu$ are related by the famous identity

$$A(\beta) = U(\beta) - \frac{1}{\beta} S(\beta).$$

Often, one is led to describe the microstate of the system with a *collective variable* (CV), also known as an order parameter or reaction coordinate. For simplicity, we consider here a one-dimensional CV, which is a map $\xi : \mathcal{E} \to \mathbb{R}$ (the extension to multi-dimensional CVs is discussed in Section 3.4.1 of Chapter 3). Generally, the CV ξ is chosen to summarize one of the microstate's key structural features: the value of some interatomic distance or angle, a measure of similarity with respect to some reference microstate, or a progress metric along a reference trajectory are all common examples of CVs. They are very useful to get an intuitive understanding of the microstate of a large molecular system. In turn, the CV induces a summarized description of the ensemble itself, via the pushforward measure $\xi_*\pi \in \mathcal{P}(\mathbb{R})$, defined by $\xi_*\pi(A) = \pi(\xi^{-1}(A))$ for any measurable subset $A \subset \mathbb{R}$.

In the case of the canonical ensemble $\pi = \mu$ (see (1.8)), and if ξ enjoys some regularity properties (for instance, it is enough to require that ξ be smooth with $\nabla\xi \neq 0$ everywhere), one can write a formula for $\xi_*\mu(A)$ using the coarea formula [199, Corollary 5.2.6]:

$$\xi_*\mu(A) = \frac{1}{Z_\mu(\beta)} \int_A \int_{\xi^{-1}(z)} \frac{\mathrm{e}^{-\beta H}}{|\nabla\xi|} \mathrm{d}\sigma_{\xi^{-1}(z)}\, \mathrm{d}z,$$

where $\sigma_{\xi^{-1}(z)}$ is the $(d-1)$-dimensional surface measure induced by the Lebesgue measure on the level set $\xi^{-1}(z)$. Defining, by analogy with (1.9), the *free-energy* associated with ξ as

$$A_\xi(z) = -\frac{1}{\beta} \log Z_\xi(z), \qquad Z_\xi(z) = \int_{\xi^{-1}(z)} \frac{\mathrm{e}^{-\beta H}}{|\nabla\xi|} \mathrm{d}\sigma_{\xi^{-1}(z)}, \tag{1.10}$$

we see that $\xi_*\mu$ has a density $Z_\mu(\beta)^{-1}\mathrm{e}^{-\beta A_\xi}$ with respect to the one-dimensional Lebesgue

measure.[1]

From the knowledge of A_ξ, one can recover the macroscopic value of any observable defined in terms of ξ. For $\varphi = \psi \circ \xi$, we have

$$\langle \varphi \rangle_\mu = \frac{\displaystyle\int_{-\infty}^{+\infty} \psi(z) \mathrm{e}^{-\beta A_\xi(z)} \, \mathrm{d}z}{\displaystyle\int_{-\infty}^{+\infty} \mathrm{e}^{-\beta A_\xi(z) \, \mathrm{d}z}}, \tag{1.11}$$

which can be computed with elementary methods. This explains why the determination of free energy A_ξ given an informative collective variable ξ is a central task in computational statistical physics. Numerous algorithms (see [229, 230], [233, Section 4] for an overview of methods) have been developed to address this specific challenge.

1.1.2 The configurational sampling problem

One of the important uses of MD is the measurement of thermodynamic properties, which corresponds to the task of computing the ensemble average (1.7) for a given microscopic observable φ. For example, so-called histogram methods [229, Section 2.5] for computing the free-energy (1.10) rely on such averages.

Since the integral in (1.7) has the same high dimensionality as the phase space (typically, $\dim \mathcal{E} = 6N$), these thermodynamic quantities cannot be computed using standard quadrature methods. Beyond the simplest cases in which (1.7) is analytically computable, one has to resort to a Monte Carlo method, which relies on the generation of sample configurations from the thermodynamic ensemble.

In the canonical ensemble, the equilibrium measure (1.8) can be written as a product measure $\mu(\mathrm{d}q \, \mathrm{d}p) = \nu(\mathrm{d}q)\kappa(\mathrm{d}p)$, where

$$\nu(\mathrm{d}q) = \frac{1}{Z_\nu(\beta)} \mathrm{e}^{-\beta V(q)} \mathrm{d}q, \qquad \kappa(\mathrm{d}p) = \left(\frac{\beta}{2\pi}\right)^{3N/2} \det M^{-1/2} \mathrm{e}^{-\frac{\beta}{2} p^\top M^{-1} p} \, \mathrm{d}p \tag{1.12}$$

are the configurational and kinetic marginal distributions under μ, respectively, and

$$Z_\nu(\beta) = \int_{\mathcal{Q}} \mathrm{e}^{-\beta V}$$

is the configurational partition function. Since κ is a simple Gaussian distribution, (pseudo-random) *i.i.d.* samples from κ can be generated very efficiently using elementary methods. Therefore the main challenge in this setting is to sample from ν, the *Gibbs measure*.

While we focus on the important case of sampling from μ or ν, some of the methods and concepts we describe are more general. To emphasize this point when needed, we introduce a generic configuration space $\mathcal{Y}$ (which will generally be $\mathcal{E}$ or $\mathcal{Q}$), and a target measure $\pi \in \mathcal{P}(\mathcal{Y})$

[1] Here, we note that adding a constant in the definition (1.10) of A_ξ only changes the normalizing constant for this density from $Z_\mu(\beta)$ to some other value. Such constants may appear depending on the chosen convention for the surface measure, for instance if one uses a $(d-1)$-dimensional Hausdorff measure. As the normalizing constant has no effect on the computation of averages via (1.11), we are primarily interested in *free-energy differences*.

(which will generally be μ or ν) possessing a density ρ with respect to some reference measure λ on $\mathcal{Y}$ (which will generally be the Lebesgue measure). In any case, the goal is to estimate, given a function $\varphi \in L^1(\mathcal{Y}, \pi)$, its average under π:

$$\pi(\varphi) = \int_{\mathcal{Y}} \varphi \, \mathrm{d}\pi = \int_{\mathcal{Y}} \varphi\rho \, \mathrm{d}\lambda. \tag{1.13}$$

Methods for estimating (1.13) generally fall into one of two categories: Markov Chain Monte Carlo (MCMC) methods [283, 238], based on the Metropolis–Hastings algorithm [247], or MD-based methods, which rely on time-discretizations of some underlying ergodic dynamics.

Link with Bayesian statistics. Before presenting MCMC methods, we stress that the task of estimating $\pi(\varphi)$ has many scientific applications beyond computational physics.

One of these is Bayesian inference. In this setting, one considers a family of probability distributions $\pi(x|\theta)\mathrm{d}x \in \mathcal{P}(\mathcal{D})$ on the set $\mathcal{D}$ of observable data, parametrized by $\theta \in \mathcal{Y}$. One also fixes a prior distribution $\Pi \in \mathcal{P}(\mathcal{Y})$ over the space of parameters. Given a realization x of the data, the *posterior distribution* $\pi(\cdot|x) \in \mathcal{P}(\mathcal{Y})$ is given by Bayes' rule: for $A \subset \mathcal{Y}$ a measurable set, it writes

$$\Pi(A|x) = \frac{\int_A \pi(x|\theta)\Pi(\mathrm{d}\theta)}{Z(x)}, \qquad Z(x) = \int_{\mathcal{Y}} \pi(x|\theta)\,\Pi(\mathrm{d}\theta).$$

Many tasks in Bayesian statistics can be viewed as computing averages with respect to the posterior distribution. For instance, the posterior predictive likelihood of observing some new realization $\widetilde{x} \in \mathcal{D}$ is given by the integral

$$\int_{\mathcal{Y}} \pi(\widetilde{x}|\theta)\Pi(\mathrm{d}\theta|x),$$

which is an ensemble average with respect to the posterior distribution. Such integrals, and others, are similar to those encountered in statistical physics in two key respects:

- The posterior distribution is typically high-dimensional, while not as high-dimensional as for MD applications.[2] The likelihood functions $\pi(\cdot|\theta)$ specify a model of the data-generation process, which may depend on a large number of parameters in many applications.
- The posterior distribution is known *up to a normalization constant*, in the sense that it has the density $Z(x)^{-1}\pi(x|\theta)$ with respect to the prior Π, where $\pi(x|\theta)$ is explicit. The only unknown quantity is the normalization constant $Z(x)$, which plays an analogous role to the partition function.

MCMC methods. Most of these methods are examples of the Metropolis–Hastings algorithm [247, 151], which provides a general method for constructing Markov chains whose

[2] The dimensionality of θ is typically of the order of 10^1–10^3, compared to the 10^4–10^6 (and sometimes more) degrees of freedom involved in modern MD systems.

stationary distribution is π, whenever the density ρ is known up to a normalization constant. MCMC methods are particularly well-suited to the problem of sampling microstates from the canonical ensemble, where the partition function is unknown, as well as from conditional distributions $\mu(\mathrm{d}q\,\mathrm{d}p|A) = \mu(A)^{-1}\mathrm{e}^{-\beta H(q,p)}\chi_A(q,p)\,\mathrm{d}q\,\mathrm{d}p$ for some subset $A \subset \mathcal{E}$.

The algorithm proceeds by generating a candidate configuration $y' \in \mathcal{Y}$ from a starting configuration $y \in \mathcal{Y}$, according to a Markov transition kernel $T(y'|y)\lambda(\mathrm{d}y')$. This proposed move is then accepted with some probability $\alpha(y'|y) \geqslant 0$, in which case the chain moves in the state y', or else is rejected, in which case the chain remains in the state y. The acceptance probability $\alpha(y'|y)$ is defined as the Metropolis ratio

$$\alpha(y'|y) = \min\left(1, \frac{\rho(y')T(y|y')}{\rho(y)T(y'|y)}\right).$$

This choice ensures that the resulting Markov chain, with transition kernel $K(y_2|y_1)\lambda(\mathrm{d}y_2)$, is reversible with respect to π, due to the *detailed balance condition*

$$\rho(y_1)K(y_2|y_1) = \rho(y_2)K(y_1|y_2).$$

Given a trajectory $(y_j)_{j\geqslant 1}$ of this chain, a natural estimator for the average (1.13) is given, for a sampled trajectory of length $J \geqslant 1$, by the trajectory average

$$\widehat{\varphi}_J = \frac{1}{J}\sum_{j=1}^{J}\varphi(y_j). \tag{1.14}$$

To justify the quality of these estimators, it is possible, under certain irreducibility conditions on the kernel K (see for instance [248, Theorem 17.0.1] or [107, Chapter 21]), to obtain ergodic and central limit theorems (CLTs)

$$\widehat{\varphi}_J \xrightarrow[\mathbb{P}_y-\text{almost surely}]{J\to+\infty} \pi(\varphi), \qquad \sqrt{J}\left(\widehat{\varphi}_J - \pi(\varphi)\right) \xrightarrow[\text{in law}]{J\to+\infty} \mathcal{G}_\varphi \sim \mathcal{N}(0, \sigma^2_{\varphi,K}),$$

for any $y \in \mathcal{Y}$, where $\mathbb{P}_y$ is the law of the chain started from $y_0 = y$, and $\sigma^2_{\varphi,K}$ is the asymptotic variance

$$\sigma^2_{\varphi,K} = \mathrm{Var}_\pi(\varphi) + 2\sum_{j=1}^{\infty}\mathrm{Cov}_\pi\left(\varphi(y_0), \varphi(y_j)\right) < +\infty. \tag{1.15}$$

Such results prove the consistency of the method, and allow in principle to construct confidence intervals for the target quantity $\pi(\varphi)$. This goal raises the question of estimating $\sigma^2_{\varphi,K}$ from trajectory averages, for which some methods have been developed, see for instance [128], [133, Appendix D] or [229, Section 2.3.1.3] and references therein.

The efficiency of the algorithm in measuring $\pi(\varphi)$ critically depends on the choice of the proposal kernel density T, which should be designed to minimize $\sigma^2_{\varphi,K}$. In turn, this is achieved by making the time series $\varphi(y_i)$ as uncorrelated as possible. This is a difficult task in MD, due to the typical structure of the Gibbs measure ν, which consists of several sparse and often anisotropic high-probability modes separated by vast low-probability regions, which have to be overcome by the trajectories of the Markov chain. Various strategies have been proposed, ranging from rather inefficient local exploration strategies, such as random-walks [247] or so-called *Metropolized numerical schemes* for continuous-time dynamics (such as MALA [286, 284],

which is based on the overdamped Langevin dynamics, or HMC [110] and gHMC [175]–which are based on Hamiltonian dynamics), to global strategies leveraging recent progress in deep generative models, see for instance [257, 134, 179] and references therein.

Langevin dynamics and its overdamped limit. The second broad class of methods are based on continuous-time dynamics which are ergodic with respect to π. Here we only consider diffusion processes, which are stochastic processes with trajectories in the configuration space $\mathcal{Y}$, defined by the stochastic differential equation (SDE):

$$\mathrm{d}Y_t = b(Y_t)\,\mathrm{d}t + \sigma(Y_t)\,\mathrm{d}W_t, \tag{1.16}$$

where b is a vector field on $\mathcal{Y}$, σ is a matrix of $m \geqslant 1$ vector fields on $\mathcal{Y}$, and W is a standard m-dimensional Brownian motion. The generic dynamics (1.16) will be called the *equilibrium dynamics*, as we will consider nonequilibrium perturbations of this SDE in Section 1.2.2. Various other processes we do not elaborate on, such as piecewise deterministic Markov processes (PDMPs), could be considered instead of the diffusion (1.16) for the configurational sampling problem, see [123].

A standard example is the *underdamped Langevin dynamics*, the model of choice to describe the motion of molecular systems in thermal equilibrium, and a very common choice in applications. Its trajectories $(q_t^\gamma, p_t^\gamma)_{t\geqslant 0}$ are governed by the following second-order system of SDEs on $\mathcal{E}$:

$$\begin{cases} \mathrm{d}q_t^\gamma = M^{-1}p_t^\gamma\,\mathrm{d}t, \\ \mathrm{d}p_t^\gamma = -\nabla V(q_t^\gamma)\,\mathrm{d}t - \gamma M^{-1}p_t^\gamma\,\mathrm{d}t + \sqrt{\dfrac{2\gamma}{\beta}}\,\mathrm{d}W_t, \end{cases} \tag{1.17}$$

where $\gamma > 0$ is a *friction* parameter, W is a standard $3N$-dimensional Brownian motion, and $V : \mathcal{Q} \to \mathbb{R}$ is the interaction potential. One can rewrite the dynamics (1.17) as a first-order SDE, in the succinct form

$$\mathrm{d}X_t^\gamma = (J - \gamma\Pi_p)\nabla H(X_t^\gamma)\,\mathrm{d}t + \sqrt{\frac{2\gamma}{\beta}}\Pi_p \mathrm{d}\widetilde{W}_t, \tag{1.18}$$

where $X_t^\gamma = (q_t^\gamma, p_t^\gamma)$, J is the symplectic matrix defined in (1.4), Π_p is the orthogonal projection onto the p coordinate (i.e. $\Pi_p(q,p) = (0,p)$), and $\widetilde{W}$ is a standard $6N$-dimensional Brownian motion. Note that setting $\gamma = 0$ yields the Hamiltonian dynamics (1.3): the underdamped Langevin dynamics can therefore be understood as a perturbation of the classical equations of motion by an Ornstein–Uhlenbeck-type evolution in the momentum variable, corresponding to the SDE $\mathrm{d}p_t^\gamma = -\gamma M^{-1}p_t^\gamma \mathrm{d}t + \sqrt{2\gamma/\beta}\mathrm{d}W_t$ (and $\mathrm{d}q_t^\gamma = 0$ in the position variable), which is easily verified to preserve μ. By Liouville's theorem and energy conservation, the Hamiltonian dynamics also preserves μ (meaning that forall $t \in \mathbb{R}$, $\phi_{t*}\mu = \mu$, where ϕ_t is the Hamiltonian flow). Therefore, μ is an invariant probability measure for the underdamped Langevin dynamics as a whole. The rigorous version of this argument is discussed below.

The friction parameter γ in (1.17) can be understood as a rate of energy exchange with a surrounding heat bath; a physical justification for this interpretation can be found in the derivation [129] of the dynamics (1.17) as the effective motion of a Hamiltonian particle

interacting with a bath of M coupled harmonic oscillators, in the limit $M \to +\infty$. Another derivation of the dynamics (1.17) consists in considering the motion of a large spherical particle of mass $M > 0$ undergoing elastic collisions with an infinite bath of non-interacting point particles of mass $m > 0$, in the limit $M/m \to +\infty$, see [111, 104]. In this derivation, the coefficients of the dynamics can be expressed in terms of the density and velocity distribution of the ideal gas bath.

In the large-friction limit $\gamma \to +\infty$, one can show (see for example [229, Section 2.2.4] or Chapter 5 below) that time-rescaled position trajectories $(q^\gamma_{\gamma t})_{0 \leqslant t \leqslant T}$ converge to solutions $(X_t)_{0 \leqslant t \leqslant T}$ of the following SDE on $\mathcal{Q}$:

$$\mathrm{d}X_t = -\nabla V(X_t)\,\mathrm{d}t + \sqrt{\frac{2}{\beta}}\mathrm{d}W_t, \tag{1.19}$$

where W is again a $3N$-dimensional Brownian motion. This equation is named the *overdamped Langevin dynamics*, and admits ν as an invariant probability measure.

Similarly to the case of discrete-time Markov chains, ensemble averages are estimated via trajectory averages. To ensure that these averages are well-defined, one should show that the trajectories of the dynamics (1.17) and (1.19) can be defined over arbitrarily long times, which requires some conditions on the potential V. To give an example, the condition

$$V \in \mathcal{C}^\infty(\mathcal{Q}), \qquad \exists\, a, b, R > 0 : \forall\, |x| > R, \quad -\nabla V(x)^\top x \leqslant a - b|x|^2, \tag{V-\textbf{Conf}}$$

guarantees, using [280, Theorem 5.9][3] or [193, Theorem 3.5] that strong solutions $(q^\gamma_t, p^\gamma_t)_{t \geqslant 0}$ and $(X_t)_{t \geqslant 0}$ to (1.17) and (1.19) exist for all times. We stress that Assumption (V-**Conf**) is sufficient, but by no means necessary: this one has the advantage of being concise and ensuring both the finiteness of $Z_\nu(\beta)$ for all $\beta > 0$ and the everywhere-positivity of $\mathrm{e}^{-\beta V}$. This condition is trivially satisfied when $\mathcal{Q}$ is compact and V is smooth.

We finally note that one can consider generalizations of these equilibrium dynamics obtained by modifying the coefficients in (1.19) and (1.17) respectively, introducing (smooth) position-dependent matrix fields γ and $\sigma : \mathcal{Q} \to \mathbb{R}^{3N \times 3N}$. More precisely, considering the modified underdamped dynamics

$$\begin{cases} \mathrm{d}q^\gamma_t = M^{-1} p^\gamma_t\,\mathrm{d}t, \\ \mathrm{d}p^\gamma_t = -\nabla V(q^\gamma_t)\,\mathrm{d}t - \gamma(q^\gamma_t) M^{-1} p^\gamma_t\,\mathrm{d}t + \sigma(q^\gamma_t)\,\mathrm{d}W_t, \end{cases} \tag{1.20}$$

and the modified overdamped dynamics

$$\mathrm{d}X_t = -\gamma(X_t)\nabla V(X_t)\,\mathrm{d}t + \frac{1}{\beta}\mathrm{div}\,\gamma(X_t)\,\mathrm{d}t + \sigma(X_t)\,\mathrm{d}W_t, \tag{1.21}$$

where div denotes the row-wise divergence operator, it is easy to show that these dynamics preserve μ and ν respectively, provided the matrix-valued functions γ and σ are related by the

[3] In the overdamped case, the Lyapunov function $W(x) = |x|^2 + c$ for some $c \geqslant 1$ will do in [280, Theorem 5.9]. The condition also implies that $V(x) \xrightarrow{|x| \to +\infty} +\infty$, so that the conditions of [280, Example 5.10] are satisfied.

fluctuation-dissipation relation

$$\sigma\sigma^\top = \frac{2\gamma}{\beta}. \tag{1.22}$$

In particular, γ must be symmetric negative semidefinite. The dynamical relevance of the coefficients γ and σ have to be assessed on a case-by-case basis. Regardless of the physical interpretation of these coefficients, these modified dynamics provide a valid sampling instrument to generate canonical microstates. A natural question in this perspective is the *optimization* of the matrix γ to improve the efficiency of the associated sampling method, see [70, 86, 226, 232] for recent works in this direction. Both the dynamics (1.21) and (1.20) play a role in this thesis, see Chapter 3 for (1.21) and Chapter 5 for (1.20).

Ergodic averages. Given an observable $\varphi \in L^1(\mathcal{Y}, \pi)$ an estimator for the average $\pi(\varphi)$ is given by the trajectory or *ergodic average*:

$$\widehat{\varphi}_T = \frac{1}{T}\int_0^T \varphi(Y_t)\,\mathrm{d}t, \tag{1.23}$$

of a continuous-time ergodic process Y with trajectories in $\mathcal{Y}$, invariant under π, typically the solution to a Brownian SDE such as (1.16). The invariance condition means that

$$\int_A \mathbb{P}_y(Y_t \in A)\,\pi(\mathrm{d}y) = \pi(A)$$

for all measurable $A \subset \mathcal{Y}$ and all $t \geqslant 0$, where $\mathbb{P}_y$ denotes the law of Y started from $Y_0 = y$. Similarly to the case of estimators coming from MCMC algorithms, the consistency and accuracy of the estimator (1.23) should be checked. This is most easily done by introducing the *infinitesimal generator* associated with the dynamics.

Infinitesimal generator. For any continuous-time process Y with trajectories in $\mathcal{Y}$ such as the equilibrium dynamics (1.16), we may define two operators:

$$T_t^Y f(y_0) = \int_{\mathcal{Y}} f(y)\mathbb{P}_{y_0}(Y_t \in \mathrm{d}y) = \mathbb{E}_{y_0}[f(Y_t)], \qquad \mathcal{L}^Y f = \lim_{t\to 0^+} \frac{T_t^Y f - f}{t}.$$

The family of operators $(T_t^Y)_{t\geqslant 0}$ forms the *transition semigroup* for the process Y. It is a semigroup of contractions on the Banach space $(\mathcal{C}_0(\mathcal{Y}), \sup_{\mathcal{Y}} |\cdot|)$ of continuous functions vanishing at infinity (or equivalently the closure of the space $\mathcal{C}_c^\infty(\mathcal{Y})$ of test functions for the sup-norm). Provided Y has the Feller property (see [279, Section III.2]), it is in fact a C_0-semigroup, with generator $\mathcal{L}^Y$. We will often use the notation $\mathrm{e}^{t\mathcal{L}^Y} := T_t^Y$.

Assuming the law $\psi(t,y)\,\mathrm{d}y$ of the time-marginal Y_t admits a $\mathcal{C}^2$ λ-density $\psi(t,\cdot)$ at any time $t \geqslant 0$, this density is a solution to the *Fokker–Planck equation*:

$$\partial_t \psi = \left(\mathcal{L}^Y\right)^\dagger \psi, \tag{1.24}$$

where the operator $\left(\mathcal{L}^Y\right)^\dagger$ denotes the formal $L^2(\lambda)$-adjoint of the generator, acting in the spatial component. When no such density exists, an equation like (1.24) applies to P_t^Y, but

only *a priori* in the sense of distributions, in which case $\left(\mathcal{L}^Y\right)^\dagger$ should be interpreted as the generator of the dual semigroup acting on $\mathcal{P}(\mathcal{Y})$.

Many stability properties of the dynamics are encoded by the generator, and can often be revealed by considering the generator's action on a well-chosen Lyapunov function, see [243, 280, 150] for some of the many applications of this strategy.

Under Assumption *V*-**Conf**, both the underdamped and overdamped dynamics are Feller processes with continuous trajectories (see [193, Theorem 3.5]), and their generators $\mathcal{L}_\gamma := \mathcal{L}^{(q^\gamma,p^\gamma)}$ and $\mathcal{L} := \mathcal{L}^X$ act on the space $\mathcal{C}_c^\infty$ of smooth compactly supported functions as second-order differential operators

$$\mathcal{L}_\gamma = A + B + \gamma O, \text{ where } \begin{cases} A = p^\top M^{-1} \nabla_q, \\ B = -\nabla V^\top \nabla_p, \\ O = -p^\top M^{-1} \nabla_p + \dfrac{1}{\beta} \Delta_p, \end{cases} \text{ and } \mathcal{L} = -\nabla V^\top \nabla + \frac{1}{\beta} \Delta, \tag{1.25}$$

where the indices under the operators $\nabla_q, \nabla_p, \Delta_p$ indicate the variable with respect to which differentials are taken. The operator $\mathcal{L}_{\text{ham}} := A + B$ is the generator of the Hamiltonian dynamics (1.3), while the operator γO is the generator of an Ornstein–Uhlenbeck process in the momentum variable. These expressions are a consequence of Itô's formula.

Given these expressions, checking that μ and ν are invariant measures for these respective dynamics simply amounts to checking, in view of (1.24), that

$$\mathcal{L}_\gamma^\dagger \mathrm{e}^{-\beta H} = \mathcal{L}^\dagger \mathrm{e}^{-\beta V} = 0. \tag{1.26}$$

Both the operators $\mathcal{L}$ and $\mathcal{L}_\gamma$ can be written in the form

$$\mathcal{A} = X_0 + \sum_{k=1}^{M} X_k^2, \tag{1.27}$$

for some first-order differential operators $(X_k)_{0 \leqslant k \leqslant M}$ satisfying *Hörmander's condition*. This condition requires that the algebra of iterated commutators associated to the decomposition (1.27) has full rank everywhere, namely

$$\dim \operatorname{Span} \left\{ X_{i_0}, [X_{i_0}, X_{i_1}], [[X_{i_0}, X_{i_1}], X_{i_2}], \dots, (i_j)_{j \geqslant 0} \in \{0, \dots, M\}^{\mathbb{N}} \right\} = D, \tag{1.28}$$

where $D = 3N$ if $\mathcal{A} = \mathcal{L}$, and $D = 6N$ if $\mathcal{A} = \mathcal{L}_\gamma$. This condition ensures that all the operators

$$\mathcal{L}, \mathcal{L}_\gamma, \mathcal{L}^\dagger, \mathcal{L}_\gamma^\dagger, \partial_t - \mathcal{L}, \partial_t - \mathcal{L}^\dagger$$

are *hypoelliptic* (see [174], [280, Section 7]), which implies in particular that the laws of the time marginals X_t and X_t^γ have smooth Lebesgue-densities for any $t > 0$. In fact $\mathcal{L}$ and $\mathcal{L}^\dagger$ are elliptic, owing to the fact that the diffusion matrix in (1.19) is non-degenerate, in contrast to the diffusion matrix in (1.18).

Convergence of trajectory averages. From the knowledge of an invariant probability measure with positive Lebesgue density (which follows from (1.26) as soon as $Z_\nu(\beta)$ is finite) and the hypoellipticity of the generators, the results of Kliemann [196] can be used to prove an ergodic theorem. [4] One can show in particular that, from any initial condition $(q,p) \in \mathcal{E}$ or $x \in \mathcal{Q}$, the trajectory average (1.23) converges almost-surely to the average of φ under the invariant measure.

To establish a CLT, one can use the results of [38] to show (see the discussion in [233, Section 3.1]) that, for $\varphi \in L^2(\mathcal{Y},\pi)$,

$$\sqrt{T}\left(\widehat{\varphi}_T - \pi(\varphi)\right) \xrightarrow[\text{in law}]{T\to+\infty} \mathcal{G} \sim \mathcal{N}\left(0,\sigma_\varphi^2\right), \qquad \sigma_\varphi^2 = 2\int_{\mathcal{Y}} \Pi\varphi(-\mathcal{L}^Y)^{-1}\Pi\varphi \,\mathrm{d}\pi, \tag{1.29}$$

where $\Pi f = f - \pi(f)$ denotes the centering projector with respect to π. The CLT is therefore valid as long as the Poisson equation $-\mathcal{L}^Y f = \Pi\varphi$ is well-posed, in the sense that such an f should exist and belong to $L^2(\mathcal{Y},\pi)$. A simple sufficient condition to this end is to establish an exponential decay bound

$$\exists \lambda, C > 0 : \forall\, t > 0, \qquad \left\| \mathrm{e}^{t\mathcal{L}^Y} \right\|_{E\to E} \leqslant C\mathrm{e}^{-\lambda t}, \tag{1.30}$$

on the operator norm of the semigroup, for some Banach space E continuously embedded in $\Pi L^2(\mathcal{Y},\pi)$. Note that bounds such as (1.30) can be used to establish the *convergence of time marginal distributions* of the process in various topologies, by duality.

The CLT (1.29) is then satisfied for any φ such that $\Pi\varphi \in E$, since the bound (1.30) ensures that

$$(-\mathcal{L}^Y)^{-1} = \int_0^{+\infty} \mathrm{e}^{t\mathcal{L}^Y}\,\mathrm{d}t \tag{1.31}$$

is a continuous inverse of $-\mathcal{L}^Y$ on E (so that the Poisson equation is well-posed), with moreover

$$\left\| \left(\mathcal{L}^Y\right)^{-1} \right\|_{E\to E} \leqslant \frac{C}{\lambda}. \tag{1.32}$$

The goal of establishing exponential decay estimates such as (1.30) motivates the study of the long-time behavior of the transition semigroup on $E = \Pi L^2(\mathcal{Q},\pi)$, which can be related to the spectrum of $\mathcal{L}^Y$ on the weighted space $L^2(\pi) := L^2(\mathcal{Y},\pi)$.

Spectral gap of the generator. Due to the invariance of π under the dual action of $\mathrm{e}^{t\mathcal{L}^Y}$, the family $(\mathrm{e}^{t\mathcal{L}^Y})_{t\geqslant 0}$ is also a C_0-semigroup of contractions on $L^2(\pi)$, whose infinitesimal generator we denote by $\mathcal{L}^Y$. We refer the reader to [240, Chapter 8] for a general discussion of the analytical properties of this semigroup and its generator in the elliptic case.

In the overdamped case, $\mathcal{C}_c^\infty(\mathcal{Q})$ is a core for $\mathcal{L}$ (see [240, Theorem 8.1.26]), and one has the equality (which follows on the core from an integration by parts, recalling the expression (1.25)

[4] The crucial point is to check Hörmander's condition (1.28). In the underdamped case, we write $\mathcal{L}_\gamma = X_0 + \frac{1}{2}\sum_{j=1}^{3N} X_j^2$ with $X_0 = A + B - \gamma p^\top M^{-1}\nabla_p$, and $X_j = \sqrt{\frac{2\gamma}{\beta}}\partial_{p_j}$ for $1 \leqslant j \leqslant 3N$. The commutator identity $\forall\, 1 \leqslant j \leqslant 3N$, $[X_0, X_j] = \left(M^{-1}(\gamma\nabla_p - \nabla_q)\right)_j$, implies that $\dim \mathrm{Span}\left\{X_1,\dots,X_{3N},[X_0,X_1],\dots,[X_0,X_{3N}]\right\} = 6N$. In the overdamped case, this condition is already verified without considering any commutators.

for $\mathcal{L}$):

$$\langle f, \mathcal{L}g \rangle_\nu = -\frac{1}{\beta} \int_{\mathcal{Q}} \nabla f^\top \nabla g \, \mathrm{d}\nu, \qquad \forall\, f \in H^1(\nu), g \in \mathcal{D}(\mathcal{L}), \tag{1.33}$$

and $\mathcal{D}(\mathcal{L}) \subset H^1(\nu)$, where the weighted Sobolev space

$$H^1(\nu) = \left\{ f \in L^2(\nu) : \nabla f \in L^2(\nu)^{3N} \right\}$$

is the form domain. The generator $\mathcal{L}$ is therefore symmetric on $L^2(\nu)$, and in fact self-adjoint, a property which reflects the reversibility of the dynamics (1.19) with respect to ν. The quadratic form (1.33) known as the *Dirichlet form* in the probability literature. Note in this case that the Fokker–Planck operator $\mathcal{L}^\dagger$ is also symmetric, but on the weighted space $L^2(\nu^{-1})$ weighted by the inverse of the Gibbs density, due to the identity $\int_{\mathcal{Q}} \mathcal{L}^\dagger \varphi \psi \mathrm{d}\nu^{-1} = \int_{\mathcal{Q}} (\varphi/\rho_\nu) \mathcal{L}(\psi/\rho_\nu) \mathrm{d}\nu$, where we write ρ_ν for the Gibbs density (1.12).

To study the spectral properties of the generator $\mathcal{L}^Y$, it is often convenient to consider a unitarily conjugated operator acting on the "flat" space $L^2(\mathcal{Y}, \lambda)$ obtained by reweighting observables, namely the operator $\rho^{1/2} \mathcal{L}^Y \rho^{-1/2}$.

Applying this conjugation to the overdamped generator $\mathcal{L}$, we obtain the so-called *Witten Laplacian*, introduced in [340], acting on $\mathcal{C}^\infty_{\mathrm{c}}(\mathcal{Q}) \subset L^2(\mathcal{Q})$ as:

$$\Delta_{V,\beta} := \mathrm{e}^{-\frac{\beta}{2}V} \mathcal{L} \mathrm{e}^{\frac{\beta}{2}V} = \frac{1}{\beta}\Delta - U_\beta, \qquad U_\beta := \frac{\beta}{4}|\nabla V|^2 - \frac{1}{2}\Delta V, \tag{1.34}$$

which now writes as a negative Schrödinger operator. The spectral properties of $\mathcal{L}$ can then be recovered from the well-developed spectral theory for quantum Hamiltonians. For example, a classical criterion (see [276, Theorem X.28]) implies that if U_β is bounded from below, the operator $\Delta_{V,\beta}$ is essentially self-adjoint on $\mathcal{C}^\infty_{\mathrm{c}}(\mathcal{Q})$, so that the (closed) operator $\mathcal{L}$ is self-adjoint. If $U_\beta(x) \xrightarrow{|x|\to+\infty} +\infty$, then the closure of $\Delta_{V,\beta}$ and therefore $\mathcal{L}$ have compact resolvents (see [277, Theorem XIII.67]), which implies that the spectrum of $\mathcal{L}$ consists of a discrete set of eigenvalues

$$0 = -\lambda_{0,\beta} > -\lambda_{1,\beta} \geqslant -\lambda_{2,\beta} \geqslant \cdots \tag{1.35}$$

enumerated with multiplicity, and such that $\lambda_{n,\beta} \xrightarrow{n\to+\infty} +\infty$. Note that the first eigenvalue, $\lambda_{0,\beta} = 0$, is simple (see for instance [277, Theorem XIII.47]), and corresponds to the subspace $\ker \mathcal{L} = \ker \Pi \subset L^2(\pi)$ of constant functions.

Under Assumption (**V-Conf**), a sufficient condition for the spectrum of $\mathcal{L}$ to be of the form (1.35) is that $\nabla^2 V$ is bounded or that $\mathcal{Q}$ is compact[5]. The Courant–Fisher characterization of $\lambda_{1,\beta}$ and the expression (1.33) then give the optimal *Poincaré inequality*:

$$\forall\, \varphi \in H^1(\nu), \qquad \|\Pi\varphi\|^2_{L^2(\nu)} \leqslant \frac{1}{\beta\lambda_{1,\beta}} \|\nabla\varphi\|^2_{L^2(\nu)}.$$

This inequality is well-known (see for instance [233, Proposition 2.3]) to be equivalent to the bound (1.30) with $E = \Pi L^2(\nu)$, $C = 1$ and $\lambda = \lambda_{1,\beta}$. In view of the bound (1.32), the asymptotic variance σ^2_φ can then be bounded in terms of the sharp exponent $\lambda_{1,\beta}$ and $\|\varphi\|^2_{L^2(\nu)}$. It is also possible to establish (suboptimal) Poincaré inequalities with direct estimates, under

[5] This follows easily from the fact that (**V-Conf**) implies $|\nabla V(x)| \geqslant b|x| - a/|x|$ for $|x| \geqslant R$.

the same growth assumption on U_β, see for example [329, Theorem A.1].

One can try to apply the same procedure to the generator $\mathcal{L}_\gamma$ of the underdamped Langevin dynamics, to obtain the *Kramers–Fokker–Planck* operator, acting on $\mathcal{C}_c^\infty(\mathcal{E}) \subset L^2(\mathcal{E})$ as:

$$P_{\gamma,V} := \mathrm{e}^{-\frac{\beta}{2}H}\mathcal{L}_\gamma \mathrm{e}^{\frac{\beta}{2}H} = \mathcal{L}_{\mathrm{ham}} + \gamma\Delta_{K(p),\beta},$$
$$\mathcal{L}_{\mathrm{ham}} = A + B, \qquad \Delta_{K(p),\beta} = \frac{1}{\beta}\Delta_p - \left(\frac{\beta}{4}|M^{-1}p|^2 - \frac{1}{2}\mathrm{Tr}(M^{-1})\right),$$

where $\Delta_{K(p),\beta}$ is a Witten Laplacian in the p-variable, associated to the kinetic energy $K(p) = \frac{1}{2}p^\top M^{-1}p$. It can be shown when $V \in \mathcal{C}^\infty(\mathcal{Q})$ that $\mathcal{C}_c^\infty(\mathcal{Q})$ is a core for $\mathcal{L}_\gamma$ [6], and that, under suitable conditions on the potential V and its derivatives, $\mathcal{L}_\gamma$ has compact resolvent, and therefore pure point spectrum[7] (see for example [254, Corollary 5.10]). Using hypoelliptic estimates related to $-P_{\gamma,V}^\dagger$, one can then establish (see [254, Theorem 6.4] or [169, 112] for earlier results) a bound such as (1.30) in $E = \Pi L^2(\mu)$, for some constant $C > 1$.

Beyond these abstract results, it is of considerable practical interest to obtain bounds of the form (1.30) which are quantitative, in the sense that the constants C and λ are explicit, or, failing this, scale in an explicit way with the physical parameters N, γ and β. It is also important to establish such bounds for dynamics other than (1.19) and (1.17), such as nonequilibrium dynamics (see Section 1.2.2 below) for which the invariant measure π is not necessarily explicit.

A variety of approaches have been developed to this end. To mention only a few, other choices of functional settings, corresponding to different choices of Banach space E can be considered, such as Lyapunov-weighted B^∞ spaces (see [280, Section 8]), including in some nonequilibrium settings [182], but the rates are rarely quantitative. Hypocoercive estimates (see for instance [329, 105, 106, 37] and references therein) offer a different route to decay bounds such as (1.30). These have the advantage of generally leading to explicit scalings of the decay exponent λ in terms of the friction parameter γ, in both the Hamiltonian limit $\gamma \to 0$ and the overdamped limit $\gamma \to +\infty$. These can also be extended perturbatively to some nonequilibrium settings [182, Theorems 1–3]. Finally, low-temperature spectral asymptotics (see [304, 195, 157, 61, 35, 166, 167, 168] and references therein) aim to give quantitative estimates of the optimal exponent λ in (1.30), in the limit $\beta \to +\infty$. Under suitable assumptions, one can derive Eyring–Kramers-type formulas for λ; broadly speaking, one can view a small value of λ as a signature of the metastability of the continuous dynamics, which therefore acts as an obstacle to efficient configurational sampling. We come back to this point in Section 1.3 below.

Discretizations of the Langevin dynamics. In practice, equations (1.17) and (1.19) cannot be solved exactly. Therefore, the trajectory averages (1.23) are approximated by ergodic averages along discrete-time trajectories generated by appropriate numerical schemes, two of

[6] A direct adaptation of the proof of [254, Proposition 5.5] shows that the closure $-\overline{P_{\gamma,V}}$ is maximally accretive in $L^2(\mathcal{E})$. Therefore, the closure $-\overline{A + B + \gamma O}$ of the differential operator (1.25) on $\mathcal{C}_c^\infty(\mathcal{E})$ is maximally accretive on $L^2(\mu)$: it must be the closed accretive operator $-\mathcal{L}_\gamma$.

[7] In fact, the *Helffer–Nier* conjecture (which is unsolved in full generality) proposes that $\mathcal{L}_\gamma$ has compact resolvent if and only if $\mathcal{L}$ has compact resolvent.

which we now present. In this paragraph, we choose a certain timestep parameter $\Delta t > 0$.

For the overdamped Langevin dynamics, a standard numerical scheme is given by the Euler–Maruyama method

$$X^{n+1} = X^n - \Delta t \nabla V(X^n) + \sqrt{\frac{2}{\beta}} \mathcal{G}^n_{\Delta t}, \qquad \mathcal{G}^n_{\Delta t} = W_{(n+1)\Delta t} - W_{n\Delta t},$$

which can be implemented easily because the Brownian increments $(\mathcal{G}^n_{\Delta t})_{n \geqslant 0}$ are *i.i.d.* with common law $\mathcal{N}(0, \Delta t \mathrm{Id}_{3N})$. This scheme therefore defines a Markov chain with transition kernel

$$P^{\mathrm{EM}}_{\Delta t}(x, \mathrm{d}x') = \left(\frac{\beta}{4\pi\Delta t}\right)^{3N/2} \mathrm{e}^{-\frac{\beta}{4\Delta t}|x - x' - \Delta t \nabla V(x)|^2} \mathrm{d}x'.$$

This scheme is also known in the MCMC literature as the unadjusted Langevin algorithm (ULA), by opposition to its Metropolis-adjusted counterpart (MALA [286, 284]).

For the underdamped Langevin dynamics, a popular family of methods is given by *splitting schemes*, which rely on the decomposition (1.25) of the generator $\mathcal{L}_{\gamma,\beta}$ as a sum of generators of explicitly solvable dynamics. Namely, simple computations show that the operators A, B and γO are the infinitesimal generators of the following transition semigroups:

$$\begin{cases} \mathrm{e}^{\Delta t A} \varphi(q,p) = \varphi\left(q + \Delta t M^{-1} p, p\right), \\ \mathrm{e}^{\Delta t B} \varphi(q,p) = \varphi\left(q, p - \Delta t \nabla V(q)\right), \\ \mathrm{e}^{\Delta t \gamma O} \varphi(q,p) = \mathbb{E}\left[\varphi\left(q, \mathrm{e}^{-\gamma \Delta t} p + \sqrt{\frac{2\gamma}{\beta}} \int_0^{\Delta t} \mathrm{e}^{-\gamma(\Delta t - s)} \mathrm{d}W_s\right)\right], \end{cases} \tag{1.36}$$

where the last operator rewrites, using Itô's isometry,

$$\mathrm{e}^{\Delta t \gamma O} \varphi(q,p) = \mathbb{E}\left[\varphi\left(q, \mathrm{e}^{-\gamma \Delta t} p + \sqrt{\frac{1 - \mathrm{e}^{-2\gamma \Delta t}}{\beta}} \mathcal{G}\right)\right], \qquad \mathcal{G} \sim \mathcal{N}(0, \mathrm{Id}_{3N}).$$

Many schemes can then be constructed based on various splittings of $\mathrm{e}^{\Delta t \mathcal{L}_\gamma}$. For example, the OBABO scheme is the Markov chain associated with the Strang splitting approximation

$$\mathrm{e}^{\Delta t \gamma O/2} \mathrm{e}^{\Delta t B/2} \mathrm{e}^{\Delta t A} \mathrm{e}^{\Delta t B/2} \mathrm{e}^{\Delta t \gamma O/2} \tag{1.37}$$

of the semigroup $\mathrm{e}^{\Delta t \mathcal{L}_\gamma}$. The transition kernel $P^{OBABO}_{\Delta t}(q, p, \mathrm{d}q', \mathrm{d}p')$ is the result of the dual action of the operator (1.37) on the Dirac measure $\delta_{(q,p)}$, and as for the case of the Euler–Maruyama scheme, it possesses a fully explicit Lebesgue-density.

In the case $\gamma = 0$, splitting schemes based on the transition operators (1.36) reduce to so-called *symplectic integrators* for the Hamiltonian dynamics (1.3). For instance, the velocity Verlet method corresponds to the splitting BAB, which is the $\gamma \to 0$ limit of the scheme (1.37). Symplectic schemes are well-known [147, 148] to mirror many of the qualitative properties of the Hamiltonian flow (in particular, they have long-term energy preservation properties) which makes them the standard choice for the integration of long trajectories of Hamiltonian systems.

Given a numerical scheme, an estimator $\widehat{\varphi}_{N,\Delta t}$ for the ensemble average (1.7) can be defined, using averages over trajectories of the associated Markov chain, just as for the MCMC estimators (1.14). In this case, the estimator $\widehat{\varphi}_{N,\Delta t}$ is associated to a time-discretization of a trajectory of the dynamics (1.17) or (1.19) of physical length $T_{\mathrm{sim}} = J\Delta t$. The existence of an invariant probability measure for the chain, and the convergence analysis for the estimator $\widehat{\varphi}_{J,\Delta t}$ can be performed using the general theory of discrete-time, continuous-space Markov chains, as in the case of MCMC estimators, see for instance [243, Section 6], [221], and references therein.

An important feature setting apart MD-based methods from MCMC-based methods is that the invariant measure $\pi_{\Delta t}$ associated to a particular numerical scheme is generically not the ensemble measure π associated with the average (1.13). As a consequence, the estimator $\widehat{\varphi}_{J,\Delta t}$ is typically not a consistent estimator of $\pi(\varphi)$ as $J \to +\infty$. To control this systematic bias, one can ensure the invariance of π by performing a Metropolis rejection step, as described above. In practice, this timestep bias is typically negligible compared to the statistical error for MD simulations. To nevertheless control this source of error, one can derive rigorous estimates in Δt for the bias $\pi_{\Delta t}(\varphi) - \pi(\varphi)$, see for instance [313], [233, Section 3.2.3], [221, Section 2.4]. In turn, these error estimates can be leveraged to reduce the systematic error, for instance by applying Richardson's extrapolation method [281], or using analytical correction schemes, see [233, Section 3.3.4].

For MD-based estimators, the asymptotic variance of the estimator $\widehat{\varphi}_{J,\Delta t}$ defined by numerical trajectory averages is given by

$$\sigma^2_{\Delta t,\varphi} = \mathrm{Var}_{\pi_{\Delta t}}(\varphi) + 2\sum_{n=1}^{+\infty} \mathrm{Cov}_{\pi_{\Delta t}}\left(\varphi(Y^0), \varphi(Y^n)\right),$$

where $(Y^n)_{n\geqslant 0}$ is the Markov chain defining the numerical scheme, with invariant measure $\pi_{\Delta t}$. This expression can be seen formally as an approximation of

$$\frac{2}{\Delta t}\int_0^{+\infty} \mathbb{E}_\pi\left[\Pi\varphi(Y_0)\Pi\varphi(Y_t)\right] \mathrm{d}t = \frac{1}{\Delta t}\sigma^2_\varphi,$$

using a trapezoidal quadrature rule for the time-integral, the substitutions $\pi_{\Delta t} \leftarrow \pi$ and $Y^n \leftarrow Y_{n\Delta t}$ for $n \geqslant 0$, and equations (1.29), (1.31) to express the continuous-time asymptotic variance σ^2_φ as an integrated autocorrelation. Considering the physical simulation time $T = J\Delta t$, this computation shows formally that the variance associated with discrete-time MD estimators is dictated (at dominant order and in the asymptotic regime $J \to +\infty$) by the variance of the corresponding continuous-time ergodic average $\widehat{\varphi}_T$ defined in (1.23). Rigorous error estimates justifying this assertion for various numerical schemes can be obtained, see for instance [233, Section 5.3.1] or [221, Section 2.5].

Enhanced sampling methods. For both MCMC and MD-based methods to estimate $\mathbb{E}_\pi[\varphi]$, the efficiency of a given estimator is determined by its asymptotic variance, respectively given by (1.15) and (1.39) for the naive trajectory estimators (1.14), (1.23). Due to the poor design of the proposition kernel K, or to the metastability of the continuous-time dynamics, these may suffer from a large asymptotic variance. Short of modifying the dynamics to improve

sampling, some alternative strategies can be implemented, inspired by classical variance reduction techniques. Enhanced sampling methods, particularly those aimed at computing the free energy (1.10), are a vast and important subject in the MD methodological literature. We refer to the perpetual review [162] for a more exhaustive overview and additional references.

- *Importance sampling* [322], [238, Section 2.5] consists in replacing the target ensemble π with a dominating probability measure $\pi' \gg \pi$, and computing the average with respect to π' of a reweighted observable. It derives from a simple identity:

$$\pi(\varphi) = \int_{\mathcal{Y}} \varphi\rho \, \mathrm{d}\lambda = \int_{\mathcal{Y}} \varphi\rho' \frac{\rho}{\rho'} \, \mathrm{d}\lambda = \pi'\left(\varphi \frac{\rho}{\rho'}\right), \tag{1.38}$$

  where $\pi'(\mathrm{d}y) = \rho'(y)\lambda(\mathrm{d}y)$. In the context of canonical sampling, i.e. when $\pi \in \{\nu, \mu\}$, a simple way to design π' is by adding a biasing potential $\widetilde{V}$ to the potential energy function V. Assuming for simplicity that φ only depends on atomic positions, the formula (1.38) writes

$$\pi(\varphi) = \frac{\displaystyle\int_{\mathcal{Q}} \varphi \, \mathrm{e}^{\beta\widetilde{V}} \mathrm{e}^{-\beta(V+\widetilde{V})}}{\displaystyle\int_{\mathcal{Q}} \mathrm{e}^{\beta\widetilde{V}} \mathrm{e}^{-\beta(V+\widetilde{V})}} = \frac{\pi'\left(\varphi \mathrm{e}^{\beta\widetilde{V}}\right)}{\pi'\left(\mathrm{e}^{\beta\widetilde{V}}\right)}.$$

  Both terms in this ratio can be estimated from trajectory averages of a *biased dynamics*, under one of the SDEs (1.17), (1.19), (1.20), (1.21) with the substitution $V \leftarrow V + \widetilde{V}$, or using MCMC methods. Often, the biasing potential is defined in terms of a collective variable, to focus sampling on a specific region of position space, or to reduce the height of free energy barriers. Importance sampling will be used in Chapter 3 of this thesis. Adaptive biasing techniques are a powerful class of related methods, we refer to [229, Chapter 5], [162, Section 7] and references therein for overviews.

- *Control variates*, in their simplest implementation, replace φ by $\varphi - c\psi$, for observables ψ such that $\pi(\psi) = 0$ and some scalar control $c \in \mathbb{R}$. One can estimate $\pi(\varphi) = \pi(\varphi - c\psi)$ with the naive estimators (1.14) or (1.23), and choose the control c to minimize the corresponding asymptotic variance, namely $\sigma^2_{K,\varphi-c\psi}$ or $\sigma^2_{\varphi-c\psi}$. In both cases, this leads to a closed-form expression for the optimal control, which in turn can be estimated from trajectory correlations. A simple way to ensure that $\pi(\psi) = 0$ is to take ψ in the range of the generator $\mathcal{L}^Y$, see for instance [233, Section 3.4.2] and [289]. Beyond this simple scheme, one can extend this strategy to multivariate controls, or controls which are themselves stochastic processes such as carefully chosen martingales, see for example [11, 161]. Martingale control variates are used extensively in Chapter 4 of this thesis.

- *Symmetrization*, in the spirit of antithetic variates, exploits symmetries in the system to construct new estimators from existing ones, by exploiting the identity

$$\pi(\varphi) = \mathbb{E}_\pi\left[\int_G \varphi \circ \psi_g \, \mu_G(\mathrm{d}g)\right],$$

  valid whenever $g \mapsto \psi_g$ is a group action of G on $\mathcal{Y}$ leaving π invariant, and $\mu_G \in \mathcal{P}(G)$ is any probability measure on G. For physical systems of indistinguishable particles, G is

typically generated by a set of rigid motions of the configuration space, and permutations of particles.

This family of methods is a simple way to ensure some amount of variance reduction, as implied by Jensen's inequality:

$$\mathbb{E}_\pi\left[\left(\int_G \varphi\circ\psi_g\,\mu_G(\mathrm{d}g)\right)^2\right] \leqslant \mathbb{E}_\pi\left[\int_G (\varphi\circ\psi_g)^2\,\mu_G(\mathrm{d}g)\right] = \mathbb{E}_\pi[\varphi^2].$$

This method is very general, as the same principle allows to use symmetries in the distribution of trajectories of the dynamics, which provides a simple approach to reducing the variance of estimators for the dynamical quantities discussed in Section 1.2 below. An example of symmetrization of dynamical averages applied to shear viscosity computations can be found in [96, 241].

- *Stratified sampling* relies on a decomposition of the configuration space in several regions, roughly corresponding to modes of π, which are sampled independently. This can be done more efficiently than sampling from π for well-defined regions. Samples from each region are then combined and reweighted according to the relative probability of each region under π. Various reweighting schemes are possible, see for instance [161, 302], and [233, Section 3.4.1] for details.

We refer to [162] for various other methods, such as so-called extended ensemble techniques, which augment the phase space with non-physical degrees of freedom allowing to bypass free-energy barriers.

1.2 The trajectorial sampling problem

In Section 1.1.2, we presented various methods for computing ensemble averages (1.7). In this section, we consider the problem of computing *dynamical properties*, which can be defined as averages over a *path ensemble* of microstate trajectories. It is intuitively clear that this is a qualitatively harder problem than the configurational sampling problem discussed in Section 1.1.2: in asking for trajectories, we traded a high but finite-dimensional space of microstates for an infinite-dimensional space of paths.

After a general approach to dynamical properties of interest, we present in Section 1.2.1 a class of methods which address the timescale problem introduced in Section 1.1, and which form a core motivation for the results of Chapters 2 and 3. Following this, we discuss the sampling of nonequilibrium response properties in Section 1.2.2, which motivate the contributions of Chapter 4.

Dynamical properties are determined by the underlying model of the molecular dynamics, which is usually an instance of one of the dynamics (1.20) or (1.21), but is at any rate given by a SDE of the form (1.16). In particular, while ensemble averages (1.13) were invariant with respect to particular choices of dynamical parameters (such as the choice of the parameter γ in the dynamics (1.17), (1.21) or (1.20)), dynamical properties are generically sensitive to these

choices, which should now therefore be regarded as physical modelling parameters, rather than hyperparameters of the sampling algorithm.

The computation of dynamical quantities is the main motivation for all the methods studied in this thesis. We begin by giving some typical examples of quantities of interest.

- *Autocorrelations.* Due to the CLT (1.29) for the ergodic average (1.23) of some $\varphi \in L^2(\pi)$, as well as the expression (1.31) for the inverse generator (which holds assuming a bound of the form (1.30)), the asymptotic variance can be written

$$\sigma_\varphi^2 = 2 \int_0^{+\infty} \mathrm{Cov}_\pi \left(\varphi(Y_t), \varphi(Y_0)\right) \, \mathrm{d}t. \tag{1.39}$$

  This integral, which is a functional of the trajectory, is the prototypical example of a dynamical property, and computing it is of practical interest to quantify the statistical uncertainty associated with estimators of the thermodynamic average $\pi(\varphi)$.

- *Path statistics.* Many quantities of interest can be reduced to path averages of the form

$$\mathbb{E}_{\pi_0} \left[f(\tau, Y_\tau) \right], \tag{1.40}$$

  where π_0 is some distribution of initial microstates, τ is a stopping time for the process Y, and $f : \mathbb{R} \times \mathcal{Y} \to \mathbb{R}$ is a measurable function. For example, given two closed disjoint subsets $A, B \subset \mathcal{Y}$, their respective hitting times τ_A, τ_B, and $C \subset \partial B$, the *committor function*, *mean first passage time* and the reactive *time distribution function* and *entering distribution kernel*, can be defined respectively as

$$\begin{aligned} h_{A\to B}(y) &= \mathbb{P}_y \left(\tau_B \leqslant \tau_A\right), \quad T_A(y) = \mathbb{E}_y \left[\tau_A\right], \\ F_{A\to B}(y,t) &= \frac{\mathbb{P}_y \left(\tau_B < t \leqslant \tau_A\right)}{h_{A\to B}(y)}, \quad \pi_{A\to B}(y, C) = \frac{\mathbb{P}_y \left(Y_{\tau_B} \in C, \tau_B \leqslant \tau_A\right)}{h_{A\to B}(y)}. \end{aligned} \tag{1.41}$$

  These are all examples of quantities which can be computed using averages of the form (1.40).

  The subsets A and B can be understood as ensembles of microstates corresponding to the reactant and product state of a given chemical reaction, or as discriminating between two metastable conformations of a molecule. Regardless of the specific interpretation, these quantities are of great interest in biology, where they can be used to estimate reaction rates, and resolve both the timescales and microscopic mechanisms underlying some of the most important biochemical processes, such as protein folding, protein-ligand binding and enzyme catalysis.

  The last two quantities in (1.41) are examples of *conditional path averages*, which can be challenging to compute with naive methods when $\mathbb{P}_y(\tau_B < \tau_A)$ is small. A variety of algorithms have been developed to address this specific problem (see for instance [97, 8, 68] and references therein).

- *Response properties* relate perturbations of the dynamics to perturbations of physical averages under these dynamics. More precisely, one considers a perturbation Y^η of the

equilibrium dynamics Y defined in (1.16), which should be thought of as a *nonequilibrium dynamics*. The associated invariant measure π_η is an example of a nonequilibrium thermodynamic ensemble, already introduced in Section 1.1. The goal is to compute perturbed thermodynamic averages $\pi_\eta(R)$ for a physically motivated response observable $R : \mathcal{Y} \to \mathbb{R}$, measuring an irreversible flux in the system. Although estimating the average flux $\pi_\eta(R)$ is conceptually precisely the configurational sampling problem from π_η we discussed in Section 1.1.2 above, the measure π_η is in general only defined implicitly by being stationary for the nonequilibrium dynamics. Sampling trajectories of these dynamics is therefore necessary to estimate the average flux. An important related quantity is the *linear response*, defined as the derivative $\alpha = \partial_\eta \pi_\eta(R)|_{\eta=0}$. The Green–Kubo formula (1.64) derived in Section 1.2.2 expresses the linear response as a specific functional of the equilibrium path ensemble, and explains why α can be viewed as a dynamical property. The computation of the linear response is the motivation for the method developed in Chapter 4 of this thesis. We elaborate on this specific and important case in Section 1.2.2 below. Finally, methods to compute alchemical free-energy differences via the Jarzynski–Crooks formula (see [229, Chapter 4]) also rely on sampling trajectories from nonequilibrium path ensembles.

The ability to measure dynamical properties hinges on the ability to sample unbiased, long trajectories of the dynamics. Sampled trajectories, to be useful, should be long enough so that the integral from a time T to $+\infty$ of the correlation in (1.39) can be neglected, or that the time τ corresponding to the event of interest is likely to have elapsed in (1.40). In most cases, sampling long trajectories is computationally prohibitive using naive methods, due to the timescale problem introduced in Section 1.1. The source of this challenge is the metastability of the system, whereby typical trajectories of the dynamics remain trapped in particular regions of the phase space for very long times before transitioning to other regions, where they remain trapped once again. These regions are called *metastable states*, and typical paths of the system alternate between long periods of residence within these metastable states and rare and rapid transitions between them.

The nature of the trapping mechanism associated to a metastable state Ω depends on the system under consideration. It may be that Ω contains some attractor y_0 for the equilibrium dynamics, whose neighborhood cannot be escaped by the dynamics, without entering regions of low likelihood according to π. This is the situation for the dynamics (1.17) or (1.19) around local energy minima of V surrounded by *energetic barriers* which are high relative to $k_\mathrm{B}T = \beta^{-1}$. It may also be the case that escaping Ω does not require crossing low-likelihood regions, but rather navigating narrow configurational pathways via a very specific realization of the driving noise. This is the typical obstacle to global conformational changes in organic molecules, which are forbidden by steric effects unless well-coordinated collective motions of atoms occur. In this case, we speak of *entropic barriers*, which are particularly pronounced in high-dimensional bonded systems.

In many cases, the presence of entropic barriers can be revealed by considering the free-energy landscape (1.10) given an appropriate collective variable $\xi : \mathcal{Y} \to \mathbb{R}$, corresponding to a *slow variable* of the system. We illustrate this point in the following example, which was suggested to us by Danny Perez.

Example 1.1 (Energetic versus entropic barriers.)**.** We consider, for $d \geqslant 1$, potentials on $\mathcal{Y} = \mathbb{R}^d$ of the form

$$V(y) = W(y_1) + k(y_1)|\hat{y}_1|^2, \tag{1.42}$$

where W, k are scalar-valued functions with $k > 0$ pointwise, and $\hat{y}_1 = (y_2, \dots, y_d)^\top \in \mathbb{R}^{d-1}$. We also choose the natural reaction coordinate $\xi(y) = y_1$, and the associated free-energy (1.10), which in this case can be computed analytically:

$$F_\xi(y_1) = W(y_1) + \frac{d-1}{2\beta} \log k(y_1) + C(d, \beta) \tag{1.43}$$

for some explicit constant $C(d, \beta)$. Different choices of W and k lead to different trapping mechanisms. The purely energetic case (see Figure 1.3 below for an example) corresponds to the choices $k(y_1) = 1$ and W possessing more than one local minimum. The purely entropic case (see Figure 1.4 below for an example) corresponds to the case where W has only one local minimum (which is therefore global), but where k displays some spatial dependence. In each case ξ is a *slow variable* of the system, with metastable states separated by *free-energy barriers* in F_ξ. In the cold regime $\beta \gg d$, the energetic barriers from W are the dominant terms in the expression (1.43), while in the high-dimensional regime $d \gg \beta$, entropic contributions from k are the primary effect.

1.2.1 Accelerated MD algorithms

The timescale problem is a direct consequence of the metastable nature of most molecular systems. As illustrated in Example 1.1, the dynamics can become trapped for long periods in metastable states corresponding to local minima of the free-energy landscape. Transitions between these states require the system to cross high free-energy barriers, which are, by definition, infrequent events. In these metastable systems, most of the wall-clock time of a sequential MD simulation will be spent in the simulation of thermal fluctuations within free-energy basins, which are typically uninformative. To overcome this issue, the family of *accelerated MD* (AMD) algorithms has been proposed to go beyond sequential MD.

Here, we choose a slightly different setup than what can be found in other reviews of AMD (see for instance [337, 267] or [233, Sections 6.3 & 6.4]), allowing for the definition of more general metastable states, which can in particular overlap. We consider a collection of subsets of $\mathcal{Y}$, denoted by $(\Omega_\alpha)_{\alpha \in I}$, each representing a distinct metastable region of the configuration space, which we call *metastable states*. We assume that for each $\alpha \in I$, $\mathcal{Y} \setminus \Omega_\alpha$ has non-empty interior. Within each state Ω_α, we define a *core-set* or *milestone* $C_\alpha \subsetneq \Omega_\alpha$. We assume that core-sets are disjoint:

$$\forall \alpha \neq \alpha', \qquad C_\alpha \cap C_{\alpha'} = \varnothing. \tag{1.44}$$

We recursively define a sequence of events, corresponding to the sequence of visits to the set of milestones. This sequence consists in a sequence of hitting times $(\tau_n)_{n \geqslant 0}$, as well as a sequence of milestone indices $(\alpha_n)_{n \geqslant 0}$. The sequence is defined as follows: let $\tau_{-1} = 0$, $\alpha_{-1} = \varnothing$

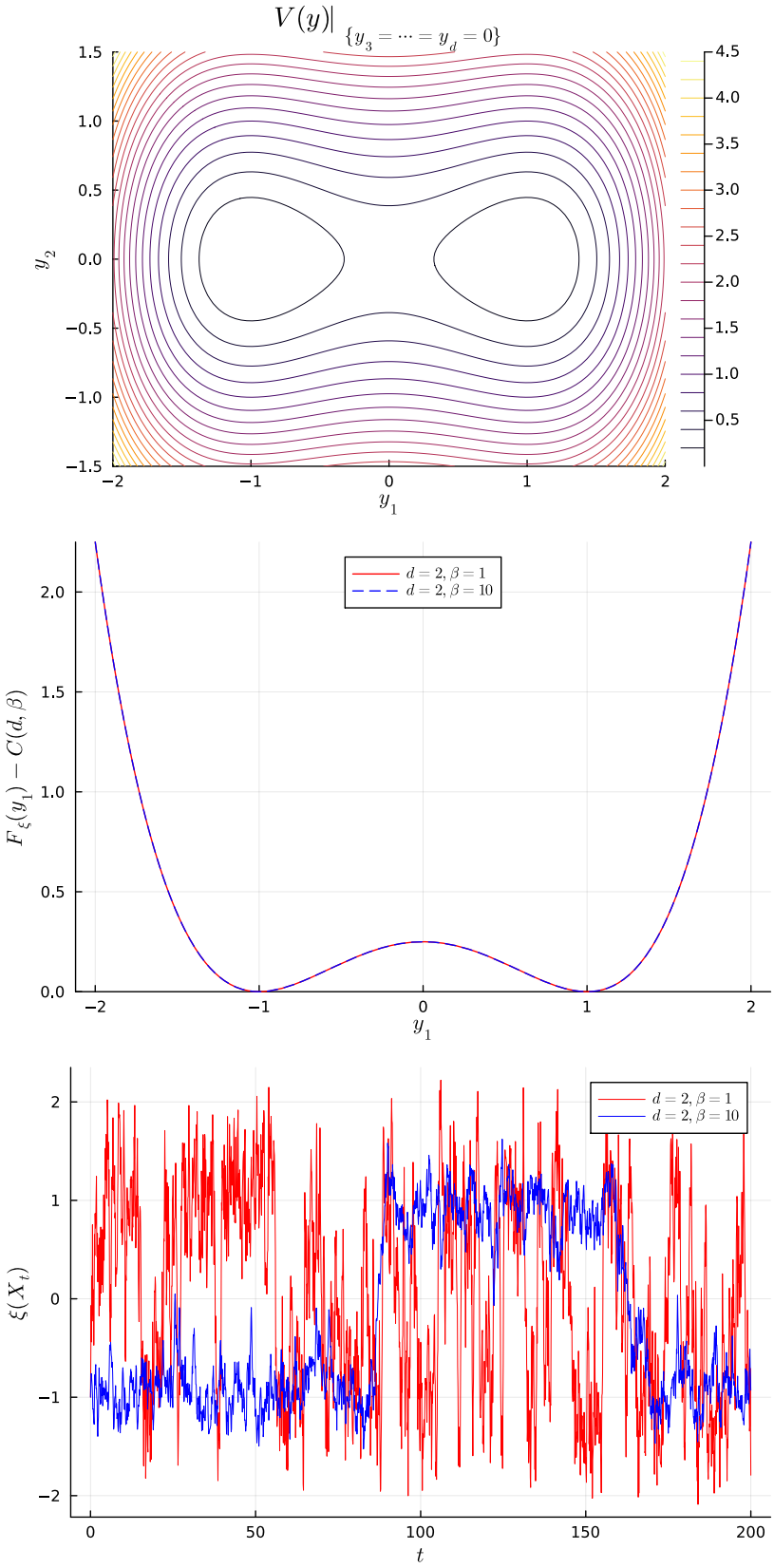

Figure 1.3: The case of a purely energetic barrier, $W(y) = \frac{1}{4}(y^2-1)^2$ and $k(y) = 1$ in (1.42). Top row: two-dimensional slice of the potential V in the (y_1, y_2)-plane. Middle row: free-energy profile for $\xi(y) = y_1$ and various values of the physical parameters d and β. The physically irrelevant constant $C(d,\beta)$ in (1.43) has been substracted. Bottom row: sample trajectories of the slow variable ξ under the dynamics (1.19) for the potential V, showcasing metastability at low temperature.

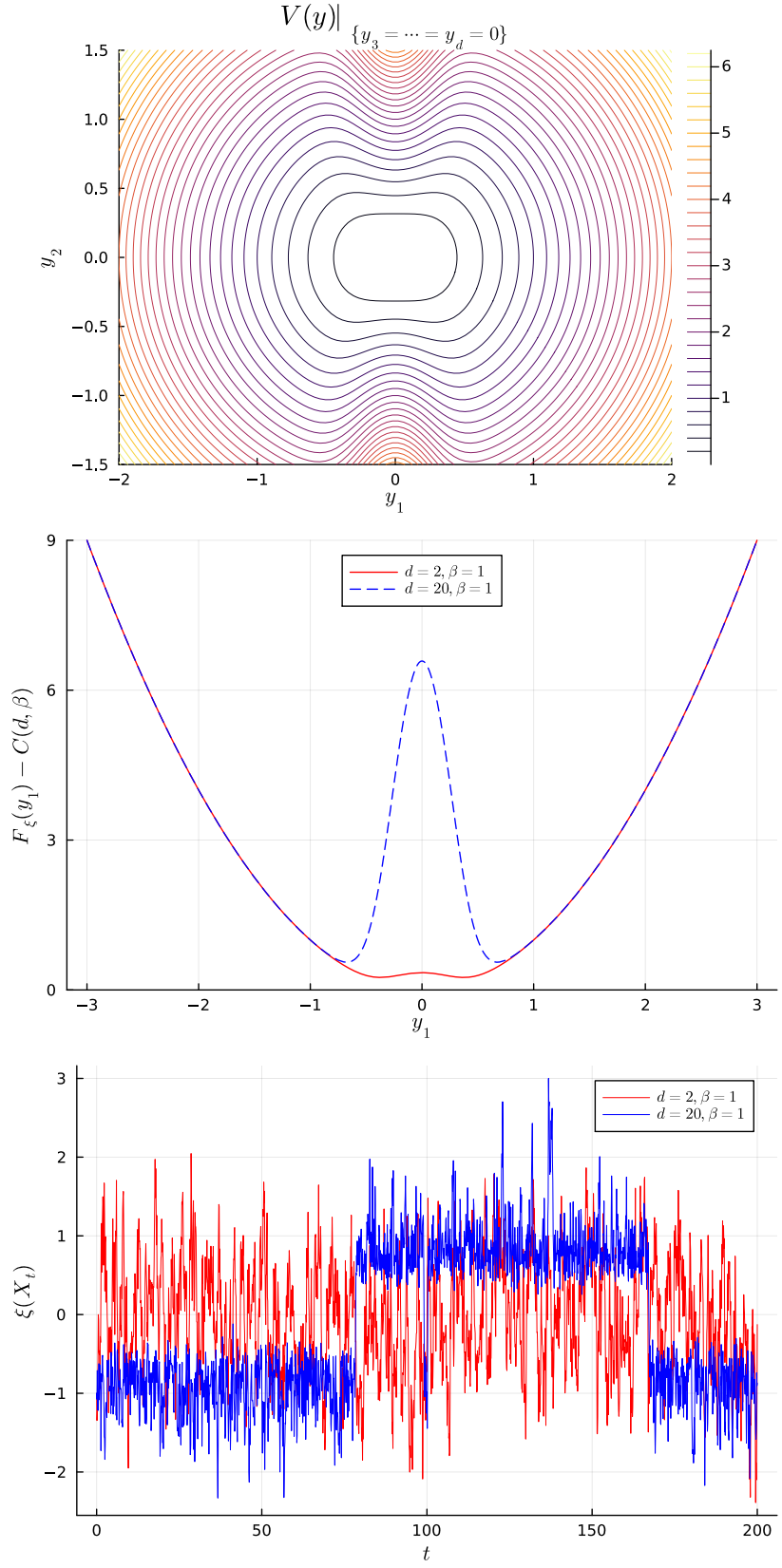

Figure 1.4: The case of a purely entropic barrier, $W(y) = \frac{1}{2}y^2$ and $k(y) = 1+\mathrm{e}^{-10y^2}$ in (1.42). Top row: two-dimensional slice of the potential in the (y_1, y_2)-plane. Middle row: free-energy profiles for $\xi(y) = y_1$. Middle row: sample trajectories of the slow variable under the dynamics (1.19), showcasing metastability in high-dimension.

be undefined, and $Y_0 \in \mathcal{Y}$ be some initial configuration. The sequence of events is initialized by

$$\tau_0 = \inf\left\{t > \tau_{-1} : Y_t \in \bigcup_{\alpha\in I} C_\alpha\right\}, \qquad \alpha_0 = \sum_{\alpha\in I} \alpha \mathbb{1}_{Y_{\tau_0}\in C_\alpha},$$

where the sum is well-defined owing to the disjointness condition (1.44). Subsequent events are defined recursively, for $n \geqslant 0$, via

$$\tau_{n+1} = \inf\left\{t > \tau_n : Y_t \in \bigcup_{\alpha\in I\setminus\{\alpha_n\}} C_\alpha\right\}, \qquad \alpha_{n+1} = \sum_{\alpha\in I\setminus\{\alpha_n\}} \alpha \mathbb{1}_{Y_{\tau_{n+1}}\in C_\alpha}.$$

We call the I-valued process

$$\left(\alpha_{n(t)}\right)_{t\geqslant 0}, \qquad n(t) = \#\{n \geqslant 0 : \tau_n \leqslant t\} - 1 \tag{1.45}$$

the *milestone-to-milestone* dynamics (it is the analog in our setting of the state-to-state dynamics, see [233, Section 6.3]). If the milestones C_α are defined to represent physically significant configurations, it can reveal the sequence of microscopic steps underlying large conformational transitions. This is invaluable in providing mechanistic insight into various biochemical and material processes.

AMD algorithms can be seen as a way to sample (approximately) unbiased trajectories of the dynamics $(\tau_n, \alpha_n)_{n\geqslant 1}$, which allow to recover the milestone-to-milestone dynamics. Note in particular that, for any milestone A, the first hitting time is given by $\tau_A = \tau_{N_A - 1}$, where $N_A = \inf\{n \geqslant 0 : C_{\alpha_n} = A\}$ so that AMD methods yield approximate samples of Y_{τ_A}, making the quantities (1.41) accessible in principle.

The central idea of accelerated MD methods is to exploit the following property of metastable systems. For reasonable definitions of the pairs $(C_\alpha, \Omega_\alpha)$, and if $Y_0 \in C_\alpha$, the time-marginal distribution of $\mathrm{Law}(Y_t)$ will converge to a *local equilibrium* $\nu_\alpha \in \mathcal{P}(\Omega_\alpha)$, conditionally on remaining trapped inside Ω_α for long enough before leaving Ω_α. One can picture C_α as lying deep inside a free-energy basin, while the metastable state Ω_α covers the whole basin. Initializing the dynamics from the local equilibrium ν_α, *exit events* from Ω_α, defined as the pair

$$(\tau_\alpha, Y_{\tau_\alpha}), \qquad \tau_\alpha := \tau_{\Omega_\alpha^c} = \inf\{t \geqslant 0 : Y_t \notin \Omega_\alpha\}, \tag{1.46}$$

are infrequent.

The three AMD methods of Arthur Voter, namely Temperature-Accelerated Dynamics (TAD, 2000, [312]), Hyperdynamics (HMD, 1997, [333, 332]) and Parallel Replica (PR, 1998, [334]), can all be understood as particular methods to sample the exit event (1.46) at a reduced cost, measured either in terms of number of floating-point operations or of wall-clock time. The notion of local equilibrium in Ω_α is formalized, for each $\alpha \in I$, by the following assumption and approximation, which are both shared by all three AMD methods, and formalize the condition that each Ω_α truly corresponds to a metastable state.

Assumption 1.2. *There exists a unique probability measure $\nu_\alpha \in \mathcal{P}(\Omega_\alpha)$ such that, for all*

measurable $A \subset \Omega_\alpha$,

$$\mathbb{P}_{\nu_\alpha}\left(Y_t \in A \,|\, \tau_\alpha > t\right) = \nu_\alpha(A). \tag{QSD}$$

A simple argument[8] shows that (**QSD**) implies the following property. There exists $\lambda_\alpha > 0$ such that for any bounded measurable function $f : \partial\Omega_\alpha \to \mathbb{R}$,

$$\mathbb{E}_{\nu_\alpha}\left[\mathbb{1}_{\tau_\alpha > t} f\left(Y_{\tau_\alpha}\right)\right] = \mathrm{e}^{-\lambda_\alpha t}\mathbb{E}_{\nu_\alpha}\left[f\left(Y_{\tau_\alpha}\right)\right].$$

This equation says that, given $Y_0 \sim \nu_\alpha$, the exit time τ_α is an exponential random variable with rate λ_α, independent from the exit point Y_{τ_α}.

The measure ν_α satisfying Assumption (**QSD**) is called the *quasi-stationary distribution* (QSD) for Y inside Ω_α. The second assumption (which implies the first) states that the law of the process converges to the QSD provided it stays trapped longer than some time $t_{\mathrm{corr}}(\alpha) > 0$.

Approximation 1.3. *Assumption* (**QSD**) *holds, and for all* $y_0 \in C_\alpha$*:*

$$\forall\, t \geqslant t_{\mathrm{corr}}(\alpha), \qquad \mathrm{Law}(Y_{t_{\mathrm{corr}}(\alpha)} \,|\tau_\alpha > t\,) = \nu_\alpha. \tag{MS($t_{\mathrm{corr}}(\alpha)$)}$$

When $t_{\mathrm{corr}}(\alpha) \ll 1/\lambda_\alpha$, Approximation (**MS**($t_{\mathrm{corr}}(\alpha)$)) is a *separation of timescales* hypothesis: it posits that convergence to the QSD occurs on a much shorter timescale than the metastable exit time.

Regardless of its specific implementation, any procedure to sample the exit event (1.46) can be used in the following algorithm to simulate the sequence $(\tau_n, \alpha_n)_{n\geqslant 1}$, and therefore the milestone-to-milestone dynamics (1.45). In the following algorithm, we assume that we can "run AMD" to sample the exit event (1.46) starting from any local equilibrium.

Algorithm 1.4 (AMD-accelerated trajectorial sampling.)**.** *We initialize a simulation clock* $T_{\mathrm{sim}} = 0$*, the index* $n = -1$ *of the last milestone transition, and* $\alpha_{\mathrm{last}} = \varnothing$*, the index of the last visited milestone. The dynamics is initialized at* $Y_0 \in \mathcal{Y}$*, and the following steps are iterated until* T_{sim}*,* n *or* α_{last} *satisfy some termination condition.*

A) Initialization step. Run sequential MD starting from $Y_{T_{\mathrm{sim}}}$ *until* T_{A}*, where* $T_A = \inf\{t > T_{\mathrm{sim}} : \exists\, \alpha \in I, Y_t \in C_\alpha\}$*. Increment* $T_{\mathrm{sim}} \leftarrow T_{\mathrm{A}}$*. Let* $\alpha \in I$ *such that* $Y_{T_{\mathrm{A}}} \in C_\alpha$*. If* $\alpha \neq \alpha_{\mathrm{last}}$*, set* $n \leftarrow n+1$*,* $\alpha_{\mathrm{last}} \leftarrow \alpha$*,* $\alpha_n \leftarrow \alpha$*, and* $\tau_n \leftarrow T_{\mathrm{sim}} + T_{\mathrm{A}}$*. Proceed to Step B.*

B) Decorrelation step. Run sequential MD starting from $Y_{T_{\mathrm{sim}}}$ *for a time* $t_{\mathrm{corr}}(\alpha_{\mathrm{last}})$*. Increment* $T_{\mathrm{sim}} \leftarrow T_{\mathrm{sim}} + t_{\mathrm{corr}}(\alpha_{\mathrm{last}})$*.*

B.1) If an exit from $\Omega_{\alpha_{\mathrm{last}}}$ *occured in step B, go back to step A.*

B.2) If not, $Y_{T_{\mathrm{sim}}} \sim \nu_{\alpha_{\mathrm{last}}}$ *by Approximation* (**MS**($t_{\mathrm{corr}}(\alpha)$))*. Proceed to step C.*

[8] Take $t, s \geqslant 0$ and compute $\mathbb{E}_\nu\left[f\left(Y_{\tau_\alpha}\right)\mathbb{1}_{\tau_\alpha > t+s}\right] = \mathbb{P}_{\nu_\alpha}\left(\tau_\alpha > s\right)\mathbb{E}_{\nu_\alpha}\left[f\left(Y_{\tau_\alpha}\right)\mathbb{1}_{\tau_\alpha > t+s} \,|\, \tau_\alpha > s\right] = \mathbb{P}_{\nu_\alpha}\left(\tau_\alpha > s\right)\mathbb{E}_{\nu_\alpha}\left[f\left(Y_{\tau_\alpha}\right)\mathbb{1}_{\tau_\alpha > t}\right]$ using the strong Markov property and (**QSD**). Taking $f = \mathbb{1}_\Omega$ and $t = 0$ respectively shows the desired exponentiality and independence properties. The fact that $\lambda_\alpha > 0$ is a consequence of the fact that $\mathcal{Y} \setminus \Omega_\alpha$ will be eventually be visited by Y with probability 1, see [84, Section 2.3].

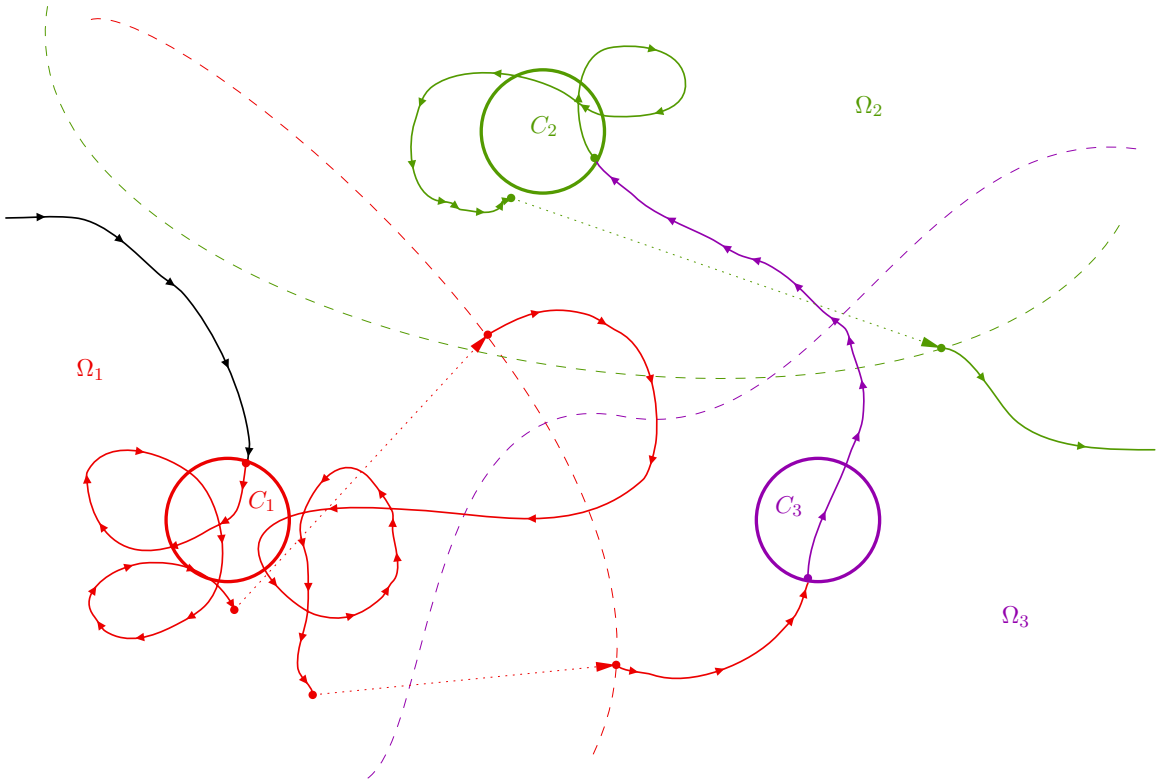

Figure 1.5: A metastable trajectory sampled using Algorithm 1.4. Boundaries of metastable states are represented with dashed lines. The state of the milestone-to-milestone dynamics is represented by the color of the solid line. AMD-accelerated portions of the trajectory, corresponding to step C in Algorithm 1.4, are represented by dotted arrows. Here, we represent a *recrossing* event: the system reaches C_1 and equilibrates under ν_1, exits Ω_1, but reenters C_1 before reaching another milestone, upon which it reequilibrates under ν_1 and finally transitions. If the metastable states are well designed, the bulk of the physical time evolution is hidden behind the "jumps" performed in step C.

C) Accelerated metastable exit step. Run any AMD procedure starting from $Y_0^{\mathrm{AMD}} = Y_{T_{\mathrm{sim}}}$. *Let* $\left(T_{\mathrm{C}}, Y_{T_{\mathrm{C}}}^{\mathrm{AMD}}\right)$ *be the sampled exit event. Increment* $T_{\mathrm{sim}} \leftarrow T_{\mathrm{sim}} + T_{\mathrm{C}}$, *set* $Y_{T_{\mathrm{sim}}} \leftarrow Y_{T_{\mathrm{C}}}^{\mathrm{AMD}}$, *and proceed from step A.*

Algorithm 1.4 generates a sequence $(\tau_n, \alpha_n)_{n \geqslant 0}$ which is statistically exact, provided the AMD-sampled metastable exit event is unbiased and Approximation (**MS($t_{\mathrm{corr}}(\alpha)$)**) is valid.[9] However, some details of the trajectories are lost in step C, and indeed most, since the bulk of a metastable system's lifetime is spent in local equilibria. However, these details consist of many excursions in the quasi-stationary regime, which can easily be sampled *a posteriori* if necessary. The most revealing portions of the trajectory, corresponding to transitions between milestones, are sampled using sequential MD. A schematic representation of a trajectory sampled using Algorithm 1.4 is given in Figure 1.5.

Before presenting the AMD methods, we give a natural choice for the sets $(\Omega_\alpha)_{\alpha \in I}$ and $(C_\alpha)_{\alpha \in I}$, which is the setting of Voter's original papers [333, 332, 334, 312].

Example 1.5 (Energy basins of attraction)**.** Assume that the local minima of the potential V

[9] In practice, this condition can only be verified in an approximate sense. Here, we choose to keep the presentation of AMD algorithms separate from concerns of their numerical analysis, and therefore speak of "approximations" rather than mathematically formalized hypotheses.

in $\mathcal{Q}$ can be enumerated by a discrete set of isolated points $\mathrm{Crit}_0 = \{x_\alpha\}_{\alpha\in I}$. To each $x_\alpha \in \mathrm{Crit}_0$, we associate the basin of attraction for the energy minimization dynamics $X'(t) = -\nabla V(X(t))$,

$$\begin{aligned} \Omega_\alpha^{\mathcal{Q}} &= \mathcal{A}(x_\alpha) = \left\{ x \in \mathcal{Q} : \phi(t,x) \xrightarrow{t\to+\infty} x_\alpha \right\}, \\ \partial_t \phi_V(t,x) &= -\nabla V(\phi_V(t,x)), \quad \phi_V(0,x) = x. \end{aligned} \tag{1.47}$$

It is often the case that the set of local minima is not countable, typically because of certain symmetry invariances of the potential function V. In this case, one can still often write $\mathrm{Crit}_0 = \bigsqcup_{\alpha\in I} \Gamma_\alpha$, where each Γ_α is a connected manifold, which is an orbit under a certain symmetry group. In this case one should take $\Omega_\alpha^{\mathcal{Q}} = \bigcup_{x\in\Gamma_\alpha} \mathcal{A}(x)$.

One can then take $\Omega_\alpha = \Omega_\alpha^{\mathcal{Q}}$ if the dynamics is given by (1.19), or $\Omega_\alpha = \Omega_\alpha^{\mathcal{Q}} \times \mathcal{P}$ if the dynamics is given by (1.17). Generically, the $(\Omega_\alpha)_{\alpha\in I}$ form a partition of configuration space, up to a set of measure zero.

Defining $C_\alpha = \Omega_\alpha$ the milestone-to-milestone dynamics (1.45) becomes a "state-to-state" dynamics.

Finally, we note that in the kinetic case, it may also be interesting to define $C_\alpha \subset \Omega_\alpha^{\mathcal{Q}} \times \mathcal{P}_\alpha$, where $\mathcal{P}_\alpha$ is a subset of momentum space (containing e.g. sufficiently small momenta "entering" $\Omega_\alpha^{\mathcal{Q}}$).

We now present the three AMD methods of Voter, listed roughly in order of decreasing computational efficiency, but increasing generality and precision.

Temperature-Accelerated Dynamics. In TAD [312], we assume that the dynamics (1.16) depends on a temperature parameter β, like (1.21) and (1.20) when the fluctuation-relation (1.22) holds. Moreover, it relies on a coarse-graining of the exit event into a finite number of disjoint *transition events*, whose probabilities are governed by an *Eyring–Kramers*-type law. We recall that the parameter $\beta = (k_{\mathrm{B}}T)^{-1}$ is inversely proportional to the temperature. The fact that the transition event obeys an Eyring–Kramers law is formalized in the following approximation.

Approximation 1.6. *There exists a critical value $\beta_0 > 0$ of the temperature parameter, and, for each $\alpha \in I$, a finite partition of the boundary*

$$\partial\Omega_\alpha = \bigsqcup_{1\leqslant i\leqslant m_\alpha} \Gamma_{i,\alpha},$$

with positive constants $(\kappa_{i,\alpha})_{1\leqslant i\leqslant m_\alpha}$ and $(\varepsilon_{i,\alpha})_{1\leqslant i\leqslant m_\alpha}$ such that, for all $1 \leqslant i \leqslant m_\alpha$ and $\beta > \beta_0$,

$$\mathbb{P}_{\nu_\alpha(\beta)}\left(Y^\beta_{\tau_\alpha} \in \Gamma_{i,\alpha}\right) = \frac{\kappa_{i,\alpha}\mathrm{e}^{-\beta\varepsilon_{i,\alpha}}}{\lambda_\alpha(\beta)}, \qquad \lambda_\alpha(\beta) = \sum_{j=1}^{m_\alpha} \kappa_{j,\alpha}\mathrm{e}^{-\beta\varepsilon_{j,\alpha}}, \tag{EK}$$

where Y^β is the dynamics with temperature parameter β, and $\nu_\alpha(\beta)$ and $\lambda_\alpha(\beta)$ are the corresponding QSD and metastable exit rate of Assumption (**QSD**).

The $(\varepsilon_{i,\alpha})_{1\leqslant i\leqslant m_\alpha}$ are called the *activation energies*, and the $(\kappa_{i,\alpha})_{1\leqslant i\leqslant m_\alpha}$ are subexponential

prefactors, which are assumed to be independent of β. Extensions to situations where the prefactors are assumed to scale in some explicit way with respect to β are straightforward. When the dynamics is given by (1.19) or (1.17), it is common to define the $\Gamma_{i,\alpha}$ as basins of attraction for the tangential energy minimization dynamics

$$X'(t) = -\Pi(X(t))\nabla V(X_t), \qquad \Pi(x) = x - (x^\top \mathrm{n}(x))\mathrm{n}(x), \qquad X(0) \in \partial\Omega_\alpha,$$

where n denotes the outward normal to $\partial\Omega_\alpha$. In this case, *harmonic transition state theory* (HTST) proposes explicit expressions for these constants in terms of local properties of the potential V, so-called *Eyring–Kramers* formulas, see Section 1.3 below.

Regardless, using the famous "alarm-clock lemma" for sums of independent exponential random variables, the combination of Assumption (**QSD**) and Approximation (**EK**) can be reformulated as assuming the following representation for τ_{Ω_α} started from $Y_0 \sim \nu_\alpha(\beta)$:

$$\tau_{\Omega_\alpha} \overset{\text{in law}}{=} \min_{1 \leqslant i \leqslant m_\alpha} \mathrm{e}^{\beta\varepsilon_{i,\alpha}} \frac{T_i}{\kappa_{i,\alpha}}, \qquad (T_i)_{1\leqslant i\leqslant m_\alpha} \text{ i.i.d. } \mathcal{E}(1). \tag{1.48}$$

Another useful way to understand this coarse-grained exit model is given by the following description: the exit event started from $Y_0 \sim \nu_\alpha$ is given by one step of a Markovian jump process into the set $(\Gamma_{i,\alpha})_{1\leqslant i\leqslant m_\alpha}$, with corresponding jump rates given by the Eyring–Kramers formula.

In the original TAD formulation, the states are defined as in Example 1.5, and it is assumed that $t_{\mathrm{corr}}(\alpha) = 0$ for each $\alpha \in I$. Furthermore, each of the boundary segments $(\Gamma_{i,\alpha})_{1\leqslant i\leqslant m_\alpha}$ are defined by the portions of the boundary separating Ω_α from some other energy basin:

$$\forall\, 1 \leqslant i \leqslant m_\alpha,\ \exists \alpha' \neq \alpha : \qquad \Gamma_{i,\alpha} = \partial\Omega_\alpha \cap \partial\Omega_{\alpha'}. \tag{1.49}$$

Therefore, the original TAD assumptions model the milestone-to-milestone dynamics (1.45) (which is a state-to-state dynamics in this case) with a Markov jump process on the set I. Markovian jump models for the milestone-to-milestone dynamics belong to the class of *Markov state models* (MSMs), see [181]. The jump process induced by the TAD assumptions is the basis of *kinetic Monte Carlo* (KMC) methods to measure dynamical properties, see [335] for example.

The core idea of TAD, to sample a metastable exit for Y^{β^-}, is to sample coarse-grained exits at a higher value of the temperature parameter $\beta^+ \in (\beta_0, \beta^-)$ for a given observation time using sequential MD. Subsequently, one uses the representation (1.48) to infer the first transition one would have observed at the target value β^-. Since the rate of transitions through $\Gamma_{i,\alpha}$ is multiplied by a factor $\mathrm{e}^{(\beta^- - \beta^+)\varepsilon_{i,\alpha}}$ when simulating the system at $\beta = \beta^+$ rather than at $\beta = \beta^-$, one can infer the order in which transitions observed at β^+ would have occured at β^- by determining the value of the activation energies $\varepsilon_{i,\alpha}$. Moreover, the transition states $(\Gamma_{i,\alpha})_{1\leqslant i\leqslant m_\alpha}$ and corresponding activation energies $(\varepsilon_{i,\alpha})_{1\leqslant i\leqslant m_\alpha}$ need not be known in advance, but can instead be detected on the fly at $\beta = \beta^+$. This discovery phase can be aborted dynamically, using statistical criteria and *a priori* bounds on the constants $(\kappa_{i,\alpha})_{1\leqslant i\leqslant m_\alpha}$ and/or $(\varepsilon_{i,\alpha})_{1\leqslant i\leqslant m_\alpha}$. All in all, the TAD procedure can lead to a significant acceleration in Ω_α if $(\min_i \varepsilon_{i,\alpha})\,(\beta^- - \beta^+)$ is sufficiently large. For convenience, we give a schematic representation

of the TAD algorithm in Figure 1.6 below.

The basic structure of the TAD algorithm to sample a transition proceeds as follows.

Algorithm 1.7 (TAD). *Initialize high-temperature observation time $T^+_{\mathrm{stop}} = +\infty$, simulation clock $T^+_{\mathrm{sim}} = 0$, first transition time $T^-_{\mathrm{min}} = +\infty$ and first transition point $Y_{\mathrm{min}} = \varnothing$. Iterate the following steps given $Y^+_0 \sim \nu_\alpha(\beta^+)$.*

A) Reinitialize $Y^+_{T^+_{\mathrm{sim}}}$ by drawing an independent sample from $\nu_\alpha(\beta^+)$. This can be ignored if $T^+_{\mathrm{sim}} = 0$.

B) Run sequential MD on Y^+ at $\beta = \beta^+$, until detecting an exit through $\Gamma_{i,\alpha}$ at time $\widetilde{T}^+_i$, for some $1 \leqslant i \leqslant m_\alpha$. Compute $\varepsilon_{i,\alpha}$.
*This requires a procedure $(i, \varepsilon_{i,\alpha}) \leftarrow$ **FindTransition**. Increment $T^+_{\mathrm{sim}} \leftarrow T^+_{\mathrm{sim}} + \widetilde{T}^+_i$.*

*B.1) If $Y^+_{\widetilde{T}^+_i}$ is the first observed transition through $\Gamma_{i,\alpha}$, set $T^+_i = \widetilde{T}^+_i$ and $T^-_i = \mathrm{e}^{(\beta^- - \beta^+)\varepsilon_{i,\alpha}} T^+_i$. If $T^-_i < T^-_{\mathrm{min}}$, update $T^-_{\mathrm{min}} \leftarrow T^-_i$, $Y_{\mathrm{min}} \leftarrow Y^+_{T^+_i}$ and $T^+_{\mathrm{stop}} \leftarrow$ **StopCriterion**$(\delta, T^-_{\mathrm{min}})$. Proceed to step C.*

B.2) If a transition through Γ_i has already been observed, proceed to step A.

C) If $T^+_{\mathrm{sim}} > T^+_{\mathrm{stop}}$, return $\left(T^-_{\mathrm{min}}, Y_{\mathrm{min}}\right)$. Otherwise proceed to step A.

Algorithm 1.7 relies on two auxiliary procedures, **FindTransition** and **StopCriterion**. The role of **FindTransition** is to determine that an exit occured through $\Gamma_{i,\alpha}$ and the associated activation energy $\varepsilon_{i,\alpha}$. In the setting of Example 1.5, when $\Gamma_{i,\alpha}$ is defined by (1.49), the activation energy $\varepsilon_{i,\alpha}$ is given by an energy difference $V(x_{i,\alpha}) - V(x_\alpha)$, where $x_{i,\alpha}$ minimizes V on $\Gamma_{i,\alpha}$, and x_α is the global minimum of V inside Ω_α. In this case, $x_{i,\alpha}$ is an index-1 saddle point for V. Upon detecting, that Y^+ has exited Ω_α (for instance by running gradient descent on V), two-sided saddle point search methods, such as the nudged-elastic band method (NEB [189]), can be used to identify $x_{i,\alpha}$, and compute the associated activation energy $V(x_{i,\alpha}) - V(x_\alpha)$.

The role of **StopCriterion** is to ensure that the probability of observing a transition $T^+ >$ **StopCriterion**$(\delta, T^-_{\mathrm{min}})$ which would extrapolate to a time $T^- < T^-_{\mathrm{min}}$ is bounded by an user-supplied confidence parameter $\delta \in (0, 1)$. Such criteria are defined using *a priori* bounds on the prefactors $(\kappa_{i,\alpha})_{1 \leqslant i \leqslant m_\alpha}$ and/or the activation energies $(\varepsilon_{i,\alpha})_{1 \leqslant i \leqslant m_\alpha}$, see [344] for additional details.

In practice, it is possible, using TAD on solid-state systems with high energy barriers, to reach acceleration factors with respect to sequential MD of the order of 10^4–10^9 [312]. The method is however both inexact and inefficient if the energy barriers are too low, or when entropic effects are significant.

Hyperdynamics. HMD [333, 332] relies on a local modification of the potential energy V, and applies to equilibrium systems evolving according to the dynamics (1.19) or (1.17). The core of the method resides in replacing the potential energy V by a biased potential $V + \delta V$ in the governing equation, and considering the resulting biased dynamics $Y^{\delta V}$. The bias potential δV is non-negative, and such that the restriction to $\delta V|_{\Omega_\alpha}$ is compactly supported inside Ω_α.

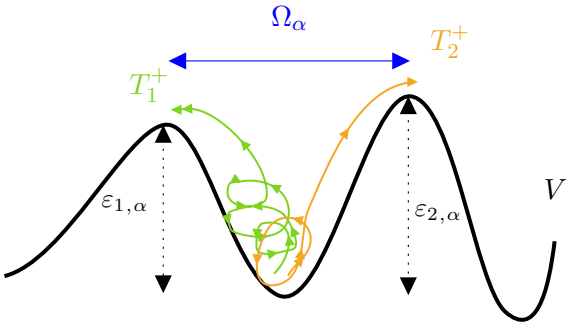

(a) Sampling at high temperature ($\beta = \beta^+$).

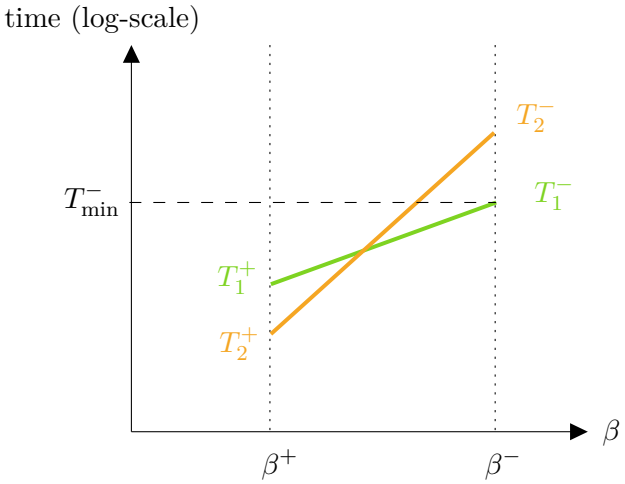

(b) Extrapolation to low temperature.

Figure 1.6: Illustration of the two-step TAD procedure in the framework of Example 1.5, consisting of (**a**), sampling metastable exits at high temperature, and (**b**), reordering these exits in time by extrapolating to a lower temperature. In this case there are $m_\alpha = 2$ transition states. The slopes of the lines in Figure (**b**) are given by the activation energies $\varepsilon_{1,\alpha}$ and $\varepsilon_{2,\alpha}$ from Figure (**a**).

If Ω_α is surrounded by energetic barriers, δV will increase the minimum energy in Ω_α, and thus effectively lower these energetic barriers, accelerating transitions. A schematic representation of a HMD-biased potential is given in Figure 1.7 below. We denote by $(\nu_\alpha^{\delta V}, \lambda_\alpha^{\delta V})$ the local equilibrium and metastable exit rate associated with the biased dynamics $Y^{\delta V}$, and $\tau_\alpha^{\delta V}$ the associated exit time. The core assumption of HMD is that the exit point distribution starting in any of the two local equilibria is the same.

Approximation 1.8. *For all measurable $A \subset \partial\Omega_\alpha$*

$$\mathbb{P}_{\nu_\alpha}\left(Y_{\tau_\alpha} \in A\right) = \mathbb{P}_{\nu_\alpha^{\delta V}}\left(Y^{\delta V}_{\tau_\alpha^{\delta V}} \in A\right). \tag{TST}$$

It is often the case (this is true for example for the case of the overdamped Langevin dynamics (1.19), see Equation 1.87 in Section 1.3.2 below), that the exiting distribution can be written explicitly as a boundary flux:

$$\mathbb{P}_{\nu_\alpha}\left(Y_{\tau_\alpha} \in A\right) = -\frac{\int_A \partial_{\mathrm{n}} u_\alpha \mathrm{e}^{-\beta V}}{\beta\lambda_\alpha \int_{\Omega_\alpha} u_\alpha \mathrm{e}^{-\beta V}}, \tag{1.50}$$

where u_α denotes the density of ν_α with respect to $\nu(x)\mathbb{1}_{\Omega_\alpha}(x)\mathrm{d}x$, and $\partial_{\mathrm{n}} u_\alpha$ denotes its outward normal derivative. Furthermore, when Ω_α is surrounded by high energy barriers, the local equilibrium is approximately equal to the restriction $\nu(x)\mathbb{1}_{\Omega_\alpha}(x)\,\mathrm{d}x$ of the equilibrium measure. This motivates the further approximation

$$\int_{\Omega_\alpha} u_\alpha \mathrm{e}^{-\beta V} \approx \int_{\Omega_\alpha} \mathrm{e}^{-\beta V}. \tag{1.51}$$

Applying (1.50) and (1.51) to (**TST**) (with $A = \partial\Omega_\alpha$ and both Y and $Y^{\delta V}$), we have

$$\frac{\lambda_\alpha}{\lambda_\alpha^{\delta V}} \approx \frac{1}{B_\alpha(\delta V)}, \qquad B_\alpha(\delta V) = \frac{\int_{\Omega_\alpha} \mathrm{e}^{-\beta V}}{\int_{\Omega_\alpha} \mathrm{e}^{-\beta(V+\delta V)}} = \frac{\int_{\Omega_\alpha} \mathrm{e}^{\beta\delta V}\mathrm{e}^{-\beta(V+\delta V)}}{\int_{\Omega_\alpha} \mathrm{e}^{-\beta(V+\delta V)}}. \tag{1.52}$$

The quantity $B_\alpha(\delta V)$ is called the *boost factor*. The last expression for the boost factor in (1.52) suggests that it can be approximated with an ergodic average of $\mathrm{e}^{\beta\delta V}$ along trajectories of $Y^{\delta V}$, prior to exiting Ω_α. Making this assumption motivates the following simple algorithm.

Algorithm 1.9 (Hyperdynamics). *A) Generate* $Y_0^{\delta V} \sim \nu_\alpha^{\delta V}$.

B) Run sequential MD on $Y^{\delta V}$ *until detecting a transition at time* $T_{\delta V}$.

C) Return $\left(\widehat{B}_\alpha(\delta V) T_{\delta V}, Y_{T_{\delta V}}^{\delta V}\right)$, *where*

$$\widehat{B}_\alpha(\delta V) = \frac{1}{T_{\delta V}} \int_0^{T_{\delta V}} \mathrm{e}^{\beta\delta V(Y_s^{\delta V})}\,\mathrm{d}s.$$

The original formulation of (**TST**) is motivated by physical heuristics from *transition state theory* (TST). The approximation (**TST**) (as well as (1.51)) can be made fully rigorously for the dynamics (1.19) in the low temperature regime $\beta \to +\infty$, in the presence of sufficiently high energetic barriers, as we further discuss in Section 1.3 below.

In the case $\Omega_\alpha = \mathcal{A}(x_\alpha)$ of Example 1.5, and if the Eyring–Kramers approximation (**EK**) correctly describes the exit event for both Y and $Y^{\delta V}$, one can perform the following sanity check. Since the activation energies can be written $\varepsilon_{i,\alpha} = V(x_{i,\alpha}) - V(x_\alpha)$ for some saddle point $x_{i,\alpha} \in \Gamma_{i,\alpha}$, raising the energy level inside the well by some constant value $E > 0$, so that $V(x_\alpha) \leftarrow V(x_\alpha) + E$, will not affect the probabilities of exiting through each of the $\Gamma_{i,\alpha}$, but will multiply the overall exit rate by $\mathrm{e}^{\beta E}$, which is indeed consistent with the estimated boost factor in step C of Algorithm 1.9.

Although Algorithm 1.9 is conceptually simple, it is not so easy to implement in practice, because of the need to design a biasing potential δV satisfying $\delta V|_{\partial\Omega_\alpha} \equiv 0$, whose gradient can be computed at an affordable computational cost, and for which Approximation (**TST**) is valid. We refer to [333, Section II.B] and [332] for a discussion of various strategies in the case $\Omega_\alpha = \mathcal{A}(x_\alpha)$. Nevertheless, boost factors of order 10^4 were reported for the simulation of an atomic cluster diffusing on a crystalline surface in [332], which translated to accelerations with respect to sequential MD of order 10^2, due to the high cost of evaluating $\nabla\delta V$.

The original version of HMD was limited to the simulation of relatively small systems, due to poor scaling in the computational cost associated with δV, but this issue has been subsequently

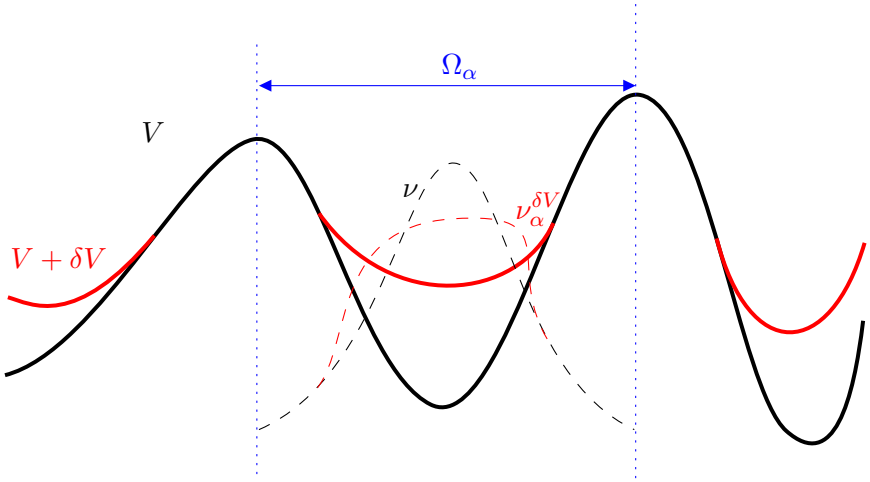

Figure 1.7: Schematic representation of the HMD bias in an energy basin Ω_α (see Example 1.5). The original potential V (black curve) is modified into $V + \delta V$ (red curve) by adding a bias potential $\delta V \geqslant 0$, compactly supported inside Ω. The corresponding local equilibria distributions ν and $\nu^{\delta V}$ are represented by dashed lines. Note that the normal derivatives of the two local equilibrium densities coincide on $\partial\Omega_\alpha$, implying that the metastable exit distributions are the same for both the biased and unbiased dynamics.

addressed, see e.g. [249, 194] for practical choices of biasing potentials.

Parallel Replica Dynamics. The third of Voter's AMD methods is the Parallel Replica (PR) [334] method, and is also the most general, since it only relies on the validity of the Approximation **MS($t_{\mathrm{corr}}(\alpha)$)**. It is based on the following simple observation. Since τ_α is exponentially distributed and independent from Y_{τ_α} if $Y_0 \sim \nu_\alpha$, the following equality in law holds:

$$\left(N\tau_{N,\alpha}, Y^{(I_N)}_{\tau_{N,\alpha}}\right) \overset{\text{in law}}{=} (\tau_\alpha, Y_{\tau_\alpha}), \tag{1.53}$$

whenever $N \geqslant 1$ and $\left(Y^{(i)}\right)_{1\leqslant i\leqslant N}$ are *i.i.d.* replicas of the dynamics such that $Y_0^{(i)} \sim \nu_\alpha$ for all i, with respective exit times $\left(\tau_\alpha^{(i)}\right)_{1\leqslant i\leqslant N}$, and

$$\tau_{N,\alpha} = \min_{1\leqslant i\leqslant N} \tau_\alpha^{(i)}, \qquad I_N = \operatorname*{argmin}_{1\leqslant i\leqslant N} \tau_\alpha^{(i)}.$$

Since $\tau_{N,\alpha}$ is exponentially distributed with rate $N\lambda_\alpha$, one obtains an expected acceleration or order N in the wall-clock time needed to sample the exit event, by simulating the independent replicas $(Y^{(i)})_{1\leqslant i\leqslant N}$ in parallel. A schematic representation of the procedure is given in Figure 1.8 below.

This observation leads to the following algorithm.

Algorithm 1.10 (Parallel Replica)**.** *A. Dephasing step. Prepare N independent initial conditions $(Y_0^{(i)})_{1\leqslant i\leqslant N}$, each distributed according to ν_α.*

B. Parallel step. Compute $(I_N, \tau_{N,\alpha})$ by evolving the replicas $(Y^{(i)})_{1\leqslant i\leqslant N}$ on parallel processors, running sequential MD with independent Brownian motions. All simulations are aborted at time $\tau_{N,\alpha}$.

C. Return $\left(N\tau_{N,\alpha}, Y^{(I_N)}_{\tau_{N,\alpha}}\right)$.

Note that, contrarily to Algorithms 1.7 and 1.9, PR does not lead to a greater efficiency in terms of computational cost, but only in terms of wall-clock time.[10] The expected wall-clock time spent in step C of Algorithm 1.4 by combining it with Algorithm 1.10 (PR-AMD) is divided on average by N, the number of simultaneously available MD processes.

On the other hand, both TAD and HMD rely on strong physical assumptions, namely Approximations (**EK**) and (**TST**), which restrict the class of systems on which they can be applied. Efficiency concerns further restrict the class of systems on which they are useful. By contrast, PR is completely generic: it applies to any metastable system, as soon as Approximation (**MS**($t_{\mathrm{corr}}(\alpha)$)) is valid for some $t_{\mathrm{corr}}(\alpha) > 0$, regardless of the underlying dynamics. In particular, it can *in principle* be used on nonequilibrium systems [325, 268], systems with entropic barriers [156], but also discrete Markov chains [15] and PDMPs [12]. Versions of Algorithm 1.10 suitable for asynchronous computing architectures can also be formulated (see again [12]).

Wall-clock time speedups with respect to sequential MD of order 10^4 have been reported [242, 268, 294] when applying PR-AMD, to systems on which TAD and HMD cannot be used efficiently. Simulations at this scale require supercomputing clusters, providing $\mathcal{O}(10^4)$ computing cores. Additionally, PR can be combined with HMD or TAD (see [336] for an application of the combination of PR with HMD) to further accelerate sampling.

Finally, we mention that there exists another method based on the equality (1.53), ParSplice [266], which provides another powerful and general method to tackle the timescale problem in MD, but lies beyond the framework of Algorithm 1.4.

Challenges in AMD. Despite their proven potential in addressing the timescale problem, some issues have to be settled for AMD-based methods to be useful in practice.

The first challenge is theoretical, and consists in setting rigorous mathematical foundations for AMD methods.

Problem 1.11 (Theoretical foundations.)**.** The first issue concerns the validity of Assumption (**QSD**), and grounding the various Approximations (**MS**($t_{\mathrm{corr}}(\alpha)$)), (**EK**), (**TST**) in mathematical analysis, ideally with quantitative error bounds in terms of the various physical and approximation parameters.

The existence and uniqueness of the QSD ν_α has recently been established for a large class of Feller processes (see [30]), including the diffusions (1.20) (1.19), and more general hypoelliptic diffusions and PDMPs. However, these result only apply to *bounded* domains $\Omega_\alpha \subset \mathcal{Y}$. For the specific case of the underdamped Langevin dynamics (1.20), similar results have been obtained for cylindrical domains of the form $\Omega_\alpha = \Omega_\alpha^{\mathcal{Q}} \times \mathbb{R}^{3N}$ with $\Omega_\alpha^{\mathcal{Q}}$ bounded [11] , using analytic methods in [253], and probabilistic arguments in [228]. Under suitable conditions on the infinitesimal generator (see [30, Theorem 1.8] and [228, Theorem 2.22]), exponential

[10] A more in-depth discussion of ParRep-AMD, with a particular focus on its wall-clock time efficiency, is given in Appendix 3.B of Chapter 3 below.

[11] In the kinetic case, another way to define bounded metastable states consists in truncating the kinetic energy K of the system, i.e. $\Omega_\alpha = \Omega_\alpha^{\mathcal{Q}} \times K^{-1}(0, R)$ for some $R > 0$. In this case the results of [30] can be applied, even for the nonequilibrium Langevin dynamics considered in Examples 1.15 and 1.16 below.

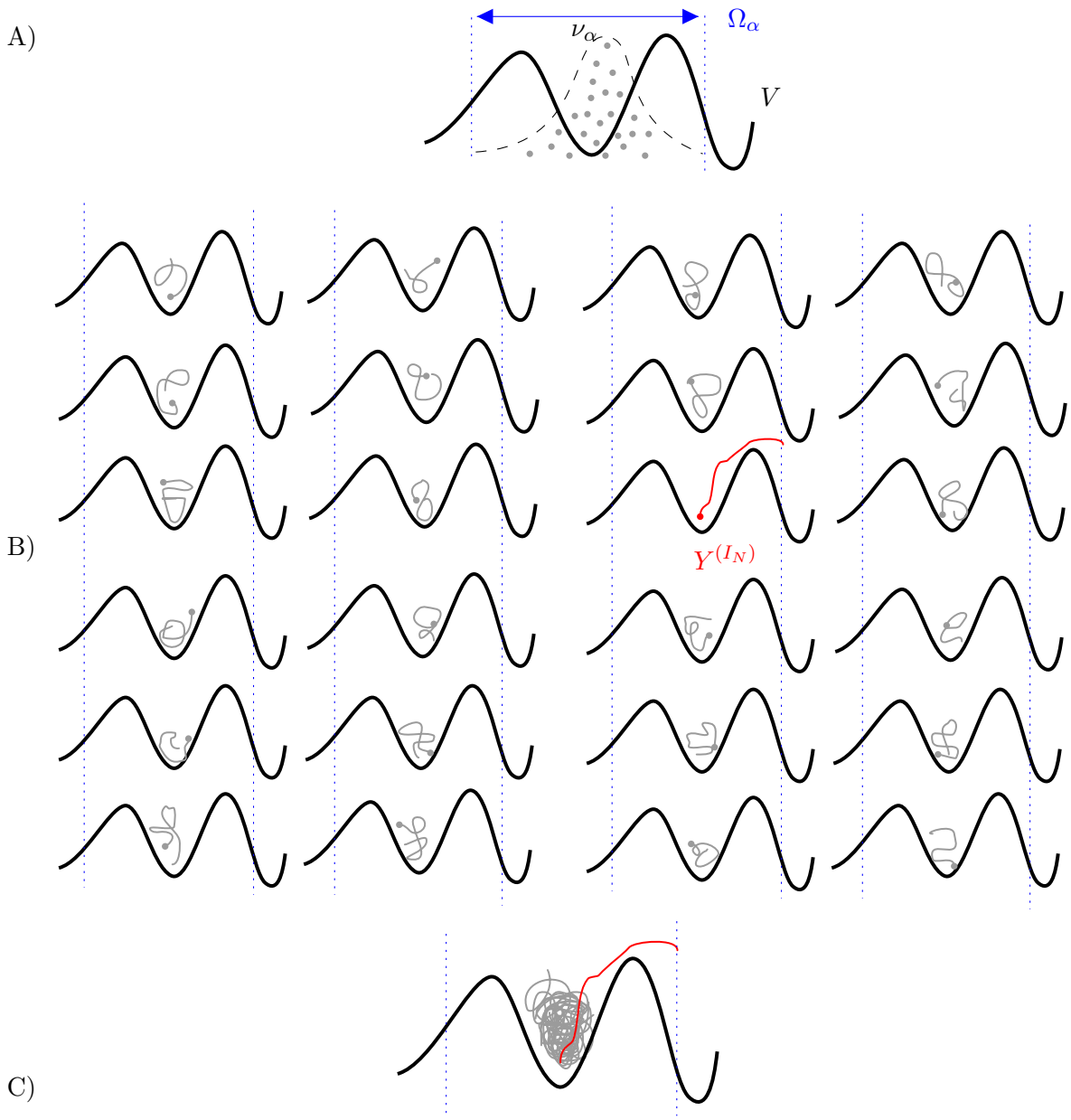

Figure 1.8: Schematic representation of Algorithm 1.10 with $N = 24$ replicas. In step A), N i.i.d. samples are drawn according to ν_α, see Problem 1.13 below for further discussion on how to achieve this. The discontinuous trajectory represented in step C), obtained by concatenating the trajectories sampled in parallel in step B), has length $N\tau_{N,\alpha}$, and its endpoint (in red) is an unbiased sample of the exit-from-Ω_α distribution starting from ν_α.

convergence to the QSD in total variation norm can be proven. Such results give the existence of a constant $r_\alpha > 0$ such that, for any initial distributions $\rho \in \mathcal{P}(\Omega_\alpha)$ and $t > 0$,

$$\mathrm{d_{TV}}\left(\mathbb{P}_\rho\left(Y_t \in \cdot \,|\, \tau_\alpha > t\right), \nu_\alpha\right) \leqslant C(\rho)\mathrm{e}^{-r_\alpha t}, \tag{1.54}$$

for some constant $C(\rho) > 0$ uniform in t, where $\mathrm{d_{TV}}$ denotes the total-variation distance on $\mathcal{P}(\Omega_\alpha)$, given by

$$\mathrm{d_{TV}}\left(\mu_1, \mu_2\right) = \sup_{\|f\|_\infty \leqslant 1} \left|\mu_1(f) - \mu_2(f)\right|.$$

The bound (1.54) provides the theoretical basis for Approximation (**MS($t_{\mathrm{corr}}(\alpha)$)**).

Justifications for Approximations (**EK**) and (**TST**) are much more difficult to obtain in general, and as far as we are aware, the only rigorous results in this directions are in the low-temperature limit of the overdamped Langevin dynamics (1.19), under restrictions on Ω_α and the potential V, see [14, 225, 99, 100, 224] and the discussion in Section 1.3 below.

The second issue is practical, and concerns the design of metastable states.

Problem 1.12 (Defining Ω_α and C_α)**.** Example 1.5 provides a general way to define the metastable states Ω_α, which is often sufficient in systems with high energetic barriers. However, the entropic case of Example 1.1 (see Figure 1.4) already shows why this definition is inadequate in general: V has a unique global minimum ($0 \in \mathbb{R}^d$), but $\mathcal{A}(0) = \mathbb{R}^d$ does not discriminate between the two metastable states. Even in the energetic case, AMD methods are known to be inefficient if the energy barriers to leave Ω_α are too small, an issue known as the *low barrier problem*. This is an issue for definitions of Ω_α based on $\mathcal{A}(x_\alpha)$, which are sensitive to low-amplitude features in the potential energy surface. Various strategies have been proposed to address this issue (see [268, Section 2.11]), such as aggregating several energetic basins into a *superbasin* surrounded by suitably high barriers, replacing energetic basins with free-energetic basins associated to a slow-moving collective variable, or hand-crafting system-specific, *ad-hoc* definitions using well-chosen order parameters. Even in the case of high potential energy barriers, definitions based on $\mathcal{A}(x_\alpha)$ are not expected to be *optimal*, because of frequent recrossings of the boundary around saddle points of the potential energy, which typically hinder the efficiency of Algorithm 1.4.

A separate question is, given a metastable state Ω_α, to define the core-set C_α. We believe that this point is less critical than the definition of Ω_α. Loosely speaking, C_α should be contained in the bulk of the QSD ν_α, so that $Y_0 \in C_\alpha$ corresponds to a typical configuration from ν_α, from which $\mathrm{Law}(Y_t)$ is expected to quickly converge to ν_α conditionally on $\{\tau_\alpha > t\}$. On the other hand, C_α should be large enough for the set $\bigcup_\alpha C_\alpha$ to be visited often by the dynamics. The question of defining good core-sets is related to the question of estimating $t_{\mathrm{corr}}(\alpha)$ (Problem 1.14 below). Note that since ν_α is defined independently of C_α, it is possible in principle to adapt the definition of the milestones (and correspondingly $t_{\mathrm{corr}}(\alpha)$) as the simulation progresses, although this changes somewhat the meaning of the milestone-to-milestone dynamics (1.45).

Finally, the milestone-hitting times $(\tau_n)_{n\geqslant 1}$ and metastable exit times τ_α for $\alpha \in I$ are particular instances of stopping times. Therefore, replacing these times with more general stopping times could lead to more flexible definitions of both metastable states and milestones. In particular, *soft killing times* have been explored in the potential-theoretic approach to

metastability, see [39, 40]

The second practical issue, which is largely solved for the purposes of AMD simulations, concerns sampling from the QSD.

Problem 1.13 (Sampling from ν_α.)**.** The second problem that each of TAD, HM and PR must address is the sampling of independent configurations under the QSD ν_α (or $\nu_\alpha^{\delta V}$ in the case of Hyperdynamics). Indeed, such samples are required in step A of each of the Algorithms 1.7, 1.9 and 1.10. In PR, $N > 1$ *i.i.d.* such samples are required to achieve accelerated sampling.

The simplest approach to tackle this problem is through rejection sampling. Under Assumptions (**QSD**), and Approximation (**MS**($t_{\mathrm{corr}}(\alpha)$)), for any $t_{\mathrm{dephase}}(\alpha) \geqslant t_{\mathrm{corr}}(\alpha)$ and $Y_0 \in C_\alpha$, the law of $Y_{t_{\mathrm{dephase}}(\alpha)}$ conditionally on $\{\tau_\alpha > t_{\mathrm{dephase}}(\alpha)\}$ is again ν_α. Therefore, one may arbitrarily sample initial conditions $(Y_0^{(i)})_{1\leqslant i\leqslant N_{\mathrm{rep}}}$ inside C_α, and simulate trajectories of the dynamics with independent driving noises for a *dephasing time* $t_{\mathrm{dephase}}(\alpha) \geqslant t_{\mathrm{corr}}(\alpha)$, eventually keeping only the $N \leqslant N_{\mathrm{rep}}$ replicas which did not transition during this phase. The procedure can be tried again if no replica survives, although this should never happen if C_α is carefully defined. To guarantee the independence of the generated samples, one should either draw the $Y_0^{(i)}$ independently, or choose $t_{\mathrm{dephase}}(\alpha)$ sufficiently large to ensure the decay of correlations between replicas. In the original paper of Voter [334], it is suggested to initialize positions by copying the position of the reference dynamics at time $t = t_{\mathrm{corr}}(\alpha)$ (at which point it is distributed under ν_α by assumption), and sample momenta independently from the kinetic marginal κ defined in (1.8).

Another possibility is to draw on ideas to approximate QSDs using empirical measures of interacting diffusions. In particular, Fleming–Viot particle systems (see [330, 95, 64]) have been proposed to generate approximately *i.i.d.* samples from the QSD ν_α. In this process, $N \geqslant 2$ replicas of the dynamics are simulated with independent Brownian motions, until a replica escapes Ω_α. Whenever this happens, the state of the exiting replica is reinitialized at the current state of a surviving replica, drawn independently and uniformly at random. Similarly to the rejection sampling case, the Fleming–Viot system is evolved for some time $t_{\mathrm{dephase}}(\alpha)$. Theoretical results (see [291]) can in some cases ensure that the marginal distribution of each replica approaches ν_α as $N, t_{\mathrm{dephase}}(\alpha) \to +\infty$, and this approach has the advantage of conserving the number of replicas. However, the final configurations of the replicas are correlated, which may introduce some bias in the final sample. This bias can be controlled using propagation of chaos results, see for instance [191]. A second approach in the stochastic approximation of QSDs uses self-interacting diffusions (see [31, 338]) whose configurations are resampled upon exiting Ω_α under their own occupation measure $\tau_\alpha^{-1} \int_0^{\tau_\alpha} \delta_{Y_s}\,\mathrm{d}s$. The practicality of this method in the specific context of AMD algorithms is unclear.

The third, important practical issue concerns the choice of a valid decorrelation time.

Problem 1.14 (Choosing $t_{\mathrm{corr}}(\alpha)$.)**.** Once Ω_α and C_α are defined, one must find $t_{\mathrm{corr}}(\alpha)$ such that Approximation **MS**($t_{\mathrm{corr}}(\alpha)$) is valid. Note that if a conservative choice is made for $t_{\mathrm{corr}}(\alpha)$, an unnecessarily large proportion of a trajectory simulated using Algorithm 1.4 will be spent in step B instead of step C. Since the acceleration from the AMD methods only occurs in step C, this will lead to suboptimal performance of the overall method. On the

other hand, setting $t_{\mathrm{corr}}(\alpha)$ to too small a value will lead to a systematic dynamical bias, since Algorithm 1.4 relies on the dynamics being distributed according to some QSD at the end of step B.

Several approaches have been suggested to handle this basic tradeoff. The original papers [333, 332, 334, 312] advocate for physically motivated choices of $t_{\mathrm{corr}}(\alpha)$. For both HMD and TAD ([333, 332, 312]), the separation of timescales was presumed to be sufficiently large to warrant the choice $t_{\mathrm{corr}}(\alpha) = 0$, meaning that the QSD ν_α is reached immediately upon entering C_α (which was equal to Ω_α in this case). For PR in solid-state systems, where the states are defined as in Example 1.5, the pragmatic recommendation [334, 268] is to set $t_{\mathrm{corr}}(\alpha)$ to a few vibrational periods of Einstein's crystalline model, on the order of one picosecond.

More principled but still heuristic approaches [268], again in the case of single energetic basins, rely on a *harmonic approximation* of the dynamics around the local minima x_α. This approximation is a time-homogeneous linear SDE, whose convergence to equilibrium can be monitored analytically. One then selects $t_{\mathrm{corr}}(\alpha)$ based on the analytical rate of convergence of this harmonic approximation.

For more general definitions of states, analytical results can still provide quantitative estimates for the exponential rate of convergence to the QSD, i.e. the exponent r_α defined in (1.54), in specific dynamical settings and physical regimes. In particular, semi-classical techniques can be used to compute the leading asymptotic behavior $\widehat{r}_\alpha(\beta)$ of the convergence rate to the QSD in the low-temperature regime $\beta \to +\infty$ for the dynamics (1.19), see for instance [159, 209, 50]. Such results may or may not confirm the validity of the harmonic approximation heuristic. A natural question concerns the estimation of the prefactor $C(\rho)$ in (1.54). This problem is still open for general initial conditions ρ.[12] These methods can be used to set $t_{\mathrm{corr}}(\alpha)$ by requiring the right hand-side of (1.54) to be less than some tolerance parameter $\epsilon > 0$, assuming some *a priori* bound on $C(\rho)$ and solving the resulting inequality.

For problems with entropic barriers, in particular most biophysical systems, such heuristics are of no use. It is therefore interesting to develop methods to estimate a valid decorrelation time *on the fly*. Since TAD and HMD are generally poorly suited to entropic barriers, this approach holds the most promise for the PR-AMD method. In [42], the authors propose applying a MCMC convergence diagnostic (or rather, non-convergence diagnostic) to the Fleming–Viot process described in Problem 1.13 above. In this approach, the decorrelation step (step B in Algorithm 1.4) is performed in parallel to the dephasing step (step A in Algorithm 1.10), with an unsuccesful decorrelation (step B.1 in Algorithm 1.4) aborting the dephasing step. This can be implemented with a "master/slave" Fleming–Viot process, in which a reference (decorrelating) replica, evolving according to sequential MD, kills all the other (dephasing) replicas whenever it exits Ω_α. The initial state of the other replicas is copied from that of the master replica, which therefore belongs to C_α. To apply MCMC convergence diagnostics, trajectories of the Fleming–Viot process $F := \left(Y^{(i)}\right)_{0 \leqslant i \leqslant N}$ (where $Y^{(0)}$ is the master replica) may be treated as independent trajectories of an underlying Markov process with values in Ω_α. In this case, it is assumed that exits during the decorrelation/dephasing stage are sufficiently rare not to invalidate this approximation. A process R_t with values

[12] In the low-temperature regime, methods have been developed in [21, 213] for certain classes of diffusions, the principal difficulty here being the conditioning in (1.54).

in $(0, +\infty)$, the *decorrelation gauge*, is then constructed as a function of $(F_s)_{0 \leqslant s \leqslant t}$, and the decorrelation/dephasing time is defined as the random time

$$T_{\mathrm{corr}}(\alpha) = \inf \{t \geqslant 0 : R_t \leqslant \epsilon\},$$

where $\epsilon > 0$ is a user-specified tolerance parameter. The gauge R should in particular be constructed such that $\mathrm{d_{TV}}\left(\mathbb{P}\left(Y_t \in \cdot \,|\, \tau_\alpha > T_{\mathrm{corr}}(\alpha)\right), \nu_\alpha\right)$ is small. The decorrelation/dephasing time is now a stopping time for the natural filtration of the Fleming–Viot process.

While [42] proposes using the so-called Gelman–Rubin diagnostic from MCMC, a number of constructions or possible: classical MCMC diagnostics (see [292] for a review), non-parametric tests, coupling-based estimators of the total variation distance (see [44]), or histograms-based methods (see Chapter 3 below) are all possibilities. Further experimentation and theory is needed to better understand which choices of (R, ϵ) are valid and perform best in practice.

Problems 1.12 and 1.14 are core motivations for some of the results in Chapters 2 and 3.

1.2.2 Computing response properties

We now turn to a second class of methods, aimed at the problem of computing particular instances of dynamical properties, namely nonequilibrium response properties. We focus in particular on the important case of transport coefficients, introducing a mathematical framework for their computation.[13] At the macroscopic scale, a transport coefficient relates the average flux (or response) of some transported physical quantity in the steady state of a system driven out of equilibrium by an external forcing (or perturbation), and the magnitude of that forcing. Such a system is known as a nonequilibrium system. Standard examples of transport coefficients include the mobility and shear viscosity of a fluid, or the thermal conductivity in atom chains and lattices.

The computation of transport coefficients is a crucial step in fitting parameters of mesoscopic and continuum models of fluids and materials at a larger scale, such as the Navier–Stokes or heat equation. However, their estimation from trajectory data can be very costly with naive methods, prompting the need for innovative numerical strategies. This topic is still the object of active research, both in the MD and mathematical communities, see [309] and references therein for another recent overview.

Broadly speaking, computational methods to measure transport coefficients from MD simulations fall in one of two categories. The first relies on the sampling of nonequilibrium microstates, and the direct measurement of various response functions under perturbations of the equilibrium dynamics. These methods include nonequilibrium molecular dynamics (NEMD)-like methods [79], as well as transient techniques such as the transient time-correlation function (TTCF [250]). The second relies on the analysis of time-dependent signals in the trajectories of the equilibrium dynamics. These include methods following the pioneering theoretical work of Green [142] and Kubo [201, 202], methods based on Einstein's relation [114, 285] for the diffusion coefficient, as well as transient methods based on relaxation to the equilibrium

[13] The content of this section is adapted from original material written for an upcoming review paper [49].

steady-state from nonequilibrium initial conditions (as in [17, 204]). Here we focus on the NEMD method and the Green–Kubo formula.

We refer to [79, 80] for early accounts of NEMD experiments, as well as [81, 172, 82, 78] and [171, Chapter 4] for reviews of the NEMD approach at various stages of historical development, as well as the books [119, 321]. Early measurements of transport coefficients from equilibrium MD trajectories can be found in [3, 234, 235].

Nonequilibrium dynamics. To formalize the physical notion of the nonequilibrium systems used in the NEMD method, we introduce perturbations of the equilibrium dynamics (1.16), which are given by a parametric family of SDEs evolving on $\mathcal{Y}$,

$$\mathrm{d}Y_t^\eta = b_\eta(Y_t^\eta)\,\mathrm{d}t + \sigma_\eta(Y_t^\eta)\,\mathrm{d}W_t, \tag{1.55}$$

indexed by a parameter $\eta > 0$ modulating the strength of the perturbation. The perturbations should be understood as being of order η as $\eta \to 0$, i.e.

$$\forall\, y \in \mathcal{Y}, \qquad |b(y) - b_\eta(y)|_{\mathcal{Y}}\,,\ |\sigma(y) - \sigma_\eta(y)|_{\mathcal{Y}} = \mathcal{O}\,(\eta)\,.$$

To be more specific, we focus on the two cases which are the most relevant in physical applications, although one could in principle consider more general classes of perturbations.

- *Non-conservative forces.* Nonequilibrium systems are often obtained by the application of a non-gradient driving force ηF, where $F : \mathcal{Q} \to \mathbb{R}^d$ is a fixed forcing field. Dynamically, this amounts to replacing the force $-\nabla V$ by

$$-\nabla V + \eta F \tag{1.56}$$

  in the governing equation (1.17) or (1.19) for the equilibrium dynamics.

- *Temperature profiles.* The second typical example consists of a spatial temperature gradient, which amounts to replacing the temperature parameter β by a positive position-dependent scalar field

$$\beta_\eta = \frac{1}{k_{\mathrm{B}}(T_0 + \eta\delta T)}, \qquad \delta T : \mathcal{Q} \to \mathbb{R}, \tag{1.57}$$

  in the equilibrium dynamics, where $T_0 = \beta^{-1}$ and $T_0 + \eta\delta T > 0$.

Nonequilibrium generator and steady states. In both examples given above, the generator of the nonequilibrium dynamics is a linear perturbation of the equilibrium generator:

$$\mathcal{L}_\eta = \mathcal{L}^Y + \eta\widetilde{\mathcal{L}}, \tag{1.58}$$

where the expression of the perturbation $\widetilde{\mathcal{L}}$ depends both on the dynamics and on the type of perturbation. Analytical expressions for $\widetilde{\mathcal{L}}$ are listed in Table 1.1.

A steady-state for the nonequilibrium dynamics (1.55) (or nonequilibrium ensemble, see

Perturbation \ Dynamics	Underdamped (1.17)	Overdamped (1.19)
Force (1.56)	$F \cdot \nabla_p$	$F \cdot \nabla$
Temperature (1.57)	$\gamma \delta T \Delta_p$	$\delta T \Delta$

Table 1.1: Nonequilibrium perturbation $\widetilde{\mathcal{L}}$ of the generator for usual dynamics and perturbation types.

Section 1.1 above) is, by definition, an invariant probability distribution $\pi_\eta \in \mathcal{P}(\mathcal{Y})$ (which we often write μ_η or ν_η depending on the underlying equilibrium dynamics). The existence and uniqueness of the steady state can often be obtained using Lyapunov techniques, in the spirit of [150], see [233, Section 5] and [280], or by a perturbative analysis (see the discussion following (1.62) below). The steady state π_η is a solution to the stationary Fokker–Planck equation (1.24), i.e.

$$\mathcal{L}_\eta^\dagger \pi_\eta = 0 \tag{1.59}$$

in the sense of distributions. Regularity properties for π_η can then usually be obtained by applying hypoelliptic or standard elliptic regularity theory, depending on whether the diffusion matrix σ_η is degenerate or not.

In turn, the results of [196] can be used, under suitable conditions on the coefficients σ_η, b_η to ensure the hypoellipticity of the generator (1.58) and the positivity of the steady state probability density, to deduce the following pathwise ergodic property: for any initial condition $y \in \mathcal{Y}$, and observable $\varphi \in L^1(\pi_\eta)$,

$$\frac{1}{T}\int_0^T \varphi(Y_t^\eta)\,\mathrm{d}t \xrightarrow{T\to+\infty} \mathbb{E}_{\pi_\eta}[\varphi] \qquad \mathbb{P}_y\text{-almost surely.} \tag{1.60}$$

A crucial distinction with the equilibrium setting is that π_η typically does not have an explicit density: since the non-conservative force F cannot be written as the gradient of a potential on $\mathcal{Q}$, or since the fluctuation-dissipation relation is generally not satisfied for a position-dependent temperature profile, one cannot write π_η as a Gibbs measure for any explicit energy function. We can nevertheless, in view of (1.60), sample from the nonequilibrium steady state, by considering sufficiently long trajectories of (1.55).

Similar to the equilibrium case, discretizations of the dynamics create bias at the level of the invariant measure of the numerical scheme and the resulting trajectory averages, but while in the equilibrium case, one can correct for this bias via Metropolization, this option is unavailable in the nonequilibrium case in all but the simplest settings, since computing the nonequilibrium stationary density up to normalization is equivalent to finding a solution to the Fokker–Planck equation (1.59).

For similar reasons, the importance sampling method (1.38) cannot be straightforwardly applied to reduce the variance of the ergodic average (1.60), because it requires an explicit expression for the likelihood ratio between the target density and modified density.

Fluxes and linear response. We now formally define transport coefficient, which measure the relative magnitude of a nonequilibrium flux with respect to the magnitude of the perturbation. The response or flux of the nonequilibrium system is measured by a scalar-valued

observable $R : \mathcal{Y} \to \mathbb{R}$, which we assume vanishes on average at equilibrium:

$$\mathbb{E}_\pi [R] = 0.$$

The transport coefficient α is then defined as the derivative of the average flux with respect to the perturbation magnitude (provided the limit exists):

$$\alpha = \lim_{\eta \to 0} \frac{\mathbb{E}_{\pi_\eta} [R]}{\eta}. \tag{1.61}$$

This definition motivates the following natural NEMD approach to estimate α.

- Pick a set of perturbation sample points $\boldsymbol{\eta} = (\eta_k)_{1 \leqslant k \leqslant K}$, and estimate the corresponding nonequilibrium steady-state flux using trajectory averages of the nonequilibrium dynamics (1.55):

  $$\forall\, 1 \leqslant k \leqslant K, \qquad \widehat{\pi}_{\eta_k,T}(R) := \frac{1}{T} \int_0^T R(Y_t^{\eta_k})\, \mathrm{d}t,$$

  for $T > 0$ sufficiently large.

- Fit an assumed functional form (e.g. a polynomial): $\eta \mapsto \widehat{R}_{\boldsymbol{\eta},T}(\eta)$ to the data $(\boldsymbol{\eta}, \widehat{\pi}_{\boldsymbol{\eta},T}(R))$, chosen so that $\widehat{R}_{\boldsymbol{\eta},T}(0) = 0$.

- The derivative

  $$\widehat{\alpha}_{\boldsymbol{\eta},T} := \widehat{R}'_{\boldsymbol{\eta},T}(0)$$

  is then used as an estimator of the transport coefficient α.

A schematic representation of a typical non-linear response profile is depicted in Figure 1.9, together with the estimators $\widehat{\pi}_{\eta_k,T}(R)$ for several values of η_k, an estimator $\eta \mapsto \widehat{R}_{\boldsymbol{\eta},T}(\eta)$ of the response profile using a quadratic functional form, and the inferred linear response $\eta \mapsto \widehat{R}'_{\boldsymbol{\eta},T}(0)$.

Connection with equilibrium fluctuations. We briefly present linear response results giving alternative expressions for the coefficient α in terms of equilibrium dynamical averages, and form the basis of numerical methods such as the celebrated Green–Kubo formula [142, 201, 202]. Here, we only give a somewhat informal presentation in the $L^2(\pi)$ functional setting, and stress that similar results can be obtained in more general situations, see for example [149] or [233, Section 5.2].

The derivation assumes that the nonequilibrium steady-state π_η admits a probability density with respect to the equilibrium steady-state π, which can be perturbatively expanded (for $|\eta|$ sufficiently small) into a power series

$$\pi_\eta = \pi \sum_{k=0}^{\infty} \eta^k \psi_k, \tag{1.62}$$

where $\psi_k \in L^2(\pi)$ for all $k \geqslant 0$.

Setting $\eta = 0$ in (1.62), it necessarily holds that $\psi_0 = \mathbb{1}_\mathcal{Y}$. The formal expansion (1.62)

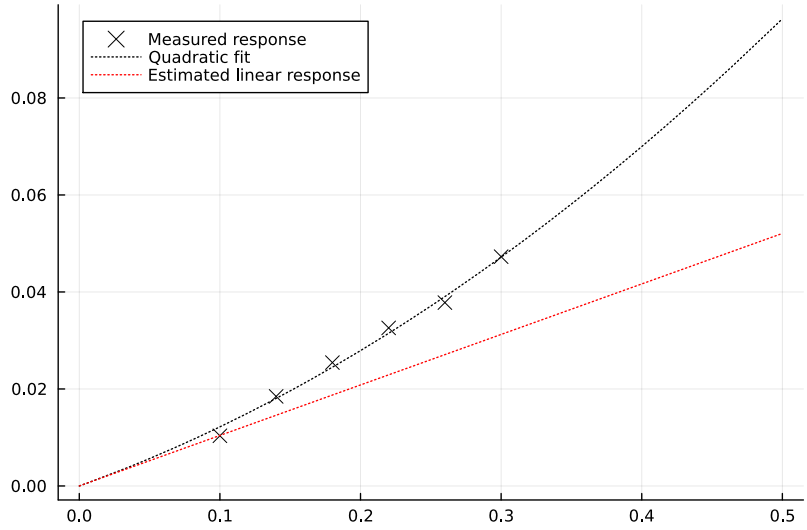

Figure 1.9: Sketch of a typical nonequilibrium response profile for a flux R with respect to the forcing magnitude, together with its linear response. In dotted lines, NEMD estimators of the nonlinear and linear response profiles, obtained by fitting a quadratic model to average responses computed via NEMD simulations. These sampled responses are represented by black crosses.

can be shown to converge when the nonequilibrium perturbation is "small", e.g. when $\widetilde{\mathcal{L}}$ is $\mathcal{L}^Y$-bounded on $L^2(\pi)$ and $|\eta|$ is small enough, see for instance the proof of [233, Theorem 5.2]. This is the case for perturbations of the dynamics by a non-conservative force F (see Table 1.1), under mild assumptions on F. For instance, it is enough to assume that F is bounded.

Assuming the validity of such an ansatz, the stationary Fokker–Planck equation (1.59) writes

$$\left(\mathcal{L}^Y + \eta\widetilde{\mathcal{L}}\right)^* \sum_{k=0}^{\infty} \eta^k \psi_k = 0,$$

where adjoints are taken with respect to the $L^2(\pi)$ scalar product. Matching terms in η, it therefore holds for any $k \geqslant 1$ that

$$\left(-\mathcal{L}^Y\right)^* \psi_k = \widetilde{\mathcal{L}}^* \psi_{k-1},$$

so that in particular $= \left(-\mathcal{L}^Y\right)^* \psi_1 = \widetilde{\mathcal{L}}^* \mathbb{1}_{\mathcal{Y}}$.

Provided the so-called conjugate flux

$$S = \widetilde{\mathcal{L}}^* \mathbb{1}_{\mathcal{Y}},$$

belongs to the space $\Pi L^2(\pi)$ of π-centered observables and $\mathcal{L}^Y$ (hence also its adjoint) is invertible on that functional space, we may write

$$\psi_1 = \left(-\mathcal{L}^{Y*}\right)^{-1} S.$$

This, in turn implies, by the definition (1.61) and the expansion (1.62) the following expression

for the transport coefficient:

$$\alpha = \lim_{\eta\to 0} \eta^{-1} \int_{\mathcal{Y}} R \mathrm{d}\pi_\eta = \lim_{\eta\to 0} \eta^{-1} \int_{\mathcal{Y}} \left(\mathbb{1}_{\mathcal{Y}} + \eta \left(-\mathcal{L}^{Y*}\right)^{-1} S \right) R \,\mathrm{d}\pi = \int_{\mathcal{Y}} S \left(-\mathcal{L}^{Y}\right)^{-1} R \,\mathrm{d}\pi. \tag{1.63}$$

Note that action of $\widetilde{\mathcal{L}}^*$, and therefore the expression for the conjugate response S, can be computed explicitly via integration by parts. The expressions of the conjugate fluxes corresponding to the perturbations given in Table 1.1 are given in Table 1.2 below, and can easily be checked to belong to $\Pi L^2(\pi)$ under mild assumptions on $V, \delta T$ and F.

The formulation (1.63) shows that the linear response α can be expressed as the equilibrium average $\pi\left(S\left(-\mathcal{L}^Y\right)^{-1} R\right)$. Unfortunately, the various equilibrium sampling methods described in Section 1.1.2 cannot be applied outright, since they require evaluating the solution $\left(-\mathcal{L}^Y\right)^{-1} R$ to a high-dimensional Poisson equation.

Instead, one can reformulate (1.63) as a dynamical average using the expression of the $\Pi L^2(\pi)$-inverse of $\mathcal{L}^Y$ given in (1.31) in terms of the integrated semigroup. This yields the celebrated Green–Kubo formula

$$\alpha = \int_0^\infty \mathbb{E}_\pi \left[S(Y_0) R(Y_t) \right] \mathrm{d}t, \tag{1.64}$$

which expresses the transport coefficient as an integrated correlation function along trajectories of the equilibrium dynamics. In this form, α is clearly a dynamical property.

Perturbation \ Dynamics	Overdamped Langevin	Underdamped Langevin
Non-conservative force	$\beta F \cdot \nabla V - \nabla \cdot F$	$\beta F \cdot M^{-1} p$
Temperature profile	$\Delta \delta T - 2\beta \nabla V \cdot \nabla \delta T$ $- \delta T \left(\beta^2 \lvert \nabla V \rvert^2 - \beta \Delta V \right)$	$\beta\gamma\delta T \left(\operatorname{Tr} M^{-1} - \beta \left\lvert M^{-1} p \right\rvert^2 \right)$

Table 1.2: Expressions for the conjugate response S, for usual dynamics and perturbation types.

It may happen, for example in the case of a nonequilibrium temperature gradient, that the perturbation $\widetilde{\mathcal{L}}$ is not $\mathcal{L}^Y$-bounded. In this case, the formal expansion (1.62) of the steady-state density does not converge in $L^2(\pi)$. One can nevertheless often recover the final expression (1.63) for the linear response, as discussed in [233, Remark 5.5].

Examples of nonequilibrium systems. We conclude this section by giving practical examples of nonequilibrium systems which can be used to compute transport coefficients in the bulk of single-species fluids. We assume the system evolves according to the underdamped Langevin dynamics (1.17) in a periodic configurational domain $\mathcal{Q} = (L\mathbb{T})^{3N}$, and that $M = m\mathrm{Id}_{3N}$ for the atomic mass $m > 0$. We also assume that the particles interact according to the Lennard–Jones potential (1.6), although the methods apply to any other pairwise potential.

Example 1.15 (Mobility of a Lennard–Jones particle)**.** Arguably the simplest example of transport coefficient is provided by the mobility a particle moving in a fluid. Physically, this quantity measures how easily mass is transported through the fluid in response to an external driving field. It is closely related to the phenomenon of self-diffusion, a relationship which is quantified by the Einstein relation (see (1.65) below and [285]).

In the framework described in Section 1.2.2 above, and keeping the same notation, this corresponds to taking a constant forcing $F \in \mathbb{R}^d$ for the configurational domain $\mathcal{Q} = (L\mathbb{T})^{3N}$. Note that F is not the gradient of a periodic function, and thus, this is indeed a nonequilibrium dynamics. We measure the average particle flux through the hyperplane perpendicular to F, defining

$$R(q,p) = m^{-1}F^\top p,$$

so that

$$S(q,p) = m^{-1}\beta F^\top p, \quad \widetilde{\mathcal{L}} = F^\top \nabla_p.$$

The mobility α_F is the corresponding linear response (1.61). In view of the Green–Kubo formula (1.64), it can also be written as

$$\alpha_F = \beta F^\top \mathfrak{C} F, \qquad \mathfrak{C} := m^{-2}\mathbb{E}_\mu\left[p_0 p_t^\top\right] \in \mathbb{R}^{d\times d}$$

in terms of the velocity autocovariance matrix $\mathfrak{C}$.

The diffusion coefficient $\mathfrak{D}$ entering in Fick's law can be computed from the linear response α_F, in the case $F = e_{x,1}$ is a unit field acting only on the first particle, via the Einstein relation [285]

$$\alpha_{e_{x,1}} = \beta\mathfrak{D}. \tag{1.65}$$

The coefficient $\alpha_{e_{x,1}}$ is called the mobility.

Example 1.16 (Shear viscosity of a Lennard–Jones fluid)**.** The second prototypical example of transport coefficient is the dynamic viscosity of a Newtonian fluid. Here, we present the computation of dynamic viscosity in monoatomic Lennard–Jones fluids, following the method described in [190], itself inspired by the sinusoidal transverse force (STF) method [141]. Another class of NEMD algorithms to measure the shear viscosity consist of boundary-driven methods, such as the direct simulation of Couette flows via shearing boundary conditions [215], see [119, Section 6.3] and [321, Section 9.3]. A schematic illustration of the STF method is given in Figure 1.10.

The STF method proceeds by analogy with Newton's macroscopic law of viscosity, for a fluid subjected to a shear force f directed along the longitudinal x-coordinate, which varies in intensity in the transverse y-coordinate. At the continuum level, the shear viscosity $\mathscr{R}$ is defined via the constitutive relation

$$\sigma_{xy} = -\mathscr{R}\frac{\mathrm{d}u_x}{\mathrm{d}y}, \tag{1.66}$$

where σ_{xy} is the (x,y) component of the local stress tensor, and u_x is the local x-velocity field of the fluid. Both σ_{xy} and u_x are functions of the y position in the fluid.

Microscopically, the action of the shear forcing on the fluid particles is defined by the following non-conservative force field:

$$\forall\, 1 \leqslant j \leqslant N, \qquad F(q)_{j,x} = f(q_{j,y}), \qquad F(q)_{j,y} = F(q)_{j,z} = 0. \tag{1.67}$$

The forcing field (1.67) acts on each component of the x-momentum variable, in a way which is

dictated by the corresponding component of the y-position variable, according to a fixed forcing profile f. The STF method derives its name from the standard choice $f(y) = \sin(2\pi y/L)$, although other profiles can be considered.

The microscopic formulation of the relation (1.66) relies on appropriate definitions of the velocity profile u_x and shear-stress profile σ_{xy}. These are defined as the linear responses (1.61) for (a limit of) y-dependent observables defined in [190] following a mathematically rigorous version of the Irving–Kirkwood procedure [183].

Using the linear response formula (1.63), one can show that the velocity and shear-stress linear response profiles u_x, σ_{xy} and forcing profile f are related as (see [190, Proposition 1])

$$\frac{1}{\rho}\frac{\mathrm{d}\sigma_{xy}(y)}{\mathrm{d}y} + \gamma u_x(y) = f(y),$$

where we recall that $\gamma > 0$ is the friction parameter in the underdamped Langevin dynamics (1.17), and $\rho = N/L^3$ is the particle density.

Formally substituting in the Newton relation (1.66), one arrives at the following differential equation for u_x:

$$-\frac{\mathscr{R}}{\rho}\frac{\mathrm{d}^2 u_x(y)}{\mathrm{d}y^2} + \gamma u_x(y) = f(y),$$

from which a Fourier analysis gives the viscosity $\mathscr{R}$ as

$$\mathscr{R} = \rho\left(\frac{\mathfrak{f}_1}{\mathfrak{u}_1} - \gamma\right)\left(\frac{L}{2\pi}\right)^2,$$

where $\mathfrak{f}_1$, $\mathfrak{u}_1$ are the first Fourier coefficients in y of the forcing profile f and the velocity linear response profile u_x respectively, on the periodic one-dimensional torus $L\mathbb{T}$. The only unknown quantity is the Fourier coefficient $\mathfrak{u}_1$, but one can formally show that it is a transport coefficient in its own right, for the "empirical Fourier flux"

$$R(q,p) = \frac{1}{Nm}\sum_{j=1}^{N} p_{j,x}\exp\left(\frac{2\mathrm{i}\pi q_{j,y}}{L}\right),$$

whose linear response can be estimated from nonequilibrium trajectory averages, or using the Green–Kubo formula with the conjugate flux

$$S(q,p) = \frac{\beta}{m}F(q)^\top p.$$

Various other approaches, relying on discretized estimates of σ_{xy}, u_x or transformations thereof, via NEMD or equilibrium-fluctuation formulas, and based on the constitutive equation (1.66), are of course possible.

1.3 Mathematical descriptions of metastability

Metastability is characterized by a timescale gap between fast thermal fluctuations within particular special regions of configuration space (metastable states) and the much slower

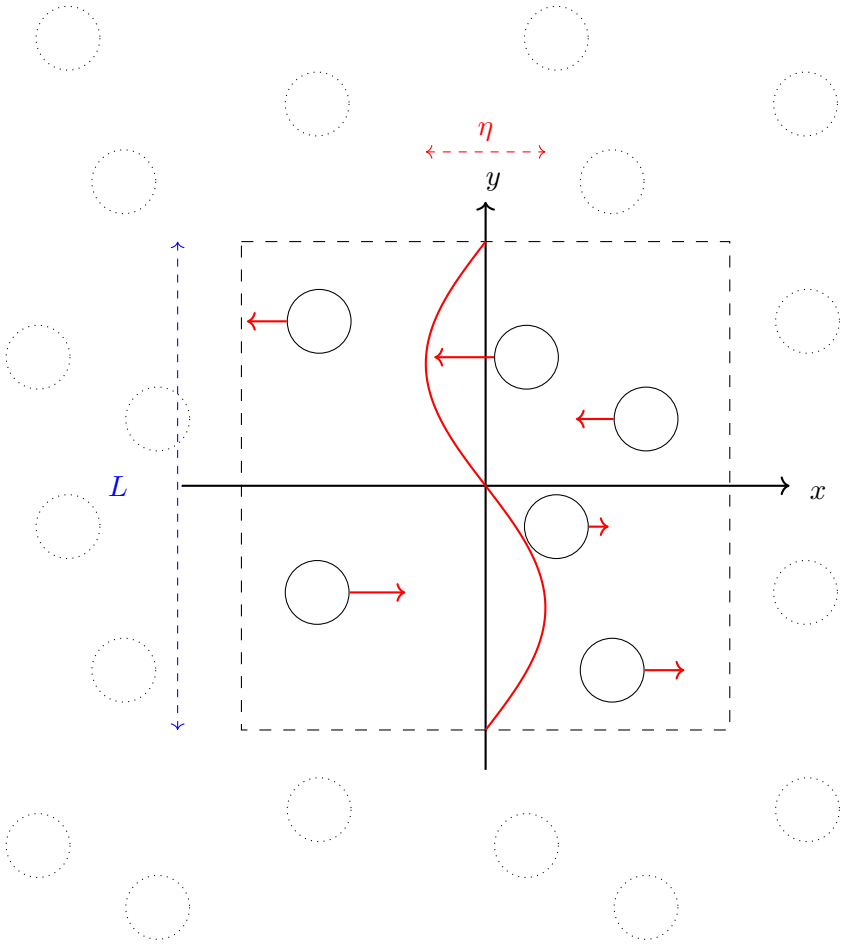

Figure 1.10: Schematic representation of the STF method. The black dashed square is the unit cell of the configurational domain $\mathcal{Q} = (L\mathbb{T})^{3N}$. Particles, represented by black circles, are subjected to an external forcing field in the longitudinal direction, represented by red arrows. The field is a function of a periodic transverse profile, plotted in the solid red line, whose amplitude is proportional to the forcing parameter η. Periodic images of the system are represented by dotted circles.

timescale at which certain rare events occur, namely configurational transitions between these states.

It is both the origin of the timescale problem in MD, as presented in Section 1.1, and the structural property behind the accelerated MD methods presented in Section 1.2. Metastability arises more generally whenever a dynamical system is subjected to random perturbations, giving continuous stochastic dynamics navigating a hilly free-energy landscape. The concept itself originates from attempts to understand the microscopic phenomenology of first-order phase transitions, and the mathematical modeling has been a long-standing concern of statistical physics, starting with Maxwell's study of the liquid-vapor phase transition [244].

A central objective in the kinetic theory of chemical reactions is to provide a microscopic foundation for the temperature dependence of reaction rates. This dependence is often described by the *Arrhenius law* [16], which states that the rate $k_{A\to B}$ of a transition event from a reactant state A to a product state B, or reaction rate, scales as:

$$k_{A\to B} \approx \kappa \exp(-\beta E_{A\to B}),$$

where $E_{A\to B}$ is an activation energy, κ is a pre-exponential factor, and we recall $\beta = (k_{\mathrm{B}}T)^{-1}$. It is of great practical interest to further derive quantitative estimates of $E_{A\to B}$ and κ, which lead to explicit Eyring–Kramers [122, 198] formulas (see (**EK**)).

Besides its interest in mathematical physics, metastability is a common feature of stochastic dynamical systems in limiting regimes. Various mathematical theories of metastability have been proposed since the 1950's.

For the dynamics (1.16), a typical setting is the small-noise regime. We focus on this example here, letting $(X^\varepsilon)_{\varepsilon>0}$ denote a family of solutions to the following SDEs on $\mathbb{R}^d$:

$$\mathrm{d}X_t^\varepsilon = b(X_t^\varepsilon)\,\mathrm{d}t + \sqrt{\varepsilon}\sigma(X_t^\varepsilon)\,\mathrm{d}W_t, \tag{1.68}$$

where $b : \mathcal{Q} \to \mathbb{R}^d$ and $\sigma : \mathcal{Q} \to \mathbb{R}^{d\times d}$ are regular coefficients, whose metastable behavior is studied in the limit $\varepsilon \to 0$. When the dynamics is given by (1.19) (i.e. $b = -\nabla V$), $\varepsilon = 2\beta^{-1}$ is proportional to the temperature. We assume for simplicity that b, σ are smooth and bounded and that σ is uniformly elliptic, meaning $\sigma\sigma^\top \geqslant c\mathrm{Id}$ for some $c > 0$, in the sense of symmetric matrices. This excludes in particular the case of the underdamped Langevin dynamics (1.17) which is important for applications, but we note that extensions to more general situations are possible.

While we focus on small-noise SDEs, some of the techniques we describe can be succesfully applied to other physical regimes (such as large system size) and other classes of models, such as spin systems (see [260, Chapter 7] and [58, Parts VI–VIII]), stochastic partial differential equations (SPDEs) (see for instance [58, Chapter IV.12] and [34]), and more.

We distinguish two distinct but related families of concerns for theories of the metastability of (1.68).

- *Global questions* are concerned with characterizing the set of metastable states, obtaining Eyring–Kramers formulas for mean first passage times between metastable states (see

Equations (1.41)), identifying transition pathways, and deriving asymptotic estimates for the rate of convergence to global equilibrium (see the discussion following Equation (1.29)). Another important objective is the justification of various *coarse-grained* models related to the continuous dynamics (such as Markovian models for the milestone-to-milestone dynamics (1.45)).

- *Local questions* study the behavior of the system within a fixed metastable state $\Omega \subset \mathcal{Y}$. Typical questions include quantifying the convergence (1.54) to ν_α, and characterizing the exit event (1.46) (from ν_α or more general initial conditions), in particular establishing Eyring–Kramers formulas for the exit time and/or exit point distribution. Such studies provide theoretical foundations for the AMD methods of Section 1.2.1, and allow to better understand their limitations and efficiency. They are therefore of great practical interest for the measurement of dynamical properties in MD.

In Section 1.3.1, we review several theoretical approaches to these questions, namely the pathwise approach, the potential-theoretic approach, the spectral approach, and related numerical approaches. In Section 1.3.2, we focus on the quasi-stationary regime, reviewing standard results concerning the QSD, and their link to the AMD algorithms of Section 1.2.1.

1.3.1 Review of approaches to metastability

Pathwise approach. The first approach is rooted in the theory of Freidlin & Wentzell. We refer to the monograph [132] for this theory, to [260] for further applications of this approach to metastability, and to [19, Course 1] for extensions to larger classes of stochastic processes.

The core of this approach is to view trajectories of X^ε as a stochastic perturbation of an ODE in the direction W. For any $\varepsilon > 0$, noise-induced fluctuations can drive the system along paths that are forbidden to the deterministic evolution

$$x'(t) = b\left(x(t)\right), \tag{1.69}$$

known as the *relaxation dynamics*. When $b = -\nabla V$, this is the gradient descent dynamics defining the energy basin (1.47).

The cornerstone of the Freidlin–Wentzell theory is a large deviation principle (LDP) on path space (see [98, Section 1.2] for an introduction to LDPs). Let $T > 0$, and $\mathcal{C}_{x,T} = \mathcal{C}([0,T], \mathcal{Q})$ denote the set of continuous functions φ such that $\varphi(0) = x \in \mathcal{Q}$, endowed with the supremum distance. We denote by $\mathbb{P}^\varepsilon_{x,T} \in \mathcal{P}(\mathcal{C}_{x,T})$ the path law of X^ε on $[0,T]$, started from $X^\varepsilon_0 = x$.

Theorem 1.17 ([132, Theorem 3.1 in Chapter 5], [260, Theorem 2.29])**.** *For any $T > 0$, the family $(\mathbb{P}^\varepsilon_{x,T})_{\varepsilon>0}$ satisfies a LDP with rate ε on $\mathcal{C}_{x,T}$, and good rate function*

$$I_{x,T}(\varphi) = \begin{cases} \dfrac{1}{2}\displaystyle\int_0^T \left(\varphi'(t) - b \circ \varphi(t)\right)^\top a^{-1} \circ \varphi(t) \left(\varphi'(t) - b \circ \varphi(t)\right) \mathrm{d}t, & \text{if } \varphi \in \mathrm{AC}\left([0,T], \mathcal{Q}\right), \\ +\infty & \text{otherwise.} \end{cases} \tag{1.70}$$

where $\mathrm{AC}([0,T], \mathcal{Q}) \subset \mathcal{C}([0,T], \mathcal{Q})$ denotes the set of absolutely continuous paths.

The functional (1.70) is called the *action functional* associated with the SDE (1.68). Theorem 1.17 has many interesting consequences for the study of rare events under the dynamics.

To give an example of how Theorem 1.17 can be used to study the behavior of the process inside a metastable state, suppose that $\Omega \subset \mathcal{Q}$ is an open bounded regular domain, which is strictly confining for the deterministic flow. This means that trajectories of the relaxation dynamics (1.69) satisfy $x(t) \in \Omega$ for all times $t \geqslant 0$ whenever $x(0) \in \Omega$, and $b(x)^\top \mathrm{n}(x) < 0$ for all $x \in \partial\Omega$. Suppose also that $x_* \in \Omega$ is such that $b(x_*) = 0$ and $x(t) \xrightarrow{t\to+\infty} x_*$ for all $x(0) \in \Omega$. We define the *quasipotential*

$$V_b(x,y) = \inf_{T,\varphi} \left\{ I_{x,T}(\varphi) \,|\, T > 0, \varphi \in \mathcal{C}_{x,T},\, \varphi(T) = y \right\}, \tag{1.71}$$

which, loosely, measures the cost of connecting x to y in arbitrarily long time for the LDP (1.17).

Let $\tau^\varepsilon = \inf\{t \geqslant 0 : X_t^\varepsilon \in \partial\Omega\}$ be the exit time from Ω. The following result can be obtained.

Theorem 1.18 ([132]). *For any $x \in \Omega$,*

$$\lim_{\varepsilon\to 0} \varepsilon \log \mathbb{E}_x\left[\tau^\varepsilon\right] = \min_{y\in\partial\Omega} V_b(x_*, y). \tag{1.72}$$

When the minimum on the right-hand-side of (1.72) is realized at a single point $y_* \in \partial\Omega$,

$$\forall\, \delta > 0, \qquad \mathbb{P}_x\left(|X^\varepsilon_{\tau^\varepsilon} - y_*| > \delta\right) \xrightarrow{\varepsilon\to 0} 0.$$

This result corresponds to the generalizations of [132, Theorems 2.4 & 4.1 in Chapter 4] discussed in [132, Chapter 5].

Informally, Theorem 1.18 says that the mean exit time is exponentially small, of order $\mathcal{O}\left(\mathrm{e}^{\frac{1}{\varepsilon}V_b(x_*,y_*)}\right)$, and the exit point distribution concentrates on the quasipotential minimum on the boundary. Moreover, it is possible to show that the exit path distribution concentrates on a half-infinite deterministic trajectory $\hat\varphi : (-\infty, 0] \to \Omega \cup \{y_*\}$ such that $\hat\varphi(-\infty) = x_*$, the *instanton*, which obeys a variational principle related to the quasipotential (1.71) (see [132, Theorem 2.3 in Chapter 4] and its generalization in Chapter 5). Finally, the LDP from Theorem 1.17 was used by Day [93] to obtain the convergence in distribution $\tau^\varepsilon / \mathbb{E}_x[\tau^\varepsilon] \xrightarrow[\varepsilon\to 0]{\text{in law}} \mathcal{E}(1)$ for any $x \in \Omega$.

In the specific case of the overdamped Langevin dynamics ($\sigma = \mathrm{Id}$, $b = -\nabla V$, $\varepsilon = 2/\beta$) one can show (see [132, Section 3 in Chapter 4]) that $V_b(x_*, y_*) = 2(V(y_*) - V(x_*))$ [14], and that $\hat\varphi$ is a half-infinite gradient flow line for V, meaning that $\hat\varphi'(t) = \nabla V(\hat\varphi(t))$ for $t \in (-\infty, 0)$. Therefore, the mean exit time is logarithmically equivalent to $\mathrm{e}^{-\beta(V(y_*)-V(x_*))}$ in the limit $\beta \to +\infty$, which is the expected Arrhenius behavior, and the instanton is a time-reversed trajectory of the steepest descent dynamics $x'(t) = -\nabla V(x(t))$ started from $x(0) = y_*$.

[14] In this, case, the action functional (1.70) is given by

$$I_{x,T}(\varphi) = \frac{1}{2}\int_0^T |\varphi'(t) + \nabla V(\varphi(t))|^2 = \frac{1}{2}\int_0^T |\varphi'(t) - \nabla V(\varphi(t))|^2 + 2\int_0^T \nabla V(\varphi(t))^\top \varphi'(t) = H(\varphi) + 2\left[V(\varphi(T)) - V(\varphi(0))\right],$$

and $H(\varphi) \geqslant 0$ vanishes whenever $\varphi'(t) = \nabla V(\varphi(t))$ for $t \in [0, T]$.

The large deviations approach therefore gives precise pathwise information in a general setting, but it fails to be fully quantitative, since (1.72) only gives a logarithmic equivalent of the mean exit time, falling short of the Eyring–Kramers formula (**EK**).

Potential theory. To obtain sharper estimates than those provided by large deviations principles, the potential-theoretic approach to metastability was developed starting in the early 2000s with works by Bovier & al. [59, 60]. This approach uses PDE techniques, expressing various path statistics (see (1.41)) in terms of solutions to Dirichlet problems, drawing from an analogy between reversible Markov processes and electrostatics, which is classical in the case of Brownian motion. We borrow from the monograph [58, Chapter 7], and refer the reader there for a complete introduction.

We restrict our scope to the reversible setting, and consider the case $b = -\nabla V$ in (1.68), corresponding to the overdamped Langevin dynamics (1.19). Assume that V satisifies the condition (V-**Conf**), so that the dynamics (1.68) is positively ergodic. In this setting, we recall that the generator and associated Dirichlet form are given respectively by

$$\mathcal{L}_\varepsilon = -\nabla V^\top \nabla + \frac{\varepsilon}{2}\Delta, \qquad \mathcal{E}_\varepsilon(f,g) = \frac{\varepsilon}{2}\int_{\mathcal{Q}} \nabla f^\top \nabla g \,\mathrm{d}\nu_\varepsilon, \qquad \forall\, f,g \in H^1(\nu_\varepsilon),$$

where $\nu_\varepsilon(\mathrm{d}x) = \mathcal{Z}_\varepsilon^{-1}\mathrm{e}^{-\frac{2}{\varepsilon}V(x)}\,\mathrm{d}x$ is the Gibbs measure (1.12).

We consider two disjoint closed domains A, B with regular boundary. We recall the commitor function for (X^ε, A, B), namely the function $h^\varepsilon_{A,B}(x) = \mathbb{P}_x(\tau^\varepsilon_A < \tau^\varepsilon_B)$ already introduced in (1.41). Using Dynkin's formula [259, Theorem 7.4.1], one can show that $h^\varepsilon_{A,B}$ is the solution $u \in \mathcal{D}(\mathcal{L}_\varepsilon)$ to the Dirichlet problem:

$$\begin{cases} -\mathcal{L}_\varepsilon u(x) = 0, & x \notin A \cup B, \\ u(x) = 1, & x \in A, \\ u(x) = 0, & x \in B. \end{cases} \tag{1.73}$$

In this context, and by analogy with electrostatics, the function $h^\varepsilon_{B\to A}$ is called the *equilibrium potential* for the capacitor (A, B). Likewise, the mean hitting time $T^\varepsilon_A(x) = \mathbb{E}_x[\tau^\varepsilon_A]$ solves the Dirichlet problem

$$\begin{cases} -\mathcal{L}_\varepsilon v(x) = 1, & x \notin A, \\ v(x) = 0, & x \in A. \end{cases}$$

Defining the *equilibrium measure* on ∂A:

$$\rho^\varepsilon_{A,B}(\mathrm{d}x) = \frac{\varepsilon}{2}\nu_\varepsilon(x)\nabla h^\varepsilon_{A,B}(x)^\top \mathrm{n}_A(x)\sigma_{\partial A}(\mathrm{d}x),$$

where $\sigma_{\partial A}$ is the surface measure on ∂A induced by the Lebesgue measure, ν_ε abusively denotes the Gibbs density, and n_A is the unit outward normal to A, one arrives, after computations using integration by parts, at the fundamental relationship [58, Corollary 7.30]

$$\int_{\partial A} T_B(y)\theta^\varepsilon_{A,B}(\mathrm{d}y) = \frac{1}{\mathrm{cap}_\varepsilon(A,B)}\int_{B^\mathrm{c}} h^\varepsilon_{A,B}(x)\nu_\varepsilon(\mathrm{d}x), \tag{1.74}$$

where $\theta^\varepsilon_{A,B} \in \mathcal{P}(\partial A)$ is a probability measure and $\mathrm{cap}_\varepsilon(A,B)$ is the *capacity*, respectively defined as

$$\theta^\varepsilon_{A,B} = \frac{\rho^\varepsilon_{A,B}}{\mathrm{cap}_\varepsilon(A,B)}, \qquad \mathrm{cap}_\varepsilon(A,B) = \mathcal{E}_\varepsilon(h^\varepsilon_{A,B}, h^\varepsilon_{A,B}) = \frac{\varepsilon}{2}\int_{\mathcal{Q}} |\nabla h^\varepsilon_{A,B}|^2 \,\mathrm{d}\nu_\varepsilon. \tag{1.75}$$

The fact that the capacity is the correct normalizing constant for $\theta^\varepsilon_{A,B}$ is itself the result of a computation, see [58, Lemma 7.26]. Moreover, the capacity satisfies the following variational principle.

Theorem 1.19 ([58, Theorems 7.33])**.** *The capacity* $\mathrm{cap}_\varepsilon(A,B)$ *satisfies the Dirichlet principle*

$$\mathrm{cap}_\varepsilon(A,B) = \inf_{f\in H^1(\mathcal{Q},\nu_\varepsilon)} \left\{\mathcal{E}_\varepsilon(f,f), f \geqslant 1 \text{ on } A,\ f \leqslant 0 \text{ on } B\right\}. \tag{1.76}$$

with minimum attained at $f = h^\varepsilon_{A,B}$*.*

In fact, $h^\varepsilon_{A,B}$ can also be defined as the supremum of another functional, yielding a complementary variational principle known as the *Thomson principle* [58, Theorem 7.35].

The relation (1.74) can be used in some cases to obtain quantitative estimates of T_A. We give an example in the case of the simplest metastable system, the bistable energetic case in the gradient case $b = -\nabla V$. We assume that V is smooth over $\mathbb{R}^d$ and goes to infinity at infinity. Suppose that V has only two non-degenerate local minima, given by points m_1, m_2, which satisfy $V(m_1) > V(m_2)$. At low temperature, the neighborhood of m_1 is a transient metastable state, while the neighborhood of m_2 corresponds to the most stable state. The height of the energy barrier to go from m_1 to m_2 is determined by the minimum energy path between m_1 and m_2. Defining

$$V^* = \inf_{\gamma\in\Gamma(m_1,m_2)} \max_{0\leqslant t\leqslant 1} V\circ\gamma(t), \qquad \Gamma(m_1,m_2) = \left\{\gamma\in\mathcal{C}([0,1];\mathbb{R}^d),\ \gamma(0)=m_1,\ \gamma(1)=m_2\right\}.$$

we see that, since V is smooth and has compact sublevel sets, it satisfies the conditions [15] of the mountain-pass theorem (see [121, Section 8.5.1]). This result ensures that V^* is a critical value of V. We make the simplifying (and generic) assumption that this critical value corresponds to a unique, non degenerate, index-1 saddle point $s\in\mathbb{R}^d$, meaning that $V^* = V(s)$, $\nabla V(s) = 0$ and $\nabla^2 V(s)$ has one negative eigenvalue and $(d-1)$ positive eigenvalue.

In other words, the energy landscape consists of two valleys, separated by a mountain. The elevation gain to go from m_1 to m_2 is given by the altitude of the pass s minus that of the valley m_1, i.e. $E_{m_1\to m_2} = V(s) - V(m_1) > 0$. The following Eyring–Kramers formula is a special case of a result by Bovier & al.

Theorem 1.20 (From [60, Theorem 3.2])**.** *For any* $\delta > 0$*,*

$$\mathbb{E}_{m_1}\left[\tau^\varepsilon_{\overline{B}_\delta(m_2)}\right] = \frac{2\pi}{|\lambda^-(s)|}\left(\frac{|\det\nabla^2 V(s)|}{\det\nabla^2 V(m_1)}\right)^{\frac{1}{2}} \mathrm{e}^{\frac{2}{\varepsilon}(V(s)-V(m_1))}\left(1+\mathcal{O}\left(\sqrt{\varepsilon}|\log\varepsilon|\right)\right), \tag{1.77}$$

where $\overline{B}_\delta(m_2)$ *denotes the closed unit ball with radius* δ *centered at* m_2*,* $\nabla^2 V$ *denotes the Hessian matrix of* V*, and* $\lambda^-(s)$ *denotes the unique negative eigenvalue of* $\nabla^2 V(s)$*.*

[15] In particular, the Palais–Smale compactness condition.

In dimension one, Theorem 1.20 can be proven directly by solving (1.73) for $h^{\varepsilon}_{A,B}$ in integral form, using the relationship (1.74) with $A = \{m_1\}$, and estimating the right-hand-side with the Laplace method. This is the original method employed by Kramers [198], see also [33] and [58, Section 7.2.5]. In higher dimensions, the proof is much more involved. Let us simply sketch the main steps.

One takes A to be a small closed ball around m_1, $B = \overline{B}_\delta(m_2)$, and one uses a priori regularity estimates to control the variations $\mathrm{osc}_A(T^{\varepsilon}_B)$, allowing to replace the left-hand-side of (1.74) by $T^{\varepsilon}_B(m_1)(1+o(1))$. One then relies on an appropriate approximation of $h^{\varepsilon}_{A,B}$ and control from the variational principle (1.76) to derive sharp estimates for $\mathrm{cap}_\varepsilon(A,B)$. Very roughly, this approximation is constructed in accordance with the probabilistic intuition: for small $\varepsilon > 0$, $h^{\varepsilon}_{A,B}$ is nearly constant in the interiors of both $\mathcal{A}(m_1)$ and $\mathcal{A}(m_2)$, with respective values 1 and 0, and with a sharp transition around s. The dominant contribution to $\mathrm{cap}_\varepsilon(A,B)$ in (1.75) is localized in a small neighborhood of s, where the Dirichlet problem (1.73) can be linearized, and the linearized problem can be solved by separation of variables. This construction gives an upper bound on the capacity using the variational principle (1.76), which, together with rough estimates for $h^{\varepsilon}_{A,B}$ around m_1 and the Laplace method, give an upper bound on the mean transition time. The lower bound on the capacity is achieved by restricting the integral (1.75) to a sufficiently small neighborhood of the saddle point, upon which delicate computations and the Laplace method finally lead to the asymptotic estimate (1.77).

Contrarily to the results obtained with the pathwise approach, the results of [60] give *sharp estimates* of the transition time with an explicit prefactor, but on the other hand give no information on the transition path. Extensions of this approach to multiple minima and multiple saddles [60], possibly degenerate [36], are also possible.

Recently, extensions of the potential-theoretic approach to non-reversible diffusions have been used to extend the Eyring–Kramers formula to more general dynamical settings, see [212] for the case of elliptic diffusions with Gibbs invariant measure, and [214] for an extension to the underdamped Langevin dynamics (1.17). The analog of the Eyring–Kramers formula for the general elliptic, non-Gibbsian, non-reversible case (1.68) was conjectured by Bouchet & Reygner in [57], and justified with formal computations. First rigorous results in this direction have been obtained very recently, see [210].

Finally, let us mention, that the potential-theoretic point of view suggests quantitative characterizations of the metastability of a given family of core-sets $(C_\alpha)_{\alpha\in I}$ in terms of certain capacity ratios, recalling the framework of Section 1.2.1. We refer to [58, Section 8.1] for a presentation of these definitions in the case of countable state spaces. Such characterizations could prompt questions regarding the shape-optimization of these criteria with respect to the choice of core-sets.

Spectral approach. The third approach to metastability is the spectral point of view. As mentioned in Section 1.1.2 above, the metastability of the dynamics, as an obstacle to efficient sampling, is reflected in a small spectral gap for the infinitesimal generator. The connections between metastability of the dynamics and structural properties of the spectrum of the generator are rich, and can first be motivated on an intuitive level.

- Invariant sets $\Omega \subset \mathcal{Y}$ for the dynamics Y are in correspondence with invariant observables under the evolution semigroup, i.e. $e^{t\mathcal{L}^Y} \mathbb{1}_\Omega = \mathbb{1}_\Omega$. Together, they span the kernel of the generator. For an ergodic Markov process, the kernel is limited to the space of constant functions, corresponding to the global stable state $\Omega = \mathcal{Y}$. In a metastable system, there exists some $\Omega \subsetneq \mathcal{Y}$ where the process remains trapped for very long times. The corresponding indicators are nearly invariant under the evolution semigroup, and can be loosely be seen as approximate eigenfunctions of the generator, with eigenvalues close to zero.

- When the infinitesimal generator is self-adjoint, its spectrum consists of inverse timescales, corresponding to rates of various relaxation processes. The spectrum of a reversible, ergodic, metastable Markov process (i.e. of its infinitesimal generator) should consist of the zero eigenvalue, as many small eigenvalues as there are transitions from metastable states to longer-lived states, and finally higher eigenvalues corresponding to fast relaxation within metastable states. Therefore, the separation of timescales in reversible metastable systems is reflected in a gap in the spectrum of the generator, between inter-state transition rates and intra-state relaxation rates.

- If physical (or any other) insight permits us to identify good metastable states, we can approximate the low-lying spectrum by constructing approximate eigenfunctions, and quantify the timescale gap. Conversely, if we can approximate the spectrum, the structure of approximate eigenvectors can reveal metastable states. Eigenvectors for low-lying eigenvalues, corresponding to *slow modes* of the system, can also be used to build reaction coordinates. Variations around this principle are behind many modern data-driven methods for spatial coarse-graining, model reduction and collective-variable learning, some of which we discuss in the next paragraph.

Early results in this perspective are given by Davies [90, 91]. In particular, the main result of [91] is the following theorem.

Theorem 1.21 ([91, Theorem 19])**.** *Assume that the infinitesimal generator $-\mathcal{L}^Y$ is self-adjoint on $L^2(\pi)$, satisfying the spectral gap assumption*[16]

$$\mathrm{Sp}(-\mathcal{L}^Y) \subseteq [0, \delta] \cup [1, \infty).$$

for some $\delta > 0$. We denote by Π_δ the spectral projection on $[0, \delta]$. Assume finally that $\Pi_\delta L^2(\pi) \in L^\infty(\mathcal{Y})$.

Then, $\dim \Pi_\delta L^2(\pi) = n$ for some finite $n \geqslant 1$. If δ is sufficiently small, there exists a partition $(E_j)_{1 \leqslant j \leqslant n}$ of $\mathcal{Y}$ into n metastable states and a basis $(u_j)_{1 \leqslant j \leqslant n}$ of $\Pi_\delta L^2(\pi)$ such that

$$\forall\, 1 \leqslant j \leqslant n, \qquad \|u_j - \mathbb{1}_{E_j}\|_{L^2(\pi)} \leqslant 4n^{3/2}\sqrt{\delta}.$$

This result states that, in the limit of a large separation of timescales, eigenfunctions of $\mathcal{L}^Y$ corresponding to small eignvalues can be well-approximated by piecewise-constant functions on each metastable state, namely linear combinations of the indicators $\mathbb{1}_{E_j}$. The strength of

[16] The existence of a spectral gap always implies a bound of this form by a change of time units.

this result is that it is rather generic (in fact [91, Theorem 17] is an abstract result which applies to more general Markovian dynamics), but it gives little quantitative information on the timescales.

More precise estimates can be computed in the low-temperature regime. In the case of the overdamped Langevin dynamics, where $(b, \sigma) = (-\nabla V, \mathrm{Id})$, the spectral approach studies the spectrum of the Witten Laplacian (1.34) on $L^2(\mathcal{Q})$. We recall its expression in terms of $\varepsilon = 2/\beta$:

$$\Delta_{V,\varepsilon} = \frac{1}{2\varepsilon}\left(-\varepsilon^2\Delta - \varepsilon\Delta V + |\nabla V|^2\right). \tag{1.78}$$

The low-temperature regime corresponds to the *semiclassical limit* $\varepsilon \to 0$. It is convenient to consider the case of energetic metastable states, corresponding to local minima of the energy function. The analysis is also simpler if V is assumed to be a Morse function, meaning that the Hessian $\nabla^2 V(x)$ is non-degenerate for each point $x \in \mathcal{Q}$ such that $\nabla V(x) = 0$. Such points are called critical points, and the Morse property implies that critical points are isolated.

In this context, one can obtain precise results on the spectrum $\mathrm{Sp}(\Delta_{V,\varepsilon}) = \mathrm{Sp}(-\mathcal{L}_\varepsilon)$. The first result concerns the overall structure of the spectrum, and shows that $\Delta_{V,\varepsilon}$ can be approximated by a block-diagonal operator, with each block being a quantum harmonic oscillator attached to a specific local minimum of V. We assume that the condition (**V-Conf**) is satisfied and that $\nabla^2 V$ is uniformly bounded, so that $\mathrm{Sp}(\Delta_{V,\varepsilon})$ consists of finite-multiplicity isolated eigenvalues $(\lambda_{k,\varepsilon})_{k\geqslant 0}$ (see the discussion following equation (1.34)), and that V has finitely many critical points $(x_j)_{1\leqslant i\leqslant N}$ in $\mathcal{Q}$. Then the following result holds.

Theorem 1.22 ([195, Theorem 11.1])**.** *It holds, for any $k \geqslant 0$:*

$$\lim_{\varepsilon\to 0} \lambda_{k,\varepsilon} = \lambda_k^{\mathrm{HA}},$$

where λ_k^{HA} is the k-th eigenvalue, counted with multiplicity, of the direct sum of shifted harmonic oscillators

$$\Delta_{V,\varepsilon}^{\mathrm{HA}} := \bigoplus_{i=1}^{N} H^{(i)}, \qquad H^{(i)} = -\Delta + \frac{1}{4}x^\top \left(\nabla^2 V(x_i)\right)^2 x - \frac{1}{2}\Delta V(x_i).$$

The operator $\Delta_{V,\varepsilon}^{\mathrm{HA}}$ is called the *harmonic approximation*, and its spectrum can be computed from that of the local harmonic models:

$$\mathrm{Sp}(\Delta_{V,\varepsilon}^{\mathrm{HA}}) = \bigcup_{i=1}^{N} \mathrm{Sp}(H^{(i)}).$$

when x_i is a local minimum, the ground state energy $\min \mathrm{Sp}(H^{(i)})$ is equal to 0, and if not, it is strictly positive. Therefore, the harmonic approximation shows that $\mathcal{L}_\varepsilon$ has as many small eigenvalues in the limit $\varepsilon \to 0$ as they are local minima of V. Furthermore, the harmonic spectra $(\mathrm{Sp}(H^{(i)}))_{1\leqslant i\leqslant N}$ can be computed by diagonalizing $\nabla^2 V$ around each critical point.

In fact, it is possible to show with rather crude estimates that the small eigenvalues are of order $\mathrm{e}^{-\frac{c}{\varepsilon}}$ for some $c > 0$, and to prove the existence of asymptotic expansions with respect to ε (see [157]). In the bistable case discussed in the previous paragraph (in which case there

are two small eigenvalues, $\lambda_{0,\varepsilon} = 0$ and $\lambda_{1,\varepsilon} \to 0$), the results of [157], in particular, imply the following Eyring–Kramers formula for $\lambda_{1,\varepsilon} > 0$:

$$\lambda_{1,\varepsilon} = \frac{|\lambda^-(s)|}{2\pi} \left(\frac{\det \nabla^2 V(m_1)}{|\det \nabla^2 V(s)|} \right)^{\frac{1}{2}} \mathrm{e}^{-\frac{2}{\varepsilon}(V(s)-V(m_1))} \left(1 + \mathcal{O}\left(\varepsilon\right)\right), \tag{1.79}$$

which is consistent with the potential-theoretic result (1.77) and the interpretation of $\lambda_{1,\varepsilon}$ as a relaxation rate corresponding to an inter-state transition. In fact, potential-theoretic approaches also allow to recover results such as (1.79), but with a worse error term. See [61, Theorem 1.2] and [58, Section 8.4.2] for a more general discussion of the link between spectral properties and potential theory.

When there are multiple wells, an explicit formula can also be derived [61, 158], and explicitly computed at the cost of a labelling procedure. Extensions to more general dynamical settings, such as non-reversible or non-elliptic dynamics (in particular the underdamped Langevin dynamics) are possible, see [166, 167, 168, 208, 55] for various results in this direction.

Numerical approaches. Many numerical methods, beyond the AMD algorithms discussed in Section 1.2.1, have been proposed to address the problem of metastability. Statistical learning methods for time-lagged propagators form a large class of methods, which aim to infer timescales, metastable states, and proporse coarse-grained dynamics from sampled trajectory data. We refer the reader to [298] for an extensive review of this type of approach.

The aim of these methods is in each case to construct a finite-dimensional approximation for an infinite-dimensional operator, generally one of

$$\mathcal{K}_\tau = \mathrm{e}^{\tau \mathcal{L}^Y}, \qquad \mathcal{T}_\tau = \mathrm{e}^{\tau \mathcal{L}^{Y\dagger}}, \tag{1.80}$$

where the semigroup $\mathcal{K}_\tau$ is known in this context as the *Koopman operator*, and its dual $\mathcal{T}_\tau$ *Perron–Frobenius or transfer operator*.

We assume that we are in a metastable situation such as the one assumed in Theorem 1.21. Namely, the generator is self-adjoint, with a spectral gap $\delta \ll 1$. For times $\tau = \mathcal{O}(\delta^{-1})$, the operators (1.80) can be well-approximated with a rank-n operator, given by the spectral projection $\Pi_{[\mathrm{e}^{-\tau/\delta},1]}\mathcal{K}_\tau$ (and its L^2-adjoint), where n is the number of metastable modes given by Theorem 1.21. For non-reversible dynamics, a similar approximation can be constructed using the singular value decomposition, see [298, Section 3.1.2].

Estimators for these finite-rank operators can be obtained from time-lagged samples of the dynamics, $\mathbb{X} = \left(Y_0^{(j)}, Y_\tau^{(j)}\right)_{1 \leqslant j \leqslant J}$, where $Y_\tau^{(j)}$ is a sample of the dynamics at time τ, started from $Y_0^{(j)}$ for each $1 \leqslant j \leqslant J$. The estimation task is generally performed in two steps. First, a rank $M \gg n$ model for $\mathcal{A}_\tau \in \{\mathcal{K}_\tau, \mathcal{T}_\tau\}$ is constructed, using feature transformation $\Psi(\mathbb{X})$ of the trajectory data, from which a matrix approximation $\widehat{A}_{\tau,\mathbb{X}} \in \mathbb{R}^{M \times M}$ is constructed. Second, the dominant eigenvalues of $\widehat{A}_{\tau,\mathbb{X}}$ are computed, and used to approximate relaxation timescales. Corresponding eigenvectors may be reconstructed using the input features. If a spectral gap is detected in the spectrum, the model $\widehat{A}_{\tau,\mathbb{X}}$ itself can be truncated, giving the final low-rank approximation, which can be used as a propagator for a coarse-grained,

low-dimensional dynamics.

Specific instances of this general yield different methods. A popular family are Markov state models (MSMs [272, 181]), which approximate the transfer operator with an empirical transition matrix associated with a coarse-graining of configuration space, see [298, Section 4.2.3]. The variational approach to conformation dynamics (VAC [256]) and its non-reversible extension, the variational approach to Markov processes (VAMP [341]), rely on variational principles satisfied by the projected propagators, see [298, Section 4.3].

1.3.2 The quasi-stationary regime

In this section, we focus on a specific tool to study local questions regarding the metastability of (1.68). As discussed in Section 1.2.1, and formalized in Assumption **QSD**, for typical initial conditions inside a metastable state Ω_α, a local equilibrium ν_α is reached after some time. Starting from this local equilibrium, the exit event $(\tau_\alpha, Y_{\tau_\alpha})$ is Markovian: the exit time τ_α is exponentially distributed with rate λ_α, and the exit point Y_{τ_α} is independent from the exit time.

Similarly to the previous paragraph, the degree of metastability of Ω_α corresponds to a *local separation of timescales*, timescales which in turn are encoded by the spectrum of the infinitesimal generator, when endowed with appropriate boundary conditions. We begin by introducing quasi-stationary distributions, as well as the spectral point of view on these objects, focusing on the reversible setting, namely that of the overdamped Langevin dynamics. Finally, we review how the spectral point of view, and in particular the use of semiclassical methods, can justify the AMD methods introduced in Section 1.2.1 and provide insight into how to optimize their efficiency.

Quasi-stationary distributions. The study of quasi-stationary behavior is attributed to Yaglom [343] to study the behavior of some critical branching processes before their extinction. QSDs are useful for instance in the mathematical modelling of ecosystems, where they allow to study the behavior of populations in the pre-extinction regime. We refer to [245] for a survey of QSDs with a focus on the applications to population dynamics, and to the book [84] for extensive background material on QSDs.

Let Y be a continuous-time Markov process on some Polish configuration space $S = \Omega \cup \partial$, and let τ_∂ be the first hitting time of a *cemetery point* ∂. The stopping time τ_∂ is called the *killing time*. The cemetery point ∂ is absorbing, in the sense that $\mathbb{P}(\forall t \geqslant \tau_\partial,\, Y_t \in \partial) = 1$ and $\mathbb{P}_y(\tau_\partial < +\infty) = 1$ for all $y \in S$. For instance, Y could model the size of a population, in which case $\Omega = (0, +\infty)$ with $\partial = \{0\}$ corresponding to the state of extinction, or the configuration of a metastable system, in which case $\Omega \subset \mathcal{E}$ is a metastable state, whose topological boundary is identified with the cemetery point: $\partial = \partial\Omega$. These following definitions can be found in [245, Section 2]. A measure $\nu_\Omega \in \mathcal{P}(E)$ is called

- A *Yaglom limit* for Y starting from $y \in \Omega$ if for all measurable $A \subset \Omega$,

$$\lim_{t \to +\infty} \mathbb{P}_y \left(Y_t \in A \,|\, \tau_\partial > t \right) = \nu_\Omega(A).$$

- A *quasi-limiting distribution* (QLD) for Y if there exists $\mu_0 \in \mathcal{P}(\Omega)$ such that for all measurable $A \subset \Omega$,
$$\lim_{t\to+\infty} \mathbb{P}_{\mu_0}\left(Y_t \in A \,|\, \tau_\partial > t\right) = \nu_\Omega(A).$$
- A *quasi-stationary distribution* (QSD) for Y if for all measurable $A \subset \Omega$, and $t \geqslant 0$,
$$\mathbb{P}_{\nu_\Omega}\left(Y_t \in A \,|\, \tau_\partial > t\right) = \nu_\Omega(A).$$

If there exists a unique Yaglom limit starting from any $y \in E$, it is *the* Yaglom limit for Y inside Ω. One can then show [245, Proposition 1] that ν_Ω is a QLD if and only if it is a QSD. Since a Yaglom limit is obviously a QLD, it is also a QSD.

QSDs are related to spectral properties. Defining, for f in the space $B^\infty(\Omega)$ of bounded measurable functions defined on Ω, the family of operators
$$\forall\, t \geqslant 0, \qquad P_t f(x) = \mathbb{E}_x\left[f(Y_t)\mathbb{1}_{t<\tau_\partial}\right],$$
the Markov property entails that $(P_t)_{t\geqslant 0}$ forms a sub-Markovian semigroup, called the *killed semigroup*. One can easily show (see [84, Chapter 2] or Section 1.2.1) that, for any QSD ν_Ω, there exists $\lambda(\nu_\Omega) > 0$ such that
$$\mathbb{E}_{\nu_\Omega}\left(f(Y_{\tau_\partial})\mathbb{1}_{t<\tau_\partial}\right) = \mathrm{e}^{-\lambda(\nu_\Omega)t}\mathbb{E}_{\nu_\Omega}\left[f(Y_{\tau_\partial})\right],$$
so that starting under a QSD ν_Ω, the killing time is exponentially distributed with rate $\lambda(\nu_\Omega)$, and independent of the killing point. Moreover, any QSD is a left-eigenvector for the killed semigroup, namely
$$\forall\, f \in B^\infty(\Omega),\, t \geqslant 0, \qquad \nu_\Omega\left(P_t f\right) = \mathrm{e}^{-\lambda(\nu_\Omega)t}\nu_\Omega(f). \tag{1.81}$$
A proof can be found in [84, Section 2.3].

Many works have focused on proving the existence of a unique QSD ν_Ω in increasingly general settings, as well as obtaining criteria for the exponential convergence to ν_Ω of the conditional distributions
$$\mu_t = \mathbb{P}_{\mu_0}\left(Y_t \in \cdot \,|\, t < \tau_\partial\right) = \frac{\mu_0 P_t}{\mu_0 P_t \mathbb{1}_\Omega} \tag{1.82}$$
for any $\mu_0 \in \mathcal{P}(\Omega)$. Probabilistic approaches by Champagnat & Villemonais, starting in [72], finding suitable analogs of the Lyapunov and local minorization conditions used in Harris' theorem (see [150]), establish the following result for elliptic SDEs.

Theorem 1.23 ([73, Theorem 1.1])**.** *Let Y be a solution to the SDE (1.16) on $\mathcal{Y} = \mathbb{R}^d$ with Hölder-continuous coefficients b and σ, with σ uniformly elliptic. Assume that Ω is a bounded, connected, open domain of $\mathcal{Y}$. Then there exists a unique QLD $\nu_\Omega \in \mathcal{P}(\Omega)$ (which is therefore the unique QSD) and constants $C, r > 0$ such that for all $\mu_0 \in \mathcal{P}(\Omega)$,*
$$\mathrm{d_{TV}}\left(\mu_t, \nu_\Omega\right) \leqslant \frac{C}{\mu_0(\eta)}\mathrm{e}^{-rt} \qquad \forall\, t \geqslant 0, \tag{1.83}$$
where $\eta : \Omega \to [0, +\infty)$ is a $\mathcal{C}^2$-eigenfunction for the infinitesimal generator, with eigenvalue

equal to the negative killing (or exit) rate, namely $-\mathcal{L}^Y \eta = \lambda(\nu_\Omega)\eta$, *defined by*

$$\eta(y) = \lim_{t\to+\infty} \mathrm{e}^{\lambda(\nu_\Omega)t}\mathbb{P}_y(t < \tau_\partial).$$

Exponential convergence bounds such as (1.83) have been obtained for elliptic diffusions on compact Riemannian manifolds [71], general Feller processes in regular bounded domains [30], and some kinetic SDEs in cylindrical domains [228, 145]. We refer to [30, Section 1.1] for a recent survey.

Spectrum of the Dirichlet generator. Analytical methods, based on spectral analysis, are also effective to study QSDs, obtain more explicit rates of convergence in (1.83), and study the metastable exit distribution $\mathbb{P}_\nu(X_{\tau_\partial} \in \cdot)$. Just as the rate of convergence to global equilibrium is dictated by a spectral gap of the infinitesimal generator, so is convergence to local equilibrium, when the infinitesimal generator is supplemented with Dirichlet boundary conditions.

For simplicity, we consider here the case of reversible elliptic diffusions. A similar approach can be followed, using the Krein–Rutman theorem for non-reversible elliptic diffusions, see [270] and [271, Chapter 3]. We assume that X is a solution to the SDE (1.21) on $\mathcal{Q} = \mathbb{R}^d$, where V, σ and γ are smooth, with σ uniformly elliptic. The fluctuation-dissipation relation (1.22) implies in particular that γ is symmetric positive-definite. To use results of elliptic regularity, we assume that Ω is a smooth, bounded, connected open domain of $\mathbb{R}^d$. The generator, as a formal operator, writes

$$\mathcal{L}_\beta = \frac{\mathrm{e}^{-\beta V}}{\beta} \mathrm{div}\left(\mathrm{e}^{-\beta V}\gamma\nabla\right).$$

We use frequently the integration by parts formula

$$\forall\, f, g \in \mathcal{C}^\infty(\overline{\Omega}), \qquad \int_\Omega f\,(\mathcal{L}_\beta g)\,\mathrm{e}^{-\beta V} = \frac{1}{\beta}\int_{\partial\Omega} f\left(\nabla g^\top \gamma \mathrm{n}\right)\mathrm{e}^{-\beta V} - \frac{1}{\beta}\int_\Omega \nabla f^\top \gamma \nabla g\,\mathrm{e}^{-\beta V}, \quad (1.84)$$

where n denotes the unit outward normal, and the boundary integral is with respect to the Lebesgue (surface) measure on $\partial\Omega$.

For f, g vanishing on the boundary of Ω, the boundary term is omitted from (1.84), so that $-\mathcal{L}_\beta$ defines a symmetric, positive, elliptic quadratic form on $L^2_\beta(\Omega) := L^2(\Omega, \mathrm{e}^{-\beta V}\,\mathrm{d}x)$. We consider the *Dirichlet realization* of $-\mathcal{L}_\beta$ on $L^2_\beta(\Omega)$, defined as Friedrichs' extension (see [276, Theorem 10.23]) of the form (1.84) on $\mathcal{C}^\infty_{\mathrm{c}}(\Omega)$. It is by definition a strictly positive self-adjoint operator, with domain contained in $H^1_0(\Omega)$, the closure of $\mathcal{C}^\infty_{\mathrm{c}}(\Omega)$ for the form-norm. Since the injection $H^1_0(\Omega) \to L^2_\beta(\Omega)$ is compact by the smoothness of V and the Rellich–Kondrachov theorem (see [121, Theorem 1 in Section 5.7]), $\mathcal{L}_\beta^{-1}$ is $(L^2_\beta(\Omega) \to L^2_\beta(\Omega))$- compact, which implies that the spectrum of $-\mathcal{L}_\beta$ is given by a sequence of positive eigenvalues, which we enumerate with multiplicity:

$$0 < \lambda_{1,\beta} \leqslant \lambda_{2,\beta} \leqslant \cdots.$$

Each eigenvalue has finite multiplicity and there are no accumulation points in the spectrum, so that $\lambda_{n,\beta} \xrightarrow{n\to\infty} +\infty$. To this sequence of eigenvalues, we associate an orthonormal

sequence $(u_{n,\beta})_{n\geqslant 1}$ of eigenfunctions, satisfying

$$\forall n, m \geqslant 1, \qquad -\mathcal{L}_\beta u_{n,\beta} = \lambda_{n,\beta} u_{n,\beta}, \qquad \int_\Omega u_{n,\beta} u_{m,\beta} \, \mathrm{e}^{-\beta V} = \delta_{nm}. \tag{1.85}$$

It is classical (see [121, Section 6.5.1]) that $\lambda_{1,\beta} < \lambda_{2,\beta}$ and that $u_{1,\beta}$ is the unique signed eigenfunction, and does not vanish inside Ω. We may assume without loss of generality that $u_{1,\beta} > 0$. Finally, elliptic regularity arguments (see [121, Theorem 6 in Section 6.3.2]) show that for all $n \geqslant 1$, $u_{n,\beta} \in \mathcal{C}^\infty(\overline{\Omega})$.

The knowledge of a spectral decomposition allows for many explicit computations, using the following Feynman–Kac representation. Writing $\tau_\Omega = \tau_\partial$ for the hitting time of $\partial\Omega$, we define

$$v(t,x) = \mathbb{E}_x \left[\mathbb{1}_{\tau_\Omega \leqslant t} \varphi(X_{\tau_\Omega}) + \mathbb{1}_{\tau_\Omega > t} \psi(X_t) \right] \tag{1.86}$$

for some $\varphi, \psi \in \mathcal{C}^\infty(\overline{\Omega})$. The function v is the smooth solution to the PDE problem

$$\begin{cases} \partial_t v = \mathcal{L}_\beta v, & (t,x) \in (0,+\infty) \times \Omega, \\ v = \varphi, & (t,x) \in (0,+\infty) \times \partial\Omega, \\ v = \psi, & (t,x) \in \{0\} \times \overline{\Omega}. \end{cases}$$

The fact that a unique smooth solution exists follows from the general theory of parabolic evolution equations, see [121, Chapter 7], and the probabilistic representation (1.86) then follows from Itô's formula, see [206, Proposition 1].

It follows from this Feynman–Kac formula that the probability measure

$$\nu_\Omega(\mathrm{d}x) = \frac{u_1(x) \mathrm{e}^{-\beta V(x)}}{\int_\Omega u_1 \mathrm{e}^{-\beta V}} \, \mathrm{d}x \in \mathcal{P}(\Omega)$$

is a QSD for X in Ω (see [206, Proposition 2]). Moreover, the exit rate $\lambda(\nu_\Omega)$ is equal to $\lambda_{1,\beta}$, and its density (which we again denote ν_Ω) is an eigenfunction of the Fokker–Planck operator $\mathcal{L}_\beta^\dagger$ with Dirichlet boundary conditions, for the same eigenvalue.

The formula (1.84) gives an expression for the exit point distribution starting from ν_Ω (see [206, Proposition 3]) as

$$\mathbb{E}_{\nu_\Omega} \left[\varphi(X_{\tau_\Omega}) \right] = \int_{\partial\Omega} \varphi \rho, \qquad \rho = - \left(\beta \lambda_{1,\beta} \int_\Omega u_{1,\beta} \mathrm{e}^{-\beta V} \right)^{-1} \left(\nabla u_{1,\beta}^\top \gamma \mathrm{n} \right) \mathrm{e}^{-\beta V}. \tag{1.87}$$

Since, starting from ν_Ω, $\tau_\Omega \sim \mathcal{E}(\lambda_{1,\beta})$ is independent from X_{τ_Ω}, the joint distribution of the exit event is in this case completely explicit in terms of the principal Dirichlet eigenpair.

For $\varphi = 0$ in (1.86), the solution $v(t,x) = P_t\psi(x)$ can be expanded in the Dirichlet eigenbasis, i.e.

$$P_t \psi(x) = \sum_{n=1}^{+\infty} \mathrm{e}^{-\lambda_{n,\beta} t} \left(\int_\Omega \psi u_{n,\beta} \mathrm{e}^{-\beta V} \right) u_{n,\beta}(x). \tag{1.88}$$

Using this expansion, one can estimate the total variation distance between the conditional

measure (1.82) and ν_Ω, and show (see for instance [305, Theorem 3.1]) that

$$\forall\, t \geqslant 0, \qquad \mathrm{d_{TV}}\left(\mu_t, \nu_\Omega\right) \leqslant C(\mu_0)\mathrm{e}^{-(\lambda_{2,\beta}-\lambda_{1,\beta})t}, \tag{1.89}$$

for some constant $C(\mu_0) > 0$ independent from t, for a large class of initial distributions $\mu_0 \in \mathcal{P}(\Omega)$ which includes Dirac distributions. In particular ν_Ω is the Yaglom limit for X inside Ω. The uniqueness of the QSD is a consequence of the simplicity of $\lambda_{1,\beta}$, the fact that $u_{1,\beta} > 0$ inside Ω, and the property (1.81).

The convergence bound (1.89) shows that the asymptotic convergence rate to the QSD is given by the spectral gap $\lambda_{2,\beta} - \lambda_{1,\beta} > 0$. Furthermore this rate is essentially sharp: taking μ_0 proportional to $(u_{1,\beta} + \varepsilon u_{2,\beta})\mathrm{e}^{-\beta V}$ for a sufficiently small ε, we get an explicit initial condition which converges at exactly this rate to the QSD in the $L^2(\Omega)$-norm.

Foundations and numerical analysis for AMD algorithms. The results reviewed in the previous two paragraphs can be used to study the AMD algorithms of Section 1.2.1. Existence and uniqueness results for the QSD justify Assumption (**QSD**). The convergence bounds (1.83) and (1.89) justify Approximation (**MS($t_{\mathrm{corr}}(\alpha)$)**).

To justify the physical assumptions behind TAD and HMD, namely Approximations (**EK**) and (**TST**), one has to study the metastable exit event in the low-temperature regime $\beta \to +\infty$, so that energetic barriers are high relative to thermal fluctuations. This is equivalent to study spectral properties of the Dirichlet realization of the Witten Laplacian (1.78) in the semiclassical limit $\varepsilon \to 0$. The main difficulty lies in constructing sufficiently accurate approximations of the principal eigenvector $u_{1,\beta}$ and its normal derivative $\nabla u_{1,\beta}^\top \gamma \mathrm{n}$ to get useful estimates on $\lambda_{1,\beta}$ and the exit distribution (1.87). Such approximations are called *quasimodes*, and are the central tool in semiclassical analysis.

Semiclassical techniques have been used in [14, 99, 100, 101, 224] to study the validity Assumption (**EK**). In particular all these works assume some restrictions on the domain Ω. The early results of [14] are in dimension 1, while positive results (justifying Approximation (**EK**)) for higher-dimensional systems exist under non-local assumptions on V, which may be hard to verify in practice. Justifications for Approximation (**TST**) can be found in [225], again in the low-temperature regime with various restrictions on V, δV and Ω.

Estimating the bias in AMD methods arising from choices of various approximation parameters is also a natural question, see [14] for a numerical analysis of TAD and [206, 233] for a numerical analysis of the Parallel Replica algorithm.

TAD and HMD are often valid and useful in the presence of high energetic barriers, but fail when the metastability has an entropic origin. Recently, the semiclassical approach has been extended to study models of entropic confinement. In these so-called narrow escape problems, high-energy transition states around an energetic basin are replaced with narrow exit pathways at the boundary of a domain Ω. In this setting, the dynamics consist in a simple Brownian motion, which is reflected on the boundary $\partial\Omega$, except on a subset $\Gamma_\varepsilon \subset \partial\Omega$, on which absorption occurs. The spectral approach to the QSD leads to eigenvalue problems for the Laplacian with mixed Dirichlet–Neumann boundary conditions. The probabilistic

interpretation of the principal eigenpair and spectral gap allows to study quasistationarity in a toy model of entropic barriers. Analogs of the Eyring–Kramers formula, when Γ_ε consists of multiple regions of varying size, have been established in a two-dimensional situation, when $|\Gamma_\varepsilon| \xrightarrow{\varepsilon \to 0} 0$, see [227]. The question has also been considered from a potential-theoretic point of view, see [124]. The question of formulating entropic equivalents of TAD in a general setting is a natural question, which has yet to be studied.

The spectral point of view is helpful in parameter selection for AMD methods. For instance, the bound (1.89) suggests one should choose the decorrelation time $t_{\mathrm{corr}}(\Omega) > \frac{C}{\lambda_{2,\beta} - \lambda_{1,\beta}}$ for some $C > 0$. For Ω to be a "good" metastable state (see Problem 1.12), the local separation of timescales should be maximized, ensuring that the timescale on which the conditionned process converges to the QSD is small compared to the timescale on which is subsequently transitions. This naturally leads to the question of maximizing $(\lambda_{2,\beta} - \lambda_{1,\beta})/\lambda_{1,\beta}$ with respect to Ω, which itself is a parameter of the algorithm. This objective was initially proposed by practitioners of AMD simulations, see [268] for example. Questions of parameter selection for AMD methods are a core motivation for the contributions of Chapters 2 and 3 of this thesis, and will be further motivated there.

1.4 Contributions of this thesis

In this section, we summarize the contributions of the following chapters. In Section 1.4.1, we present our contributions pertaining to the study of metastability reviewed in Section 1.3, motivated by applications to the accelerated MD methods of Section 1.2.1. In Section 1.4.2, we present our other contributions to the sampling of trajectorial properties, in particular the nonequilibrium properties of Section 1.2.2

1.4.1 Analysis and optimization of quasistationary timescales

The results we introduced in this section correspond to Chapters 2 and 3 of this thesis. The overarching motivation for these contributions is a problem of parameter selection for the accelerated MD algorithms of Section 1.2.1, particularly the most generic of Voter's methods, namely the parallel replica algorithm. This is the metastable state design problem (Problem 1.12). In [268], for the case of reversible elliptic diffusions, the authors argue that metastable states should be chosen as local maxima of the ratio

$$N^*(\Omega) = \frac{\lambda_{2,\beta}(\Omega) - \lambda_{1,\beta}(\Omega)}{\lambda_{1,\beta}(\Omega)}, \tag{1.90}$$

where $\lambda_{k,\beta}(\Omega)$ denotes the k-th Dirichlet eigenvalue of the infinitesimal generator inside Ω, see (1.85), where we make the dependence on Ω explicit. In this context, $N^*(\Omega)$ roughly measures the number of replicas one can use in the Parallel Replica algorithm (Algorithm 1.10 in Section 1.2.1) inside Ω while maintaining a proportionate speedup in wall-clock time, therefore warranting its name of *scalability metric*.

This ratio also measures a separation of timescales, between the exit rate when the dynamics

is initially distributed according to the QSD ν_Ω and the slowest relaxation timescale of the renormalized killed semigroup, according to the representation (1.88), which is the asymptotic rate of convergence to the local equilibrium ν_Ω. Therefore $N^*(\Omega)$ can also be understood as a natural *local measure of metastability* associated to the state Ω.

It is neither true nor expected that standard energetic definitions for Ω (see Example 1.5 in Section 1.2.1) are particularly good at maximizing N^*. This is particularly true at high temperature, or in the presence of low energy barriers, where thermal fluctuations make transitions between energy basins rather frequent. Besides, when entropic effects significantly contribute to metastability, these definitions make it impossible to separate metastable states (see Problem 1.12 in Section 1.2.1).

A core contribution of this thesis is to propose two complementary approaches to tackle the state definition problem, with the aim of locally maximizing $N^*(\Omega)$ with respect to Ω, which we regard as a shape-optimization problem.

- The first approach is based on theoretical results obtained in Chapter 2, computing spectral asymptotics for the generator

$$\mathcal{L}_\beta = -\nabla V^\top \nabla + \frac{1}{\beta}\Delta$$

  of the overdamped Langevin dynamics (1.19) with Dirichlet boundary conditions at the boundary of a temperature-dependent domain, in the low-temperature limit $\beta \to +\infty$. A set of geometric assumptions is considered concerning the temperature dependence of the domain geometry, which ensures that i) the asymptotics are sensitive to the choice of the boundary geometry and ii) the leading asymptotic behavior can be computed in practice. These shape-sensitive asymptotics may be plugged into (1.90) to optimize the leading-order asymptotic of the scalability metric N^* in the low-temperature regime, within the class of domains satisfying our geometric assumptions.

- The second approach, presented in Chapter 3, is a numerical shape-optimization method for the Dirichlet eigenvalues for the generator

$$\left(-\gamma\nabla V + \frac{1}{\beta}\operatorname{div}\gamma\right)^\top \nabla + \frac{1}{\beta}\gamma : \nabla^2$$

  of the general reversible elliptic dynamics (1.21). To make the optimization tractable in a high-dimensional system, we propose a dynamical coarse-graining approach.

Before giving details on these contributions, let us briefly comment on the implications of these results for the AMD algorithms of Section 1.2.1. These two approaches offer strategies to address Problem 1.12 in different situations.

- The low-temperature analysis applies in situations where energetic barriers are by definition the main contributors to metastability, in which case the energetic definitions of Example 1.5 are known to lead to significantly accelerated sampling via AMD methods. In fact, the geometric setting of the analysis restricts the class of domains to variations

(in a sense to be made precise later) of the energetic basin $\mathcal{A}(z_0)$ associated with a local minimum z_0 for V. Therefore the asymptotic optimization approach can be viewed as a *fine-tuning* strategy for the state definition, to maximize the scalability in a situation where reasonable performance is already guaranteed. Besides, a byproduct of the analysis is an asymptotically exact estimate of the spectral gap $\lambda_{2,\beta}(\Omega) - \lambda_{1,\beta}(\Omega)$, which is directly relevant to Problem 1.14.

- By contrast, the numerical shape-optimization approach makes no assumption on the origin of metastability, and therefore also applies to situations where the separation of timescales is induced by entropic effects. As such, it is more general, and should be viewed as an *enabling* strategy, for situations where no reasonable state definitions are available. However, it is also generically inexact for realistic systems, as it relies on approximation parameters which are hard to control. In particular, its practical implications with regards to Problem 1.14 are still unclear, and should be further investigated.

Finally, although the guiding objective is the maximization of N^*, both approaches can be applied to any functional of the Dirichlet eigenvalues.

Low-temperature spectral asymptotics. Chapter 2, which was preprinted as [50] and is currently under review, provides new asymptotic results concerning the Dirichlet eigenvalues of $\mathcal{L}_\beta$, where V is a smooth Morse function, $\beta \to +\infty$, and Dirichlet boundary conditions are imposed at the boundary of a regular bounded domain representing a metastable state. The novelty with respect to previous analyses in this setting [158, 14, 99, 100, 101, 224, 209] is that the domain is not a fixed set $\Omega \subset \mathbb{R}^d$, but rather a temperature-dependent family of domains $(\Omega_\beta)_{\beta>0}$.

Besides the shape-optimization problem, another more theoretical motivation to study spectral asymptotics in this non-standard setting is the fact that the leading-order asymptotic formulas for Dirichlet eigenvalues obtained in the case of fixed domains (such as those given in [209]) are discontinuous with respect to the boundary geometry. In particular, discontinuities in the leading-order term appear when the boundary crosses certain critical points of V. On the other hand, results of perturbation theory (for instance those given in Chapter 3) show that the spectrum is continuous with respect to deformations of the boundary. Studying the Dirichlet spectrum in temperature-dependent domains allows to better understand these sharp spectral transitions which must occur at low-temperature.

The contributions of Chapter 2 are as follows.

- We construct a set of geometric assumptions under which the asymptotics can be shown to be valid and computed in practice. The main geometric assumption states that, for a fixed set $(z_i)_{0\leqslant i<N_V}$ of critical points for V, and for all β sufficiently large, the domain Ω_β can be approximated locally around each z_i by a half-space. Moreover, the boundary of the approximating half-space around each critical point z_i is assumed to be orthogonal to an eigenvector of the Hessian $\nabla^2 V(z_i)$, and at a signed distance $\alpha^{(i)}/\sqrt{\beta}$ from z_i in this eigendirection, for some $\alpha^{(i)} \in (-\infty, +\infty]$.

The leading order asymptotics of the Dirichlet spectrum are derived as a function of the parameter $\alpha = (\alpha^{(i)})_{1\leqslant i\leqslant N_V}$ and the temperature parameter β. This has the major advantage of replacing the infinite-dimensional shape functional N^* by a finite-dimensional function in the asymptotic regime.

Other critical points of V are assumed to be far from all the domains Ω_β and therefore do not enter into the analysis.

- Under these assumptions, we show the counterpart of the harmonic approximation (Theorem 1.22) in our setting, namely that, for each $k \geqslant 1$, we have the limit

$$\lim_{\beta\to+\infty} \lambda_{k,\beta}(\Omega_\beta) \xrightarrow{\beta\to+\infty} \lambda_k^{\mathrm{H}}(\alpha),$$

where $\lambda_k^{\mathrm{H}}(\alpha)$ is the k-th eigenvalue of some temperature-independent, block-diagonal operator, the harmonic approximation, given by a direct sum of local harmonic models, endowed with appropriate Dirichlet boundary conditions. Crucially, the $\lambda_k^{\mathrm{H}}(\alpha)$ can be computed numerically as a function of α, at a negligible computational cost.

- Under an additional set of assumptions ensuring, amongst other technical conditions, that the principal eigenvalue $\lambda_{1,\beta}(\Omega_\beta)$ is exponentially small as $\beta \to +\infty$, and that the second eigenvalue $\lambda_{2,\beta}(\Omega_\beta)$ is bounded away from zero uniformly in β, we prove a shape-sensitive Eyring–Kramers formula:

$$\lambda_{1,\beta}(\Omega_\beta) = \mathrm{e}^{-\beta(V^*-V(z_0))} \left[\sum_{i\in I_{\min}} \frac{|\nu_1^{(i)}|}{2\pi\Phi\left(|\nu_1^{(i)}|^{\frac{1}{2}}\alpha^{(i)}\right)} \sqrt{\frac{\det \nabla^2 V(z_0)}{|\det \nabla^2 V(z_i)|}} \right] (1+\mathcal{O}(1)), \quad (1.91)$$

where

$$\Phi(x) = \frac{1}{\sqrt{2\pi}} \int_{-\infty}^{x} \mathrm{e}^{-\frac{t^2}{2}}\, \mathrm{d}t, \qquad \Phi(+\infty) = 1,$$

the critical point z_0 is a distinguished local minimum of V, and the $(z_i)_{i\in I_{\min}}$ are index-1 saddle points of V bordering the basin of attraction $\mathcal{A}(z_0)$ (see Example 1.5) at the energy level V^*. In the formula (1.91), $\nu_1^{(i)}$ is the sole negative eigenvalue of $\nabla^2 V(z_i)$ for $i \in I_{\min}$, and corresponds to the eigenvector perpendicular to the approximating half-space around z_i.

- From a technical perspective, the proofs of these two results adapt well-established strategies for approximating eigenvectors in the semiclassical analysis of the Witten Laplacian, such as the construction of harmonic quasimodes performed in [195], or the construction of Gaussian quasimodes used in [61, 209]. However one aspect of the analysis is significantly different from previous works. While prior approaches to the Eyring–Kramers formula on fixed domains relied on local changes of variables around critical point to reduce the analysis to the study of a model operator in a simple geometric situation. While this is always possible in the case of a fixed domain, this approach cannot be adapted in the case of temperature-dependent boundaries without making additional regularity assumptions on the family $(\Omega_\beta)_{\beta>0}$, which would restrict the genericity of the result. Instead, our approach relies heavily on deformations of the domain itself, combined with well-known domain monotonicity principles for Dirichlet eigenvalues to control the error induced by these deformations. In fact, when applied to the case of

a constant domain $\Omega_\beta = \Omega$ for all $\beta > 0$, our method gives an alternative proof of these classical Eyring–Kramers formulas, with a slightly degraded error term. Another technical contribution is the derivation of a suitable Laplace method for the case of moving integration domains.

Shape-optimization of metastable states. Chapter 3, which was preprinted as [51] and is currently under review, studies the shape optimization problem from a numerical perspective. It proposes a novel framework to define metastable states by directly optimizing a spectral metric for timescale separation, which is closely related to the efficiency of accelerated sampling algorithms. The contributions are as follows.

- We argue that the scalability metric (1.90) indeed quantifies the efficiency of the Parallel Replica algorithm, using an idealized choice of the decorrelation time t_{corr}, and a specific implementation of the dephasing step (step A in Algorithm 1.10).
- To optimize the domain, we require gradients of Dirichlet eigenvalues with respect to geometric perturbations of the domain. A known difficulty in the optimization of eigenvalue functionals is the loss of differentiability which occurs at points where the eigenvalues become degenerate. We devise the necessary regularity results for the Dirichlet eigenvalues $\lambda_{k,\beta}(\Omega)$ with respect to shape-perturbations, and compute in particular analytical formulas giving the Gateaux derivatives for clusters of degenerate eigenvalues. As for the Dirichlet Laplacian, this directional derivative is given by the spectrum of a small, symmetric matrix $M^{\Omega,k}(\theta)$ (Theorem 3.2), where θ is a shape-perturbation field.
- Using these formulas, we construct a robust ascent algorithm (Algorithm 3.5) to locally maximize $N^*(\Omega)$. The algorithm is based on a finite-element (FEM) discretization of the domain and the Dirichlet eigenproblem. Its robustness stems from its ability to handle degenerate eigenvalues: it uses a numerical criterion to detect near-degeneracies, and adaptively chooses a steepest ascent direction θ^* by formulating a secondary optimization problem related to the spectrum of some matrix-valued functional $S^\Omega(\theta)$, which fortunately can be efficiently solved. This effectively avoids oscillations and the slow convergence that would otherwise plague the optimization procedure.
- For realistic high-dimensional molecular systems, where a direct FEM discretization is computationally intractable, we propose a coarse-graining strategy. Given a low-dimensional collective variable (CV) $\xi : \mathbb{R}^d \to \mathbb{R}^m$ (with $m \leqslant 3$), states are defined as preimages $\Omega = \xi^{-1}(\Omega_\xi)$. The optimization problem is approached by performing a Galerkin approximation, restricting the variational search space for the Dirichlet eigenproblem to functions of the form $\varphi \circ \xi$, considering the subspace

$$\left\{\varphi \circ \xi,\, \varphi \in H^1_{0,\beta}(\Omega_\xi)\right\} \subset H^1_{0,\beta}(\Omega).$$

  This reduces the intractable high-dimensional PDE on Ω to an effective, low-dimensional Dirichlet eigenproblem on $\Omega_\xi \subset \mathbb{R}^m$, which can be readily solved with FEM. In fact, this eigenproblem is precisely the Dirichlet eigenproblem for the generator $\mathcal{L}^\xi_\beta$ of another reversible elliptic dynamics in $\mathbb{R}^m$, which is again of the form (1.21). Its coefficients are

given by the free energy F_ξ and an effective diffusion tensor a_ξ, whose expressions are

$$F_\xi(z) = -\frac{1}{\beta}\log\left(\int_{\Sigma_z} \mathrm{e}^{-\beta V}\left(\det \nabla\xi^\top\nabla\xi\right)^{-1/2}\mathrm{d}\sigma_{\Sigma_z}\right) \in \mathbb{R},$$
$$a_\xi(z) = \int_{\Sigma_z} \nabla\xi^\top\gamma\nabla\xi\,\mathrm{d}\nu_z \in \mathbb{R}^{m\times m},$$

where $\Sigma_z = \xi^{-1}(z)$, σ_{Σ_z} denotes the surface Lebesgue measure, and ν_z denotes the conditional Gibbs measure on Σ_z, given by

$$\nu_z(\mathrm{d}y) = \frac{\mathrm{e}^{-\beta V(y)}\left(\det \nabla\xi(y)^\top\nabla\xi(y)\right)^{-1/2}}{\displaystyle\int_{\Sigma_z}\mathrm{e}^{-\beta V}\left(\det \nabla\xi^\top\nabla\xi\right)^{-1/2}\mathrm{d}\sigma_{\Sigma_z}}\sigma_{\Sigma_z}(\mathrm{d}y).$$

These effective dynamics have been considered previously for dynamical coarse-graining, see for instance [346], but never in the context of absorbing boundary conditions. While any reversible model for the low-dimensional dynamics $\xi(X_t)$ could be used instead, this particular choice has the advantage that its coefficients F_ξ, a_ξ can be efficiently estimated from sample configurations, with no need for statistically correct trajectories.

- We first validate our approach on small numerical examples, showing that when the reaction coordinate is able to resolve the relevant free-energy basins, the coarse-grained optimization procedure is in very good agreement with the optimum domain of the form $\xi^{-1}(\Omega_\xi)$, in a toy two-dimensional potential. We also validate the semiclassical asymptotics of Chapter 2 on a one-dimensional potential, and find that the asymptotics-optimization problem (as a function of the shape parameter α) resembles the true shape-optimization problem, and can be solved at a fraction of the computational cost.

- We finally deploy our methodology on a biophysical system, solvated alanine dipeptide (see Figure 1.2), a system with 1857 configurational degrees of freedom. We show through numerical experiments that the shape-optimization procedure increases the local separation of timescales, compared to a natural ad-hoc definition of states, for the underdamped Langevin dynamics, in a range of dynamical settings, and for several choices of the core-set.

1.4.2 Nonequilibrium sampling and pathwise properties

A dual approach to computing transport coefficients. Chapter 4, which was published in [52], provides a generalization to the setting of the NEMD stochastic dynamics (1.55) of ideas from works of Evans & Morriss [118, 117, 120, 116, 115] and [119, Section 6.7] in nonequilibrium statistical mechanics. The goal is to compute linear response properties such as (1.61), using a constant-flux approach, named the *Norton* method. This name comes from an analogy with electrical-circuit theory, because the Norton method measures a resistance, contrarily to the constant-forcing NEMD (or *Thévenin*) method which measures a current.

The spirit of this method is based on the observation that, although physical intuition suggests that the steady-state response is *caused* by the nonequilibrium driving force – this

is indeed reflected in the choice of terminology – from the macroscopic point of view, there is no reason to suppose this is the case. Instead, the flux and the forcing co-occur, and one could equivalently think of the nonequilibrium flux as creating a resisting force opposing the drive out of equilibrium. This shift in perspective suggests the following approach: instead of fixing the magnitude of the nonequilibrium perturbation, and measuring the average flux in the nonequilibrium steady-state, as in standard NEMD methods, one could *fix the flux*, and measure the *average forcing magnitude* needed to sustain it. The average forcing is therefore measured in a constant-flux ensemble. The Norton and NEMD nonequilibrium ensembles are in a dual relationship with respect to the pair of flux/forcing variables: one's value is fixed exactly, while the other's is fixed on average by the nonequilibrium steady-state. This duality is analogous to the relationship between the NVE and NVT equilibrium ensembles with respect to the Hamiltonian/temperature pair of thermodynamic variables.

One objective of this work is to place this dual approach in a clear stochastic setting, in which one could subsequently hope to obtain rigorous theoretical results concerning its validity and efficiency, contrarily to the original deterministic framework of Evans & Morriss. Another objective is to ascertain with numerical experiments whether the approach is promising for applications, beyond academic toy models.

This results in the following contributions.

- We derive a formal framework for these constant-flux nonequilibrium dynamics in the case of perturbations of the drift, i.e. $b_\eta = b + \eta F$ for some $F : \mathcal{Q} \to \mathbb{R}^d$ and $\sigma_\eta = \sigma$ in (1.55). This allows to cover the relevant examples of mobility and shear viscosity discussed in Examples 1.15 and 1.16. The framework is based on the constrained SDE

$$\mathrm{d}Z_t^r = b(Z_t^r)\,\mathrm{d}t + \sigma(Z_t^r)\mathrm{d}W_t + F(Z_t^r)\,\mathrm{d}\Lambda_t^r, \tag{1.92}$$

  which has same basic form as the NEMD dynamics (1.55), except that the perturbation parameter η has been replaced by the increment of a stochastic process $(\Lambda_t)_{t\geqslant 0}$, where the forcing magnitude process Λ_t^r is determined by the constant-flux constraint

$$R(Z_t^r) = R(Z_0^r) = r, \qquad \forall\, t \geqslant 0,$$

  and the parameter $r > 0$ fixes the value of the flux. In fact, Λ^r is a W-adapted Itô process, satisfying the SDE

$$\Lambda_t^r = \int_0^t \lambda(Z_s^r)\,\mathrm{d}s + \int_0^t \widetilde{\lambda}(Z_s^r)\,\mathrm{d}W_s,$$

  for explicit observables $\lambda : \mathcal{Y} \to \mathbb{R}$ and $\widetilde{\lambda} : \mathcal{Y} \to \mathbb{R}^{1\times d}$. We also derive explicit Norton dynamics in the case of multiple and time-dependent flux constraints.

  As a result, one may measure the average forcing magnitude using an ergodic average

$$\frac{1}{T}\int_0^T \lambda(Z_t^r)\,\mathrm{d}t \xrightarrow{T\to\infty} \mathbb{E}_{\pi^r}\left[\lambda\right], \tag{1.93}$$

  where π^r denotes the Norton steady-state, defined as the invariant probability distribution of the dynamics (1.92).

Because the trajectory average on the left-hand side of (1.93) neglects the contribution of the observable $\widetilde{\lambda}$, corresponding to the martingale component of Λ^r, the dual approach incorporates variance reduction in its estimation of nonequilibrium response properties. It amounts to using the predictable process $-\frac{1}{T}\int_0^T \widetilde{\lambda}(Z_t^r)\,\mathrm{d}W_t$ as a control variate in the estimation of the average forcing magnitude.

By analogy with the macroscopic transport law, we define the Norton linear response as the reciprocal derivative of the forcing with respect to the flux, provided the following limit exists:

$$\alpha^* = \lim_{r\to 0} \frac{r}{\mathbb{E}_{\pi^r}[\lambda]}.$$

- Specializing this framework to the case where the equilibrium dynamics is given by the underdamped Langevin SDE (1.17), we give a physical interpretation of the Norton dynamics as satisfying an "oblique" version of Gauss' principle of least constraints, which itself had been previously proposed as a principled way to construct nonequilibrium ensembles [117, 173].

- Drawing on (A, B, O) splitting schemes for Langevin dynamics (see (1.36)), we construct a family of flux-preserving numerical schemes for the underdamped Langevin–Norton dynamics, and explain how to efficiently construct an estimator for the average forcing directly from the integration procedure, incorporating variance reduction and avoiding the potentially costly evaluation of λ. These schemes were implemented in the molecular simulation package Molly [143].

- We perform various numerical experiments on Lennard–Jones fluids, which reveal that the dual approach allows to compute both mobility and shear viscosity in these systems. Furthermore, this equivalence extends beyond the linear regime for the pairs (F, R) we consider, suggesting that the dual approach provides an alternative way to compute response properties far from equilibrium in some systems.

- We show that in the case of shear viscosity, the dual method is more efficient, and that the efficiency gap increases with the system size. This is caused by the fact that the fluctuation behavior of the forcing process $\lambda(Z_t^r)$ is often quite different from that of response process $R(Y_t^\eta)$ in NEMD. Roughly speaking, the former tends to display large instantaneous fluctuations over short correlation times, while in NEMD, smaller fluctuations occur, but which dissipate over much longer times. In Lennard–Jones fluids, we show evidence of anomalous concentration for the forcing distribution; namely the variance of the shear forcing distribution, which is the pushforward measure $\lambda_*\pi^r \in \mathcal{P}(\mathbb{R})$, scales as $N^{-5/3}$ as the number of particles $N \to +\infty$, at fixed density and temperature. The variance of its NEMD counterpart, the Fourier flux distribution $R_*\pi_\eta$, on the other hand, scales as N^{-1}, which is the expected CLT behavior. A possible explanation of this phenomenon lies in the fact that, for typical choices of (R, F), the forcing variable λ is coupled to the system through a mean-field-type interaction, but a rigorous analysis remains an open question.

Finally, we raise several theoretical questions regarding the dual method for future work. In particular, the method suggests an approach to the equivalence of nonequilibrium ensembles

results, which is expected to hold in specific, but nevertheless practically relevant, limiting regimes. The upcoming work [89] addresses some of these questions in a mean-field setting.

Since publication, our framework has been specialized to dissipative particle dynamics (DPD, [342]), and similar numerical results have been obtained therein regarding the efficiency of the Norton dynamics and the anomalous scaling of the variance in the constant-shear-flow ensemble. The qualitative difference in fluctuation behavior between constant-force and constant-flux ensembles has also been observed in recent simulations [315, 296] using deterministic Norton dynamics with Nosé-Hoover thermostats.

More generally, the idea of choosing from equivalent statistical ensembles those which possess the most desirable fluctuation behavior for a target property is classical in equilibrium statistical mechanics [211, 66]. Norton dynamics aim to extend this possibility to the nonequilibrium setting by proposing an equivalent nonequilibrium ensemble to sample from, with different fluctuation properties. Overall, variance reduction for constant-flux ensemble estimators of various transport coefficients have indeed been observed in [118, 315, 52, 296, 342].

A hypocoercive approach to the overdamped approximation of the Langevin dynamics with position-dependent friction matrices. Chapter 5 corresponds to contents of an upcoming research note [48]. The purpose of this note is to study the dynamical behavior of the general underdamped Langevin dynamics

$$\begin{cases} \mathrm{d}q_t^\lambda = M^{-1} p_t^\lambda \mathrm{d}t, \\ \mathrm{d}p_t^\lambda = -\nabla V(q_t^\lambda)\mathrm{d}t - \lambda D(q_t^\lambda)^{-1} M^{-1} p_t^\lambda \,\mathrm{d}t + \sqrt{\frac{2\lambda}{\beta}} D(q_t^\lambda)^{-1/2} \,\mathrm{d}W_t^\lambda, \end{cases} \tag{1.94}$$

which corresponds to (1.20) with $\gamma = \lambda D^{-1}$, in the large friction regime $\lambda \to +\infty$. In this equation, $D^{-1} : \mathcal{Q} \to \mathcal{S}_d^{++}$ is a position-dependent, matrix-valued friction coefficient.

Under suitable assumptions on the coefficients of these dynamics and the initial data, we show that the rescaled position process $(q_{\lambda t}^\lambda)_{0 \leqslant t \leqslant T}$ converges in law to the solution $(X_t)_{0 \leqslant t \leqslant T}$ of the SDE

$$\mathrm{d}X_t = -\left[D(X_t)\nabla V(X_t) - \frac{1}{\beta} \operatorname{div} D(X_t) \right] \mathrm{d}t + \sqrt{\frac{2}{\beta}} D^{1/2}(X_t) \mathrm{d}W_t, \tag{1.95}$$

which corresponds to (1.21) with $\gamma = D$, and is the dynamics studied in Chapter 3.

While similar results are well-known in the small-mass regime $M \to 0$, and have been shown to hold in very general settings [130, 131, 177, 339], the main contribution of this work is the method of proof, which relies on the control of a well-chosen Poisson problem via L^2-hypocoercivity estimates. As a result, the structure of the argument is very simple, and gives an intuitive explanation for the form of the limiting dynamics. As an intermediate technical step, the proof involves extending known hypocoercivity results to a setting with multiplicative noise, and obtaining uniform in λ estimates for the inverse generator, results which may be of independent interest. Along the way, we identify a gap in the proof of a previous result in the small-mass case ([339, Lemma 3.1]), and provide a correct argument for an analogous step in our setting.

The second contribution of the work consists in the application of the result to a case where the kinetic energy, given by $\frac{1}{2}p^\top M^{-1}(q)p$, where $M : \mathcal{Q} \to \mathcal{S}_d^{++}$ is itself position-dependent. These dynamics are for instance useful when considering molecular dynamics in internal coordinates, see [326]. We show, under suitable assumptions on M, that the main result can be applied, via an appropriate change of coordinates, to derive the overdamped limit. This allows in particular the treatment of the general one-dimensional case.

Chapter 2

Quantitative spectral asymptotics for reversible diffusions in temperature-dependent domains.

At the still point of the turning world.
... at the still point, there the dance is ...
—T.S. Eliot, *Burnt Norton*, 1936

Abstract. *We derive novel low-temperature asymptotics for the spectrum of the infinitesimal generator of the overdamped Langevin dynamics. The novelty is that this operator is endowed with homogeneous Dirichlet conditions at the boundary of a domain which depends on the temperature. From the point of view of stochastic processes, this gives information on the long-time behavior of the diffusion conditioned on non-absorption at the boundary, in the so-called quasi-stationary regime. Our results provide precise estimates of the spectral gap and principal eigenvalue, extending the Eyring–Kramers formula. The phenomenology is richer than in the case of a fixed boundary and gives new insight into the sensitivity of the spectrum with respect to the shape of the domain near critical points of the energy function. Our work is motivated by–and is relevant to–the problem of finding optimal hyperparameters for accelerated molecular dynamics algorithms.*

2.1 Introduction

We study characteristic timescales of the diffusion process defined as the strong solution $(X_t^\beta)_{t\geqslant 0}$ to the stochastic differential equation

$$\mathrm{d}X_t^\beta = -\nabla V(X_t^\beta)\,\mathrm{d}t + \sqrt{\frac{2}{\beta}}\,\mathrm{d}W_t, \tag{2.1}$$

where $(W_t)_{t\geqslant 0}$ is a standard Brownian motion on $\mathbb{R}^d$, $V : \mathbb{R}^d \to \mathbb{R}$ is a smooth function, and $\beta > 0$ is a parameter modulating the magnitude of the noise. In the context of atomistic simulation, the process (2.1) is called the overdamped Langevin dynamics, and is commonly used to model the motion of particles subject to an interaction potential V at thermal equilibrium with inverse temperature $\beta = (kT)^{-1}$.

More generally, the function V is, up to an additive constant, the log-likelihood of the Gibbs measure

$$\mu(\mathrm{d}x) = \mathcal{Z}_\beta^{-1}\mathrm{e}^{-\beta V(x)}\,\mathrm{d}x, \tag{2.2}$$

which is a probability measure with respect to which the dynamics (2.1) is known to be reversible, and, under a general set of assumptions, ergodic. We refer the reader to [280] for sufficient conditions ensuring the well-posedness and ergodicity of (2.1) with respect to μ.

As it allows sampling from probability measures whose densities are explicit up to the normalization constant $\mathcal{Z}_\beta$, the dynamics (2.1) is also used in Bayesian statistics to sample from the posterior distribution. In theoretical machine learning, the process (2.1) can also be seen as an idealized model for the stochastic gradient descent algorithm, after an appropriate normalization of the data, in which case V plays the role of the loss function.

The local approach to metastability. In many cases, the trajectories of (2.1) are subject to the phenomenon of metastability, which is indicated by the presence of a wide range of well-separated timescales, often exponentially wide in the inverse temperature. This corresponds to the regime in which the Arrhenius law (see [16]) applies. Longer timescales correspond to rare transitions between attractive regions of the configuration space $\mathbb{R}^d$, which trap the dynamics into long-lived local ensembles of configurations, which we refer to as metastable states. The shorter timescales correspond to thermal fluctuations inside these states.

The nature of the trapping mechanism itself may vary. It may be that energetic barriers tend to confine the dynamics inside a potential well for long times, which is the case on which we focus in this work. It may also happen that different subdomains are joined by low-energy paths, but in narrow configurational corridors, which require well-coordinated collective motion of the system's degrees of freedom to successfully navigate. In this case, the obstacle is of an entropic nature, and the dynamics is in fact confined in a free-energetic rather than purely energetic well.

Moreover, in molecular dynamics (MD) simulations, monitoring the long-time behaviour of the dynamics (2.1) is of crucial importance to reliably estimate macroscopic dynamical properties of materials and biomolecules, as well as parametrizing models on larger scales,

such as discrete Markov models or PDEs.

Drawing meaningful long trajectories from metastable dynamics is however challenging with naive techniques. To alleviate this, so-called accelerated dynamics methods [332, 334, 312] have been proposed by Arthur Voter in the late 1990's, all of which rely on a local approach to metastability.

In this local approach, the notion of metastable state can be formalized using the quasi-stationary distribution (QSD), which, given an arbitrary bounded subset of configuration space $\Omega \subset \mathbb{R}^d$, can be loosely understood as the long time limiting distribution of the process conditioned on staying trapped inside Ω. Defining the so-called Yaglom limit:

$$\nu = \lim_{t\to\infty} \mu_t, \qquad \mu_t := \mathrm{Law}\left(X_t^\beta \middle| \forall\, 0 \leqslant s \leqslant t,\, X_s^\beta \in \Omega\right),$$

it can be shown under mild assumptions (see [245]) that the limit ν is well-defined, and that it is the unique QSD for the process (2.1) in Ω, with moreover μ_t converging exponentially fast to ν in total variation norm. Local metastability inside Ω can then be understood as a large separation between two natural timescales related to the QSD. The first timescale is the average exit time from Ω for the dynamics X_t^β with initial distribution ν:

$$\tau_1(\Omega) = \mathbb{E}^\nu\left[\inf\{t > 0 :\, X_t^\beta \notin \Omega\}\right].$$

The second timescale $\tau_2(\Omega)$ is that at which μ_t reaches the QSD and the process X_t^β thus forgets its initial distribution conditionally on not exiting Ω. If $\tau_1(\Omega) \gg \tau_2(\Omega)$, then the domain Ω acts as a metastable trap for the dynamics X_t^β. Conditionally on $\{X_s^\beta \in \Omega,\, \forall\, 0 \leqslant s \leqslant t\}$, for $\tau_2(\Omega) \ll t \ll \tau_1(\Omega)$, the state of the dynamics at time t is distributed according to the local equilibrium ν, and remains distributed according to ν before the dynamics exits once again.

It is possible to show (see [206] and Propositions 2.2 and 2.3 below) that the two local timescales associated with the metastable behavior of the process X_t^β inside Ω can be related to the spectrum of the infinitesimal generator of the dynamics (2.1), supplemented with Dirichlet boundary conditions on $\partial\Omega$. Namely, writing $-\lambda_{k,\beta}(\Omega)$ for the k-th smallest Dirichlet eigenvalue, the following holds:

- The metastable exit rate is given by $\lambda_{1,\beta}(\Omega)$.
- The asymptotic convergence rate to the QSD is given by $\lambda_{2,\beta}(\Omega) - \lambda_{1,\beta}(\Omega)$.

Strictly speaking, Proposition 2.3 only provides an upper bound on the convergence rate, which we expect in practice to depend on the initial condition. Nevertheless, these spectral characterization provide us with a natural and tractable measure of the local metastability associated with Ω, namely the separation of timescales

$$J(\Omega) := \frac{\lambda_{2,\beta}(\Omega) - \lambda_{1,\beta}(\Omega)}{\lambda_{1,\beta}(\Omega)}. \tag{2.3}$$

If $J(\Omega) \gg 1$, i.e. $\lambda_{2,\beta}(\Omega) - \lambda_{1,\beta}(\Omega) \gg \lambda_{1,\beta}(\Omega)$, then Ω acts as highly locally metastable trap for the dynamics (2.1). The link between characteristic timescales for conformational

dynamics and the spectrum of various operators has been widely discussed in the literature, see [178, 256, 157] for an overview of various approaches.

Shape optimization for the timescale separation. A natural question arises: how to choose the shape of the domain Ω in order to maximize $J(\Omega)$? In other words: how to choose Ω in order for the process $(X_t^\beta)_{t\geqslant 0}$ to be as locally metastable as possible ? This line of investigation is interesting from a theoretical point of view, as it generalizes the problem of finding extremal shapes for ratios of eigenvalues of the Dirichlet Laplacian (which corresponds to setting $V = 0$ in our context), which has been addressed with tools from spectral geometry, see for example the Payne–Polyá–Weinberger conjecture [263] and its solution by Ashbaugh and Benguria in [18].

It is, in addition of practical interest, since it has recently been shown in [2, 13] that metastable diffusions such as (2.1) may be described with an arbitrary accuracy by coarse-grained dynamics consisting of Markov renewal processes. In this context, the timescale separations (2.3) associated with each coarse state appears as a parameter governing the convergence of this approximation. More generally, it is expected that a large separation of local timescales in Ω will lead to dynamics which are prone to be approximated by simpler processes to simulate and analyze, such as jump Markov processes. From the point of view of acceleration algorithms in MD simulation, the timescale separation has also been related to the efficiency of the parallel replica algorithm (ParRep) (see [206, 305, 268]), and thus, finding definitions of metastable subsets Ω for which the separation of timescales is large has relevance to applications in MD. In particular, deriving quantitative estimates of $\lambda_{1,\beta}(\Omega)$ and $\lambda_{2,\beta}(\Omega)$ is an important question in the numerical analysis of ParRep and its variants.

In low-dimensional settings, or when low-dimensional representations of the dynamics are available, it is possible to locally optimize the shape of an initial domain Ω, using shape perturbation results for eigenvalues see [152, 153, 154, 164, 165]. Indeed, it is possible to show that the ratio (2.3) is shape-differentiable with respect to Ω, by adapting arguments developed to treat the case of the Dirichlet Laplacian (see [165, 164] for the Laplacian, and the companion work [51], treating the case of a general V with a position-dependent diffusion matrix, as well as a Galerkin approximation method given a reaction coordinate).

However, the exact computation of shape perturbations of eigenvalues is generally intractable for systems of practical interest, because it involves solving a high-dimensional boundary value problem, and the numerical representation of the shape itself is a non-trivial question. To circumvent these difficulties, an alternative approach relies on choosing a limiting regime, and finding asymptotically optimal shapes within a low-dimensional parametric family of shapes. In this work, we perform the mathematical analysis necessary to realize this strategy in the low-temperature regime $\beta \to \infty$, for a class of parametrizations which allow for explicit computations.

This problem motivates the study of eigenvalue asymptotics for temperature-dependent domains, in which the dependence of the shape of the boundary depends on only a handful of relevant parameters. In fact, numerical experiments, as well as our theoretical results, suggest that, in the limit $\beta \to \infty$ and at dominant order, the low-lying eigenvalues are rather

insensitive to the geometry of the domain far away from critical points of V, so that the shape optimization problem may become tractable in the limit $\beta \to \infty$. The relevant parameters should fix the shape of the boundary near critical points of V. This is the framework in which we work, and which we make precise in Section 2.2.3.

Let us finally mention that the application of shape-differentiation methods and spectral asymptotics to the state optimization problem is the subject of an upcoming work [51].

Low-temperature spectral asymptotics for metastable stochastic processes. In the low-temperature limit, methods from semi-classical analysis, potential theory and large deviations have been successfully leveraged in previous works to address the problem of finding quantitative spectral estimates for the dynamics (2.1) as well as the associated Dirichlet eigenvalue problem on a fixed domain Ω, see for instance [157, 61, 159, 225, 223, 100, 209, 224]. In particular, many efforts have been dedicated to rigorously derive precise asymptotics for the principal eigenvalue:

$$\lambda_{1,\beta}(\Omega) \overset{\beta\to\infty}{\sim} C(\Omega,\beta)\,\mathrm{e}^{-\beta E(\Omega)},$$

where $E(\Omega)$ is analogous to the activation energy in the Arrhenius law, and $C(\Omega,\beta)$ is a pre-exponential factor whose expression generally depends on both the temperature and the domain, but which can, under various sets of assumptions, be computed, at least to first order in β. Such results are known as Eyring–Kramers formulæ, following first proposals concerning the behavior of reaction rates [122] guided by chemical intuition, and early computations [198] supported by physical modeling. Eyring–Kramers type results have, since the early 2000s, been rigorously proven and generalized in the mathematical community, using tools from dynamical systems, quantum theory, and stochastic processes. We refer to [33] for an overview.

The link with the classical Eyring–Kramers formula, which concerns the closely related problem of computing asymptotics for the exit rate $\mathbb{E}_x[\tau_\Omega]^{-1}$ for some deterministic initial condition $x \in \Omega$, requires some discussions. It is justified by the interpretation of $1/\lambda_{1,\beta}(\Omega)$ as a metastable exit time, i.e. $1/\lambda_{1,\beta}(\Omega) = \int_\Omega \mathbb{E}_x[\tau_\Omega]\mathrm{d}\nu$ (see Proposition 2.2 below). The connection can be made fully rigorous by exploiting exponential leveling results, see for instance [252]. In the context of deterministic initial conditions, let us mention that tools from the theory of Freidlin and Wentzell (see [132]) relying on large deviations are capable of identifying the activation energy $E(\Omega)$ under very general conditions, including non-reversible diffusions, and these techniques have also been recently extended to a class of non-Markovian processes (so-called self-interacting diffusions, see [5]).

Let us stress that our results are limited to the setting of the overdamped Langevin dynamics (2.1), but various extensions to other dynamics would be of practical interest but are not addressed in this work. For instance, extending the computation of quantitative spectral asymptotics with absorbing boundaries to the case of the underdamped Langevin dynamics (see [166, 167, 168, 55] for the case without boundary), or treating the case of non-reversible diffusions with non-degenerate noise, as in [57, 205, 208, 212].

Because of the fact that energetic barriers contribute exponentially to the slowest timescales in the small-noise limit $\beta \to \infty$, the literature has focused on the case where metastability occurs in the presence of energetic barriers, and this is also the case for this work. However,

entropic barriers are often relevant to applications, most notably in the context of cellular biology, and recent works have started to tackle rigorously spectral asymptotics for the so-called narrow escape problem, for systems in which the asymptotic parameter is not the temperature but instead the size of a vanishing exit region for a Brownian motion in a confining spatial domain (which corresponds to a purely entropic trapping mechanism). For rigorous results in this direction, we cite [124] where coarse asymptotics of the spectrum of the Laplacian with mixed Dirichlet–Neumann boundary conditions are given in the limit of a vanishing absorbing region, as well [9, 227] where finer asymptotics of low-lying eigenvalues and normal derivatives of the associated eigenmodes are derived, in a model two-dimensional situation.

We finally mention that the previous works [225, 100] have applied semiclassical techniques to the Witten Laplacian, motivated by the numerical analysis of Arthur Voter's accelerated dynamics methods, respectively Hyperdynamics and Temperature Accelerated Dynamics. In this work, we pursue this path, deriving useful results to analyze the third and last of the accelerated dynamics methods of Voter, namely the Parallel Replica method, in the low-temperature regime.

Contributions and outline. The purpose of this work is to extend previous results on low-temperature spectral asymptotics for the dynamics (2.1) in the framework of temperature-dependent Dirichlet boundary conditions. We develop a set of geometric assumptions on these temperature-dependent boundaries which ensure that these asymptotics can be easily computed. This allows to asymptotically optimize various functionals of the spectrum with respect to the shape of the boundary, within a particular class of domains. We then identify the first-order behavior of the spectrum (Theorem 2.16), extending to β-dependent Dirichlet boundary conditions the so-called harmonic limit from the semi-classical analysis of the Witten Laplacian. We finally generalize the Eyring–Kramers formula (Theorem 2.17) to the case of temperature-dependent boundaries and a single-well domain, and obtain an explicit expression for the prefactor.

This work is organized as follows. In Section 2.2, we introduce the necessary notation and present our geometric framework. In Section 2.3, we state and discuss our main results. In Section 2.4, we construct the harmonic approximation and prove the first spectral asymptotics. We finally prove in Section 2.5 the modified Eyring–Kramers formula.

2.2 Setting and notation

In this section, we introduce various notation (see Section 2.2.1), define the QSD in Section 2.2.2, and present in 2.2.3 the geometric framework which will be used throughout this work. In Section 2.2.4, we motivate these assumptions, discuss their genericity and compare them with previous related works.

2.2.1 Notation

We introduce various notation and classical properties which will be used throughout this work.

Temperature-dependent domains. The basic setting we work in, and the main novelty compared to previous related works, is the presence of a temperature-dependent boundary. To this end, we introduce a family of domains $(\Omega_\beta)_{\beta>0}$ which will be considered throughout this work, and which we will always assume to be smooth, open and bounded. In fact, we make the following stronger assumption.

Assumption 2.1. *For all $\beta > 0$, the domain Ω_β is a smooth open set, and there exists a compact set $\mathcal{K} \subset \mathbb{R}^d$ such that*

$$\forall\, \beta > 0, \qquad \Omega_\beta \subset \mathcal{K}. \tag{H0}$$

We denote by σ_{Ω_β} the signed Euclidean distance to the boundary of Ω_β:

$$\sigma_{\Omega_\beta}(x) = \begin{cases} d(x, \partial\Omega_\beta) & \text{for } x \in \Omega_\beta, \\ -d(x, \partial\Omega_\beta) & \text{for } x \notin \Omega_\beta. \end{cases} \tag{2.4}$$

While the opposite sign is sometimes preferred in the definition of the signed distance, our choice of convention is motivated by the identities $A \cap B = (\sigma_A \wedge \sigma_B)^{-1}(\mathbb{R}_+^*)$, $A \cup B = (\sigma_A \vee \sigma_B)^{-1}(\mathbb{R}_+^*)$ for two open sets $A, B \subset \mathbb{R}^d$. We denote the unit outward normal at a point $x \in \partial\Omega_\beta$ by $\mathrm{n}_{\Omega_\beta}(x) = -\nabla\sigma_{\Omega_\beta}(x)$.

Various other assumptions which will enter in the statement of our results are given in Section 2.2.3.

Critical points of the potential. We assume throughout this work that the potential V is a smooth Morse function over $\mathbb{R}^d$, meaning that at each point z such that $\nabla V(z) = 0$, the Hessian $\nabla^2 V(z)$ is non-degenerate. This condition implies in particular that critical points of V are isolated, and are therefore finitely many inside $\mathcal{K}$. We also assume that V is globally bounded from below. We recall that the index of a critical point $z \in \mathbb{R}^d$ for V is the number of negative eigenvalues of $\nabla^2 V(z)$:

$$\mathrm{Ind}(z) = \#\left[\mathrm{Spec}(\nabla^2 V(z)) \cap (-\infty, 0)\right].$$

For $0 \leqslant k \leqslant d$, denote by N_k the number of critical points of index k located in $\mathcal{K}$:

$$N_k = \#\left\{z \in \mathcal{K} \,|\, \nabla V(z) = 0,\, \mathrm{Ind}(z) = k\right\}, \qquad N := \sum_{k=0}^{d} N_k.$$

Thus, V has N critical points in $\mathcal{K}$, and, for instance, N_0 local minima. Finally, we fix an enumeration $(z_i)_{0\leqslant i<N}$ of the critical points of V in $\mathcal{K}$, chosen so that (with the convention $N_0 + \cdots + N_{k-1} = 0$ for $k = 0$):

$$\{z_i \,|\, N_0 + \cdots + N_{k-1} \leqslant i < N_0 + \cdots + N_k\} = \{z \in \mathcal{K} \,|\, \nabla V(z) = 0,\, \mathrm{Ind}(z) = k\}.$$

Such a finite enumeration is guaranteed to exist, owing to the Morse property of V and the compactness of $\mathcal{K}$. In particular, the local minima of V in $\mathcal{K}$ are enumerated as $z_0, \dots, z_{N_0-1}$.

We also fix an eigendecomposition of the Hessian $\nabla^2 V$ at each critical point z_i, letting

$$\mathrm{Spec}(\nabla^2 V(z_i)) = \left\{\nu_1^{(i)}, \nu_2^{(i)}, \cdots, \nu_d^{(i)}\right\} \tag{2.5}$$

denote the spectrum of $\nabla^2 V$ at z_i, with an associated orthonormal eigenbasis:

$$U^{(i)} = \begin{pmatrix} v_1^{(i)} & \cdots & v_d^{(i)} \end{pmatrix} \in \mathbb{R}^{d\times d}, \quad \mathrm{diag}(\nu_1^{(i)}, \cdots, \nu_d^{(i)}) = U^{(i)\intercal} \nabla^2 V(z_i) U^{(i)}. \tag{2.6}$$

Since V has the Morse property, $\nu_j^{(i)} \neq 0$ for all $1 \leqslant j \leqslant d$ and $0 \leqslant i < N$. Let us also assume that, in the case where $\mathrm{Ind}(z_i) = 1$, $\nu_1^{(i)} < 0$ is the unique negative eigenvalue of $\nabla^2 V(z_i)$. The orientation convention for the first eigenvector $v_1^{(i)}$ is either fixed by the geometry of the domains Ω_β (see Assumption (**H2**) below), or else plays no role in the analysis.

The eigenrotation induces a unitary transformation in L^2, via:

$$\left(\mathcal{U}^{(i)} f\right)(x) = f\left(U^{(i)\intercal} x\right), \quad \left(\mathcal{U}^{(i)*} f\right)(x) = f\left(U^{(i)} x\right). \tag{2.7}$$

We will make repeated use of the following half-spaces associated with each critical point, defined for $\theta \in (-\infty, +\infty]$ by:

$$E^{(i)}(\theta) = U^{(i)}\left[(-\infty, \theta) \times \mathbb{R}^{d-1}\right]. \tag{2.8}$$

Of course, one simply has $E^{(i)}(+\infty) = \mathbb{R}^d$.

For notational convenience, we also introduce the following local coordinates, adapted to the quadratic behavior of V near z_i:

$$y^{(i)}(x) = U^{(i)\intercal}(x - z_i) = \left(y_1^{(i)}(x), y^{(i)\prime}(x)\right) \in \mathbb{R} \times \mathbb{R}^{d-1}. \tag{2.9}$$

Note that $y^{(i)}$ is a linear isometry, with $\nabla y_j^{(i)} = v_j^{(i)}$ and $\nabla^2 y^{(i)} = 0$.

Gradient flow and invariant manifolds. We denote by $(\phi_t)_{t\in\mathbb{R}}$ the flow associated with the dynamics $X'(t) = -\nabla V(X(t))$, which can be seen as the formal limit of the process (2.1) as $\beta \to +\infty$. For $0 \leqslant i < N$, we introduce the following sets:

$$\mathcal{W}^{\pm}(z_i) = \left\{ x \in \mathbb{R}^d \,\middle|\, \lim_{t\to\pm\infty} \phi_t(x) = z_i \right\}. \tag{2.10}$$

The stable manifold theorem (see [317, Section 9.2]) asserts that these sets are smooth submanifolds with boundary. The manifold $\mathcal{W}^+(z_i)$ is called the stable manifold and $\mathcal{W}^-(z_i)$ is called the unstable manifold. Moreover their tangent spaces at z_i are given by

$$T_{z_i}(\mathcal{W}^{\pm}) = \mathrm{Vect}\left\{ v_j^{(i)},\ 1 \leqslant j \leqslant d : \pm\nu_j^{(i)} > 0 \right\},$$

so that $\mathcal{W}^+(z_i)$ and $\mathcal{W}^-(z_i)$ are of dimensions $d - \mathrm{Ind}(z_i)$ and $\mathrm{Ind}(z_i)$, respectively.

For $0 \leqslant i < N_0$, we alternatively denote

$$\mathcal{A}(z_i) := \mathcal{W}^+(z_i), \tag{2.11}$$

which we refer to as the basin of attraction for the critical point z_i.

Weighted Sobolev spaces. Let us introduce the following Hilbert spaces, defined for an open set $\Omega \subset \mathbb{R}^d$ by

$$L^2_\beta(\Omega_\beta) = \left\{ u \text{ measurable} \,\middle|\, \|u\|^2_{L^2_\beta(\Omega_\beta)} := \int_{\Omega_\beta} u^2 \, \mathrm{e}^{-\beta V} < +\infty \right\},$$
$$H^k_\beta(\Omega_\beta) = \left\{ u \in L^2_\beta(\Omega_\beta) \,\middle|\, \partial^\alpha u \in L^2_\beta(\Omega_\beta), \, \forall\, |\alpha| \leqslant k \right\},$$

where $\partial^\alpha = \partial^{\alpha_1}_{x_1} \dots \partial^{\alpha_d}_{x_d}$ denotes the weak differentiation operator associated to a multi-index $\alpha = (\alpha_1, \dots, \alpha_d) \in \mathbb{R}^d$. For the flat case (i.e. when $V \equiv 0$), we simply write $L^2(\Omega_\beta)$ and $H^k(\Omega_\beta)$. As in the flat case, we let $H^k_{0,\beta}(\Omega_\beta)$ denote the $H^k_\beta(\Omega_\beta)$-norm closure of $\mathcal{C}^\infty_{\mathrm{c}}(\Omega_\beta)$.

Dirichlet realizations of the generator. The infinitesimal generator $\mathcal{L}_\beta$ of the evolution semigroup associated with the dynamics (2.1) is formally defined by:

$$\forall u \in \mathcal{C}^\infty_{\mathrm{c}}(\mathbb{R}^d), \qquad -\mathcal{L}_\beta u = -\frac{1}{\beta}\Delta u + \nabla V \cdot \nabla u. \tag{2.12}$$

A direct computation shows that $-\mathcal{L}_\beta$ is a symmetric positive operator on $L^2_\beta(\mathbb{R}^d)$, with associated quadratic form:

$$\langle -\mathcal{L}_\beta u, u \rangle_{L^2_\beta(\mathbb{R}^d)} = \frac{1}{\beta} \int_{\mathbb{R}^d} |\nabla u|^2 \, \mathrm{e}^{-\beta V}. \tag{2.13}$$

This identity is the analytic formulation of the reversibility of the dynamics (2.1) with respect to μ.

For bounded open domains $\Omega_\beta \subset \mathbb{R}^d$ with Lipschitz boundary, we will still denote by $\mathcal{L}_\beta$ the Dirichlet realization of the generator, defined as the Friedrichs extension (see [276]) of the quadratic form (2.13) on $\mathcal{C}^\infty_{\mathrm{c}}(\Omega_\beta)$. This is a self-adjoint operator, with domain

$$\mathcal{D}(\mathcal{L}_\beta) = H^1_{0,\beta}(\Omega_\beta) \cap H^2_\beta(\Omega_\beta) \subset L^2_\beta(\Omega_\beta).$$

We will also consider the Dirichlet realization of the differential operator $\mathcal{L}_\beta$ on other domains than Ω_β, this will be made precise when needed.

The compact injection $H^1_{0,\beta}(\Omega_\beta) \to L^2_\beta(\Omega_\beta)$ (which follows immediately from the Rellich–Kondrachov theorem since V is smooth and Ω_β is smooth and bounded) implies that $-\mathcal{L}_\beta$ seen as an operator on $L^2_\beta(\Omega_\beta)$ has a compact resolvent, so that its spectrum consists of non-negative, isolated eigenvalues of finite multiplicity tending to $+\infty$:

$$0 \leqslant \lambda_{1,\beta} \leqslant \lambda_{2,\beta} \leqslant \dots \leqslant \lambda_{N,\beta} \xrightarrow{N\to\infty} +\infty,$$

where for $k \geqslant 1$, $\lambda_{k,\beta}$ denotes the k-th smallest eigenvalue counted with multiplicity. Furthermore, standard arguments (see [206]) show that the first eigenvalue is strictly positive and non-degenerate, so that $0 < \lambda_{1,\beta} < \lambda_{2,\beta}$, with an associated eigenmode $u_{1,\beta} > 0$ on Ω_β.

We also consider eigenmodes $u_{k,\beta}$ associated with $\lambda_{k,\beta}$ with, for any integers $i, j \geqslant 1$, the normalization convention:

$$\int_{\Omega_\beta} u_{i,\beta} u_{j,\beta} \mathrm{e}^{-\beta V} = \delta_{ij}.$$

When considering the Dirichlet realization of $\mathcal{L}_\beta$ on a domain $A \subset \mathbb{R}^d$ other than Ω_β, we will explicitly denote the dependence of the eigenelements on A as follows: for all $k, \ell \geqslant 1$,

$$-\mathcal{L}_\beta u_{k,\beta}(A) = \lambda_{k,\beta}(A) u_{k,\beta}(A), \qquad \int_A u_{k,\beta}(A) u_{\ell,\beta}(A)\, \mathrm{e}^{-\beta V} = \delta_{k\ell}.$$

Witten Laplacian. It it sometimes convenient to change representations to a flat L^2 setting, using the unitary map $u \mapsto \mathrm{e}^{-\frac{\beta V}{2}} u$ from $L^2_\beta(\Omega_\beta)$ to $L^2(\Omega_\beta)$. The conjugated operator associated to $-\mathcal{L}_\beta$ is proportional to the celebrated Witten Laplacian [340] acting on 0-forms (or functions):

$$H_\beta = -\beta \mathrm{e}^{-\frac{\beta V}{2}} \mathcal{L}_\beta \mathrm{e}^{\frac{\beta V}{2}} \cdot = -\Delta + U_\beta, \qquad U_\beta = \frac{\beta^2}{4} |\nabla V|^2 - \frac{\beta}{2} \Delta V, \tag{2.14}$$

with domain $\mathcal{D}(H_\beta) = H^1_0(\Omega_\beta) \cap H^2(\Omega_\beta) \subset L^2(\Omega_\beta)$. The operator $\beta^{-2} H_\beta$ closely resembles a Schrödinger operator (with the semiclassical parameter h proportional to $1/\beta$), and a potential perturbed by an order h term. For convenience, we give the correspondence with the notation commonly used in the semiclassical literature for the Witten Laplacian, following [157]:

$$\beta^{-2} H_\beta = \Delta^{(0)}_{f,h} := -h^2 \Delta + |\nabla f|^2 - h \Delta f, \quad \text{with } h := 1/\beta \text{ and } f := V/2.$$

We finally denote by

$$Q_\beta(u) = \langle H_\beta u, u \rangle_{L^2(\Omega_\beta)} = \|\nabla u\|^2_{L^2(\Omega_\beta)} + \langle U_\beta u, u \rangle_{L^2(\Omega_\beta)},$$

the quadratic form associated with H_β, with form domain $\mathcal{D}(Q_\beta) = H^1_0(\Omega_\beta)$.

2.2.2 Quasi-stationary distributions and the Dirichlet spectrum

Given a subdomain $\Omega_\beta \subset \mathbb{R}^d$, define the first exit time out of Ω_β by

$$\tau_{\Omega_\beta} = \inf \left\{ t \in \mathbb{R}_+ \,\middle|\, X^\beta_t \notin \Omega_\beta \right\}.$$

A QSD in Ω_β is a probability measure ν satisfying:

$$\forall\, t > 0,\, \forall\, A \in \mathcal{B}(\Omega_\beta), \qquad \mathbb{P}^\nu \left(X^\beta_t \in A \,\middle|\, \tau_{\Omega_\beta} > t \right) = \nu(A).$$

In other words, the QSD is stationary for the process X^β_t conditioned on not being absorbed at the boundary of Ω_β up to the time t. Under generic assumptions, ν may also be defined by

the Yaglom limit:

$$\forall x_0 \in \Omega_\beta, \qquad \nu(A) = \lim_{t\to\infty} \mathbb{P}^{x_0}\left(X_t^\beta \in A \,\middle|\, \tau_{\Omega_\beta} > t\right).$$

Quasi-stationary distributions were initially introduced to study long-lived phases of populations in the pre-extinction time regime. We refer to [245] for a review and examples on this topic, as well as [84] for general background material on QSDs.

It happens that the QSD inside a smooth bounded domain Ω_β is directly related to the spectrum of the Dirichlet realization of the infinitesimal generator (2.12). More precisely, the following result, adapted from [206], holds.

Proposition 2.2 ([206]). *Let $(\lambda_{1,\beta}, u_{1,\beta})$ be the principal Dirichlet eigenpair of $-\mathcal{L}_\beta$ in Ω_β (which is unique up to the sign of $u_{1,\beta}$), i.e.*

$$\lambda_{1,\beta} = \inf_{u\in H^1_{0,\beta}(\Omega_\beta)} \frac{\langle -\mathcal{L}_\beta u, u\rangle_{L^2_\beta(\Omega_\beta)}}{\|u\|^2_{L^2_\beta(\Omega_\beta)}} = \frac{1}{\beta}\int_{\Omega_\beta} |\nabla u_{1,\beta}|^2 \,\mathrm{e}^{-\beta V}.$$

Then the probability measure

$$A \mapsto \nu(A) = \frac{\displaystyle\int_A u_{1,\beta}\,\mathrm{e}^{-\beta V}}{\displaystyle\int_{\Omega_\beta} u_{1,\beta}\,\mathrm{e}^{-\beta V}}$$

is the unique QSD for the process (2.1) on Ω_β. Moreover, the exit time τ_{Ω_β} is exponentially distributed with rate $\lambda_{1,\beta}$ when the initial conditions follow ν, and is independent from the exit point:

$$\forall\, \varphi \in L^\infty(\partial\Omega_\beta), \qquad \mathbb{E}^\nu\left[\varphi(X^\beta_{\tau_{\Omega_\beta}})\mathbb{1}_{\tau_{\Omega_\beta}>t}\right] = \mathrm{e}^{-\lambda_{1,\beta}t}\mathbb{E}^\nu\left[\varphi(X^\beta_{\tau_{\Omega_\beta}})\right].$$

The Dirichlet spectrum also provides an upper bound on the relaxation timescale to the QSD. Let us define the total variation distance between signed measures $\nu, \nu' \in \mathcal{M}(\Omega_\beta)$ by

$$\|\nu - \nu'\|_{\mathrm{TV}} = \sup_{A\in\mathcal{B}(\Omega_\beta)} |\nu(A) - \nu'(A)|.$$

We have the following result, adapted again from [206].

Proposition 2.3 ([206]). *Assume that the initial law $\mu_0 := \mathrm{Law}(X_0^\beta)$ has an $L^2_\beta(\Omega_\beta)$ Radon–Nikodym derivative with respect to $\mathrm{e}^{-\beta V(x)}\,\mathrm{d}x$. Then there exist $C_1, C_2 > 0$ such that, for all $t > 0$,*

$$\left\|\mathrm{Law}^{\mu_0}\left[X_t^\beta \,\middle|\, \tau_{\Omega_\beta} > t\right] - \nu\right\|_{\mathrm{TV}} \leqslant C_1\mathrm{e}^{-(\lambda_{2,\beta}-\lambda_{1,\beta})t}, \tag{2.15}$$

$$\left\|\mathrm{Law}^{\mu_0}\left[\left(X^\beta_{\tau_{\Omega_\beta}}, \tau_{\Omega_\beta} - t\right) \,\middle|\, \tau_{\Omega_\beta} > t\right] - \mathrm{Law}^\nu\left[\left(X^\beta_{\tau_{\Omega_\beta}}, \tau_{\Omega_\beta}\right)\right]\right\|_{\mathrm{TV}} \leqslant C_2\mathrm{e}^{-(\lambda_{2,\beta}-\lambda_{1,\beta})t}. \tag{2.16}$$

Equation (2.15) states that the time-marginal of the process X_t^β, conditioned on remaining in the domain during a positive time t converges to the QSD exponentially fast, and Equation (2.16) states an analogous result for the law of the exit event. The requirement on the initial condition can be considerably weakened by using estimates on the heat semigroup for the diffusion process (2.1), see for example [305].

2.2.3 Geometric assumptions

We now discuss the geometric setting and basic assumptions which will be used in the remainder of this work. When considering a Gaussian approximation of the Gibbs measure (2.2) around a minimum of V, one finds that the covariance matrix scales as β^{-1} when $\beta \to +\infty$. Thus, it appears that the relevant scale to analyze the localization of low-temperature distributions is $\beta^{-\frac{1}{2}}$. This heuristic is justified by analysis, and motivates the scaling with respect to β in the following geometric hypothesis.

Assumption 2.4. *The following limit is well-defined in* $\mathbb{R} \cup \{+\infty\}$ *for each* $0 \leqslant i < N$*:*

$$\alpha^{(i)} = \lim_{\beta \to \infty} \sqrt{\beta} \sigma_{\Omega_\beta}(z_i) \in (-\infty, +\infty]. \tag{H1}$$

Let $0 \leqslant i < N$. We distinguish two regimes depending on the nature of $\alpha^{(i)}$:

- If $\alpha^{(i)} = +\infty$, we say that z_i is **far** from the boundary.
- If $\alpha^{(i)}$ is finite, we say that z_i is **close** to the boundary.

Remark 2.5. Note that (**H1**), excludes the case $\alpha^{(i)} = -\infty$, so that critical points which are far from the boundary but outside the domain do not appear. This is merely for convenience, since the forthcoming analysis would be unaffected by the presence of such points. Notice in particular that if z is a critical point of V such that $\mathrm{d}(z, \Omega_\beta) > c$ for some $c > 0$ and all β sufficiently large, one may ignore it by considering $\mathcal{K} \setminus B(z, c)$ instead of $\mathcal{K}$.

If a critical point $z_i \in \Omega_\beta$ is far from the boundary, Ω_β contains a ball centered around z_i of radius much larger than $\beta^{-\frac{1}{2}}$, namely of radius $\frac{\sigma_{\Omega_\beta}(z_i)}{2}$. When z_i is close to the boundary, this is not the case. In order to make quantitative statements on the spectrum, we need to constrain the local geometry of $\partial\Omega_\beta$ around z_i.

Assumption 2.6. *There exist functions* $\delta, \gamma : \mathbb{R}_+^* \to \mathbb{R}_+$ *such that the following holds for* β *large enough and each* $0 \leqslant i < N$*:*

$$\begin{cases} \sqrt{\beta}\delta(\beta) \xrightarrow{\beta \to \infty} +\infty, \\ \sqrt{\beta}\gamma(\beta) \xrightarrow{\beta \to \infty} 0, \\ \mathcal{O}_i^-(\beta) \subseteq B(z_i, \delta(\beta)) \cap \Omega_\beta \subseteq \mathcal{O}_i^+(\beta), \end{cases} \tag{H2}$$

where we denote

$$\mathcal{O}_i^\pm(\beta) = z_i + \left[B(0, \delta(\beta)) \cap E^{(i)} \left(\frac{\alpha^{(i)}}{\sqrt{\beta}} \pm \gamma(\beta) \right) \right], \tag{2.17}$$

recalling the definition (2.8) *of the half-space.*

In the case $\alpha^{(i)} = +\infty$, one has $\mathcal{O}_i^\pm(\beta) = B(z_i, \delta(\beta))$, and so Assumption (**H2**) only imposes $B(z_i, \delta(\beta)) \subset \Omega_\beta$. We schematically represent in Figure 2.1 the local geometry of $\partial\Omega_\beta$ under Assumption (**H2**), in a case where z_i is close to and inside the boundary.

Geometrically, the sets (2.17) correspond to hyperspherical caps centered around z_i and cut in the eigendirection $v_1^{(i)}$ of $\nabla^2 V(z_i)$. Thus, the condition (**H2**) fixes the orientation convention

for $v_1^{(i)}$ in the case where z_i is close to the boundary, namely that $v_1^{(i)}$ always points outwards from $\partial\Omega_\beta$ (including when z_i is outside the domain). The content of Assumption (**H2**) is that the boundary can be approximated by a hyperplane normal to $v_1^{(i)}$, up to negligible perturbations relative to $\beta^{-\frac{1}{2}}$, in a local neighborhood of size $\delta(\beta)$ around z_i. Note that in the case $d = 1$, Assumption (**H2**) is a direct consequence of Assumption (**H1**). Moreover, from the boundedness (**H0**), $\mathcal{O}_i^-(\beta) \subset \mathcal{K}$ and $\delta(\beta)$ is necessarily uniformly bounded with respect to β under Assumption (**H2**).

Remark 2.7. We will sometimes need $\delta(\beta)$ to be sufficiently small so that various local approximations are sufficiently precise. This desideratum is not restrictive, as Assumption (**H2**) remains valid upon reducing δ or augmenting γ by a constant multiplicative factor. Consequently, we will often assume at no cost to generality that δ is sufficiently small or that γ is sufficiently large for the purposes of the analysis.

Let us also note that since $\mathcal{K}$ contains only finitely many critical points, (**H2**) needs only to be verified locally around each critical point in order to hold globally.

The second geometric assumption we make is more technical in nature and relates to the scaling of the quantity δ constraining the local geometry of the domains in (2.17). More precisely, we will sometimes need $\sqrt{\beta}\delta(\beta)$ to grow sufficiently fast for the neighborhoods (2.17) to contain the bulk of the support for various quasimodes.

The rather mild growth condition on $\sqrt{\beta}\delta(\beta)$ we will require is the following.

Assumption 2.8. *The following limit holds for any $0 \leqslant i < N$:*

$$\lim_{\beta\to\infty} \delta(\beta)\sqrt{\frac{\beta}{\log\beta}} = +\infty. \tag{H3}$$

We stress that (**H3**) forces in particular critical points which are far from $\partial\Omega_\beta$ to be sufficiently far relatively to $1/\sqrt{\beta}$, namely further than $\sqrt{\log\beta}/\sqrt{\beta}$. Slower rates of divergence lie outside the scope of our analysis. We summarize relevant length scales of Assumptions (**H2**), (**H3**) by the following chain of scaling inequalities:

$$\gamma(\beta) \ll \beta^{-\frac{1}{2}} \ll \sqrt{\frac{\log\beta}{\beta}} \ll \delta(\beta).$$

Assumptions (**H0**), (**H1**), (**H2**) and (**H3**) are assumed to hold for the remainder of this work.

Additional assumptions in Theorem 2.17. For the purpose of deriving asymptotics for the metastable exit time $\lambda_{1,\beta}^{-1}$, we will restrict our setting to the case of domains containing essentially a unique local minimum z_0 far from the boundary (see (**EK1**) below), which moreover contains sufficiently large sublevel sets of V (see (**EK3**) below). Let us make this precise. Formally, we first assume the following.

Assumption 2.9. *The point z_0 is the only local minimum of V in $\mathcal{K}$ which is far from the boundary:*

$$N_0 \geqslant 1, \qquad \alpha^{(0)} = +\infty, \qquad \forall\, 1 \leqslant i < N_0, \quad \alpha^{(i)} < +\infty. \tag{EK1}$$

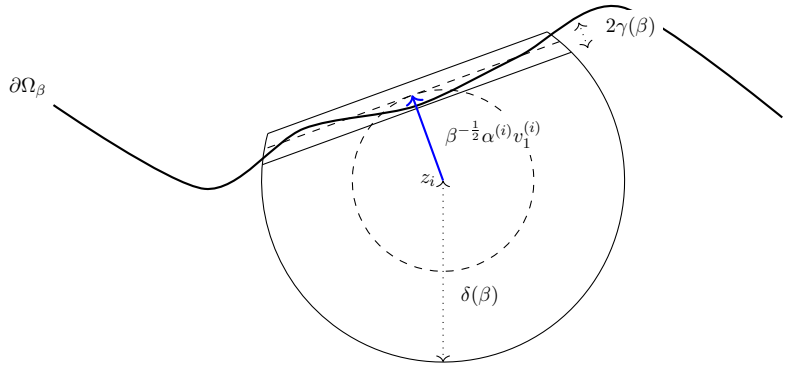

Figure 2.1: Local geometry of Ω_β in the neighborhood of a critical point z_i close to the boundary and inside the domain Ω_β. The relevant length scales are $\gamma(\beta) \ll \beta^{-\frac{1}{2}} \ll \delta(\beta)$.

Note that the basin of attraction $\mathcal{A}(z_0)$ (see Equation (2.11)) is a natural candidate for the metastable state associated with the potential well around z_0. It is also a convenient implicit definition from a numerical perspective, since determining whether x belongs to $\mathcal{A}(z_0)$ is as simple as estimating the gradient flow $\phi_t(x)$ for a sufficiently long time. The definition $\Omega_\beta = \mathcal{A}(z_0)$ is actually commonly used in accelerated MD, see [334]. However, in the context of the ParRep algorithm (see [334]), this definition is not expected to be optimal, and one of the motivations of this work is to rigorously show this and derive improved definitions for the metastable well associated with an energy minimum.

Our analysis almost applies to this special case, with the slight caveat that $\mathcal{A}(z_0)$ is typically not a smooth domain, but is instead piecewise smooth (see the proof of Lemma 2.28 below). However, the points at which the boundary $\partial\mathcal{A}(z_0)$ fails to be smooth are critical points of V of index greater than 1, which are typically too high in energy to be visited by the dynamics (2.1) in any reasonable amount of time. Thus, one can often circumvent this technical obstacle by considering a local regularization of the boundary excluding higher index saddle points from Ω. In our geometric setting, this situation corresponds to the following parameter values: $N_0 = 1$, $N = N_0 + N_1$, $\alpha^{(0)} = +\infty$ and $\alpha^{(i)} = 0$ for $1 \leqslant i < N$.

It is shown in [100, 224] that when the domain coincides with the basin $\mathcal{A}(z_0)$ (up to a local regularization), the exit distribution starting from the QSD concentrates on the index 1 saddle points of lowest energy separating $\mathcal{A}(z_0)$ from the basin of attraction of another local minimum for V. These so-called separating saddle points will also play a distinguished role in our analysis, as in [160, 157, 61, 209, 224].

Indeed, we relate the asymptotic behavior of the eigenvalues with local perturbations of the domain near critical points, as formalized by the geometric assumptions (**H1**) and (**H2**). In this context, the asymptotic behavior of the smallest eigenvalue will be especially sensitive to the shape of the boundary near separating critical points with the lowest energy, which turn out to be index 1 saddle points.

Let $\mathcal{M}(V)$ denote the set of local minima of V over $\mathbb{R}^d$, which is discrete since V is Morse.

It is natural to introduce the following quantity

$$V^* = \inf_{z \in \mathcal{S}(z_0)} V(z), \qquad \mathcal{S}(z_0) = \partial \mathcal{A}(z_0) \cap \left(\bigcup_{m \in \mathcal{M}(V) \setminus \{z_0\}} \partial \mathcal{A}(m) \right), \tag{2.18}$$

so that $V^* - V(z_0)$ gives the height of the energy barrier separating z_0 from some other basin of attraction for the steepest descent dynamics. The set $\mathcal{S}(z_0)$ loosely coincides with $\partial \mathcal{A}(z_0)$, up to a submanifold consisting of the union of the stable manifolds for critical points separating $\mathcal{A}(z_0)$ from itself. We refer to [246, Theorem B.13] or the proof of Lemma 2.28 below for more precision on this point. In particular, it holds that

$$\mathcal{S}(z_0) = \partial \overline{\mathcal{A}(z_0)}. \tag{2.19}$$

We refer to Figure 2.2 for a schematic representation of the set $\mathcal{S}(z_0)$ in a two-dimensional setting. We will make the following boundedness assumption.

Assumption 2.10.

The set $\mathcal{A}(z_0) \cap \{V < V^*\}$ is bounded. **(EK2)**

In the case $V^* < +\infty$ (which is of course the case of interest), a natural sufficient condition to ensure (**EK2**) is to assume growth conditions on V at infinity, which are standard in the theoretical study of the stochastic process (2.1).

In turn, by the regularity of V, (**EK2**) implies that $V^* < +\infty$, and thus the set

$$\operatorname*{Argmin}_{z \in \mathcal{S}(z_0)} V(z)$$

is non-empty. In fact, by virtue of Lemma 2.28 below and the Morse property satisfied by V, the infimum in (2.18) is attained at index 1 saddle points of V. Let us denote by $I_{\min}$ the indices associated with these low-energy saddle points, so that we may also write

$$I_{\min} = \operatorname*{Argmin}_{\substack{1 \leqslant i < N_1 \\ z_i \in \mathcal{S}(z_0)}} V(z_i), \qquad V^* = \min_{\substack{1 \leqslant i < N_1 \\ z_i \in \mathcal{S}(z_0)}} V(z_i). \tag{2.20}$$

Notice that, for $i \in I_{\min}$ such that $\alpha^{(i)} = +\infty$, the orientation convention for $v_1^{(i)}$ has not yet been fixed. However, since in this case $z_i \in \partial \mathcal{A}(z_0) \cap \partial \left[\mathbb{R}^d \setminus \mathcal{A}(z_0) \right]$, the stable manifold theorem implies that the outward normal $\mathrm{n}_{\mathcal{A}(z_0)}(z_i)$ to $\partial \mathcal{A}(z_0)$ is well-defined at z_i, and is furthermore a unit eigenvector of $\nabla^2 V(z_i)$ for the negative eigenvalue $\nu_1^{(i)}$. We therefore convene that in this case $v_1^{(i)} = \mathrm{n}_{\mathcal{A}(z_0)}(z_i)$.

We require that the domains Ω_β contain a small energetic neighborhood of the principal energy well $\mathcal{A}(z_0) \cap \{V < V^*\}$.

Assumption 2.11. *There exists $C_V, \beta_0 > 0$ such that, for all $\beta > \beta_0$,*

$$\left[\mathcal{A}(z_0) \cap \{V < V^* + C_V \delta(\beta)^2\} \right] \setminus \bigcup_{i \in I_{\min}} B(z_i, \delta(\beta)) \subset \Omega_\beta. \tag{EK3}$$

Assumption (**EK3**) serves as a counterpart to (**H2**), mildly constraining the geometry of $\partial\Omega_\beta$ away from the low-energy saddle points. We schematize its meaning in Figure 2.3.

For technical reasons, we finally require that the quantity $\delta(\beta)$ appearing in Assumption (**H2**) to be sufficiently small asymptotically, namely smaller than a positive constant $\varepsilon_0(V, z_0) > 0$ depending only on V and z_0, whose expression is given in the proof of Proposition 2.30 (see Section 2.5.1 below).

Assumption 2.12. *There exists $\beta > \beta_0$ such that for all $\beta > \beta_0$,*

$$\delta(\beta) < \varepsilon_0(V, z_0), \tag{EK4}$$

where $\varepsilon_0(V, z_0)$ is introduced in Proposition 2.30 below. Additionally, for each $0 \leqslant i < N$, z_i is the unique critical point of V in $B(z_i, 2\varepsilon_0(V, z_0))$.

The role of this hypothesis is to ensure that V is sufficiently well approximated by its second-order expansion on the $\delta(\beta)$ scale around each $(z_i)_{i\in I_{\min}}$. Since (**H2**) only constrains the geometry on the scale $\delta(\beta)$, Assumption (**EK4**) is rather non-restrictive.

Remark 2.13. Let us note that, together with the regularity of Ω_β, Assumption (**EK3**) may force critical points which are low in energy to be far from the boundary, i.e. $\alpha^{(i)} = +\infty$. This may occur when the set

$$\mathcal{X}(z_0) = \{\, 1 \leqslant i < N \,|\, z_i \in \partial\mathcal{A}(z_0) \setminus \mathcal{S}(z_0) : V(z_i) < V^*\} \tag{2.21}$$

is non-empty. Indeed, recall that $\partial\mathcal{A}(z_0)$ has Lebesgue measure 0 (see the proof of Lemma 2.29 below). It follows that for $i \in \mathcal{X}(z_0)$, there exists $h > 0$ such that almost all points in $B(z_i, h)$ are contained in $\mathcal{A}(z_0)$. If not, $z_i \in \overline{\mathcal{A}(m)}$ for some local minimum $m \neq z_0$ (since V is bounded from below), which is forbidden by the definitions of $\mathcal{X}(z_0)$ and $\mathcal{S}(z_0)$. By continuity, we may assume that $B(z_i, h) \subset \{V < V^*\}$ and $h < \varepsilon_0(V, z_0)$, so that, for sufficiently large β, almost all points in $B(z_i, h)$ are contained in Ω_β by Assumption (**EK3**) (because $h < \varepsilon_0(V, z_0) \implies B(z_i, h) \cap \bigcup_{i\in I_{\min}} B(z_i, \delta(\beta)) = \varnothing$ by Assumption (**EK4**)). Thus $z_i \in \overline{\Omega}_\beta$, but since $\overline{\Omega_\beta}$ is a smooth manifold with boundary, it must in fact hold that $B(z_i, h) \subset \Omega_\beta$. This obviously implies $\alpha^{(i)} = +\infty$.

Note that, since minima lie in the interior of their basin of attraction, $i \geqslant N_0$ for any $i \in \mathcal{X}(z_0)$, so that Assumption (**EK3**) can never lead to a situation in which Assumption (**EK1**) cannot be verified. In Figure 2.2, we depict a situation in which $\mathcal{X}(z_0) \neq \varnothing$.

2.2.4 Genericity of the assumptions and comparison with previous work

Let us briefly discuss how the assumptions listed in Sections 2.2.1 to 2.2.3 relate to previous works on the spectral asymptotics of the Witten Laplacian. We stress that our choice of geometric setting is heavily biased towards the optimization problem for (2.3) mentioned in the introduction. A such, it would be possible to obtain Eyring–Kramers-type asymptotics in more general settings, but for which the separation of timescales (2.3) would be asymptotically smaller than those domains to which we restrict ourselves, and so we filter out many such cases through our choice of geometric framework.

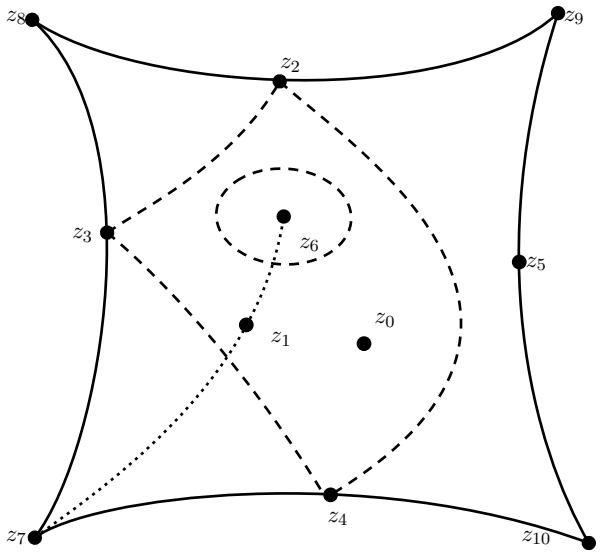

Figure 2.2: Depiction of a basin $\mathcal{A}(z_0)$ in dimension $d = 2$. In solid lines, the set $\mathcal{S}(z_0)$ defined in (2.18). The dotted line is the set $\partial\mathcal{A}(z_0) \setminus \mathcal{S}(z_0)$. The dashed line is the level set $\{V = V^*\}$. There are eleven critical points including the minimum z_0, five index 1 saddle points z_1, z_2, z_3, z_4 and z_5. The point z_1 is a non-separating saddle point. The remaining points are index-2 saddle points (local maxima). Here $I_{\min} = \{2, 3, 4\}$, and $\mathcal{X}(z_0) = \{1\}$. Under (**EK3**), it holds $\alpha^{(1)} = +\infty$. Note however that one could even change the sets $\mathcal{K}$ and Ω_β to have $z_6 \notin \mathcal{K}$ and hence not be considered as a critical point.

Euclidean setting. First, we stress that our results are for the time being restricted to the case of parameter dependent subsets of the Euclidean space $\mathbb{R}^d$, whereas many works from the semiclassical literature [157, 207, 225, 209, 100] consider the more general setting of Riemannian manifolds, with or without boundaries. The distinction is not entirely anecdotal, since the presence of a metric introduces another technical difficulty, which is typically taken care of by a suitable choice of local coordinates.

Since the natural counterpart of the main geometric assumption (**H2**) would most likely involve expressing the asymptotic shape of the boundary in such a system of local coordinates, this would lead to conditions which would be difficult to verify in practice. We avoid this difficulty by considering for now the Euclidean case. However, extending the results to the genuine Riemannian case would be of practical interest, since many atomistic trajectories evolve on manifolds (a minima, flat tori), and would also allow to analyze the case of effective metastable dynamics in free-energy wells, which involve multiplicative noise in the associated diffusion process, see for instance the discussion in [346, Section 2.3].

On the choice of the local geometry. Assumption (**H2**) is of course restrictive, since it states that the shape of the boundary may be roughly parametrized in the local neighborhood of a critical point z_i close to the boundary by a single scalar parameter $\alpha^{(i)}$. If z_i is far from the boundary, there is no particular assumption on the local shape of the boundary, except that it must be sufficiently far from z_i, according to (**H3**). However, all works on spectral asymptotics

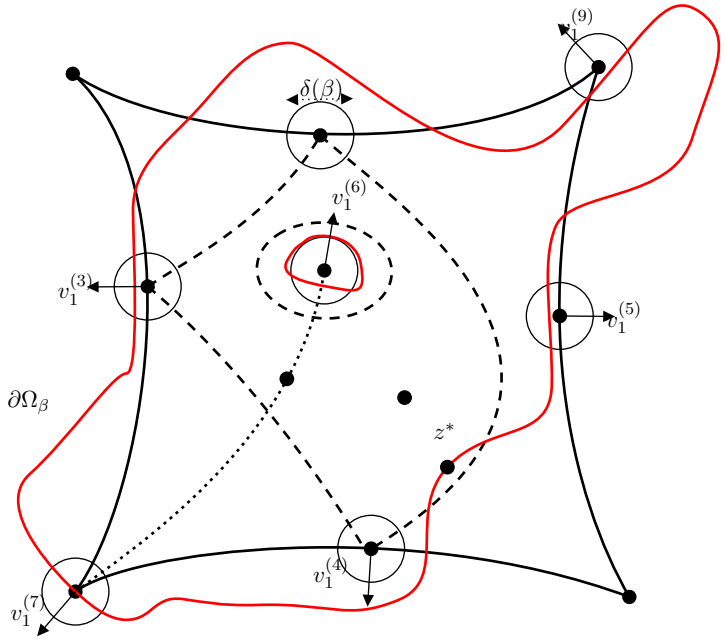

Figure 2.3: Illustration of the hypothesis (**EK3**) around the basin depicted in Figure 2.2. In red, the boundary of a domain satisfying the geometric constraint (**H2**) (at a fixed value of β), but violating (**EK3**) is depicted. The boundary crosses the level set $\{V = V^*\}$, and z^* is therefore a low-energy generalized saddle point (see Section 2.2.4 below) for this domain. The critical points z_8 and z_{10} are assumed not to be in the englobing set $\mathcal{K}$. The points z_0, z_1, z_2 and z_4 are far from the boundary, while the others are close. Note that the orientation convention for $v_1^{(4)}$ is fixed by the geometry of $\mathcal{A}(z_0)$.

of the Witten Laplacian dealing with boundary conditions impose geometric restrictions at the boundary, either for technical reasons, or for the sake of obtaining analytical formulæ. To assess the restrictiveness of the condition (**H2**), and compare it to previous works, it is thus helpful to consider the standard case $\Omega_\beta = \Omega$ for all $\beta > 0$, where $\Omega \subset \mathbb{R}^d$ is a fixed smooth, bounded and open domain. Let $z_i \in \overline{\Omega}$ be a critical point. We may ignore all critical points in $\mathbb{R}^d \setminus \overline{\Omega}$ by considering $\mathcal{K}$ to be a sufficiently small closed neighborhood of $\overline{\Omega}$ in (**H0**). We distinguish two cases.

1. If $z_i \in \Omega$, then $\sigma_\Omega(z_i) > 0$ and z_i is thus far from the boundary. Then, (**H2**) and (**H3**) hold locally without restriction by setting $\delta(\beta) = \frac{\sigma_\Omega(z_i)}{2}$, and $\gamma(\beta) = 0$ for all $\beta > 0$.

2. If $z_i \in \partial\Omega$, then z_i is close to the boundary with $\alpha^{(i)} = 0$. This is the case of critical points on the boundary analyzed in [209, 224]. In [209], it is assumed that for each $z_i \in \partial\Omega$ such that $\mathrm{Ind}(z_i) = 1$, the outward normal $\mathrm{n}_\Omega(z_i)$ is an eigenvector for the unique negative eigenvalue of $\mathrm{Hess}\, V(z_i)$. As we show in Lemma 2.14 below, this requirement is equivalent to (**H2**) in the case of a fixed domain for the order-one saddle points lying on the boundary. In [224], for the purpose of obtaining finer estimates on the normal derivative of low-lying eigenmodes, this condition is replaced with the much stronger requirement that $\partial\Omega$ coincides with the stable manifold $\mathcal{W}^+(z_i)$ in a neighborhood of z_i.

Lemma 2.14. *Let $\Omega \subset \mathbb{R}^d$ be a smooth open domain, and set $\Omega_\beta = \Omega$ for all $\beta > 0$. Then* (**H0**)*,* (**H1**)*,* (**H2**) *and* (**H3**) *hold if and only if Ω is bounded, and for each $z_i \in \overline{\Omega}$ such that $\nabla V(z_i) = 0$, either $z_i \in \Omega$ or $\mathrm{n}_\Omega(z_i) = v_1^{(i)}$.*

Proof. Assume that (**H0**)–(**H3**) hold. Then Ω is bounded, according to (**H0**). We only need to check the case of a critical point $z_i \in \partial\Omega$, in which case $\alpha^{(i)} = 0$. Since Ω is smooth, $\mathrm{n}_\Omega(z_i) = -\nabla\sigma_\Omega(z_i) \neq 0$. Let $u \in \mathbb{R}^d$ with $|u| = 1$ and $u^\intercal v_1^{(i)} = 0$. According to (**H2**), for $\beta > \beta_0$ such that $\beta^{-\frac{1}{2}} < \delta(\beta)$ for all $\beta > \beta_0$, the ball $B(z_i + \beta^{-\frac{1}{2}}u, 2\gamma(\beta))$ intersects both $\mathcal{O}_i^-(\beta) \subset \Omega$ and $B(z_i, \delta(\beta)) \setminus \mathcal{O}_i^+(\beta) \subset \Omega^c$. It follows that $\mathrm{d}(z_i + \beta^{-\frac{1}{2}}u, \partial\Omega) \leqslant 2\gamma(\beta)$, hence:

$$|u^\intercal \nabla\sigma_\Omega(z_i)| \leqslant \limsup_{\beta\to\infty} \frac{\mathrm{d}(z_i + \beta^{-\frac{1}{2}}u, \partial\Omega)}{\beta^{-\frac{1}{2}}} \leqslant \limsup_{\beta\to\infty} 2\sqrt{\beta}\gamma(\beta) = 0.$$

Since u was arbitrary orthogonal to $v_1^{(i)}$, and $\nabla\sigma_\Omega(z_i) \neq 0$, $v_1^{(i)}$ is collinear with the unit outward normal $\mathrm{n}_\Omega = -\nabla\sigma_\Omega$, so that they are in fact equal, according to the orientation convention imposed by (**H2**).

For the reverse implication, since Ω is bounded, (**H0**) holds with $\mathcal{K} = \overline{\Omega}$. For a critical point $z_i \in \Omega$, (**H1**), (**H2**) hold locally with $\alpha^{(i)} = +\infty, \delta(\beta) = \sigma_\Omega(z_i)/2$ and $\gamma(\beta) = 0$.

If $z_i \in \partial\Omega$, (**H1**) holds locally with $\alpha^{(i)} = 0$, and by hypothesis $\mathrm{n}_\Omega(z_i) = v_1^{(i)}$. We once again rely on the smoothness of $\partial\Omega$ to write the Taylor expansion

$$\sigma_\Omega(z_i + h) = \sigma_\Omega(z_i) + \nabla\sigma_\Omega(z_i)^\intercal h + R_i(h) = -h^\intercal v_1^{(i)} + R_i(h),$$

where there exists $C_i, h_{0,i} > 0$ such that $|R_i(h)| \leqslant C_i|h|^2$ for all $|h| < h_{0,i}$. Set $\delta(\beta) = \beta^{s-\frac{1}{2}}$, $\gamma(\beta) = \beta^{t-1}$ with $0 < 2s < t < \frac{1}{2}$. Then δ, γ satisfy the scaling assumptions of (**H2**) and (**H3**). Recalling the definition of the capped balls (2.17), we have $\sigma_\Omega(\mathcal{O}_i^-) \subset [\gamma(\beta) - C_i\delta(\beta)^2, +\infty)$ for $\beta > h_{0,i}^{\frac{1}{s-1/2}}$, and likewise $\sigma_\Omega(B(z_i, \delta^{(i)}(\beta)) \setminus \mathcal{O}_i^+) \subset (-\infty, -\gamma(\beta) + C_i\delta(\beta)^2]$. It is thus clear that the inclusion (**H2**) holds locally around z_i for $\beta > \beta_{0,i} := \max\{h_{0,i}^{\frac{1}{s-1/2}}, C_i^{\frac{1}{t-2s}}\}$.

Since V has finitely many critical points in $\overline{\Omega}$, the functions δ and γ satisfy by construction the requirements of Assumption (**H2**) with $\beta_0 := \max_{0\leqslant i<N} \beta_{0,i}$.

□

Lemma 2.14 shows that our setting can be understood as a generalization of that of [209] in the case of temperature-dependent domains in Euclidean space.

Remark 2.15. In the general case, the geometry of the boundary $\partial\Omega_\beta$ may be quite degenerate under (**H2**), even close to critical points, as no particular restrictions on $\partial\Omega_\beta$ are imposed in the strip $\mathcal{O}_i^+(\beta) \setminus \mathcal{O}_i^-(\beta)$, except for its smoothness at each $\beta > 0$. In particular, the curvature at any point in the strip may diverge arbitrarily fast as $\beta \to \infty$, and it may happen that $z_i \in \partial\Omega_\beta$ for all $\beta > 0$ and some $0 \leqslant i < N$, but that $\mathrm{n}_{\Omega_\beta}(z_i) \neq v_1^{(i)}$ for any $\beta > 0$. In this respect, our analysis goes beyond the standard setting used for example in [209].

On Assumptions (EK1) and (EK3). A phenomenon of interest in the semiclassical approach to metastability is the interaction between potential wells, see [160, 102, 157, 61, 225, 224]. However, we consider here, as in [100], the case where the unique local minimum of V in $\mathcal{K}$ which is far from the boundary is z_0 (we stress however that this minimum need not be global nor unique on $\mathcal{K}$, provided the other local minima are close to the boundary),

and thus there is in some sense only one potential well. The motivation for concentrating on this setting is the conclusion of Theorem 2.17 below, which shows that the modification to the standard Eyring–Kramers formula arises when low-lying index 1 saddle points are close to the boundary, which therefore prevents any interaction between energy wells separated by these critical points.

Besides, from the perspective of the shape optimization problem mentioned in the introduction, the more interesting situation occurs when both the first and second eigenvalues are sensitive to the position of the boundary. In the context of MD, domains containing multiple energy minima can be seen as energy superbasins, for which the relaxation timescale is related to the crossing of energy barriers internal to the domain, and which will therefore be insensitive to the position of the boundary. We believe however that the analysis can be extended to handle the case of multiple energy wells, by adapting standard arguments (see for instance [209]) to our temperature-dependent setting.

In the analysis of the Witten Laplacian with Dirichlet boundary [159, 225, 100, 209], the interesting phenomenon of so-called generalized saddle points (which are not genuine critical points) also plays a role. These are local minima z of $V|_{\partial\Omega_\beta}$ for which the normal derivative of V is positive, i.e. $\nabla V(z) \cdot \mathrm{n}_{\Omega_\beta}(z) > 0$. In particular, such points are not critical points of V, and can be seen informally as index-one saddle points for the extension of V by $-\infty$ outside of Ω_β. The role of Assumption (**EK3**) is to ensure that generalized saddle points are sufficiently high in energy so that their contribution to the smallest eigenvalue is negligible, and that the main contribution comes from intrinsic low-lying saddle points, indexed by $I_{\min}$.

Since the definition of generalized saddle points depends on the geometry of $\partial\Omega_\beta$ which varies as $\beta \to \infty$, one way to analyze their contribution would be to place strong geometric constraints on the domains, using analogs of Assumption (**H2**) and Proposition 2.36 in the $1/\beta$ scaling around a predetermined limiting geometry. However, we do not pursue this direction. Besides, the contribution of non-critical generalized saddle points to the pre-exponential factor is of order $\sqrt{\beta}$ rather than 1 in the case of a usual saddle point (see for example [159]), while they do not contribute to the harmonic spectrum. From the point of view of maximizing the separation of timescales (2.3), it is therefore always asymptotically preferable to consider domains Ω_β which do not contain generalized order 1 saddle points at the energy level V^*.

2.3 Statement of the main results

We present in this section the main results of this work, giving the leading-order asymptotics of the eigenvalues of $-\mathcal{L}_\beta$ in the small temperature limit. The resulting formulas are explicit in terms of easily computable functions, and give in particular quantitative estimates for crucial timescales related to the dynamics (2.1) conditioned on non-absorption at the boundary, namely the metastable exit timescale $\lambda_{1,\beta}(\Omega_\beta)^{-1}$, and the local relaxation timescale $(\lambda_{2,\beta}(\Omega_\beta) - \lambda_{1,\beta}(\Omega_\beta))^{-1}$. As noted in the introduction, this is of practical interest for assessing the efficiency of acceleration methods in MD, such as ParRep [334, 268, 206] and ParSplice [266], as well as providing quantitative estimates for the decorrelation time. To estimate $\lambda_{2,\beta}(\Omega_\beta)$, we make use of a harmonic approximation result (Theorem 2.16), which

we state in Section 2.3.1. Under (**EK1**), the harmonic approximation shows that $\lambda_{1,\beta} \to 0$ in the limit $\beta \to \infty$, but without any estimate on the asymptotic rate of decay. To get useful estimates of the separation of timescales (2.3), we therefore derive finer asymptotics for $\lambda_{1,\beta}(\Omega_\beta)$, extending the Eyring–Kramers formula (Theorem 2.17). This result is discussed in Section 2.3.2. In Section 2.3.3, we briefly discuss the main implications of these two results for the optimization of the efficiency of parallel replica methods from accelerated MD, with respect to the definitions of the metastable states.

2.3.1 Harmonic approximation of the Dirichlet spectrum

We generalize the harmonic approximation of [303, 195] to the case of a homogeneous Dirichlet conditions in a temperature-dependent domain, treating the case in which the asymptotic geometry near critical points is prescribed by the assumptions of Section 2.2.3. More precisely, we show the following result.

Theorem 2.16. *Assume that* (**H0**) (**H1**), (**H2**) *and* (**H3**) *hold. For any* $k \geqslant 1$*, the following limit holds:*

$$\lim_{\beta\to\infty} \lambda_{k,\beta} = \lambda^{\mathrm{H}}_{k,\alpha}, \tag{2.22}$$

where

$$\alpha = \left(\alpha^{(i)}\right)_{0\leqslant i<N} \tag{2.23}$$

where the $\alpha^{(i)}$ *are defined in* (**H1**) *and* $\lambda^{\mathrm{H}}_{k,\alpha}$ *is defined in* (2.45)*, while* $\lambda_{k,\beta}$ *is the* k*-th Dirichlet eigenvalue of the operator* (2.12) *considered on* $L^2_\beta(\Omega_\beta)$*.*

In the above, $\lambda^{\mathrm{H}}_{k,\alpha}$ denotes the k-th eigenvalue of some operator with a temperature-independent spectrum defined in (2.44), the so-called harmonic approximation. The vector $\alpha \in (-\infty, +\infty]^N = (\alpha^{(i)})_{0\leqslant i<N}$ encodes the asymptotic distance to the boundary of each critical points in the semiclassical scaling, where we recall Assumption (**H1**). Crucially, the limiting eigenvalue $\lambda^{\mathrm{H}}_{k,\alpha}$ can be expressed in terms of the eigenvalues of one-dimensional harmonic oscillators on the real-half line, with homogeneous Dirichlet boundary conditions, which makes their numerical approximation computationally feasible.

In fact, the proof Theorem 2.16 relies on the estimation of Dirichlet eigenvalues for the operator H_β defined in (2.14), which grow linearly in β in the low-temperature limit (as suggested by the conjugation (2.14)).

The proof of Theorem 2.16, which relies on the construction of approximate eigenvectors for the Witten Laplacian, or so-called harmonic quasimodes, is given in Section 2.4.

In the case where there is only one minimum far from the boundary (i.e. (**EK1**) is satisfied), then $\lambda^{\mathrm{H}}_2 > 0$, and Theorem 2.16 is sufficient to determine the leading-order asymptotic of the second eigenvalue $\lambda_{2,\beta}$. However, $\lambda^{\mathrm{H}}_1 = 0$, and so a finer analysis is necessary to treat the first eigenvalue.

2.3.2 A modified Eyring–Kramers formula

The second main result provides exact asymptotics of the smallest eigenvalue $\lambda_{1,\beta}$, up to a multiplicative factor converging to 1, under the additional assumptions discussed in Section 2.2.3.

Theorem 2.17. *Assume that the hypotheses of Theorem 2.16 hold, as well as* (**EK1**), (**EK2**), (**EK3**) *and* (**EK4**). *The following estimate holds in the limit $\beta \to +\infty$:*

$$\lambda_{1,\beta} = \mathrm{e}^{-\beta(V^*-V(z_0))}\left[\sum_{i\in I_{\min}} \frac{|\nu_1^{(i)}|}{2\pi\Phi\left(|\nu_1^{(i)}|^{\frac{1}{2}}\alpha^{(i)}\right)}\sqrt{\frac{\det\nabla^2V(z_0)}{|\det\nabla^2V(z_i)|}}\,(1+\varepsilon_i(\beta))\right], \tag{2.24}$$

where

$$\Phi(x) = \frac{1}{\sqrt{2\pi}}\int_{-\infty}^{x}\mathrm{e}^{-\frac{t^2}{2}}\,\mathrm{d}t, \qquad \Phi(+\infty) = 1, \tag{2.25}$$

and

$$\varepsilon_i(\beta) = \begin{cases} \mathcal{O}(\beta^{-1}\delta(\beta)^{-2}), & \alpha^{(i)} = +\infty, \\ \mathcal{O}(\sqrt{\beta}\gamma(\beta) + \beta^{-1}\delta(\beta)^{-2} + \beta^{-\frac{1}{2}}), & \alpha^{(i)} < +\infty. \end{cases} \tag{2.26}$$

According to Proposition 2.2, Theorem 2.17 gives an asymptotic equivalent for the inverse of the mean exit time of the dynamics (2.1) initially distributed according to the QSD in Ω_β.

Remark 2.18. By restricting oneself to the geometric setting in which the boundary is flat in a positive neighborhood of each $(z_i)_{i\in I_{\min}}$ (that is $\gamma(\beta) = 0$ and $\delta(\beta) = \eta$ in (**H2**) for some small $\eta > 0$), one recovers the optimal error terms

$$\varepsilon_i(\beta) = \begin{cases} \mathcal{O}(\beta^{-1}), & \alpha^{(i)} = +\infty \\ \mathcal{O}(\beta^{-\frac{1}{2}}), & \alpha^{(i)} < +\infty, \end{cases}$$

in accordance with the analysis performed in [209]. On the other hand, aiming for maximum geometric flexibility, Assumptions (**H2**) and (**H3**) only imply that, in the limit $\beta \to \infty$,

$$\sqrt{\beta}\gamma(\beta) = o(1), \qquad \beta^{-1}\delta(\beta)^{-2} = \mathcal{O}(|\log\beta|^{-1}),$$

and thus the remainder (2.26) is $\mathcal{O}(|\log\beta|^{-1})$ in the case $\alpha^{(i)} = +\infty$, and not quantitative in the case $\alpha^{(i)} < +\infty$.

Remark 2.19. The modification with respect to the Eyring–Kramers formula obtained in the boundaryless case in [160, 61, 157] and in the case with boundary in [159, 209] concerns the prefactor which depends on the asymptotic distances of the low-lying saddle points to the boundary. Let us fix a family of domains $(\Omega_t)_{t\in[-1,1]}$ and $i \in I_{\min}$ such that $\sigma_{\Omega_t}(z_i) = at$ for all $-1 \leqslant t \leqslant 1$, i.e. the boundary crosses z_i in such a way that the geometry of the boundary is prescribed by (**H2**) (say with $\alpha^{(i)}(t) = at\sqrt{\beta}$, $\delta(\beta) = \varepsilon > 0$ and $\gamma(\beta) = 0$) for some large β. One can informally see Theorem 2.17 as an analysis of the transition in the pre-exponential factor of $\lambda_{1,\beta}(\Omega_t)$ as the saddle point crosses the boundary. Assuming for simplicity that $I_{\min} = \{i\}$, writing $\lambda_{1,\beta}(\Omega_t) = C(t)\mathrm{e}^{-\beta(V^*-V(z_0))}$, and formally substituting $\alpha^{(i)}(t)$ in (2.24), Theorem 2.17 suggests that

$$C(t) \approx \frac{|\nu_1^{(i)}|}{2\pi\Phi\left(|\nu_1^{(i)}|^{\frac{1}{2}}at\sqrt{\beta}\right)}\sqrt{\frac{\det\nabla^2V(z_0)}{|\det\nabla^2V(z_i)|}}.$$

We stress this is only a formal interpretation, since the remainder term (2.26) depends non-uniformly on t. The prefactor is halved as t goes from 0 to 1, with a sharp transition occurring on the scale $\left(\beta|\nu_1^{(i)}|\right)^{-\frac{1}{2}}$. This is in accordance with the probabilistic interpretation of $\lambda_{1,\beta}$, since half of the trajectories of the dynamics (2.1) which reach z_i are expected to return to a small neighborhood of z_0 before transitioning to another potential well. On the other hand, the asymptotic estimate, in the limit $x \to -\infty$,

$$\Phi(x) = \frac{1 + \mathcal{O}(|x|^{-2})}{|x|\sqrt{2\pi}} \mathrm{e}^{-\frac{x^2}{2}} \tag{2.27}$$

suggests again that

$$\lambda_{1,\beta}(\Omega_{-1}) \approx a\sqrt{\frac{\beta}{2\pi}}|\nu_1^{(i)}|^{\frac{3}{2}}\sqrt{\frac{\det\,\nabla^2 V(z_0)}{|\det\,\nabla^2 V(z_i)|}}\mathrm{e}^{-\beta(V^* - \frac{1}{2}|\nu_1^{(i)}|a^2 - V(z_0))}.$$

Although the case $\alpha^{(i)} = -\infty$ is not covered in this work (we nevertheless expect that our setting can be extended to handle this case as well), we note that this heuristic is in agreement with the results of [159]. Indeed, writing $z^*(a) = z_i - a v_1^{(i)}$, for small a, this approximation corresponds to

$$\lambda_{1,\beta}(\Omega_{-1}) \approx \sqrt{\frac{\beta}{2\pi}}|\nabla V(z^*(a))|\sqrt{\frac{\det\,\nabla^2 V(z_0)}{\det\,\nabla^2_{\partial\Omega_{-1}} V(z^*(a))}}\mathrm{e}^{-\beta(V(z^*(a)) - V(z_0))},$$

where $\nabla^2_{\partial\Omega_{-1}}$ denotes the Hessian on the submanifold $\partial\Omega_{-1}$. This corresponds to the standard asymptotic behavior in the case where $z^*(a) \in \partial\Omega_{-1}$ is a so-called generalized saddle point (see for instance [159, 209]).

The proof of Theorem 2.17, which relies on the construction of accurate quasimodes for the principal Dirichlet eigenvector inspired by [209], and a modified Laplace method (Proposition 2.36), is performed in Section 2.5.

Before proving Theorems 2.16 and 2.17, we briefly and informally discuss some implications of these results for the problem of maximizing the timescale separation (2.3).

2.3.3 Practical implications of the asymptotic analysis.

In this section, we briefly and informally highlight the key implications of our results for the selection of metastable states and the estimation of associated timescales in MD simulations. For this purpose, we assume in this section that Assumptions (**H0**)–(**H3**) and (**EK1**)–(**EK4**) are satisfied.

Theorems 2.16 and 2.17 give asymptotic equivalents for the metastable exit rate $\lambda_{1,\beta}$ and the convergence rate $\lambda_{2,\beta} - \lambda_{1,\beta}$ to the QSD inside Ω_β (also known as the decorrelation rate). In the small temperature regime, $\lambda_{1,\beta}$ converges exponentially fast to zero, and $\lambda_{2,\beta}$ is asymptotically bounded from below. Explicitly, we obtain from the statement of Theorem 2.17 and the proof

of Theorem 2.16 (see Equation (2.47) in Section 2.4.3 below) that

$$\begin{aligned}
\lambda_{1,\beta} &\overset{\beta\to\infty}{\sim} \mathrm{e}^{-\beta(V^*-V(z_0))} \left[\sum_{i\in I_{\min}} \frac{|\nu_1^{(i)}|}{2\pi\Phi\left(|\nu_1^{(i)}|^{\frac{1}{2}}\alpha^{(i)}\right)} \sqrt{\frac{\det\nabla^2 V(z_0)}{|\det\nabla^2 V(z_i)|}}\right], \\
\lambda_{2,\beta} &\overset{\beta\to\infty}{\sim} \min\left\{\min_{1\leqslant j\leqslant d}\nu_j^{(0)}, \min_{1\leqslant i<N}\left[\left|\nu_1^{(i)}\right|\mu_i(\alpha^{(i)}) - \frac{\nu_1^{(i)}}{2} + \sum_{2\leqslant j\leqslant d}\left|\nu_j^{(i)}\right|\mathbb{1}_{\nu_j^{(i)}<0}\right]\right\},
\end{aligned} \tag{2.28}$$

where $\mu_i(\alpha^{(i)})$ is the principal eigenvalue of the canonical harmonic oscillator $-\frac{1}{2}\left(\partial_x^2 - x^2\right)$ acting on the spatial domain $\left(-\infty, \alpha^{(i)}\sqrt{|\nu_1^{(i)}|/2}\right)$ with homogeneous Dirichlet boundary conditions. Both these quantities can therefore be easily computed in practice, given the knowledge of all the critical points of V inside $\mathcal{K}$ and the eigenvalues of the Hessian $\nabla^2 V$ at these points. The formulas (2.28) provide insight into how to tune acceleration methods such as ParRep in the limit of small temperature.

Harmonic approximation of the decorrelation time. A key choice in ParRep-like algorithms is the selection of a decorrelation time associated to a domain Ω_β (which here we take for the sake of generality to be temperature-dependent). Heuristically, Proposition 2.2 suggests that a natural decorrelation time is given by $n_{\mathrm{corr}}/(\lambda_{2,\beta} - \lambda_{1,\beta})$, where $n_{\mathrm{corr}} > 0$ is a tolerance hyperparameter of our choosing. This choice is common in materials science, and $\lambda_{2,\beta}$ is then usually further approximated by modelling the basin of attraction $\mathcal{A}(z_0)$ as a harmonic potential well, see for instance [268, Section 2.10]. In our setting, this corresponds to the approximation $\lambda_{2,\beta} \approx \min_{1\leqslant j\leqslant d}\nu_j^{(0)}$. The formula (2.28) shows that this approximation is however not valid in general (even in the case $\Omega_\beta = \mathcal{A}(z_0)$), but that it is possible to get a valid approximation by taking into account the eigenvalues of harmonic oscillators at the other critical points.

Optimization of the asymptotic timescale separation (2.3) with respect to $\left(\alpha^{(i)}\right)_{i\in I_{\min}}$. The formulas (2.28) also provide insight into the problem of maximizing the separation of timescales $(\lambda_{2,\beta} - \lambda_{1,\beta})/\lambda_{1,\beta}$ with respect to the shape of the domain. Equivalently, we aim to maximize $\lambda_{2,\beta}/\lambda_{1,\beta}$. As mentioned in the introduction, this optimization problem can be addressed using numerical methods, at least in cases where low-dimensional representations of the system can be used, see [51]. Here we focus on the optimization in the semiclassical limit. Obviously, there is a caveat in the fact that our geometric assumptions (see Section 2.2.3) restrict the class of domains with respect to which we optimize, and our results only give asymptotically optimal prescriptions in the limit $\beta\to\infty$ for the choice of $(\alpha^{(i)})_{0\leqslant i<N}$. We can nevertheless make some observations.

Note firstly that the ratio $\lambda_{2,\beta}/\lambda_{1,\beta}$ diverges at an exponential rate which is independent of the parameter α in the limit $\beta\to\infty$. However, the prefactor $\mathrm{e}^{-\beta(V^*-V(z_0)}\lambda_{2,\beta}/\lambda_{1,\beta}$ converges to a finite limit, which is a function of α, and thus it is in fact this quantity that we wish to maximize. Second, the parameters $\left(\alpha^{(i)}\right)_{i\in\{0\}\cup\mathcal{X}(z_0)}$ are set to $+\infty$ by our geometric assumptions, where we recall the definition (2.21) of the set $\mathcal{X}(z_0)$. Next, each critical point z_i

with $1 \leqslant i < N$ contributes a lowest eigenvalue

$$\lambda_i(\alpha^{(i)}) := \left|\nu_1^{(i)}\right| \mu_i(\alpha^{(i)}) - \frac{\nu_1^{(i)}}{2} + \sum_{2 \leqslant j \leqslant d} \left|\nu_j^{(i)}\right| \mathbb{1}_{\nu_j^{(i)} < 0}$$

to the harmonic spectrum. These last two facts imply that there is an upper bound on the asymptotics of $\lambda_{2,\beta}$, with respect to $(\alpha^{(i)})_{i \in I_{\min}}$, namely

$$\begin{aligned} \ell(z_0) &= \min \left\{ \min_{1 \leqslant j \leqslant d} \nu_j^{(0)}, \min_{i \in \mathcal{X}(z_0)} \lambda_i(+\infty) \right\} \\ &= \min \left\{ \min_{1 \leqslant j \leqslant d} \nu_j^{(0)}, \min_{i \in \mathcal{X}(z_0)} \sum_{1 \leqslant j \leqslant d} \left|\nu_j^{(i)}\right| \mathbb{1}_{\nu_j^{(i)} < 0} \right\} > 0. \end{aligned}$$

In many cases, the set $\mathcal{X}(z_0)$ is empty, and so $\ell(z_0)$ is in this case simply given by the smallest eigenvalue of the Hessian $\nabla^2 V(z_0)$ at the minimum. If, for $i \in I_{\min}$, it holds that $\lambda_i(+\infty) = |v_1^{(i)}| \geqslant \ell(z_0)$ (i.e. when the unstable mode at the saddle point is sharp enough), then the choice $\alpha^{(i)} = +\infty$ is in fact optimal, since it maximally decreases the asymptotic behavior of $\lambda_{1,\beta}$ without affecting that of $\lambda_{2,\beta}$. If for one or more z_i with $i \in I_{\min}$, it holds that $\lambda_i(+\infty) < \ell(z_0)$, then there is a genuine optimization problem, but which typically involves a small number of parameters.

In the latter case, there exists indeed an optimal value $\left(\alpha^{(i)\star}\right)_{i \in I_{\min}} \in (-\infty, +\infty]^{|I_{\min}|}$. To see this, we rely on the Gaussian tail estimate (2.27) and Lemma 2.22 to show that, as $\alpha^{(i)}$ tends to $-\infty$, the value $\lambda_i(\alpha^{(i)})$ will eventually become larger than $\ell(z_0)$, whereas the prefactor for $\lambda_{1,\beta}$ will tend to $+\infty$. This implies that any maximizing sequence of parameters is bounded from below by some $C > -\infty$ in each of its components. We endow $(-\infty, +\infty]$ with the one-point compactified topology at $+\infty$. In this topology, the claim then follows from compactness of $[C, +\infty]^{|I_{\min}|}$, the continuity at $+\infty$ of Φ (defined in (2.25)) and of the principal Dirichlet eigenvalue μ_i of the harmonic oscillator (which follows from (2.36) in Lemma 2.22).

Optimization with respect to the other parameters. The remaining tunable parameters are those not corresponding to low-lying separating saddle points. These are given by the vector of parameters $\mathcal{P}(\alpha) = \left(\alpha^{(i)},\, i \notin \{0\} \cup \mathcal{X}(z_0) \cup I_{\min}\right)$. Indeed for $i \in \{0\} \cup \mathcal{X}(z_0)$, it necessarily holds that $\alpha^{(i)} = +\infty$ (see Remark 2.13 above), and the case $i \in I_{\min}$ is treated in the previous paragraph. Noticing that the asymptotic behavior of $\lambda_{1,\beta}$ is only a function of $(\alpha^{(i)})_{i \in I_{\min}}$, it follows that the asymptotic optimization problem reduces to a maximization of $\lim_{\beta \to \infty} \lambda_{2,\beta}$ with respect to the parameter $\mathcal{P}(\alpha)$. By domain monotonicity (see Proposition 2.33), all the quantities $\lambda_i(\alpha^{(i)})$ are decreasing functions of $\alpha^{(i)}$. In particular, the components of $\mathcal{P}(\alpha)$ may be sent to $-\infty$ without affecting the asymptotic prefactor $\mathrm{e}^{-\beta(V^* - V(z_0))} \lambda_{2,\beta} / \lambda_{1,\beta}$.

One option is to entirely disregard the corresponding critical points by not including them in $\mathcal{K}$ from the start. This reduces the problem to that of finding an asymptotically optimal perturbation of the set $\mathcal{A}(z_0) \cap \{V < V^*\}$.

However, in general, many values of $\mathcal{P}(\alpha)$ will yield asymptotically optimal parameters. We now describe a full optimization procedure using the following steps.

- First, solve the optimization problem with respect to $(\alpha^{(i)})_{i\in I_{\min}}$, following the procedure described in the previous paragraph, and neglecting the contribution of critical points which are not low energy separating saddle points. In other words, find

$$\alpha^\star_{I_{\min}} \in \operatorname*{Argmax}_{\alpha\in(-\infty,+\infty]^{|I_{\min}|}} \frac{\min\left\{\ell(z_0), \min\limits_{i\in I_{\min}} \lambda_i(\alpha^{(i)})\right\}}{\displaystyle\sum_{i\in I_{\min}} \frac{|\nu_1^{(i)}|}{2\pi\Phi\left(|\nu_1^{(i)}|^{\frac{1}{2}}\alpha^{(i)}\right)}\sqrt{\frac{\det\nabla^2 V(z_0)}{|\det\nabla^2 V(z_i)|}}}.$$

  For each optimum $\alpha^\star_{I_{\min}} = (\alpha^{(i)\star})_{i\in I_{\min}}$, there exists an associated optimal harmonic eigenvalue

$$\lambda\left(\alpha^\star_{I_{\min}}\right) = \min\left\{\ell(z_0), \min_{i\in I_{\min}} \lambda_i(\alpha^{(i)\star})\right\}.$$

- Then, any value of $\alpha^{(i)} \in \mathcal{P}(\alpha)$ for which $\lambda_i(\alpha^{(i)})$ is larger than $\lambda(\alpha^\star_{I_{\min}})$ is optimal. In other words, the structure of the set of optimal parameters with respect to $\mathcal{P}(\alpha)$ is particularly simple: it is simply the Cartesian product

$$\prod_{i\notin\{0\}\cup\mathcal{X}(z_0)\cup I_{\min}} (-\infty, \alpha^{(i)\star}], \qquad \text{where } \lambda_i(\alpha^{(i)\star}) = \lambda(\alpha^\star_{I_{\min}}).$$

  The full set of optimal α can be deduced by taking a union over the set of optimizers $\alpha^\star_{I_{\min}}$.

For a system which is reasonably isotropic (in the sense that the $\nu_j^{(i)}$ do not span many orders of magnitude), it is sensible to expect that for many saddle points z_i such that $\alpha^{(i)} \in \mathcal{P}(\alpha)$, any $\alpha^{(i)\star} \in (-\infty, +\infty]$ is optimal, particularly if $\mathrm{Ind}(z_i) \gg 1$. For such points, the asymptotic separation of timescales is insensitive at leading order to the choice of $\alpha^{(i)}$.

The effect of other minima. In the particular case that z_i is a local minimum (i.e. $1 \leqslant i < N_0$), it holds from the second item in Lemma 2.22 that $\lim\limits_{\alpha^{(i)}\to+\infty} \lambda_i(\alpha^{(i)}) = 0$, and thus $\alpha^{(i)\star}$ is finite. This indicates that, in the low-temperature regime, the separation of timescales ultimately degrades when moving from a domain containing one minimum far from the boundary (such as a neighborhood of $\mathcal{A}(z_0)$) to one containing several, such as an energy superbasin. This suggests the existence of a locally optimal domain around $\mathcal{A}(z_0)$, which is indeed observed numerically in [51]. This observation also motivates a posteriori the choice of Assumption (**EK1**), which restricts the class of considered domains to the vicinity of $\mathcal{A}(z_0) \cap \{V < V^*\}$.

2.4 Proof of Theorem 2.16

In this section, we perform the construction of the harmonic approximation to the Witten Laplacian (2.44), and give the proof of Theorem 2.16. The construction relies on the definition of local models for the Witten Laplacian H_β defined in (2.14), and a family of approximate eigenmodes, or quasimodes, thereof. These quasimodes correspond in fact to exact eigenmodes of the harmonic approximation, or of a carefully chosen realization thereof, pointwise multiplied

by a smooth cutoff function to localize the analysis. The harmonic approximation itself is obtained by considering a direct sum of local models around each critical point z_i, which are quantum harmonic oscillators supplemented with appropriate Dirichlet boundary conditions, depending on the value of the limit $\alpha^{(i)} \in (-\infty, +\infty]$.

In Section 2.4.1, we define formally the local models serving in the construction of the harmonic approximation, before discussing in Section 2.4.2 their Dirichlet realization and obtaining the required properties of their spectral decomposition. In Section 2.4.3, we define the global harmonic approximation and the associated harmonic quasimodes in Section 2.4.4, obtaining also crucial localization estimates. In Section 2.4.5, we derive a key technical result related to the construction of an extended domain with a precise control on the shape of the boundary near critical points, and finally prove Theorem 2.16 in Section 2.4.6.

2.4.1 Local harmonic models

The potential part of $H_\beta = -\Delta + U_\beta$, given by $U_\beta = \frac{1}{2}\left(\beta^2 \frac{|\nabla V|^2}{2} - \beta \Delta V\right)$ is, at dominant order in β, comprised of wells centered around the critical points of V, which become steeper as $\beta \to \infty$. The purpose of the harmonic approximation is to approximate H_β using independent local models consisting of shifted harmonic oscillators centered around each one of these wells, with frequencies prescribed by the eigenvalues of the Hessian $\nabla^2 V$ at z_i. This very simple approximation is sufficient to estimate the first-order behavior of the bottom of the spectrum of $-\mathcal{L}_\beta$.

Introduce

$$\Sigma^{(i)} = \frac{1}{2}\nabla^2\left(\frac{1}{4}|\nabla V|^2\right)(z_i) = \frac{1}{2}\left[\frac{1}{2}D^3 V \nabla V + \frac{1}{2}\left(\nabla^2 V\right)^2\right](z_i) = \frac{1}{4}\left(\nabla^2 V\right)^2(z_i).$$

We define local harmonic approximations to H_β around each critical point as

$$H_\beta^{(i)} = -\Delta + \beta^2 (x - z_i)^\intercal \Sigma^{(i)} (x - z_i) - \beta \frac{\Delta V(z_i)}{2}. \tag{2.29}$$

Remark 2.20. The operators $H_\beta^{(i)}$ have a natural interpretation in terms of the original stochastic dynamics (2.1). Indeed, a direct computation shows that $\beta^{-1} H_\beta^{(i)}$ is formally conjugate (up to an additive constant) to

$$-\mathcal{L}_\beta^{(i)} = -\frac{1}{\beta}\Delta + x^\intercal \nabla^2 V(z_i) \nabla,$$

under the change of representation $u \mapsto \mathrm{e}^{-\beta V^{(i)}/2} u(z_i + \cdot)$ to the flat L^2 coordinates, where $V^{(i)}(x)$ is the local harmonic approximation to V, namely $V^{(i)}(x) = V(z_i) + x^\intercal \frac{\nabla^2 V(z_i)}{2} x$. Hence, $\mathcal{L}_\beta^{(i)}$ may be seen as the generator of a diffusion of the form (2.1), in which the potential has been replaced by its harmonic approximation around z_i, so that the resulting stochastic process is a generalized Ornstein–Uhlenbeck process. We stress that this interpretation is merely formal, as the operator $\mathcal{L}_\beta^{(i)}$ is typically not well-behaved, since the measure $\mathrm{e}^{-\beta V^{(i)}(x)}\,\mathrm{d}x$ is not even finite if $i \geqslant N_0$, due to the presence of repulsive modes in the harmonic approximation.

We then define the shifted harmonic oscillators:

$$K^{(i)} = -\Delta + x^{\intercal}\mathcal{D}^{(i)}x - \frac{\Delta V(z_i)}{2},$$

where $\mathcal{D}^{(i)}$ denotes the diagonal matrix $\mathcal{D}^{(i)} = \operatorname{diag}\left(\nu_j^{(i)2}/4\right)_{j=1,\dots,d}$. By dilation $D_\lambda f(x) = \lambda^{d/2} f(\lambda x)$, translation $T_b f(x) = f(x-b)$ and rotation $\mathcal{U}^{(i)}$, where we recall the notation (2.7), a direct computation shows that the Dirichlet realization of $H_\beta^{(i)}$ on $L^2(\Omega_\beta)$ is unitarily equivalent to that of $\beta K^{(i)}$ on $L^2(\sqrt{\beta}U^{(i)\intercal}(\Omega_\beta - z_i))$:

$$H_\beta^{(i)} = T_{z_i} D_{\sqrt{\beta}} \mathcal{U}^{(i)} \left(\beta K^{(i)}\right) \mathcal{U}^{(i)*} D_{1/\sqrt{\beta}} T_{-z_i}. \tag{2.30}$$

This is precisely the construction performed in [195] on $L^2(\mathbb{R}^d)$, up to our choice of conjugating $H_\beta^{(i)}$ by $\mathcal{U}^{(i)}$ to simplify the explicit form of tensorized eigenmodes. We next proceed in Section 2.4.2 to compute the eigendecomposition for a family of self-adjoint realizations of the harmonic oscillators $K^{(i)}$, corresponding to specific Dirichlet boundary conditions in which the boundary is a hyperplane transverse to the eigendirection $v_1^{(i)}$ whenever $\alpha^{(i)} < +\infty$. These operators in turn will serve as local approximations of H_β around each critical point, allowing the construction of approximate low-temperature quasimodes for H_β.

Before this, we recall standard results concerning the full one-dimensional harmonic oscillator, see for instance [318], and introduce some notation. The operator $\frac{1}{2}\left(-\partial_x^2 + x^2\right)$ considered on $L^2(\mathbb{R})$, the canonical oscillator, which we denote by $\mathfrak{H}_\infty$, is self-adjoint as the Friedrich extension of a positive quadratic form. We denote, for $k \in \mathbb{N}$,

$$v_{k,\infty}(x) = \frac{1}{\sqrt{2^k k! \sqrt{\pi}}} \mathrm{e}^{-\frac{x^2}{2}} H_k(x), \qquad H_k(x) = \mathrm{e}^{x^2} \partial_x^k \, \mathrm{e}^{-x^2} \tag{2.31}$$

where H_k is the k-th Hermite polynomial. The function $v_{k,\infty}$ is the k-th eigenstate of $\mathfrak{H}_\infty$, with

$$\mathfrak{H}_\infty v_{k,\infty} = \mu_{k,\infty} v_{k,\infty}, \qquad \mu_{k,\infty} = k + \frac{1}{2}.$$

The full harmonic oscillator will serve, as in [195, Chapter 11], as the base operator to construct local models for H_β associated with critical points which are far from the boundary, and will also be useful to capture the behavior of modes transverse to the first eigendirection of the Hessian for critical points which are close to the boundary. For the first eigendirection, however, we need to use another model, which is a harmonic oscillator with a Dirichlet boundary condition on the asymptotic hyperplane $z_i + \partial E(\alpha^{(i)}/\sqrt{\beta})$. In fact, to handle the possibly irregular nature of $\partial\Omega_\beta$ in the vicinity of critical points which are close to the boundary, we need to define these Dirichlet oscillators for a range of boundary conditions.

2.4.2 Dirichlet oscillators

In this section, we introduce the appropriate Dirichlet realizations for the harmonic oscillator, which serve as the basis for the construction of local models for H_β around critical points

which are close to the boundary. We consider the following dense subspace of $L^2(\mathbb{R}_+^*)$:

$$\mathcal{D}(\widetilde{\mathfrak{H}_0}) = \left\{ f : x^2 f \in L^2(\mathbb{R}_+^*),\ f \in \mathcal{C}^1(\mathbb{R}_+^*), f' \in \mathrm{AC}(\mathbb{R}_+^*),\ f'' \in L^2(\mathbb{R}_+^*),\ f(0) = 0 \right\}.$$

We first recall classical properties of the Dirichlet harmonic half-oscillator (see for instance [276, Chapter X.1] or [32, Section 5.1.2] for a closely related construction): the symmetric operator

$$\widetilde{\mathfrak{H}}_0 = \frac{1}{2}(-\partial_x^2 + x^2)$$

with domain $\mathcal{D}(\widetilde{\mathfrak{H}}_0)$ is essentially self-adjoint. Its closure, denoted by $\mathfrak{H}_0$, has a complete family of eigenfunctions which are given explicitly by the odd states of the full harmonic oscillator:

$$\mathfrak{H}_0 v_{2k+1,\infty} = \left(2k + \frac{3}{2}\right) v_{2k+1,\infty}, \qquad k \in \mathbb{N}.$$

The family $(\sqrt{2}v_{2k+1,\infty})_{k\geqslant 0}$ is an orthonormal eigenbasis for $\mathfrak{H}_0$, where the factor $\sqrt{2}$ enforces normalization in $L^2(\mathbb{R}_+)$. Furthermore, $\mathfrak{H}_0$ has compact resolvent, with $\mathcal{D}(\mathfrak{H}_0) \subset H_0^1(\mathbb{R}_+)$. Our aim is to make precise, for $\theta \in \mathbb{R}$, the spectrum of a self-adjoint realization of the canonical oscillator $\frac{1}{2}(-\partial_x^2 + x^2)$ with Dirichlet boundary conditions on $[-\theta, +\infty)$. Specifically, we show that the spectrum is well-defined, purely discrete, and depends continuously on the position of the boundary θ. To this end, we use analytic perturbation theory, noticing that by translation, the spectral properties of the operator

$$\widetilde{\mathfrak{H}}_\theta = \frac{1}{2}(-\partial_x^2 + x^2), \qquad \mathcal{D}(\widetilde{\mathfrak{H}}_\theta) = T_{-\theta}\mathcal{D}(\widetilde{\mathfrak{H}}_0)$$

can be deduced from those of the conjugate operator

$$T_\theta \widetilde{\mathfrak{H}}_\theta T_{-\theta} = \frac{1}{2}(-\partial_x^2 + x^2) - \theta x + \frac{\theta^2}{2}, \tag{2.32}$$

with domain $\mathcal{D}(\widetilde{\mathfrak{H}_0})$. Since the constant $\frac{\theta^2}{2}$ only shifts the spectrum by an analytic function of θ, it is sufficient to study the operator

$$\widetilde{\mathfrak{G}}_\theta = \widetilde{\mathfrak{H}}_0 - \theta x.$$

We show the following result.

Lemma 2.21. *The operator $\widetilde{\mathfrak{G}}_\theta$ is essentially self-adjoint, and its closure $\mathfrak{G}_\theta$ has compact resolvent. For any $k \geqslant 0$, the normalized eigenpairs $(\widetilde{\mu}_{k,\theta}, \widetilde{v}_{k,\theta}) \in \mathbb{R} \times L^2(\mathbb{R}_+)$ are defined by*

$$\mathfrak{G}_\theta \widetilde{v}_{k,\theta} = \widetilde{\mu}_{k,\theta}\widetilde{v}_{k,\theta}, \qquad \|\widetilde{v}_{k,\theta}\|^2_{L^2(\mathbb{R}_+)} = 1, \tag{2.33}$$

furthermore, the eigenpairs $(\mu_{k,\theta}, \widetilde{v}_{k,\theta})$ can be chosen to be holomorphic functions of θ. Their enumeration convention is fixed by the condition that $\widetilde{v}_{k,0}$ is an eigenstate of the half-harmonic oscillator: $\widetilde{v}_{k,0} = \sqrt{2}v_{2k+1,\infty}$.

Proof. We check that θx is $\widetilde{\mathfrak{H}}_0$-bounded with relative bound 0. In the following, norms and

inner products are for $L^2(0,\infty)$. For $\varphi \in \mathcal{C}_c^\infty([0,+\infty))$ and any $M > 0$, we compute:

$$\begin{aligned}\|\theta x\varphi\|^2 &= \theta^2\langle x^2\varphi,\varphi\rangle \\ &\leqslant 2\theta^2\left\langle \widetilde{\mathfrak{H}}_0\varphi,\varphi\right\rangle \\ &\leqslant \theta^2M^2\|\varphi\|^2 + \frac{\theta^2}{M^2}\|\widetilde{\mathfrak{H}}_0\varphi\|^2,\end{aligned}$$

using Cauchy–Schwarz and Young inequalities in the last line. It follows that

$$\|\theta x\varphi\| \leqslant |\theta|M\|\varphi\| + \frac{|\theta|}{M}\left\|\widetilde{\mathfrak{H}}_0\varphi\right\|, \tag{2.34}$$

and the claim follows by taking $M \to \infty$.

Since θx is $\widetilde{\mathfrak{H}}_0$-bounded with relative bound 0, by the Kato–Rellich theorem (see for instance [318, Theorem 6.4]), the operator $\widetilde{\mathfrak{G}}_\theta = \widetilde{\mathfrak{H}}_0 + \theta x$ is essentially self-adjoint on $\mathcal{D}(\widetilde{\mathfrak{H}}_0)$, and its unique self-adjoint extension has domain $\mathcal{D}(\mathfrak{G}_\theta) = \mathcal{D}(\mathfrak{H}_0) \subset H_0^1(\mathbb{R}_+)$ independently of θ. We denote by $\mathfrak{G}_\theta$ the closure of $\widetilde{\mathfrak{G}}_\theta$. A straightforward consequence of the relative bound (2.34) (which extends to the closures of the operators at play) and the compactness of the resolvent of $\mathfrak{H}_0$ is that, for fixed $\theta \in \mathbb{R}$ and $\operatorname{Im}\lambda \neq 0$, the resolvent $(\mathfrak{G}_\theta - \lambda)^{-1}$ is a compact operator. Hence $\mathfrak{G}_\theta$ also has a compact resolvent, and therefore purely discrete a spectrum. Since this spectrum is manifestly bounded from below, it consists of isolated eigenvalues of finite multiplicity tending to $+\infty$. Standard results of perturbation theory (see [192, Chapter VII]) apply. In particular, we get from (2.34) and [192, Theorems VII.2.6 and VII.3.9] that $\mathfrak{G}_\theta$ defines a self-adjoint holomorphic family of type (A) for $\theta \in \mathbb{R}$, and that there exists, for every $k \in \mathbb{N}$, holomorphic functions of θ $\widetilde{\mu}_{k,\theta}$, $\widetilde{v}_{k,\theta}$ satisfying (2.33). □

Let us denote by $\mathfrak{H}_\theta$ the self-adjoint operator on $L^2([-\theta,+\infty))$ obtained by translating back and appropriately shifting the spectrum by $\theta^2/2$ (recalling (2.32)):

$$\mathfrak{H}_\theta := T_{-\theta}\mathfrak{G}_\theta T_\theta + \frac{\theta^2}{2}.$$

We compute its eigenpairs $\mu_{k,\theta} = \widetilde{\mu}_{k,\theta} + \frac{\theta^2}{2}$, and $v_{k,\theta} = T_{-\theta}\widetilde{v}_{k,\theta}$, satisfying the relation:

$$\mathfrak{H}_\theta v_{k,\theta} = \mu_{k,\theta}v_{k,\theta},$$

where $(v_{k,\theta})_{k\in\mathbb{N}}$ is a dense orthonormal family in $L^2([-\theta,+\infty))$. Moreover, the enumeration of these eigenpairs is fixed by the convention chosen for the harmonic half-oscillator, namely:

$$v_{k,0} = \sqrt{2}v_{2k+1}, \qquad \mu_{k,0} = 2k + \frac{3}{2},$$

and the eigenvalues $\mu_{k,\theta}$ depend holomorphically, hence continuously, on θ.

We provide the following estimates on the principal eigenvalue $\mu_{0,\theta}$ in the regimes $\theta \to \pm\infty$, which are useful for the application of our results to asymptotic shape optimization (see Section 2.3.3).

Lemma 2.22. *It holds*

$$\mu_{0,\theta} = \frac{\theta^2}{2} + \mathcal{O}(|\theta|^{2/3}) \text{ in the limit } \theta \to -\infty, \tag{2.35}$$

$$\text{and } \lim_{\theta\to+\infty} \mu_{0,\theta} = \mu_{0,\infty} = \frac{1}{2}. \tag{2.36}$$

Proof. By unitary transformation, we equivalently estimate the principal Dirichlet eigenvalue of $\mathfrak{H}_\theta$ on $L^2(-\theta, +\infty)$.

Let us show (2.35). Note first that, since $x^2/2$ is bounded from below by $\theta^2/2$ on $(-\theta, +\infty)$, it clearly holds that $\mu_{0,\theta} \geqslant \theta^2/2$, so there is a trivial lower bound. The proof of the estimate 2.35 given below does not rely on a variational argument, but rather on a connection with the asymptotics of Hermite polynomials. Let, for any $n \geqslant 1$, $\zeta_n \geqslant 0$ be the largest root of the n-th Hermite polynomial H_n, where we recall the definition (2.31) of the eigenmodes for the full harmonic oscillator $\mathfrak{H}_\infty$. Then, it holds that $\mu_{0,-\zeta_n} = n + \frac{1}{2}$. Indeed, the restriction of the n-th eigenfunction $w_{n,\infty}$ to the nodal domain $(\zeta_n, +\infty)$ is a signed eigenfunction of $\mathfrak{H}_{-\zeta_n}$, with eigenvalue $\omega_{n,\infty} = n + \frac{1}{2}$. By standard arguments, it must in fact be a principal eigenfunction. Indeed, if u minimizes the quadratic form, so does $|u|$, hence there exist a signed principal eigenfunction. If v is an eigenfunction for some higher eigenvalue, it may therefore not be signed without violating the orthogonality condition.

From the domain monotonicity property of Dirichlet eigenvalues (see Proposition 2.33), it holds for $-\zeta_{n+1} \leqslant \theta \leqslant -\zeta_n$, that $n + \frac{3}{2} \geqslant \mu_{0,\theta} \geqslant n + \frac{1}{2}$. Therefore, $n(\theta) + \frac{3}{2} \geqslant \mu_{0,\theta} \geqslant n(\theta) + \frac{1}{2}$, where $n(\theta) = \max\{n \geqslant 1 : \theta \leqslant -\zeta_n\}$.

In [311, Theorem 6.32], Szegö gives the estimate $\zeta_n = \sqrt{2n+1} + \mathcal{O}(n^{-1/6})$, from which we get
$\sqrt{2n(\theta)}(1 + o(1)) = |\theta|$ and $\theta^2/C \leqslant n(\theta) \leqslant C\theta^2$ for some $C > 0$. Using Szegö's estimate once again,

$$\sqrt{2n(\theta)+1} + \mathcal{O}(|\theta|^{-1/3}) \leqslant |\theta| < \sqrt{2n(\theta)+3} + \mathcal{O}(|\theta|^{-1/3}),$$

from which $n(\theta) = \frac{\theta^2}{2} + \mathcal{O}(|\theta|^{2/3})$ and the final estimate (2.35) easily follows.

We now show (2.36). The domain monotonicity principle yields the lower bound $\mu_{0,\theta} \geqslant \mu_{0,\infty} = \frac{1}{2}$. Let us show an asymptotic upper bound. We introduce $\chi_\theta : \mathbb{R} \to \mathbb{R}$ a $\mathcal{C}^\infty$ cutoff function such that

$$\mathbb{1}_{(-\theta+1,+\infty)} \leqslant \chi_\theta \leqslant \mathbb{1}_{(-\theta,+\infty)},$$

and denote by $\overline{\chi}_\theta = \sqrt{1-\chi_\theta^2}$. We may choose χ_θ such that $\|\partial_x \chi_\theta\|_{L^\infty(\mathbb{R})}, \|\partial_x \overline{\chi}_\theta\|_{L^\infty(\mathbb{R})} \leqslant C$ for some $C > 0$ independent of θ. This may be enforced simply by setting $\chi_\theta = \chi_0(\cdot + \theta)$ for a suitably chosen χ_0.

Consider the trial quasimode $u_\theta = \chi_\theta v_{0,\infty} \in \mathcal{D}(\mathfrak{H}_\theta)$, where $v_{0,\infty}(x) = \pi^{-1/4} \mathrm{e}^{-\frac{x^2}{2}}$ is defined in (2.31). It first holds that

$$1 = \|v_{0,\infty}\|^2_{L^2(\mathbb{R})} = \|u_\theta\|^2_{L^2(\mathbb{R})} + \|\overline{\chi}_\theta v_{0,\infty}\|^2_{L^2(\mathbb{R})},$$

using $\chi_\theta^2 + \overline{\chi}_\theta^2 = 1$. Then, since $\overline{\chi_\theta} \leqslant \mathbb{1}_{(-\infty,-\theta+1)}$, we obtain $\|\overline{\chi_\theta} v_{0,\infty}\|^2_{L^2(\mathbb{R})} = \mathcal{O}\left(\mathrm{e}^{-(\theta-1)^2}\right) =$

$\mathcal{O}\left(\mathrm{e}^{-\theta^2/2}\right)$ as $\theta \to +\infty$ by a Gaussian tail bound. Hence, $\|u_\theta\|^2_{L^2(-\theta,+\infty)} = \|u_\theta\|^2_{L^2(\mathbb{R})} = 1 + \mathcal{O}(\mathrm{e}^{-\theta^2/2})$.

The IMS localization formula (see [303, 195]) then gives

$$\begin{aligned}\frac{1}{2} &= \langle \mathfrak{H}_\infty v_{0,\infty}, v_{0,\infty}\rangle_{L^2(\mathbb{R})} \\ &= \langle \mathfrak{H}_\infty u_\theta, u_\theta\rangle_{L^2(\mathbb{R})} + \langle \mathfrak{H}_\infty \overline{\chi}_\theta v_{0,\infty}, \overline{\chi}_\theta v_{0,\infty}\rangle_{L^2(\mathbb{R})} - \frac{1}{2}\left\|\sqrt{(\partial_x\chi_\theta)^2 + (\partial_x\overline{\chi}_\theta)^2}\, v_{0,\infty}\right\|^2_{L^2(\mathbb{R})}.\end{aligned}$$

Since $\operatorname{supp}\partial_x\chi_\theta$, $\operatorname{supp}\partial_x\overline{\chi}_\theta \subset (-\theta, -\theta+1)$ and these derivatives are uniformly bounded in θ, it holds that $\left\|\sqrt{(\partial_x\chi_\theta)^2 + (\partial_x\overline{\chi}_\theta)^2}\, v_{0,\infty}\right\|^2_{L^2(\mathbb{R})} = \mathcal{O}(\mathrm{e}^{-\theta^2/2})$ by the same Gaussian estimate. Finally,

$$\langle \mathfrak{H}_\infty \overline{\chi}_\theta v_{0,\infty}, \overline{\chi}_\theta v_{0,\infty}\rangle_{L^2(\mathbb{R})} = \frac{1}{2}\|\partial_x(\overline{\chi_\theta} v_{0,\infty})\|^2_{L^2(\mathbb{R})} + \frac{1}{2}\|x\overline{\chi_\theta} v_{0,\infty}\|^2_{L^2(\mathbb{R})} = \mathcal{O}(\mathrm{e}^{-\theta^2/3}),$$

using again $\operatorname{supp}\partial_x\overline{\chi}_\theta \subset (-\theta, -\theta+1)$, $\overline{\chi}_\theta \leqslant \mathbb{1}_{(-\infty,-\theta+1)}$ and $\|\partial_x\overline{\chi}_\theta\|^2_{L^\infty(\mathbb{R})} \leqslant C$. The loss of a multiplicative constant in the exponent is due to the absorption of the $\frac{x^2}{2}$ term from the potential.

It follows that

$$\mu_{0,\theta} \leqslant \frac{\langle \mathfrak{H}_\theta u_\theta, u_\theta\rangle_{L^2(-\theta,+\infty)}}{\|u_\theta\|^2_{L^2(-\theta,+\infty)}} = \frac{\langle \mathfrak{H}_\infty u_\theta, u_\theta\rangle_{L^2(\mathbb{R})}}{\|u_\theta\|^2_{L^2(\mathbb{R})}} = \frac{1}{2}\left(1 + \mathcal{O}(\mathrm{e}^{-\theta^2/3})\right),$$

and (2.36) follows upon taking the lim sup as $\theta \to +\infty$ on both sides of this inequality. □

Note that the strategies to show (2.35) and (2.36) can easily be adapted to treat the asymptotics of higher eigenvalues $\mu_{k,\theta}$ of the Dirichlet oscillators $\mathfrak{H}_\theta$, using respectively estimates on the k-th largest root of the Hermite polynomials, and the trial family of quasi-modes $\{\chi_\theta v_{0,\infty}, \dots, \chi_\theta v_{k,\infty}\}$. We now construct the local harmonic oscillators entering in the harmonic approximation to the Witten Laplacian (2.14), by considering tensorized eigenmodes of one-dimensional oscillators. As many notations are used, we provide for convenience Table 2.1, which summarizes the notations used for the various operators at play.

One-dimensional case. In view of the change of variables $z = \sqrt{\frac{|\nu_1^{(i)}|}{2}}x$ which is such that $\frac{\nu_1^{(i)2}}{4}x^2 - \partial_x^2 = |\nu_1^{(i)}|\frac{1}{2}\left(z^2 - \partial_z^2\right)$, we denote, for $k \geqslant 0$ and $\theta \in \mathbb{R}\cup\{+\infty\}$,

$$K_\theta^{(i)} = |\nu_1^{(i)}| R D_{|\nu_1^{(i)}/2|^{\frac{1}{2}}} \mathfrak{H}_{\theta|\nu_1^{(i)}/2|^{1/2}} D_{|\nu_1^{(i)}/2|^{-\frac{1}{2}}} R - \frac{\nu_1^{(i)}}{2},$$

where $Ru(x) = u(-x)$ denotes the reflection operator, which accounts for the orientation convention chosen for $v_1^{(i)}$. The spectrum of $K_\theta^{(i)}$ is explicit in terms of the $\mu_{k,\theta}$, with the

following expressions for the eigenpairs:

$$w_{k,\theta}^{(i)}(x) = \left(\frac{|\nu_1^{(i)}|}{2}\right)^{\frac{1}{4}} v_{k,\theta(|\nu_1^{(i)}|/2)^{\frac{1}{2}}}\left(-\sqrt{\frac{|\nu_1^{(i)}|}{2}}x\right), \qquad \omega_{k,\theta}^{(i)} = |\nu_1^{(i)}|\mu_{k,\theta(|\nu_1^{(i)}|/2)^{\frac{1}{2}}} - \frac{\nu_1^{(i)}}{2}. \quad (2.37)$$

It is immediate, from the construction performed above, that $(w_{k,\theta}^{(i)})_{k\geqslant 0}$ forms a complete orthonormal eigenbasis for the Dirichlet realization of the oscillator $K_\theta^{(i)}$ on $L^2((-\infty,\theta))$, hence $K_\theta^{(i)}$ is self-adjoint with

$$\mathcal{D}(K_\theta^{(i)}) \subset H_0^1(-\infty,\theta).$$

Multidimensional case. The higher dimensional case is obtained by considering a separable Schrödinger operator acting on the first coordinate as a one-dimensional Dirichlet oscillator, and on the $(d-1)$ transverse coordinates as full one-dimensional (scaled) harmonic oscillators. More precisely, we define $K_\theta^{(i)}$ as the closure of the essentially self-adjoint operator (see e.g. [276, Chapter X] for background on self-adjoint extensions)

$$\begin{aligned}&\left[|\nu_1^{(i)}|RD_{|\nu_1^{(i)}/2|^{\frac{1}{2}}}\mathfrak{H}_{\theta|\nu_1^{(i)}/2|^{1/2}}D_{|\nu_1^{(i)}/2|^{-\frac{1}{2}}}R\right]_1 \otimes \mathbb{I}_1\\ &+\sum_{j=2}^{d}\left[|\nu_j^{(i)}|D_{|\nu_j^{(i)}/2|^{\frac{1}{2}}}\mathfrak{H}_\infty D_{|\nu_j^{(i)}/2|^{-\frac{1}{2}}}\right]_j \otimes \mathbb{I}_j - \frac{\Delta V(z_i)}{2},\end{aligned}$$

where we define, given d Hilbert spaces $(\mathcal{H}_j)_{j=1,\dots,d}$ and an unbounded operator A on $\mathcal{H}_j$, the operator $A_j \otimes \mathbb{I}_j$ acting on $\bigotimes_{j=1}^d \mathcal{H}_j$ via

$$A_j \otimes \mathbb{I}_j(f_1 \otimes \cdots \otimes f_j) = f_1 \otimes \cdots \otimes f_{j-1} \otimes Af_j \otimes f_{j+1} \otimes \cdots \otimes f_d.$$

We naturally identify $K_\theta^{(i)}$ with a self-adjoint operator on $L^2((-\infty,\theta)\times\mathbb{R}^{d-1})$. Its eigendecomposition is explicit, and enumerated by $n=(n_1,\dots,n_d)\in\mathbb{N}^d$:

$$\begin{aligned}\lambda_{n,\theta}^{(i)} &= \omega_{n_1,\theta}^{(i)} + \sum_{j=2}^{d}\left[|\nu_j^{(i)}|\mu_{n_j,\infty} - \frac{\nu_j^{(i)}}{2}\right],\\ \psi_{n,\theta}^{(i)}(x) &= w_{n_1,\theta}^{(i)}(x_1)\prod_{j=2}^{d}\left[\left(\frac{|\nu_j^{(i)}|}{2}\right)^{\frac{1}{4}} v_{n_j,\infty}\left(\sqrt{\frac{|\nu_j^{(i)}|}{2}}x_j\right)\right].\end{aligned} \quad (2.38)$$

Moreover, the domain satisfies the inclusion

$$\mathcal{D}(K_\theta^{(i)}) \subset H_0^1\left[(-\infty,\theta)\times\mathbb{R}^{d-1}\right].$$

It is often more convenient to enumerate the spectrum of $K_\theta^{(i)}$ with integers instead. Here we slightly abuse notation, and again write the spectrum

$$\mathrm{Spec}(K_\theta^{(i)}) = \left(\lambda_{n,\theta}^{(i)}\right)_{n\geqslant 1} \quad (2.39)$$

in a non-decreasing sequence of eigenvalues. The indexing convention used will be clear from the context.

Operator	Spatial domain	Eigenstates	Eigenvalues
$\frac{1}{2}(-\partial_x^2 + x^2)$	$(-\theta, +\infty)$	$v_{k,\theta}$	$\mu_{k,\theta}$
$K_\theta^{(i)}$, $d = 1, \theta \in \mathbb{R} \cup \{+\infty\}$	$(-\infty, \theta)$	$w_{k,\theta}^{(i)}, k \geqslant 0$	$\omega_{k,\theta}^{(i)}, k \geqslant 0$
$K_\theta^{(i)}$, $d \geqslant 2, \theta \in \mathbb{R} \cup \{+\infty\}$	$(-\infty, \theta) \times \mathbb{R}^{d-1}$	$\psi_{k,\theta}^{(i)}$, $k \in \mathbb{N}^d$ or $\mathbb{N}^*$	$\lambda_{k,\theta}^{(i)}$, $k \in \mathbb{N}^d$ or $\mathbb{N}^*$
$H_{\beta,\theta}^{(i)}$, $\theta \in \mathbb{R} \cup \{+\infty\}$	$z_i + E^{(i)}\left(\frac{\theta}{\sqrt{\beta}}\right)$	$\psi_{\beta,k,\theta}^{(i)}, k \geqslant 1$	$\beta\lambda_{k,\theta}^{(i)}, k \geqslant 1$
$H_{\beta,\alpha}^{\mathrm{H}}$, $\alpha \in (\mathbb{R} \cup \{+\infty\})^N$	$\prod_{i=0}^{N-1}\left[z_i + E^{(i)}\left(\frac{\alpha_i}{\sqrt{\beta}}\right)\right]$	$\psi_{\beta,k,\alpha}^{\mathrm{H}} = \psi_{\beta,n_k,\alpha_{i_k}}^{(i_k)}, k \geqslant 1$	$\beta\lambda_{k,\alpha}^{\mathrm{H}} = \beta\lambda_{n_k,\alpha_{i_k}}^{(i_k)}, k \geqslant 1$

Table 2.1: Notations used in the definition of the harmonic approximation

When the need arises, we will consider $\psi_{n,\theta}^{(i)}$ as an element of $L^2(\mathbb{R}^d)$ by extending it by zero outside of $(-\infty, \theta) \times \mathbb{R}^{d-1}$. A crucial tool in our analysis is the following pointwise decay estimate for these harmonic Dirichlet eigenmodes.

Lemma 2.23. *For any $n \in \mathbb{N}^d$, $\theta \in (-\infty, \infty]$ and $0 \leqslant i < N$, there exists a constant $C_{i,n,\theta} > 0$ such that the following inequality holds for every $x \in \mathbb{R}^d$:*

$$|\psi_{n,\theta}^{(i)}(x)| \leqslant C_{i,n,\theta}\, \mathrm{e}^{-\frac{|x|^2}{C_{i,n,\theta}}}. \tag{2.40}$$

Proof. The proof relies on a probabilistic estimate obtained in [67], and a reflection argument. We consider the following anti-symmetrization of the eigenmode $\psi_{n,\theta}^{(i)}$:

$$\widetilde{\psi}_{n,\theta}^{(i)}(x) = \psi_{n,\theta}^{(i)}(x)\mathbb{1}_{x_1 \leqslant \theta} - \psi_{n,\theta}^{(i)}(\iota_\theta x)\mathbb{1}_{x_1 > \theta},$$

where $\iota_\theta(x) = (2\theta - x_1, \dots, x_d)$ denotes the reflection with respect to the $\{x_1 = \theta\}$ hyperplane. Then, it is easy to check that $\widetilde{\psi}_{n,\theta}^{(i)}$ is also an eigenmode (for the same eigenvalue $\lambda_{n,\theta}^{(i)}$) of the Schrödinger operator associated with the symmetrized potential:

$$\widetilde{K}_\theta^{(i)} = -\Delta + \widetilde{W}^{(i)}, \quad \widetilde{W}^{(i)}(x) = W^{(i)}(x)\mathbb{1}_{x_1 \leqslant \theta} + W^{(i)}(\iota_\theta x)\mathbb{1}_{x_1 > \theta},$$

where $W^{(i)}(x) = x^\intercal \Sigma^{(i)} x$. Note that there exist $\varepsilon > 0$ and a compact set $B \subset \mathbb{R}^d$ such that

$$\widetilde{W}^{(i)} \geqslant \varepsilon |x|^2, \qquad \forall\, x \in \mathbb{R}^d \setminus B, \tag{2.41}$$

owing to the strict positivity of $\Sigma^{(i)}$ (recalling that z_i is a non-degenerate critical point). We consider $K_{\theta,\mathrm{sym}}^{(i)}$ to be the self-adjoint operator obtained by the Friedrichs extension of the lower-bounded quadratic form associated with $\widetilde{K}_\theta^{(i)}$. Then, it immediately follows from [67, Proposition 3.1] and the lower bound (2.41) that the pointwise estimate (2.40) holds for $\widetilde{\psi}_{n,\theta}^{(i)}$ and some constant $C_{i,n,\theta} > 0$. The proof is concluded, in view of the inequality $|\psi_{n,,\theta}^{(i)}(x)| \leqslant |\widetilde{\psi}_{n,\theta}^{(i)}(x)|$ for all $x \in \mathbb{R}^d$. □

2.4.3 Global harmonic approximation

We now define global harmonic approximations to H_β defined in (2.14). Because of the geometric flexibility afforded by Assumption (**H2**), we will in fact use this harmonic approximation for a variety of Dirichlet boundary conditions. Each of these boundary conditions will be encoded with a vector of extended real numbers $\alpha' = (\alpha'_i)_{0\leqslant i<N} \in (-\infty,\infty]^N$. In this context, a distinguished role is played by $\alpha' = \alpha$, where we recall the definition (2.23). Its components correspond to the asymptotic signed distance of each critical point to the boundary, on the scale $\beta^{-\frac{1}{2}}$, in view of Assumption (**H1**).

For general α', we define local oscillators $H^{(i)}_{\beta,\alpha'_i}$ from the definition $K^{(i)}_{\alpha'_i}$ (in the d-dimensional case) using the unitary equivalence (2.30). In particular, the domain of $H^{(i)}_{\beta,\alpha'_i}$ is given by

$$\mathcal{D}(H^{(i)}_{\beta,\alpha'_i}) = T_{z_i} D_{\sqrt{\beta}} \mathcal{U}^{(i)} \mathcal{D}\left(K^{(i)}_{\alpha'_i}\right) \subset H^1_0\left[z_i + E^{(i)}\left(\frac{\alpha'_i}{\sqrt{\beta}}\right)\right]. \tag{2.42}$$

We denote, for $n \in \mathbb{N}^d$,

$$\psi^{(i)}_{\beta,n,\alpha'_i}(x) = \beta^{\frac{d}{4}} \psi^{(i)}_{n,\alpha'_i}\left(\sqrt{\beta} U^{(i)\intercal}(x - z_i)\right), \tag{2.43}$$

the eigenmode of $H^{(i)}_{\beta,\alpha'_i}$ with the eigenvalue $\beta\lambda^{(i)}_{n,\alpha'_i}$ associated with $\psi^{(i)}_{n,\alpha'_i}$ under this correspondence. Notice that we introduce a prefactor β in the definition of the eigenvalues of $H^{(i)}_{\beta,\alpha'_i}$, which is related to the fact that $\mathcal{L}_\beta$ is unitarily equivalent to $-H_\beta/\beta$, see (2.14). Note the $\beta^{\frac{d}{4}}$ factor in (2.43), which accounts for L^2 normalization.

The global approximation is formed by a direct sum of these local oscillators:

$$H^{\mathrm{H}}_{\beta,\alpha'} = \bigoplus_{i=0}^{N-1} H^{(i)}_{\beta,\alpha'_i}, \qquad \mathcal{D}(H^{\mathrm{H}}_{\beta,\alpha'}) = \prod_{i=0}^{N-1} \mathcal{D}(H^{(i)}_{\beta,\alpha'_i}), \tag{2.44}$$

hence the harmonic spectrum is given by

$$\mathrm{Spec}(H^{\mathrm{H}}_{\beta,\alpha'}) = \left\{\beta\lambda^{(i)}_{n,\alpha'_i}\right\}_{\substack{0\leqslant i<N \\ n\in\mathbb{N}^d}}.$$

Let us specify the convention we use to enumerate the various spectra at play. First, we enumerate the spectrum of $K^{(i)}_{\alpha'_i}$ in non-decreasing order, according to the convention (2.39), with corresponding eigenmodes $(\psi^{(i)}_{m,\alpha})_{m\geqslant 1}$. We then enumerate the full harmonic spectrum in non-decreasing order, by defining two integer-valued sequences

$$(n_j)_{j\geqslant 1} \in (\mathbb{N}^*)^{\mathbb{N}^*}, \qquad (i_j)_{j\geqslant 1} \in \{0,\dots,N-1\}^{\mathbb{N}^*},$$

defined by the condition that the j-th largest eigenvalue of H^{H}_β, counted with multiplicity, is given by

$$\beta\lambda^{\mathrm{H}}_{j,\alpha'} = \beta\lambda^{(i_j)}_{n_j,\alpha'_{i_j}}, \tag{2.45}$$

where we first defer to the ordering on $\{0,\dots,N-1\}$ and then to the ordering on each $\mathrm{Spec}(K^{(i)}_{\alpha'_i})$

to resolve ambiguities due to degenerate eigenvalues. We note that this choice is arbitrary, since the ordering convention plays no particular part in the analysis. For convenience, we also define, for each $0 \leqslant i < N$, the function which gives for a $n \geqslant 1$ the number of states with energy lower than $\lambda^{\mathrm{H}}_{n,\alpha'}$ and localized around z_i:

$$\mathfrak{N}_i(n) = \#\{1 \leqslant j \leqslant n : i_j = i\}.$$

To lighten the notation, we have omitted to include the dependence of $\mathfrak{N}_i$, i_j and n_j in α', which will be clear from the context. We also note the following equalities, valid by definition for any $n \geqslant 1$:

$$\max_{0\leqslant i<N} \lambda^{(i)}_{\mathfrak{N}_i(n),\alpha'_i} = \lambda^{\mathrm{H}}_{n,\alpha'}, \qquad \min_{0\leqslant i<N} \lambda^{(i)}_{\mathfrak{N}_i(n)+1,\alpha'_i} = \lambda^{\mathrm{H}}_{n+1,\alpha'}, \qquad \sum_{i=0}^{N-1} \mathfrak{N}_i(n) = n. \tag{2.46}$$

In particular, an expression for the second eigenvalue of the harmonic approximation is available.

Remark 2.24. In the case where the bottom eigenvalue is associated to a local minimum z_0, i.e. $\mathfrak{N}_0(1) = 1$, $\mathfrak{N}_i(1) = 0$ for $0 < i < N$, then it holds

$$\lambda^{\mathrm{H}}_{2,\alpha'} = \min\left\{\lambda^{(0)}_{1,\alpha'_0}, \min_{0<i<N} \lambda^{(i)}_{0,\alpha'_i}\right\}.$$

In the particular case $\alpha'_0 = +\infty$, this gives, using the expression (2.38) and $\mu_{0,\infty} = 1/2$,

$$\begin{aligned}\lambda^{\mathrm{H}}_{2,\alpha'} &= \min\left\{\min_{1\leqslant j\leqslant d} \nu^{(0)}_j, \min_{0<i<N} \omega^{(i)}_{0,\alpha'_i} + \sum_{j=2}^{d} |\nu^{(i)}_j| \mathbb{1}_{\nu^{(i)}_j<0}\right\} \\ &= \min\left\{\min_{1\leqslant j\leqslant d} \nu^{(0)}_j, \min_{0<i<N} |\nu^{(i)}_1| \mu_{k,\theta(|\nu^{(i)}_1|/2)^{\frac{1}{2}}} - \frac{\nu^{(i)}_1}{2} + \sum_{j=2}^{d} |\nu^{(i)}_j| \mathbb{1}_{\nu^{(i)}_j<0}\right\},\end{aligned} \tag{2.47}$$

using equation (2.37) in the last line.

Finally, we note that the analyticity of the map $\alpha \mapsto \mu_{k,\alpha}$ obtained for all $k \in \mathbb{N}$ in Lemma 2.21 implies the continuity of the mapping $\alpha' \mapsto \lambda^{\mathrm{H}}_{n,\alpha'}$ for any $n \geqslant 1$.

2.4.4 Construction of harmonic quasimodes and associated localization estimates

Approximate eigenmodes of H_β may be obtained by localizing the eigenmodes of the harmonic approximation around the corresponding critical point, in such a way that the Dirichlet boundary conditions in Ω_β are met. We consider, for $\theta \in \mathbb{R} \cup \{+\infty\}$, so-called quasimodes of the form

$$\widetilde{\psi}^{(i)}_{\beta,n,\theta} = \frac{\chi^{(i)}_\beta \psi^{(i)}_{\beta,n,\theta}}{\|\chi^{(i)}_\beta \psi^{(i)}_{\beta,n,\theta}\|_{L^2(\Omega_\beta)}}, \tag{2.48}$$

where $\psi^{(i)}_{\beta,n,\theta}$ is a harmonic mode of $H^{(i)}_{\beta,\theta}$, defined in (2.43) multiplied by the cutoff function $\chi^{(i)}_\beta$, and normalized in $L^2(\Omega_\beta)$. The role of $\chi^{(i)}_\beta$ is to localize the quasimode in the vicinity of z_i.

To this effect, we fix a reference $\mathcal{C}^\infty_{\rm c}(\mathbb{R})$ cutoff function χ such that

$$\mathbb{1}_{[-\frac{1}{2},\frac{1}{2}]} \leqslant \chi \leqslant \mathbb{1}_{[-1,1]}. \tag{2.49}$$

We furthermore require that

$$\left\| \frac{\mathrm{d}}{\mathrm{d}x}\left[\sqrt{1-\chi^2}\right]\right\|_{L^\infty(\mathbb{R})} < +\infty. \tag{2.50}$$

Let us next define the localized cutoff function:

$$\chi^{(i)}_\beta(x) = \chi\left(\delta(\beta)^{-1}|x-z_i|\right). \tag{2.51}$$

Recalling that $\sqrt{\beta}\delta(\beta) \xrightarrow{\beta\to\infty} +\infty$, we have that $\operatorname{supp}\chi^{(i)}_\beta$ is contained in a ball around z_i whose radius is large with respect to $\frac{1}{\sqrt{\beta}}$, while $\operatorname{supp}\nabla\chi^{(i)}_\beta$ is contained in a hyperspherical shell around z_i:

$$\operatorname{supp}\chi^{(i)}_\beta \subset B(z_i,\delta(\beta)), \qquad \operatorname{supp}\nabla\chi^{(i)}_\beta \subset B(z_i,\delta(\beta)) \setminus B\left(z_i,\frac{1}{2}\delta(\beta)\right). \tag{2.52}$$

In fact we will assume in the proof of the Theorem 2.16 that (**H2**) is satisfied with $\delta(\beta) \ll \beta^{-\frac{1}{3}}$ (this comes at no cost of generality), so that the support of $\chi^{(i)}_\beta$ is localized around z_i. We have the bounds

$$\left\|\partial^p\chi^{(i)}_\beta\right\|_\infty = \|\partial^p\chi\|_\infty\delta(\beta)^{-|p|}, \tag{2.53}$$

for any multi-index $p\in\mathbb{N}^d$, and thus $\|\partial^p\chi^{(i)}_\beta\|_\infty = \mathcal{O}\left(\beta^{\frac{|p|}{2}}\right)$.

We stress that, assuming that β is large enough for (**H2**) to hold, although $\chi^{(i)}_\beta$ does not necessarily vanish on $\partial\Omega_\beta$ when $\alpha^{(i)} < +\infty$, we still have $\widetilde{\psi}^{(i)}_{\beta,k,\theta} \in H^1_0(\Omega_\beta)$ (the form domain of Q_β) provided $\theta < \alpha^{(i)} - \sqrt{\beta}\gamma^{(i)}(\beta)$ and for β large enough.

The following result records some crucial localization estimates.

Lemma 2.25. *We consider, for $n\in\mathbb{N}^d$, eigenvectors $\psi^{(i)}_{\beta,n,\theta}$ of $H^{(i)}_{\beta,\theta}$ normalized in $L^2\left(z_i + E^{(i)}(\frac{\theta}{\sqrt{\beta}})\right)$, extended by 0 in $L^2(\mathbb{R}^d)$, and define the associated quasimodes $\widetilde{\psi}^{(i)}_{\beta,n,\theta}$ according to (2.48). Then, for any $n,m\in\mathbb{N}^d$, there exists $\beta_0>0$ and constants $M_{i,n,\theta}, M_{i,n,m,\theta}>0$, independent of β such that the following estimates hold for any $\beta>\beta_0$.*

$$\left\|\left(1-\chi^{(i)}_\beta\right)\psi^{(i)}_{\beta,n,\theta}\right\|_{L^2(\mathbb{R}^d)} = \mathcal{O}\left(\mathrm{e}^{-\frac{\beta\delta(\beta)^2}{M_{i,n,\theta}}}\right), \tag{2.54}$$

$$\left|\left\langle\widetilde{\psi}^{(i)}_{\beta,n,\theta},\widetilde{\psi}^{(i)}_{\beta,m,\theta}\right\rangle_{L^2(\mathbb{R}^d)} - \delta_{nm}\right| = \mathcal{O}\left(\mathrm{e}^{-\frac{\beta\delta(\beta)^2}{M_{i,n,m,\theta}}}\right), \tag{2.55}$$

$$\left|\left\langle H^{(i)}_\beta(1-\chi^{(i)}_\beta)\psi^{(i)}_{\beta,n,\theta},(1-\chi^{(i)}_\beta)\psi^{(i)}_{\beta,m,\theta}\right\rangle_{L^2(\mathbb{R}^d)}\right| = \mathcal{O}\left(\beta\mathrm{e}^{-\frac{2\beta\delta(\beta)^2}{M_{i,n,m,\theta}}}\right). \tag{2.56}$$

If the scaling (**H3**) *holds, the upper bounds decay superpolynomially in* β.

Proof. We begin by proving (2.54). Changing coordinates with $y = \sqrt{\beta}U^{(i)\intercal}(x - z_i)$, we get, in view of (2.43),

$$\begin{aligned}\left\|(1-\chi_\beta^{(i)})\psi_{\beta,n,\theta}^{(i)}\right\|_{L^2(\mathbb{R}^d)}^2 &= \int_{\mathbb{R}^d}(1-\chi)\left(\frac{1}{\sqrt{\beta}\delta(\beta)}\left|U^{(i)}y\right|\right)\psi_{n,\theta}^{(i)}(y)^2\,\mathrm{d}y\\ &\leqslant \int_{\mathbb{R}^d\setminus B\left(0,\frac{1}{2}\sqrt{\beta}\delta(\beta)\right)}\psi_{n,\theta}^{(i)}(y)^2\,\mathrm{d}y\\ &\leqslant |\mathbb{S}^{d-1}|C_{i,n,\theta}^2\int_{\frac{1}{2}\sqrt{\beta}\delta(\beta)}^{\infty}s^{d-1}\mathrm{e}^{-\frac{2s^2}{C_{i,n,\theta}}}\,\mathrm{d}s,\\ &= \mathcal{O}\left(\int_{\frac{1}{2}\sqrt{\beta}\delta(\beta)}^{\infty}\mathrm{e}^{-\frac{s^2}{C_{i,n,\theta}}}\,\mathrm{d}s\right),\end{aligned}$$

where we used respectively the lower bound in (2.49) and the pointwise exponential decay estimate (2.40) to obtain the first and second inequalities. Applying, for $t > 1$, a standard Gaussian tail bound

$$\int_t^\infty \mathrm{e}^{-s^2/2}\,\mathrm{d}s \leqslant t^{-1}\int_t^\infty s\mathrm{e}^{-s^2/2}\,\mathrm{d}s \leqslant \mathrm{e}^{-t^2/2}$$

yields the desired bound (2.54) for β sufficiently large, since $\sqrt{\beta}\delta(\beta) \to +\infty$, and where we set $M_{i,n,\theta} = 2C_{i,n,\theta}$.

Unless otherwise specified, the norms and inner products in the remainder of the proof are on $L^2(\mathbb{R}^d)$. To show (2.55), we first note that, since $\|\psi_{\beta,n,\theta}^{(i)}\| = 1$ and $0 \leqslant \chi_\beta^{(i)} \leqslant 1$, a triangle inequality gives

$$0 \leqslant 1 - \left\|\chi_\beta^{(i)}\psi_{\beta,n,\theta}^{(i)}\right\| \leqslant \left\|(1-\chi_\beta^{(i)})\psi_{\beta,n,\theta}^{(i)}\right\|,$$

so that

$$1 \leqslant \frac{1}{\left\|\chi_\beta^{(i)}\psi_{\beta,n,\theta}^{(i)}\right\|} \leqslant \frac{1}{1-\left\|(1-\chi_\beta^{(i)})\psi_{\beta,n,\theta}^{(i)}\right\|} \leqslant 1 + 2\left\|(1-\chi_\beta^{(i)})\psi_{\beta,n,\theta}^{(i)}\right\| \tag{2.57}$$

for β sufficiently large, where we use (2.54) to obtain the final inequality.

For convenience, we write $\psi_{\beta,n,\theta}^{(i)} = \psi_n$, $\psi_{\beta,m,\theta}^{(i)} = \psi_m$ and $\chi_\beta^{(i)} = \chi$. Then,

$$\langle\chi\psi_n, \chi\psi_m\rangle = \langle\psi_n,\psi_m\rangle - 2\langle\psi_n,(1-\chi)\psi_m\rangle + \left\langle\psi_n,(1-\chi)^2\psi_m\right\rangle.$$

Thus, by Cauchy–Schwarz inequalities, and using the orthonormality of ψ_n and ψ_m, we obtain:

$$|\langle\chi\psi_n,\chi\psi_m\rangle - \delta_{n,m}| \leqslant 2\|\psi_n\|\|(1-\chi)\psi_m\| + \|\psi_n\|\|(1-\chi)^2\psi_m\| \leqslant 3\|(1-\chi)\psi_m\|,$$

since $(1-\chi)^2 \leqslant (1-\chi)$. It follows by symmetry that

$$|\langle\chi\psi_n,\chi\psi_m\rangle - \delta_{n,m}| \leqslant \frac{3}{2}\left(\|(1-\chi)\psi_n\| + \|(1-\chi)\psi_m\|\right). \tag{2.58}$$

Denoting by $\widetilde{\psi}_n = \chi\psi_n\|\chi\psi_n\|^{-1}$ and $\widetilde{\psi}_m = \chi\psi_m\|\chi\psi_m\|^{-1}$, we obtain

$$\left|\left\langle\widetilde{\psi}_n,\widetilde{\psi}_m\right\rangle - \delta_{nm}\right| \leqslant |\langle\chi\psi_n,\chi\psi_m\rangle - \delta_{n,m}| + \left|1 - \left(\|\chi\psi_n\|\,\|\chi\psi_m\|\right)^{-1}\right||\langle\chi\psi_n,\chi\psi_m\rangle|,$$

and it follows from (2.57), (2.58) that

$$\left|\left\langle \widetilde{\psi}_n, \widetilde{\psi}_m \right\rangle - \delta_{nm}\right| = \mathcal{O}\left(\|(1-\chi)\psi_n\| + \|(1-\chi)\psi_m\|\right)$$

in the limit $\beta \to \infty$. The estimate (2.54) then implies (2.55) with $M_{i,n,m,\theta} = \max\{M_{i,n,\theta}, M_{i,m,\theta}\}$.

For (2.56), we start with an algebraic computation for a Schrödinger operator $H = -\Delta + V$ with domain $\mathcal{D}(H) \subset H^1(\mathbb{R}^d)$, two eigenstates u, v with respective eigenvalues λ_u, λ_v, and $\eta \in \mathcal{C}^2(\mathbb{R}^d)$ with uniformly bounded derivatives. Using the relation

$$H(\eta u) = \eta H u - 2\nabla\eta \cdot \nabla u - u\Delta\eta = \lambda_u \eta u - 2\nabla\eta \cdot \nabla u - u\Delta\eta,$$

we get by integrating against ηv,

$$\langle H\eta u, \eta v\rangle = \lambda_u \left\langle u, \eta^2 v\right\rangle - \langle u, (\eta\Delta\eta)\, v\rangle - 2\,\langle \nabla u, (\eta\nabla\eta)\, v\rangle\,.$$

Thus, by symmetry and an integration by parts,

$$\begin{aligned}\langle H\eta u, \eta v\rangle &= \left\langle u, \left(\frac{\lambda_u+\lambda_v}{2}\eta^2 - \eta\Delta\eta\right) v\right\rangle - \frac{1}{2}\left\langle \nabla[uv], \nabla[\eta^2]\right\rangle_{\mathcal{D}'(\mathbb{R}^d)\times\mathcal{D}(\mathbb{R}^d)} \\ &= \left\langle u, \left(\frac{\lambda_u+\lambda_v}{2}\eta^2 + |\nabla\eta|^2\right) v\right\rangle.\end{aligned} \tag{2.59}$$

Applying (2.59) to $H = H^{(i)}_{\beta,\theta}$ with $\eta = 1 - \chi^{(i)}_\beta$, we get, noting that the function $\frac{\lambda_u+\lambda_v}{2}\eta^2 + |\nabla\eta|^2$ is supported in $S^{(i)}_\beta := \mathbb{R}^d \setminus B\left(z_i, \frac{1}{2}\sqrt{\beta}\delta(\beta)\right)$ and using (2.53), that there exists a constant $C_{n,m} > 0$ such that

$$\left\| \frac{\lambda_n+\lambda_m}{2}(1-\chi^{(i)}_\beta)^2 + |\nabla(1-\chi^{(i)}_\beta)|^2 \right\|_{L^\infty(\mathbb{R}^d)} \leqslant \frac{C_{n,m}}{\delta(\beta)^2}.$$

By a Cauchy–Schwarz inequality, it follows that

$$\left|\left\langle H^{(i)}_\beta(1-\chi^{(i)}_\beta)\psi^{(i)}_{\beta,n,\theta}, (1-\chi^{(i)}_\beta)\psi^{(i)}_{\beta,m,\theta}\right\rangle\right| \leqslant \frac{C_{n,m}}{\delta(\beta)^2}\|\psi^{(i)}_{\beta,n,\theta}\|_{L^2\left(S^{(i)}_\beta\right)}\|\psi^{(i)}_{\beta,m,\theta}\|_{L^2\left(S^{(i)}_\beta\right)},$$

and identical arguments as the ones leading to (2.54) give

$$\|\psi^{(i)}_{\beta,n,\theta}\|_{L^2\left(S^{(i)}_\beta\right)}\|\psi^{(i)}_{\beta,m,\theta}\|_{L^2\left(S^{(i)}_\beta\right)} = \mathcal{O}\left(\mathrm{e}^{-\frac{2\beta\delta(\beta)^2}{M_{i,n,m,\theta}}}\right),$$

which implies (2.56) upon using the scaling $\delta(\beta) \gg \beta^{-\frac{1}{2}}$. □

The following lemma, adapting [195, Equations 11.5–7] to the Dirichlet context, justifies the local approximation of H_β by $H^{(i)}_\beta$ around z_i to the order β.

Lemma 2.26. *Fix $0 \leqslant i < N$, $u \in L^2(\Omega_\beta)$, and assume that $\delta(\beta) < \beta^{s-\frac{1}{2}}$ for some $0 < s < \frac{1}{6}$ in (**H2**). For any $\theta \in (-\infty, +\infty]$, the operator $H_\beta - H^{(i)}_{\beta,\theta}$ extends to a bounded operator in $L^2(\Omega_\beta)$, and there exist $C > 0$ and $\beta_0 > 0$ independent of θ such that, for all $\beta > \beta_0$, the*

following estimate holds:

$$\left\|(H_\beta - H^{(i)}_{\beta,\theta})\chi^{(i)}_\beta u\right\|_{L^2(\Omega_\beta)} \leqslant C\beta^{3s+\frac{1}{2}}\|\chi^{(i)}_\beta u\|_{L^2(\Omega_\beta)} = o(\beta)\|\chi^{(i)}_\beta u\|_{L^2(\Omega_\beta)}.$$

Proof. Since $H_\beta - H^{(i)}_\beta$ is a multiplication operator by a smooth function over a bounded domain, it is bounded in $L^2(\Omega_\beta)$, and we therefore only need to control the L^∞-norm of the difference in the potential parts

$$U_\beta - \beta^2(x-z_i)^\intercal\Sigma^{(i)}(x-z_i) + \beta\frac{\Delta V(z_i)}{2}$$

on $\Omega_\beta \cap \operatorname{supp}\chi^{(i)}_\beta \subset B(z_i,\delta(\beta))$. We estimate separately the two contributions

$$\beta^2\left(\frac{|\nabla V(x)|^2}{4} - (x-z_i)^\intercal\Sigma^{(i)}(x-z_i)\right) - \frac{\beta}{2}(\Delta V(x) - \Delta V(z_i)).$$

Using a second-order Taylor expansion around z_i, there exist $\beta_0 > 0$ and $C_1 > 0$ depending only on V and i such that, for all $\beta > \beta_0$ and every $x \in \operatorname{supp}\chi^{(i)}_\beta$,

$$\left|\frac{|\nabla V(x)|^2}{4} - (x-z_i)^\intercal\Sigma^{(i)}(x-z_i)\right| \leqslant C_1|x-z_i|^3 \leqslant \beta^{3s-\frac{3}{2}}.$$

For the Laplacian term, since V is C^∞ and ΔV is thus locally Lipschitz, we have, for β large enough, and for some constant $C_2 > 0$,

$$|\Delta V(x) - \Delta V(z_i)| \leqslant C_2|x-z_i| \leqslant C_2\beta^{s-\frac{1}{2}}.$$

By gathering these estimates and setting $C = \max\{C_1, C_2\}$,

$$\left\|(H_\beta - H^{(i)}_\beta)\chi^{(i)}_\beta u\right\|_{L^2(\Omega_\beta)} \leqslant C\max\{\beta^{3s+\frac{1}{2}}, \beta^{s+\frac{1}{2}}\}\|\chi^{(i)}_\beta u\|_{L^2(\Omega_\beta)},$$

which yields the desired bound. Note that $\beta^{3s+\frac{1}{2}} = o(\beta)$ since $0 < s < \frac{1}{6}$. □

2.4.5 Local perturbations of the boundary

In both the proofs of the harmonic approximation (Theorem 2.16) and of the modified Eyring–Kramers formula (Theorem 2.17), we make use of the following technical result, which guarantees the existence of local extensions and contractions of the domains Ω_β, whose geometry around each critical point close to the boundary is precisely that of a half-space. More precisely, the existence of such an extension is used in the proof of Theorem 2.16 to obtain a lower bound on the spectrum, using a domain monotonicity result (see Proposition 2.33 below). In the proof of Theorem 2.17, both the extension and contraction are used to provide asymptotic bounds on the principal eigenvalue. Besides, the construction of approximate eigenmodes is greatly simplified on these perturbed domains.

Proposition 2.27. *Let $(\Omega_\beta)_{\beta\geqslant 0}$ be a family of smooth domains satisfying* (**H2**)*, and let ρ be*

a non-negative function such that

$$\gamma(\beta) < \rho(\beta) = o(\delta(\beta)). \tag{2.60}$$

Then, there exists $\beta_0 > 0$*, and for each* $\beta > \beta_0$*, bounded, smooth, open domains* $\Omega^{\pm}_{\beta,\rho}$ *with*

$$\Omega^{-}_{\beta,\rho} \subseteq \Omega_\beta \subseteq \Omega^{+}_{\beta,\rho},$$

such that

$$B\left(z_i, \frac{1}{2}\delta(\beta)\right) \cap \Omega^{\pm}_{\beta,\rho} = B\left(z_i, \frac{1}{2}\delta(\beta)\right) \cap \left[z_i + E^{(i)}\left(\frac{\alpha^{(i)}}{\sqrt{\beta}} \pm \rho(\beta)\right)\right] \tag{2.61}$$

for all $0 \leqslant i < N$ *for which* z_i *is close to the boundary (i.e.* $\alpha^{(i)} < +\infty$*).*

The proof of Proposition 2.27 is given in Appendix 2.A below.

2.4.6 Conclusion of the proof of Theorem 2.16

We conclude this section by giving the proof of the harmonic approximation in the case of a temperature-dependent boundary, which shows that the first-order asymptotics of any given eigenvalue at the bottom of the spectrum of H_β is given by the corresponding eigenvalue of $H^{\mathrm{H}}_{\beta,\alpha}$ defined in the limit $\beta \to \infty$. The proof extends the results of [195, 303] to the case of moving Dirichlet boundary conditions, allowing the computation of first-order spectral asymptotics for eigenstates localized (in the Witten representation) around critical points which are close to the boundary. To show (2.22), we study the eigenvalues of the Witten Laplacian (2.14), since these are equal to those of $-\mathcal{L}_\beta$ up to a factor of β. The (standard) strategy we follow is to construct approximate eigenvectors for H_β, which (roughly speaking) consist of eigenvectors of each of the local oscillators $H^{(i)}_{\beta,\alpha^{(i)}}$, localized around the critical points z_i by appropriate cutoff functions. The main technical novelty compared to previous works, besides the construction of critical harmonic models performed in Section 2.4.2, is the technique used to ensure that the quasimodes belong to the form domain of the Dirichlet Witten Laplacian on Ω_β, relying namely on Proposition 2.27, rather than on the fact that the domain is locally diffeomorphic to a half-space, as in [159] and [224].

Once we have constructed valid quasimodes, we obtain coarse estimates similar to those of [195, 303], at the level of the quadratic form and Courant–Fischer variational principles, allowing to compute the limit spectrum of $\mathcal{L}_\beta$ as $\beta \to \infty$, explicitly in terms of the spectra of the Dirichlet oscillators of Section 2.4.2. The constant $\beta_0 > 0$ will be increased a finite number of times in the following proof, without changing notation.

Proof of Theorem 2.16. Without loss of generality, we assume in this proof that $\delta(\beta) < \beta^{s-\frac{1}{2}}$ in (**H2**) for some $0 < s < \frac{1}{6}$, so that the assumptions of Lemma 2.25 are satisfied.

Step 1: Upper bound on $\lambda_{k,\beta}$

The proof of the upper bound proceeds in two steps. First, we choose an appropriate realization of the harmonic approximation (2.44) so that the associated quasimodes are in the form domain $H_0^1(\Omega_\beta)$. The second step is essentially identical to the analysis performed in [195, Theorem 11.1], given the localization estimates of Lemma 2.25. We include it for the sake of completeness.

Step 1a: Perturbation of the local oscillators.

We fix $k \geqslant 1$. We construct families of quasimodes $\{\varphi_1, \dots, \varphi_k\}$ for H_β associated to the first k harmonic eigenvalues $\beta\lambda^{\mathrm{H}}_{1,\alpha}, \dots, \beta\lambda^{\mathrm{H}}_{k,\alpha}$. Recall Table 2.1 for notation used in the definition of the harmonic approximation. The functions φ_j are of the general form (2.48). We must however be careful with the choice of realization for the formal operator $H_\beta^{(i_j)}$ defined in (2.29), to ensure that the quasimodes are in the form domain of H_β. In fact we need, for each $0 \leqslant i < N$, to distinguish between two cases:

a) If z_i is far from the boundary, then by Assumption (**H2**), $\chi_\beta^{(i)}$ is supported inside Ω_β, and thus the associated quasimodes are indeed in $H_0^1(\Omega_\beta)$ (and indeed in the domain of $\mathcal{L}_\beta$).

b) If z_i is close to the boundary, then by the third condition in Assumption (**H2**), $\mathcal{O}_i^-(\beta) \subseteq B(z_i, \delta(\beta)) \cap \Omega_\beta$ for β large enough. In this case, the construction presented below yields again a quasimode in $H_0^1(\Omega_\beta)$.

Let $0 \leqslant i < N$, and $0 < h < \alpha^{(i)}$. Then, Assumption (**H2**) implies that there exists $\beta_0 > 0$ such that, for all $\beta > \beta_0$, we have the inclusion:

$$B(z_i, \delta(\beta)) \cap \left[z_i + E^{(i)} \left(\frac{\alpha^{(i)} - h}{\sqrt{\beta}} \right) \right] \subseteq \mathcal{O}_i^-(\beta) \subseteq \Omega_\beta.$$

Defining the vector

$$\alpha^{h,-} = (\alpha^{(i)} - h \mathbb{1}_{\alpha^{(i)} < +\infty})_{0 \leqslant i < N},$$

we consider the perturbed harmonic approximation corresponding to the operator $H^{\mathrm{H}}_{\beta,\alpha^{h,-}}$, as defined in (2.44). By construction, for all $\beta > \beta_0$, eigenmodes $\psi^{(i_j)}_{\beta,n_j,\alpha^{h,-}_{i_j}}$ of $H^{(i_j)}_{\beta,\alpha^{h,-}_{i_j}}$, are supported in $z_{i_j} + E^{(i_j)}\left(\frac{\alpha^{(i_j)}-h}{\sqrt{\beta}}\right)$, as noted in (2.42), and it follows that the associated quasimode $\widetilde{\psi}^{(i_j)}_{\beta,n_j,\alpha^{h,-}_{i_j}}$, as defined by (2.48), belongs to $H_0^1(\mathcal{O}_{i_j}^-(\beta)) \subset H_0^1(\Omega_\beta)$.

Step 1b: Energy upper bound.

The aim of this step is to show the upper bound for all $k \geqslant 1$:

$$\overline{\lim_{\beta\to\infty}} \lambda_{k,\beta} \leqslant \lambda^{\mathrm{H}}_{k,\alpha}. \tag{2.62}$$

For a fixed $k \geqslant 1$, we consider the quasimodes

$$\varphi_j = \widetilde{\psi}^{(i_j)}_{\beta,n_j,\alpha^{h,-}_{i_j}} \qquad \text{for } 1 \leqslant j \leqslant k.$$

Note that $(\varphi_j)_{1\leqslant j\leqslant k}$ span a k-dimensional subspace of $H^1_0(\Omega_\beta)$, since the Gram matrix

$$\left(\langle \varphi_j, \varphi_{j'}\rangle_{L^2(\Omega_\beta)}\right)_{1\leqslant j,j'\leqslant k}$$

is quasi-unitary, i.e. can be written in the form $I+\mathcal{o}(1)$ as $\beta\to\infty$. Indeed, since the φ_j are normalized in $L^2(\Omega_\beta)$, it suffices to check that the off-diagonal entries of the Gram matrix vanish in this limit. Fixing $1\leqslant j,j'\leqslant k$, this is clear for $i_j\neq i_{j'}$, since the corresponding test functions $\chi_\beta^{(i_j)}$, $\chi_\beta^{(i_{j'})}$ have disjoint supports. If $i_j=i_{j'}$, the statement is an immediate consequence of the quasi-orthogonality estimate (2.55).

By the Min-Max Courant–Fischer principle, it suffices to show that

$$\forall\, u\in \mathrm{Span}\{\varphi_j\}_{1\leqslant j\leqslant k},\qquad Q_\beta(u)\leqslant (\beta\lambda^{\mathrm{H}}_{k,\alpha^{h,-}}+\mathcal{o}(\beta))\|u\|^2_{L^2(\Omega_\beta)}, \tag{2.63}$$

to conclude

$$\overline{\lim_{\beta\to\infty}}\ \lambda_{k,\beta}\leqslant \lambda^{\mathrm{H}}_{k,\alpha^{h,-}}.$$

Since the map $h\mapsto \lambda^{\mathrm{H}}_{k,\alpha^{h,-}}$ is continuous and $\alpha^{h,-}\xrightarrow{h\to 0}\alpha$, and therefore $\lambda^{\mathrm{H}}_{k,\alpha^{h,-}}\xrightarrow{h\to 0}\lambda^{\mathrm{H}}_{k,\alpha}$, the latter inequality implies (2.62).

Let us prove (2.63). Unless otherwise specified, in Step 1, norms and inner products are on $L^2(\Omega_\beta)$. For a fixed $1\leqslant j\leqslant k$, first consider $u=\chi_\beta^{(i_j)}\psi^{(i_j)}_{\beta,n_j,\alpha^{h,-}}\in\mathrm{Span}\{\varphi_j\}$. Recall that $H^{(i_j)}_{\beta,\alpha^{h,-}_{i_j}}\psi^{(i_j)}_{\beta,n_j,\alpha^{h,-}}=\beta\lambda^{(i_j)}_{n_j,\alpha^{h,-}}\psi^{(i_j)}_{\beta,n_j,\alpha^{h,-}}$. For convenience, we drop the indices and superscripts in the following computation, so that $u=\chi\psi$, with $H\psi=\beta\lambda\psi$. By our choice of $(\varphi_j)_{1\leqslant j\leqslant k}$, we have $\lambda\in\left\{\lambda^{\mathrm{H}}_{j,\alpha^{h,-}}\right\}_{1\leqslant j\leqslant k}$, and so $\lambda\leqslant\lambda^{\mathrm{H}}_{k,\alpha^{h,-}}$.

$$Q_\beta(u)=\langle H_\beta u,u\rangle=\langle Hu,u\rangle+\langle (H_\beta-H)u,u\rangle,$$

and since $|\langle (H_\beta-H)u,u\rangle|\leqslant C_{j,\alpha,h}\beta^{3s+\frac12}\|u\|^2=\mathcal{o}(\beta)\|u\|^2$ for some constant $C_{j,\alpha,h}>0$ by Lemma 2.26, the only remaining task is to estimate the first term. Expanding the quadratic form, we get:

$$\begin{aligned}\langle H\chi\psi,\chi\psi\rangle&=\langle H\psi,\psi\rangle-2\langle H\psi,(1-\chi)\psi\rangle+\langle H(1-\chi)\psi,(1-\chi)\psi\rangle\\&=\beta\lambda\|\psi\|^2-2\langle H\psi,(1-\chi)\psi\rangle+\langle H(1-\chi)\psi,(1-\chi)\psi\rangle\\&\leqslant\beta\lambda\|u\|^2+\mathcal{O}(\beta\|(1-\chi)\psi\|)+\langle H(1-\chi)\psi,(1-\chi)\psi\rangle,\end{aligned}\tag{2.64}$$

where we used a Cauchy–Schwarz inequality and the estimate (see (2.54))

$$\|\psi\|^2=\|u\|^2+2\langle u,(1-\chi)\psi\rangle+\|(1-\chi)\psi\|^2=\|u\|^2+\mathcal{O}(\|(1-\chi)\psi\|).$$

We next use the localization estimates given in Lemma 2.25 to control the two rightmost terms in the last line of (2.64). Here, we make crucial use of the hypothesis (**H3**), which gives the superpolynomial decay of the bound (2.54), implying that $\beta\|(1-\chi)\psi\|=\mathcal{o}(\beta)$, and similarly $\langle H(1-\chi)\psi,(1-\chi)\psi\rangle=\mathcal{o}(\beta)$, using (2.56). Finally, (2.55) implies that $\|u\|^2=1+\mathcal{o}(\beta)$, so that we may write $Q_\beta(u)\leqslant\|u\|^2(\beta\lambda+\mathcal{o}(\beta))$. Since $\lambda\leqslant\lambda^{\mathrm{H}}_{k,\alpha^{h,-}}$, this implies the upper bound (2.63) for this particular choice of u, and thus for any $u\in\mathrm{Span}\{\varphi_j\}$, as we now show.

For $u = \sum_{j=1}^k g_j \varphi_j \in \mathrm{Span}\{\varphi_j\}_{1\leqslant j\leqslant k}$, in view of the previous estimate, it is enough to show that the cross terms

$$g_j g_{j'} \left\langle H^{(i_j)}_{\beta,\alpha^h_{i_j}} \varphi_j, \varphi_{j'} \right\rangle$$

are small whenever $i_j = i_{j'}$ with $j \neq j'$, since the terms for which $i_j \neq i_{j'}$ vanish for β large enough as the corresponding cutoff functions have disjoint supports. To check that the non-zero terms decay superpolynomially in β, we denote, for convenience $H^{(i_j)}_{\beta,\alpha^h_{i_j}} = H$, $\chi = \chi^{(i_j)}_\beta$, and $\psi = \psi^{(i_j)}_{\beta,n_j,\alpha^{h,-}}$, $\psi' = \psi^{(i_{j'})}_{\beta,k_{j'},\alpha^{h,-}}$, so that $\varphi_j = \chi\psi/Z$, $\varphi_{j'} = \chi\psi'/Z'$, where Z, Z' are normalizing constants ensuring that the quasimodes have unit $L^2(\Omega_\beta)$-norm. With this notation,

$$\begin{aligned}
\langle H\chi\psi, \chi\psi'\rangle &= \langle H\psi, \psi'\rangle - \langle H\psi, (1-\chi)\psi'\rangle - \langle H(1-\chi)\psi, \psi'\rangle + \langle H(1-\chi)\psi, (1-\chi)\psi'\rangle \\
&= \langle H\psi, \psi'\rangle - \lambda\langle \psi, (1-\chi)\psi'\rangle - \lambda'\langle (1-\chi)\psi, \psi'\rangle + \langle H(1-\chi)\psi, (1-\chi)\psi'\rangle \\
&= 0 + \mathcal{O}(\beta)\|\psi\|\|\psi'\|,
\end{aligned}$$

where we used again Cauchy–Schwarz inequalities and the superpolynomial decay of the estimates (2.54) and (2.56) under (**H3**), as well as the orthogonality relation $\langle \psi, \psi'\rangle = 0$. Since $Z, Z' = 1 + \mathcal{O}(\beta)$ by (2.55), it follows that (2.63) holds, which concludes the proof of (2.62).

Step 2: Lower bound on $\lambda_{k,\beta}$

We show the lower bound in (2.22), namely that for all $k \geqslant 1$,

$$\varliminf_{\beta\to\infty} \lambda_{k,\beta} \geqslant \lambda^{\mathrm{H}}_{k,\alpha}. \tag{2.65}$$

As in the proof of the upper bound, we proceed in two steps. The first step is to construct an appropriate extension of the domain Ω_β around critical points which are close to the boundary, relying on Proposition 2.27. The second step is similar to what is done in related proofs of [303, 195] in the boundaryless case, and we include it for completeness.

Step 2a: Perturbation of the domain.

Our analysis requires to consider, in addition to perturbed harmonic eigenvalues, a perturbed domain Ω^h_β which contains Ω_β, parametrized by some small $h > 0$. We construct Ω^h_β to be smooth and bounded, so that the Dirichlet realization of H_β in Ω^h_β is self-adjoint on $L^2(\Omega^h_\beta)$, with compact resolvent and form domain $H^1_0(\Omega^h_\beta)$. This domain is constructed by a direct application of Proposition 2.27 with $\rho(\beta) = \frac{h}{\sqrt{\beta}}$, that is,

$$\Omega^h_\beta = \Omega^+_{\beta,h/\sqrt{\beta}}.$$

Crucially, it satisfies the inclusion (2.61), which corresponds to the requirement that, locally around each z_i close to the boundary, $\partial\Omega^h_\beta$ coincides precisely with a hyperplane located at a distance $\beta^{-\frac{1}{2}}(\alpha^{(i)} + h)$ away from the saddle in the direction $v^{(i)}_1$, and normal to the same vector. In the remainder of the proof, norms and inner products are by default on $L^2(\Omega^h_\beta)$.

We denote by $\lambda^h_{k,\beta} := \lambda_{k,\beta}(\Omega^h_\beta)$ its k-th eigenvalue, which is positive with finite multiplicity, and by H^h_β the Dirichlet realization of H_β on Ω^h_β, with Q^h_β its associated quadratic form. By the comparison principle given in Proposition 2.33, it holds that $\lambda_{k,\beta}(\Omega_\beta) \geqslant \lambda_{k,\beta}(\Omega^h_\beta)$, and so it is sufficient to prove (2.65) with $\lambda_{k,\beta} = \lambda^h_{k,\beta}$.

Step 2b: Energy lower bound.
From now on, $\alpha^{h,+}$ denotes the vector $(\alpha^{(i)} + h\mathbb{1}_{\alpha^{(i)}<+\infty})_{0\leqslant i<N}$, and φ_j, for $1 \leqslant j \leqslant k-1$ are $k-1$ harmonic quasimodes, associated with the Dirichlet harmonic approximation $H^{\mathrm{H}}_{\beta,\alpha^{h,+}}$. However, due to the construction performed in the previous step, one must slightly adjust the definition (2.48), and more precisely the support of the cutoff function. For this, we set:

$$\varphi_j = \frac{\eta^{(i)}_\beta \psi^{(i_j)}_{\beta,n_j,\alpha^{h,+}_{i_j}}}{\|\eta^{(i)}_\beta \psi^{(i_j)}_{\beta,n_j,\alpha^{h,+}_{i_j}}\|} \, 1 \leqslant j \leqslant k-1,$$

where $\eta^{(i)}_\beta(x - z_i) = \chi^{(i)}_\beta(2(x - z_i))$. By construction, each φ_j is supported in $B(z_i, \frac{1}{2}\delta(\beta))$, and thus belongs to $H^1_0(\Omega^h_\beta)$, by the inclusion (2.61) and the fact that $\psi^{(i_j)}_{\beta,n_j,\alpha^{h,+}_{i_j}}$ has support in $z_{i_j} + E^{(i_j)}\left(\frac{\alpha^{(i_j)}+h}{\sqrt{\beta}}\right)$ whenever $\alpha^{(i_j)} < +\infty$. We note that this choice of quasimodes amounts to rescaling $\delta(\beta)$ by a factor $\frac{1}{2}$, and consequently has no impact on the superpolynomial decay of the estimates of Lemma 2.25, nor on the conclusion of Lemma 2.26, which we will use freely in the remainder of the proof, upon replacing $\chi^{(i)}_\beta$ by $\eta^{(i)}_\beta$, Ω_β by Ω^h_β and H_β by H^h_β. As in Step 1b, for β large enough, the φ_j span a $(k-1)$-dimensional subspace of $L^2(\Omega^h_\beta)$.

This time, we rely on the Courant–Fischer principle in its Max-Min form: it suffices to show that, for any $u \in H^1_0(\Omega^h_\beta) \cap \mathrm{Span}\{\varphi_j\}^\perp_{1\leqslant j\leqslant k-1}$, the following inequality holds:

$$Q^h_\beta(u) \geqslant (\beta\lambda^{\mathrm{H}}_{k,\alpha^{h,+}} + o(\beta))\|u\|^2.$$

This will indeed imply:

$$\varliminf_{\beta\to\infty} \lambda_{k,\beta} \geqslant \varliminf_{\beta\to\infty} \lambda^h_{k,\beta} \geqslant \lambda^{\mathrm{H}}_{k,\alpha^{h,+}},$$

and the desired lower bound (2.65) follows by continuity of the harmonic eigenvalues with respect to the boundary position $\alpha^{h,+}$, taking the limit $h \to 0$. Hence, let $u \in H^1_0(\Omega^h_\beta)$ be orthogonal to φ_j for every $1 \leqslant j \leqslant k-1$. The IMS localization formula (see for instance [195, Chapter 3]) gives:

$$Q^h_\beta(u) = \sum_{i=0}^{N} Q^h_\beta\left(\eta^{(i)}_\beta u\right) - \left\|u\nabla\eta^{(i)}_\beta\right\|^2, \tag{2.66}$$

with $\eta^{(N)}_\beta = \sqrt{\mathbb{1}_{\Omega^h_\beta} - \sum_{i=0}^{N-1} \eta^{(i)2}_\beta}$. We first estimate, for $0 \leqslant i < N$, the terms

$$Q^h_\beta\left(\eta^{(i)}_\beta u\right) - \left\langle H^{(i)}_{\beta,\alpha^{h,+}_i}\eta^{(i)}_\beta u, \eta^{(i)}_\beta u\right\rangle = \left\langle (H^h_\beta - H^{(i)}_{\beta,\alpha^{h,+}_i})\eta^{(i)}_\beta u, \eta^{(i)}_\beta u\right\rangle = o(\beta)\|u\|^2,$$

using Lemma 2.26. On the other hand, the assumption that u is $L^2(\Omega^h_\beta)$-orthogonal to the φ_j for $1 \leqslant j \leqslant k-1$ implies, for all $0 \leqslant i < N$ and all $1 \leqslant n \leqslant \mathfrak{N}_i(k-1)$, that $\eta^{(i)}_\beta u$

is $L^2\left[z_i + E^{(i)}\left(\frac{\alpha^{(i)}+h}{\sqrt{\beta}}\right)\right]$-orthogonal to $\psi^{(i)}_{\beta,n,\alpha_i^{h,+}}$. Here, we made crucial use of the property (2.61) of the extended domain. Furthermore, $\eta_\beta^{(i)}u$ is in the form domain of the self-adjoint operator $H^{(i)}_{\beta,\alpha_i^{h,+}}$, and thus the Courant–Fischer principle implies:

$$\left\langle H^{(i)}_{\beta,\alpha_i^{h,+}}\eta_\beta^{(i)}u, \eta_\beta^{(i)}u\right\rangle \geqslant \beta\lambda^{(i)}_{\mathfrak{N}_i(k-1)+1,\alpha_i^{h,+}}\|\eta_\beta^{(i)}u\|^2 \geqslant \beta\lambda^{\mathrm{H}}_{k,\alpha^{h,+}}\|\eta_\beta^{(i)}u\|^2,$$

where we used the identity (2.46). The crude L^∞ bound (2.53) implies, since $\delta(\beta)^{-1} = \mathcal{O}\left(\sqrt{\beta}\right)$, that $\left\|u\nabla\eta_\beta^{(i)}\right\|^2 = \mathcal{O}(\beta)\|u\|^2$. At this point, we have shown that

$$\sum_{i=0}^{N-1} Q^h_\beta\left(\eta_\beta^{(i)}u\right) - \left\|u\nabla\eta_\beta^{(i)}\right\|^2 \geqslant \beta\lambda^{\mathrm{H}}_{k,\alpha^{h,+}}\sum_{i=0}^{N-1}\|\eta_\beta^{(i)}u\|^2 + \mathcal{O}(\beta)\|u\|^2$$

We are left with the following term in (2.66):

$$\left\langle H^h_\beta\eta_\beta^{(N)}u, \eta_\beta^{(N)}u\right\rangle - \left\|u\nabla\eta_\beta^{(N)}\right\|^2.$$

Note that, since

$$\operatorname{supp}\eta_\beta^{(N)} \subset \mathbb{R}^d \setminus \bigcup_{i=0}^m B\left(z_i, \frac{1}{2}\delta(\beta)\right),$$

the fact that V is a smooth Morse function in Ω^h_β ensures that there exist $C, \beta_0 > 0$ such that, for all $\beta > \beta_0$,

$$|\nabla V|^2_{\left|\operatorname{supp}\eta_\beta^{(N)}\right.} \geqslant \frac{1}{C}\delta(\beta)^2, \qquad |\Delta V|_{\left|\operatorname{supp}\eta_\beta^{(N)}\right.} \leqslant C,$$

hence:

$$\forall\, x \in \operatorname{supp}\eta_\beta^{(N)}, \qquad U_\beta(x) = \frac{\beta^2}{4}|\nabla V(x)|^2 - \frac{\beta}{2}\Delta V(x) \geqslant \frac{\beta^2\delta(\beta)^2}{4C} - \beta C,$$

The following ground state estimate then shows that, for $\beta > \beta_0$ and any $v \in H^1_0(\operatorname{supp}\eta_\beta^{(N)})$:

$$\left\langle H^h_\beta v, v\right\rangle_{L^2(\operatorname{supp}\eta_\beta^{(N)})} \geqslant \langle U_\beta v, v\rangle^2_{L^2(\operatorname{supp}\eta_\beta^{(N)})} \geqslant \beta\left(\frac{\beta\delta(\beta)^2}{4C} - C\right)\|v\|^2_{L^2(\operatorname{supp}\eta_\beta^{(N)})}.$$

Since $\sqrt{\beta}\delta(\beta) \xrightarrow{\beta\to\infty} +\infty$, we conclude that, for β large enough, and since $\eta_\beta^{(N)}u$ belongs to $H^1_0(\operatorname{supp}\eta_\beta^{(N)})$, we have:

$$\left\langle H^h_\beta\eta_\beta^{(N)}u, \eta_\beta^{(N)}u\right\rangle \geqslant \beta\lambda^{\mathrm{H}}_{k,\alpha^{h,+}}\left\|\eta_\beta^{(N)}u\right\|^2.$$

Finally, we note that, owing to the condition (2.50), and the fact that the $\eta_\beta^{(i)}$ have disjoint supports for $i = 0, \dots, N-1$, it also holds:

$$\|\nabla\eta_\beta^{(N)}u\|^2 = \mathcal{O}(\beta)\|u\|^2.$$

In conclusion, we have shown that

$$\left\langle H_\beta^h u, u \right\rangle \geqslant \beta \lambda^{\mathrm{H}}_{k,a^{h,+}} \sum_{i=0}^{N} \|\eta_\beta^{(i)} u\|^2_{L^2(\Omega_\beta^h)} + o(\beta)\|u\|^2_{L^2(\Omega_\beta^h)}.$$

The lower bound (2.65) follows easily since the $\eta_\beta^{(i)}$ form a quadratic partition of unity on Ω_β^h, that is

$$\forall\, v \in L^2(\Omega_\beta^h), \quad \|v\|^2_{L^2(\Omega_\beta^h)} = \sum_{i=0}^{N} \|\eta_\beta^{(i)} v\|^2_{L^2(\Omega_\beta^h)}.$$

□

2.5 Proof of Theorem 2.17

In this section, we derive finer asymptotics for the first Dirichlet eigenvalue $\lambda_{\beta,1}$ of $-\mathcal{L}_\beta$, in the regime $\beta \to \infty$, as described by Theorem 2.17. The proof of (2.24), inspired by a construction performed in [209] in the case of a static domain, relies on the definition of accurate approximations of the first Dirichlet eigenvector for $-\mathcal{L}_\beta$, so-called quasimodes. In Section 2.5.1, we derive the necessary local estimates to ensure the well-posedness of the construction, in the presence of a temperature-dependent boundary. In Section 2.5.2, we perform the construction of precise quasimodes, on slightly perturbed domains chosen so that the Dirichlet boundary condition is satisfied. In Section 2.5.3, we present a technical result to deal with Laplace asymptotics in the presence of moving boundaries. In Section 2.5.4, we prove the key semiclassical estimates needed to conclude the proof of Theorem 2.17, which is done in Section 2.5.5.

2.5.1 Local energy estimates

A technical detail one has to address in this construction is that in order for the quasimodes (2.75) introduced below to be smooth and supported in $\Omega_\beta^{\pm}$, we may need to reduce the value of $\delta(\beta)$ in Assumption (**H2**) in order for various energy estimates to hold in the neighborhoods $B(z_i, \delta(\beta))$ of low-energy saddle points. In fact, we show in Proposition 2.35 that there exists some constant $\varepsilon_0(V, z_0) > 0$ independent of β such that requiring $\delta(\beta) < \varepsilon_0(V, z_0)$ ((**EK4**)) allows for the construction of valid quasimodes.

We begin by recalling some facts concerning the geometry of the basin of attraction $\mathcal{A}(z_0)$ and the behavior of V near low-energy critical points. Recall the definition (2.18).

Lemma 2.28. *Let $z \in \partial\mathcal{A}(z_0)$ be a local minimum for $V|_{\mathcal{S}(z_0)}$. Then, $\nabla V(z) = 0$ and $\mathrm{Ind}(z) = 1$.*

Proof. From [246, Theorem B.13], we may write $\mathcal{S}(z_0)$ as an at most countable disjoint union of submanifolds

$$\mathcal{S}(z_0) = \bigcup_{\mathbf{m} \in \mathcal{Z}(z_0)} \mathcal{W}^+(\mathbf{m}), \tag{2.67}$$

where $\mathcal{Z}(z_0)$ is the set of critical points of V on $\mathcal{S}(z_0) = \partial\mathcal{A}(z_0) \cap \bigcup_{z\in\mathcal{M}(V)\setminus\{z_0\}} \partial\mathcal{A}(z)$, which all have index at least 1, and we recall the definition (2.10) of the stable manifold $\mathcal{W}^+$. Moreover, $\mathcal{W}^+(\mathbf{m})$ is a $(d - \mathrm{Ind}(\mathbf{m}))$-dimensional manifold.

From (2.67), there exists a unique critical point $\mathbf{m}$ of V such that $z \in \mathcal{W}^+(\mathbf{m})$, so that by definition the gradient flow $\phi_t(z)$ converges to $\mathbf{m}$ in the limit $t \to \infty$, and is included in $\mathcal{S}(z_0)$, which is positively stable for the gradient flow, as a union of stable manifolds. Since V decreases along trajectories of ϕ and z is a local minimum of V on $\mathcal{S}(z_0)$, it must hold that $\nabla V(z) = 0$. In particular, $\mathbf{m} = z$.

It only remains to check that $\mathrm{Ind}(z) = 1$. We first show that there exists $\mathbf{m}_1 \in \mathcal{Z}(z_0)$ with $\mathrm{Ind}(\mathbf{m}_1) = 1$ such that $z \in \overline{\mathcal{W}^+(\mathbf{m}_1)}$. Assume for the sake of contradiction that this is not the case, hence there exists $r > 0$ such that

$$\mathcal{S}(z_0) \cap B(z, r) \subset \bigcup_{\substack{\mathbf{m}\in\mathcal{Z}(z_0)\\ \mathrm{Ind}(\mathbf{m})\geqslant 2}} \mathcal{W}^+(\mathbf{m}).$$

Since the set on the right-hand side has dimension at most $d-2$, the set $B(z,r) \setminus \mathcal{S}(z_0)$ is connected (see [180, Theorem IV 4, Corollary 1]). On the other hand, the sets

$$\mathcal{A}'(y) := \overline{\mathcal{A}(y)} \setminus \mathcal{S}(y), \qquad y \in \mathcal{M}(V)$$

are open and pairwise disjoint, and the disjoint open cover

$$B(z, r) \setminus \mathcal{S}(z_0) \subset \bigcup_{y\in\mathcal{M}(V)} \mathcal{A}'(y)$$

has at least two non-empty components by definition of $\mathcal{S}(z_0)$, and therefore cannot be connected.

We finally show that $\mathrm{Ind}(z) = 1$. We already know that $\mathrm{Ind}(z) \geqslant 1$, and again assume for the sake of contradiction that $\mathrm{Ind}(z) > 1$. Since $\dim(\mathcal{W}^-(z)) = \mathrm{Ind}(z)$ and $\dim(\mathcal{W}^+(\mathbf{m}_1)) = d-1$, there exists $v \in T_z\mathcal{W}^+(\mathbf{m}_1) \cap T_z\mathcal{W}^-(z)$ such that $v \neq 0$. Here, $T_z\mathcal{W}^+(\mathbf{m}_1)$ denotes the tangent half-space at the boundary, consisting of initial velocities of paths entering $\mathcal{W}^+(\mathbf{m}_1)$ starting from z. Let then f be a $\mathcal{C}^\infty$ map $[0,1) \to \{z\} \cup \mathcal{W}^+(\mathbf{m}_1) \subset \mathcal{S}(z_0)$ such that $f(0) = z$ and $f'(0^+) = v$. Expanding, we get

$$V(f(t)) = V(z) + \frac{t^2}{2} v^\intercal \nabla^2 V(z) v + \mathcal{O}(t^3),$$

where we used $\nabla V(z) = 0$ twice. Since $V(f(t)) \geqslant V(z)$ for t sufficiently small, this implies $v^\intercal \nabla^2 V(z) v \geqslant 0$. We have reached a contradiction, since $T_z\mathcal{W}^-(z)$ is spanned by the negative eigendirections of $\nabla^2 V(z)$. □

This leads to the following estimation on the position of $\partial\mathcal{A}(z_0)$ near a low-energy separating saddle point. Recall the definition of the local coordinates (2.9).

Lemma 2.29. *For all $T > 0$, there exists $\varepsilon_0(T), K(T) > 0$ such that for all $\varepsilon < \varepsilon_0(T)$ and*

all $i \in I_{\min}$,

$$\begin{aligned} &\{y_1^{(i)} < -T\varepsilon\} \cap B(z_i, K(T)\sqrt{\varepsilon}) \subset \overline{\mathcal{A}(z_0)}, \\ &\{y_1^{(i)} > T\varepsilon\} \cap B(z_i, K(T)\sqrt{\varepsilon}) \subset \mathbb{R}^d \setminus \overline{\mathcal{A}(z_0)}. \end{aligned} \tag{2.68}$$

Proof. Let $T > 0$ and $i \in I_{\min}$. In a neighborhood of z_i, the decomposition (2.67) shows that $\partial\overline{\mathcal{A}(z_0)} = \mathcal{S}(z_0)$ coincides with $\mathcal{W}^+(z_i)$.The stable manifold theorem (see [317, Section 9.2]) implies that $\mathcal{S}(z_0)$ is smooth in a neighborhood of z_i, with furthermore $\mathrm{n}_{\overline{\mathcal{A}(z_0)}}(z_i) = v_1^{(i)}$. Recall that $\sigma_{\overline{\mathcal{A}(z_0)}}$ denotes the signed distance function to $\partial\overline{\mathcal{A}(z_0)}$ with the convention (2.4). Its regularity in a neighborhood of z_i is guaranteed by the fact that, according to the definition (2.20), z_i is a separating saddle point. Note that in the case where $z \in \partial\mathcal{A}(z_0)$ is a non-separating saddle point, the outward normal $\mathrm{n}_{\mathcal{A}(z_0)}(z) = -\nabla\sigma_{\mathcal{A}(z_0)}(z)$ is not well-defined. A Taylor expansion gives

$$\sigma_{\overline{\mathcal{A}(z_0)}}(z_i + h) = \sigma_{\overline{\mathcal{A}(z_0)}}(z_i) - h^\intercal \mathrm{n}_{\overline{\mathcal{A}(z_0)}}(z_i) + R(h) = -h^\intercal v_1^{(i)} + R(h) = -y_1^{(i)}(z_i + h) + R(h),$$

where $|R(h)| < M_i|h|^2$ for some constant $M_i > 0$ and for all $|h| < M_i^{-1}$. Choosing $\varepsilon_{0,i} = \frac{T}{M_i}$, we get, for all $0 < \varepsilon < \varepsilon_{0,i}$ and all $x \in \{y_1^{(i)} < -T\varepsilon\} \cap B(z_i, K_i\sqrt{\varepsilon})$,

$$\sigma_{\overline{\mathcal{A}(z_0)}}(x) \geqslant T\varepsilon - K_i^2 M_i \varepsilon > 0$$

for $K_i < \sqrt{T/M_i}$, thus $x \in \overline{\mathcal{A}(z_0)}$ for K_i sufficiently small.

Setting $\varepsilon_0(T) = \min_i \varepsilon_{0,i}$ and $K(T) = \min_i K_i$, we obtain the first inclusion in (2.68). The second inclusion follows along the same lines. □

The following proposition allows to multiply $\delta(\beta)$ by an arbitrarily small positive constant factor in Assumption (**EK3**), which will be convenient for the construction of accurate quasimodes.

Proposition 2.30. *There exists* $\varepsilon_0(V, z_0), C(V, z_0), \beta_0 > 0$ *such that, provided* (**EK3**) *holds and* $\delta(\beta) < \varepsilon_0(V, z_0)$*, for all* $0 < \rho_0 < 1$*, there exists* $\rho < \rho_0$ *such that for all* $\beta > \beta_0$*, Assumption* (**EK3**) *again holds upon replacing* $\delta(\beta)$ *by* $\rho\delta(\beta)$ *and* C_V *by* $C(V, z_0)\rho^2$*, i.e.*

$$\Big[\mathcal{A}(z_0) \cap \{V < V^* + C(V, z_0)\rho^2\delta(\beta)^2\}\Big] \setminus \bigcup_{i \in I_{\min}} B(z_i, \rho\delta(\beta)) \subset \Omega_\beta. \tag{**EK3'**}$$

Furthermore, $\varepsilon_0(V, z_0)$ *can be chosen such that, for each* $0 \leqslant i < N$*,* z_i *is the only critical point of* V *in* $B(z_i, 2\varepsilon_0(V, z_0))$*.*

Proof. We assume (**EK3**), and show (**EK3'**). For any $C < C_V$, the inclusion $\{V < V^* + C\rho^2\delta(\beta)^2\} \subset \{V < V^* + C_V\delta(\beta)^2\}$ implies that it is sufficient to show that, for each $i \in I_{\min}$, it holds, for some $C > 0$ and $0 < \rho < 1$, that

$$\mathscr{S}^{(i)}(\rho, C) := \mathcal{A}(z_0) \cap \left\{V < V^* + C\rho^2\delta(\beta)^2\right\} \cap [B(z_i, \delta(\beta)) \setminus B(z_i, \rho\delta(\beta))] \subset \Omega_\beta. \tag{2.69}$$

The Taylor expansion of V in the coordinates (2.9) around z_i gives (recalling $V(z_i) = V^*$)

$$\begin{aligned} V - V^* &= \frac{1}{2}\sum_{j=1}^{d} \nu_j^{(i)} y_j^{(i)2} + \frac{1}{2}\int_0^1 (1-t)^2 D^3 V\left(y^{(i)-1}\left(ty^{(i)}\right)\right) : y^{(i)\otimes 3}\,\mathrm{d}t \\ &= \frac{1}{2}\sum_{j=1}^{d} \nu_j^{(i)} y_j^{(i)2} + \mathcal{O}(|y^{(i)}|^3). \end{aligned} \tag{2.70}$$

It follows that the following estimate holds for all $i \in I_{\min}$ and for some $M > 0$ on $B(z_i, \frac{1}{M})$:

$$Q_-(y^{(i)}) \leqslant V - V^*, \tag{2.71}$$

where we denote

$$Q_-(y) = M^{-1}|y'|^2 - My_1^2 = M^{-1}|y|^2 - (M + M^{-1})y_1^2.$$

We note that the set $\{Q_- > 0\}$ is simply given by the cone $\{|y_1| < M^{-1}|y'|\}$.

We assume that $\delta(\beta) < M^{-1}$ for sufficiently large β, and let $x \in \mathscr{S}^{(i)}(\rho, C)$. It follows from (2.71) and $V(x) < V^* + C\rho^2\delta(\beta)^2$ that $Q_-(y^{(i)}(x)) < C\rho^2\delta(\beta)^2$, from which we gather

$$\frac{M^{-1}|y^{(i)}(x)|^2 - C\rho^2\delta(\beta)^2}{M + M^{-1}} < y_1^{(i)2}(x).$$

Therefore, for $0 < C < M^{-1}$, and since $|y^{(i)}(x)| > \rho\delta(\beta)$, it holds that $|y_1^{(i)}(x)| > \sqrt{\frac{M^{-1}-C}{M+M^{-1}}}\rho\delta(\beta)$. We take $C(V, z_0) = C = \min(C_V, M^{-1}/2)$, and set $\zeta := \sqrt{\frac{M^{-1}-C}{M+M^{-1}}} > 0$. We distinguish two cases

- If $y_1^{(i)}(x) < -\zeta\rho\delta(\beta) < \alpha^{(i)}/\sqrt{\beta} - \gamma(\beta)$, which holds for β sufficiently large, it holds asymptotically that $x \in \Omega_\beta$ by (**H2**). This fixes β_0.
- On the other hand, if $y_1^{(i)}(x) > \zeta\rho\delta(\beta)$ and $\delta(\beta) < K(\zeta)\sqrt{\varepsilon_0(\zeta)}$, applying Lemma 2.29 with $T = \zeta$ and $\varepsilon = \delta(\beta)^2/K(T)^2$, it holds that $x \notin \mathcal{A}(z_0)$ provided $\rho > \delta(\beta)/K(\zeta)^2$. This in turn implies $x \notin \mathscr{S}^{(i)}(\rho, C)$, which contradicts the assumption on x and precludes this case.

It follows that, provided $\delta(\beta) < \varepsilon_0(V, z_0) := \min\{M^{-1}, K(\zeta)^2/2, K(\zeta)\sqrt{\varepsilon_0(\zeta)}\}$, there exists $0 < \rho \leqslant 1/2$ and $C > 0$, such that for sufficiently large β, the required inclusion (2.69) holds. The conclusion of Proposition 2.30 follows by iterating this argument a finite number of times.

The final condition on $\varepsilon_0(V, z_0)$ can clearly be satisfied, since V has finitely many isolated critical points in $\mathcal{K}$. □

Remark 2.31. The constant $\varepsilon_0(V, z_0)$ is actually a function of $\min_{i\in I_{\min}} \min_{1\leqslant j\leqslant d} |\nu_j^{(i)}|$, where we recall the definition (2.5).

We finally state the following simple estimates.

Lemma 2.32. *There exists $\varepsilon_0 > 0$ and $0 < C_\xi < 1$ and $0 < M(V, z_0)$ such that, for all $i \in I_{\min}$ and all $0 < \varepsilon < \varepsilon_0$, it holds*

$$\left[B(z_i, \varepsilon) \setminus B\left(z_i, \frac{1}{2}\varepsilon\right)\right] \cap \left\{|y_1^{(i)}| < C_\xi \varepsilon\right\} \subset \left\{V > V^* + M(V, z_0)\varepsilon^2\right\}, \tag{2.72}$$

$$\mathcal{S}(z_0) \setminus \bigcup_{i \in I_{\min}} B(z_i, \varepsilon) \subset \left\{V > V^* + M(V, z_0)\varepsilon^2\right\}. \tag{2.73}$$

Proof. We recall the bound (2.71). We first find $C_\xi > 0$ so that for all $0 < \varepsilon < \varepsilon_0' := M^{-1}$, (2.72) holds. For any $0 < C_\xi < 1$ and all $x \in \{|y_1^{(i)}| < C_\xi \varepsilon\} \cap \left[B(z_i, \varepsilon) \setminus B\left(z_i, \frac{1}{2}\varepsilon\right)\right]$, it holds that

$$Q_-(y^{(i)}(x)) \geqslant \left[\frac{1}{4M} - C_\xi^2\left(M + \frac{1}{M}\right)\right]\varepsilon^2.$$

In particular, choosing $C_\xi < \frac{1}{2\sqrt{1+M^2}}$ ensures that $V(x) - V^* > Q_-(y^{(i)}(x)) > 0$, and taking $M(V, z_0) < \frac{1}{4M} - C_\xi^2\left(M + \frac{1}{M}\right)$ ensures (2.72).

Let us next show (2.73). Since V is decreasing along trajectories of the gradient flow ϕ_t, it follows that $V|_{\overline{\mathcal{A}(z_0)}}$ is bounded from below by $V(z_0)$. From the boundedness of $\mathcal{A}(z_0) \cap \{V < V^*\}$ (see Assumption (**EK2**)) and the Morse property of V, the set $I_{\min}$ is finite, and by Lemma 2.28 above, the points $(z_i)_{i \in I_{\min}}$ are the unique minimizers of $V|_{\mathcal{S}(z_0)}$. Since $I_{\min}$ is finite, the stable manifold theorem implies that the restricted Hessian $\nabla^2 V|_{\mathcal{S}(z_0)}$ is positive definite in a neighborhood of $\{z_i\}_{i \in I_{\min}}$. It therefore holds that there exists constants $C', \varepsilon_0 > 0$ with $\varepsilon_0 \leqslant \varepsilon_0'$ such that for all $0 < \varepsilon < \varepsilon_0$, it holds

$$\mathcal{S}(z_0) \setminus \bigcup_{i \in I_{\min}} B(z_i, \varepsilon) \subset \left\{V > V^* + C'\varepsilon^2\right\},$$

and choosing $M(V, z_0) < C'$ suffices to ensure (2.73). □

2.5.2 Construction of the quasimodes on perturbed domains

From now on, we assume that assumptions (**EK1**), (**EK2**) (**EK3**) and (**EK4**) hold.

In the literature dealing with semiclassical asymptotics in the presence of a Dirichlet boundary (see e.g. [159, 209]), a common way to define quasimodes relies on expressing them in a dedicated set of local coordinates around each (generalized) critical point of interest, which is adapted to the local quadratic behavior of V and in which the geometry of the boundary becomes locally linear. This allows to perform the analysis in a simpler geometric setting. However, the flexibility regarding the specific geometry of the boundary afforded by Assumption (**H2**) makes the definition of such a set of local coordinates rather difficult. Instead, we base our argument on the following comparison principle for Dirichlet eigenvalues, or so-called domain monotonicity, which is well-known in the case of the Laplacian $V = 0$.

Proposition 2.33. *Let $A \subset B$ be bounded open subsets of $\mathbb{R}^d$, $\beta > 0$ and $k \in \mathbb{N}^*$. Then*

$$\lambda_{k,\beta}(B) \leqslant \lambda_{k,\beta}(A),$$

where we recall $\lambda_{k,\beta}(A)$ is the k-th eigenvalue of $-\mathcal{L}_\beta$ with Dirichlet boundary conditions on ∂A.

Proof. The fact that $X \in \{A, B\}$ is bounded and open ensures that the Dirichlet realization of $-\mathcal{L}_\beta$ on X has pure point spectrum tending to $+\infty$, due to the compact injections $H^1_0(X) \hookrightarrow L^2(X)$, and $\lambda_{k,\beta}(X)$ is therefore well-defined. The inequality follows immediately from the Min-Max Courant–Fischer principle and the inclusion of form domains:

$$H^1_{0,\beta}(A) \subset H^1_{0,\beta}(B).$$

□

Our approach relies on the construction, for sufficiently large β, of two modified domains $\Omega^\pm_\beta$ such that

$$\Omega^-_\beta \subseteq \Omega_\beta \subseteq \Omega^+_\beta,$$

and whose boundaries are flat in the neighborhood of low-lying separating saddle points close to the boundary. These domains are defined using Proposition 2.27 with $\rho(\beta) = 2\gamma(\beta)$, and their boundaries are shaped like hyperplanes in the neighborhood of each z_i such that $\alpha^{(i)} < +\infty$, as made precise by Equation (2.61).

Remark 2.34. Since (**EK3**) holds for Ω_β, it also holds for $\Omega^\pm_\beta$. For Ω^+_β, this is immediate since $\Omega_\beta \subset \Omega^+_\beta$. For Ω^-_β, the proof of Proposition 2.27 shows that one can take Ω^-_β to be a $\mathcal{O}(\delta(\beta)^2)$-perturbation of Ω_β outside of $\bigcup_{i\in I_{\min}} B\left(z_i, \delta(\beta)\right)$. Since V is uniformly Lipschitz on $\mathcal{K}$, this implies that (**EK3**) still holds, possibly with a smaller constant C_V.

For similar reasons, choosing Ω^-_β to be an $\mathcal{O}(\delta(\beta))$-perturbation of Ω_β near critical points z_i such that $\alpha^{(i)} = +\infty$, we may assume that $B(z_i, \delta(\beta)) \subset \Omega^-_\beta$ for β sufficiently large, after possibly reducing $\delta(\beta)$ by a constant factor. We will henceforth assume that both these properties hold for Ω^-_β.

Upon replacing $\delta(\beta)$ by $c\delta(\beta)$ for some $c \leqslant \frac{1}{2}$ in Assumption (**H2**) (which is allowed according to (**EK4**) and Proposition 2.30), we henceforth assume that, for β sufficiently large,

$$\forall\, i \in I_{\min}, \qquad \Omega^\pm_\beta \cap B(z_i, \delta(\beta)) = \left[z_i + E^{(i)}\left(\frac{\alpha^{(i)}}{\sqrt{\beta}} \pm 2\gamma(\beta)\right)\right] \cap B(z_i, \delta(\beta)), \tag{2.74}$$

which will somewhat simplify the presentation.

The proof of Theorem 2.17 relies on the construction, inspired by [61, 208, 209], of approximate eigenmodes $\psi^\pm_\beta$ for the Dirichlet realization of $-\mathcal{L}_\beta$ on each of the domains $\Omega^\pm_\beta$, which will be sufficiently precise to provide an asymptotic equivalent for $\lambda_{1,\beta}\left(\Omega^\pm_\beta\right)$. The comparison principle of Proposition 2.33 will finally yield the conclusion of Theorem 2.17. More precisely, solutions to an elliptic PDE, obtained by linearizing $\mathcal{L}_\beta$ in the neighborhood of each of the $\{z_i,\, i \in I_{\min}\}$, are used to define these quasimodes locally, which are then rather crudely extended to define elements of the operator domains $H^1_{0,\beta}(\Omega^\pm_\beta) \cap H^2_\beta(\Omega^\pm_\beta)$. Using Theorem 2.16 to ensure that a spectral gap exists, one can then use a resolvent estimate (Lemma 2.39 below) to control the error incurred by projecting the quasimodes onto the

subspace spanned by the first eigenmode of the Dirichlet realization of $-\mathcal{L}_\beta$ on $\Omega_\beta^\pm$. This allows to derive the Eyring–Kramers formula in a straightforward way.

Our quasimodes are defined by the following convex combinations

$$\psi_\beta^\pm = \frac{1}{Z_\beta^\pm}\left[\eta_\beta + \sum_{i\in I_{\min}} \chi_\beta^{(i)}\left(\varphi_\beta^{(i),\pm} - \eta_\beta\right)\right], \tag{2.75}$$

where the χ_β are defined in (2.51), and where $Z_\beta^\pm$ are normalizing constants imposing

$$\int_{\Omega_\beta^\pm} {\psi_\beta^\pm}^2 \mathrm{e}^{-\beta V} = 1.$$

This definition uses auxiliary functions η_β and $\left(\varphi_\beta^{(i),\pm}\right)_{i\in I_{\min}}$.

The function η_β is a crude cutoff function used to localize the analysis in some small neighborhood of the energy basin separating the minimum z_0 from the low energy saddle points $\{z_i,\, i \in I_{\min}\}$. More precisely, we define the energy cutoff η_β by

$$\eta_\beta(x) = \eta\left(\frac{V(x) - V^*}{C_\eta \delta(\beta)^2}\right) \mathbb{1}_{\overline{\mathcal{A}(z_0)}}(x), \tag{2.76}$$

where $\eta \in \mathcal{C}_{\mathrm{c}}^\infty(\mathbb{R})$ is a model cutoff function chosen such that

$$\mathbb{1}_{(-\infty,\frac{1}{2})} \leqslant \eta \leqslant \mathbb{1}_{(-\infty,1)}, \tag{2.77}$$

and $C_\eta > 0$ is a constant we make precise in Proposition 2.35 below. This rough construction is, in the neighborhood of low-energy saddle points, replaced by a finer local approximation, which one can (roughly) view as the solution to a linearized Dirichlet problem.

The functions $\varphi_\beta^{(i),\pm}$ are defined, for $i \in I_{\min}$, by

$$\varphi_\beta^{(i),\pm}(x) = \frac{\displaystyle\int_{y_1^{(i)}(x)}^{\frac{\alpha^{(i)}}{\sqrt{\beta}}\pm 2\gamma(\beta)} \mathrm{e}^{-\beta\frac{|\nu_1^{(i)}|}{2}t^2}\xi_\beta(t)\,\mathrm{d}t}{\displaystyle\int_{-\infty}^{\frac{\alpha^{(i)}}{\sqrt{\beta}}\pm 2\gamma(\beta)} \mathrm{e}^{-\beta\frac{|\nu_1^{(i)}|}{2}t^2}\xi_\beta(t)\,\mathrm{d}t} \tag{2.78}$$

where ξ_β is again a $\mathcal{C}_{\mathrm{c}}^\infty(\mathbb{R})$ cutoff function used to localize the support of $\nabla\varphi_\beta^{(i)}$. It is convenient for the analysis to work with a $\varphi_\beta^{(i),\pm}$ whose gradient is localized around z_i. We thus take $\xi_\beta \in \mathcal{C}_{\mathrm{c}}^\infty(\mathbb{R})$ to be an even, smooth cutoff function satisfying

$$\mathbb{1}_{\left(-\frac{C_\xi}{2}\delta(\beta),\frac{C_\xi}{2}\delta(\beta)\right)} \leqslant \xi_\beta \leqslant \mathbb{1}_{\left(-C_\xi\delta(\beta),C_\xi\delta(\beta)\right)} \tag{2.79}$$

where $C_\xi > 0$ is a constant whose value we make precise in Proposition 2.35 below.

Observe that, upon formally taking $\xi_\beta = \mathbb{1}_{\mathbb{R}}$, and $\gamma(\beta) = 0$ in the definition (2.78), an easy

computation gives

$$\begin{cases} \left((x-z_i)^\intercal \nabla^2 V(z_i)\nabla - \frac{1}{\beta}\Delta\right)\varphi_\beta^{(i)} = 0 \text{ on } E^{(i)}\left(\frac{\alpha^{(i)}}{\sqrt{\beta}}\right), \\ \varphi_\beta^{(i)} = 0 \text{ on } \partial E^{(i)}\left(\frac{\alpha^{(i)}}{\sqrt{\beta}}\right). \end{cases}$$

Notice that if z_i is far from the boundary, that is if $\alpha^{(i)} = +\infty$, then $E^{(i)}\left(\frac{\alpha^{(i)}}{\sqrt{\beta}}\right) = \mathbb{R}^d$, so that the boundary condition disappears. Since the operator $(x-z_i)^\intercal \nabla^2 V(z_i)\nabla - \frac{1}{\beta}\Delta$ is a linearization of $-\mathcal{L}_\beta$ around z_i, the definition (2.78) is a natural local approximation for the Dirichlet eigenvector associated with the smallest eigenvalue $\lambda_{1,\beta}$ (which goes to zero as $\beta \to \infty$, by Theorem 2.16).

Proposition 2.35. *There exist a bounded open set $\mathcal{U}_0 \subset \mathbb{R}^d$, and positive constants $\beta_0, C_\xi, C_\eta > 0$, such that for all $\beta > \beta_0$, the functions $\psi_\beta^\pm$ defined in (2.75) and η_β defined in (2.76) satisfy the following conditions:*

$$\operatorname{supp}\psi_\beta^\pm \subset \overline{\mathcal{U}_0} \text{ and } z_0 \text{ is the unique minimum of } V \text{ in } \overline{\mathcal{U}_0}, \tag{2.80}$$

$$\psi_\beta^\pm \in \mathcal{C}_c^\infty\left(\mathbb{R}^d\right), \tag{2.81}$$

$$\psi_\beta^\pm \in H^1_{0,\beta}(\Omega_\beta^\pm) \cap H^2_\beta(\Omega_\beta^\pm), \tag{2.82}$$

$$\forall\, i \in I_{\min}, \quad \operatorname{supp}\eta_\beta \cap \left[B(z_i,\delta(\beta)) \setminus B\left(z_i, \frac{1}{2}\delta(\beta)\right)\right] \subset \{y_1^{(i)} < -C_\xi\delta(\beta)\}, \tag{2.83}$$

$$\operatorname{supp}\nabla\psi_\beta^\pm \setminus \bigcup_{i\in I_{\min}} B\left(z_i,\delta(\beta)\right) \subset \left\{V \geqslant V^* + \frac{C_\eta}{2}\delta(\beta)^2\right\} \cap \overline{\mathcal{A}(z_0)}, \tag{2.84}$$

$$\psi_\beta^\pm \equiv \frac{1}{Z_\beta^\pm}\varphi_\beta^{(i),\pm} \text{ on } B\left(z_i, \frac{1}{2}\delta(\beta)\right), \tag{2.85}$$

$$\psi_\beta^\pm \equiv \frac{1}{Z_\beta^\pm} \text{ on } \left[\Omega_\beta^\pm \setminus \bigcup_{i\in I_{\min}} B\left(z_i,\delta(\beta)\right)\right] \cap \left\{V < V^* + \frac{C_\eta}{2}\delta(\beta)^2\right\} \cap \overline{\mathcal{A}(z_0)}. \tag{2.86}$$

Proof. We take C_ξ as in Lemma 2.32, and $C_\eta < \min\{C_V, C(V,z_0), M(V,z_0)\}$, where C_V is given in (**EK3**), $C(V,z_0)$ is given in Proposition 2.30 and $M(V,z_0)$ is given in Lemma 2.32. In the following proof, we reduce the value of $\delta(\beta)$ several times by invoking (**EK4**) and Proposition 2.30.

The properties (2.84), (2.85) and (2.86) are immediate consequences of the definitions (2.75), (2.76), and are verified by construction regardless of the value of $\delta(\beta)$.

The property (2.83) follows from (2.76), (2.68) and (2.72), once one imposes $\delta(\beta)$ to be smaller than $\varepsilon_0(C_\xi)$ obtained in Lemma 2.29 and than ε_0 from Lemma 2.32, at least for β sufficiently large.

Let us now define $\mathcal{U}_0$ and prove (2.80). For any local minimum $m \in \mathbb{R}^d$ of V, standard arguments (see [317, Chapter 8]) show that the basin $\mathcal{A}(z_0)$ is open and its boundary contains no local minimum of V. Furthermore, for $\varepsilon < 2\varepsilon_0(V, z_0)$, $\overline{B(z_i, \varepsilon)}$ contains no local minimum of V for any $i \in I_{\min}$. Let us then define

$$\mathcal{U}_0 = [(\overline{\mathcal{A}(z_0)} \setminus \mathcal{S}(z_0)) \cap \{V < V^* + \varepsilon\}] \cup \bigcup_{i \in I_{\min}} B(z_i, \varepsilon).$$

Note that, according to (**EK2**) and for ε sufficiently small, this set is bounded and since $V^* > V(z_0)$, we may also choose ε sufficiently small so that z_0 is the unique minimum of V in $\overline{\mathcal{U}_0}$.

Let us check that $\operatorname{supp} \psi_\beta^\pm \subset \overline{\mathcal{U}_0}$. For $i \in I_{\min}$, $\psi_\beta^\pm$ writes

$$\psi_\beta^\pm = \begin{cases} \chi_\beta^{(i)} \varphi_\beta^{(i),\pm} \equiv \varphi_\beta^{(i)} \text{ on } B\left(z_i, \frac{1}{2}\delta(\beta)\right), \\ (1 - \chi_\beta^{(i)})\eta_\beta + \chi_\beta^{(i)} \varphi_\beta^{(i),\pm} \text{ on } B\left(z_i, \delta(\beta)\right) \setminus B\left(z_i, \frac{1}{2}\delta(\beta)\right), \\ \eta_\beta \text{ on } \mathbb{R}^d \setminus \bigcup_{i \in I_{\min}} B\left(z_i, \delta(\beta)\right), \end{cases}$$

using, (2.49), (2.52) and the definition (2.75).

Therefore, it is clear that, for $C_\eta \delta(\beta)^2, \delta(\beta) < \varepsilon$, it is the case that $\operatorname{supp} \psi_\beta^\pm \subset \overline{\mathcal{U}_0}$: the first condition ensures $\operatorname{supp} \eta_\beta \subset \overline{\mathcal{U}_0}$, while the second ensures $\operatorname{supp} \sum_{i \in I_{\min}} \chi_\beta^{(i)} \subset \overline{\mathcal{U}_0}$. Reducing $\delta(\beta)$ once again to satisfy these constraints, using (**EK4**) and Proposition 2.30, (2.80) follows.

Let us show (2.81). From (2.80), $\psi_\beta^\pm$ is compactly supported, and from the definition (2.75) and the smoothness, for each $i \in I_{\min}$, of $\varphi_\beta^{(i),\pm} \chi_\beta^{(i)}$ on $B(z_i, \delta(\beta))$, and since $\psi_\beta^\pm$ coincides with $\varphi_\beta^{(i),\pm}$ on $B\left(z_i, \frac{1}{2}\delta(\beta)\right)$, it is sufficient to check that η_β is smooth on $\mathbb{R}^d \setminus \bigcup_{i \in I_{\min}} B\left(z_i, \frac{1}{2}\delta(\beta)\right)$. In turn, it is sufficient to show, from the definition (2.76), that $\mathcal{S}(z_0) \cap \{V < V^* + C_\eta \delta(\beta)^2\}$ is contained in $\bigcup_{i \in I_{\min}} B\left(z_i, \frac{1}{2}\delta(\beta)\right)$ for β sufficiently large, where we use (2.19). This in turn follows immediately from the estimate (2.73), and from the choice $C_\eta < M(V, z_0)$, provided $\delta(\beta)/2 < \varepsilon_0$ from Lemma 2.32.

We finally show (2.82). From (2.81), it is clear that $\psi_\beta^\pm \in H^2_\beta(\Omega_\beta^\pm) \cap H^1_\beta(\Omega_\beta^\pm)$. Thus it only remains to show $\psi_\beta^\pm \in H^1_{0,\beta}(\Omega_\beta)$, for which we in fact show that $\psi_\beta^\pm|_{\partial\Omega_\beta^\pm} \equiv 0$ holds. Again, we decompose the argument. On $\partial\Omega_\beta^\pm \setminus \left[\overline{\mathcal{A}(z_0)} \bigcup_{i \in I_{\min}} B(z_i, \delta(\beta))\right]$, it holds that $\psi_\beta^\pm \equiv \eta_\beta \equiv 0$, and on $\left[\partial\Omega_\beta^\pm \setminus \bigcup_{i \in I_{\min}} B(z_i, \delta(\beta))\right] \cap \overline{\mathcal{A}(z_0)}$, it holds that $\psi_\beta^\pm \equiv \eta_\beta \equiv 0$ from the inclusion (**EK3**) and the choice $C_\eta < C_V$. Now let $i \in I_{\min}$. If $\alpha^{(i)} = +\infty$, then $B(z_i, \delta(\beta)) \subset \Omega_\beta \subset \Omega_\beta^+$ by (**H2**). By slightly reducing $\delta(\beta)$ if necessary, it is possible to ensure that $B(z_i, \delta(\beta)) \subset \Omega_\beta^-$ (see Remark 2.34). Thus, in this case, $\partial\Omega_\beta^\pm \cap B(z_i, \delta(\beta)) = \varnothing$. We now assume $\alpha^{(i)} < +\infty$. From (2.74) and (2.78), the boundary condition $\psi_\beta^\pm|_{\partial\Omega_\beta^\pm} \equiv 0$ is satisfied on $\partial\Omega_\beta^\pm \cap B(z_i, \frac{1}{2}\delta(\beta))$, since on this set, $\psi_\beta^\pm \equiv \varphi_\beta^{(i),\pm}$. On $\partial\Omega_\beta^\pm \cap \left[B(z_i, \delta(\beta)) \setminus B\left(z_i, \frac{1}{2}\delta(\beta)\right)\right]$, this finally follows, for β

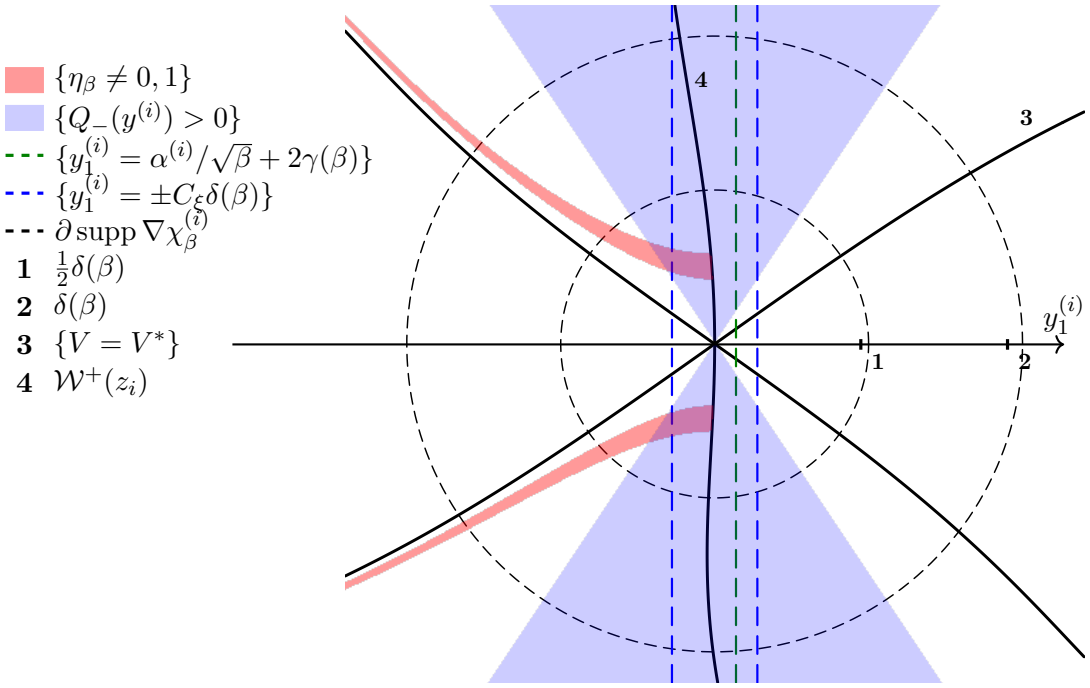

Figure 2.4: Construction of the quasimode (2.75) in the neighborhood of the low-energy saddle point z_i, depicted in the adapted $y^{(i)}$ coordinates. Here, we depict the elements entering into the construction of ψ_β^+, in the case $\alpha^{(i)} < +\infty$. The shaded blue cone corresponds to the positive superlevel set of the quadratic form Q_- from the proof of Proposition 2.30.

sufficiently large, from the energy estimate (2.72), the choices $\delta(\beta) < \varepsilon$, $C_\eta < M(V, z_0)$ and the fact that, on this set $\left|y_1^{(i)}\right| = \left|\alpha^{(i)}/\sqrt{\beta} \pm 2\gamma(\beta)\right| \ll C_\xi \delta(\beta)$. Since $\Omega_\beta^\pm$ are regular domains from Proposition 2.27, $\psi_\beta^\pm \in H_0^1(\Omega_\beta^\pm) = H_{0,\beta}^1(\Omega_\beta^\pm)$ by the trace theorem. The latter equality follows from the smoothness of V and the boundedness of $\Omega_\beta^\pm$. This concludes the proof of (2.82). □

We assume, for the remainder of this work, and without loss of generality, that $\delta(\beta)$ is asymptotically sufficiently small for the conclusions of Proposition 2.35 to hold. We now derive the first preliminary result for the proof of the formula (2.24), which is a variant of the Laplace method for in moving domains.

2.5.3 Laplace's method on moving domains

We present in this section a key technical tool, a variant of the Laplace method for exponential integrals in the case where the domain of integration varies with the asymptotic parameter. Moreover, we allow for a minimum of the argument of the exponential lying outside of the domain, but close to the boundary in some scaling made precise in Proposition 2.36. We recall the symmetric difference of sets, which we denote by

$$A \triangle B := (A \cup B) \setminus (A \cap B) = (A \setminus B) \cup (B \setminus A).$$

We show the following result.

Proposition 2.36. *Consider a family $(A_\lambda)_{\lambda>0}$ of Borel sets. Assume that there exists $\mathcal{K}, A_\infty \in \mathcal{B}(\mathbb{R}^d)$ with non-empty interiors, $x_0 \in \overset{\circ}{\mathcal{K}}$, and $\epsilon > 0$ such that the following properties hold:*

- *The set $\mathcal{K}$ is compact, and the following inclusion holds:*

$$\forall\, \lambda > 0, \qquad A_\lambda \subseteq \mathcal{K}. \tag{L1}$$

- *The functions*

$$f \in \mathcal{C}^4(\mathcal{K}), \qquad g \in \mathcal{C}^2(\mathcal{K}) \tag{L2}$$

  are such that

$$\operatorname*{Argmin}_{x\in\mathcal{K}} f(x) = \{x_0\}, \qquad \nabla^2 f(x_0) \geqslant \epsilon \mathrm{Id}, \qquad g(x_0) \neq 0. \tag{L3}$$

- *The domains admit a limit in the semiclassical scaling around x_0:*

$$\mathbb{1}_{\sqrt{\lambda}(A_\lambda - x_0)} \xrightarrow[\lambda\to+\infty]{a.e.} \mathbb{1}_{A_\infty}. \tag{L4}$$

Then,

$$\int_{A_\lambda} \mathrm{e}^{-\lambda f(x)} g(x)\,\mathrm{d}x = \left(\frac{2\pi}{\lambda}\right)^{\frac{d}{2}} \mathrm{e}^{-\lambda f(x_0)} \left(\det \nabla^2 f(x_0)\right)^{-\frac{1}{2}} g(x_0) \mathbb{P}(\mathcal{G} \in A_\infty) \left(1 + \mathcal{O}(\varepsilon(\lambda)) + \mathcal{O}(\lambda^{-\frac{r}{2}})\right) \tag{2.87}$$

as $\lambda \to +\infty$, where $\mathcal{G}$ is a Gaussian random variable with distribution $\mathcal{N}\left(0, \nabla^2 f(x_0)^{-1}\right)$, and the dominant error terms are determined by:

$$\varepsilon(\lambda) = \mathbb{P}\left(\mathcal{G} \in \left[\sqrt{\lambda}\,(A_\lambda - x_0)\right] \triangle\, A_\infty\right),$$

and

$$\begin{cases} r = 2, & \text{if } A_\infty = -A_\infty, \\ r = 1 & \text{otherwise.} \end{cases}$$

The proof of Proposition 2.36 is postponed to Appendix 2.B below.

Remark 2.37. The conclusion of Proposition 2.36 still holds true assuming only that $\mathcal{K}$ is closed but not necessarily bounded, requiring instead that $g \in L^1(\mathcal{K})$, and that there exists $\delta_0 > 0$ such that, for any $0 < \delta < \delta_0$,

$$\gamma(\delta) := \inf_{x\in\mathcal{K}\setminus B(x_0,\delta)} \{f(x) - f(x_0)\} > 0.$$

The proof of this variant is verbatim the same as the one given in Appendix 2.B below, upon replacing γ by $\gamma(\delta)$ with $\delta < \delta_0$ in (2.114).

2.5.4 Low-temperature estimates

We obtain in this section the key estimates on the quasimode (2.75) needed to compute the asymptotic behavior of $\|\nabla\psi_\beta\|_{L^2_\beta(\Omega_\beta)}$ and $\|\mathcal{L}_\beta\psi_\beta\|_{L^2_\beta(\Omega_\beta)}$ in the limit $\beta \to \infty$. Good estimates

for these quantities, summarized in Proposition 2.38, together with a resolvent estimate given by Lemma 2.39 below, will yield the modified Eyring–Kramers formula (2.24) in the proof of Theorem 2.17, concluded in section 2.5.5.

For convenience, we decompose the analysis according to the following partition of the domain Ω_β:

$$\Omega_\beta^\pm = \bigcup_{i\in I_{\min}} \left[\mathbf{A}_\beta^{(i)} \cup \mathbf{B}_\beta^{(i),\pm} \cup \mathbf{C}_\beta^{(i)} \cup \mathbf{D}_\beta^{(i),\pm}\right] \cup \mathbf{E}_\beta \cup \mathbf{F}_\beta \cup \mathbf{G}_\beta^\pm, \tag{2.88}$$

where, for $i \in I_{\min}$:

$$\mathbf{A}_\beta^{(i)} = \left[B\left(z_i, \delta(\beta)\right) \setminus B\left(z_i, \frac{1}{2}\delta(\beta)\right)\right] \cap \left\{y_1^{(i)} < -C_\xi \delta(\beta)\right\} \cap \left\{V - V^* \geqslant C_\eta \delta(\beta)^2\right\}, \tag{2.89}$$

$$\mathbf{B}_\beta^{(i),\pm} = \Omega_\beta^\pm \cap \left[B\left(z_i, \delta(\beta)\right) \setminus B\left(z_i, \frac{1}{2}\delta(\beta)\right)\right] \cap \left\{|y_1^{(i)}| \leqslant C_\xi \delta(\beta)\right\}, \tag{2.90}$$

$$\mathbf{C}_\beta^{(i)} = \left[B\left(z_i, \delta(\beta)\right) \setminus B\left(z_i, \frac{1}{2}\delta(\beta)\right)\right] \cap \left\{\frac{1}{2}C_\eta \delta(\beta)^2 < V - V^* < C_\eta \delta(\beta)^2\right\} \cap \left\{y_1^{(i)} < -C_\xi \delta(\beta)\right\}, \tag{2.91}$$

$$\mathbf{D}_\beta^{(i),\pm} = \Omega_\beta^\pm \cap B\left(z_i, \frac{1}{2}\delta(\beta)\right),$$

$$\mathbf{E}_\beta = \left[\overline{\mathcal{A}(z_0)} \cap \left\{\frac{C_\eta}{2}\delta(\beta)^2 \leqslant V - V^* \leqslant C_\eta \delta(\beta)^2\right\}\right] \setminus \bigcup_{i\in I_{\min}} B\left(z_i, \delta(\beta)\right),$$

$$\mathbf{F}_\beta = \left[\overline{\mathcal{A}(z_0)} \cap \left\{V - V^* < \frac{C_\eta}{2}\delta(\beta)^2\right\}\right] \setminus \bigcup_{i\in I_{\min}} B\left(z_i, \frac{1}{2}\delta(\beta)\right),$$

$$\mathbf{G}_\beta^\pm = \Omega_\beta \setminus \left(\bigcup_{i\in I_{\min}} \left[\mathbf{A}_\beta^{(i)} \cup \mathbf{B}_\beta^{(i),\pm} \cup \mathbf{C}_\beta^{(i)} \cup \mathbf{D}_\beta^{(i),\pm}\right] \cup \mathbf{E}_\beta \cup \mathbf{F}_\beta\right).$$

Note that, according to (2.74), the sets $\mathbf{B}_\beta^{(i),\pm}$ and $\mathbf{D}_\beta^{(i),\pm}$ have simple representations, namely

$$\mathbf{D}_\beta^{(i),\pm} = \left\{y_1^{(i)} < \alpha^{(i)}/\sqrt{\beta} \pm 2\gamma(\beta)\right\} \cap B\left(z_i, \frac{1}{2}\delta(\beta)\right),$$

$$\mathbf{B}_\beta^{(i),\pm} = \left\{y_1^{(i)} < \alpha^{(i)}/\sqrt{\beta} \pm 2\gamma(\beta)\right\} \cap \left[B\left(z_i, \delta(\beta)\right) \setminus B\left(z_i, \frac{1}{2}\delta(\beta)\right)\right] \cap \left\{|y_1^{(i)}| \leqslant C_\xi \delta(\beta)\right\}.$$

We refer the reader to Figure 2.5 for a pictorial representation of these sets. Before the statements and proof of the necessary estimates, let us give some informal indications of our strategy. On the high-energy sets $\mathbf{A}_\beta^{(i)}$, $\mathbf{B}_\beta^{(i),\pm}$, $\mathbf{C}_\beta^{(i)}$ and $\mathbf{E}_\beta$ (contained in $\{V \geqslant V^* + C_\eta\delta(\beta)^2/2\}$), crude uniform bounds on the derivatives of $\chi_\beta^{(i)}$, η_β and $\varphi_\beta^{(i)}$ will suffice to identify the contribution of these sets to the $L^2_\beta(\Omega_\beta)$-norms of both $\nabla\psi_\beta^\pm$ and $\mathcal{L}_\beta\psi_\beta^\pm$ as superpolynomially decaying error terms. The sets $\mathbf{F}_\beta$ and $\mathbf{G}_\beta^\pm$ are constructed so that $\psi_\beta^\pm$ is constant on each

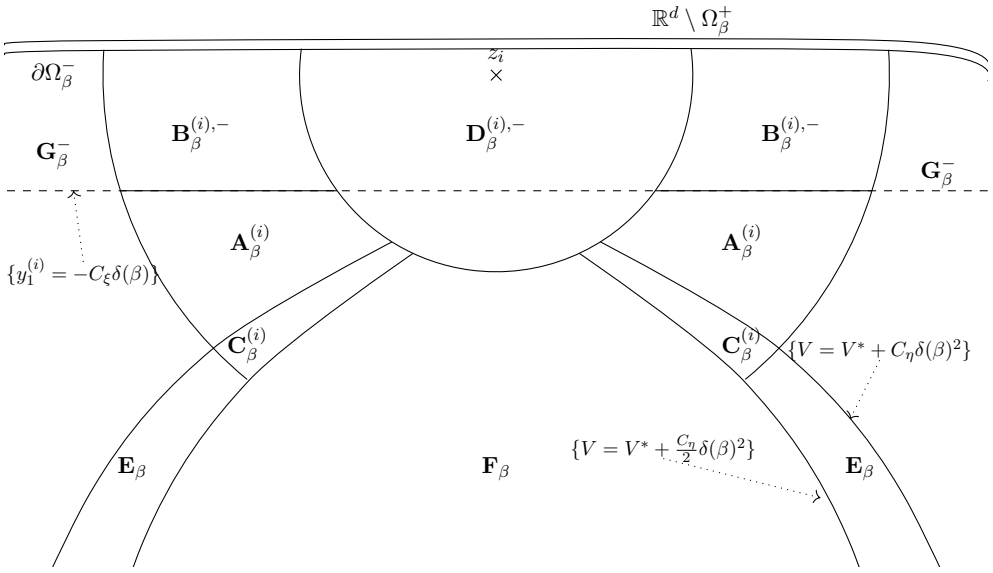

(a) The case $\alpha^{(i)} < +\infty$. The boundaries $\partial\Omega_\beta^\pm$ are hyperplanes inside $B(z_i, \delta(\beta))$, separated by a distance $4\gamma(\beta)$, as described in (2.74).

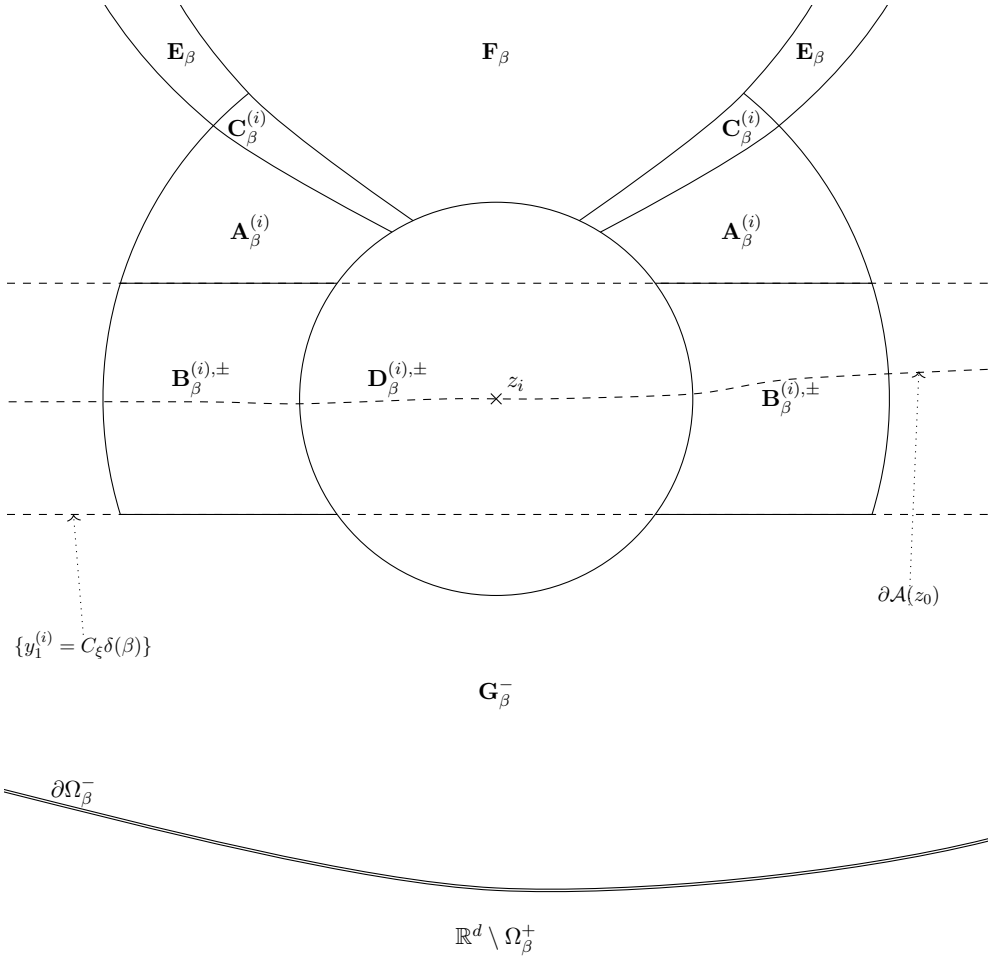

(b) The case $\alpha^{(i)} = +\infty$. The width of the shell $\Omega_\beta^+ \setminus \Omega_\beta^-$ is of order $\varepsilon_1(\beta)$ around z_i, as in the proof of Proposition 2.27.

Figure 2.5: Schematic representation of the partition (2.88).

of them, with respective values $1/Z_\beta^\pm$ and 0, and will not contribute to the estimates. The only contribution left are from $\mathbf{D}_\beta^{(i),\pm}$, on which the $\psi_\beta^\pm$ coincide with the finer approximations $\frac{1}{Z_\beta^\pm}\varphi_\beta^{(i),\pm}$, according to (2.85). The contribution of this set to the $L^2_\beta(\Omega_\beta^\pm)$-norm of $\nabla\psi_\beta^\pm$ is more finely analyzed using Proposition 2.36, giving sufficiently precise asymptotics.

We now state the required estimates.

Proposition 2.38. *The following estimates hold:*

$$Z_\beta^\pm = \mathrm{e}^{-\frac{\beta}{2}V(z_0)}\left(\frac{2\pi}{\beta}\right)^{\frac{d}{4}} |\det\nabla^2 V(z_0)|^{-\frac{1}{4}}\left(1+\mathcal{O}(\beta^{-1})\right), \tag{2.92}$$

$$\left\|\nabla\psi_\beta^\pm\right\|^2_{L^2_\beta\left(\Omega_\beta^\pm\setminus\bigcup_{i\in I_{\min}}\mathbf{D}_\beta^{(i),\pm}\right)} = \mathcal{O}\left(\mathrm{e}^{-\beta\left(V^*-V(z_0)+\frac{C_\eta}{3}\delta(\beta)^2\right)}\right), \tag{2.93}$$

$$\|\mathcal{L}_\beta\psi_\beta^\pm\|^2_{L^2_\beta\left(\Omega_\beta^\pm\setminus\bigcup_{i\in I_{\min}}\mathbf{D}_\beta^{(i),\pm}\right)} = \mathcal{O}\left(\mathrm{e}^{-\beta\left(V^*-V(z_0)+\frac{C_\eta}{3}\delta(\beta)^2\right)}\right), \tag{2.94}$$

and for all $i\in I_{\min}$, the following hold:

$$\left\|\nabla\psi_\beta^\pm\right\|^2_{L^2_\beta(\mathbf{D}_\beta^{(i),\pm})} = \frac{\beta|\nu_1^{(i)}|}{2\pi\Phi\left(|\nu_1^{(i)}|^{\frac{1}{2}}\alpha^{(i)}\right)}\sqrt{\frac{\det\nabla^2V(z_0)}{|\det\nabla^2V(z_i)|}}\mathrm{e}^{-\beta(V^*-V(z_0))}\left(1+\mathcal{O}(r_i(\beta))\right), \tag{2.95}$$

where Φ is given by (2.25), and the dominant error term r_i is given by:

$$r_i(\beta) = \begin{cases}\beta^{-1}, & \alpha^{(i)}=+\infty,\\ \sqrt{\beta}\gamma(\beta)+\beta^{-\frac{1}{2}}, & \alpha^{(i)}<+\infty.\end{cases} \tag{2.96}$$

Finally, we have

$$\|\mathcal{L}_\beta\psi_\beta^\pm\|^2_{L^2_\beta(\mathbf{D}_\beta^{(i),\pm})} = \mathcal{O}\left(\beta^{-2}\delta(\beta)^{-2}\right)\left\|\nabla\psi_\beta^\pm\right\|^2_{L^2_\beta(\mathbf{D}_\beta^{(i),\pm})} \tag{2.97}$$

Proof. As a first step, we derive the asymptotic behavior of the normalizing constant as stated in (2.92).

Asymptotic behavior of $Z_\beta^\pm$.

Using (2.80), and since $B(z_0,\delta(\beta))\subset\Omega_\beta$ for sufficiently large β by Assumptions (**EK1**) and (**H2**), a direct application of Proposition 2.36 to the inequality

$$\begin{aligned}&\int_{B(z_0,\delta(\beta))}\left[\eta_\beta+\sum_{i\in I_{\min}}\chi_\beta^{(i)}\left(\varphi_\beta^{(i),\pm}-\eta_\beta\right)\right]^2\mathrm{e}^{-\beta V}\leqslant Z_\beta^{\pm 2}\\ &\leqslant\int_{\mathcal{U}_0}\left[\eta_\beta+\sum_{i\in I_{\min}}\chi_\beta^{(i)}\left(\varphi_\beta^{(i),\pm}-\eta_\beta\right)\right]^2\mathrm{e}^{-\beta V},\end{aligned}$$

since $\mathbb{1}_{B(z_0,\delta(\beta))} \leqslant \left[\eta_\beta + \sum_{i\in I_{\min}} \chi_\beta^{(i)}\left(\varphi_\beta^{(i)} - \eta_\beta\right)\right] \leqslant \mathbb{1}_{\overline{\mathcal{U}_0}}$, gives (2.92). Indeed, by a standard Gaussian decay estimate, for $\xi \sim \mathcal{N}(0, \nabla^2 V(z_0)^{-1})$, $\mathbb{P}(\xi \notin B(0, \sqrt{\beta}\delta(\beta))) = \mathcal{O}\left(\mathrm{e}^{-c\beta\delta(\beta)^2}\right)$, and $\mathbb{P}(\xi \notin B(0, \sqrt{\beta}\mathcal{U}_0)) = \mathcal{O}\left(\mathrm{e}^{-c\beta}\right)$ for some $c > 0$.
It follows from the scaling (**H3**) that the error term $\epsilon(\beta)$ in (2.87) decays superpolynomially, while the $\mathcal{O}(\beta^{-\frac{1}{2}})$ term vanishes by symmetry of the limiting domains $B(0, \sqrt{\beta}\delta(\beta))$, $\sqrt{\beta}\,(\mathcal{U}_0 - z_0) \to \mathbb{R}^d$, leaving a dominant error term in $\mathcal{O}(\beta^{-1})$. This, of course, corresponds to the usual Laplace method.

As announced, the remainder of the analysis is split according to the partition (2.88). We now let $i \in I_{\min}$ throughout the remainder of the proof.

Analysis on $\mathbf{F}_\beta \cup \mathbf{G}_\beta^\pm$.

These sets do not contributes to the estimates (2.93), (2.94), since $\left(\mathbf{F}_\beta \cup \mathbf{G}_\beta^\pm\right) \cap \operatorname{supp} \nabla\psi_\beta^\pm = \varnothing$ and $\operatorname{supp} \mathcal{L}_\beta\psi_\beta^\pm \subseteq \operatorname{supp} \nabla\psi_\beta^\pm$.

Indeed, on $\mathbf{G}_\beta^\pm$, it holds that both $\chi_\beta^{(i)}$ and η_β are zero, since $\mathbf{G}_\beta^\pm \cap \bigcup_{i\in I_{\min}} B(z_i, \delta(\beta)) = \varnothing$, which ensures $\chi_\beta^{(i)} \equiv 0$ according to (2.52), and $\mathbf{G}_\beta^\pm \subset \left(\mathbb{R}^d \setminus \overline{\mathcal{A}(z_0)}\right) \cup \{V \geqslant V^* + C_\beta\delta(\beta)^2\}$, which ensures $\eta_\beta \equiv 0$ according to (2.76). On $\mathbf{F}_\beta$, it holds that $\varphi_\beta^{(i),\pm} \equiv 1$ for all $i \in I_{\min}$, according to (2.83) and $\eta_\beta \equiv 1$. Thus, $\psi_\beta^\pm \equiv 1$ as well as a convex combination of η_β and the $\varphi_\beta^{(i),\pm}$. Therefore, for $x \in \mathbf{F}_\beta \cup \mathbf{G}_\beta^\pm$, one has $\nabla\psi_\beta^\pm = 0$ and $\mathcal{L}_\beta\psi_\beta^\pm = 0$.

Analysis on $\mathbf{A}_\beta^{(i)}$.

From (2.76),(2.77) and (2.89), we have $\eta_\beta \equiv 0$ on $\mathbf{A}_\beta^{(i)}$. Furthermore, from (2.79), $\varphi_\beta^{(i),\pm} \equiv 1$ in this set, hence $\psi_\beta^\pm$ coincides with $\frac{1}{Z_\beta^\pm}\chi_\beta^{(i)}$ on $\mathbf{A}_\beta^{(i)}$, which gives

$$\nabla\psi_\beta^\pm = \frac{1}{Z_\beta^\pm}\nabla\chi_\beta^{(i)}, \quad \mathcal{L}_\beta\psi_\beta^\pm = \frac{1}{Z_\beta^\pm}\left(-\nabla V\cdot\nabla\chi_\beta^{(i)} + \frac{1}{\beta}\Delta\chi_\beta^{(i)}\right),$$

from which it follows that

$$\|\nabla\psi_\beta^\pm\|_{L^\infty(\mathbf{A}_\beta^{(i)})} = \mathcal{O}\left(\mathrm{e}^{\frac{\beta}{2}V(z_0)}\beta^{\frac{d}{4}}\delta(\beta)^{-1}\right), \|\mathcal{L}_\beta\psi_\beta^\pm\|_{L^\infty(\mathbf{A}_\beta^{(i)})} = \mathcal{O}\left(\mathrm{e}^{\frac{\beta}{2}V(z_0)}\beta^{\frac{d}{4}}\right),$$

where we used the estimates (2.92) and (2.53), the first-order estimate $\nabla V\cdot\nabla\chi_\beta^{(i)} = \mathcal{O}(1)$ on the domain $\mathbf{A}_\beta^{(i)}$, and $\beta^{-1}\delta(\beta)^{-2} = o(1)$ to absorb the contribution of the Laplacian term $\Delta\chi_\beta^{(i)}/\beta$. We then estimate

$$\|\nabla\psi_\beta^\pm\|^2_{L^2_\beta(\mathbf{A}_\beta^{(i)})} = \mathcal{O}\left(\beta^{\frac{d}{2}}\delta(\beta)^{d-2}\mathrm{e}^{-\beta(V^*-V(z_0)+C_\eta\delta(\beta)^2)}\right) = \mathcal{O}\left(\mathrm{e}^{-\beta(V^*-V(z_0)+\frac{C_\eta}{3}\delta(\beta)^2)}\right),$$

$$\|\mathcal{L}_\beta\psi_\beta^\pm\|^2_{L^2_\beta(\mathbf{A}_\beta^{(i)})} = \mathcal{O}\left(\beta^{\frac{d}{2}}\delta(\beta)^{d}\mathrm{e}^{-\beta(V^*-V(z_0)+C_\eta\delta(\beta)^2)}\right) = \mathcal{O}\left(\mathrm{e}^{-\beta(V^*-V(z_0)+\frac{C_\eta}{3}\delta(\beta)^2)}\right),$$

using the inclusions $\mathbf{A}_\beta^{(i)} \subset \{V - V^* \geqslant C_\eta\delta(\beta)^2\}$, $\mathbf{A}_\beta^{(i)} \subset B(z_i, \delta(\beta))$, the fact that $\delta(\beta)$ is bounded by ε, and the superpolynomial decay of $\mathrm{e}^{-\beta\delta(\beta)^2}$ which follows from (**H3**).

Analysis on $\mathbf{B}_\beta^{(i),\pm}$.

From (2.76), (2.83) and (2.90), we still have $\eta_\beta \equiv 0$ on $\mathbf{B}_\beta^{(i),\pm}$, however $\varphi_\beta^{(i),\pm}$ is not constant over this set. Thus, $\psi_\beta^\pm$ is given by $\frac{1}{Z_\beta^\pm}\chi_\beta^{(i)}\varphi_\beta^{(i),\pm}$ on $\mathbf{B}_\beta^{(i),\pm}$, which yields

$$\nabla\psi_\beta^\pm = \frac{1}{Z_\beta^\pm}\left(\varphi_\beta^{(i),\pm}\nabla\chi_\beta^{(i)} + \chi_\beta^{(i)}\nabla\varphi_\beta^{(i),\pm}\right),$$

$$\mathcal{L}_\beta\psi_\beta^\pm = \frac{1}{Z_\beta^\pm}\left(\varphi_\beta^{(i),\pm}\mathcal{L}_\beta\chi_\beta^{(i)} + \chi_\beta^{(i)}\mathcal{L}_\beta\varphi_\beta^{(i),\pm} + \frac{2}{\beta}\nabla\varphi_\beta^{(i),\pm}\cdot\nabla\chi_\beta^{(i)}\right).$$

At this point, we need uniform estimates in $\mathbf{B}_\beta^{(i),\pm}$ for derivatives $\partial^\alpha\varphi_\beta^{(i),\pm}$ for $|\alpha| \leqslant 2$. Since $\varphi_\beta^{(i),\pm}$ is in fact simply a function of the affine map $y_1^{(i)}$, the problem is that of bounding the first two derivatives of

$$y_1 \mapsto \frac{1}{C_\beta^{(i),\pm}}\int_{y_1}^{\frac{\alpha^{(i)}}{\sqrt{\beta}}\pm 2\gamma(\beta)} \mathrm{e}^{-\beta\frac{|\nu_1^{(i)}|}{2}t^2}\xi_\beta(t)\,\mathrm{d}t, \quad C_\beta^{(i),\pm} := \int_{-\infty}^{\frac{\alpha^{(i)}}{\sqrt{\beta}}\pm 2\gamma(\beta)} \mathrm{e}^{-\beta\frac{|\nu_1^{(i)}|}{2}t^2}\xi_\beta(t)\,\mathrm{d}t.$$

We first estimate $C_\beta^{(i),\pm}$ by a direct application of Proposition 2.36 in the one-dimensional case. It gives

$$C_\beta^{(i),\pm} = \sqrt{\frac{2\pi}{\beta|\nu_1^{(i)}|}}\Phi\left(|\nu_1^{(i)}|^{\frac{1}{2}}\alpha^{(i)}\right)(1+e_i(\beta)), \tag{2.98}$$

where

$$\begin{cases} e_i(\beta) = \mathcal{O}\left(\sqrt{\beta}\gamma(\beta) + \beta^{-\frac{1}{2}}\right), & \alpha^{(i)} < +\infty, \\ e_i(\beta) = \mathcal{O}\left(\beta^{-1}\right), & \alpha^{(i)} = +\infty. \end{cases} \tag{2.99}$$

To obtain the formula, we note that for $\mathcal{G} \sim \mathcal{N}(0, |\nu_1^{(i)}|^{-1})$,

$$\mathbb{P}\left(\mathcal{G} \in \left(-\infty, \alpha^{(i)} \pm 2\sqrt{\beta}\gamma(\beta)\right)\right) \xrightarrow{\beta\to\infty} \Phi\left(|\nu_1^{(i)}|^{\frac{1}{2}}\alpha^{(i)}\right),$$

and

$$\mathbb{P}\left(\mathcal{G} \in \left(-\infty, \alpha^{(i)}\right) \triangle \left(-\infty, \alpha^{(i)} \pm 2\sqrt{\beta}\gamma(\beta)\right)\right) = \mathcal{O}\left(\sqrt{\beta}\gamma(\beta)\right) \tag{2.100}$$

in the case $\alpha^{(i)} < +\infty$. In the case $\alpha^{(i)} = +\infty$, note that the domain of integration is identically equal to $\mathbb{R}$ for any β, and thus the integration error vanishes, leaving only an error term in β^{-1} corresponding to the symmetry of the limiting domain. In any case, $C_\beta^{(i),\pm} = \mathcal{O}\left(\beta^{-\frac{1}{2}}\right)$, which is sufficient for our purposes, although the finer estimate (2.98) will be useful for the analysis on $\mathbf{D}_\beta^{(i),\pm}$.

We then compute

$$\begin{aligned} \nabla\varphi_\beta^{(i),\pm} &= -\frac{1}{C_\beta^{(i),\pm}}\mathrm{e}^{-\beta\frac{|\nu_1^{(i)}|}{2}y_1^{(i)2}}\xi_\beta(y_1^{(i)})v_1^{(i)}, \\ \Delta\varphi_\beta^{(i),\pm} &= \frac{1}{C_\beta^{(i),\pm}}\left[\beta|\nu_1^{(i)}|y_1^{(i)}\xi_\beta(y_1^{(i)}) - \xi_\beta'(y_1^{(i)})\right]\mathrm{e}^{-\beta\frac{|\nu_1^{(i)}|}{2}y_1^{(i)2}}, \end{aligned} \tag{2.101}$$

using $\nabla y_1^{(i)} \equiv v_1^{(i)}$ and $|v_1^{(i)}| = 1$. It follows from $0 \leqslant \mathrm{e}^{-\beta \frac{|\nu_1^{(i)}|}{2} y_1^2}, \xi_\beta^{(i)}(y_1) \leqslant 1$ that

$$\|\nabla \varphi_\beta^{(i),\pm}\|_{L^\infty(\mathbf{B}_\beta^{(i),\pm})} = \mathcal{O}(\beta^{\frac{1}{2}}), \qquad \|\Delta \varphi_\beta^{(i),\pm}\|_{L^\infty(\mathbf{B}_\beta^{(i),\pm})} = \mathcal{O}\left(\beta^{\frac{1}{2}}\left[\beta\delta(\beta) + \delta(\beta)^{-1}\right]\right) = \mathcal{O}(\beta^{\frac{3}{2}}),$$

using $\|\xi_\beta^{(i)\prime}\|_\infty = \mathcal{O}\left(\delta(\beta)^{-1}\right)$, $y_1^{(i)} = \mathcal{O}(\delta(\beta))$ on $\mathbf{B}_\beta^{(i),\pm}$, $\delta(\beta) = \mathcal{O}(1)$ and the scaling $\beta^{\frac{1}{2}}\delta(\beta)^{-1} \ll \beta/\sqrt{\log\beta}$ given by Assumption (**H3**). It follows that $\|\mathcal{L}_\beta \varphi_\beta^{(i),\pm}\|_{L^\infty(\mathbf{B}_\beta^{(i),\pm})} = \mathcal{O}(\beta^{\frac{1}{2}})$.

Plugging in these estimates and collecting terms (reusing the estimates $\nabla\chi_\beta^{(i)} = \mathcal{O}(\delta(\beta)^{-1})$, $\mathcal{L}_\beta\chi_\beta^{(i)} = \mathcal{O}(1)$ on $\mathbf{B}_\beta^{(i),\pm}$) gives, using $0 \leqslant \chi_\beta^{(i)}, \varphi_\beta^{(i),\pm} \leqslant 1$:

$$\|\nabla\psi_\beta^\pm\|_{L^\infty(\mathbf{B}_\beta^{(i),\pm})} = \mathcal{O}\left(\mathrm{e}^{\frac{\beta}{2}V(z_0)}\beta^{\frac{d}{4}}\left[\delta(\beta)^{-1} + \beta^{\frac{1}{2}}\right]\right) = \mathcal{O}\left(\mathrm{e}^{\frac{\beta}{2}V(z_0)}\beta^{\frac{d}{4}+\frac{1}{2}}\right),$$

$$\|\mathcal{L}_\beta\psi_\beta^\pm\|_{L^\infty(\mathbf{B}_\beta^{(i),\pm})} = \mathcal{O}\left(\mathrm{e}^{\frac{\beta}{2}V(z_0)}\beta^{\frac{d}{4}}\left[1 + \beta^{\frac{1}{2}} + \beta^{-\frac{1}{2}}\delta(\beta)^{-1}\right]\right) = \mathcal{O}\left(\mathrm{e}^{\frac{\beta}{2}V(z_0)}\beta^{\frac{d}{4}+\frac{1}{2}}\right),$$

using $\delta(\beta)^{-1} = o\left(\beta^{\frac{1}{2}}\right)$ to estimate the square bracketed terms. This leads to

$$\begin{aligned}\|\nabla\psi_\beta^\pm\|^2_{L^2_\beta(\mathbf{B}_\beta^{(i),\pm})}, \|\mathcal{L}_\beta\psi_\beta^\pm\|^2_{L^2_\beta(\mathbf{B}_\beta^{(i),\pm})} &= \mathcal{O}\left(\beta^{\frac{d}{2}+1}\delta(\beta)^d\mathrm{e}^{-\beta(V^*-V(z_0)+C_\eta\delta(\beta)^2)}\right)\\ &= \mathcal{O}\left(\mathrm{e}^{-\beta(V^*-V(z_0)+\frac{C_\eta}{3}\delta(\beta)^2)}\right),\end{aligned}$$

similarly to the analysis on $\mathbf{A}_\beta^{(i)}$, since $\mathbf{B}_\beta^{(i),\pm} \subset B(z_i, \delta(\beta))$ and $\mathbf{B}_\beta^{(i),\pm} \subset \{V > V^* + C_\eta\delta(\beta)^2\}$ using (2.72).

Analysis on $\mathbf{C}_\beta^{(i)}$.

By the definition (2.91), $\mathbf{C}_\beta^{(i)} \subset \{y_1^{(i)} < -C_\xi\delta(\beta)\}$, hence $\varphi_\beta^{(i)} \equiv 1$ on this set. Thus, we have locally:

$$\psi_\beta = \frac{1}{Z_\beta^\pm}\left(\eta_\beta + \chi_\beta^{(i)}(1-\eta_\beta)\right),$$

whence

$$\nabla\psi_\beta^\pm = \frac{1}{Z_\beta^\pm}\left(\left[1-\eta_\beta\right]\nabla\chi_\beta^{(i)} + \left[1-\chi_\beta^{(i)}\right]\nabla\eta_\beta\right),$$

$$\mathcal{L}_\beta\psi_\beta^\pm = \frac{1}{Z_\beta^\pm}\left(\left[1-\eta_\beta\right]\mathcal{L}_\beta\chi_\beta^{(i)} + \left[1-\chi_\beta^{(i)}\right]\mathcal{L}_\beta\eta_\beta - \frac{2}{\beta}\nabla\chi_\beta^{(i)}\cdot\nabla\eta_\beta\right),$$

by straightforward manipulations. One then only needs to check that

$$\|\nabla\eta_\beta\|_{L^\infty(\mathbf{C}_\beta^{(i)})} = \mathcal{O}\left(\delta(\beta)^{-2}\right), \quad \|\Delta\eta_\beta\|_{L^\infty(\mathbf{C}_\beta^{(i)})} = \mathcal{O}\left(\delta(\beta)^{-4}\right)$$

to obtain by similar arguments:

$$\begin{aligned}\|\nabla\psi_\beta^\pm\|^2_{L^2_\beta(\mathbf{C}_\beta^{(i)})}, \|\mathcal{L}_\beta\psi_\beta^\pm\|^2_{L^2_\beta(\mathbf{C}_\beta^{(i)})} &= \mathcal{O}\left(\beta^{\frac{d}{2}}\delta(\beta)^{d-4}\mathrm{e}^{-\beta(V^*-V(z_0)+\frac{C_\eta}{2}\delta(\beta)^2)}\right)\\ &= \mathcal{O}\left(\mathrm{e}^{-\beta(V^*-V(z_0)+\frac{C_\eta}{3}\delta(\beta)^2)}\right),\end{aligned}$$

using the inclusions $\mathbf{C}_\beta^{(i)} \subset B(z_i, \delta(\beta))$, $\mathbf{C}_\beta^{(i)} \subset \left\{V - V^* \geqslant \frac{C_\eta}{2}\delta(\beta)^2\right\}$.

Analysis on $\mathbf{E}_\beta$.

On the set $\mathbf{E}_\beta$, we have $\chi_\beta^{(i)} \equiv 0$ for all $i \in I_{\min}$, hence $\psi_\beta^\pm$ coincides with $\frac{1}{Z_\beta^\pm}\eta_\beta$. Reusing the bounds on the derivatives of η_β from the analysis on $\mathbf{C}_\beta^{(i)}$ (here the fact that $\mathbf{E}_\beta \subset \mathcal{K}$ is bounded), we obtain once again:

$$\begin{aligned}\|\nabla\psi_\beta^\pm\|^2_{L^2_\beta(\mathbf{E}_\beta)}, \|\mathcal{L}_\beta\psi_\beta^\pm\|^2_{L^2_\beta(\mathbf{E}_\beta)} &= \mathcal{O}\left(\beta^{\frac{d}{2}}\delta(\beta)^{-4}\mathrm{e}^{-\beta(V^*-V(z_0)+\frac{C_\eta}{2}\delta(\beta)^2)}\right)\\ &= \mathcal{O}\left(\mathrm{e}^{-\beta(V^*-V(z_0)+\frac{C_\eta}{3}\delta(\beta)^2)}\right),\end{aligned}$$

Summing the estimates on $\mathbf{A}_\beta^{(i)}$, $\mathbf{B}_\beta^{(i),\pm}$, $\mathbf{C}_\beta^{(i)}$ and $\mathbf{E}_\beta$, we obtain (2.93) and (2.94).

Analysis on $\mathbf{D}_\beta^{(i),\pm}$.

By (2.85), $\psi_\beta^\pm$ coincides with $\frac{1}{Z_\beta^\pm}\varphi_\beta^{(i),\pm}$ on $\mathbf{D}_\beta^{(i),\pm}$, and here we turn to the finer estimates provided by Proposition 2.36. Using the computation (2.101) once again, we get

$$|\nabla\varphi_\beta^{(i),\pm}|^2\mathrm{e}^{-\beta V} = \frac{1}{\left(C_\beta^{(i),\pm}\right)^2}\mathrm{e}^{-\beta\left(|\nu_1^{(i)}|y_1^{(i)2}+V\right)}\xi_\beta(y_1^{(i)})^2.$$

We next note using the Taylor expansion (2.70) that $W_i(x) := |\nu_1^{(i)}|y_1^{(i)}(x)^2 + V(x)$ has a strict local minimum at z_i, with a Hessian given by

$$\nabla^2 W_i(z_i) = \mathrm{abs}\left(\nabla^2 V(z_i)\right) = U^{(i)}\mathrm{diag}\left(|\nu_1^{(i)}|, \ldots, \nu_d^{(i)}\right)U^{(i)\top},$$

see (2.6). Moreover, this minimum is unique in $B\left(z_i, \frac{1}{2}\delta(\beta)\right)$ for $\delta(\beta)$ sufficiently small, which we may assume upon reducing $\delta(\beta)$ once again.

Since $\xi_\beta(y_1^{(i)}(z_i))^2 = \xi_\beta(0) = 1$ we may estimate $\|\nabla\varphi_\beta^{(i),\pm}\|_{L^2_\beta(\mathbf{D}_\beta^{(i),\pm})}$ using Proposition 2.36.

Let us first note that, according to (2.74) and (**H2**), $\sqrt{\beta}\left(\mathbf{D}_\beta^{(i),\pm} - z_i\right) \xrightarrow{\beta\to\infty} E^{(i)}(\alpha^{(i)})$ in the sense of (**L4**). Let $\mathcal{G} \sim \mathcal{N}\left(0, \mathrm{abs}\left(\nabla^2 V(z_i)\right)^{-1}\right)$. It is then easy to check that

$$\mathbb{P}\left(\mathcal{G} \in E^{(i)}(\alpha^{(i)})\right) = \mathbb{P}\left(\mathcal{G}^\top v_1^{(i)} < \alpha^{(i)}\right) = \Phi\left(|\nu_1^{(i)}|^{\frac{1}{2}}\alpha^{(i)}\right),$$

since $\mathcal{G}^\top v_1^{(i)} \sim \mathcal{N}(0, |\nu_1^{(i)}|^{-1})$. Furthermore,

$$h_i(\beta) := \mathbb{P}\left(\mathcal{G} \in \sqrt{\beta}\left[\mathbf{D}_\beta^{(i),\pm} - z_i\right] \triangle E^{(i)}(\alpha^{(i)})\right) = \begin{cases}\mathcal{O}\left(\sqrt{\beta}\gamma(\beta) + \mathrm{e}^{-c\beta\delta(\beta)^2}\right), & \alpha^{(i)} < +\infty,\\ \mathcal{O}\left(\mathrm{e}^{-c\beta\delta(\beta)^2}\right), & \alpha^{(i)} = +\infty.\end{cases} \tag{2.102}$$

Indeed, it follows from (2.74) and (**H2**) that the following inclusion holds:

$$\sqrt{\beta}\left(\mathbf{D}_\beta^{(i),\pm} - z_i\right) \triangle E^{(i)}(\alpha^{(i)}) \subset \left[E^{(i)}(\alpha^{(i)}) \triangle E^{(i)}(\alpha^{(i)} \pm \sqrt{\beta} 2\gamma(\beta))\right] \cup B\left(0, \frac{\sqrt{\beta}}{2}\delta(\beta)\right)^{\mathrm{c}}, \tag{2.103}$$

which we use to estimate $h_i(\beta)$ with the union bound. In the case $\alpha^{(i)} = +\infty$, the leftmost set in (2.103) is empty and the only contribution is from the second term, which is handled using a standard Gaussian estimate

$$\mathbb{P}\left(\mathcal{G} \notin B\left(0, \frac{\sqrt{\beta}\delta(\beta)}{2}\right)\right) = \mathcal{O}\left(\mathrm{e}^{-c\beta\delta(\beta)^2}\right)$$

for some $c > 0$ depending only on i.

In the case $\alpha^{(i)} < +\infty$, we have a contribution from the leftmost set in (2.103)

$$\mathbb{P}\left(\mathcal{G} \in E^{(i)}(\alpha^{(i)}) \triangle E^{(i)}(\alpha^{(i)} \pm \sqrt{\beta}\gamma(\beta))\right) = \mathbb{P}\left(\mathcal{G}^\top v_1^{(i)} \in \left(\alpha^{(i)}, \alpha^{(i)} \pm 2\gamma(\beta)\right)\right),$$

whose asymptotic behavior has already been computed in (2.100). The union bound yields (2.102).

Apply Proposition 2.36, we estimate

$$\begin{aligned}
\|\nabla\varphi_\beta^{(i),\pm}\|^2_{L^2_\beta(\mathbf{D}_\beta^{(i),\pm})} &= (C_\beta^{(i),\pm})^{-2}\left(\frac{2\pi}{\beta}\right)^{\frac{d}{2}} \mathrm{e}^{-\beta V^*}\left|\det\nabla^2 V(z_i)\right|^{-\frac{1}{2}} \Phi\left(|\nu_1^{(i)}|^{\frac{1}{2}}\alpha^{(i)}\right)(1+e_i(\beta)), \\
&= \frac{\beta|\nu_1^{(i)}|^{\frac{1}{2}}}{\Phi\left(|\nu_1^{(i)}|^{\frac{1}{2}}\alpha^{(i)}\right)}\left(\frac{2\pi}{\beta}\right)^{\frac{d}{2}} \mathrm{e}^{-\beta V^*}\left|\det\nabla^2 V(z_i)\right|^{-\frac{1}{2}}(1+e_i(\beta)).
\end{aligned}$$

The error term e_i is once again given by (2.99) (since the limiting domain is symmetric if and only if $\alpha^{(i)} = +\infty$), and we used (2.98) in the final line. Combining this estimate with (2.92) finally yields (2.95).

Let us show (2.97). We write, for $x \in \mathbf{D}_\beta^{(i),\pm} \subseteq B\left(z_i, \frac{1}{2}\delta(\beta)\right)$, in the $y^{(i)}$-coordinates and for $\delta(\beta)$ sufficiently small,

$$\begin{aligned}
\mathcal{L}_\beta\psi_\beta^\pm &= \frac{1}{Z_\beta^\pm}\left(-\nabla V\cdot\nabla\varphi_\beta^{(i),\pm} + \frac{1}{\beta}\Delta\varphi_\beta^{(i),\pm}\right) \\
&= \frac{\mathrm{e}^{-\beta\frac{|\nu_1^{(i)}|}{2}y_1^{(i)2}}}{Z_\beta^\pm C_\beta^{(i),\pm}}\begin{pmatrix}\xi_\beta(y_1^{(i)})\nabla V\cdot\nabla y_1^{(i)} \\ +\frac{1}{\beta}\left[-\xi_\beta(y_1^{(i)})\Delta y_1^{(i)} + \left(-\xi_\beta'(y_1^{(i)}) + \beta\xi_\beta(y_1^{(i)})|\nu_1^{(i)}|y_1^{(i)}\right)\left|\nabla y_1^{(i)}\right|^2\right]\end{pmatrix} \\
&= \frac{\mathrm{e}^{-\beta\frac{|\nu_1^{(i)}|}{2}y_1^{(i)2}}}{Z_\beta^\pm C_\beta^{(i),\pm}}\left(\xi_\beta(y_1^{(i)})v_1^{(i)}\cdot\left[\nabla V + |\nu_1^{(i)}|y_1^{(i)}v_1^{(i)}\right] + \mathcal{O}\left(\beta^{-1}\|\xi_\beta'\|_{L^\infty(\mathbb{R})}\right)\right) \\
&= \frac{\mathrm{e}^{-\beta\frac{|\nu_1^{(i)}|}{2}y_1^{(i)2}}}{Z_\beta^\pm C_\beta^{(i),\pm}}\left(\mathcal{O}\left(|y^{(i)}|^2\right) + \mathcal{O}\left(\beta^{-1}\delta(\beta)^{-1}\right)\right)
\end{aligned}$$

using a first-order Taylor expansion of ∇V around z_i in the last line. We now estimate

the $L^2_\beta\left(\mathbf{D}^{(i),\pm}_\beta\right)$-norms. Noting that, by the change of variables $z = \sqrt{\beta}y^{(i)}$,

$$\int_{\mathbf{D}^{(i),\pm}_\beta} |y^{(i)}|^4 \mathrm{e}^{-\beta\left(|\nu_1^{(i)}|y_1^{(i)2}+V\right)} = \mathcal{O}\left(\beta^{-\frac{d}{2}-2}\mathrm{e}^{-\beta V^*}\right),$$

we get

$$\begin{aligned}\|\mathcal{L}_\beta\psi^\pm_\beta\|^2_{L^2_\beta(\mathbf{D}^{(i),\pm}_\beta)} &= \left(Z^\pm_\beta C^{(i),\pm}_\beta\right)^{-2}\left[\mathcal{O}\left(\beta^{-\frac{d}{2}-2}\mathrm{e}^{-\beta V^*}\right) + \beta^{-2}\delta(\beta)^{-2}\left\|\mathrm{e}^{-\beta\frac{|\nu_1^{(i)}|}{2}y_1^{(i)2}}\right\|^2_{L^2_\beta(\mathbf{D}^{(i),\pm}_\beta)}\right]\\ &= \left(Z^\pm_\beta C^{(i),\pm}_\beta\right)^{-2}\mathcal{O}\left(\beta^{-2}\delta(\beta)^{-2}\right)\beta^{-\frac{d}{2}}\mathrm{e}^{-\beta V^*}\\ &= \mathcal{O}\left(\beta^{-2}\delta(\beta)^{-2}\right)\|\nabla\psi^\pm_\beta\|^2_{L^2_\beta(\mathbf{D}^{(i),\pm}_\beta)},\end{aligned}$$

where we used the same change of variables in the second line, and the estimates (2.92), (2.98) and (2.95) in the last line. This concludes the proof of (2.97). □

2.5.5 Conclusion of the proof of Theorem 2.17

The last tool for the proof is the following resolvent estimate, which was already used for the estimation of metastable exit times in the semiclassical approach, see [209, Proposition 27] and [227, Proposition 3.4]. We include its proof (in our weighted L^2_β setting) for the sake of completeness.

Throughout this section, let us denote by

$$\lambda^\pm_{1,\beta} := \lambda_{1,\beta}(\Omega^\pm_\beta), \qquad u^\pm_{1,\beta} := u_{1,\beta}(\Omega^\pm_\beta),$$

the principal Dirichlet eigenpairs of $-\mathcal{L}_\beta$ in $\Omega^\pm_\beta$.

We introduce the spectral projectors associated with the principal eigenspaces: for all $\varphi \in L^2_\beta(\Omega^\pm_\beta)$,

$$\pi^\pm_\beta\varphi := \frac{\left\langle u^\pm_{1,\beta},\varphi\right\rangle_{L^2_\beta(\Omega^\pm_\beta)}}{\|u^\pm_{1,\beta}\|^2_{L^2_\beta(\Omega^\pm_\beta)}}u^\pm_{1,\beta}.$$

Lemma 2.39. *Fix $u \in H^1_{0,\beta}(\Omega^\pm_\beta)\cap H^2_\beta(\Omega^\pm_\beta)$. Then,*

$$\|(1-\pi^\pm_\beta)u\|_{L^2_\beta(\Omega^\pm_\beta)} = \mathcal{O}(\|\mathcal{L}_\beta u\|_{L^2_\beta(\Omega^\pm_\beta)}), \tag{2.104}$$

$$\left\|\nabla\pi^\pm_\beta u\right\|^2_{L^2_\beta(\Omega^\pm_\beta)} = \|\nabla u\|^2_{L^2_\beta(\Omega^\pm_\beta)} + \mathcal{O}\left(\beta\|\mathcal{L}_\beta u\|^2_{L^2_\beta(\Omega^\pm_\beta)}\right). \tag{2.105}$$

Proof. Let us first check that, thanks to Assumption (**EK1**), $\lambda^{\mathrm{H}}_1 = 0$ and $\lambda^{\mathrm{H}}_2 > 0$, where we recall λ^{H}_j is defined in (2.45). We recall the expressions (2.37) and (2.38) for the harmonic eigenvalues. In the following, we use the multi-index enumeration convention for the spectra, i.e. $\mathrm{Spec}\left(K^{(i)}_{\alpha^{(i)}}\right) = \left\{\lambda^{(i)}_{n,\alpha^{(i)}}\right\}_{n\in\mathbb{N}^d}$. Note that the ground state energy of each of these operators is given by $\lambda^{(i)}_{(0,\dots,0),\alpha^{(i)}} \geqslant 0$, which implies that $\lambda^{\mathrm{H}}_1 = 0$. Let us now show that $\lambda^{\mathrm{H}}_2 > 0$.

It is clear that $\lambda^{(0)}_{n,\infty} > 0$ for $n \neq 0 \in \mathbb{N}^d$. Besides, for $i \geqslant N_0$, it holds

$$\lambda^{(i)}_{(0,\dots,0),\alpha^{(i)}} = |\nu_1^{(i)}|\mu_{0,\alpha^{(i)}(|\nu_1^{(i)}|/2)^{1/2}} - \frac{\nu_1^{(i)}}{2} + \frac{1}{2}\sum_{j=2}^{d}\left[|\nu_j^{(i)}| - \nu_j^{(i)}\right] \geqslant \frac{1}{2}\sum_{j=1}^{d}\left[|\nu_j^{(i)}| - \nu_j^{(i)}\right] > 0,$$

since $\mathrm{Ind}(z_i) \geqslant 1$. We used the inequality $\mu_{0,\theta} \geqslant \mu_{0,\infty} = \frac{1}{2}$ for any $\theta \in \mathbb{R} \cup \{\infty\}$, which follows directly from the Courant–Fischer principle, similarly to the proof of Proposition 2.33.
To get $\lambda_2^{\mathrm{H}} > 0$, is therefore remains to show that $\lambda^{(i)}_{(0,\dots,0),\alpha^{(i)}} > 0$ for $1 \leqslant i < N_0$. For these local minima z_i, it holds that $\alpha^{(i)} < +\infty$ by Assumption (**EK1**). It is thus sufficient to check that $\mu_{0,\theta} > \frac{1}{2} = \mu_{0,\infty}$ for any $\theta \in \mathbb{R}$. In fact it holds more generally that $\mu_{k,\theta} > \mu_{k,\infty}$ for $k \in \mathbb{N}$. The inequality $\mu_{k,\theta} \geqslant \mu_{k,\infty}$ follows again from the domain monotonicity of Dirichlet eigenvalues. For the strict inequality, we note that the identity $\mathfrak{H}_\theta v_{k,\theta} = \mu_{k,\infty} v_{k,\theta}$ would contradict the fact that $\mu_{k,\infty}$ is a simple eigenvalue of $\mathfrak{H}_\infty$, since $v_{k,\infty}$ and the trivial extension of $v_{k,\theta}$ are linearly independent in $L^2(\mathbb{R})$. This concludes the proof of $\lambda_2^{\mathrm{H}} > 0$.

Hence, by Theorem 2.16, there exists $r, \beta_0 > 0$ such that for all $\beta > \beta_0$:

$$|\lambda_{1,\beta}| < r, \quad \lambda_{2,\beta} > 3r,$$

so that the circular contour $\Gamma_{2r} = \{2r\mathrm{e}^{2i\pi t}, 0 \leqslant t \leqslant 1\}$ is at distance at least r from the Dirichlet spectrum of $-\mathcal{L}_\beta$ on $\Omega_\beta^\pm$. When needed, in this proof, we indicate explicitly by $\mathcal{L}_\beta^\pm$ the fact that we consider the Dirichlet realization of $\mathcal{L}_\beta$ on $\Omega_\beta^\pm$.
A standard corollary of the spectral theorem then yields the following uniform resolvent estimate:

$$\forall z \in \Gamma_{2r}, \quad \|(-\mathcal{L}_\beta^\pm - z)^{-1}\|_{\mathcal{B}(L^2_\beta(\Omega_\beta^\pm))} \leqslant \frac{1}{r}.$$

Furthermore, $\pi_\beta^\pm$ may be expressed using the contour integral

$$\pi_\beta^\pm = -\frac{1}{2i\pi}\oint_{\Gamma_{2r}} (\mathcal{L}_\beta^\pm - z)^{-1}\,\mathrm{d}z,$$

so that, for all $u \in H^1_{0,\beta}(\Omega_\beta^\pm) \cap H^2_\beta(\Omega_\beta^\pm)$,

$$\begin{aligned}(1-\pi_\beta^\pm)u &= -\frac{1}{2i\pi}\oint_{\Gamma_{2r}}\left[z^{-1} - (\mathcal{L}_\beta^\pm - z)^{-1}\right]u\,\mathrm{d}z \\ &= -\left(\frac{1}{2i\pi}\oint_{\Gamma_{2r}} z^{-1}(\mathcal{L}_\beta^\pm - z)^{-1}\,\mathrm{d}z\right)\mathcal{L}_\beta^\pm u,\end{aligned}$$

where we used the second resolvent identity in the last line. Estimating the L^2_β norm then yields (2.104):

$$\|(1-\pi_\beta^\pm)u\|_{L^2_\beta(\Omega_\beta^\pm)} \leqslant \frac{1}{r}\|\mathcal{L}_\beta u\|_{L^2_\beta(\Omega_\beta^\pm)}.$$

For (2.105), we use commutativity and the projector identity $\pi_\beta^\pm \mathcal{L}_\beta^\pm \pi_\beta^\pm = \pi_\beta^\pm \mathcal{L}_\beta^\pm$ to write:

$$\begin{aligned}\left\|\nabla \pi_\beta^\pm u\right\|^2_{L^2_\beta(\Omega_\beta^\pm)} &= -\beta \left\langle \pi_\beta^\pm u, \mathcal{L}_\beta \pi_\beta^\pm u\right\rangle_{L^2_\beta(\Omega_\beta^\pm)} \\ &= -\beta \left\langle \pi_\beta^\pm u, \mathcal{L}_\beta u\right\rangle_{L^2_\beta(\Omega_\beta^\pm)} \\ &= -\beta \left\langle u, \mathcal{L}_\beta u\right\rangle_{L^2_\beta(\Omega_\beta^\pm)} - \beta \left\langle (\pi_\beta^\pm - 1)u, \mathcal{L}_\beta u\right\rangle_{L^2_\beta(\Omega_\beta^\pm)} \\ &= \|\nabla u\|^2_{L^2_\beta(\Omega_\beta^\pm)} + \mathcal{O}(\beta \|\mathcal{L}_\beta u\|^2_{L^2_\beta(\Omega_\beta^\pm)}),\end{aligned}$$

where we used a Cauchy–Schwarz inequality and (2.104) to obtain the last equality. □

We are now in a position to derive the modified Eyring–Kramers formula (2.24).

Proof of Theorem 2.17. Recall that $\psi_\beta^\pm$ denotes the quasimode defined in Section 2.5.2. We write, using (2.104) and (2.105):

$$\begin{aligned}\lambda_{1,\beta}^\pm &= \frac{1}{\beta} \frac{\left\|\nabla \pi_\beta^\pm \psi_\beta^\pm\right\|^2_{L^2_\beta(\Omega_\beta^\pm)}}{\|\pi_\beta^\pm \psi_\beta^\pm\|^2_{L^2_\beta(\Omega_\beta^\pm)}} \\ &= \frac{1}{\beta} \frac{\|\nabla \psi_\beta^\pm\|^2_{L^2_\beta(\Omega_\beta^\pm)} + \mathcal{O}(\beta \|\mathcal{L}_\beta \psi_\beta^\pm\|^2_{L^2_\beta(\Omega_\beta^\pm)})}{\|\psi_\beta^\pm - (1-\pi_\beta^\pm)\psi_\beta^\pm\|^2_{L^2_\beta(\Omega_\beta^\pm)}} \\ &= \frac{1}{\beta} \frac{\|\nabla \psi_\beta^\pm\|^2_{L^2_\beta(\Omega_\beta^\pm)} + \mathcal{O}(\beta \|\mathcal{L}_\beta \psi_\beta^\pm\|^2_{L^2_\beta(\Omega_\beta^\pm)})}{1 - \|(1-\pi_\beta^\pm)\psi_\beta^\pm\|^2_{L^2_\beta(\Omega_\beta^\pm)}} \\ &= \frac{1}{\beta} \frac{\|\nabla \psi_\beta^\pm\|^2_{L^2_\beta(\Omega_\beta^\pm)} + \mathcal{O}(\beta \|\mathcal{L}_\beta \psi_\beta^\pm\|^2_{L^2_\beta(\Omega_\beta^\pm)})}{1 + \mathcal{O}(\|\mathcal{L}_\beta \psi_\beta^\pm\|^2_{L^2_\beta(\Omega_\beta^\pm)})} \\ &= \frac{1}{\beta} \|\nabla \psi_\beta^\pm\|^2_{L^2_\beta(\Omega_\beta^\pm)} \left(1 + \mathcal{O}(\|\mathcal{L}_\beta \psi_\beta^\pm\|^2_{L^2_\beta(\Omega_\beta^\pm)})\right) + \mathcal{O}(\|\mathcal{L}_\beta \psi_\beta^\pm\|^2_{L^2_\beta(\Omega_\beta^\pm)}),\end{aligned}$$

where used (2.104) in the penultimate line, and the fact that $\|\mathcal{L}_\beta \psi_\beta^\pm\|_{L^2_\beta(\Omega_\beta^\pm)} = o(1)$ to conclude. Now, using the estimates (2.93), (2.95) of Proposition 2.38 yields

$$\begin{aligned}\|\nabla \psi_\beta^\pm\|^2_{L^2_\beta(\Omega_\beta^\pm)} &= \sum_{i \in I_{\min}} \|\nabla \psi_\beta^\pm\|^2_{L^2_\beta(\mathbf{D}_\beta^{(i),\pm})} + \mathcal{O}\left(\mathrm{e}^{-\beta\left(V^* - V(z_0) + \frac{C_\eta}{3}\delta(\beta)^2\right)}\right) \\ &= \mathrm{e}^{-\beta(V^* - V(z_0))} \left[\sum_{i \in I_{\min}} \frac{\beta |\nu_1^{(i)}|}{2\pi \Phi\left(|\nu_1^{(i)}|^{\frac{1}{2}} \alpha^{(i)}\right)} \sqrt{\frac{\det \nabla^2 V(z_0)}{|\det \nabla^2 V(z_i)|}} \left[1 + \mathcal{O}\left(r_i(\beta)\right)\right] \right. \\ &\qquad \left. + \mathcal{O}\left(\mathrm{e}^{-\beta \frac{C_\eta}{3}\delta(\beta)^2}\right)\right] \\ &= \mathrm{e}^{-\beta(V^* - V(z_0))} \left[\sum_{i \in I_{\min}} \frac{\beta |\nu_1^{(i)}|}{2\pi \Phi\left(|\nu_1^{(i)}|^{\frac{1}{2}} \alpha^{(i)}\right)} \sqrt{\frac{\det \nabla^2 V(z_0)}{|\det \nabla^2 V(z_i)|}} \left[1 + \mathcal{O}\left(r_i(\beta)\right)\right]\right],\end{aligned}$$

using the fact that $\mathrm{e}^{-\beta\frac{C_\eta}{3}\delta(\beta)^2} = \mathcal{O}\left(\beta r_i(\beta)\right)$. The estimates (2.94) and (2.97) give

$$\begin{aligned}
\|\mathcal{L}_\beta\psi_\beta^\pm\|^2_{L^2_\beta(\Omega_\beta^\pm)} &= \sum_{i\in I_{\min}} \mathcal{O}(\beta^{-2}\delta(\beta)^{-2})\|\nabla\psi_\beta^\pm\|^2_{L^2_\beta(\mathbf{D}_\beta^{(i),\pm})} + \mathcal{O}\left(\mathrm{e}^{-\beta\left(V^*-V(z_0)+\frac{C_\eta}{3}\delta(\beta)^2\right)}\right)\\
&= \mathcal{O}(\beta^{-2}\delta(\beta)^{-2})\left(\|\nabla\psi_\beta^\pm\|^2_{L^2_\beta(\Omega_\beta^\pm)} - \|\nabla\psi_\beta^\pm\|^2_{L^2_\beta(\Omega_\beta^\pm\setminus\bigcup_{i\in I_{\min}}\mathbf{D}_\beta^{(i),\pm})}\right)\\
&\quad + \mathcal{O}\left(\mathrm{e}^{-\beta\left(V^*-V(z_0)+\frac{C_\eta}{3}\delta(\beta)^2\right)}\right)\\
&= \mathcal{O}(\beta^{-2}\delta(\beta)^{-2})\|\nabla\psi_\beta^\pm\|^2_{L^2_\beta(\Omega_\beta^\pm)} + \mathcal{O}\left(\mathrm{e}^{-\beta\left(V^*-V(z_0)+\frac{C_\eta}{3}\delta(\beta)^2\right)}\right)\\
&= \mathcal{O}(\beta^{-2}\delta(\beta)^{-2})\|\nabla\psi_\beta^\pm\|^2_{L^2_\beta(\Omega_\beta^\pm)}.
\end{aligned}$$

In the third line, we used (**EK4**) to write $\beta^{-2}\delta(\beta)^{-2}\mathrm{e}^{-\beta\left(V^*-V(z_0)+\frac{C_\eta}{3}\delta(\beta)^2\right)} = \mathcal{O}\left(\mathrm{e}^{-\beta\left(V^*-V(z_0)+\frac{C_\eta}{3}\delta(\beta)^2\right)}\right)$. In the last line, we use the previous estimate $\|\nabla\psi_\beta^\pm\|^2_{L^2_\beta(\Omega_\beta^\pm)} = \mathcal{O}(\beta\mathrm{e}^{-\beta(V^*-V(z_0))})$ to absorb the exponential error term in the prefactor $\mathcal{O}(\beta^{-2}\delta(\beta)^{-2})$. Combining these two estimates, we obtain

$$\begin{aligned}
\lambda_{1,\beta}^\pm &= \frac{1}{\beta}\|\nabla\psi_\beta^\pm\|^2_{L^2_\beta(\Omega_\beta^\pm)}\left(1+\mathcal{O}(\|\mathcal{L}_\beta\psi_\beta^\pm\|^2_{L^2_\beta(\Omega_\beta^\pm)}) + \mathcal{O}\left(\beta^{-1}\delta(\beta)^{-2}\right)\right)\\
&= \mathrm{e}^{-\beta(V^*-V(z_0))}\left[\sum_{i\in I_{\min}}\frac{|\nu_1^{(i)}|}{2\pi\Phi\left(|\nu_1^{(i)}|^{\frac12}\alpha^{(i)}\right)}\sqrt{\frac{\det\nabla^2V(z_0)}{|\det\nabla^2V(z_i)|}}\left[1+\mathcal{O}\left(r_i(\beta)\right)\right]\right]\left(1+\mathcal{O}(\beta^{-1}\delta(\beta)^{-2})\right)\\
&= \mathrm{e}^{-\beta(V^*-V(z_0))}\left[\sum_{i\in I_{\min}}\frac{|\nu_1^{(i)}|}{2\pi\Phi\left(|\nu_1^{(i)}|^{\frac12}\alpha^{(i)}\right)}\sqrt{\frac{\det\nabla^2V(z_0)}{|\det\nabla^2V(z_i)|}}\left[1+\mathcal{O}\left(r_i(\beta)+\beta^{-1}\delta(\beta)^{-2}\right)\right]\right].
\end{aligned}$$

We note that, according to (2.96)

$$r_i(\beta)+\beta^{-1}\delta(\beta)^{-2} = \begin{cases}\beta^{-1}\delta(\beta)^{-2}, & \alpha^{(i)}=+\infty,\\ \sqrt{\beta}\gamma(\beta)+\beta^{-1}\delta(\beta)^{-2}+\beta^{-\frac12}, & \alpha^{(i)}<+\infty.\end{cases}$$

This concludes the proof of Theorem 2.17 upon applying the comparison principle for Dirichlet eigenvalues (see Proposition 2.33). □

We conclude this chapter by giving the proof of two key technical results.

Appendix 2.A: Proof of Proposition 2.27

We prove Proposition 2.27 in this appendix.

Proof of Proposition 2.27. To simplify the presentation, we provide the construction assuming that z_i is the single critical point of V close to the boundary. Since the construction is local, and critical points of V are isolated because of the Morse property, our proof can be straightforwardly adapted to the case of multiple critical points.

Because Ω_β may be viewed as the positive superlevel set of the signed distance function, namely

$$\Omega_\beta = \sigma_{\Omega_\beta}^{-1}(0, +\infty),$$

a natural approach is to construct the extended domain $\Omega^+_{\beta,\rho}$ as the positive superlevel set of a local perturbation of σ_{Ω_β} around each z_i close to the boundary. This is roughly this construction we perform. However, making this precise requires some technicalities to ensure the regularity of the boundary level set. For visual reference, the construction of the extension $\Omega^+_{\beta,\rho}$ is sketched in Figures 2.6a and 2.6b.

Let us assume for simplicity that $z_i = 0$ is the only critical point of V close to the boundary. We consider the signed distance functions f_β to $\partial\Omega_\beta$, g_β to $\partial B(0, \delta(\beta))$, and h_β to the half-space $\partial E^{(i)}\left(\frac{\alpha^{(i)}}{\sqrt{\beta}} + \rho(\beta)\right)$. Since $\Omega_\beta = f_\beta^{-1}(0, +\infty)$ and $B(0, \delta(\beta)) = g_\beta^{-1}(0, +\infty)$ are smooth and bounded domains, there exists $r_\beta > 0$ such that f_β, g_β are C^∞ respectively on $\{|f_\beta| < r_\beta\}$ and $\mathbb{R}^d \setminus \{0\}$ (see for example [137, Lemma 14.16]) whereas h_β as an affine map is smooth on $\mathbb{R}^d$.

The zero level-set of the function $f_\beta \vee (g_\beta \wedge h_\beta)$ coincides with the boundary of the set

$$\widetilde{\Omega}^+_{\beta,\rho} := \Omega_\beta \cup \left[B(0, \delta(\beta)) \cap E^{(i)}\left(\frac{\alpha^{(i)}}{\sqrt{\beta}} + \rho(\beta)\right)\right].$$

It satisfies (2.61), the inclusion $\Omega_\beta \subseteq \widetilde{\Omega}^+_{\beta,\rho}$ and is bounded, but is generally not smooth.

To enforce the regularity of the extended domain, we work with smooth versions of the min and max functions, constructed as follows. Take any $\varepsilon > 0$ and let $a^\pm_\varepsilon \in \mathcal{C}^\infty(\mathbb{R})$ be such that $|x| \leqslant a^+_\varepsilon(x) \leqslant |x| + \varepsilon$, and $|x| - \varepsilon \leqslant a^-_\varepsilon(x) \leqslant |x|$, with moreover $a^\pm_\varepsilon(x) = |x|$ for all $|x| \geqslant \varepsilon$. Define

$$m^\pm_\varepsilon(x, y) = \frac{x + y \pm a^\pm_\varepsilon(x - y)}{2},$$

which are smooth functions on $\mathbb{R}^2$ satisfying the inequalities:

$$x \wedge y \leqslant m^-_\varepsilon(x, y) \leqslant x \wedge y + \frac{\varepsilon}{2}, \qquad x \vee y \leqslant m^+_\varepsilon(x, y) \leqslant x \vee y + \frac{\varepsilon}{2}, \tag{2.106}$$

with moreover

$$\forall\, (x, y) \in \mathbb{R}^2 \text{ such that } |x - y| \geqslant \varepsilon, \qquad m^-_\varepsilon(x, y) = x \wedge y, \qquad m^+_\varepsilon(x, y) = x \vee y. \tag{2.107}$$

We introduce a temperature-dependent parameter $\varepsilon_0(\beta) > 0$, which will be reduced several times in the following proof. In order not to overburden the notation, we sometimes omit the dependence of ε_0 on β. We then define:

$$\sigma_{\varepsilon_0} = m^+_{\varepsilon_0}(f_\beta, m^-_{\varepsilon_0}(g_\beta, h_\beta)).$$

From (2.106), we have by construction that:

$$f_\beta \vee (g_\beta \wedge h_\beta) \leqslant \sigma_{\varepsilon_0} \leqslant f_\beta \vee (g_\beta \wedge h_\beta) + \varepsilon_0(\beta), \tag{2.108}$$

We will prove that, if $\delta(\beta) > \alpha^{(i)}/\sqrt{\beta} + \rho(\beta)$ (which holds in the limit $\beta \to \infty$ according to (**H2**)

and (2.60)), then for a sufficiently small $\varepsilon_0(\beta)$, the function σ_{ε_0} is smooth on a small outward neighborhood $\sigma_{\varepsilon_0}^{-1}(-\varepsilon_0(\beta),0)$ of its zero level set. Let us first write $\sigma_{\varepsilon_0} = m_{\varepsilon_0}^+(f_\beta, \psi_{\varepsilon_0})$, where we define $\psi_{\varepsilon_0} = m_{\varepsilon_0}^-(g_\beta, h_\beta)$. The claimed regularity follows from the following observations. The function ψ_{ε_0} is smooth on $\mathbb{R}^d$ for $\varepsilon_0(\beta) < \delta(\beta) - \alpha^{(i)}/\sqrt{\beta} - \rho(\beta)$: by the regularities of $m_{\varepsilon_0}^-$, f_β and g_β, it is enough to check that ψ_{ε_0} is smooth at 0. But $h_\beta(0) = \frac{\alpha^{(i)}}{\sqrt{\beta}} + \rho(\beta)$ and $g_\beta(0) = \delta(\beta)$, so for $0 < \varepsilon_0(\beta) < \delta(\beta) - \alpha^{(i)}/\sqrt{\beta} - \rho(\beta)$ it holds $h_\beta(0) < g_\beta(0) - \varepsilon_0(\beta)$ and ψ_{ε_0} thus coincides with h_β in a neighborhood of 0 by (2.107), and is therefore smooth at 0.

Furthermore, the rightmost inequality in (2.106) implies the inclusion

$$\sigma_{\varepsilon_0}^{-1}(-\varepsilon_0(\beta),0) \subset (f_\beta \vee \psi_{\varepsilon_0})^{-1}(-3\varepsilon_0(\beta)/2, 0),$$

and so it suffices to show the smoothness of σ_{ε_0} over this larger set. To achieve this, let $x \in (f_\beta \vee \psi_{\varepsilon_0})^{-1}(-3\varepsilon_0(\beta)/2, 0)$, and distinguish between four cases.

- **Case** $\psi_{\varepsilon_0}(x) > f_\beta(x) + \varepsilon_0(\beta)$. Then, σ_{ε_0} coincides with ψ_{ε_0} in a neighborhood of x, and is smooth at x.
- **Case** $f_\beta(x) > \psi_{\varepsilon_0}(x) + \varepsilon_0(\beta)$. Then, σ_{ε_0} coincides with f_β in a neighborhood of x, and is smooth at x provided $3\varepsilon_0(\beta)/2 < r_\beta$.
- **Case** $\psi_{\varepsilon_0}(x) \leqslant f_\beta(x) \leqslant \psi_{\varepsilon_0}(x) + \varepsilon_0(\beta)$. Then, $f_\beta(x) = f_\beta(x) \vee \psi_{\varepsilon_0}(x) \in (-3\varepsilon_0(\beta)/2, 0)$, thus f_β is smooth at x, and likewise σ_{ε_0}, provided $3\varepsilon_0(\beta)/2 < r_\beta$.
- **Case** $\psi_{\varepsilon_0}(x) - \varepsilon_0(\beta) \leqslant f_\beta(x) < \psi_{\varepsilon_0}(x)$. Then $\psi_{\varepsilon_0}(x) \in (-3\varepsilon_0(\beta)/2, 0)$ and $f_\beta(x) \in (-5\varepsilon_0(\beta)/2, 0)$. It follows that f_β and therefore σ_{ε_0} are smooth at x provided $5\varepsilon_0(\beta)/2 < r_\beta$.

We now assume here and in the following that $\varepsilon_0(\beta) < \min\{\frac{2}{5} r_\beta, \delta(\beta) - \frac{\alpha^{(i)}}{\sqrt{\beta}} - \rho(\beta)\}$, and that β is large enough so that $\varepsilon_0(\beta)$ can be chosen to be positive. The regularity of σ_{ε_0} on $\sigma_{\varepsilon_0}^{-1}(-\varepsilon_0(\beta),0)$ allows for the construction of a smooth extended domain, as follows. By Sard's theorem [295], there exists $\varepsilon_1(\beta) < \varepsilon_0(\beta)$ such that the level set $\sigma_{\varepsilon_0}^{-1}\{-\varepsilon_1(\beta)\}$ contains no critical points of σ_{ε_0}, and hence defines a smooth hypersurface of $\mathbb{R}^d$ by the implicit function theorem. Therefore, the superlevel set $\Omega^+_{\beta,\rho,\varepsilon_1} := \sigma_{\varepsilon_0}^{-1}(-\varepsilon_1(\beta), +\infty)$, is a smooth open domain satisfying:

$$(f_\beta \vee (g_\beta \wedge h_\beta))^{-1}(-\varepsilon_1(\beta), +\infty) \subseteq \Omega^+_{\beta,\rho,\varepsilon_1} \subseteq (f_\beta \vee (g_\beta \wedge h_\beta))^{-1}(-\varepsilon_1(\beta) - \varepsilon_0(\beta), +\infty),$$

where we used the inequality (2.108). It follows that $\Omega^+_{\beta,\rho,\varepsilon_1}$ is bounded and contains $(f_\beta \vee (g_\beta \wedge h_\beta))^{-1}(0, +\infty) = \widetilde{\Omega}^+_{\beta,\rho} \supseteq \Omega_\beta$. Note that our construction (and in particular Sard's theorem) implies the existence of an appropriate $\varepsilon_1(\beta) < \varepsilon_0(\beta)$ for any $\varepsilon_0(\beta) > 0$ sufficiently small, and so the existence of a smooth extension $\Omega_\beta \subseteq \Omega^+_{\beta,\rho,\varepsilon_1}$ remains valid upon further reduction of $\varepsilon_0(\beta)$.

At this point, we will show that we can fix $\beta_0 > 0$ to be sufficiently large and $\varepsilon_0(\beta)$ sufficiently

small so that the inclusion

$$\begin{aligned}\mathcal{O}_{\beta,\varepsilon_0} &:= B\left(0,\delta(\beta)-2\varepsilon_0(\beta)\right)\cap E^{(i)}\left(\frac{\alpha^{(i)}}{\sqrt{\beta}}+\rho(\beta)+\varepsilon_0(\beta)\right)\setminus \overline{E}^{(i)}\left(\frac{\alpha^{(i)}}{\sqrt{\beta}}+\rho(\beta)\right)\\ &\subset \{f_\beta+\varepsilon_0(\beta)<h_\beta<g_\beta-\varepsilon_0(\beta)\}\end{aligned} \tag{2.109}$$

holds for all $\beta>\beta_0$, where $\overline{E}^{(i)}$ denotes the closure of $E^{(i)}$. The purpose of (2.109) is to locate a set on which the geometry of the modified domain may be modified to enforce (2.61). Let us check that taking $\varepsilon_0(\beta)<\frac{\rho(\beta)-\gamma(\beta)}{2}<\frac{\delta(\beta)}{2}$ suffices to ensure (2.109). Let $x\in\mathcal{O}_{\beta,\varepsilon_0}$: from $x\in B(0,\delta(\beta)-2\varepsilon_0(\beta))$, we get $g_\beta(x)>2\varepsilon_0(\beta)$, and from $x\in E^{(i)}\left(\frac{\alpha^{(i)}}{\sqrt{\beta}}+\rho(\beta)+\varepsilon_0(\beta)\right)\setminus \overline{E}^{(i)}\left(\frac{\alpha^{(i)}}{\sqrt{\beta}}+\rho(\beta)\right)$, we get $-\varepsilon_0(\beta)<h_\beta(x)<0$, whence $\mathcal{O}_{\beta,\varepsilon_0(\beta)}\subset\{-\varepsilon_0(\beta)<h_\beta<g_\beta-\varepsilon_0(\beta)\}$. From $x\in B(0,\delta(\beta)-2\varepsilon_0(\beta))\setminus \overline{E}^{(i)}\left(\frac{\alpha^{(i)}}{\sqrt{\beta}}+\rho(\beta)\right)$, we deduce by (**H2**) that $x\notin\Omega_\beta$, with furthermore:

$$d(x,\partial\Omega_\beta\setminus B(0,\delta(\beta)))>2\varepsilon_0(\beta),$$

$$d\left(x,\partial\Omega_\beta\cap B(0,\delta(\beta))\right)>d\left(x,\partial E^{(i)}\left(\frac{\alpha^{(i)}}{\sqrt{\beta}}+\gamma(\beta)\right)\right)>2\varepsilon_0(\beta),$$

where the last inequality is obtained using $\rho(\beta)-\gamma(\beta)>2\varepsilon_0(\beta)$ and $x\notin\overline{E}^{(i)}\left(\frac{\alpha^{(i)}}{\sqrt{\beta}}+\rho(\beta)\right)$. Thus $f_\beta(x)<-2\varepsilon_0(\beta)$, so that $\mathcal{O}_{\beta,\varepsilon_0}\subset\{f_\beta<-2\varepsilon_0(\beta)\}$, and

$$\mathcal{O}_{\beta,\varepsilon_0}\subset\{f_\beta<-2\varepsilon_0(\beta)\}\cap\{-\varepsilon_0(\beta)<h_\beta<g_\beta-\varepsilon_0(\beta)\},$$

from which (2.109) follows easily.

We assume at no cost of generality upon taking β_0 once again larger that for all $\beta>\beta_0$, it holds $\delta(\beta)>\frac{\alpha^{(i)}}{\sqrt{\beta}}+\rho(\beta)$, $\delta(\beta)/4>\rho(\beta)-\gamma(\beta)>0$, and

$$\varepsilon_0(\beta)<\min\left\{\frac{2}{5}r_\beta,\delta(\beta)-\frac{\alpha^{(i)}}{\sqrt{\beta}}-\rho(\beta),\frac{\rho(\beta)-\gamma(\beta)}{2}\right\}.$$

The previous construction can still be performed for this potentially smaller $\varepsilon_0(\beta)$, upon accordingly updating $\varepsilon_1(\beta)$. Furthermore, from the inclusion (2.109) and (2.107), the boundary of the so-constructed set $\Omega^+_{\beta,\rho,\varepsilon_1(\beta)}$ locally coincides with the hyperplane:

$$\partial\Omega^+_{\beta,\rho,\varepsilon_1(\beta)}\cap\mathcal{O}_{\beta,\varepsilon_0}=\partial E^{(i)}\left(\frac{\alpha^{(i)}}{\sqrt{\beta}}+\rho(\beta)+\varepsilon_1(\beta)\right)\cap\mathcal{O}_{\beta,\varepsilon_0}.$$

The last step in the construction consists in indenting this hyperplane locally in $\mathcal{O}_{\beta,\varepsilon_0}$, so that it coincides with $\partial E^{(i)}\left(\frac{\alpha^{(i)}}{\sqrt{\beta}}+\rho(\beta)\right)$ inside $B\left(0,\frac{1}{2}\delta(\beta)\right)$.

This indentation amounts to setting:

$$\Omega^+_\beta=\left[\Omega^+_{\beta,\rho,\varepsilon_1(\beta)}\setminus\mathcal{O}_{\beta,\varepsilon_0}\right]\cup\left[U^{(i)}\mathcal{H}^{(i)}_\beta\cap\mathcal{O}_{\beta,\varepsilon_0}\right],$$

where $\mathcal{H}_\beta^{(i)}$ is the hypograph:

$$\mathcal{H}_\beta^{(i)} = \left\{(x,x') \in \mathbb{R}\times\mathbb{R}^{d-1} : x < \frac{\alpha^{(i)}}{\sqrt{\beta}} + \rho(\beta) + \varepsilon_1(\beta)\eta(|x'|)\right\},$$

with $\eta \in \mathcal{C}_c^\infty(\mathbb{R})$, $0 \leqslant \eta \leqslant 1$ is chosen such that:

$$\begin{cases} \eta(|x'|) = 0, & \text{for } |x'|^2 \leqslant \frac{\delta(\beta)^2}{4} - \left(\frac{\alpha^{(i)}}{\sqrt{\beta}} + \rho(\beta) + \varepsilon_1(\beta)\right)^2, \\ \eta(|x'|) = 1, & \text{for } |x'|^2 > (\delta(\beta) - 3\varepsilon_0(\beta))^2 - \left(\frac{\alpha^{(i)}}{\sqrt{\beta}} + \rho(\beta) + \varepsilon_1(\beta)\right)^2. \end{cases} \tag{2.110}$$

In the second line, one could possibly replace $3\varepsilon_0(\beta)$ by $(2+t)\varepsilon_0(\beta)$ for some other $t > 0$. This is related to the fact that $\mathcal{O}_{\beta,\varepsilon_0} \subset B\left(0, \delta(\beta) - 2\varepsilon_0(\beta)\right)$ by (2.109).

The requirement (2.110) places additional constraints on $\varepsilon_0(\beta)$ (and thus on $\varepsilon_1(\beta)$). Namely, one must ensure that $\frac{\delta(\beta)^2}{4} > \left(\frac{\alpha^{(i)}}{\sqrt{\beta}} + \rho(\beta) + \varepsilon_1(\beta)\right)^2$, and that $(\delta(\beta) - 3\varepsilon_0(\beta))^2 > \frac{\delta(\beta)^2}{4}$, which lead to the condition $0 < \varepsilon_1(\beta) < \varepsilon_0(\beta) < \min\left\{\frac{\delta(\beta)}{2} - \frac{\alpha^{(i)}}{\sqrt{\beta}} - \rho(\beta), \frac{\delta(\beta)}{6}\right\}$. It is then easily checked that the first condition on η in (2.110) ensures the property (2.61), and the second the smoothness of Ω_β^+.

Therefore, choosing $\beta_0 > 0$ sufficiently large, $\varepsilon_0(\beta)$ sufficiently small and $0 < \varepsilon_1(\beta) < \varepsilon_0(\beta)$ such that $\Omega_{\beta,\varepsilon_1}^+$ is smooth, we have shown, since $\mathcal{O}_{\beta,\varepsilon_0}$ is bounded and disjoint from Ω_β (which follows from (**H2**)), the inclusions $\Omega_\beta \subset \Omega_\beta^+$ and (2.61), as well as the boundedness of Ω_β^+.

To construct the included domains $\Omega_\beta^- \subseteq \Omega_\beta$, one can perform precisely the same construction, working instead on the open complement $\mathbb{R}^d \setminus \overline{\Omega_\beta}$, which satisfies a symmetric version of Assumption (**H2**) for each z_i such that $\alpha^{(i)} < +\infty$. Denoting the resulting extension by $\mathbb{R}^d \setminus \overline{\Omega_\beta} \subseteq \Omega_\beta^{-,c}$, which by construction satisfies the condition

$$B\left(z_i, \frac{1}{2}\delta(\beta)\right) \cap \Omega_\beta^{-,c} = B\left(z_i, \frac{1}{2}\delta(\beta)\right) \cap \mathbb{R}^d \setminus \left[z_i + \overline{E^{(i)}}\left(\frac{\alpha^{(i)}}{\sqrt{\beta}} - \rho(\beta)\right)\right]$$

for each i such that $\alpha^{(i)} < +\infty$, we define

$$\Omega_\beta^- := \mathbb{R}^d \setminus \overline{\Omega_\beta^{-,c}},$$

and indeed recover equation (2.61) for $\Omega_\beta^- \subset \Omega_\beta$, which is also clearly bounded. □

Appendix 2.B: Proof of Proposition 2.36

We prove Proposition 2.36 in this appendix.

Proof of Proposition 2.36. Up to a translation by x_0 and considering instead $\tilde{f}(x) = f(x) - f(x_0)$ and $\tilde{g}(x) = g(x)/g(x_0)$, we may assume without loss of generality that $x_0 = 0$, $f(0) = 0$ and $g(0) = 1$.

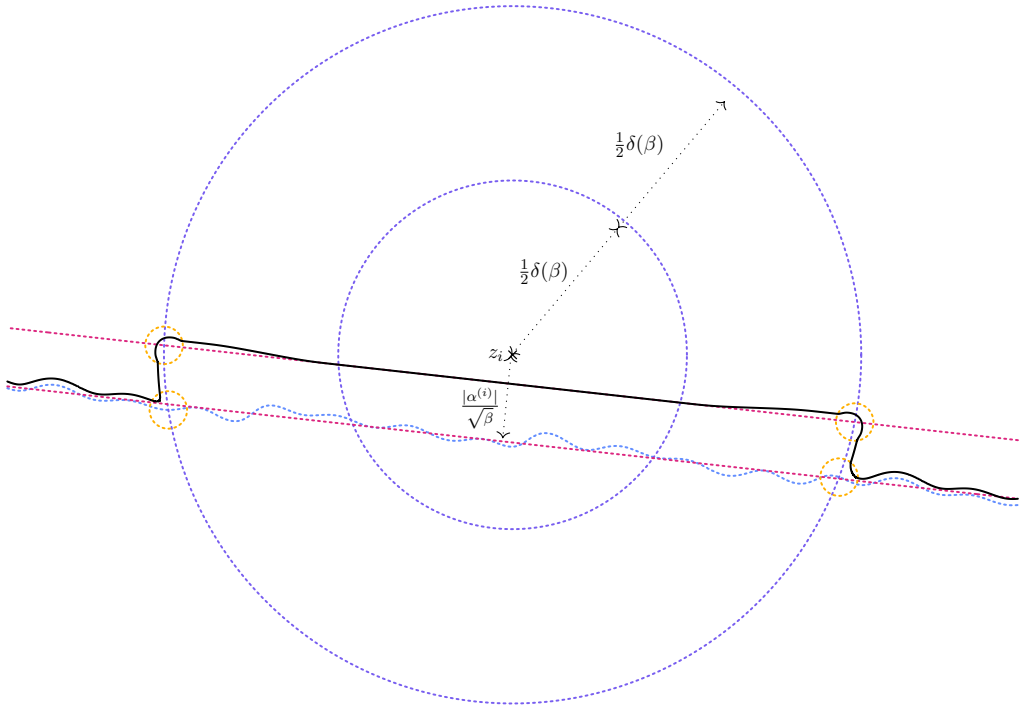

(a) Schematic representation of the boundary of the extended domain $\partial\Omega_\beta^h$ in the case $\alpha^{(i)} < 0$.

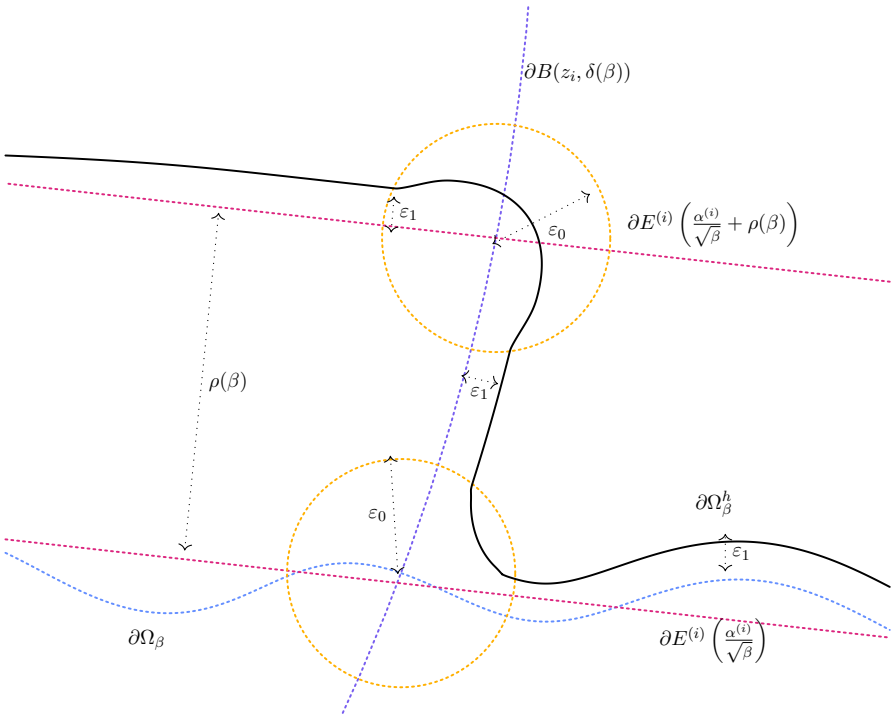

(b) Enlarged view of the construction in the rightmost region of interest.

Figure 2.6: Schematic representation of the extended domain Ω_β^+ satisfying (2.61), depicted here in the vicinity of z_i, a critical point close to, but outside, the boundary of $\partial\Omega_\beta$.

Let us denote by $\mathcal{Q} := \nabla^2 f(0)$ the Hessian of f at the minimum, which, according to (**L3**), is bounded from below by $\epsilon > 0$. We make use of the following Taylor expansions, which are valid in view of (**L2**):

$$f(x) = \frac{1}{2} x^\intercal \mathcal{Q} x + R_f(x), \qquad R_f(x) = \frac{1}{2} \int_0^1 (1-t)^2 D^3 f(tx) : x^{\otimes 3} \, \mathrm{d}t, \tag{2.111}$$

$$g(x) = 1 + x^\intercal \nabla g(0) + R_g(x), \qquad R_g(x) = \int_0^1 (1-t) x^\intercal \nabla^2 g(tx) x \, \mathrm{d}t. \tag{2.112}$$

Let $\delta > 0$ be such that $B(0,\delta) \subset \mathcal{K}$, which exists since $x_0 \in \mathring{\mathcal{K}}$. We may furthermore assume (upon possibly reducing δ), according to (2.111), that for some $C > 0$,

$$\forall\, x \in B(0,\delta), \qquad f(x) \geqslant \frac{1}{C}|x|^2, \qquad |R_f(x)| \leqslant C|x|^3, \qquad |R_g(x)| \leqslant C|x|^2. \tag{2.113}$$

In addition, by (**L3**) and the compactness of $\mathcal{K}$:

$$\gamma := \min_{x \in \mathcal{K} \setminus B(0,\delta)} f(x) > 0. \tag{2.114}$$

Then, using the inclusion (**L1**):

$$\left| \int_{A_\lambda \setminus B(0,\delta)} \mathrm{e}^{-\lambda f(x)} g(x) \, \mathrm{d}x \right| \leqslant \mathrm{e}^{-\lambda\gamma} \|g\|_{L^1(\mathcal{K})} = \mathcal{O}(\mathrm{e}^{-\lambda\gamma}),$$

since g is integrable on $\mathcal{K}$ by (**L2**).

It remains to estimate

$$I(\lambda, 1) := \int_{A_\lambda \cap B(0,\delta)} \mathrm{e}^{-\lambda f(x)} g(x) \, \mathrm{d}x,$$

for which we introduce the following parametric integral, for $0 \leqslant t \leqslant 1$:

$$I(\lambda, t) := \int_{A_\lambda \cap B(0,\delta)} \mathrm{e}^{-\lambda\left(\frac{1}{2} x^\intercal \mathcal{Q} x + t R_f(x)\right)} g(x) \, \mathrm{d}x.$$

The role of t is to interpolate between the quadratic approximation of f around the minimum and f itself.

From (2.113) and (**L3**), we deduce that $c = \min\{\frac{1}{C}, \epsilon/2\} > 0$ is such that

$$\forall\, x \in B(0,\delta),\ \forall\, 0 \leqslant t \leqslant 1, \qquad \frac{1}{2} x^\intercal \mathcal{Q} x + t R_f(x) = \frac{1-t}{2} x^\intercal \mathcal{Q} x + t f(x) \geqslant c|x|^2. \tag{2.115}$$

We then write, by Taylor's theorem:

$$I(\lambda, 1) = I(\lambda, 0) + \frac{\partial I}{\partial t}(\lambda, 0) + \int_0^1 \frac{\partial^2 I}{\partial t^2}(\lambda, t)(1-t) \, \mathrm{d}t,$$

with

$$\frac{\partial^k I}{\partial t^k}(\lambda, t) = (-\lambda)^k \int_{A_\lambda \cap B(0,\delta)} \mathrm{e}^{-\lambda\left(\frac{1}{2} x^\intercal \mathcal{Q} x + t R_f(x)\right)} R_f(x)^k g(x) \, \mathrm{d}x.$$

We can then estimate, for $k = 2$, in view of (2.115):

$$\begin{aligned}\left|\frac{\partial^2 I}{\partial t^2}(\lambda,t)\right| &\leqslant \|g\|_{L^\infty(B(0,\delta))}\lambda^2 \int_{B(0,\delta)} \mathrm{e}^{-\lambda c|x|^2} R_f(x)^2 \,\mathrm{d}x \\ &\leqslant K\lambda^2 \int_{B(0,\delta)} \mathrm{e}^{-\lambda c|x|^2}|x|^6 \,\mathrm{d}x = \lambda^{-\frac{d}{2}}\mathcal{O}(\lambda^{-1}),\end{aligned} \tag{2.116}$$

uniformly in $t \in (0,1)$, where we used the change of variables $y = \sqrt{\lambda}x$ to obtain the last equality. It follows that

$$I(\lambda,1) = \left[I + \frac{\partial I}{\partial t}\right](\lambda,0) + \lambda^{-\frac{d}{2}}\mathcal{O}(\lambda^{-1}).$$

The bracketed term may be rewritten as a Gaussian expectation:

$$\begin{aligned}\left[I + \frac{\partial I}{\partial t}\right](\lambda,0) &= \int_{A_\lambda \cap B(0,\delta)} \mathrm{e}^{-\lambda\frac{1}{2}x^\intercal \mathcal{Q} x}\left(1 - \lambda R_f(x)\right) g(x)\,\mathrm{d}x \\ &= \left(\frac{2\pi}{\lambda}\right)^{\frac{d}{2}} |\det \mathcal{Q}|^{-\frac{1}{2}} \mathbb{E}\left[\left(1 - \lambda R_f(\mathcal{G}/\sqrt{\lambda})\right) g(\mathcal{G}/\sqrt{\lambda}) \mathbb{1}_{\mathcal{G}\in\sqrt{\lambda}A_\lambda \cap B(0,\sqrt{\lambda}\delta)}\right],\end{aligned}$$

where $\mathcal{G} \sim \mathcal{N}(0, \mathcal{Q}^{-1})$. Before estimating the expectation, we write the following expansion allowed by (**L2**):

$$R_f(x) = \frac{1}{6}D^3 f(0) : x^{\otimes 3} + \widetilde{R}_f(x), \qquad \left|\widetilde{R}_f(x)\right| \leqslant \widetilde{C}|x|^4 \text{ on } B(0,\delta), \tag{2.117}$$

which, together with (2.112), gives almost surely:

$$\begin{aligned}\left(1 - \lambda R_f(\mathcal{G}/\sqrt{\lambda})\right) g(\mathcal{G}/\sqrt{\lambda}) &= \left(1 - \frac{\lambda^{-\frac{1}{2}}}{6} D^3 f(0) : \mathcal{G}^{\otimes 3} - \lambda \widetilde{R}_f(\mathcal{G}/\sqrt{\lambda})\right) \\ \times \left(1 + \lambda^{-\frac{1}{2}}\mathcal{G}^\intercal \nabla g(0) + R_g(\mathcal{G}/\sqrt{\lambda})\right) & \\ &= 1 + \lambda^{-\frac{1}{2}}\left[\mathcal{G}^\intercal \nabla g(0) - \frac{1}{6}D^3 f(0) : \mathcal{G}^{\otimes 3}\right] + \lambda^{-1} S(\mathcal{G},\lambda).\end{aligned}$$

A straightforward computation and estimation using the bounds (2.113) and (2.117) shows that there exist $K, \lambda_0 > 0$ such that, for all $\lambda > \lambda_0$, it holds, almost surely,

$$|S(\mathcal{G},\lambda)| \leqslant K\left(1 + |\mathcal{G}|^6\right).$$

In particular $\mathbb{E}[|S(\mathcal{G},\lambda)|] = \mathcal{O}(1)$ in the limit $\lambda \to \infty$. It follows that

$$\begin{aligned}&\mathbb{E}\left[\left(1 - \lambda R_f(\mathcal{G}/\sqrt{\lambda})\right) g(\mathcal{G}/\sqrt{\lambda}) \mathbb{1}_{\mathcal{G}\in\sqrt{\lambda}A_\lambda \cap B(0,\sqrt{\lambda}\delta)}\right] \\ &= \mathbb{E}\left[\left(1 + \lambda^{-\frac{1}{2}}P(\mathcal{G})\right)\mathbb{1}_{\mathcal{G}\in A_\infty}\right] + \mathbb{E}\left[\left(1 + \lambda^{-\frac{1}{2}}P(\mathcal{G})\right)\left(\mathbb{1}_{\mathcal{G}\in\sqrt{\lambda}A_\lambda\cap B(0,\sqrt{\lambda}\delta)} - \mathbb{1}_{\mathcal{G}\in A_\infty}\right)\right] + \mathcal{O}(\lambda^{-1}),\end{aligned}$$

where $P(\mathcal{G}) = \mathcal{G}^\intercal\nabla g(0) - \frac{1}{6}D^3 f(0) : \mathcal{G}^{\otimes 3}$ is a polynomial involving only odd moments of $\mathcal{G}$. By symmetry, the first term in the sum is then given by:

$$\mathbb{E}\left[(1 + \lambda^{-\frac{1}{2}}P(\mathcal{G}))\mathbb{1}_{\mathcal{G}\in A_\infty}\right] = \begin{cases}\mathbb{P}(\mathcal{G}\in A_\infty) & \text{if } A_\infty = -A_\infty, \\ \mathbb{P}(\mathcal{G}\in A_\infty)\left(1 + \mathcal{O}(\lambda^{-\frac{1}{2}})\right) & \text{otherwise.}\end{cases} \tag{2.118}$$

We are left with the task of estimating

$$\left|\mathbb{E}\left[(1+\lambda^{-\frac{1}{2}}P(\mathcal{G}))\left(\mathbb{1}_{\mathcal{G}\in\sqrt{\lambda}A_\lambda\cap B(0,\sqrt{\lambda}\delta)}-\mathbb{1}_{\mathcal{G}\in A_\infty}\right)\right]\right| \leqslant \mathbb{E}\left[\left|1+\lambda^{-\frac{1}{2}}P(\mathcal{G})\right|\mathbb{1}_{\mathcal{G}\in\sqrt{\lambda}A_\lambda\setminus B(0,\sqrt{\lambda}\delta)}\right] + \mathbb{E}\left[\left|1+\lambda^{-\frac{1}{2}}P(\mathcal{G})\right|\left|\mathbb{1}_{\mathcal{G}\in\sqrt{\lambda}A_\lambda}-\mathbb{1}_{\mathcal{G}\in A_\infty}\right|\right]. \tag{2.119}$$

By a standard Gaussian decay estimate and the second condition in (**L3**), the term

$$\mathbb{E}\left[\left|1+\lambda^{-\frac{1}{2}}P(\mathcal{G})\right|\mathbb{1}_{\mathcal{G}\in\sqrt{\lambda}A_\lambda\setminus B(0,\sqrt{\lambda}\delta)}\right]=\mathcal{O}(\mathrm{e}^{-\frac{\lambda}{3}\epsilon\delta^2})$$

is negligible with respect to λ^{-1}. Noting that $\mathbb{1}_{\mathcal{G}\in\sqrt{\lambda}A_\lambda\triangle A_\infty}=\left|\mathbb{1}_{\mathcal{G}\in\sqrt{\lambda}A_\lambda}-\mathbb{1}_{\mathcal{G}\in A_\infty}\right|$, we further obtain by a triangle inequality

$$\mathbb{E}\left[\left|1+\lambda^{-\frac{1}{2}}P(\mathcal{G})\right|\left|\mathbb{1}_{\mathcal{G}\in\sqrt{\lambda}A_\lambda}-\mathbb{1}_{\mathcal{G}\in A_\infty}\right|\right]\leqslant\mathbb{P}\left(\mathcal{G}\in\sqrt{\lambda}A_\lambda\triangle A_\infty\right)+\mathbb{E}\left[\lambda^{-\frac{1}{2}}|P(\mathcal{G})|\mathbb{1}_{\mathcal{G}\in\sqrt{\lambda}A_\lambda\triangle A_\infty}\right].$$

The term $\varepsilon(\lambda)=\mathbb{P}\left(\mathcal{G}\in\sqrt{\lambda}A_\lambda\triangle A_\infty\right)=o(1)$ by Assumption (**L4**).
Let us show that $\mathbb{E}\left[\lambda^{-\frac{1}{2}}|P(\mathcal{G})|\mathbb{1}_{\mathcal{G}\in\sqrt{\lambda}A_\lambda\triangle A_\infty}\right]=\mathcal{O}(\lambda^{-1})$. Decomposing this term, we obtain

$$\mathbb{E}\left[\lambda^{-\frac{1}{2}}|P(\mathcal{G})|\mathbb{1}_{\mathcal{G}\in\sqrt{\lambda}A_\lambda\triangle A_\infty}\mathbb{1}_{|P(\mathcal{G})|\leqslant\lambda^{\frac{1}{2}}}\right]+\mathbb{E}\left[\lambda^{-\frac{1}{2}}|P(\mathcal{G})|\mathbb{1}_{\mathcal{G}\in\sqrt{\lambda}A_\lambda\triangle A_\infty}\mathbb{1}_{|P(\mathcal{G})|>\lambda^{\frac{1}{2}}}\right] \leqslant\mathbb{P}\left(\mathcal{G}\in\sqrt{\lambda}A_\lambda\triangle A_\infty\right)+\mathbb{E}\left[\lambda^{-\frac{1}{2}}|P(\mathcal{G})|\mathbb{1}_{|P(\mathcal{G})|>\lambda^{\frac{1}{2}}}\right]. \tag{2.120}$$

Furthermore, since $P(x)$ is bounded by $C_{d,f}|x|^3$ for some constant $C_{d,f}>0$ outside of a compact set, it holds, for sufficiently large λ, that

$$\mathbb{E}\left[\lambda^{-\frac{1}{2}}|P(\mathcal{G})|\mathbb{1}_{|P(\mathcal{G})|>\lambda^{\frac{1}{2}}}\right]\leqslant C_{d,f}\mathbb{E}\left[\lambda^{-\frac{1}{2}}|\mathcal{G}|^3\mathbb{1}_{|\mathcal{G}|^3>C_{d,f}^{-1}\lambda^{\frac{1}{2}}}\right]=\mathcal{O}(\lambda^{-\frac{1}{2}}\mathrm{e}^{-\epsilon\lambda^{1/3}/3})=\mathcal{O}(\lambda^{-1}), \tag{2.121}$$

by a Gaussian decay estimate.

In view of (2.87), and collecting the estimates (2.116), (2.118), (2.119), (2.120) and (2.121) we conclude that

$$I(\lambda,1)=\left(\frac{2\pi}{\lambda}\right)^{\frac{d}{2}}\det\mathcal{Q}^{-\frac{1}{2}}\mathbb{P}(\mathcal{G}\in A_\infty)\left(1+\mathcal{O}(\lambda^{-1})+\mathcal{O}(\varepsilon(\lambda))+\mathcal{O}(\lambda^{-\frac{1}{2}})\mathbb{1}_{A_\infty\neq -A_\infty}\right),$$

which gives the claimed asymptotic behavior (2.87). □

Note that the same strategy of proof can be deployed to compute higher order terms in the asymptotic expansion.

Acknowledgments. The authors thank Dorian Le Peutrec, Boris Nectoux, Danny Perez, Mohamad Rachid and Julien Reygner for helpful discussions and insightful comments. This work received funding from the European Research Council (ERC) under the European Union's Horizon 2020 research and innovation programme (project EMC2, grant agreement No 810367), and from the Agence Nationale de la Recherche, under grants ANR-19-CE40-0010-01

(QuAMProcs) and ANR-21-CE40-0006 (SINEQ).

Chapter 3

Shape optimization of metastable states

He move in space with minimum waste and maximum joy.
—Sade Adu & Ray St. John, *Smooth Operator*, 1984

Abstract. *The definition of metastable states is a ubiquitous task in the design and analysis of molecular simulation, and is a crucial input in a variety of acceleration methods for the sampling of long configurational trajectories. Although standard definitions based on local energy minimization procedures can sometimes be used, these definitions are typically suboptimal, or entirely inadequate when entropic effects are significant, or when the lowest energy barriers are quickly overcome by thermal fluctuations. In this work, we propose an approach to the definition of metastable states, based on the shape-optimization of a local separation of timescale metric directly linked to the efficiency of a class of accelerated molecular dynamics algorithms. To realize this approach, we derive analytic expressions for shape-variations of Dirichlet eigenvalues for a class of operators associated with reversible elliptic diffusions, and use them to construct a local ascent algorithm, explicitly treating the case of multiple eigenvalues. We propose two methods to make our method tractable in high-dimensional systems: one based on dynamical coarse-graining, the other on recently obtained low-temperature shape-sensitive spectral asymptotics. We validate our method on a benchmark biomolecular system, showcasing a significant improvement over conventional definitions of metastable states.*

3.1 Introduction

Molecular Dynamics (MD) [7, 220] is one of the workhorses of modern computational statistical physics, enabling the exploration of complex biomolecular systems at atomistic resolution. By numerically integrating equations of motion, MD generates trajectories that sample the system's

configuration space according to target statistical ensembles, typically the Boltzmann-Gibbs distribution relevant to canonical (NVT) or isothermal-isobaric (NPT) conditions. Understanding phenomena such as protein folding or conformational transitions between functional states hinges on accurately capturing these dynamics over biologically relevant timescales. However, the inherent separation of timescales characterizing transitions between metastable states often presents significant computational challenges, motivating the development of enhanced sampling and analysis methodologies to efficiently probe rare events.

In this work, we are concerned with the definition of these metastable states. It is often convenient to associate with a given local minimum of the energy function its basin of attraction for a zero-temperature dynamics. Although this procedure, which provides a natural and numerically convenient definition of metastable states, is often unsatisfactory, for instance in many biological applications where the energy landscape displays many local minima separated by shallow energy barriers. In this setting, one seeks alternative, better descriptions, often by replacing the energy with the free energy associated with a given reaction coordinate. In this work, we provide a general and principled approach to define "good" metastable states, using techniques of shape optimization originally developed for problems in continuum mechanics. More precisely, we optimize the boundary of configurational domains in phase-space, with respect to a certain spectral criterion relating the shape of the domain with so-called quasi-stationary timescales within the state. One of the motivations of this work is to maximize the efficiency of a class of algorithms aimed at sampling long, unbiased molecular trajectories, an example of which is discussed in detail in Appendix 3.B below.

Dynamical setting. To formalize this problem, we first specify the class of models we consider for conformational molecular dynamics, namely reversible elliptic diffusions. More precisely, we consider in this work strong solutions to the stochastic differential equation (SDE)

$$\mathrm{d}X_t = \left[-a(X_t)\nabla V(X_t) + \frac{1}{\beta}\mathrm{div}\, a(X_t)\right]\mathrm{d}t + \sqrt{\frac{2}{\beta}}a(X_t)^{1/2}\,\mathrm{d}W_t, \tag{3.1}$$

where $a : \mathbb{R}^d \to \mathbb{R}^{d\times d}$ is a symmetric positive-definite matrix field, $\nabla V : \mathbb{R}^d \to \mathbb{R}^d$ is a locally Lipschitz vector field which is the gradient of a potential $V : \mathbb{R}^d \to \mathbb{R}$, $\mathrm{div}\, a$ denotes the row-wise divergence operator, and W is a standard d-dimensional Brownian motion. The usefulness of the dynamics (3.1) comes from the fact that it is reversible, and thus invariant, for the Gibbs probability measure

$$\mu(\mathrm{d}x) = \frac{1}{\mathcal{Z}_\beta}\mathrm{e}^{-\beta V(x)}\,\mathrm{d}x, \qquad \mathcal{Z}_\beta = \int_{\mathbb{R}^d}\mathrm{e}^{-\beta V},$$

which is the configurational marginal of the canonical (NVT) ensemble at inverse temperature $\beta = (k_\mathrm{B}\theta)^{-1}$ (where k_B is Boltzmann's constant and θ is the temperature)– provided $\mathcal{Z}_\beta$ is finite, which we will always assume. As such, it may be used to sample the NVT ensemble. The case $a = \mathrm{Id}$ corresponds to what is known as the overdamped Langevin equation. As all the dynamics (3.1) sample the same target measure, the free parameter a can be optimized to accelerate various metrics associated to the efficiency of MCMC samplers, see [226, 232, 86]. In this work, we consider the problem of sampling trajectories of (3.1), with a fixed. The dy-

namics (3.1) also arises as the Kramers–Smoluchowski approximation, or so-called overdamped limit, of the kinetic Langevin dynamics, defined by the SDE

$$\begin{cases} \mathrm{d}q_t^\gamma = M^{-1} p_t^\gamma \, \mathrm{d}t, \\ \mathrm{d}p_t^\gamma = -\nabla V(q_t^\gamma) \, \mathrm{d}t - \gamma \Gamma(q_t^\gamma) M^{-1} p_t^\gamma \, \mathrm{d}t + \sqrt{\frac{2\gamma}{\beta}} \Sigma(q_t^\gamma) \, \mathrm{d}W_t^\gamma, \end{cases} \tag{3.2}$$

where the momentum process p_t^γ takes values in $\mathbb{R}^d$, W_t^γ is a standard d-dimensional Brownian motion, V is as in (3.1), and $M \in \mathbb{R}^{d \times d}$ is a positive-definite mass matrix (typically a diagonal matrix with entries equal to the atomic masses in the system). The matrix fields $\Gamma, S : \mathbb{R}^d \to \mathbb{R}^{d \times d}$ define fluctuation and dissipation profiles. They are assumed to be non-degenerate, and to satisfy the fluctuation-dissipation condition $\Sigma\Sigma^\top = \Gamma$, which ensures that the Boltzmann–Gibbs distribution with density proportional to $\mathrm{e}^{-\beta(\frac{1}{2}p^\top M^{-1} p + V(q))} \, \mathrm{d}p \, \mathrm{d}q$ is invariant under the dynamics. The parameter $\gamma > 0$ modulates the rate of momentum dissipation, and in this context, the matrix field $a = \Gamma^{-1}$ arises naturally as the limiting diffusion matrix in the large friction regime. More exactly, it can be shown that the finite-time trajectories of the time-rescaled position process $(q_{\gamma t}^\gamma)_{0 \leqslant t \leqslant T}$ converge to solutions $(X_t)_{0 \leqslant t \leqslant T}$ of (3.1) in the limit $\gamma \to +\infty$, see for example [177], with $a = \Gamma^{-1} = \left(\Sigma\Sigma^\top\right)^{-1}$.

In most MD packages, the Langevin dynamics (3.2) is implemented with $\Gamma = M$, in which case $a = M^{-1}$ in (3.1). We therefore use (3.1) as a model of the underlying underdamped Langevin dynamics with which simulations are typically run, keeping in mind that any timescale inferred at the level of the dynamics (3.1) should be divided by a factor γ to obtain the corresponding timescale for the underdamped dynamics, in order to account for the rescaling involved in the Kramers–Smoluchowski approximation.

The infinitesimal generator of the evolution semigroup for the dynamics (3.1) is the operator

$$\mathcal{L}_\beta = \left(-a\nabla V + \frac{1}{\beta} \mathrm{div}\, a\right)^\top \nabla + \frac{1}{\beta} a : \nabla^2 = \frac{1}{\beta} \mathrm{e}^{\beta V} \mathrm{div}\left(\mathrm{e}^{-\beta V} a \nabla \cdot\right). \tag{3.3}$$

In an appropriate functional setting (see Section 3.2.1 below), it can be shown to be self-adjoint with pure point spectrum.

Local metastability and quasi-stationary timescales. The main difficulty in sampling long trajectories from the process (3.1) (as well as from (3.2), for that matter) is the phenomenon of metastability, which often arises from the presence of energy wells separated by high-energy barriers (relative to the characteristic thermal fluctuation scale β^{-1}), or from entropic traps, see [233, Section 1.2.3]. More generically, this phenomenon can be understood as the presence of subsets of the configuration space in which the dynamics resides for long times before abruptly transitioning and settling in the next metastable state. This property is characterized by the existence of a separation of timescales between intra-state fluctuations and inter-state transitions. In full generality, there may be a hierarchy of timescales, corresponding to states, superstates (energy superbasins), etc. In the local approach to metastability, one fixes such a subset $\Omega \subset \mathbb{R}^d$, and studies local dynamical properties of the system inside Ω. A central object of interest in this study is the quasi-stationary distribution (QSD) of the dynamics

inside Ω, which formalizes the notion of the local equilibrium that the dynamics reaches inside Ω, provided it remains trapped for a sufficiently long time. More formally, the QSD inside Ω for the dynamics (3.1) is defined as a probability measure $\nu \in \mathcal{P}_1(\Omega)$ such that, for any $A \subset \Omega$ measurable,

$$\nu(A) = \int_\Omega \mathbb{P}_x \left(X_t \in A | \, \tau > t\right) \nu(\mathrm{d}x), \qquad \tau = \inf \left\{t \geqslant 0 : X_t \notin \Omega\right\}.$$

Under mild assumptions on Ω, V and a (see [206] and Assumptions (**Ell**), (**Reg**) below), the QSD is unique, and coincides with the Yaglom limit:

$$\nu(A) = \lim_{t\to\infty} \mu_{t,x}(A), \qquad \mu_{t,x}(A) := \mathbb{P}_x \left(X_t \in A \,|\, \tau > t\right), \tag{3.4}$$

for an arbitrary initial condition $x \in \Omega$.

From this definition alone, it is not entirely clear which domains Ω correspond to metastable states. A natural albeit informal answer to this question is to require that for most visits in Ω, convergence to the QSD in (3.4) occurs much faster than the typical metastable exit time $\mathbb{E}_\nu[\tau]$. This definition suggests a quantitative measure of the local metastability of a given domain Ω, namely the ratio between the metastable exit time and the convergence time to the QSD. Moreover, these timescales can be analyzed by relating them to the eigenvalues of the operator (3.3), endowed with Dirichlet boundary conditions on $\partial\Omega$. Indeed, on the one hand it is shown in [206, Propositions 2 & 3] that the QSD in Ω has an explicit density in terms of the principal Dirichlet eigenfunction $u_1(\Omega)$ of $\mathcal{L}_\beta$ in Ω:

$$\nu(\mathrm{d}x) = Z_{\beta,\Omega}^{-1} \mathrm{e}^{-\beta V(x)} u_1(\Omega)(x) \, \mathrm{d}x, \qquad \begin{cases} \mathcal{L}_\beta u_1(\Omega) = -\lambda_1(\Omega) u_1(\Omega) & \text{in } \Omega, \\ u_1(\Omega) = 0 & \text{on } \partial\Omega, \end{cases}$$

and that the exit time starting from the QSD is an exponential random variable with rate $\lambda_1(\Omega)$ and independent from the exit point: for all Borel sets $A \subset \partial\Omega$, it holds

$$\mathbb{P}_\nu(\tau > t, X_\tau \in A) = \mathrm{e}^{-t\lambda_1(\Omega)} \mathbb{P}_\nu(X_\tau \in A). \tag{3.5}$$

In particular, the expected exit time from the QSD (or metastable exit time) is given by $\mathbb{E}_\nu[\tau] = 1/\lambda_1(\Omega)$. In fact, for regular domains, the law of X_τ starting under ν is also explicit in terms of the normal derivative of the density $\frac{\mathrm{d}\nu}{\mathrm{d}x}$ on $\partial\Omega$, see the proof of Proposition 3 in [206].

Moreover, on the other hand, bounds on the total variation distance between $\mu_{t,x}$ and ν are also available in terms of the spectral gap $\lambda_2(\Omega) - \lambda_1(\Omega)$. Namely, a spectral expansion argument (see the proof of [305, Theorem 1.1]) shows that there exists $C(x), t(x) > 0$ such that

$$\mathrm{d}_{\mathrm{TV}} \left(\mu_{t,x}, \nu\right) \leqslant C(x) \mathrm{e}^{-t(\lambda_2(\Omega) - \lambda_1(\Omega))}, \qquad \forall \, t > t(x), \tag{3.6}$$

where d_{TV} denotes the total variation distance between two probability measures: $\mathrm{d}_{\mathrm{TV}}(\pi, \rho) = \sup_{\|f\|_\infty \leqslant 1} |\pi(f) - \rho(f)|$. The restriction of the estimate (3.6) to times larger than $t(x)$ is technical, and is related to the lack of regularity of $\mu_{0,x} = \delta_x$. If one considers initial conditions with sufficient regularity, a similar estimate holds for all $t > 0$. It can be shown, e.g. by taking $X_0 \sim C\mathrm{e}^{-\beta V} \left(u_1(\Omega) + \varepsilon u_2(\Omega)\right) \mathrm{d}x$ for some appropriate $C, \varepsilon > 0$, that the rate $\lambda_2(\Omega) - \lambda_1(\Omega)$ in (3.6)

is sharp, and therefore corresponds to the asymptotic rate of convergence of $\mu_{t,x}$ to ν.

In view of the above discussion on the exit rate $\lambda_1(\Omega)$ and the convergence rate to the QSD $\lambda_2(\Omega) - \lambda_1(\Omega)$, a natural measure of the metastability of the dynamics inside Ω is given by the ratio:

$$N^*(\Omega) = \frac{\lambda_2(\Omega) - \lambda_1(\Omega)}{\lambda_1(\Omega)}. \tag{3.7}$$

In this work, our aim is to optimize the shape of the domain Ω in order to make $N^*(\Omega)$ as large as possible, see problem (3.8) below. The quantity $N^*(\Omega)$ has been identified in [334, 268] as a "scalability metric" associated with a given definition of metastable state Ω, which quantifies the efficiency of a class of accelerated MD algorithms, the so-called "Parallel Replica" methods. We discuss the link between the separation metric (3.7) and the Parallel Replica method in Appendix 3.B below.

Beyond the family of Parallel Replica methods, the other accelerated MD methods developed by Arthur Voter (see [332, 312]) also rely on definitions of metastable states, and a separation of timescales hypothesis within these states. Although our main motivation stems from algorithmic efficiency concerns, we stress that other, more theoretical motivations lead one to consider the problem (3.8). It is indeed expected that identifying highly locally metastable domains (in the sense of a large separation of timescales) leads to configurational dynamics amenable to approximation by various simpler, discrete-space dynamics, such as Markov jump processes. The quantity (3.7) has for instance been identified as the key approximation parameter in an approach to reduced-state dynamics using Markov renewal processes (see [13]). It is therefore of more general interest to investigate how much freedom one has in defining more general states than simple energy basins, and how to ensure a large separation of timescales. Let us finally mention that the case $V = 0$, which amounts to maximizing the ratio of the first two Dirichlet eigenvalues of the Laplacian, also arises in the field of spectral geometry as the Payne–Polya–Weinberger conjecture, see [263, 18].

We consider the shape-optimization problem

$$\max_{\Omega \in \mathcal{S}} N^*(\Omega), \qquad \mathcal{S} = \left\{ \Omega \subset \mathbb{R}^d \text{ bounded, Lipschitz and connected} \right\}. \tag{3.8}$$

The optimization problem as formulated in (3.8) is typically not well-posed. Whenever the operator (3.3) acting on $L^2(\mathbb{R}^d, \nu(\mathrm{d}x))$ has compact resolvent, a simple argument involving the sequence of domains $\Omega_n = B_{\mathbb{R}^d}(0, n)$ shows that $\lambda_1(\Omega_n) \xrightarrow{n\to\infty} 0$ and $\lambda_2(\Omega_n) \xrightarrow{n\to\infty} \lambda_2(\mathbb{R}^d) > 0$, so that there is generically no bounded domain maximizing (3.7). This situation is somewhat standard in the numerical optimization of eigenvalue functionals, and well-posedness is generally only obtained upon imposing various normalizing constraints on the design variable. In this work, we address practical methods to numerically optimize N^* *locally* around a given domain Ω_0, and we make no attempt to solve the optimization problem (3.8) globally. We therefore look for local maxima of $N^*(\Omega)$.

More precisely, it has been observed (see [268] or Figure 3.9b below for a simple example) that the shape optimization landscape for the separation of timescales typically displays local maxima around single energy wells (which we define loosely as domains containing a local energy minimum z_0, and an energetic neighborhood of several βs thereof), i.e. domains for

which arbitrary perturbations of the boundary locally decrease the separation of timescales. This numerical evidence is also supported by theoretical results, see [50, Section 3.3] or Section 3.4.2 below.

Main contributions of this work. In this work, we introduce a novel and principled approach to the definition of metastable states in MD. In so doing, we make several methodological advances.

- We introduce the spectral criterion (3.7) and link it to the efficiency of Parallel Replica dynamics.
- We provide in Theorem 3.2 and Corollary 3.4 explicit expressions for shape variations of Dirichlet eigenvalues of a large class of diffusions. These formulas also cover the case of degenerate eigenvalues.
- We define a robust steepest ascent method (Algorithm 3.5) to optimize $N^*(\Omega)$ in low dimension, taking in particular account the degeneracy of the eigenvalues, and adaptively selecting an ascent direction accordingly.
- We propose two projection techniques to adapt the algorithm to high-dimensional problems. One is based on a coarse-graining strategy, using a collective variable. The other is based on exact, shape-sensitive spectral asymptotics obtained in the recent work [50].
- We validate our methods with numerical experiments, which demonstrate the interest of the approach on various problems of increasing complexity, including a biomolecular system.

Outline of the work. In Section 3.2 we present our main theoretical results, Theorem 3.2 and Corollary 3.4, which form the basis of our numerical method. In Section 3.3, we describe the ascent method using the results of Section 3.2. In Section 3.4, we discuss two practical methods to approach the shape-optimization problem in high-dimensional systems, which is the standard setting in MD. In Section 3.5, we present various numerical results to validate our methods. Some conclusions and perspectives are gathered in Section 3.6. Finally, we conclude this work with two appendices: Appendix 3.A, in which we give a full proof of Theorem 3.2, and Appendix 3.B, in which we discuss the relevance to the Parallel Replica algorithm.

3.2 Main results

In this section, we present the main theoretical results which form the basis of our optimization method. In Section 3.2.1, we introduce various notation and useful notions. In Section 3.2.2, we state our main result, before proving a reformulation in 3.2.3.

3.2.1 Framework and notation

Assumptions on V and a. We assume that the diffusion matrix a is locally elliptic: for any compact set $K \subset \mathbb{R}^d$,

$$\exists\, \varepsilon_a(K) > 0 : \qquad u^\top a(x) u \geqslant \varepsilon_a(K)|u|^2 \qquad \forall u \in \mathbb{R}^d, \text{ for almost all } x \in K. \tag{Ell}$$

We also assume that V and a have locally bounded derivatives up to order 2:

$$V \in \mathcal{W}^{2,\infty}_{\mathrm{loc}}\left(\mathbb{R}^d\right), \qquad a \in \mathcal{W}^{2,\infty}_{\mathrm{loc}}(\mathbb{R}^d; \mathcal{M}_d). \tag{Reg}$$

Functional spaces. Throughout this work, we consider the following Hilbert spaces, defined for an open Lipschitz domain $\Omega \subset \mathbb{R}^d$ by

$$\begin{aligned} L^2_\beta(\Omega) &= \left\{ u \text{ measurable} \,\middle|\, \|u\|^2_{L^2_\beta(\Omega)} := \int_\Omega u^2 \, \mathrm{e}^{-\beta V} < +\infty \right\}, \\ H^k_\beta(\Omega) &= \left\{ u \in L^2_\beta(\Omega) \middle| \, \partial^\alpha u \in L^2_\beta(\Omega),\, \forall\, |\alpha| \leqslant k \right\}, \end{aligned} \tag{3.9}$$

where $\partial^\alpha = \partial^{\alpha_1}_{x_1} \dots \partial^{\alpha_d}_{x_d}$ denotes the weak differentiation operator associated to a multi-index $\alpha = (\alpha_1, \dots, \alpha_d) \in \mathbb{R}^d$. For the flat case (i.e. when $V \equiv 0$), we simply write $L^2(\Omega)$ and $H^k(\Omega)$. As in the flat case, $H^k_{0,\beta}(\Omega)$ denotes the $H^k_\beta(\Omega)$-norm closure of $\mathcal{C}^\infty_{\mathrm{c}}(\Omega)$.

If Ω is bounded (which will be the case in the following) and for any $k \in \mathbb{N}$, the sets $H^k_\beta(\Omega)$ and $H^k(\Omega)$ are equal as Banach spaces, but are endowed with different inner products.

Lipschitz shape perturbations. For the purpose of studying shape perturbations of eigenvalues, we introduce an appropriate Banach space of deformation fields. We denote by $\mathcal{W}^{1,\infty}(\mathbb{R}^d; \mathbb{R}^d)$ (or simply $\mathcal{W}^{1,\infty}$) the set of essentially bounded vector fields with essentially bounded weak differential:

$$\left\{ \theta : \mathbb{R}^d \to \mathbb{R}^d \text{ measurable} \,\middle|\, \|\theta\|_{\mathcal{W}^{1,\infty}} := \|\theta\|_{L^\infty\left(\mathbb{R}^d;\mathbb{R}^d\right)} + \|\nabla\theta\|_{L^\infty\left(\mathbb{R}^d;\mathcal{M}_d\right)} < +\infty \right\},$$

where $\mathbb{R}^d$ is endowed with the Euclidean norm and where $\mathcal{M}_d$ denotes the space of $d \times d$ matrices, which is endowed with the induced operator norm. For any finite-dimensional vector space E and $\theta \in \mathcal{W}^{1,\infty}(\mathbb{R}^d; E)$, θ has a Lipschitz-continuous representative (see for example [121, Section 5.8.2.b, Theorem 4]). We will therefore identify throughout this work elements of $\mathcal{W}^{1,\infty}(\mathbb{R}^d; E)$ with their Lipschitz representatives. The normed vector space $(\mathcal{W}^{1,\infty}, \|\cdot\|_{\mathcal{W}^{1,\infty}})$ is a Banach space, and due to Rademacher's theorem, $\theta \in \mathcal{W}^{1,\infty}$ is differentiable almost everywhere. We use the convention $(\nabla\theta)_{ij} = \partial_i \theta_j$, so that $\nabla\theta = D\theta^\top \in \mathbb{R}^{d\times d}$ is the transpose of the Jacobian matrix.

The interest of this class of perturbations is the stability of the class of Lipschitz domains under $\mathcal{W}^{1,\infty}$ shape perturbations, as formalized by the following result.

Proposition 3.1. *Let $\Omega \subset \mathbb{R}^d$ be a bounded, open Lipschitz domain, and $k \geqslant 1$. There exists $h_0 > 0$ such that, for all $\theta \in B_{\mathcal{W}^{1,\infty}}(0, h_0)$,*

$$\Omega_\theta := (\mathrm{Id} + \theta)\Omega = \{x + \theta(x), x \in \Omega\} \tag{3.10}$$

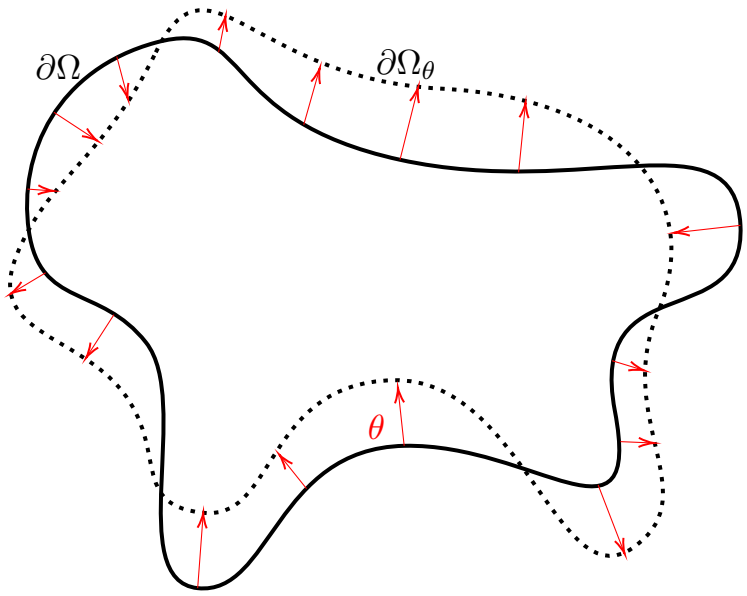

Figure 3.1: The standard framework of the Hadamard shape derivative: a reference domain Ω is deformed into Ω_θ defined in (3.10) following a perturbation field $\theta \in \mathcal{W}^{1,\infty}$. Regularity properties of a shape functional $J(\Omega)$ are studied via those of the map $\theta \mapsto J(\Omega_\theta)$.

is still a bounded, open Lipschitz domain.

We depict schematically the perturbed domain (3.10) in Figure 3.1. The proof of Proposition 3.1 relies on the fact that bounded Lipschitz domains are characterized by a geometric condition in the class of so-called uniform ε-cone conditions, which is stable under bi-Lipschitz homeomorphisms. We refer to [75, Section III] for a proof of this result. Another straightforward but important property of this class of perturbations is that the composition mapping

$$\begin{cases} H^1_0(\Omega_\theta) \to H^1_0(\Omega) \\ \qquad v \mapsto v \circ \Phi_\theta, \end{cases} \tag{3.11}$$

where $\Phi_\theta(x) = x + \theta(x)$, is a Banach space isomorphism for $\|\theta\|_{\mathcal{W}^{1,\infty}}$ sufficiently small, with inverse $v_\theta \mapsto v_\theta \circ \Phi_\theta^{-1}$.

Spectral properties of the Dirichlet generator. We recall that the evolution semigroup associated with the diffusion (3.1) is generated by the operator (3.3). Given a bounded open domain Ω, the Dirichlet realization of $-\mathcal{L}_\beta$ on $L^2_\beta(\Omega)$, also denoted by $-\mathcal{L}_\beta$, is defined as the Friedrichs extension (see [318]) of the positive quadratic form

$$\mathcal{C}^\infty_{\mathrm{c}}(\Omega) \ni u \mapsto \frac{1}{\beta} \int_\Omega \nabla u^\top a \nabla u \, \mathrm{e}^{-\beta V}.$$

It is a self-adjoint operator with domain $\mathcal{D}(\mathcal{L}_\beta) = \left\{ u \in H^1_{0,\beta}(\Omega) : \mathcal{L}_\beta u \in L^2_\beta(\Omega) \right\}$. If Ω is a smooth domain, we simply have $\mathcal{D}(\mathcal{L}_\beta) = H_{2,\beta}(\Omega) \cap H^1_{0,\beta}(\Omega)$.

Since $\mathcal{D}(\mathcal{L}_\beta) \subset H^1_{0,\beta}(\Omega)$ is compactly embedded in $L^2_\beta(\Omega)$, $-\mathcal{L}_\beta$ has compact resolvent, and

its spectrum is composed of a sequence

$$0 < \lambda_1(\Omega) \leqslant \lambda_2(\Omega) \dots$$

of eigenvalues with finite multiplicities tending to $+\infty$. We enumerate the spectrum with multiplicity, and consider the following normalization for eigenvectors: for any integers $i, j \geqslant 1$,

$$\int_\Omega u_i(\Omega) u_j(\Omega) \mathrm{e}^{-\beta V} = \delta_{ij}, \tag{3.12}$$

where for any $k \geqslant 1$, $u_k(\Omega) \in L^2_\beta(\Omega)$ satisfies the eigenrelation $-\mathcal{L}_\beta u_k(\Omega) = \lambda_k(\Omega) u_k(\Omega)$. It can also be shown that the eigenfunction associated with $\lambda_1(\Omega)$ is a signed function $u_1(\Omega)$ (since $|u_1(\Omega)| \in \mathcal{D}(\mathcal{L}_\beta)$ is also a minimizer of the quadratic form), which is unique up to normalization, and the Harnack inequality implies that $u_1(\Omega)$ does not vanish inside Ω. Therefore, the orthogonality constraint (3.12) forces the principal eigenvalue to be simple, i.e. $0 < \lambda_1(\Omega) < \lambda_2(\Omega)$. Moreover, one can choose $u_1(\Omega)$ to be positive in Ω, which will be our convention throughout this work.

Precise statements regarding the spectral properties of $\mathcal{L}_\beta$ will be given in the proof of Theorem 3.2 below.

Shape perturbation analysis. In Section 3.2, we derive regularity results (Theorem 3.2) for the Dirichlet eigenvalues of the generator $-\mathcal{L}_\beta$ with respect to Lipschitz shape perturbations. To do so, we adopt the standard framework of shape calculus, considering mappings from perturbations of the domain to eigenvalues

$$\theta \mapsto \lambda_k(\Omega_\theta), \qquad \forall\, k \geqslant 1,$$

and obtain regularity results with respect to $\theta \in \mathcal{W}^{1,\infty}$ with explicit first-order formulas.

To illustrate the main difficulty when dealing with eigenvalues, we consider the following two-dimensional example, which already gives insight into the infinite-dimensional situation. Consider the following matrix-valued map $\mathbb{R}^2 \to \mathbb{R}^{2\times 2}$ (which depends on two independent parameters, and therefore lies outside the scope of analytic perturbation theory):

$$A(\theta) = \begin{pmatrix} -\theta_1 & \theta_2 \\ \theta_2 & \theta_1 \end{pmatrix}, \qquad \operatorname{Spec} A(\theta) = \left\{ \pm\sqrt{\theta_1^2 + \theta_2^2} \right\}.$$

Simple eigenvalues remain Fréchet-differentiable with respect to θ. One does not however have Fréchet differentiability for degenerate eigenvalues (as 0 for $\theta = 0$ above), even if one is free to choose the ordering of the eigenvalues. Indeed, there is no local parametrization of $\operatorname{Spec} A(\theta)$ as the union of two differentiable surfaces in a neighborhood of $\theta = 0$: geometrically, it is a double cone in $\mathbb{R}^3$ with a vertex at $\theta = 0$. However, it is simple to see that, for a fixed perturbation direction $\theta \in \mathbb{R}^2$, the set $\operatorname{Spec} A(t\theta)$ may be parametrized as the union of two differentiable graphs, namely $t \mapsto \pm t|\theta|$, and in this sense the degenerate eigenvalue is Gateaux-differentiable. If one moreover orders the eigenvalues, one gets the parametrization $t \mapsto \pm|t\theta|$, and the eigenvalues are again non-differentiable at $t = 0$ (even in the sense of Gateaux), but only semi-differentiable, with well-defined left and right derivatives. This is simply an artifact of

the non-differentiability of the ordering map, which nevertheless is semi-differentiable on the diagonal $\{(x,y) \in \mathbb{R}^2 : x = y\}$.

The case of the Dirichlet eigenvalues of $-\mathcal{L}_\beta$ is similar. Namely, for a degenerate eigenvalue $\lambda_k(\Omega)$ of multiplicity m and a fixed perturbation direction $\theta \in \mathcal{W}^{1,\infty}$, the spectral cluster

$$\{\lambda_{k+\ell}(\Omega_{t\theta}), 0 \leqslant \ell < m, \, |t| \text{ small}\}$$

around $\lambda_k(\Omega)$ depends differentiably on t, in a sense made precise in Theorem 3.2 below. It is also the case that, if $\lambda_k(\Omega)$ is simple, then $\theta \mapsto \lambda_k(\Omega_\theta)$ has $\mathcal{C}^1(\mathcal{W}^{1,\infty})$-regularity in a neighborhood of 0, a property known as shape-differentiability. In both the simple and degenerate cases, explicit formulas for the directional one-sided derivatives (and thus also the Fréchet derivative in the simple case) of the ordered eigenvalues $\lambda_{k+\ell}(\Omega_\theta)$ with respect to θ at $\theta = 0$ are available for $0 \leqslant \ell < m$. These results justify formal computations (see Corollary 3.4 below), generalizing those of Hadamard [146] for the Laplacian, and allowing for the identification of shape-ascent directions for smooth functionals of the Dirichlet spectrum. This forms the crux of our numerical method, see Section 3.3 below. The general strategy we follow was proposed by Haug and Rousselet in [152, 153, 290, 154] for problems in structural mechanics.

However, besides the fact that the operators we consider here are different from those in [290, 154], the regularity results we prove are stronger than those derived in [152, 153, 290, 154] (for instance, we show Fréchet-differentiability of simple eigenvalues in a $\mathcal{W}^{1,\infty}$-neighborhood of $\theta = 0$). These results require locally uniform-in-θ estimates throughout the proof, and we therefore give a self-contained derivation.

Let us also mention the books [164, Section 5.7] and [163, Section 2.5] for a more pedagogical and somewhat less technical approach than our proof in the case of the Laplacian, but which only applies to the case of simple eigenvalues.

3.2.2 Shape perturbation formulas

Our main result is the following theorem, which summarizes the regularity properties for the Dirichlet ordered eigenvalue maps $\theta \mapsto \lambda_k(\Omega_\theta)$, with explicit expressions for the directional derivatives at $\theta = 0$ in terms of a $L^2_\beta(\Omega)$-orthonormal basis of eigenvectors. Crucially, formulas are still available in the case of degenerate eigenvalues.

Theorem 3.2. *Let $\Omega \subset \mathbb{R}^d$ be a bounded Lipschitz domain, and $\lambda_k(\Omega) = \lambda_{k+\ell}(\Omega)$ for $0 \leqslant \ell < m$ be a multiplicity $m \geqslant 1$ eigenvalue for the operator $-\mathcal{L}_\beta$ on Ω with Dirichlet boundary conditions. Let $\left(u_k^{(i)}(\Omega)\right)_{1 \leqslant i \leqslant m}$ be a basis of eigenvectors for the associated invariant subspace of $L^2_\beta(\Omega)$, satisfying the normalization convention (3.12). We recall that, for $\theta \in \mathcal{W}^{1,\infty}\left(\mathbb{R}^d, \mathbb{R}^d\right)$, the transported domain is denoted $\Omega_\theta = (\mathrm{Id} + \theta)\Omega$. The following properties hold.*

i) The map $\theta \mapsto (\lambda_{k+\ell}(\Omega_\theta))_{0 \leqslant \ell < m}$ is Lipschitz in a $\mathcal{W}^{1,\infty}$-neighborhood of $\theta = 0$.

ii) Fix $\theta \in \mathcal{W}^{1,\infty}\left(\mathbb{R}^d, \mathbb{R}^d\right)$. There exist $t_\theta > 0$ and m differentiable maps

$$(-t_\theta, t_\theta) \ni t \mapsto \mu_\ell(t), \qquad 1 \leqslant \ell \leqslant m$$

such that

$$\{\mu_\ell(t),\, 1 \leqslant \ell \leqslant m\} = \{\lambda_{k+\ell}(\Omega_{t\theta}),\, 0 \leqslant \ell < m\}\,. \tag{3.13}$$

Moreover, the set $\{\mu'_\ell(0),\, 1 \leqslant \ell \leqslant m\}$ *of derivatives at* $t = 0$ *is the spectrum of the symmetric matrix* $M^{\Omega,k}(\theta)$ *with entries, for* $1 \leqslant i, j \leqslant m$*:*

$$\begin{aligned} M^{\Omega,k}_{ij}(\theta) =& \frac{1}{\beta}\int_\Omega \nabla u_k^{(i)}(\Omega)^\top \left(\nabla a^\top \theta - a\nabla\theta - \nabla\theta^\top a\right)\nabla u_k^{(j)}(\Omega)\mathrm{e}^{-\beta V} \\ &+ \frac{1}{\beta}\int_\Omega \nabla u_k^{(i)}(\Omega)^\top a \nabla u_k^{(j)}(\Omega)\mathrm{div}\left(\theta \mathrm{e}^{-\beta V}\right) \\ &- \lambda_k(\Omega)\int_\Omega u_k^{(i)}(\Omega) u_k^{(j)}(\Omega)\mathrm{div}\left(\theta \mathrm{e}^{-\beta V}\right). \end{aligned} \tag{3.14}$$

iii) If $\lambda_k(\Omega)$ *is a simple eigenvalue, i.e.* $m = 1$*, then the map* $\theta \mapsto \lambda_k(\Omega_\theta)$ *is* $\mathcal{C}^1(\mathcal{W}^{1,\infty};\mathbb{R})$ *in a* $\mathcal{W}^{1,\infty}$*-neighborhood of* $\theta = 0$*.*

In the expression (3.14) above, we use the shorthand $\nabla a^\top\theta$ *for the matrix with entries* $\sum_{\alpha=1}^d \partial_\alpha a_{ij}\theta_\alpha$*.*

Remark 3.3. Note that, from the second item in Theorem 3.2, the Gateaux right-derivatives of the ordered eigenvalues can be deduced from the ordering of the eigenvalues of the matrix $M^{\Omega,k}$ defined in (3.14). Namely, for any $0 \leqslant \ell < m$, the right-derivative $\frac{\mathrm{d}}{\mathrm{d}t}\lambda_{k+\ell}(\Omega_{t\theta})\big|_{t=0^+}$ is given by the ℓ-th smallest eigenvalue of $M^{\Omega,k}(\theta)$, counted with multiplicity. This simply follows by comparing the first-order expansions of the eigenvalues given in (3.13). It may happen that $M^{\Omega,k}(\theta)$ has degenerate eigenvalues, in which case some eigenvalue branches are tangent to one another, and $\lambda_k(\Omega_{t\theta})$ remains degenerate to first-order in t around $t = 0$. Such a situation is depicted in Figure 3.2 below.

As the proof of Theorem 3.2 is somewhat lengthy, it is postponed to Appendix 3.A below.

3.2.3 Revisiting eigenvalue derivatives as boundary integrals

The next result states that the components of the matrix (3.14) defining the directional derivatives of a multiple eigenvalue have a simpler form, provided that the boundary has sufficient regularity.

Corollary 3.4. *Assume that* Ω *is convex or has a* $\mathcal{C}^{1,1}$ *boundary. Then the components (3.14) can be rewritten as the following boundary integrals for* $1 \leqslant i, j \leqslant m$*:*

$$M^{\Omega,k}_{ij}(\theta) = -\frac{1}{\beta}\int_{\partial\Omega} \frac{\partial u_k^{(i)}}{\partial \mathrm{n}}\frac{\partial u_k^{(j)}}{\partial \mathrm{n}}\left(\mathrm{n}^\top a \mathrm{n}\right)\left(\theta^\top \mathrm{n}\right)\mathrm{e}^{-\beta V}, \tag{3.15}$$

where n *denotes the unit outward normal to* $\partial\Omega$ *and* $\frac{\partial u}{\partial \mathrm{n}} = \nabla u^\top \mathrm{n}$ *denotes the normal derivative.*

Compared to (3.14), the form (3.15) is useful from the numerical point of view, since it does not involve any derivative of the diffusion tensor a or of the perturbation field θ. As such, it is the one we use for the purpose of numerical shape optimization, see Section 3.3 below.

Proof of Corollary 3.4. We fix $1 \leqslant i, j \leqslant m$ and for simplicity, we denote by $u_k^{(i)}(\Omega) = u$, $u_k^{(j)}(\Omega) = v$ and $\lambda_k(\Omega) = \lambda$. By standard results of elliptic regularity (see [144, Theorems

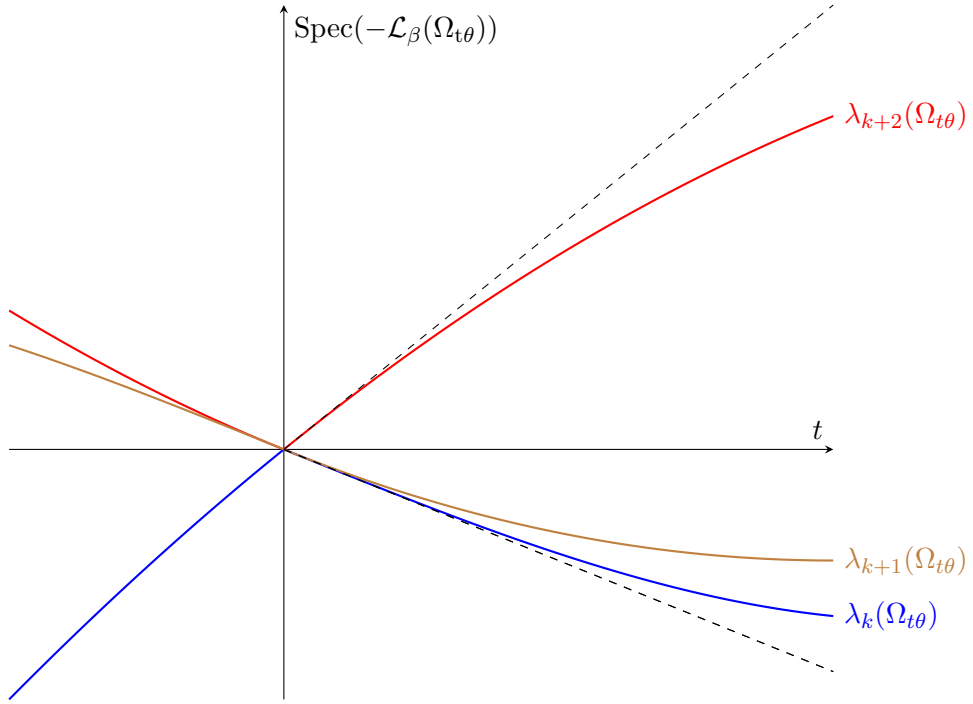

Figure 3.2: Directional shape perturbation of the triple Dirichlet eigenvalue $\lambda_k(\Omega)$ in the direction θ. The slopes of the Gateaux right-tangents (in black dashed lines) correspond to the eigenvalues of the matrix $M^{\Omega,k}(\theta)$ (counted with multiplicity). In this case, the bottom eigenvalue has multiplicity two, and two half-tangents coincide.

2.4.2.5 and 3.2.1.3]), the regularity of $\partial\Omega$ or the convexity of Ω ensure that u and v belong to $H^2(\Omega)$, so that $\nabla u, \nabla v, \theta \in L^2(\partial\Omega)$ by the Sobolev trace theorem, with furthermore, since $u, v \in H^1_0(\Omega)$,

$$\nabla u = \frac{\partial u}{\partial \mathrm{n}}\mathrm{n}, \quad \nabla v = \frac{\partial v}{\partial \mathrm{n}}\mathrm{n} \qquad \text{in } L^2(\partial\Omega)^d, \tag{3.16}$$

where $\nabla u, \nabla v$ are defined in $L^2(\partial\Omega)$ in the sense of the trace. We recall a Green-like identity for $f \in H^1(\Omega)$ and $g \in \mathcal{D}(\mathcal{L}_\beta)$. In view of the following equality in $L^1(\Omega)$

$$\begin{aligned}\frac{1}{\beta}\mathrm{div}\left(f\mathrm{e}^{-\beta V}a\nabla g\right) &= \frac{1}{\beta}f\mathrm{div}\left(\mathrm{e}^{-\beta V}a\nabla g\right) + \frac{1}{\beta}\nabla f^\top a\nabla g\mathrm{e}^{-\beta V}\\ &= \left(f\mathcal{L}_\beta g + \frac{1}{\beta}\nabla f^\top a\nabla g\right)\mathrm{e}^{-\beta V},\end{aligned}$$

the Green–Ostrogradski formula gives

$$\frac{1}{\beta}\int_{\partial\Omega} f\mathrm{n}^\top a\nabla g\,\mathrm{e}^{-\beta V} = \int_\Omega f\mathcal{L}_\beta g\,\mathrm{e}^{-\beta V} + \frac{1}{\beta}\int_\Omega \nabla f^\top a\nabla g\,\mathrm{e}^{-\beta V}. \tag{3.17}$$

Applying (3.17) with $f = \theta^\top\nabla u$ and $g = v$, observing that $\theta^\top\nabla u \in H^1(\Omega)$ and using (3.16) as well as the eigenrelation $\mathcal{L}_\beta v = -\lambda v$, we obtain

$$\begin{aligned}\frac{1}{\beta}\int_{\partial\Omega}\frac{\partial u}{\partial \mathrm{n}}\frac{\partial v}{\partial \mathrm{n}}\mathrm{n}^\top a\mathrm{n}\theta^\top\mathrm{n}\,\mathrm{e}^{-\beta V} &= -\lambda\int_\Omega \theta^\top\nabla uv\,\mathrm{e}^{-\beta V} + \frac{1}{\beta}\int_\Omega \nabla\left(\theta^\top\nabla u\right)^\top a\nabla v\,\mathrm{e}^{-\beta V}\\ &= -\lambda\int_\Omega \theta^\top\nabla uv\,\mathrm{e}^{-\beta V} + \frac{1}{\beta}\int_\Omega \nabla u^\top\nabla\theta^\top a\nabla v\,\mathrm{e}^{-\beta V}\\ &\quad + \frac{1}{\beta}\int_\Omega \theta^\top\nabla^2 ua\nabla v\,\mathrm{e}^{-\beta V}.\end{aligned}$$

Applying this identity to (3.14) twice (exchanging the roles of u and v the second time), we get

$$\begin{aligned} M_{ij}^{\Omega,k}(\theta) = \frac{1}{\beta}\int_\Omega \nabla u^\top \nabla a^\top \theta \nabla v \, \mathrm{e}^{-\beta V} - \frac{2}{\beta}\int_{\partial\Omega} \frac{\partial u}{\partial \mathrm{n}}\frac{\partial v}{\partial \mathrm{n}} \mathrm{n}^\top a \mathrm{n} \theta^\top \mathrm{n} \, \mathrm{e}^{-\beta V} \\ - \lambda \int_\Omega \theta^\top \nabla(uv) \, \mathrm{e}^{-\beta V} - \lambda \int_\Omega uv \, \mathrm{div}\left(\theta \mathrm{e}^{-\beta V}\right) \\ + \frac{1}{\beta}\int_\Omega \theta^\top \left(\nabla^2 u a \nabla v + \nabla^2 v a \nabla u\right) \mathrm{e}^{-\beta V} + \frac{1}{\beta}\int_\Omega \nabla u^\top a \nabla v \, \mathrm{div}\left(\theta \mathrm{e}^{-\beta V}\right). \end{aligned}$$

Note that the second line is equal to

$$-\lambda \int_\Omega \mathrm{div}\left(uv\theta \mathrm{e}^{-\beta V}\right) = 0,$$

by the Green–Ostrogradski formula and the boundary condition $u, v \in H_0^1(\Omega)$. It then suffices to notice that

$$\begin{aligned} \mathrm{div}\left(\nabla u^\top a \nabla v \theta \mathrm{e}^{-\beta V}\right) = \theta^\top \left(\nabla^2 u a \nabla v + \nabla^2 v a \nabla u\right) \mathrm{e}^{-\beta V} \\ + \nabla u^\top \nabla a^\top \theta \nabla v \, \mathrm{e}^{-\beta V} + \nabla u^\top a \nabla v \, \mathrm{div}\left(\theta \mathrm{e}^{-\beta V}\right), \end{aligned}$$

to conclude that

$$\begin{aligned} M_{ij}^{\Omega,k}(\theta) &= \frac{1}{\beta}\int_{\partial\Omega} \nabla u^\top a \nabla v \theta^\top \mathrm{n} \, \mathrm{e}^{-\beta V} - \frac{2}{\beta}\int_{\partial\Omega} \frac{\partial u}{\partial \mathrm{n}}\frac{\partial v}{\partial \mathrm{n}} \mathrm{n}^\top a \mathrm{n} \theta^\top \mathrm{n} \, \mathrm{e}^{-\beta V} \\ &= -\frac{1}{\beta}\int_{\partial\Omega} \frac{\partial u}{\partial \mathrm{n}}\frac{\partial v}{\partial \mathrm{n}} \mathrm{n}^\top a \mathrm{n} \theta^\top \mathrm{n} \, \mathrm{e}^{-\beta V} \end{aligned}$$

as claimed. □

3.3 Numerical optimization

Using the results of Section 3.2, we describe in this section an ascent algorithm to numerically optimize smooth functionals of the eigenvalues of the Dirichlet generator $\mathcal{L}_\beta$. We first present in Section 3.3.1 the discretization procedure used to solve the Dirichlet eigenproblem. In Section 3.3.2, we describe the local ascent method we use, and detail the choice of ascent direction in Section 3.3.3.

Throughout this section, we fix a smooth function J of $k \in \mathbb{N}^*$ ordered Dirichlet eigenvalues, which we seek to maximize:

$$\max_{\Omega \subset \mathbb{R}^d} J\left(\lambda_1(\Omega), \dots, \lambda_k(\Omega)\right), \qquad J \in \mathcal{C}^\infty\left(\left(\mathbb{R}_+^*\right)^k, \mathbb{R}\right).$$

By an abuse of notation, we also write the shorthands $J(\Omega) := J\left(\lambda_1(\Omega), \dots, \lambda_k(\Omega)\right)$, $\partial_{\lambda_i} J(\Omega) := \partial_{\lambda_i} J(\lambda_1(\Omega), \dots, \lambda_k(\Omega))$ for $1 \leqslant i \leqslant k$ and denote by $DJ(\Omega;\theta)$ the Gateaux right-derivative at point θ of the map $\theta \mapsto J\left(\lambda_1(\Omega_\theta), \dots, \lambda_k(\Omega_\theta)\right)$, which exists by the second item in Theorem 3.2, or its Fréchet derivative whenever it is defined.

3.3.1 Finite-element discretization of the eigenproblem

The numerical method we propose is based on a finite-element (FEM) approximation of the spectrum. As such, it is computationally affordable in the low-dimensional setting $d \leqslant 3$. For higher dimensional systems, one may resort to a low-dimensional representation of the dynamics, see Section 3.4.1 below where this is illustrated in a case when a good low-dimensional collective variable is available.

Finite-element meshes. All the shapes we consider in this work are parametrized by simplicial meshes. A mesh Σ for a given polyhedral domain Ω consists for our purposes of the data

$$\Sigma = (\mathcal{V}, \mathcal{T}), \qquad \mathcal{V} = (x_i)_{1 \leqslant i \leqslant N_V}, \qquad \mathcal{T} = (T_i)_{1 \leqslant i \leqslant N_T},$$

where $\mathcal{V} \in \left(\mathbb{R}^d\right)^{N_V}$ is the set of 0-cells or vertices, and $\mathcal{T} \in \left(\mathcal{V}^{d+1}\right)^{N_T}$ defines the set of d-cells, namely triangles for $d = 2$ or tetrahedra for $d = 3$. We assume the usual finite-element method (FEM) conditions on $\mathcal{T}$:

$$\overline{\Omega} = \bigcup_{i=1}^{N_T} \operatorname{co} T_i, \qquad \forall\, 1 \leqslant i < j \leqslant N_T, \qquad \mathring{\operatorname{co}}\, T_i \cap \mathring{\operatorname{co}}\, T_j = \varnothing, \tag{3.18}$$

where co (resp. $\mathring{\text{co}}$) denotes the closed (resp. open) convex hull. The set $\operatorname{co} T$ is the (closed) d-cell associated with any $T \in \mathcal{T}$.

Dirichlet eigenvalues are approximated using the following procedure.

Rayleigh–Ritz approximation of the Dirichlet spectrum. Given a mesh Σ, the Rayleigh–Ritz method for the Dirichlet eigenproblem consists in performing the following steps.

A. Fix a finite-dimensional subspace $E_0(\Sigma) \subset H^1_0(\Omega)$, spanned by a set of basis functions $\Phi(\Sigma) = (\phi_i)_{1 \leqslant i \leqslant d_\Sigma}$. A typical choice is the set of $\mathbb{P}_1$ elements for the interior vertices $\mathcal{V} \cap \Omega$. Another approach is to take $E_0(\Sigma) \subset H^1(\Omega)$ and enforce the Dirichlet boundary condition by adding a penalization term to the weak formulation. We use the latter method, which is implemented by default in FreeFem++ [155] (with the default value of the penalization parameter).

B. Form the matrices

$$A(\Sigma) = \left(\int_\Omega \nabla \phi_i^\top a \nabla \phi_j \, \mathrm{e}^{-\beta V} \right)_{1 \leqslant i,j \leqslant d_\Sigma}, \qquad B(\Sigma) = \left(\int_\Omega \phi_i \phi_j \, \mathrm{e}^{-\beta V} \right)_{1 \leqslant i,j \leqslant d_\Sigma}. \tag{3.19}$$

In practice the integrals can be restricted to the set $\operatorname{supp} \phi_i \cap \operatorname{supp} \phi_j = \cup_{n \in \mathcal{N}_{ij}} \operatorname{co} T_n$, where $\mathcal{N}_{ij}$ is a set indexing the cells on which both ϕ_i and ϕ_j are non-zero. Generally, the integrals in (3.19) consist in the sum of integrals over only a handful of cells in $\mathcal{T}$, which are approximated by quadrature rules. The resulting matrices are sparse, which makes the computation of the bottom eigenvalues tractable with iterative methods.

C. Solve the generalized eigenvalue problem (e.g. using a Lanczos algorithm) for $1 \leqslant \ell \leqslant k$:

$$A(\Sigma)w_\ell(\Sigma) = -\lambda_\ell(\Sigma)B(\Sigma)w_\ell(\Sigma), \qquad w_\ell(\Sigma) \in \mathbb{R}^{d_\Sigma}.$$

The Rayleigh–Ritz eigenpair $\big(\lambda_\ell(\Sigma), w_\ell(\Sigma)^\top \Phi(\Sigma)\big)$ can then be used as an approximation of the Dirichlet eigenpair $(\lambda_\ell(\Omega), u_\ell(\Omega))$. We denote by $u_\ell(\Sigma) = w_\ell(\Sigma)^\top \Phi(\Sigma)$ the approximated eigenfunction, and convene that the eigenvalues are listed in increasing order.

We also select the shape perturbation θ (see Figure 3.1) in a finite-dimensional space $W(\Sigma) \subset \mathcal{W}^{1,\infty}(\mathbb{R}^d;\mathbb{R}^d)$. In practice, we take $W(\Sigma) \subset H^1(\Omega)^d$ to be the finite-dimensional space spanned by the set of $\mathbb{P}_1$ vector-valued elements associated with Σ.

We finally introduce the following notion of numerical degeneracy for Rayleigh–Ritz eigenvalues: we say that $\lambda_\ell(\Sigma)$ has ε-multiplicity $m \geqslant 1$ if

$$\frac{\lambda_\ell(\Sigma) - \lambda_{\ell-1}(\Sigma)}{\lambda_{\ell-1}(\Sigma)} > \varepsilon, \qquad \frac{\lambda_{\ell+m-1}(\Sigma) - \lambda_\ell(\Sigma)}{\lambda_\ell(\Sigma)} \leqslant \varepsilon < \frac{\lambda_{\ell+m}(\Sigma) - \lambda_\ell(\Sigma)}{\lambda_\ell(\Sigma)}.$$

3.3.2 Local optimization procedure.

The algorithm starts from the choice of some initial mesh-like open domain Ω_0, with an underlying mesh Σ_0. The ascent algorithm used to solve (3.8) takes the following parameters as input.

Parameter	**Description**
Ω_0, $\Sigma_0 = (\mathcal{V}_0, \mathcal{T}_0)$	Initial polyhedral domain and its mesh
$\varepsilon_{\text{degen}} > 0$	Degeneracy tolerance parameter
$m_{\max} \geqslant 2$	Maximal degeneracy rank
$\eta_{\max} > 0$	Maximal step size
$0 < \alpha < 1$	Step size multiplier
$\varepsilon_{\text{term}} > 0$	Termination criterion tolerance
$M_{\text{grad}} > 0$	Gradient normalization parameter
$N_{\text{search}} > 0$	Number of search points in the degenerate case

Input parameters for Algorithm 3.5.

We proceed by iterating the following steps.

Algorithm 3.5 (Ascent iteration.)**.** *At step $n \geqslant 0$:*

A. Approximate the $k + m_{\max} + 1$ first eigenpairs for Σ_n using the finite-element Rayleigh–Ritz procedure from Section 3.3.1 above.

B. Identify an ascent direction $\theta_n \in \mathcal{W}(\Sigma_n)$ such that $\widehat{DJ}(\Sigma_n;\theta_n) > 0$, where

$$\widehat{DJ}(\Sigma;\theta) = \nabla J(\lambda_1(\Sigma),\dots,\lambda_k(\Sigma))^\top \widehat{D\Lambda}(\Sigma;\theta), \qquad \widehat{D\Lambda}(\Sigma;\theta) = \Big(\widehat{D\lambda_i}(\Sigma;\theta)\Big)_{1\leqslant i\leqslant k}$$

and where $\widehat{D\lambda_i}(\Sigma;\theta)$ *is the approximation of the right-Gateaux derivative of* $\lambda_i(\Omega)$ *in the direction* θ *from step A., i.e.*

$$\widehat{D\lambda_i}(\Sigma;\theta) = -\frac{1}{\beta}\int_{\partial\Omega}\left(\frac{\partial u_i(\Sigma)}{\partial \mathrm{n}}\right)^2 \mathrm{n}^\top a \mathrm{n} \mathrm{e}^{-\beta V}\theta^\top \mathrm{n} \text{ if } \lambda_i(\Sigma) \text{ has } \varepsilon_{\mathrm{degen}}\text{-multiplicity } 1,$$

and otherwise is given by the ℓ*-th smallest eigenvalue of the matrix*

$$\left(-\frac{1}{\beta}\int_{\partial\Omega}\frac{\partial u_\sigma(\Sigma)}{\partial \mathrm{n}}\frac{\partial u_\tau(\Sigma)}{\partial \mathrm{n}}\mathrm{n}^\top a \mathrm{n}\theta^\top \mathrm{n}\,\mathrm{e}^{-\beta V}\right)_{i-\ell+1\leqslant\sigma,\tau\leqslant i-\ell+m} \tag{3.20}$$

if $\lambda_{i-\ell+1}(\Sigma)$ *has* $\varepsilon_{\mathrm{degen}}$*-multiplicity* $m \geqslant \ell$ *for some* $2 \leqslant \ell \leqslant m_{\max}$*. If* $\lambda_{i-\ell+1}(\Sigma)$ *has* $\varepsilon_{\mathrm{degen}}$ *greater than* $m_{\max}$*, the iteration fails. The choice of* θ_n *and its discretization are the crucial features of the algorithm, and are made precise in Section 3.3.3 below.*

C. *Set the step size* $\eta_n = \eta_{\max}$*, and displace the vertices of the mesh via* $\widetilde{\mathcal{V}}_{n+1} = \mathcal{V}_n + \eta_n\theta_n(\mathcal{V}_n)$*. The geometry of the mesh* $\widetilde{\Sigma}_{n+1}$ *is defined by the set of new vertices* $\widetilde{\mathcal{V}}_{n+1}$*, inheriting its combinatorial structure from* Σ_n*. If* $\widetilde{\Sigma}_{n+1}$ *is a valid mesh for a domain* Ω_{n+1}*, i.e. satisfies the FEM conditions (3.18), set* $\Sigma_{n+1} = \mathcal{A}\left(\widetilde{\Sigma}_{n+1}\right)$*, where* $\mathcal{A}$ *is a local mesh refinement procedure designed to preserve meshing quality, namely the* `adaptmesh` *function from FreeFem++. Otherwise, set* $\eta_n \leftarrow \alpha\eta_n$ *and repeat this step. For the sake of computational efficiency and simplicity, we limit ourselves to a fixed maximal step size* $\eta_{\max}$*, although various other strategies to select* η_n *are a classical topic in numerical optimization, see [255, Chapter 3].*

D. *Set* $n \leftarrow n+1$ *and proceed from step A., unless the termination condition*

$$\widehat{DJ}(\Sigma_n;\theta_n) < \varepsilon_{\mathrm{term}}$$

is met. Other termination criteria are possible and are again a classical topic, see [255].

3.3.3 Choice of ascent directions

We now detail how to find ascent directions θ_n in step B. of Algorithm 3.5. Following the standard reading on numerical shape optimization (see for instance [6, Section 6.5]), we take a "solve-then-discretize" approach. We first describe how to identify steepest ascent directions at the continuous level (for both simple and multiple eigenvalues), and then make precise the discretization procedure. For the purpose of this discussion, we assume to avoid undue technical difficulties that Ω is a smooth domain and the coefficients a, V are smooth, ensuring by elliptic regularity that the Dirichlet eigenfunctions are smooth on $\overline{\Omega}$, and therefore smooth and bounded on $\partial\Omega$.

Case of simple eigenvalues. We first handle the case where each of the $\lambda_i(\Omega)$ have multiplicity 1. In this case, according to Corollary 3.4, the differential of J with respect to the perturbation θ can be expressed as a continuous linear form of the normal perturbation $\theta^\top \mathrm{n}$ on $\partial\Omega$, i.e.

$$DJ(\Omega;\theta) = \int_{\partial\Omega}\phi_J(\Omega)\theta^\top \mathrm{n},$$

for the scalar-valued map $\phi_J(\Omega)$ defined on $\partial\Omega$ by

$$\phi_J(\Omega) = -\frac{1}{\beta}\left[\sum_{i=1}^{k} \partial_i J(\lambda_1(\Omega), \dots, \lambda_k(\Omega)) \left(\frac{\partial u_i(\Omega)}{\partial \mathrm{n}}\right)^2\right] \mathrm{n}^\top a \mathrm{n} e^{-\beta V}. \tag{3.21}$$

The vector field $\phi_J(\Omega)\mathrm{n}$ is therefore the $L^2(\partial\Omega)$-gradient of J with respect to θ, which is why $\phi_J(\Omega)$ is also called the shape-gradient of J at Ω. A natural approach to shape-optimization is to approximate the $L^2(\partial\Omega)$-gradient flow by an explicit Euler discretization, setting $\widetilde{\Omega} = (\mathrm{Id} + \eta\theta)\Omega$, where θ is chosen so that $\theta^\top \mathrm{n}\big|_{\partial\Omega} = \phi_J(\Omega)$. When using mesh-discretizations of Ω, two difficulties arise with this approach. Firstly, one must specify how to displace the internal vertices of the mesh, or in other words how to extend $\phi_J(\Omega)\mathrm{n}$ to Ω. Secondly, the normal derivative n is an irregular field on the boundary of a mesh. In practice, one observes that displacements of the boundary vertices along the mesh normal field leads to rapid collapse in mesh quality, which prevents the naive method from being useful.

To overcome both difficulties, a standard approach (see for instance [94]) is to resort to an extension-regularization procedure, seeking a Riesz representative of $\theta \mapsto DJ(\Omega;\theta)$ in a Hilbert space $\mathcal{H}(\Omega) \subset L^2(\Omega)$ consisting of more regular shape-perturbations, defined on the whole of Ω. To ensure that this is possible, $\mathcal{H}(\Omega)$ should be continuously embedded in $L^2(\partial\Omega)$. A common choice, which we use in this work, is to take

$$\mathcal{H}(\Omega) = H^1(\Omega)^d, \qquad \langle \theta, \psi \rangle_{\mathcal{H}(\Omega)} = \int_\Omega \left(\varepsilon_{\mathrm{reg}}^2 \nabla\theta : \nabla\psi + \theta^\top \psi\right), \tag{3.22}$$

where $\varepsilon_{\mathrm{reg}} > 0$ is a regularization scale, which is chosen of the order of a few cell widths for the underlying mesh. Therefore, the problem of finding a Riesz representative of $\theta \mapsto DJ(\Omega;\theta)$ amounts to solving

$$\langle \theta_{\mathrm{reg}}, \theta \rangle_{\mathcal{H}(\Omega)} = \int_{\partial\Omega} \phi_J(\Omega)\theta^\top \mathrm{n}, \qquad \forall\, \theta \in \mathcal{H}(\Omega). \tag{3.23}$$

Solving and taking $\theta = \theta_{\mathrm{reg}}$, one finds that $DJ(\Omega;\theta_{\mathrm{reg}}) = \|\theta_{\mathrm{reg}}\|^2_{\mathcal{H}(\Omega)}$, so that θ_{reg} is indeed a valid descent direction defined on the whole of Ω, and moreover $\theta_{\mathrm{reg}} = 0$ if and only if Ω is a critical shape of J. Note that this approach is still valid whenever $\phi_J(\Omega)\mathrm{n} \in H^{-1/2}(\partial\Omega)^d$ and Ω is a Lipschitz domain, since the Sobolev trace theorem then gives the continuity of the trace $\gamma : \mathcal{H}(\Omega) \to H^{1/2}(\partial\Omega)^d$. In practice, the problem (3.23) is solved by a Galerkin method, which we discuss below.

For our choice of $\mathcal{H}(\Omega)$, the requirement (3.23) is the weak formulation of the following Neumann boundary value problem:

$$\begin{cases} -\varepsilon_{\mathrm{reg}}^2 \Delta\theta_{\mathrm{reg}} + \theta_{\mathrm{reg}} = 0 \text{ in } \Omega, \\ \qquad \varepsilon_{\mathrm{reg}}^2 \nabla\theta_{\mathrm{reg}} \mathrm{n} = \phi_J(\Omega)\mathrm{n} \text{ on } \partial\Omega. \end{cases} \tag{3.24}$$

where Δ is the component-wise Laplace operator. Let us denote by

$$R_{\varepsilon_{\mathrm{reg}}} : \begin{cases} H^{-1/2}(\partial\Omega)^d \to \mathcal{H}(\Omega), \\ \qquad \phi_J(\Omega)\mathrm{n} \mapsto \theta_{\mathrm{reg}} \quad \text{solution to equation (3.24)} \end{cases}$$

the operator which maps the boundary data $\Phi_J(\Omega)\mathrm{n}$ to the solution θ of the above Neumann problem.

Various other approaches to the extension-regularization procedure, tailored to preserve mesh quality over many iterations, are sometimes preferred, see [87, Section 3.5]. They simply correspond to other choices of $\mathcal{H}(\Omega)$ and the associated inner product.

Case of multiple eigenvalues. The case of multiple eigenvalues is more challenging. To simplify the presentation, and motivated by the maximization of (3.7), we focus on the case where J depends only on the first two Dirichlet eigenvalues, and $\lambda_2(\Omega)$ has multiplicity $m = 2$ ($\lambda_1(\Omega)$ is always simple by theory), and $\partial_{\lambda_2} J(\Omega) \geqslant 0$. The generalization to more eigenvalues and/or other local monotonicity properties of J is straightforward, although the computational cost of the method increases with the total multiplicity.

According to the third item in Theorem 3.14, multiple eigenvalues are no longer Fréchet-differentiable, and one therefore loses any natural notion of shape gradient. However, the objective is still directionally differentiable. The natural counterpart to the shape gradient is given by the steepest ascent perturbation

$$\theta^* \in \operatorname*{Argmax}_{\|\theta\|_{\mathcal{H}(\Omega)}=1} DJ(\Omega;\theta). \tag{3.25}$$

Note that one seeks a steepest ascent perturbation in the space $\mathcal{H}(\Omega)$ of regular perturbations defined in (3.22). This is done to ultimately preserve mesh quality, just as in the case of simple eigenvalues. It is however not immediately clear that the problem (3.25) is well-posed or tractable. Fortunately, this turns out to be the case in our setting. First, we write

$$\begin{aligned} DJ(\Omega;\theta) &= \partial_{\lambda_1} J(\Omega) D\lambda_1(\Omega;\theta) + \partial_{\lambda_2} J(\Omega) \min_{|u|=1} u^\top M^{\Omega,2}(\theta) u \\ &= \min_{|u|=1} u^\top \left[\partial_{\lambda_1} J(\Omega) D\lambda_1(\Omega;\theta) \mathrm{I}_2 + \partial_{\lambda_2} J(\Omega) M^{\Omega,2}(\theta) \right] u, \end{aligned}$$

using $\partial_{\lambda_2} J(\Omega) \geqslant 0$ and the fact that $D\lambda_2(\Omega;\theta)$ is the smallest eigenvalue of the 2×2 matrix $M^{\Omega,2}(\theta)$ defined in (3.14). The problem (3.25) is therefore to maximize with respect to θ the smallest eigenvalue of the symmetric matrix $Q^\Omega(\theta)$ whose (i,j)-th component is given by

$$\begin{aligned} Q^\Omega_{ij}(\theta) &= \langle \phi^{ij}_J(\Omega)\mathrm{n}, \theta \rangle_{L^2(\partial\Omega)}, \\ \phi^{ij}_J(\Omega) &= -\frac{1}{\beta} \left[\partial_{\lambda_2} J(\Omega) \frac{\partial u_2^{(i)}}{\partial \mathrm{n}} \frac{\partial u_2^{(j)}}{\partial \mathrm{n}} + \delta_{ij} \partial_{\lambda_1} J(\Omega) \left(\frac{\partial u_1}{\partial \mathrm{n}} \right)^2 \right] \mathrm{n}^\top a \mathrm{n} e^{-\beta V}, \end{aligned} \tag{3.26}$$

where we write $u_1 = u_1(\Omega)$, $u_2^{(i)} = u_2^{(i)}(\Omega)$ for $i = 1, 2$, and use the formula (3.15). Crucially, this matrix depends linearly on θ, although its smallest eigenvalue does not.

By the regularization procedure detailed in the previous paragraph, we may also write

$$Q^\Omega_{ij}(\theta) = \langle R_{\varepsilon_{\mathrm{reg}}} \phi^{ij}_J(\Omega)\mathrm{n}, \theta \rangle_{\mathcal{H}(\Omega)}, \qquad \forall\, 1 \leqslant i, j \leqslant 2. \tag{3.27}$$

Let us denote by $\psi_{ij} := R_{\varepsilon_{\mathrm{reg}}} \phi^{ij}_J(\Omega)\mathrm{n} \in \mathcal{H}(\Omega)$, $G := \mathrm{Span}_{\mathcal{H}(\Omega)}\{\psi_{ij},\, 1 \leqslant i \leqslant j \leqslant 2\}$, and Π_G

the $\mathcal{H}(\Omega)$-orthogonal projector onto G.

To solve (3.25), we distinguish between two cases.

- If $\sup_{\|\theta\|_{\mathcal{H}(\Omega)}=1} DJ(\Omega;\theta) \leqslant 0$, then the sup is equal to 0, and is attained for any $\theta \in G^\perp$ with unit norm. Note this is a first-order optimality condition: to first order, any shape perturbation can only decrease the value of J.
- If $\sup_{\|\theta\|_{\mathcal{H}(\Omega)}=1} DJ(\Omega;\theta) > 0$ then by positive homogeneity of the smallest eigenvalue with respect to θ and the identity $Q^\Omega(\theta) = Q^\Omega(\Pi_G\theta)$, we rewrite

$$\sup_{\|\theta\|_{\mathcal{H}(\Omega)=1}} DJ(\Omega;\theta) = \sup_{\|\theta\|_{\mathcal{H}(\Omega)\leqslant 1}} DJ(\Omega;\theta) = \max_{\substack{\|\theta\|_{\mathcal{H}(\Omega)\leqslant 1}\\ \theta\in G}} DJ(\Omega;\theta).$$

In the second case, the sup is replaced by a max, since the supremum is taken over the compact set $\overline{B_{\mathcal{H}(\Omega)}(0,1)} \cap G$. Hence, in both cases, a maximizer for (3.25) is attained. In fact, we can check that, in the second case, the maximizer is unique, as implied by the following elementary lemma.

Lemma 3.6. *Let B be the closed unit ball in a finite-dimensional Hilbert space E, and let $f : B \to \mathbb{R}$ be a concave function which is not identically 0 on B, and is furthermore positively homogeneous of degree $\alpha > 0$. Then, there exists a unique maximizer $\theta^* \in \partial B$ for the problem*

$$\sup_{\theta\in B} f(\theta).$$

Proof. Since B is compact, there exists a maximizer. Assume for the sake of contradiction the existence of two distinct maximizers $\theta_1 \neq \theta_2$. Letting $\theta = \frac{1}{2}(\theta_1 + \theta_2)$, we note that $\|\theta\|_E < 1$ and next that

$$\begin{aligned} f(\theta/\|\theta\|_E) &= \|\theta\|_E^{-\alpha} f(\theta) > f(\theta) \\ &= f\left(\frac{1}{2}(\theta_1+\theta_2)\right) \geqslant \frac{1}{2}\left(f(\theta_1)+f(\theta_2)\right) \\ &= \max_B f, \end{aligned}$$

using homogeneity in the first inequality and concavity in the second inequality. We have reached a contradiction, therefore there exists a unique maximizer θ^*, which necessarily satisfies $\|\theta^*\| = 1$ by homogeneity. □

In our setting, we let $E = G$, and notice that, since $\theta \mapsto u^\top Q^\Omega(\theta)u$ is linear for any $u \in \mathbb{R}^2$, the map

$$\theta \mapsto DJ(\Omega;\theta) = \min_{|u|=1} u^\top Q^\Omega(\theta)u$$

is concave and positively homogeneous of degree $\alpha = 1$. Under the assumption $\sup_{\|\theta\|_{\mathcal{H}}=1} DJ(\Omega;\theta) > 0$, it is non-identically equal to zero on the closed unit ball of G, which proves the existence of a unique θ^* solving (3.25).

In practice, finding θ^* is tractable by a direct search method. Letting $g = (g_1, g_2, g_3) \in \mathcal{H}(\Omega)^3$ be a $\mathcal{H}(\Omega)$-orthonormal basis for G, obtained by applying a Gram–Schmidt procedure to

the $\{\psi_{ij}, 1 \leqslant i \leqslant j \leqslant 2\}$, the problem (3.25) reduces to an optimization with respect to a parameter α on the unit sphere $\mathbb{S}^2 \subset \mathbb{R}^3$. If we fail to find $\alpha \in \mathbb{S}^2$ such that $DJ(\Omega; \alpha^\top g) > 0$, we deduce that Ω satisfies a first-order optimality condition, although this case never came up in our examples.

Remark 3.7. We note that, even for objectives J involving several eigenvalues with multiplicities greater than 2, the optimization problem (3.25) can still be reduced to a finite-dimensional optimization problem. However, the dimensionality of the problem may be large, and is related to the number of linearly independent components of the perturbation matrix (3.27), namely

$$\dim G \leqslant \sum_{j=1}^{\ell} \frac{m_j(m_j+1)}{2},$$

where ℓ denotes the number of distinct degenerate eigenvalue involved in the definition of J, and the set $\{m_j, 1 \leqslant j \leqslant \ell\}$ enumerates their respective multiplicities. Moreover, the finite-dimensional problem will generally not be concave, in which case the optimum θ^* may not be unique, and the problem may be itself hard to solve, especially if dim G is large.

Discretization of ascent directions. We now explain how we discretize the choice of ascent direction at the k-th iteration of Algorithm 3.5. The domain Ω_k is approximated by a mesh $\Sigma_k = (\mathcal{V}_k, \mathcal{T}_k)$, and the extension-regularization operator $R_{\varepsilon_{\text{reg}}}$ is replaced by a Galerkin approximation $\widehat{R}_{\varepsilon_{\text{reg}}}$

We consider the subspace $W(\Sigma_k)$ spanned by the basis Θ_k of $\mathbb{P}_1$ vector-valued elements associated with Σ_k, and compute its Gram matrix $G_{\text{reg}}(\Sigma_k)$ with respect to the $\mathcal{H}(\Omega_k)$-inner product (3.22) for the basis Θ_k. This costly step only needs to be performed once, regardless of the number of extension-regularization calls (which is determined by the degeneracy of the eigenvalues, as (3.27) needs to be computed). For any $f \in H^{-1/2}(\partial\Omega_k)^d$, we compute the components $b_f(\Sigma_k)$ of $\theta \mapsto \langle f, \theta\rangle_{L^2(\partial\Omega_k)^d}$ in the basis Θ_k, solve $G_{\text{reg}}(\Sigma_k)\alpha = b_f(\Sigma_k)$ for $\alpha \in \mathbb{R}^{|\Theta_k|}$, and take $\widehat{R}_{\varepsilon_{\text{reg}}}(f) := \Theta_k^\top \alpha$. In practice, the components of $b_f(\Sigma_k)$ are further approximated by quadrature rules. All spectral quantities, namely the eigenvalues $\lambda_j(\Omega)$ and the eigenvectors $u_j(\Omega)$ for $1 \leqslant j \leqslant k$, are replaced by their Rayleigh–Ritz counterparts $\lambda_j(\Sigma)$ and $u_j(\Sigma)$, as well as the corresponding normal derivatives.

Numerically, exactly degenerate eigenvalues are never encountered. However, when λ_2 is almost degenerate, i.e. $(\lambda_3(\Sigma_k) - \lambda_2(\Sigma_k))/\lambda_2(\Sigma_k) \ll 1$, the displacement in step $C.$ of the ascent algorithm 3.5 may lead to the crossing of the eigenvalue branches, in such a way that it leads in fact to a local decrease in the value of J. This manifests itself through local oscillations in the eigenvalues and objective functions throughout the ascent algorithm, see Figure 3.15 below. This is a well-known problem in the numerical optimization of non-smooth objective functions, and decreasing the step size η_k to ensure local ascent is not a viable solution, as it may lead to very slow convergence to a local minimum, or altogether prevent it. In the context of numerical optimization of eigenvalues, this behavior has been for example observed in [86], where Nesterov-type acceleration techniques are suggested.

We follow another approach, assuming exact degeneracy when detecting $\varepsilon_{\text{degen}}$-degeneracy, and choosing an ascent direction within a low-dimensional space of perturbations, according

to the analytical prescription of the previous paragraph. See the work [94] for a closely related method applied to an exactly degenerate eigenvalue problem.

More precisely, in the case of $\varepsilon_{\text{degen}}$-simple eigenvalues, we set

$$\theta_k := \widehat{R}_{\varepsilon_{\text{reg}}}(\phi_J(\Sigma_k)\mathrm{n}) / \max\left(M_{\text{grad}}, \|\widehat{R}_{\varepsilon_{\text{reg}}}(\phi_J(\Sigma_k)\mathrm{n})\|_{\mathcal{H}(\Sigma_k)}\right),$$

where $\phi_J(\Sigma_k)$ is obtained by substituting Rayleigh–Ritz approximations in the definition (3.21) of the shape gradient $\phi_J(\Omega_k)$, and we recall $M_{\text{grad}} > 0$ is a hyperparameter. In other words, if the shape gradient is larger than M_{grad} in the $\mathcal{H}(\Sigma_k)$-norm, the ascent perturbation is normalized. This procedure is equivalent to step size adaptation in an explicit Euler discretization of the underlying geometric flow, and corresponds to some time reparameterization (in the limit $\eta_{\max} \to 0$) of the trajectories generated by Algorithm 3.5. We found this choice convenient to stabilize the numerical flow, since the gradient varies by several orders of magnitude throughout the numerical trajectories for the problem we considered. To ensure convergence near local maxima, this normalization is capped at $M_{\text{grad}} > 0$.

For the case of $\varepsilon_{\text{degen}}$-degenerate eigenvalues, we first solve

$$\forall\, 1 \leqslant i, j \leqslant 2, \qquad \psi_{ij}(\Sigma_k) = \widehat{R}_{\varepsilon_{\text{reg}}}(\phi_J^{ij}(\Sigma_k)\mathrm{n}),$$

where the $\phi_J^{ij}(\Sigma_k)$ are obtained from (3.26) by substituting Rayleigh–Ritz approximations in place of exact eigenelements. We then apply the Gram–Schmidt algorithm (for the $\mathcal{H}(\Sigma_k)$-scalar product (3.22)) to this set of perturbations, yielding a basis $g(\Sigma_k) = (g_1(\Sigma_k), g_2(\Sigma_k), g_3(\Sigma_k)) \in \mathcal{H}(\Sigma_k)^3$ of regular perturbations defined on Ω_k. We then solve

$$\alpha^* = \max_{\alpha \in L_{N_{\text{search}}}} \widehat{DJ}(\Sigma_k; \alpha^\top g(\Sigma_k)),$$

where $\widehat{DJ}(\Sigma_k; \cdot)$ is defined in (3.20), and $L_{N_{\text{search}}} \subset \mathbb{S}^2$ is a set of N_{search} points on the sphere. In practice, we use a Fibonacci lattice (see [140]), which is simple to implement and distributes points quasi-uniformly. This optimization step is extremely cheap, after having precomputed the matrix elements

$$\langle \phi_J^{ij}(\Sigma_k)\mathrm{n}, g_k(\Sigma_k)\rangle_{L^2(\partial\Omega_k)}, \qquad 1 \leqslant i, j \leqslant 2,\ 1 \leqslant k \leqslant 3.$$

Note that one could use the equivalent volume form (3.27), but since boundary integrals are cheaper to compute and give good results in practice, we work with the latter instead. After this precomputation step, the cost of evaluating the value of $DJ(\Omega_k; \alpha^\top g)$ for $\alpha \in \mathbb{S}^2$ becomes negligible, and one can deduce the optimal perturbation $\theta^*(\Sigma) = \alpha^{*\top} g(\Sigma)$ at virtually no cost. We set $\theta_k = \theta^*(\Sigma)$, which is by construction normalized in $\mathcal{H}(\Sigma)$.

It would be of interest to obtain rigorous consistency results in the regimes $\varepsilon_{\text{degen}} \to 0$ and $|\mathcal{T}|, N_{\text{search}} \to +\infty$, as well as proving local convergence results for the algorithm and/or the underlying geometric flow. We leave this delicate question up for future work.

3.4 Practical methods for high-dimensional systems

Although Theorem 3.2 is interesting from a theoretical perspective, its applicability to the numerical shape optimization of spectral functionals is limited to settings for which the eigenelements of $\mathcal{L}_\beta$ are available. For high-dimensional systems, which are typical in molecular simulation, this is hardly the case. It is therefore necessary to provide alternative numerical approaches. In this section, we discuss such methods. The first one, discussed in Section 3.4.1, relies on optimizing the separation of timescales for an effective dynamics through a given collective variable. The second one, discussed in Section 3.4.2, relies on the optimization of asymptotic expressions derived in the low-temperature regime, in the recent results of [50].

3.4.1 Coarse graining of dynamical rates

In this section, we propose a numerical strategy based on a Galerkin method and Theorem 3.2, after projecting the infinitesimal generator onto a collective variable (CV) or reaction coordinate.

In practical cases from molecular dynamics, the process (3.1) evolves in a high-dimensional space $\mathbb{R}^d$ with $d \gg 1$. In order to interpret trajectories in configurational space, it is often useful to view them through a low-dimensional map $\xi : \mathbb{R}^d \to \mathbb{R}^m$, also known as a collective variable or reaction coordinate. Classical examples include geometric quantities such as dihedral angles, well-chosen interatomic distances, coordination numbers, path collective variables, which all derive from chemical intuition, and thus generally have a good physical interpretation. In recent years, machine learning techniques have been applied to the automatic construction of CVs optimized for a variety of purposes, see for instance [125, 138, 74, 139] for a review of recent approaches.

Here we assume that a collective variable ξ is given, and consider the new problem of optimizing the effective separation of timescales with respect to a domain defined in collective variable space. The effective objective is defined with respect to a surrogate dynamics (see (3.30)), which is already studied in [217, 346, 258], although the methodology could in principle be applied to other reduced order models of the dynamics as well (see Remark 3.10 below).

Assumptions on the collective variable. From now on, we assume that ξ is smooth, with $\nabla\xi$ of full rank m everywhere. In particular, the Gram matrix $G_\xi = \nabla\xi^\top \nabla\xi \in \mathbb{R}^{m\times m}$ is everywhere invertible. This condition ensures, by the implicit function theorem, that ξ foliates $\mathbb{R}^d$ into a disjoint union of smooth submanifolds, which are given by the level sets $\Sigma_z := \xi^{-1}(z)$, for $z \in \mathbb{R}^m$. We denote by μ_z the canonical measure conditioned on Σ_z. It corresponds to the probability measure defined by

$$\mu_z \in \mathcal{M}_1(\Sigma_z), \qquad \frac{\mathrm{d}\mu_z}{\mathrm{d}\mathcal{H}_{\Sigma_z}} = \mathrm{e}^{-\beta V} \left(\det G_\xi\right)^{-1/2} \mathrm{e}^{\beta F_\xi(z)},$$

where $\mathcal{H}_{\Sigma_z}$ is the $(d-m)$-dimensional Hausdorff measure on the submanifold Σ_z. The factor $\mathrm{e}^{-\beta F_\xi(z)}$ is a normalization constant expressed in terms of the free energy $F_\xi : \mathbb{R}^m \to \mathbb{R}$ defined as

$$F_\xi(z) := -\frac{1}{\beta} \log \int_{\Sigma_z} \mathrm{e}^{-\beta V} \left(\det G_\xi\right)^{-1/2} \mathrm{d}\mathcal{H}_{\Sigma_z}. \tag{3.28}$$

The collective variable will serve two purposes. Firstly, states will be defined in collective variable space, i.e. by fixing $\Omega_\xi \subset \mathbb{R}^m$, and considering the preimage $\xi^{-1}(\Omega_\xi)$. Secondly, the variational principle defining Dirichlet eigenvalues for the generator $-\mathcal{L}_\beta$ will be restricted to functions which are only a function of the collective variable ξ. This will define, for each domain Ω_ξ, a set of Rayleigh–Ritz eigenvalues which will serve as effective eigenvalues associated with $\xi^{-1}(\Omega_\xi)$.

Introduce the weighted space $L^2_\beta(\Omega_\xi) = L^2(\Omega_\xi, \mathrm{e}^{-\beta F_\xi(z)}\,\mathrm{d}z)$, and the associated weighted Sobolev spaces as in (3.9). We denote, for $\Omega_\xi \subset \mathbb{R}^m$ and $\varphi \in H^1_{0,\beta}(\Omega_\xi)$,

$$R_\xi\left(\varphi;\Omega_\xi\right) = R\left(\varphi\circ\xi;\xi^{-1}(\Omega_\xi)\right),$$

where $R(\cdot;\Omega)$ is the Rayleigh quotient associated with the Dirichlet realization of $\mathcal{L}_\beta$ on Ω, i.e.

$$R(\psi;\Omega) = \frac{1}{\beta}\frac{\displaystyle\int_\Omega \nabla\psi^\top a\nabla\psi \mathrm{e}^{-\beta V}}{\displaystyle\int_\Omega \psi^2 \mathrm{e}^{-\beta V}} \qquad \forall \psi \in H^1_{0,\beta}(\Omega).$$

Then, the coarea formula (see [199, Corollary 5.2.6]) allows us to write

$$\begin{aligned} R_\xi\left(\varphi;\Omega_\xi\right) &= \frac{1}{\beta}\frac{\displaystyle\int_{\xi^{-1}(\Omega_\xi)} \nabla(\varphi\circ\xi)^\top a\nabla(\varphi\circ\xi)\mathrm{e}^{-\beta V}}{\displaystyle\int_{\xi^{-1}(\Omega_\xi)} (\varphi\circ\xi)^2\mathrm{e}^{-\beta V}} \\ &= \frac{1}{\beta}\frac{\displaystyle\int_{\Omega_\xi}\int_{\Sigma_z} \left[\nabla\varphi\circ\xi\right]^\top \nabla\xi^\top a\nabla\xi\left[\nabla\varphi\circ\xi\right]\mathrm{e}^{-\beta F_\xi\circ\xi}\,\mathrm{d}\mu_z\,\mathrm{d}z}{\displaystyle\int_{\Omega_\xi}\int_{\Sigma_z} (\varphi\circ\xi)^2\,\mathrm{e}^{-\beta F_\xi\circ\xi}\,\mathrm{d}\mu_z\,\mathrm{d}z} \\ &= \frac{1}{\beta}\frac{\displaystyle\int_{\Omega_\xi} \nabla\varphi^\top a_\xi\nabla\varphi\,\mathrm{e}^{-\beta F_\xi}}{\displaystyle\int_{\Omega_\xi}\varphi^2\,\mathrm{e}^{-\beta F_\xi}} \end{aligned}$$

where a_ξ denotes the symmetric, positive-definite matrix-valued map

$$a_\xi(z) = \int_{\Sigma_z} \nabla\xi^\top a\nabla\xi \mathrm{d}\mu_z \in \mathbb{R}^{m\times m}. \tag{3.29}$$

It follows that R_ξ, which we interpret as a family of coarse-grained Rayleigh quotients on the lower-dimensional space $\mathbb{R}^m$, has the same basic structure as R. Indeed, it corresponds to the family of Dirichlet Rayleigh quotients associated with a reversible diffusion on $\mathbb{R}^m$ of the form (3.1), where the potential V and diffusion matrix a have been replaced by their lower-dimensional analogs defined in terms of conditional expectations with respect to the reference dynamics:

$$\mathrm{d}Z^\xi_t = \left(-a_\xi(Z^\xi_t)\nabla F_\xi(Z^\xi_t) + \frac{1}{\beta}\mathrm{div}\, a_\xi(Z^\xi_t)\right)\mathrm{d}t + \sqrt{\frac{2}{\beta}}a_\xi(Z^\xi_t)^{1/2}\,\mathrm{d}B_t, \tag{3.30}$$

where B is a m-dimensional standard Brownian motion. The dynamics (3.30) can be understood as a Markovian model for the dynamics of $\xi(X_t)$, which is also reversible with respect to the

Gibbs measure associated with the free energy. We refer to [217, 346] for additional details on the mathematical properties of the effective dynamics.

A natural question is whether one can hope to approximate the true dynamical rates with those predicted by the effective dynamics (3.30). The answer has practical implications, since in the case where m is sufficiently low-dimensional, the eigenvalue problem associated with R_ξ becomes numerically tractable, and one may then optimize the separation of timescales $N^*(\Omega)$ with respect to domains Ω defined in terms of the CV. It should be noted that it is anyway common practice to define configurational states in terms of a CV.

These considerations motivate the following Galerkin approach, already discussed in [346, Section 3.3.2] for the case $\Omega_\xi = \mathbb{R}^m$. We introduce the following linear subspace

$$V_\xi = \{\varphi \circ \xi, \varphi \in H^1_{0,\beta}(\Omega_\xi)\} \subset H^1_{0,\beta}\left(\xi^{-1}(\Omega_\xi)\right),$$

and define the local coarse-grained rates

$$\lambda_k^\xi(\Omega_\xi) := \min_{E_\xi} \max_{\varphi \in E_\xi} R_\xi(\varphi, \varphi; \Omega_\xi) = \min_{E} \max_{\varphi \in E} R\left(\varphi, \varphi; \xi^{-1}(\Omega_\xi)\right),$$

where E_ξ ranges over the set of k-dimensional subspaces of $H^1_{0,\beta}(\Omega_\xi)$ in the first equality, and E ranges over the set of k-dimensional subspaces of $\mathcal{E}_\xi$ in the second. In other words, λ_k^ξ is the k-th eigenvalue of the following operator acting on the weighted space $L^2(\Omega_\xi, \mathrm{e}^{-\beta F_\xi}\,\mathrm{d}z)$ with Dirichlet boundary conditions:

$$-\mathcal{L}_\beta^\xi \varphi = -\frac{1}{\beta} \mathrm{e}^{\beta F_\xi} \mathrm{div}\left(\mathrm{e}^{-\beta F_\xi} a_\xi \nabla \varphi\right).$$

It follows easily from the Courant–Fischer principle that $\lambda_k^\xi(\Omega_\xi) \geqslant \lambda_k(\xi^{-1}(\Omega_\xi))$, and moreover that if $\{u_1(\xi^{-1}(\Omega_\xi)), \ldots, u_k(\xi^{-1}(\Omega_\xi))\} \subset \mathcal{V}_\xi$ for some $k \leqslant m$, it holds that $\lambda_k^\xi(\Omega_\xi) = \lambda_k(\xi^{-1}(\Omega_\xi))$. Thus, the dynamical rates associated with the effective dynamics will systematically overestimate the true rates. However, these will still be accurate if the Dirichlet eigenfunctions for $\mathcal{L}_\beta$ on $\xi^{-1}(\Omega_\xi)$ can be well approximated in the class $\mathcal{V}_\xi$.

More precisely, we have the following result, adapted from [346, Proposition 5].

Proposition 3.8. *Let $k \geqslant 1$ and λ_k^ξ (respectively, λ_k) be the k-th principal eigenvalue of $-\mathcal{L}_\beta^\xi$ (resp. $-\mathcal{L}_\beta$) in Ω_ξ (resp. $\xi^{-1}(\Omega_\xi)$), with associated eigenfunction u_k^ξ (resp. u_k), with the normalization (3.12). Then,*

$$\lambda_k \leqslant \lambda_k^\xi \leqslant \lambda_k + \frac{1}{\beta} \int_{\xi^{-1}(\Omega_\xi)} \nabla\left[u_k - u_k^\xi \circ \xi\right]^\top a \nabla\left[u_k - u_k^\xi \circ \xi\right] \mathrm{e}^{-\beta V}. \tag{3.31}$$

The proof of Proposition 3.8 is a straightforward adaptation of [346, Proposition 5] to the case of absorbing Dirichlet boundary conditions on $\partial\Omega_\xi$ and is therefore omitted.

A useful corollary of Theorem 3.2 is the following result.

Proposition 3.9. *Let $\Omega_\xi \subset \mathbb{R}^m$ be a bounded open domain which is convex or has a $\mathcal{C}^{1,1}$ boundary. Assume that ξ is such that Assumptions (**Ell**) and (**Reg**) are satisfied with $d = m$, $V = F_\xi$ and $a = a_\xi$. Let $\lambda_k^\xi = \lambda_k^\xi(\Omega_\xi)$ be an eigenvalue for $\mathcal{L}_\beta^\xi$ of multiplicity $m_k^\xi \geqslant 1$,*

satisfying the normalization

$$\int_{\Omega_\xi} u_k^{(i),\xi}(\Omega_\xi) u_k^{(j),\xi}(\Omega_\xi) \mathrm{e}^{-\beta F_\xi} = \delta_{ij}, \qquad 1 \leqslant i,j \leqslant m_k^\xi,$$

where the $u_k^{(i),\xi}(\Omega_\xi)$ *for* $1 \leqslant i \leqslant m_k^\xi$ *are a basis of corresponding eigenvectors in* $L^2(\Omega_\xi, \mathrm{e}^{-\beta F_\xi})$. *Then, for* $\theta \in \mathcal{W}^{1,\infty}(\mathbb{R}^m;\mathbb{R}^m)$ *and* $0 \leqslant \ell < m$, *the map* $t \mapsto \lambda_{k+\ell}^\xi((\mathrm{Id}+t\theta)\Omega_\xi)$ *is semi-differentiable at* $t=0$, *and the right-differential is the* $(\ell+1)$*-th smallest eigenvalue of the matrix*

$$M_{ij}^\xi(\theta) = -\frac{1}{\beta}\int_{\partial\Omega_\xi} \frac{\partial u_k^{(i),\xi}(\Omega_\xi)}{\partial \mathrm{n}} \frac{\partial u_k^{(j),\xi}(\Omega_\xi)}{\partial \mathrm{n}} n^\top a_\xi \mathrm{n} \theta^\top \mathrm{n}\, \mathrm{e}^{-\beta F_\xi} \qquad 1 \leqslant i,j \leqslant m.$$

Proof. The result is a direct application of Theorem 3.2 and Corollary 3.4. □

We discuss sufficient conditions for the assumptions of Proposition 3.9 in Appendix 3.C below.

Proposition 3.9 suggests a practical approach to the shape optimization of spectral functionals $\mathcal{F}(\lambda_1(\Omega),\dots,\lambda_k(\Omega))$ in a high-dimensional setting, replacing the original objective with the coarse-grained objective $\mathcal{F}(\lambda_1^\xi(\Omega_\xi),\dots,\lambda_k^\xi(\Omega_\xi))$. The computational implementation of this approach however requires access to the free energy F_ξ and the matrix a_ξ, for which a number of sampling methods are available, see [229] for an overview. Due to the approximation error in (3.31), we cannot expect the resulting shapes to be optimal for the original objective in the class of domains defined in CV space. They can nevertheless be used as input in acceleration methods such as ParRep, since this algorithm is dynamically unbiased by construction (in the limit of long decorrelation times).

Remark 3.10. The quality of the approximation (3.31) is quite sensitive to the choice of collective variable ξ, and so, for a poor choice of ξ, the effective dynamics (3.30) and its associated eigenvalues may give little insight into the original timescales (see Section 3.5.1 below for an example).

However, one could in principle apply the same methodology to other reversible, elliptic diffusions in $\mathbb{R}^m$ besides (3.30), designed to better replicate the dynamical properties of $\xi(X_t)$. In particular, instead of directly measuring F_ξ and a_ξ using thermodynamic averages, one can use a parametric approach to fit drift and diffusion coefficients of a dynamical model in $\mathbb{R}^m$ directly from trajectories of $\xi(X_t)$ in CV space, see for instance [200]. This option has the advantage of being available even when the underlying dynamics in configurational space is not of the form (3.1), as long as the model enforces the form of a reversible diffusion (3.1) in $\mathbb{R}^m$. We leave this line of investigation to future work.

This method is numerically validated in Section 3.5.1 below, and is applied to a molecular system in Section 3.5.3.

3.4.2 Optimization in the semiclassical limit

In this section, we briefly summarize a second approach to make the shape optimization problem tractable, based on low-temperature spectral asymptotic results obtained in [50, Section 2.5]. These results are proved in [50] under a set of assumptions which we simplify here for the sake of clarity, while keeping the main ideas intact. We restrict ourselves to the case of a constant diffusion coefficient $a = \mathrm{Id}$. The dynamics follows therefore a standard overdamped Langevin equation:

$$\mathrm{d}X_t^\beta = -\nabla V\left(X_t^\beta\right)\,\mathrm{d}t + \sqrt{\frac{2}{\beta}}\,\mathrm{d}W_t. \tag{3.32}$$

We additionally note the dependence of the dynamics on β, which is inversely proportional to the temperature. In this section, it is an asymptotic parameter considered in the limit $\beta \to +\infty$.

The use of semiclassical techniques to approximate spectral properties of metastable diffusions is a well-established topic in the probabilistic literature, see for example [160, 61, 158, 225, 100, 101, 209, 227, 50] and references therein.

Asymptotic shape optimization of eigenvalue functionals. We consider the general problem of maximizing with respect to a shape Ω a functional of the Dirichlet eigenvalues of $-\mathcal{L}_\beta$ on Ω:

$$J(\Omega) = \mathcal{F}(\lambda_1(\Omega), \dots, \lambda_k(\Omega)),$$

where $\mathcal{F} : \mathbb{R}^k \to \mathbb{R}$ is continuous. When $d \gg 1$, the numerical optimization of J is generally numerically intractable, since the objective involves solving a high-dimensional boundary eigenvalue problem.

The low-temperature asymptotic approach to this problem consists in fixing a family of domains $(\Omega_{\alpha,\beta})_{\beta>0,\alpha\in\mathcal{S}}$, whose boundary geometry is jointly parametrized by the asymptotic parameter β, and a shape parameter α in the design space $\mathcal{S}$. Assume that the asymptotic behavior of $J(\Omega_{\alpha,\beta})$ is dictated, at dominant order, only by β and α in the limit $\beta \to +\infty$:

$$\mathcal{F}\left(\lambda_1(\Omega_{\alpha,\beta}), \dots, \lambda_k(\Omega_{\alpha,\beta})\right) = \mathcal{F}_\infty(\alpha,\beta)(1 + o(1)) \tag{3.33}$$

for some function $\mathcal{F}_\infty : \mathcal{S} \times \mathbb{R}_+^* \to \mathbb{R}$. At fixed $\beta > 0$, we say the domain $\Omega_{\alpha_\beta^*,\beta}$ is asymptotically optimal if

$$\alpha_\beta^* \in \operatorname*{Argmax}_{\alpha\in\mathcal{S}} \mathcal{F}_\infty(\alpha,\beta). \tag{3.34}$$

The difficulty in this approach lies in computing spectral asymptotics for domains with temperature-dependent boundaries. In [50], we define a set of geometric assumptions under which these spectral asymptotics can be derived, computed in practice, and ultimately optimized to solve the asymptotic problem (3.34). The derivation of these shape-sensitive asymptotic formulas relies on the construction of approximate eigenmodes (or quasimodes in the semiclassical terminology) for $\mathcal{L}_\beta$, which form the crux of identifying $\mathcal{F}_\infty$ in (3.33).

Geometrical setting. We now present a slightly simplified version of the geometrical setting used in [50], which will allow to express the asymptotic results as clearly as possible. We refer to [50] for a weaker set of assumptions for which the asymptotic results remain valid. Throughout this section, we assume that V is a $\mathcal{C}^\infty$ Morse function over $\mathbb{R}^d$. This means that at each point $z \in \mathbb{R}^d$ such that $\nabla V(z) = 0$, the Hessian matrix $\nabla^2 V(z)$ is non-degenerate. For $0 \leqslant i < N$, we denote the eigenvalues of the Hessian $\nabla^2 V(z_i)$ by

$$\mathrm{Spec}(\nabla^2 V(z_i)) = \left\{\nu_1^{(i)}, \nu_2^{(i)}, \cdots, \nu_d^{(i)}\right\}.$$

We make no assumption on the ordering of these eigenvalues, except that, if z_i is an index-1 saddle point, meaning that $\nabla^2 V(z_i)$ has a unique negative eigenvalue, one has $\nu_1^{(i)} < 0$ (i.e. the negative eigenvalue is the first one).

The Morse property implies that V has finitely many critical points in $\mathcal{K}_\alpha$, which we enumerate as $(z_i)_{0\leqslant i<N}$ for some $N > 0$. Among the critical points of V in $\mathcal{K}$, we distinguish the local minima and index-1 saddle points, respectively given by the sets

$$\{z_i,\, 0 \leqslant i < N_0\}, \qquad \{z_i,\, N_0 \leqslant i < N_0 + N_1\}.$$

For a given $x \in \mathbb{R}^d$, we denote by $\mathcal{A}(x)$ the basin of attraction of x for the steepest descent dynamics, i.e.

$$\mathcal{A}(x) = \left\{z \in \mathbb{R}^d :\, X(t) \xrightarrow{t\to\infty} x,\, X'(t) = -\nabla V(X(t)),\, X(0) = z\right\}. \tag{3.35}$$

The set $\mathcal{A}(x)$ is non-empty if and only if $\nabla V(x) = 0$, and in this case $\mathcal{A}(x)$ is a d-dimensional subset of $\mathbb{R}^d$, where d is the number of positive eigenvalues of $\nabla^2 V(x)$.

We now introduce the parameter $\alpha = \left(\alpha^{(i)}\right)_{0\leqslant i<N} \in (-\infty, +\infty]^N := \mathcal{S}$, which controls the asymptotic geometry of the domains near critical points of V. The value of the parameter $\alpha \in \mathcal{S}$ is fixed, its link with the domain geometry will be made explicit in Assumption 3.11 below. We first assume that the domains $\Omega_{\alpha,\beta}$ are smooth, and uniformly bounded, i.e. there exists a compact set $\mathcal{K}_\alpha \subset \mathbb{R}^d$ such that, $\Omega_{\alpha,\beta} \subset \mathcal{K}_\alpha$ for all $\beta > 0$.

Assumption 3.11. *In a small neighborhood of each critical point z_i and for β sufficiently large, the domain $\Omega_{\alpha,\beta}$ is shaped like a half-space:*

$$\Omega_{\alpha,\beta} \cap B(z_i, \varepsilon) = z_i + \left\{x \in \mathbb{R}^d :\, (x - z_i)^\top v_1^{(i)} < \alpha^{(i)}/\sqrt{\beta}\right\},$$

where $\varepsilon > 0$ is a fixed parameter which depends only on V, and $v_1^{(i)}$ is a unit eigenvector of $\nabla^2 V(z_i)$ for the eigenvalue $\nu_1^{(i)}$ (pointing outward of $\Omega_{\alpha,\beta}$ for $\alpha^{(i)} < +\infty$).

When $\alpha^{(i)} < +\infty$, the orientation convention for $v_1^{(i)}$ ensures that decreasing $\alpha^{(i)}$ locally retracts the domain. When z_i is an index-1 saddle point, Assumption (3.11) is physically motivated by the fact that $v_1^{(i)}$ gives the direction of the minimum energy path through z_i connecting a local minimum in the domain with a local minimum outside the domain (that is, the gradient flow lines joining the minima lying on both sides of the saddle point z_i). Informally, the parameter α encodes the position of the boundary along these paths, on the length scale $1/\sqrt{\beta}$.

The second assumption is that there is only one local minimum far from the boundary, in the following sense.

Assumption 3.12. *The point z_0 is the only local minimum of V in $\mathcal{K}$ such that $\alpha^{(0)} = +\infty$.*

Informally, this assumption forces the QSD inside $\Omega_{\alpha,\beta}$ to be unimodal, and to concentrate around z_0 in the limit $\beta \to \infty$.

In order to state the last hypothesis, we introduce the sets

$$\mathrm{SSP}(z_0) = \left\{ z_i : N_0 \leqslant i < N_0 + N_1,\ \exists m \neq z_0 \text{ a local minimum of } V \text{ s.t. } z_i \in \overline{\mathcal{A}(z_0)} \cap \overline{\mathcal{A}(m)} \right\},$$

$$I_{\min} = \left\{ N_0 \leqslant i < N_0 + N_1 :\ z_i \in \operatorname*{Argmin}_{i \in \mathrm{SSP}(z_0)} V \right\}, \qquad V^* = \min_{i \in \mathrm{SSP}(z_0)} V(z_i).$$

The set $\mathrm{SSP}(z_0)$ corresponds to so-called separating saddle points, which lie on the boundary of the basin of attraction of z_0, and the boundary of the basin of attraction for some other local minimum. Physically, these points correspond to the lowest-energy transition states on the boundary of $\mathcal{A}(z_0)$. The set $I_{\min}$ contains the indices of these low-energy separating saddle points, and the associated minimal energy is given by V^*.

The final assumption is the following.

Assumption 3.13. *There exists $c > 0$ such that, for β sufficiently large, it holds*

$$\mathcal{A}(z_0) \cap \{V < V^* + c\} \subset \Omega_{\alpha,\beta} \setminus \bigcup_{i \in I_{\min}} B(z_i, \varepsilon).$$

This assumption ensures that the boundary of $\Omega_{\alpha,\beta}$ does not enter below the energy level V^*, except perhaps near low-energy separating saddle points. The role of this assumption is to avoid the introduction of spurious low-energy transition states, corresponding to local minima of V on the boundary which have no relation to the physically relevant transition pathways. Assumption 3.13 ensures that these so-called generalized saddle points are higher in energy than the low-energy transition states, and do not pollute the dominant asymptotic behavior of the metastable exit time. This assumption is crucial in ensuring that the asymptotics are, at dominant order, only a function of β and α, as in the desideratum (3.33). However, it is expected in [50] that a similar analysis can be performed even if Assumption (3.13) does not hold, but at the cost of introducing a global counterpart to the local geometric Assumption (3.11). Relaxing Assumption 3.13 therefore leads once again to a high-dimensional (if not infinite-dimensional) design space $\mathcal{S}$, and besides cannot improve upon the maximizers of (3.34) in the case $\mathcal{F}(\lambda_1, \lambda_2) = (\lambda_2 - \lambda_1)/\lambda_1$, which is why we enforce it.

Harmonic approximation of the spectral gap. The first main result of [50] gives a quantitative and computable estimate of the spectral gap of the Dirichlet generator on $\Omega_{\alpha,\beta}$, in the limit $\beta \to +\infty$. In fact, it more generally shows that, for each $k \geqslant 1$, the k-th eigenvalue $\lambda_{k,\beta}(\Omega_{\alpha,\beta})$ converges to the k-th eigenvalue of a temperature-independent operator, the so-called harmonic approximation.

Theorem 3.14. *Under Assumption 3.11, it holds*

$$\lambda_{k,\beta}(\Omega_{\alpha,\beta}) \xrightarrow{\beta\to+\infty} \lambda^{\mathrm{H}}_{k,\alpha}, \tag{3.36}$$

where $\lambda^{\mathrm{H}}_{k,\alpha}$ is the k-th eigenvalue of the operator

$$K_\alpha = \bigoplus_{i=0}^{N} K^{(i)}_{\alpha^{(i)}}, \qquad K^{(i)}_{\alpha^{(i)}} = -\Delta + \frac{1}{4}x^\top \mathcal{D}^{(i)} x - \frac{\Delta V(z_i)}{2}, \tag{3.37}$$

with $\mathcal{D}^{(i)} = \operatorname{diag}\left(\nu_j^{(i)2}\right)_{j=1}^{d}$, and where the operator $K^{(i)}_{\alpha^{(i)}}$ is the Dirichlet realization of a quantum harmonic oscillator acting on the half-space $(-\infty, \alpha^{(i)}) \times \mathbb{R}^{d-1}$.

The local operators $K^{(i)}_{\alpha^{(i)}}$ serve as (appropriately rescaled) local models for the action of $-\mathcal{L}_\beta$ near critical points of V. The proof of Theorem 3.14 relies on a variational argument similar to the one used in [195, Theorem 11.1] or [303]. Using the eigenmodes of K_α, we construct variational test families for $\mathcal{L}_\beta$, so-called harmonic quasimodes. The convergence (3.36) follows from localization estimates on these quasimodes and the Courant–Fischer principle.

Crucially, the geometric assumptions outlined in the previous paragraph ensure that the eigenvalues $\lambda^{\mathrm{H}}_{k,\alpha}$ can be explicitly computed, as they belong to the spectrum of one of the local oscillators $K^{(i)}_{\alpha^{(i)}}$ for some $0 \leqslant i < N$. Indeed (see [50, Section 4.2]), the spectrum of $K^{(i)}_{\alpha^{(i)}}$ can be enumerated (with multiplicities) by

$$\operatorname{Spec} K^{(i)}_{\alpha^{(i)}} = \left(|\nu_1^{(i)}| \mu_{n_1, \alpha^{(i)}\left(|\nu_1^{(i)}|/2\right)^{1/2}} - \frac{\nu_1^{(i)}}{2} + \sum_{j=2}^{d} \left[|\nu_j^{(i)}| (n_j + 1/2) - \frac{\nu_j^{(i)}}{2} \right] \right)_{n \in \mathbb{N}^d}, \tag{3.38}$$

where $\mu_{n,a}$ is the $(n+1)$-th eigenvalue of the one-dimensional quantum oscillator $\frac{1}{2}(-\partial_x^2 - x^2)$ acting on $L^2(-\infty, a)$ with Dirichlet boundary conditions. The particular values $\mu_{n,\infty} = n + 1/2$ and $\mu_{n,0} = 2n + 3/2$ are well-known, so that the spectrum of the harmonic approximation is fully explicit in terms of eigenvalues of the Hessian $\nabla^2 V(z_i)$ in the case all the critical points z_i of V in $\mathcal{K}$ lie either on the boundary (i.e. $\alpha^{(i)} = 0$) or ε-inside $\partial\Omega_{\alpha,\beta}$ (i.e. $\alpha^{(i)} = +\infty$) for all $\beta > 0$. Otherwise, one generally has to compute the values of $\mu_{n,a}$ numerically. The (nonincreasing) functions $a \mapsto \mu_{n,a}$ can be computed once and for all with high precision for a range of integers n.

The value of $\lambda^{\mathrm{H}}_{k,\alpha}$ can then be easily obtained by taking the k-th largest element from the union with multiplicity (i.e. the multiset union) of each of the sets $\operatorname{Spec} K^{(i)}_{\alpha^{(i)}}$.

Modified Eyring–Kramers formula for the metastable exit rate. When z_i is a local minimum of V such that $\alpha^{(i)} = +\infty$, the bottom eigenvalue of $K^{(i)}_{\alpha^{(i)}}$ is 0. Thus, the harmonic approximation predicts a metastable rate of 0, which calls for finer asymptotics. The following result fulfills this need.

Theorem 3.15. *Under Assumptions 3.11, 3.12 and 3.13, it holds, in the limit $\beta \to \infty$:*

$$\lambda_{1,\beta}(\Omega_\beta) = \mathrm{e}^{-\beta(V^*-V(z_0))}\left[\sum_{i\in I_{\min}} \frac{|\nu_1^{(i)}|}{2\pi\Phi\left(\sqrt{|\nu_1^{(i)}|}\alpha_i\right)}\sqrt{\frac{\det\nabla^2 V(z_0)}{|\det\nabla^2 V(z_i)|}}\right]\left(1+\mathcal{O}(\beta^{-\frac{1}{2}})\right), \quad (3.39)$$

where $\Phi(x) = (2\pi)^{-\frac{1}{2}}\int_{-\infty}^{x}\mathrm{e}^{-\frac{t^2}{2}}\,\mathrm{d}t$, and $\nu_1^{(i)}$ is the unique negative eigenvalue of the Hessian matrix $\nabla^2 V(z_i)$ at the saddle point z_i.

For a full proof of this result, see the proof of [50, Theorem 5]. It relies on the construction of a precise approximation ψ_β of the principal Dirichlet eigenmode $u_1(\Omega_\beta)$.

Roughly speaking, ψ_β is constructed by combining a smoothed indicator of the set $\mathcal{A}(z_0)\cap\{V<V^*\}$ with, near each low-energy saddle points $(z_i)_{i\in I_{\min}}$, a finer construction based on formal eigenmodes for the linearization of the dynamics (3.32), which corresponds to an unstable Ornstein–Uhlenbeck process. Due to the geometric structure of the domain $\Omega_{\alpha,\beta}$ given by Assumption 3.11, one can separate variables in the unstable direction, leading to an explicit expression for these formal eigenmodes in terms of the unstable coordinate

$$\xi_\beta^{(i)}(x) = \sqrt{\beta}(x-z_i)^\top v_1^{(i)}.$$

The quasimode is then projected onto the principal eigenspace $\mathrm{Span}(u_1(\Omega_{\alpha,\beta}))$, yielding $\lambda_{1,\beta}(\Omega_{\alpha,\beta})$ as a Rayleigh quotient associated with the projected quasimode. Quantitative estimates based on a modification of Laplace's method and a resolvent estimate then allows to bound the projection error, which is sufficiently small to give sharp estimates on $\lambda_{1,\beta}(\Omega_{\alpha,\beta})$.

Application to the separation of timescales. We briefly discuss the implications of Theorems 3.14 and 3.15 for the problem of maximizing the separation of timescales (3.7). We refer to [50, Section 3.3] for additional details.

The first point of interest is that Theorem 3.14 gives a quantitative estimate of the spectral gap $\lambda_2(\Omega_{\alpha,\beta})-\lambda_1(\Omega_{\alpha,\beta})$ for large β, and, in view of (3.6), of the asymptotic rate of convergence to the QSD. This estimate is solely a function of the asymptotic shape parameter α, and of the eigenvalues of the Hessian $\nabla^2 V$ of the potential at some critical points. As such, it can be used to choose decorrelation times in Algorithm 3.18 for highly metastable systems. Explicitly, the second harmonic eigenvalue is given by:

$$\lambda_2^{\mathrm{H}} = \min\left\{\min_{1\leqslant j\leqslant d}\nu_j^{(0)}, \min_{1\leqslant i<N}\left[\left|\nu_1^{(i)}\right|\mu\left(\alpha^{(i)}\sqrt{\nu_1^{(i)}/2}\right)-\frac{\nu_1^{(i)}}{2}+\sum_{2\leqslant j\leqslant d}\left|\nu_j^{(i)}\right|\mathbb{1}_{\nu_j^{(i)}<0}\right]\right\}, \quad (3.40)$$

where we set $\mu(\theta) := \mu_{1,\theta}$ to be the principal eigenvalue of the Dirichlet harmonic oscillator on $(-\infty,\theta)$. The limiting eigenvalue λ_2^{H} is positive under Assumption 3.12. Interestingly, this estimate is not always in agreement with standard numerical practice, which relies on a harmonic approximation of the energy basin at the local minimum to set the decorrelation time (see for instance [268]). This approximation neglects the possible effect of higher-order saddle points. It can be shown to fail when the Hessian $\nabla^2 V$ has sufficiently soft modes around

such critical points, and these are low enough in energy to be visited during decorrelation to the QSD.

Theorem 3.15 provides a quantitative estimate of the exit time starting from the QSD as a function of α. Combined with the previous estimate, we therefore obtain an estimate for the separation of timescales (3.7) as a function of α and β. In view of (3.38) and (3.39), one finds that the asymptotic separation of timescales, for the class of domains satisfying Assumptions 3.11–3.13, is of order $e^{\beta(V^*-V(z_0))}$, with a β-independent prefactor $C(\alpha)$ (neglecting error terms). Therefore, the asymptotic shape optimization problem (3.34) for the separation of timescales can only hope to improve on the prefactor.

We show in [50, Section 3.3] that there exist asymptotically optimal domains, and indeed many in general. Qualitatively, these optimal domains are found to have the following properties. Firstly, they spill out beyond low-energy separating saddle points, on geometric scales of the order $1/\sqrt{\beta}$ in the unstable direction. This means that one should wait for the system to reach an energy level lower than V^* (in the next basin of attraction) by a multiple of the characteristic thermal fluctuation β before declaring that a transition has occurred. The value of the multiplicative constant depends on the geometry of the energy landscape, but can be computed numerically. Secondly, one can show that they can never absorb other local energy minima, in the sense that the asymptotic separation of timescales necessarily decreases when continuously growing the domain so as to include any other minima far (i.e. at distances $\gg 1/\sqrt{\beta}$) inside the domain. This gives some theoretical indication that there indeed exist local shape optima surrounding basins of attraction of local minima for the steepest descent dynamics.

We present validations of Theorems 3.14 and 3.15 in Section 3.5.2 below, and connect the asymptotic problem (3.34) to a shape-optimization problem in one spatial dimension.

3.5 Numerical experiments

In this section, we present various numerical experiments to illustrate and validate the results and methodology presented in Sections 3.4, 3.4.1, and 3.4.2. In Section 3.5.1, we verify, on a model two-dimensional situation that, given a suitable choice of CV, the coarse-grained Dirichlet eigenvalues provide a good approximation for the true eigenvalues of the Dirichlet generator. In Section 3.5.2, we show how the results of Section 3.4.2 can be used to approximate the shape optimization problem in the semiclassical limit, and verify in particulars the spectral asymptotics given by Theorems 3.15 and 3.14. In Section 3.5.3, we finally apply the coarse-grained shape optimization methodology to a realistic molecular system, and estimate the gain in the separation of timescales in the practical setting of underdamped Langevin dynamics.

The code used to generate the numerical results of this paper are publicly available in the paper repository [46]. Data generated from the various simulations and optimization runs can moreover be obtained from the repository [47].

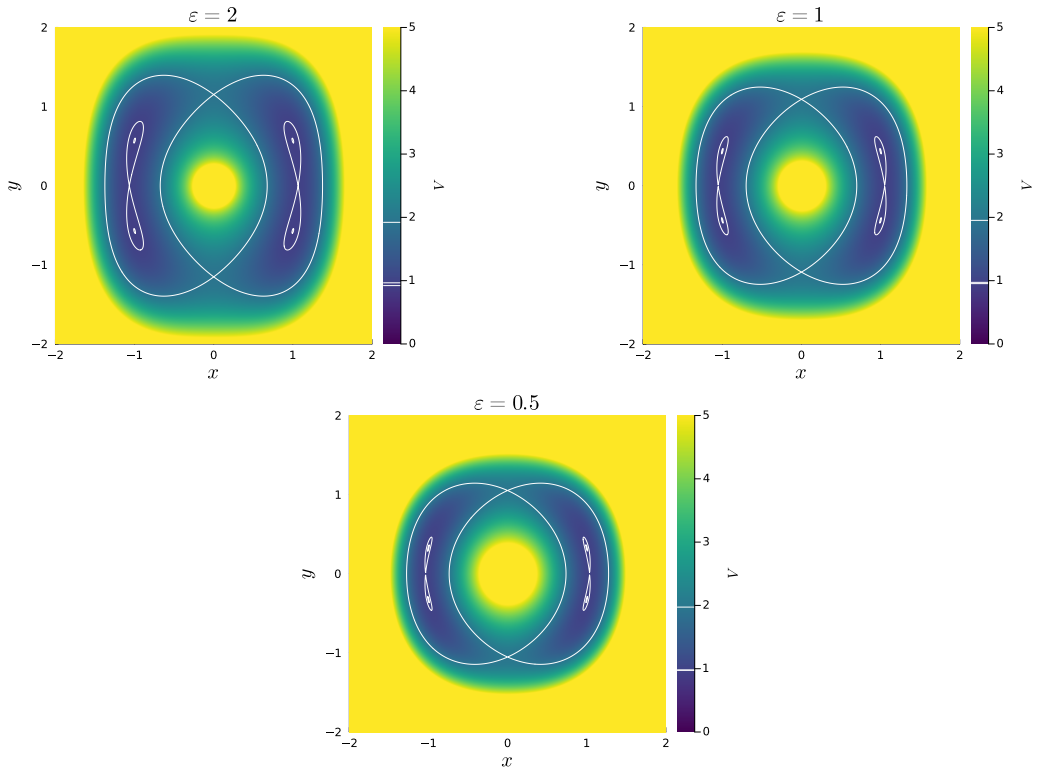

Figure 3.3: Two-dimensional potentials (3.41), for decreasing values of the parameter ε. In each case, the potential has a local minimum in each quadrant of the plane, and two saddles on each axis. The saddles on the y-axis separate two deep energy basins, while the saddle points on the x-axis form shallow energy barriers inside these basins. Some energy level sets, in thin white lines, highlight the well structure.

3.5.1 Validation of the coarse-graining approximation

In this section, we demonstrate numerically that, for an appropriate choice of CV, the coarse-grained Dirichlet eigenvalues defined in Section 3.4.1 provide a good approximation for the lowest eigenvalues of the Dirichlet generators. As such, they can be used as a proxy to optimize the separation of timescales.

Two-dimensional system and collective variables. We consider, for a parameter $\varepsilon > 0$, the following family of potential functions defined on the configurational space $\mathbb{R}^2 \setminus \{0\}$:

$$V_\varepsilon(x, y) = (x^2 - 1)^2 + \frac{1}{\varepsilon}(x^2 + y^2 - 1)^2 + \frac{1}{\sqrt{x^2 + y^2}}. \tag{3.41}$$

The potential V_ε is the sum of a quartic double-well potential in the variable x, and of a harmonic energy in the squared radial coordinate $r^2 = x^2 + y^2$, whose sharpness is modulated by ε, confining the dynamics to the unit circle. The additional repulsion term $1/r$ ensures that the effective diffusion coefficient a_{ξ_1} is well-defined, as discussed below. The potential is depicted in Figure 3.3 for the three values of ε we consider in this experiment.

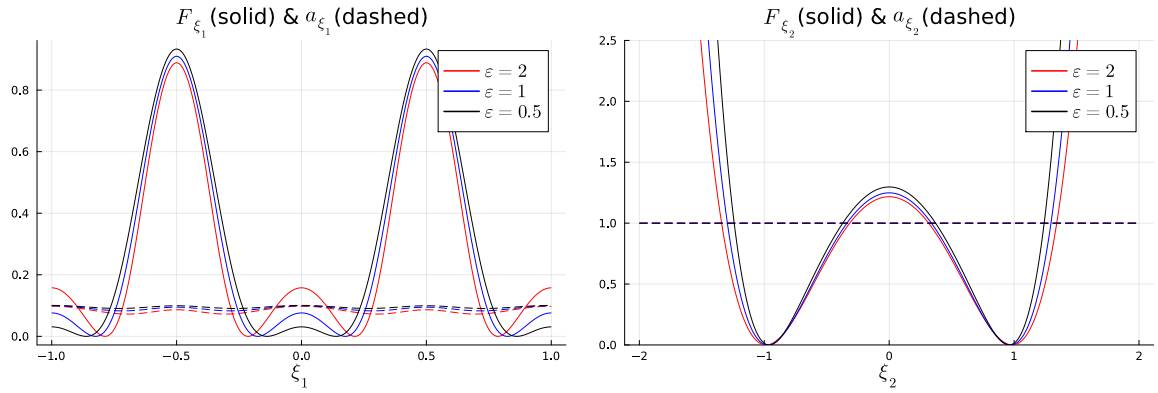

Figure 3.4: Free energy profiles and effective diffusion coefficients for the CVs ξ_1 and ξ_2 defined in (3.42), and for the potential (3.41). Various values of the parameter ε are color-coded. Free energy profiles are depicted in solid lines and effective diffusion coefficients are plotted in dashed lines.

We compare the two following CVs:

$$\xi_1(x,y) = \frac{2}{\pi}\operatorname{atan}\left(\frac{y}{x+\sqrt{x^2+y^2}}\right), \qquad \xi_2(x,y) = x. \tag{3.42}$$

The variable ξ_1 is equal to θ/π, where (r,θ) is the image of (x,y) via a polar change of variables. In particular, the CV ξ_1 takes values in the compact interval $[-1,1]$, while ξ_2 is unbounded. In the limit $\varepsilon \to 0$, we expect the effective dynamics through ξ_1 to provide a good one-dimensional description of the original dynamics, and ξ_2, while able to resolve the main energy barrier, is blind to the shape of the energy minima (e.g. the shallow energy barriers separating the two rightmost local minima), leading to a poor model for the local decorrelation inside the rightmost well.

For each of these functions, the value of the free energy and diffusion coefficient, given respectively by (3.28) and (3.29), are computed at values of z corresponding to $N = 1000$ points on a regular grid (on the interval $[-2,2]$ for ξ_2), by numerical quadrature (using the Gauss–Kronrod rule as implemented in the Julia package Cubature.jl) on the manifold Σ_z, which for both our choices of CV (3.42) have a simple linear parametrization. The resulting free energy and diffusion profiles are presented in Figure 3.4.

Computation of the coarse-grained Dirichlet eigenvalues. For $\xi \in \{\xi_1, \xi_2\}$, we discretize the effective generator $\mathcal{L}^{\xi}_{\beta}$ as the generator of a reversible jump process on a regular grid $(z_i)_{i\in\mathbb{L}_N}$ in collective variable space, where $\mathbb{L}_N$ is either a periodic lattice $\mathbb{L}_N = \mathbb{Z}/N\mathbb{Z}$ if $\xi = \xi_1$ or $\mathbb{L}_N = \{0,\dots,N-1\}$ if $\xi = \xi_2$. In both cases, we set $N = 1000$. The grid points are defined by $z_i = \xi_{\max}\left(\frac{2i+1}{N} - 1\right)$, where $\xi_{\max} = 1$ for $\xi = \xi_1$, and 2 for $\xi = \xi_2$. The jump rates are only positive for nearest neighbors:

$$\mathcal{L}^{\xi}_{N,\beta,ij} = \left(\beta(2\xi_{\max}/N)^2\right)^{-1} \mathrm{e}^{-\frac{\beta}{2}(F_{j,\xi}-F_{i,\xi})}\left(\frac{a_{i,\xi}+a_{j,\xi}}{2}\right), \qquad \forall\, |i-j|_{\mathbb{L}_N} = 1, \tag{3.43}$$

where $F_{i,\xi} = F_\xi(z_i)$ $a_{i,\xi} = a_\xi(z_i)$ for any $i \in \mathbb{Z}^m$, and $|\cdot|_{\mathbb{L}_N}$ is the nearest-neighbor graph metric on $\mathbb{L}_N$. A simple computation shows that the jump process (3.43) is reversible for the

on-site Boltzmann distribution, defined by

$$\mu_N(\{z_i\}) = \frac{\mathrm{e}^{-\beta F_{i,\xi}}}{\sum_{j\in\mathbb{L}} \mathrm{e}^{-\beta F_{j,\xi}}}, \qquad \forall\, i \in \mathbb{L}.$$

The factor $\left(\beta(2\xi_{\max}/N)^2\right)^{-1}$ ensures that (3.43) is a consistent approximation of the generator associated with the SDE (3.30). Given an open domain $\Omega \subset [-\xi_{\max}, \xi_{\max}]$, the effective eigenvalues are approximated by computing the eigenvalues of the generator for the process killed outside Ω:

$$\left(\mathcal{L}^{\xi}_{N,\beta,ij}\right)_{i,j\in I_\Omega}, \qquad I_\Omega = \{i \in \mathbb{L} : z_i \in \Omega\}. \tag{3.44}$$

The eigenvalues of the sparse matrix (3.44) were numerically computed using the Julia interface to the Arpack module [218].

Validation of the approximation. In Figure 3.5, we compare the approximation obtained from (3.44) with Dirichlet eigenvalues of the generator $\mathcal{L}$ approximated using Algorithm 3.3.1 in FreeFem++ [155]. The FreeFem++ implementation, including the parameters we used for geometry parametrization and meshing (which are the default parameters in the provided code), are available on GitHub [46]. We compute the values of the first four Dirichlet eigenvalues for domains of the form $\Omega(b) = (a, b)$, for a fixed value of a and for a range of values of b, and for several values of the parameter ε (see Figure 3.3). We compare these eigenvalues to those of the effective generator, using the jump-process approximation (3.43). We observe that, for ξ_1, even for relatively large values of ε, the effective eigenvalues give a good approximation to the true eigenvalues of the generator, across a wide range of boundary conditions. The error appears to decrease for low values of ε, as expected. However, the effective eigenvalues for ξ_2 significantly depart from the true eigenvalues. This is especially true for the higher eigenvalues, confirming that the effective diffusion through ξ_2 is unable to correctly model the decorrelation inside the energy wells.

These results suggest that ξ_1 may be used for the purpose of shape optimization of the separation of timescales N^* defined in (3.7). In Figure 3.6, we compare the (locally) optimal domain of the effective generator (3.43) with the (locally) optimal domain of the true generator in the class of domains defined in terms of the CV ξ_1, and for the value $\varepsilon = 0.5$. These optima were found by a full grid-search over the set of domains of the form (a, b) for $-\xi_{\max} < a < b < \xi_{\max}$ in the case of the effective generator, and an iteratively refined grid search over domains of the form $\xi_1^{-1}(a, b)$ for the case of the FEM generator, for the same range of a and b. The iterative refinement procedure consisted in searching for optimal domains for values (a, b) on a regularly spaced 6×6 grid, and iterating this procedure, restricting the search at the next iteration to the cell of the maximizer and its nearest-neighbors. The procedure stopped once a target grid resolution of $\delta\xi = 0.01$ was reached. We find the result of both these optimization procedures to give almost indistinguishable optimal values of a and b, showcasing the usefulness of the effective generator, whose Dirichlet eigenvalues are significantly cheaper to compute.

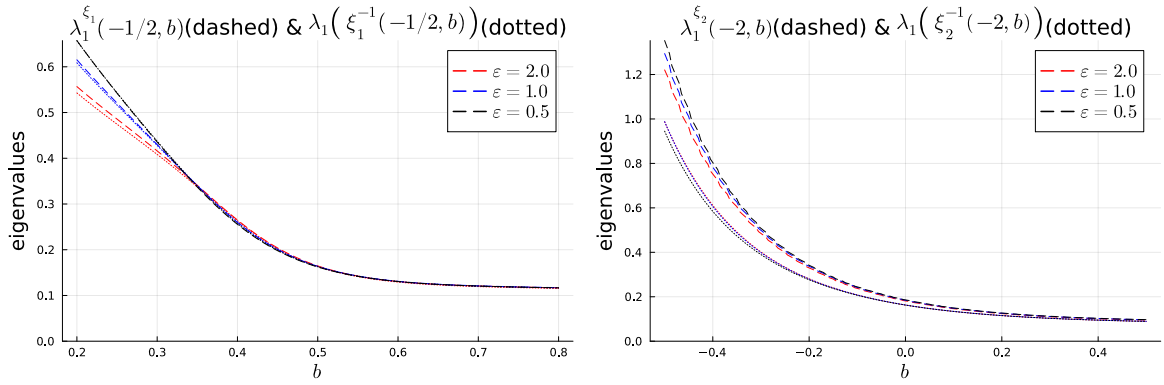

(a) Approximation of the first Dirichlet eigenvalue.

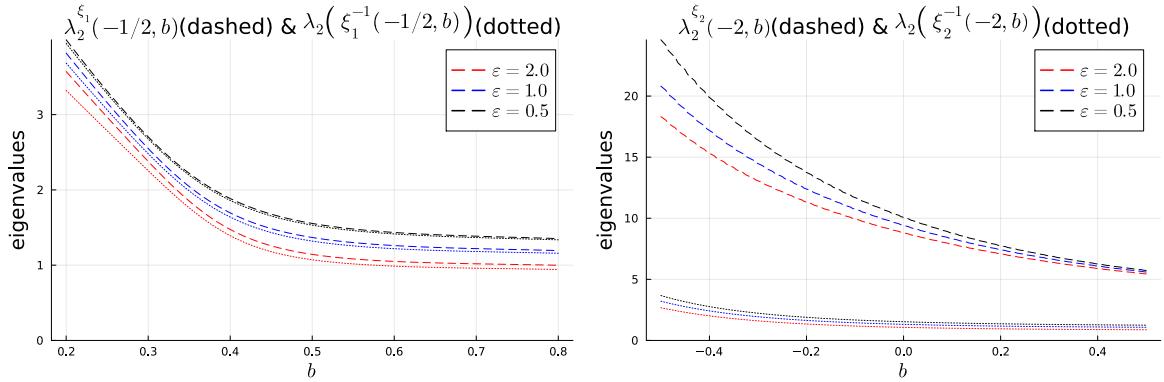

(b) Approximation of the second Dirichlet eigenvalue.

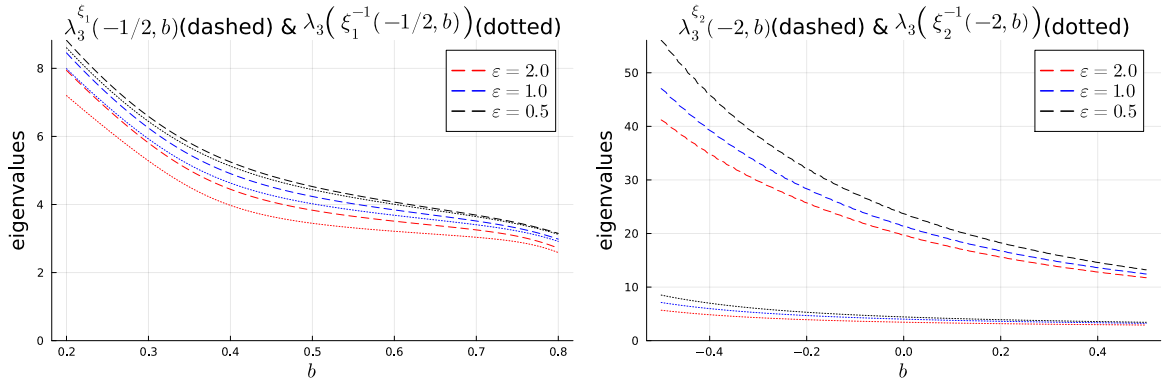

(c) Approximation of the third Dirichlet eigenvalue.

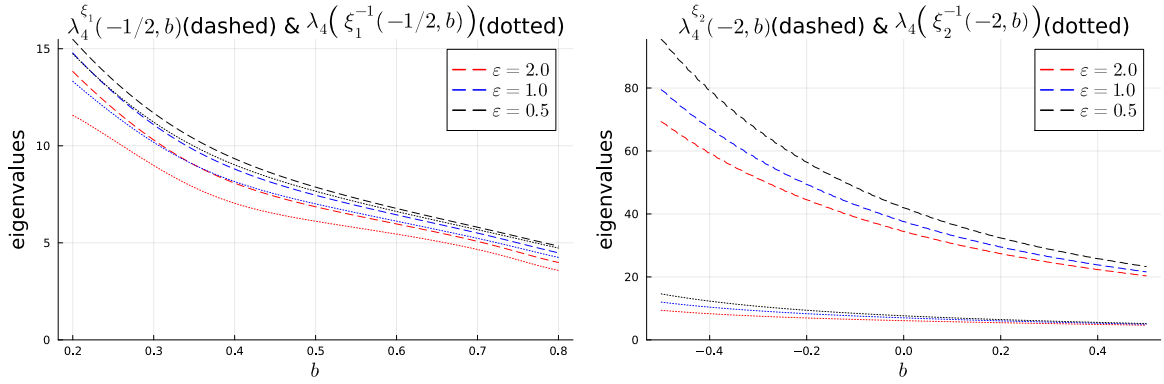

(d) Approximation of the fourth Dirichlet eigenvalue.

Figure 3.5: Domain-dependent eigenvalues (dotted lines) and their coarse-grained approximations (dashed lines), for parametric families of domains defined in CV space.

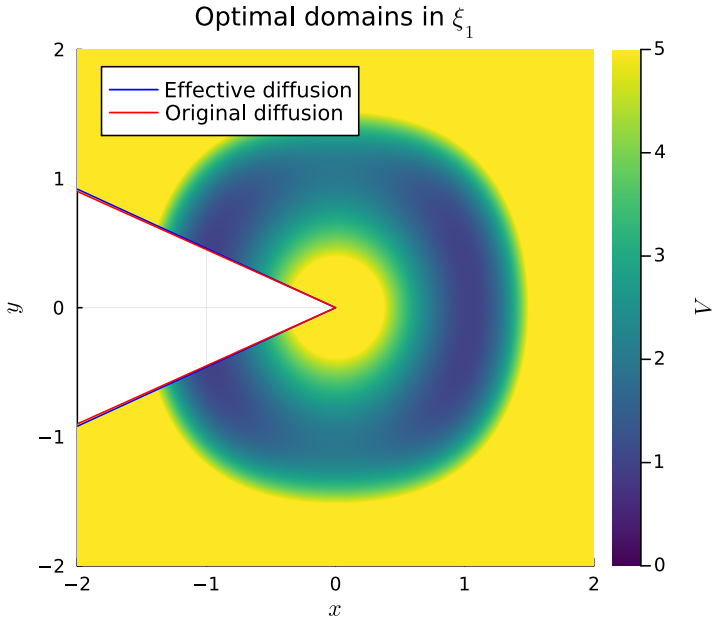

Figure 3.6: Optimal domain for the effective dynamics, and optimal domain for the original generator, in the class of domains defined in terms of ξ_1, for the value of the parameter $\varepsilon = 0.5$. Points outside both of these domains lie in the white region. The optimized domains are almost indistinguishable.

3.5.2 Validation of the semiclassical asymptotics

In this section, we give a numerical verification of the semiclassical results obtained in [50] (which corresponds to Theorems 3.14 and 3.15 here), and assess their usefulness for the state definition problem, in a model one-dimensional situation.

Definition of the toy system. The potential V is defined by

$$V(x) = \epsilon \left(1 - \cos \frac{x}{\sigma} + \exp\left(-\frac{1}{2} \left(\frac{x}{\sigma} - 1 \right)^2 \right) + \ell x \right), \tag{3.45}$$

where $(\epsilon, \sigma) = (0.7, 1/4)$ are energy and scale parameters, and $\ell \approx 0.01293$ is a constant factor chosen so that V has two index-one saddle points at $z_1 \approx -0.7824$ and $z_2 \approx 0.8286$, satisfying $V(z_1) = V(z_2) = V^*$, so that $I_{\min} = \{1, 2\}$. Additionally V admits a local minimum at $z_0 \approx 0.1166$. The corresponding eigenvalues of the Hessian are given by $(\nu_1^{(0)}, \nu_1^{(1)}, \nu_1^{(2)}) \approx (16.9532, -11.2348, -14.3845)$. We consider, for a parameter $\alpha = (\alpha^{(1)}, \alpha^{(2)}) \in \mathbb{R}^2$, temperature-dependent domains defined by

$$\Omega_{\alpha,\beta} = \left(z_1 - \frac{\alpha^{(1)}}{\sqrt{\beta}}, z_2 + \frac{\alpha^{(2)}}{\sqrt{\beta}} \right), \tag{3.46}$$

which satisfy the assumptions of Theorems 3.14 and 3.15. The potential and domains (for a fixed value of β) are depicted in Figure 3.7.

We aim to maximize

$$\frac{\lambda_{2,\beta}(\Omega_{\alpha,\beta}) - \lambda_{1,\beta}(\Omega_{\alpha,\beta})}{\lambda_{1,\beta}(\Omega_{\alpha,\beta})}$$

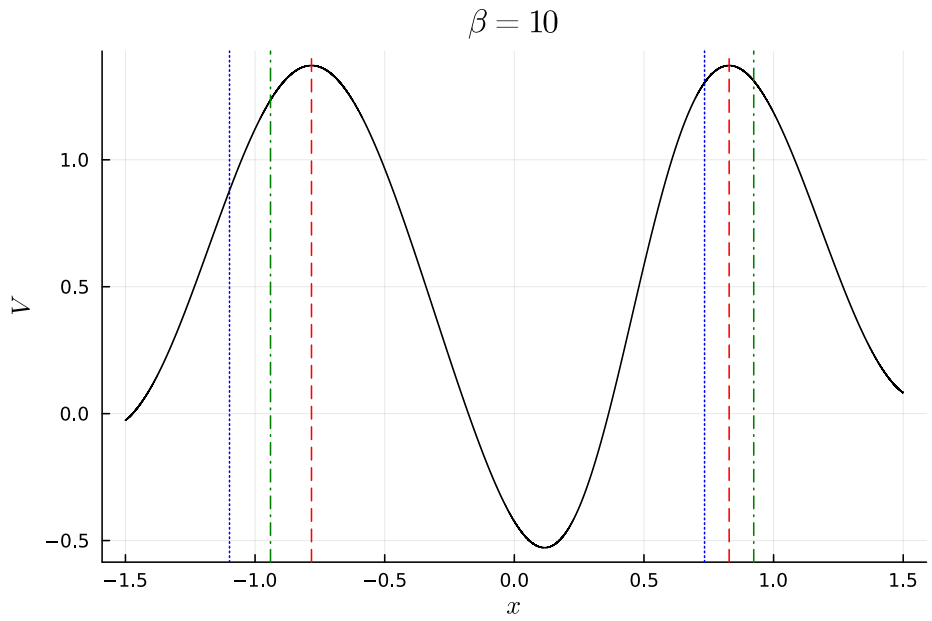

Figure 3.7: Potential landscape and domains $\Omega_{\alpha,\beta}$ used in Figures 3.8a and 3.8b, as defined by (3.46), at the fixed value of the temperature parameter $\beta = 10$. The color coding is the same as that used in Figure 3.8, i.e. $\alpha = (0.5, 0.3)$ in green, $\alpha = (1.0, -0.3)$ in blue and $\alpha = (0.0, 0.0)$ in red, which correponds to the basin of attraction $\mathcal{A}(z_0)$.

with respect to α. Fixing β, it is equivalent to maximize the quantity

$$J_\beta(\alpha) = \frac{\lambda_{2,\beta}(\Omega_{\alpha,\beta})\lambda_{1,\beta}(\mathcal{A}(z_0))}{\lambda_{1,\beta}(\Omega_{\alpha,\beta})\lambda_{2,\beta}(\mathcal{A}(z_0))}, \tag{3.47}$$

where we recall $\mathcal{A}(z_0) = \Omega_{0,\beta}$ is the basin of attraction for the local minimum z_0, see (3.35). The interest of considering this objective J_β is that, according to Theorems 3.14 and 3.15, $J_\beta \xrightarrow{\beta\to+\infty} J_\infty$ pointwise, where

$$J_\infty(\alpha) = \frac{\lambda^{\mathrm{H}}_{2,\alpha} C(0)}{\lambda^{\mathrm{H}}_{2,0} C(\alpha)}, \qquad C(\alpha) = \sum_{i \in I_{\min}} \frac{|\nu_1^{(i)}|}{2\pi\Phi\left(\sqrt{|\nu_1^{(i)}|}\alpha_i\right)} \sqrt{\frac{\det \nabla^2 V(z_0)}{|\det \nabla^2 V(z_i)|}}, \tag{3.48}$$

where $C(\alpha)$ is the pre-exponential factor in (3.39). Substituting the expression (3.40) in (3.48), we find explicitly:

$$J_\infty(\alpha) = 2\frac{\min\left\{\nu_1^{(0)}, |\nu_1^{(1)}|\left(\mu\left(\sqrt{|\nu_1^{(1)}|/2}\alpha^{(1)}\right) + \frac{1}{2}\right), |\nu_1^{(2)}|\left(\mu\left(\sqrt{|\nu_1^{(2)}|/2}\alpha^{(2)}\right) + \frac{1}{2}\right)\right\}\left(\sqrt{|\nu_1^{(1)}|} + \sqrt{|\nu_1^{(2)}|}\right)}{\min\left\{\nu_1^{(0)}, 2|\nu_1^{(1)}|, 2|\nu_1^{(2)}|\right\}\left(\frac{\sqrt{|\nu_1^{(1)}|}}{\Phi\left(\sqrt{|\nu_1^{(1)}|}\alpha^{(1)}\right)} + \frac{\sqrt{|\nu_1^{(2)}|}}{\Phi\left(\sqrt{|\nu_1^{(2)}|}\alpha^{(2)}\right)}\right)}, \tag{3.49}$$

where we recall that $\mu(\theta)$ is the principal Dirichlet eigenvalue of the one-dimensional Dirichlet harmonic oscillator $\frac{1}{2}(-\partial_x^2 + x^2)$ on $(-\infty, \theta)$.

Numerical results. We approximate the generator $\mathcal{L}_\beta$ using the same procedure as for the effective generator in Section 3.5.1. In Figure 3.8a, we illustrate the validity of the modified

Eyring–Kramers formula. The α-dependent prefactor correctly predicts fine effects of the boundary geometry near the saddle points. The asymptotic regime is reached for relatively small values of β. In Figure 3.8b, we illustrate the harmonic approximation of Theorem 3.14. Eigenvalues appear to converge to the prediction of the harmonic approximation in the limit $\beta \to \infty$. For domains in which the second harmonic eigenvalue corresponds to a local model around an index-1 saddle point (the blue and green domains in Figure 3.7), this convergence appears to occur faster, though we have no explanation for why this should be the case.

In Figure 3.9, we compare two quantities, for a fixed value of $\beta = 10$ (see Figure 3.7 for examples of corresponding domains): the low-temperature approximation J_∞ to the shape-optimization landscape defined in (3.49), and the actual optimization landscape obtained by numerically approximating the reduced objective (3.47). The low-temperature approximation and the true objective agree, making the low-temperature approximation an acceptable surrogate objective in the low-temperature regime, which can be maximized at a much smaller computational cost.

3.5.3 Application to a molecular system

In this section, we apply our shape-optimization method to the energy landscape of a small molecule commonly used to benchmark methods in MD, namely alanine dipeptide solvated in water. The system is composed of $N = d/3 = 619$ atoms, in fact 22 atoms in the peptide chain and 199 water molecules. Atomic positions are restricted to a periodic cubic box of length $L = 18.643\,\text{Å}$. As a collective variable, we use the dihedral angles (a standard choice, see [54]),

$$\xi = (\phi, \psi).$$

The values and gradients of ϕ and ψ are available through the Tinker-HP [203] interface to the Colvars library [127].

Simulation parameters. All simulation runs were performed using a modified version of Tinker-HP [203] allowing to simulate the Fleming–Viot process (see 3.16 below) inside an arbitrary domain defined in CV space.

Unless otherwise specified, simulations of the underdamped Langevin dynamics (3.2) (with $\Gamma = M$) were performed at $T = 300\,\text{K}$ ($\beta = 1.677\,\text{mol} \cdot \text{kcal}^{-1}$) and discretized with the BAOAB scheme, setting the time step to $\Delta t = 2$ fs, using the Amberff99 force field, and the SHAKE method [293] to fix the geometry of the solvent molecules.

Experiments were performed across a range of friction parameters, $\gamma \in \{1, 2, 5, 10\}\,\text{ps}^{-1}$, to assess the effectiveness of the methodology in various dynamical settings. Since our methodology requires a low-dimensional reversible diffusion (3.1) as input, we use the effective dynamics (3.30) associated with the Kramers–Smoluchowski approximation (3.1) of the underdamped Langevin dynamics (where $a = M^{-1}$). In other words, the (rescaled by γ) effective generator whose

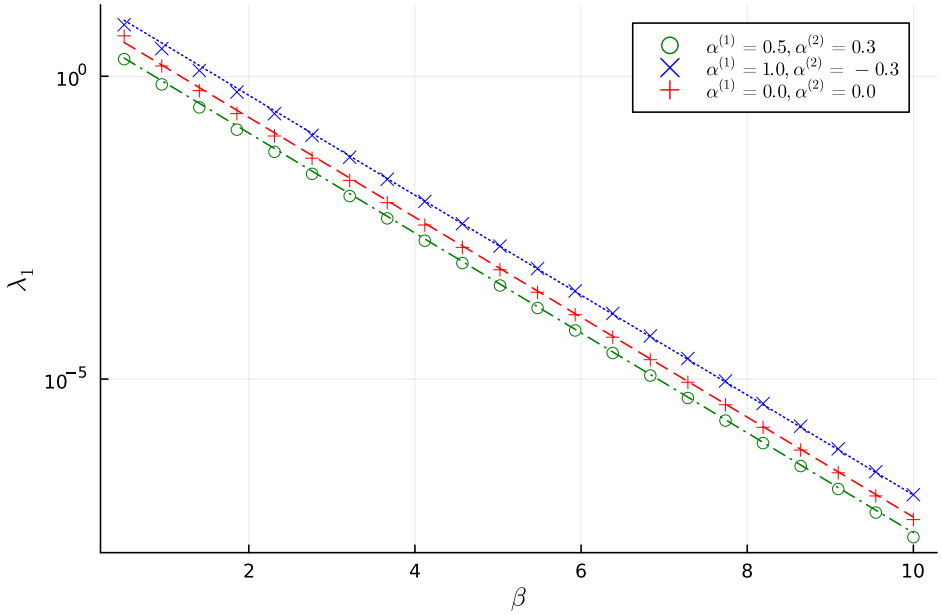

(a) Principal Dirichlet eigenvalue of $\mathcal{L}_\beta$ on $\Omega_{\alpha,\beta}$, for various values of the shape parameter α. The theoretical leading-order asymptotic of Theorem 3.15 is represented with a dotted line.

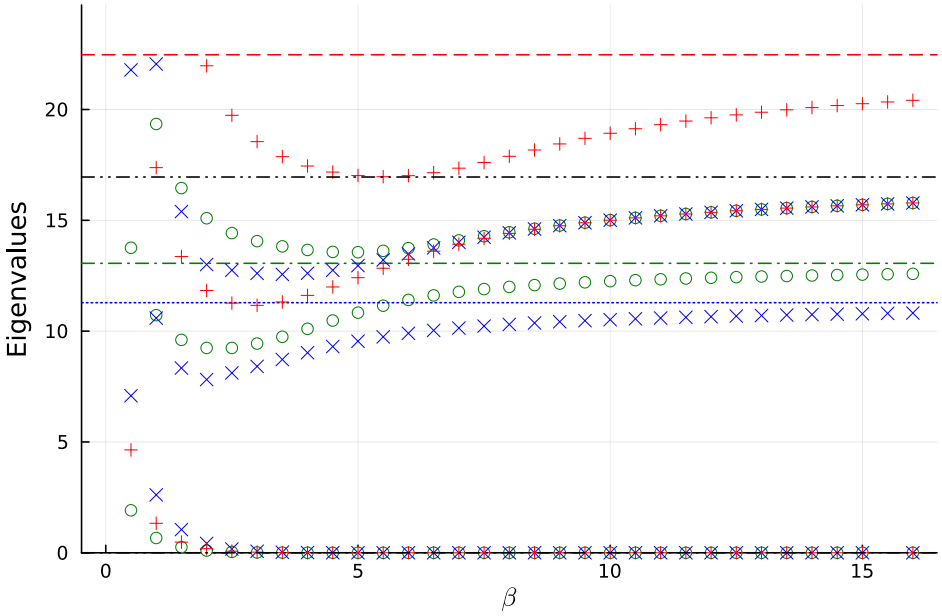

(b) First three Dirichlet eigenvalues of $-\mathcal{L}_\beta$ on $\Omega_{\alpha,\beta}$, for the three values of α from Figure 3.8a. Horizontal lines correspond to the theoretical limiting values from Theorem 3.14. The black line (–··–) corresponds to a harmonic eigenvalue shared between all the domains. Missing values failed to converge. We observe convergence to the limiting regime, with eigenvalues corresponding to a lower asymptotic value appearing to converge faster.

Figure 3.8: Numerical validation of the low-temperature asymptotics of Theorems 3.15 and 3.14 from [50], for the one-dimensional potential depicted in Figure 3.7.

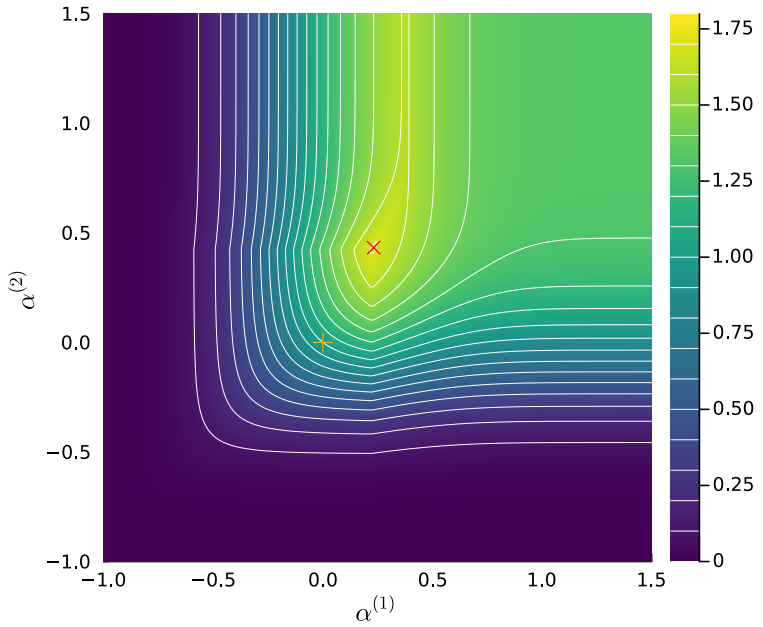

(a) Semiclassical approximation of the shape optimization landscape. The limiting objective $J_\infty(\alpha)$ defined in (3.48) is plotted for the potential V defined in (3.45) and depicted in Figure 3.7. The optimal $\alpha^\star_\infty$ is marked by ×, and the basin of attraction $\mathcal{A}(z_0)$ is marked by +. Ridge-like features are discernible, and correspond to the loci of eigenvalue crossings for the harmonic approximation K_α defined in (3.37). The optimal value is attained for $\alpha^\star_\infty \approx (0.23116, 0.43216)$ with $J_\infty(\alpha^\star_\infty) \approx 1.71$.

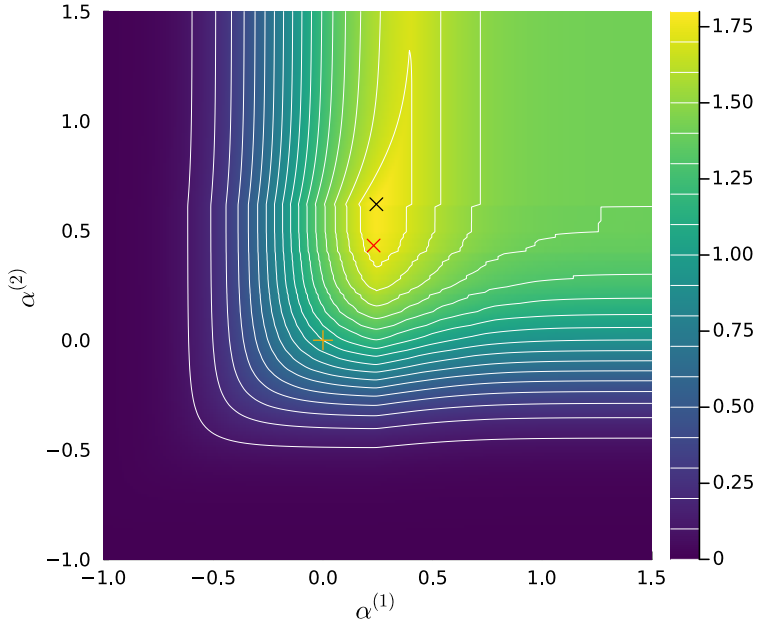

(b) Shape-optimization landscape for the reduced objective $J_\beta(\alpha)$ defined in (3.47) for the value $\beta = 10$. The optimal shape $\alpha^\star_\beta$ is marked by ×, the basin of attraction $\mathcal{A}(z_0)$ is marked by + and the semiclassical prescription $\alpha^\star_\infty$ is marked by ×. The optimal value is attained for $\alpha^\star_\beta \approx (0.24372, 0.6206)$ with $J_\beta(\alpha^\star_\beta) \approx 1.81$. By comparison $J_\beta(\alpha^\star_\infty) \approx 1.76$.

Figure 3.9: Asymptotic approach to the shape optimization problem for the potential (3.45) and the objective (3.47). At low temperature, the semiclassical approximation (Figure 3.9a) faithfully captures the features of the true optimization landscape (Figure 3.9b). In particular, the semiclassical optimizer is close, both in argument and value of the objective function, to the true optimizer.

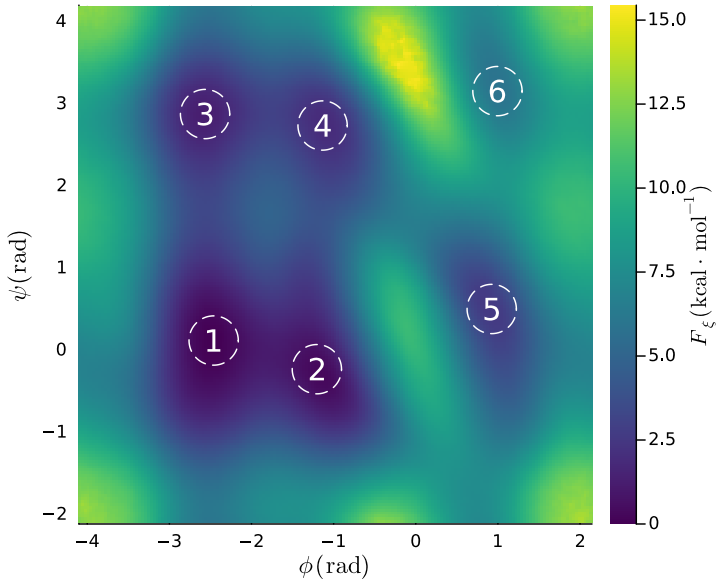

Figure 3.10: Free energy landscape in the dihedral angles (ϕ, ψ). We identify and label six local minima.

eigenvalues we optimize is given by

$$\mathcal{L}_\beta^\xi = \frac{1}{\gamma\beta} e^{\beta F_\xi} \operatorname{div}\left(e^{-\beta F_\xi} a_\xi \nabla \cdot\right), \qquad a_\xi(z) = \int_{\Sigma_z} \nabla\xi^\top M^{-1} \nabla\xi \, \mathrm{d}\mu_z. \tag{3.50}$$

It has been observed in previous studies of realistic molecular systems (see for instance [251, Sections 4.2.2 and 4.3.2]) that the dynamical rates inferred by the Kramers–Smoluchowski approximation often differ greatly from those associated with the underlying underdamped Langevin dynamics, even when accounting for rescaling by the friction parameter γ. Therefore we shall not use our reduced model to directly infer timescales for the original dynamics, but merely as a proxy to define good metastable states. The effectiveness of these states, in the sense of maximizing the separation of timescales, will therefore be assessed at the level of the original dynamics, and not of the reduced model.

Free energy landscape and effective diffusion. We first compute the free energy F_ξ and effective diffusion tensor a_ξ entering in the definition of the effective dynamics (3.30). The free energy landscape is represented in Figure 3.10, and was precomputed using a multiple-replica adaptive biasing force dynamics (see [85]), with four replicas, for a total of $t = 600$ ps of simulation time. The effective diffusion tensor was estimated using an importance sampling scheme using a family of harmonically biased potentials. More precisely, the collective variable space $(-\pi, \pi)^2$ was divided into a set $\mathcal{W}$ of square-shaped windows of side-length $\Delta\phi_\mathcal{W} = \Delta\psi_\mathcal{W} = \pi/36$ rad. For each window $w \in \mathcal{W}$, we performed a biased simulation of the underdamped Langevin dynamics (3.2) using a harmonic biasing potential

$$V^w = V + U^w, \qquad U^w(q) = \frac{1}{2\eta}|\xi(q) - z_w|^2,$$

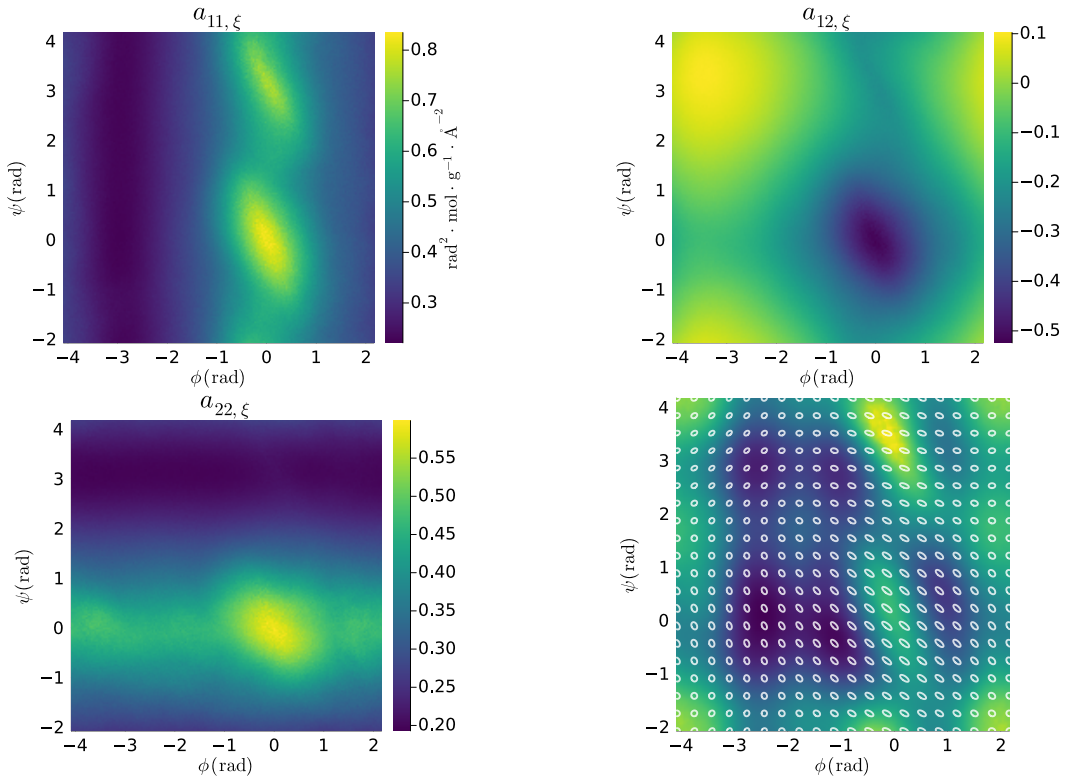

Figure 3.11: Components of the effective diffusion tensor a_ξ (top row and left-bottom row), and corresponding ellipsoid glyph representation (right-bottom row).

where z_w is the center of the window w, and $\eta = 40\,\mathrm{mol}\cdot\mathrm{kcal}^{-1}$ is the inverse force constant. For $z \in (-\pi,\pi)^2$, we use the estimator

$$\widehat{a}_\xi(z) = \sum_{w\in\mathcal{W}} \rho_w(z) \frac{\sum_{k=1}^{N_{\mathrm{sim}}} \nabla\xi(X_k^w)^\top M^{-1} \nabla\xi(X_k^w) \mathrm{e}^{\beta U^w(X_k^w)} \mathbb{1}_{|\xi(X_k^w)-z|_\infty < h/2}}{\sum_{k=0}^{N_{\mathrm{sim}}} \mathrm{e}^{\beta U^w(X_k^w)} \mathbb{1}_{|\xi(X_k^w)-z|_\infty < h/2}}, \tag{3.51}$$

where $(X_k^w)_{k=1,\dots,N_{\mathrm{sim}}}$ are sample points of the numerical trajectory for the biased dynamics in the window $w \in \mathcal{W}$, $h = \pi/90\,\mathrm{rad}$ is the histogram resolution and ρ_w is a weighting function chosen so that $\sum_{w\in\mathcal{W}} \rho_w(z) = 1$ for all z. For simplicity, we chose $\rho_w(z)$ to give uniform weight to each window for which the ratio in (3.51) was well-defined.

The initial condition X_0^w was prepared by running a harmonically steered-MD simulation from a reference configuration toward the value $\xi = z_w$, followed by a 5 ps equilibration run, both with a value of the friction parameter $\gamma = 1\,\mathrm{ps}^{-1}$. The values of the CV, biasing energy and instantaneous tensor $\nabla\xi^\top M^{-1}\nabla\xi$ were recorded every 10 fs. The overall computation can be straightforwardly parallelized, as the estimators within each window are independent of one another. The results of the computation of the effective diffusion tensor are shown in Figure 3.11.

Shape optimization of eigenvalues for the effective dynamics. We apply Algorithm 3.5 to obtain optimized domains in the two-dimensional space of dihedral angles (ϕ,ψ), using

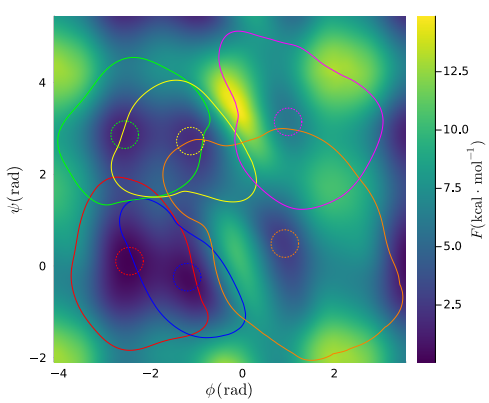

(a) Numerically optimized metastable states for alanine dipeptide using Algorithm 3.5.

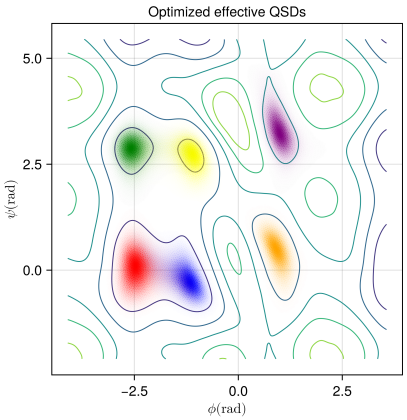

(b) QSDs for the effective dynamics (3.30).

Figure 3.12: In Figure 3.12a, solid lines correspond to the boundaries of the optimized domains, with corresponding initial domains in dotted lines. In Figure 3.12b, higher densities map to lower transparency values, with the same color-coding as in Figure 3.12. QSDs have been normalized in L^∞. In both figures, the free energy landscape from Figure 3.10 is plotted for reference.

the thermodynamic quantities computed in the previous paragraph and Corollary 3.9 for shape-variation formulas. Algorithm 3.5 was implemented in FreeFem++. Its code is available in the paper repository [46].

The algorithm was run six times, each time initialized with $\Omega_0 = B((\phi_0, \psi_0), 0.3)$ in CV space, where (ϕ_0, ψ_0) ranged across the six free energy local minima displayed in Figure 3.10. All optimization runs were performed with the parameters $\varepsilon_{\text{reg}} = \sqrt{0.1}$, $\varepsilon_{\text{degen}} = 0.01$, $m_{\max} = 2$, $\eta_{\max} = 0.004$, $\alpha = 0.8$, $\varepsilon_{\text{term}} = 0.005$, $M_{\text{grad}} = 2$ and $N_{\text{search}} = 1000$, except for the optimization of state 2, for which a value $\eta_{\max} = 0.001$ was necessary to achieve convergence. The mesh adaptation procedure $\mathcal{A}$ from step C. of Algorithm 3.5 enforced a maximal cell width of $h_{\max} = 0.03$ throughout the runs.

The initial domains are plotted alongside the corresponding numerically optimized domains in Figure 3.12a, together with the associated QSDs for the effective dynamics (3.30).

In Figure 3.13, we plot the evolution of the effective separation of timescales during the optimization process, for the six runs of Algorithm 3.5. State 5 is the most locally metastable state for the effective diffusion, with an effective separation of timescales of nearly 500.

In Figure 3.14, we plot the evolution of the first four Dirichlet eigenvalues of the effective generator during the six runs of Algorithm 3.5, showcasing frequent eigenvalue crossings. In all cases, we observe that the second and third Dirichlet eigenvalues coalesce during an early phase of the optimization process, which suggests that encountering degenerate eigenvalues is the rule rather than the exception. For the purpose of fixing a timescale in Figure 3.14, we (somewhat arbitrarily) set $\gamma = 5\,\text{ps}^{-1}$ in the definition of the effective generator (3.50).

In Figure 3.15, we illustrate the usefulness of the choice of ascent direction in Algorithm 3.5 using the numerical degeneracy parameter $\varepsilon_{\text{degen}}$. Omitting the numerical degeneracy parameter and trusting the non-degenerate shape gradients may lead to oscillations in the objective function, due to non-differentiable features of the objective landscape near points of near-degeneracy. The algorithm adapting the choice of ascent direction in the case of approximately

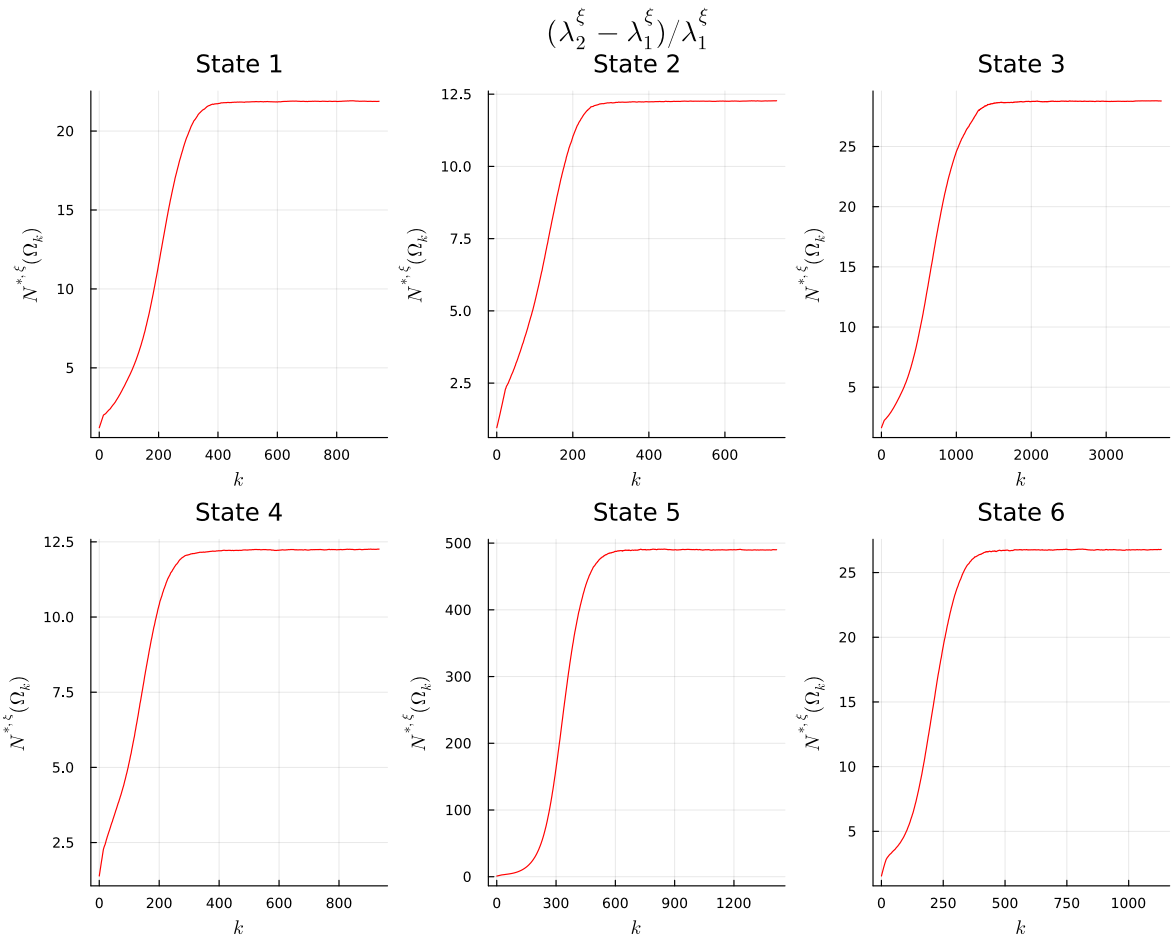

Figure 3.13: Effective separation of timescales throughout six runs of Algorithm 3.5, initialized with coresets around the six free energy minima depicted in Figure 3.10.

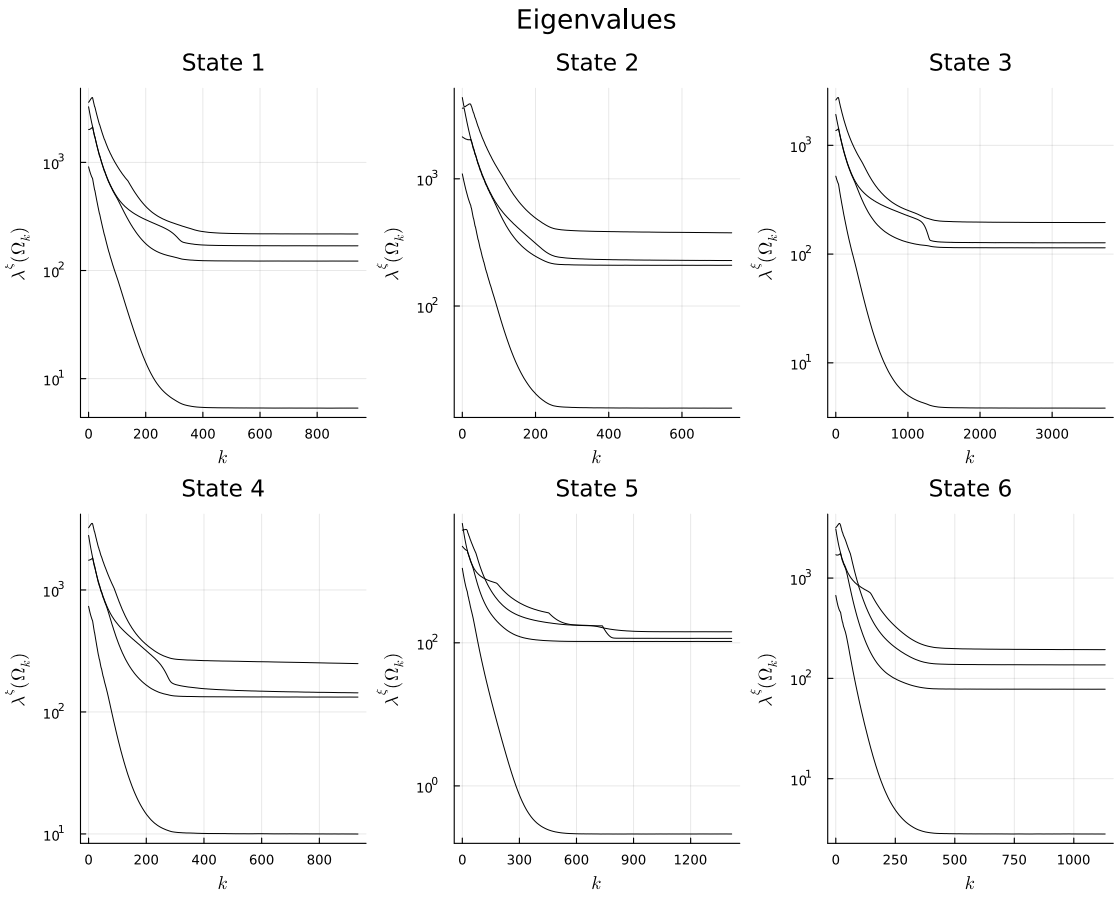

Figure 3.14: Behavior of the four smallest Dirichlet eigenvalues throughout the six runs of Algorithm 3.5 depicted in Figure 3.13, displaying frequent eigenvalue coalescence and crossings.

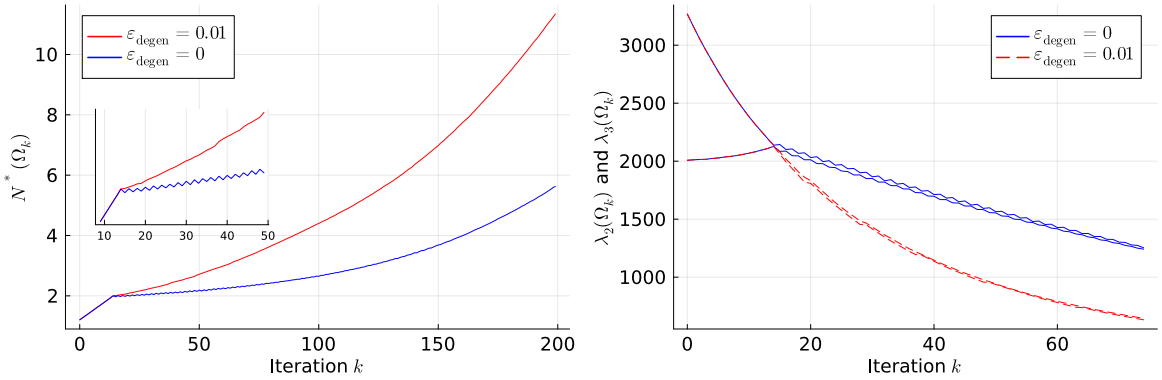

(a) Value of the objective function versus number of iterations, with zoom on iterations 10–50.

(b) Second and third Dirichlet eigenvalue versus number of iterations.

Figure 3.15: Effect of the numerical degeneracy parameter $\varepsilon_{\text{degen}}$ in Algorithm 3.5, during the optimization of state 1 (see Figure 3.10). Setting $\varepsilon_{\text{degen}} > 0$ ensures local ascent of the objective function, leading to an overall improvement in the convergence behavior (Figure 3.15a), and effectively suppresses eigenvalue crossings (Figure 3.15b).

degenerate eigenvalues leads to a significant improvement in the speed of increase of the objective function, and successfully suppresses eigenvalue crossings and oscillations in the value of the objective.

Parametrization of the states. The boundary vertices $(\phi_i, \psi_i)_{1 \leqslant i \leqslant N_{\text{V}}}$ of the optimized mesh for state 5 were transformed from (ϕ, ψ)-space into $(r_i, \theta_i)_{1 \leqslant i \leqslant N_{\text{V}}}$ for a system (r, θ) of polar coordinates centered at the free energy minimum inside state 5. A finite Fourier series

$$R(t) := \sum_{k=0}^{N_{\text{modes}}} [a_k \cos(kt) + b_k \sin(kt)]$$

was then fitted to these points via ordinary least squares with $N_{\text{modes}} = 20$, and the final definition we took for the optimized state was

$$\Omega = \{(r, \theta) : r < R(\theta)\}.$$

This definition assumes that the domain is star-shaped around the minimum, which is indeed the case here. The boundary of the free energy basin, which was computed using finite-difference gradient descent on the estimated free energy (see Figure 3.10), was similarly fitted with a Fourier series.

The Fleming–Viot process. To quantify the performance gained from using optimized definitions of metastable states at the level of the original high-dimensional dynamics, we must quantify the separation of timescale directly. We focus on state 5, the most locally metastable domain according to the effective dynamics, and argue numerically that the state optimized with the surrogate coarse-grained objective leads to a significant improvement in the separation of timescales, when compared with a reference domain given by the basin of attraction of the local minimum in state 5, for a steepest-descent dynamics on the free energy landscape.

We achieve this by using a Fleming–Viot process (see for instance [95]), which allows to infer both metastable timescales of interest, namely the exit rate starting from the QSD and the convergence rate to the QSD.

Algorithm 3.16 (Discrete-time Fleming–Viot process)**.** *One step of the Fleming–Viot process with hard-killing, given a domain $\Omega \subset \mathbb{R}^d$, a stride length Δt_{FV}, and given a number $N_{\mathrm{proc}} \geqslant 1$ of replicas in state $(X_{t_0}^{(i)})_{1 \leqslant i \leqslant N_{\mathrm{proc}}}$, consists in iterating the following procedure from $k = 0$.*

A. At step k: evolve each replica with independent Brownian motions for a physical time Δt_{FV} using a discretization of the underdamped Langevin dynamics.

B. For any $1 \leqslant i \leqslant N_{\mathrm{proc}}$, if $X_{t_0+k\Delta t_{\mathrm{FV}}}^{(i)} \notin \Omega$, kill this replica, and branch it in the next step from the state of a replica chosen uniformly at random among the survivors (that is, the set of replicas which did not exit Ω in step k).

C. Set $k \leftarrow k+1$ and proceed from step A.

This algorithm corresponds to the Fleming–Viot process with hard-killing for the discrete-time Markov chain obtained by subsampling the numerical trajectories in time at integer multiples of Δt_{FV}. Algorithm 3.16 should be understood as a particle approximation of the dynamics conditioned on remaining inside Ω, in the sense that the empirical distribution of replicas at time t converges to the conditional distribution μ_{t,X_0} (recall (3.4)) as $N_{\mathrm{proc}} \to \infty$, see [330, Theorem 2.2]. This convergence can in some cases be controlled uniformly in time, see [291, Theorem 3.1] for an early approach, and [191, Theorem 2] for a recent result in the overdamped case. In particular, the empirical stationary distribution of the Fleming–Viot process approaches the QSD as $N \to \infty$.

The time evolution of a single particle from the Fleming–Viot process (say $X^{(1)}$), resembles a ν-return process (where ν is the QSD): it evolves according to the dynamics until it reaches the boundary of the state, and is then instantly resurrected according to the empirical distribution of the Fleming–Viot process whose invariant measure approximates $\nu^{\otimes N_{\mathrm{proc}}}$. This approximation underpins the estimation of the exit rate from Ω starting from ν, and also step C. of Algorithm 3.18.

For each value of the friction parameter γ and the two definitions of the state, we sample N_γ independent trajectories of the Fleming–Viot process (starting from a random initial condition X_0 which we make precise below), lasting $t_{\mathrm{sim}} = 60\,\mathrm{ps}$ in total. The first $t_{\mathrm{eq}} = 30\,\mathrm{ps}$ were used to probe the decorrelation behavior to the QSD, and the last 30 ps were used to sample the QSD (or an approximation thereof), and stationary exit events.

Estimation of the exit rate. To estimate the metastable exit rate $\lambda_1(\Omega)$, we compute the empirical stationary exit rate for the Fleming–Viot process by counting the number $N_{\mathrm{exit},\Omega}(t)$ of branching events recorded after time t. The exit rate is estimated (for each value of γ and definition of the state) as

$$\widehat{\lambda}_1(\Omega) = \frac{N_{\mathrm{exit},\Omega}(t_{\mathrm{sim}}) - N_{\mathrm{exit},\Omega}(t_{\mathrm{eq}})}{N_{\mathrm{proc}}\,(t_{\mathrm{sim}} - t_{\mathrm{eq}})}. \tag{3.52}$$

Under the approximation that the stationary Fleming–Viot process is a collection of N_{proc} independent ν-return processes, the counting process $N_{\mathrm{exit},\Omega}$ is a Poisson process with rate measure $\lambda_1(\Omega)N_{\mathrm{proc}}\,\mathrm{d}t$, which motivates the choice of estimator (3.52). Confidence intervals for this exit rate were constructed from the independent realizations of the Fleming–Viot process.

Estimation of the convergence rate to the QSD. We assess the convergence of the conditional measure μ_{t,X_0} (see (3.4)) to the QSD ν at the level of convergence in total variation distance for their ϕ and ψ marginals (and not their (ϕ,ψ)-marginals, due to data scarcity). This choice is motivated by the assumption that the CVs ϕ and ψ correspond to the "slow" variables in the system, meaning that other degrees of freedom should have relaxed to their quasi-stationary state by the time ϕ and ψ do. We first approximate the conditional law μ_{t,X_0} and the QSD ν with empirical approximations $\widehat{\mu}_{t,X_0}$ and $\widehat{\nu}$. The approximations $\widehat{\nu}$ (or rather their ϕ and ψ marginal histograms) were constructed by aggregating samples of the CV values recorded over all realizations of the Fleming–Viot process and the last 60 ps of their trajectories. The approximations $\widehat{\mu}_{k\Delta t_{\mathrm{hist}}}$ (rather, their histograms) were constructed for $k \geqslant 1$ at regular time intervals of length $\Delta t_{\mathrm{hist}} = 0.2\,\mathrm{ps}$ by aggregating samples of the CV values across realizations, and on the time interval $((k-1)\Delta t_{\mathrm{hist}}, k\Delta t_{\mathrm{hist}}]$.

We estimate the total variation distances between marginals (where $f\sharp\mu$ denotes the push-forward of the measure μ by the function f):

$$\|\phi\sharp\mu_{k\Delta t_{\mathrm{hist}}} - \phi\sharp\nu\|_{\mathrm{TV}}, \qquad \|\psi\sharp\mu_{k\Delta t_{\mathrm{hist}}} - \psi\sharp\nu\|_{\mathrm{TV}}$$

by considering the L^1-distances between the one-dimensional histograms, constructed using 50 regular bins. We denote by $e_{k\Delta t_{\mathrm{hist}}}(\phi)$, $e_{k\Delta t_{\mathrm{hist}}}(\psi)$ the corresponding estimators, and define $e_t(\phi)$, $e_t(\psi)$ for any $t \geqslant \Delta t_{\mathrm{hist}}$ by linear interpolation.

Values of the "mixing-time" at level $\varepsilon = 0.05$, defined as $\mathrm{MT}_\varepsilon(f) = \inf\{t \geqslant \Delta t_{\mathrm{hist}} : e_t(f) < \varepsilon\}$, for $f \in \{\phi,\psi\}$ were computed. Additionally, we inferred a "decorrelation rate", by performing an affine fit on $\log \mathrm{e}_t(f)$ on $t \in [1, \mathrm{MT}_{0.1}(f)]\,\mathrm{ps}$ if $\mathrm{MT}_{0.1} - 1 \geqslant 4\,\mathrm{ps}$. Otherwise, no fit was performed. We give an example of convergence curves for the value of the friction parameter $\gamma = 10\,\mathrm{ps}^{-1}$ in Figures 3.16a and 3.16b, for the free energy basin and the optimized state, respectively. The horizontal line correspond to the value $\varepsilon = 0.05$ of the tolerance threshold for the mixing time. The regression line corresponding to the smallest decorrelation rate is also plotted. Error curves are color-coded according to the procedure with which the initial configuration is sampled, as made precise in the next paragraph.

Sampling of initial configurations. To assess the dependence of the decorrelation errors $e_t(\phi)$, $e_t(\psi)$ on the initial configuration of the system, we compute a realization of $e_t(\phi)$, $e_t(\psi)$ for various distributions of initial configurations X_0, each one corresponding to a critical point of the free energy.

- Four distributions corresponding to the four free energy saddle points surrounding state 5 (see Figure 3.10). First, a steered MD simulation was performed to bring the system close to the target critical point, following which a harmonically restrained simulation was

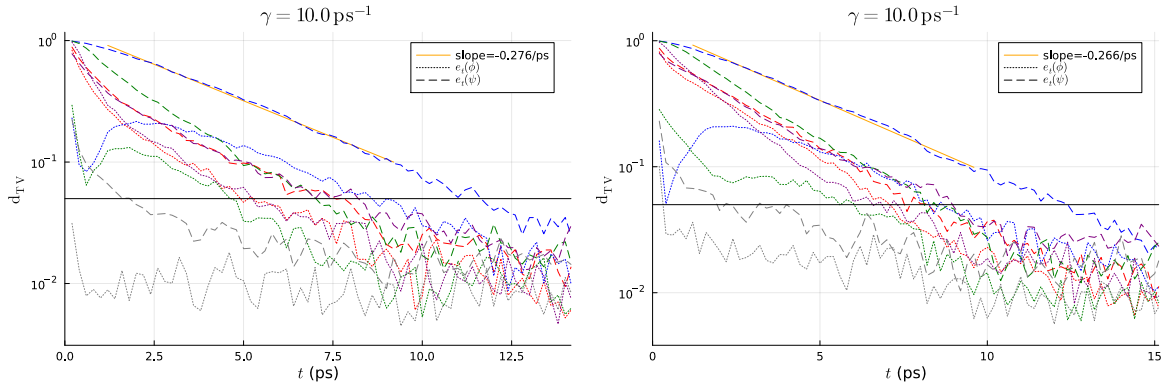

(a) Free-energy basin.

(b) Optimized domain.

Figure 3.16: Convergence of the marginals of the Fleming–Viot process to the corresponding quasi-stationary marginals for $\gamma = 10\,\mathrm{ps}^{-1}$. The dependence on the initial condition is color-coded as in Figure 3.17, except for the gray curves which correspond to initial conditions close to the free energy minimum. We observe, after a short transient phase, exponential convergence to the quasi-stationary marginals, and also a slight decrease in the decorrelation rate for the optimized state.

performed, with a biasing potential centered at the critical point. Only initial conditions with "entering" velocities were considered. We mean by this that, for the purposes of this experiment, we discarded samples which moved away from the free energy minimum in CV space during an equilibrium MD simulation of 2 fs, or which had a final configuration outside of the free energy basin.

- One distribution corresponding to the local free energy minimum in state 5. Again, a steered MD simulation was performed to bring the system close to the free energy minimum, followed by a harmonically restrained simulation. However, no "velocity check" was performed in this case.

In both cases, the steering phase was performed for 1 ps, and the harmonically restrained phase for 5 ps, both with an inverse force constant of $\eta = 40\,\mathrm{mol}\cdot\mathrm{kcal}^{-1}$. Timesteps of 0.5 fs and 1 fs were used respectively for the steering phase and the harmonically-restrained equilibration phase.

These two families of initial conditions correspond roughly to two natural definitions of the core-set $\mathcal{C}$ from Algorithm 3.16 associated with Ω. Initial conditions associated with free energy saddle points correspond to a coreset $\mathcal{C} = \mathcal{A}(z_5) \cap \Omega$, where z_5 is the free energy minimum associated with Ω, and $\mathcal{A}(z_5)$ denotes the corresponding free energy basin. Initial conditions steered towards the free energy minimum correspond to the definition $\mathcal{C} = B(z_5, r_c)$ for some small $r_c > 0$ in CV space. In the case where $\Omega = \mathcal{A}(z_5)$, the first core-set corresponds to the state itself: $\mathcal{C} = \Omega$, which is the standard situation in ParRep.

In Figure 3.17, we show the empirical stationary ξ-marginal $\xi_*\widehat{\nu}$ of the Fleming–Viot process, for the two state definitions we compare, and the value of the friction parameter $\gamma = 5\,\mathrm{ps}^{-1}$. Additionally, the sampled initial values of the collective variable are scattered, and color-coded according to the associated free energy saddle point. The color coding is the same as in Figures 3.16a and 3.16b.

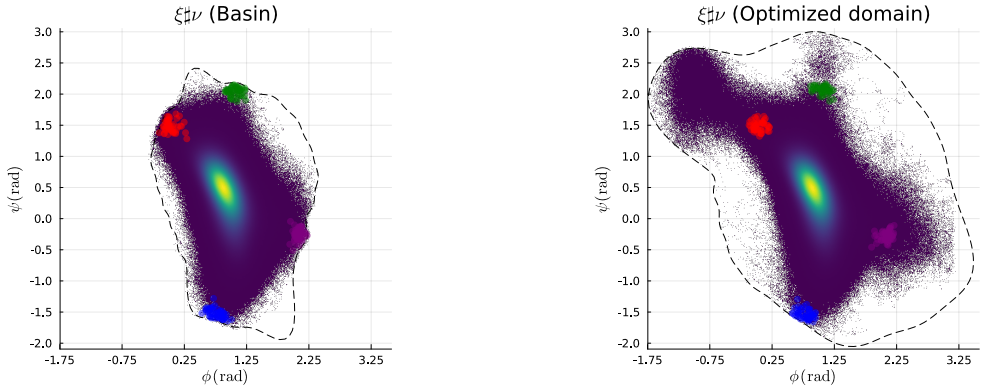

Figure 3.17: Empirical ξ-marginal for the stationary Fleming–Viot process for $\gamma = 10\,\mathrm{ps}^{-1}$. Left: free energy basin. Right: numerically optimized domain. On both figures, sampled initial configurations for the Fleming–Viot process are overlaid on the stationary histogram, and distinguished by color according to the corresponding free energy saddle point. Initial conditions sampled around the free energy minimum are not depicted.

Results. We present the results in Table 3.18: for each of the states and values of $\gamma \in \{1, 2, 5, 10, 20\}\,\mathrm{ps}^{-1}$, we report the estimated exit rate (ER) $\widehat{\lambda}_1(\Omega)$, in ps^{-1}, as well as various metrics quantifying the speed of convergence to the QSD.

- The decorrelation rate (DR) in ps^{-1}, defined as the least infered decorrelation rate among the observables ϕ, ψ and ensembles of initial configurations.
- The mixing time from saddle points (MT^{s}) in ps, defined as the largest mixing time $\mathrm{MT}_{0.05}(f)$ for $f \in \{\phi, \psi\}$ and initial conditions steered towards one of the four free energy saddle points according to the procedure described in the previous paragraph.
- The mixing time from the minimum (MT^{m}) in ps, defined as the largest mixing time $\mathrm{MT}_{0.05}(f)$ for $f \in \{\phi, \psi\}$, and initial conditions steered towards the free energy minimum.

To each of these metrics, we associate a corresponding measure of the separation of metastable timescales, namely the respective ratios DR/ER, $1/(\mathrm{MT}^{\mathrm{s}} \cdot \mathrm{ER})$ and $1/(\mathrm{MT}^{\mathrm{m}} \cdot \mathrm{ER})$ (where the inverse mixing times are interpreted as "mixing rates"). The full results are given in Tables 3.18a and 3.18b, for the free energy basin and optimized state, respectively. The timescale ratios are also plotted for visual comparison in Figure 3.18. We consistently observe a gain in timescale separation when using the optimized state, especially for higher values of the friction parameter, where the gain is estimated to be about $\times 3$ for the optimized state, across all measures of timescale separation. At lower values of the friction parameter, the gain is less pronounced, but still substantial. The improvements in timescale separation are reported in Figure 3.18c. The various timescale separation metrics are generally in agreement about this improvement.

3.6 Conclusions and perspectives

This work raises a number of perspectives which could prove interesting for future research.

(a) Free-energy basin.

γ	ER	DR	DR/ER	MT^{s}	$(\mathrm{ER}\cdot\mathrm{MT}^{\mathrm{s}})^{-1}$	MT^{m}	$(\mathrm{ER}\cdot\mathrm{MT}^{\mathrm{m}})^{-1}$
1	$(4.31 \pm 0.20) \times 10^{-3}$	0.48	111.7	6.8	34.1	0.8	290.0
2	$(4.21 \pm 0.21) \times 10^{-3}$	0.47	110.5	7.2	33.0	1.0	237.0
5	$(3.69 \pm 0.21) \times 10^{-3}$	0.36	97.1	9.4	28.8	1.8	150.6
10	$(3.26 \pm 0.19) \times 10^{-3}$	0.28	84.9	11.8	26.0	2.0	153.6
20	$(2.52 \pm 0.16) \times 10^{-3}$	0.19	72.4	16.8	23.6	3.0	132.1

(b) Optimized domain.

γ	ER	DR	DR/ER	MT^{s}	$(\mathrm{ER}\cdot\mathrm{MT}^{\mathrm{s}})^{-1}$	MT^{m}	$(\mathrm{ER}\cdot\mathrm{MT}^{\mathrm{m}})^{-1}$
1	$(1.86 \pm 0.15) \times 10^{-3}$	0.25	134.0	8.6	62.5	1.6	336.0
2	$(1.70 \pm 0.13) \times 10^{-3}$	0.40	237.0	7.6	77.6	1.2	491.0
5	$(1.43 \pm 0.12) \times 10^{-3}$	0.26	184.0	13.6	51.4	1.4	500.0
10	$(1.01 \pm 0.11) \times 10^{-3}$	0.27	265.0	12.6	78.9	2.0	497.0
20	$(7.55 \pm 0.92) \times 10^{-4}$	0.17	228.0	17.0	77.9	3.0	442.0

(c) Improvement of the optimized domain over the free energy basin in timescale separation metrics.

γ	DR/ER	$(\mathrm{ER}\cdot\mathrm{MT}^{\mathrm{s}})^{-1}$	$(\mathrm{ER}\cdot\mathrm{MT}^{\mathrm{m}})^{-1}$
1	1.2	1.83	1.16
2	2.14	2.35	2.07
5	1.89	1.78	3.32
10	3.12	3.03	3.24
20	3.15	3.3	3.35

Figure 3.18: Results of the Fleming–Viot simulations, showing that the optimized state consistently outperforms the free energy basin. Reported errors are at the level $\pm 1.96\sigma$.

- The most salient point is the extension of the shape perturbation results of Theorem 3.2 to the case of non-reversible and/or hypoelliptic diffusions. We expect that, due to the non-symmetry and/or non-ellipticity of the generator (3.3), this represents a significant theoretical endeavour.

- A standing question would be how to systematically optimize the definition of the core-sets in Algorithm 3.18 (see Appendix 3.B below), either numerically or in some limiting asymptotic regime. This question is related to the search for quantitative estimates of the prefactor $C(x)$ in the error estimate (3.6).

- At this point, a convergence proof for the method described in Algorithm 3.5 is lacking. It would be interesting to obtain consistency results with respect to the various approximation parameters.

- The direct shape optimization method, due to the FEM discretization, is limited to settings where low-dimensional ($m = 2$ or 3) representations of the dynamics (i.e. good CVs) are available. To go beyond this limitation, a natural approach would be to follow a parametric approach, setting $\Omega_\theta = \Phi_\theta(\mathcal{C})$ for some reference domain $\mathcal{C} \subset \mathbb{R}^d$, where $\theta \mapsto \Phi_\theta$ is a parametric family of homeomorphisms, represented for instance using a neural network. The main question becomes how to define a neural architecture for which the Dirichlet eigenvalue problem associated with the transported operator (3.58) is solvable, and for which perturbations of the eigenvalues are tractable.

- Instead of computing the thermodynamic coefficients F_ξ, a_ξ (see Equations (3.28), (3.29)) associated with the effective dynamics (3.30), one could seek kinetically-tuned effective dynamics. One approach would be to train a parametric model of a dynamics of the

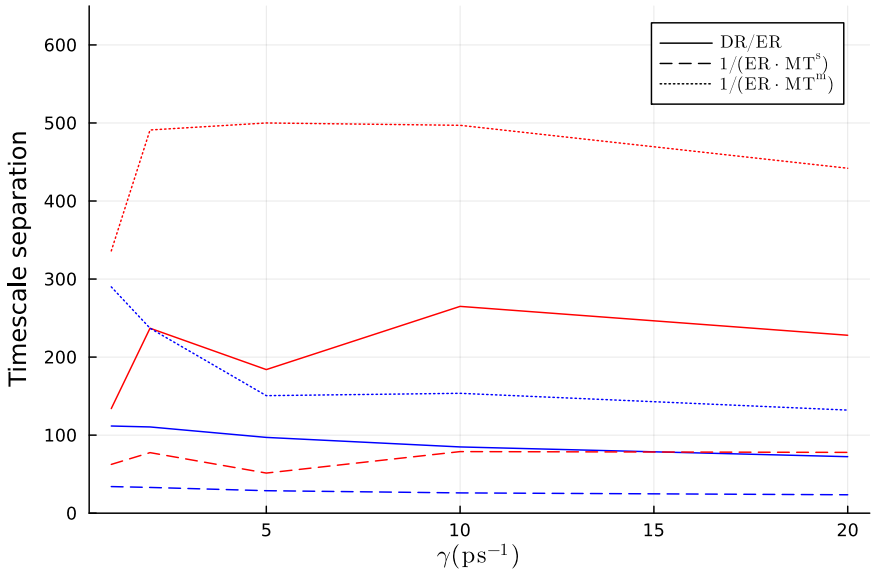

Figure 3.19: Timescale separation ratios. Blue lines correspond to the free energy basin, and red lines to the optimized domain. Across all metrics, the optimized domain outperforms the free energy basin.

form (3.1) on CV trajectory data, using EDMD-like techniques or neural SDEs in the hope of obtaining a dynamical description which is more robust to a suboptimal choice of CV. Note that the results of Theorem 3.2, since they are currently limited to the case of reversible dynamics, place a constraint on the class of allowable models.

Appendix 3.A: Proof of Theorem 3.2

We prove Theorem 3.2 in this appendix. The proof relies on the transport of the variational formulation of the generalized eigenvalue problem on Ω_θ to the reference domain Ω. This leads to the definition of a family of generalized eigenproblems associated with bilinear forms parametrized by θ. The corresponding eigenvalues are exactly the Dirichlet eigenvalues of $-\mathcal{L}_\beta$ on Ω_θ. One then proves the Fréchet-differentiability of these bilinear forms, or equivalently, by polarization, of the associated quadratic forms. Since the first-order perturbations are themselves unbounded quadratic forms, this regularity only holds with respect to the topology of relatively bounded perturbations of the reference quadratic forms. Once this has been established, classical results of perturbation theory from [192] can be leveraged to show the Fréchet differentiability of the inverse operator, and finally the Gateaux-differentiability of multiple eigenvalues.

Remark 3.17. By adapting the approach based on the implicit function theorem discussed in [164, Section 5.7] for the Dirichlet Laplacian (which corresponds to the special case $a \equiv \mathrm{Id}$ and $V \equiv 0$ in our setting), one can also show that the map $\theta \mapsto \lambda_k(\Omega_\theta)$ is $\mathcal{C}^1$ around $\theta = 0$ in a somewhat less technical manner. However, this approach is only adapted to the case of simple eigenvalues. Since the main purpose of Theorem 3.2 is to identify ascent directions for functionals of the Dirichlet eigenvalues of $\mathcal{L}_\beta$ with respect to the perturbation θ, and since multiple eigenvalues have been noted to occur in eigenvalue shape optimization problems (see e.g. [163, Theorem 2.5.10] or [261, Section 4.5]), including in our own numerical experiments

(see Figure 3.14 above), it is of practical interest to devise numerical strategies adapted to this reality.

Proof of Theorem 3.2. At various places, we assume that

$$\|\theta\|_{\mathcal{W}^{1,\infty}} < h_0$$

for some $h_0 > 0$ whose value will be reduced several times. We also fix a regular open and bounded set $\mathcal{D} \subset \mathbb{R}^d$, sufficiently large so that $\bigcup_{x\in\Omega} B_{\mathbb{R}^d}(x, h_0) \subset \mathcal{D}$. This ensures in particular that $\Omega_\theta \subset \mathcal{D}$ for all $\|\theta\|_{\mathcal{W}^{1,\infty}} < h_0$.

We say that an estimate of the form

$$J(\Omega, \theta) \leqslant C(\mathcal{D})h(\theta),$$

with $J : \mathcal{B}(\mathbb{R}^d) \times \mathcal{W}^{1,\infty} \to \mathbb{R}$, $h : \mathcal{W}^{1,\infty} \to \mathbb{R}$ and $C(\mathcal{D}) > 0$, holds "uniformly inside $\mathcal{D}$" if it holds for all pairs (Ω, θ) with $\Omega \subset \mathcal{D}$ an open Lipschitz set and $\theta \in B_{\mathcal{W}^{1,\infty}}(0, h_0)$.

Transport of the variational formulation. Introduce, for $\theta \in \mathcal{W}^{1,\infty}$, the bilinear forms

$$\forall\, u, v \in H^1_0(\Omega_\theta), \qquad \mathfrak{a}_0(u, v; \Omega_\theta) = \frac{1}{\beta}\int_{\Omega_\theta} \nabla u^\top a \nabla v\, \mathrm{e}^{-\beta V}, \qquad \mathfrak{b}_0(u, v; \Omega_\theta) = \int_{\Omega_\theta} uv\, \mathrm{e}^{-\beta V}.$$

For $\|\theta\|_{\mathcal{W}^{1,\infty}} < h_0$ sufficiently small, the map $\Phi_\theta(x) = x+\theta(x)$ is a bi-Lipschitz homeomorphism of $\mathbb{R}^d$, and using the Lebesgue change of variables formula, it holds

$$\begin{aligned}
\mathfrak{a}_0(u, v; \Omega_\theta) &= \frac{1}{\beta}\int_\Omega \left(\nabla u^\top a \nabla v\, \mathrm{e}^{-\beta V}\right) \circ \Phi_\theta \,|\det\, \nabla\Phi_\theta| \\
&= \frac{1}{\beta}\int_\Omega \nabla\left(u \circ \Phi_\theta\right)^\top \nabla\Phi_\theta^{-\top} a \circ \Phi_\theta \nabla\Phi_\theta^{-1} \nabla\left(v \circ \Phi_\theta\right) \mathrm{e}^{-\beta V\circ\Phi_\theta} \,|\det\, \nabla\Phi_\theta| \\
&:= \mathfrak{a}_\theta(u \circ \Phi_\theta, v \circ \Phi_\theta; \Omega),
\end{aligned}$$

where we used $\nabla\left(u \circ \Phi_\theta\right) = \nabla\Phi_\theta\, (\nabla u) \circ \Phi_\theta$ in the penultimate line, and $\nabla\Phi_\theta^{-1}$ denotes the matrix inverse of $\nabla\Phi_\theta$. Similarly,

$$\mathfrak{b}_0(u, v; \Omega_\theta) = \int_\Omega \left(u \circ \Phi_\theta\right)\left(v \circ \Phi_\theta\right) \mathrm{e}^{-\beta V\circ\Phi_\theta} \,|\det\, \nabla\Phi_\theta| := \mathfrak{b}_\theta(u \circ \Phi_\theta, v \circ \Phi_\theta; \Omega).$$

From now on, all bilinear forms act on the fixed domain Ω, which we therefore omit in the notation for the bilinear forms, i.e. we define for all $u, v \in H^1_0(\Omega)$,

$$\begin{aligned}
\mathfrak{a}_\theta(u, v) &= \frac{1}{\beta}\int_\Omega \nabla u^\top \nabla\Phi_\theta^{-\top} a \circ \Phi_\theta \nabla\Phi_\theta^{-1} \nabla v \mathrm{e}^{-\beta V\circ\Phi_\theta} \,|\det\, \nabla\Phi_\theta|\,, \\
\mathfrak{b}_\theta(u, v) &= \int_\Omega uv \mathrm{e}^{-\beta\circ\Phi_\theta} \,|\det\, \nabla\Phi_\theta|\,.
\end{aligned} \tag{3.53}$$

Spectral properties. Now, considering an eigenpair $(\lambda_\theta, u_\theta)$ for $-\mathcal{L}_\beta$ on $L^2_\beta(\Omega_\theta)$, it holds, for all $v \in H^1_{0,\beta}(\Omega_\theta) = H^1_0(\Omega_\theta)$, that

$$\mathfrak{a}_\theta\left(u_\theta \circ \Phi_\theta, v \circ \Phi_\theta\right) = \lambda_\theta \mathfrak{b}_\theta(u \circ \Phi_\theta, v \circ \Phi_\theta).$$

Since, using the isomorphism (3.11), any function $v \in H^1_0(\Omega)$ can be written under the form $v \circ \Phi_\theta^{-1} \circ \Phi_\theta$ with $v \circ \Phi_\theta^{-1} \in H^1_0(\Omega_\theta)$, the transported eigenvector $w_\theta = u_\theta \circ \Phi_\theta$ satisfies

$$\mathfrak{a}_\theta(w_\theta, v) = \lambda_\theta \mathfrak{b}_\theta(w_\theta, v) \qquad \forall v \in H^1_0(\Omega).$$

In other words, w_θ is a generalized eigenvector for $(\mathfrak{a}_\theta, \mathfrak{b}_\theta)$. Let us make this statement precise.

We first introduce the following estimates, which hold, for $h_0 < 1$, uniformly inside $\mathcal{D}$ for some $C_1(\mathcal{D}), C_2(\mathcal{D}) > 0$:

$$\begin{aligned} \|\nabla\Phi_\theta^{-1} - \mathrm{Id}\|_{L^\infty(\Omega;\mathcal{M}_d)} &\leqslant \frac{\|\theta\|_{\mathcal{W}^{1,\infty}}}{1 - \|\theta\|_{\mathcal{W}^{1,\infty}}} \leqslant C_1(\mathcal{D})\|\theta\|^{1,\infty}_{\mathcal{W}}, \\ \|\nabla\Phi_\theta^{-1} - (\mathrm{Id} - \nabla\theta)\,\|_{L^\infty(\Omega;\mathcal{M}_d)} &\leqslant \frac{\|\theta\|^2_{\mathcal{W}^{1,\infty}}}{1 - \|\theta\|_{\mathcal{W}^{1,\infty}}} \leqslant C_2(\mathcal{D})\|\theta\|^2_{\mathcal{W}^{1,\infty}}. \end{aligned} \tag{3.54}$$

These follow by expanding $\nabla\Phi_\theta(x)^{-1} = (\mathrm{Id} + \nabla\theta(x))^{-1}$ into a Neumann series and estimating the (submultiplicative) $\mathcal{M}_d$-norm of the first and second partial remainders respectively. In fact we can take $C_1(\mathcal{D}) = C_2(\mathcal{D}) = (1 - h_0)^{-1}$ here, but we nevertheless distinguish these constants for the sake of clarity.

Secondly, by Jacobi's formula for the Fréchet derivative of the determinant of a $d \times d$ matrix, it holds almost everywhere in $\mathbb{R}^d$ (by Rademacher's theorem) that

$$|\det \nabla\Phi_\theta(x)| = \det(1 + \nabla\theta(x)) = 1 + \mathrm{Tr}\ \nabla\theta(x) + \mathcal{O}(|\nabla\theta(x)|^2_{\mathcal{M}_d});$$

whence, uniformly inside $\mathcal{D}$ for some constants $C_3(\mathcal{D}), C_4(\mathcal{D}) > 0$, it holds

$$\begin{aligned} \|\det \nabla\Phi_\theta - 1\|_{L^\infty(\Omega)} &\leqslant C_3(\mathcal{D})\,\|\theta\|_{\mathcal{W}^{1,\infty}}\,, \\ \|\det \nabla\Phi_\theta - 1 - \mathrm{div}\,\theta\|_{L^\infty(\Omega)} &\leqslant C_4(\mathcal{D})\,\|\theta\|^2_{\mathcal{W}^{1,\infty}}\,. \end{aligned} \tag{3.55}$$

Note that we used $\mathrm{Tr}\,\nabla\theta = \mathrm{div}\,\theta$ and $|\,\mathrm{Tr}\,M| \leqslant d|M|_{\mathcal{M}_d}$ for all $M \in \mathcal{M}_d$.

From the estimates (3.54) and (3.55), we deduce that the symmetric bilinear form $\mathfrak{a}_\theta$, with domain $H^1_0(\Omega) \subset L^2(\Omega)$, satisfies the following upper bound uniformly inside $\mathcal{D}$:

$$\mathfrak{a}_\theta(u,u) \leqslant \frac{1}{\beta}\|a\|_{L^\infty(\mathcal{D};\mathcal{M}_d)}\|\mathrm{e}^{-\beta V}\|_{L^\infty(\mathcal{D})}(1 + C_3(\mathcal{D})h_0)(1 + C_1(\mathcal{D})h_0)^2\|\nabla u\|^2_{L^2(\Omega)}, \tag{3.56}$$

as well as the lower bound

$$\begin{aligned} \mathfrak{a}_\theta(u,u) &\geqslant \frac{1}{\beta}\varepsilon_a(\overline{\mathcal{D}})m_V(\mathcal{D})(1 - C_1(\mathcal{D})h_0)^2(1 - C_3(\mathcal{D})h_0)\|\nabla u\|^2_{L^2(\Omega)} \\ &\geqslant \frac{1}{\beta}\varepsilon_a(\overline{\mathcal{D}})m_V(\mathcal{D})(1 - C_1(\mathcal{D})h_0)^2(1 - C_3(\mathcal{D})h_0)\mu_0(\Omega)\|u\|^2_{L^2(\Omega)} \\ &\geqslant \frac{1}{\beta}\varepsilon_a(\overline{\mathcal{D}})m_V(\mathcal{D})(1 - C_1(\mathcal{D})h_0)^2(1 - C_3(\mathcal{D})h_0)\mu_0(\mathcal{D})\|u\|^2_{L^2(\Omega)}, \end{aligned} \tag{3.57}$$

with $\mu_0 > 0$ is the principal Dirichlet eigenvalue of the Laplacian, and where we use $\mu_0(\Omega) \geqslant \mu_0(\mathcal{D})$ in the last line (see for instance [50, Proposition 16]), and recall the definition (**Ell**)

of $\varepsilon_a(\overline{\mathcal{D}})$. In (3.57), we define

$$m_V(\mathcal{D}) := \exp\left(-\beta\left[\operatorname*{ess\,sup}_{\mathcal{D}} V\right]\right) > 0.$$

Note that the lower bound in (3.57) is positive for h_0 sufficiently small, therefore $\mathfrak{a}_\theta$ is $H^1(\Omega)$-coercive and $L^2(\Omega)$-bounded from below, uniformly inside $\mathcal{D}$. Moreover, it follows from (3.56) and (3.57) that $\mathfrak{a}_\theta$ is closed, since the squared form norm $\|u\|^2_{\mathfrak{a}_\theta} = \mathfrak{a}_\theta(u,u) + \|u\|^2_{L^2(\Omega)}$ on $H^1_0(\Omega)$ is equivalent to the squared $H^1(\Omega)$-norm. Therefore, by a representation result for positive symmetric closed forms [192, Theorem VI.2.6], there exists a self-adjoint operator A_θ satisfying

$$\mathfrak{a}_\theta(u,v) = \langle A_\theta u, v\rangle_{L^2(\Omega)}, \qquad \forall (u,v) \in D(A_\theta) \times H^1_0(\Omega),$$

with $\mathcal{D}(A_\theta) \subset \mathcal{D}(A_\theta^{1/2}) = H^1_0(\Omega)$ and A_θ being $L^2(\Omega)$-bounded from below, with the same lower bound as a_θ:

$$\langle A_\theta u, u\rangle_{L^2(\Omega)} \geqslant \frac{1}{\beta}\varepsilon_a(\overline{\mathcal{D}}) m_V(\mathcal{D})(1 - C_1(\mathcal{D})h_0)^2(1 - C_3(\mathcal{D})h_0)\mu_0(\mathcal{D})\|u\|^2_{L^2(\Omega)}.$$

In particular, the resolvent A_θ^{-1} is bounded and compact in view of the compact embedding $H^1_0(\Omega) \subset L^2(\Omega)$ given by the Rellich–Kondrachov theorem.

Note that, by integration by parts, A_θ extends the positive (for h_0 sufficiently small) operator

$$-\widetilde{\mathcal{L}}_{\beta,\theta}\varphi = -\frac{1}{\beta}\operatorname{div}\left(|\det \nabla\Phi_\theta|\, \mathrm{e}^{-\beta V\circ\Phi_\theta}\nabla\Phi_\theta^{-\top} a \circ \Phi_\theta \nabla\Phi_\theta^{-1}\nabla\varphi\right) \qquad \forall \varphi \in \mathcal{D}(\widetilde{\mathcal{L}}_{\beta,\theta}) = \mathcal{C}^\infty_{\mathrm{c}}(\Omega), \tag{3.58}$$

therefore, the closed operator A_θ, which extends $-\widetilde{\mathcal{L}}_{\beta,\theta}$, also corresponds to its Friedrichs extension (see [192, Section VI.2.3]). For the sake of consistency, we also write A_0 for the operator $-\mathcal{L}_\beta$. Similarly, $\mathfrak{b}_\theta$ has the representation $\mathfrak{b}_\theta(u,v) = \langle B_\theta u, v\rangle_{L^2(\Omega)}$, where B_θ is the bounded, positive linear operator given by multiplication by $\mathrm{e}^{-\beta V\circ\Phi_\theta}\,|\det \nabla\Phi_\theta|$, which is both bounded from above and from below uniformly inside $\mathcal{D}$:

$$m_V(\mathcal{D})(1-C_3(\mathcal{D})h_0)\|u\|^2_{L^2(\Omega)} \leqslant \mathfrak{b}_\theta(u,u) = \langle B_\theta u, u\rangle_{L^2(\Omega)} \leqslant \|\mathrm{e}^{-\beta V}\|_{L^\infty(\mathcal{D})}(1+C_3(\mathcal{D})h_0)\|u\|^2_{L^2(\Omega)}. \tag{3.59}$$

It follows (see [153, Proposition 1] or the discussion in [192, Section VII.6.1]) that the reciprocals of the eigenvalues of the compact, positive operator $A_\theta^{-1}B_\theta$ on $L^2(\Omega)$ (which is also self-adjoint for the topologically equivalent scalar product $\langle B_\theta \cdot, \cdot\rangle_{L^2(\Omega)}$) are the solutions to

$$A_\theta w_\theta = \lambda_\theta B_\theta w_\theta, \quad \lambda_\theta > 0, \quad w_\theta \in \mathcal{D}(A_\theta).$$

In fact it is more convenient than solving the latter generalized eigenvalue problem to consider the spectrum of the compact operator $A_\theta^{-1}B_\theta$, which is composed of positive, isolated eigenvalues of finite multiplicity.

Perturbation estimates. Let us define the first-order perturbations of the linear forms (3.53). More precisely, we define, for $u, v \in H^1_0(\Omega)$, the symmetric bilinear forms

$$\begin{aligned} \mathrm{d}\mathfrak{a}_0(\theta)(u,v) &= \frac{1}{\beta}\int_\Omega \nabla u^\top \left(\nabla a^\top \theta - a\nabla\theta - \nabla\theta^\top a\right)\nabla v\, \mathrm{e}^{-\beta V} + \frac{1}{\beta}\int_\Omega \nabla u^\top a \nabla v \,\mathrm{div}\left(\theta \mathrm{e}^{-\beta V}\right), \\ \mathrm{d}\mathfrak{b}_0(\theta)(u,v) &= \int_\Omega uv\,\mathrm{div}(\theta \mathrm{e}^{-\beta V}). \end{aligned} \tag{3.60}$$

Writing, for $u \in H^1_0(\Omega)$,

$$\begin{aligned} r_{\mathfrak{a}}(\theta,u) &= \mathfrak{a}_\theta(u,u) - \mathfrak{a}_0(u,u) - \mathrm{d}\mathfrak{a}_0(\theta)(u,u), \\ r_{\mathfrak{b}}(\theta,u) &= \mathfrak{b}_\theta(u,u) - \mathfrak{b}_0(u,u) - \mathrm{d}\mathfrak{b}_0(\theta)(u,u), \end{aligned} \tag{3.61}$$

we next show that the following bounds hold for all $u \in H^1_0(\Omega)$ and $\theta \in B_{\mathcal{W}^{1,\infty}}(0,h_0)$:

$$\begin{aligned} |\mathrm{d}\mathfrak{a}_0(\theta)(u,u)| &\leqslant C_{\mathfrak{a},1}(\mathcal{D})\|\theta\|_{\mathcal{W}^{1,\infty}}\mathfrak{a}_0(u,u), \quad |\mathrm{d}\mathfrak{b}_0(\theta)(u,u)| \leqslant C_{\mathfrak{b},1}(\mathcal{D})\|\theta\|_{\mathcal{W}^{1,\infty}}\mathfrak{b}_0(u,u), \\ |r_{\mathfrak{a}}(\theta,u)| &\leqslant C_{\mathfrak{a},2}(\mathcal{D})\|\theta\|^2_{\mathcal{W}^{1,\infty}}\mathfrak{a}_0(u,u), \qquad |r_{\mathfrak{b}}(\theta,u) \leqslant C_{\mathfrak{b},2}(\mathcal{D})\|\theta\|^2_{\mathcal{W}^{1,\infty}}\mathfrak{b}_0(u,u), \end{aligned} \tag{3.62}$$

where $C_{\mathfrak{a},1}(\mathcal{D}), C_{\mathfrak{a},2}(\mathcal{D}), C_{\mathfrak{b},1}(\mathcal{D}), C_{\mathfrak{b},2}(\mathcal{D})$ are positive constants. These estimates, together with the linearity of the maps $\theta \mapsto \mathrm{d}\mathfrak{a}_0(\theta)$ and $\theta \mapsto \mathrm{d}\mathfrak{b}_0(\theta)$, establish the Fréchet differentiability of the bilinear forms $\mathfrak{a}_\theta, \mathfrak{b}_\theta$, in the topology of relative $\mathfrak{a}_0$-form-boundedness and $\mathfrak{b}_0$-form-boundedness respectively, at $\theta = 0$. Note that the Kato–Rellich theorem (see for instance [318, Theorem 6.4]) then implies that $\mathcal{D}(A_\theta) = \mathcal{D}(A_0)$ in a $\mathcal{W}^{1,\infty}$-neighborhood of $\theta = 0$. Therefore, we may assume that h_0 is sufficiently small so that $\mathcal{D}(A_\theta) = \mathcal{D}(A_0)$ for all $\theta \in B_{\mathcal{W}^{1,\infty}}(0,h_0)$.

The expressions (3.60) are motivated by formal first-order expansions in θ in the expressions (3.53). In order to establish them, we first note that the following estimates hold uniformly inside $\mathcal{D}$:

$$\begin{aligned} \left\|\nabla\Phi_\theta^{-1}\right\|_{L^\infty(\Omega;\mathcal{M}_d)} &\leqslant 1 + C_1(\mathcal{D})h_0, \\ \|\det\nabla\Phi_\theta\|_{L^\infty(\Omega)} &\leqslant 1 + C_3(\mathcal{D})h_0, \\ \|a\circ\Phi_\theta\|_{L^\infty(\Omega;\mathcal{M}_d)} &\leqslant \|a\|_{L^\infty(\mathcal{D};\mathcal{M}_d)}, \\ \left\|\mathrm{e}^{-\beta V\circ\Phi_\theta}\right\|_{L^\infty(\Omega)} &\leqslant \left\|\mathrm{e}^{-\beta V}\right\|_{L^\infty(\mathcal{D})}, \\ \left\|\nabla\Phi_\theta^{-1} - (\mathrm{Id} - \nabla\theta)\right\|_{L^\infty(\Omega;\mathcal{M}_d)} &\leqslant C_2(\mathcal{D})\|\theta\|^2_{\mathcal{W}^{1,\infty}}, \\ \|\det\nabla\Phi_\theta - 1 - \mathrm{div}\,\theta\|_{L^\infty(\Omega)} &\leqslant C_4(\mathcal{D})\|\theta\|^2_{\mathcal{W}^{1,\infty}}, \\ \left\|a\circ\Phi_\theta - a - \nabla a^\top\theta\right\|_{L^\infty(\Omega;\mathcal{M}_d)} &\leqslant \frac{1}{2}\left\|\nabla^2 a\right\|_{L^\infty(\mathcal{D};\mathcal{M}_d\otimes\mathcal{M}_d)}\|\theta\|^2_{L^\infty(\mathbb{R}^d;\mathbb{R}^d)}, \\ \left\|\mathrm{e}^{-\beta V\circ\Phi_\theta} - \left(\mathrm{e}^{-\beta V} - \beta\nabla V^\top\theta\mathrm{e}^{-\beta V}\right)\right\|_{L^\infty(\Omega)} &\leqslant \frac{1}{2}\left\|\nabla^2\left(\mathrm{e}^{-\beta V}\right)\right\|_{L^\infty(\mathcal{D};\mathcal{M}_d)}\|\theta\|^2_{L^\infty(\mathbb{R}^d;\mathbb{R}^d)}, \\ \|\theta\|_{L^\infty(\Omega;\mathbb{R}^d)}, \|\nabla\theta\|_{L^\infty(\Omega;\mathcal{M}_d)} &\leqslant h_0, \\ \|\mathrm{div}\,\theta\| &\leqslant dh_0. \end{aligned} \tag{3.63}$$

The two first estimates in (3.63) follow immediately from (3.54) and (3.55). The third and fourth follow from the inclusion $\Omega_\theta \subset \mathcal{D}$, the fifth and sixth are already given in (3.54) and (3.55). The seventh and eighth follow from the regularities $V \in \mathcal{W}^{2,\infty}(\mathcal{D})$, $a \in \mathcal{W}^{2,\infty}(\mathcal{D};\mathcal{M}_d)$ given

by Assumption (**Reg**), and the inclusion $\Omega_\theta \subset \mathcal{D}$. The penultimate estimate is clear, and the last one follows from $|\operatorname{Tr} M| \leqslant d|M|_{\mathcal{M}_d}$.

From the estimates (3.54), (3.55) and (3.63), we obtain, by the Leibniz rule in the Banach algebra $L^\infty(\Omega;\mathcal{M}_d)$, that the map

$$\alpha : \begin{cases} \mathcal{W}^{1,\infty} \to L^\infty(\Omega;\mathcal{M}_d), \\ \qquad \theta \mapsto \nabla\Phi_\theta^{-\top} a \circ \Phi_\theta \nabla\Phi_\theta^{-1} |\det \nabla\Phi_\theta| \mathrm{e}^{-\beta V\circ\Phi_\theta}, \end{cases}$$

is Fréchet differentiable at $\theta = 0$, with

$$D\alpha(0)\theta = -\nabla\theta^\top a \mathrm{e}^{-\beta V} + \nabla a^\top \theta \mathrm{e}^{-\beta V} - a\nabla\theta \mathrm{e}^{-\beta V} + a \operatorname{div}\left(\theta \mathrm{e}^{-\beta V}\right).$$

Moreover, there exist $M_{\mathfrak{a},1}(\mathcal{D}), M_{\mathfrak{a},2}(\mathcal{D}) > 0$ such that, uniformly inside $\mathcal{D}$, it holds

$$\begin{aligned} \|D\alpha(0)\theta\|_{L^\infty(\Omega;\mathcal{M}_d)} &\leqslant M_{a,1}(\mathcal{D})\|\theta\|_{\mathcal{W}^{1,\infty}}, \\ \|\alpha(\theta) - \alpha(0) - D\alpha(0)\theta\|_{L^\infty(\Omega;\mathcal{M}_d)} &\leqslant M_{a,2}(\mathcal{D})\|\theta\|^2_{\mathcal{W}^{1,\infty}}. \end{aligned}$$

By a similar argument, the map

$$\gamma : \begin{cases} \mathcal{W}^{1,\infty} \to L^\infty(\Omega), \\ \qquad \theta \mapsto |\det \nabla\Phi_\theta| \mathrm{e}^{-\beta V\circ\Phi_\theta}, \end{cases}$$

is Fréchet differentiable at $\theta = 0$, with

$$D\gamma(0)\theta = \operatorname{div}\left(\theta \mathrm{e}^{-\beta V}\right),$$

and the estimates

$$\begin{aligned} \|D\gamma(0)\theta\|_{L^\infty(\Omega)} &\leqslant M_{b,1}(\mathcal{D})\|\theta\|_{\mathcal{W}^{1,\infty}}, \\ \|\gamma(\theta) - \gamma(0) - D\gamma(0)\theta\|_{L^\infty(\Omega)} &\leqslant M_{b,2}(\mathcal{D})\|\theta\|^2_{\mathcal{W}^{1,\infty}}, \end{aligned}$$

hold uniformly inside $\mathcal{D}$ for some positive constants $M_{\mathfrak{b},1}(\mathcal{D}), M_{\mathfrak{b},2}(\mathcal{D}) > 0$.

We now show (3.62). It holds

$$\begin{aligned} \mathrm{d}\mathfrak{a}_0(\theta)(u,u) &= \frac{1}{\beta}\int_\Omega \nabla u^\top D\alpha(0)\theta \nabla u, \\ r_{\mathfrak{a}}(\theta,u) &= \frac{1}{\beta}\int_\Omega \nabla u^\top \left(\alpha(\theta) - \alpha(0) - D\alpha(0)\theta\right)\nabla u, \\ \mathrm{d}\mathfrak{b}_0(\theta)(u,u) &= \int_\Omega u^2 D\gamma(0)\theta, \\ r_{\mathfrak{b}}(\theta,u) &= \int_\Omega u^2 \left(\gamma(\theta) - \gamma(0) - D\gamma(0)\theta\right), \end{aligned}$$

whence, uniformly inside $\mathcal{D}$:

$$\begin{aligned}
|\mathrm{d}\mathfrak{a}_0(\theta)(u,u)| &\leqslant \frac{M_{\mathfrak{a},1}(\mathcal{D})}{\beta}\|\theta\|_{\mathcal{W}^{1,\infty}}\|\nabla u\|^2_{L^2(\Omega;\mathbb{R}^d)},\\
|r_{\mathfrak{b}}(\theta,u)| &\leqslant \frac{M_{\mathfrak{a},2}(\mathcal{D})}{\beta}\|\theta\|^2_{\mathcal{W}^{1,\infty}}\|\nabla u\|^2_{L^2(\Omega;\mathbb{R}^d)},\\
|\mathrm{d}\mathfrak{b}_0(\theta)(u,u)| &\leqslant M_{\mathfrak{b},1}(\mathcal{D})\|\theta\|_{\mathcal{W}^{1,\infty}}\|u\|^2_{L^2(\Omega)},\\
|r_{\mathfrak{b}}(\theta,u)| &\leqslant M_{\mathfrak{b},2}(\mathcal{D})\|\theta\|^2_{\mathcal{W}^{1,\infty}}\|u\|^2_{L^2(\Omega)}.
\end{aligned}$$

Using (3.57) and likewise the lower bound in (3.59), it follows that (3.62) holds with constants

$$\begin{aligned}
C_{\mathfrak{a},1}(\mathcal{D}) &= \frac{M_{\mathfrak{a},1}(\mathcal{D})}{\varepsilon_a(\overline{\mathcal{D}})m_V(\mathcal{D})(1-C_1(\mathcal{D})h_0)^2(1-C_3(\mathcal{D})h_0)}, \quad C_{\mathfrak{b},1}(\mathcal{D}) = \frac{M_{\mathfrak{b},1}(\mathcal{D})}{m_V(\mathcal{D})(1-C_3(\mathcal{D})h_0)},\\
C_{\mathfrak{a},2}(\mathcal{D}) &= \frac{M_{\mathfrak{a},2}(\mathcal{D})}{\varepsilon_a(\overline{\mathcal{D}})m_V(\mathcal{D})(1-C_1(\mathcal{D})h_0)^2(1-C_3(\mathcal{D})h_0)}, \quad C_{\mathfrak{b},2}(\mathcal{D}) = \frac{M_{\mathfrak{b},2}(\mathcal{D})}{m_V(\mathcal{D})(1-C_3(\mathcal{D})h_0)}.
\end{aligned}$$

At this point, we have obtained the necessary estimates casting the problem in the form treated in [152, 153], using abstract arguments of perturbation theory. We next largely follow the approach of these works, but nevertheless give a full proof below, not only for the sake of self-completeness but also because we require stronger intermediate regularity results than those obtained in [152] in order to prove the third item in Theorem 3.2.

Continuous Fréchet differentiability of the inverse operator. As previously noted, $\lambda_k(\Omega_\theta)$ is the reciprocal of the k-th largest eigenvalue of the operator

$$S(\theta) := A_\theta^{-1}B_\theta.$$

To obtain the results of Theorem 3.2, it is then sufficient to study the regularity of the eigenvalues of $\theta \mapsto S(\theta)$. Assuming these are Gateaux-semi-differentiable, in order to obtain the second item in Theorem 3.2, we may indeed write, for $0 \leqslant \ell < m$:

$$\frac{\mathrm{d}}{\mathrm{d}t}\lambda_{k+\ell}(\Omega_{t\theta})\Big|_{t=0^+} = -\lambda_k(\Omega)^2\,\frac{\mathrm{d}}{\mathrm{d}t}\frac{1}{\lambda_{k+\ell}(\Omega_{t\theta})}\Big|_{t=0^+}, \tag{3.64}$$

where one recognizes right-Gateaux-derivatives of the eigenvalues of S at 0 on the right-hand side of this equality. A similar observation holds for Fréchet-differentiability.

The first step is to show that $\theta \mapsto A_\theta^{-1}B_\theta$ is $\mathcal{C}^1$ in a $\mathcal{W}^{1,\infty}$-neighborhood of $\theta = 0$ for the $L^2_\beta(\Omega)$ operator norm.

From the estimates (3.62), it holds from the representation result [192, Lemma VI.3.1] that there exists $L^2(\Omega)$-bounded operator-valued maps $\theta \mapsto D^{(1)}_{A_0}\theta, R_{A_0}(\theta), D^{(1)}_{B_0}\theta, R_{B_0}(\theta) \in \mathcal{B}(L^2(\Omega))$ such that

$$\begin{aligned}
\mathrm{d}\mathfrak{a}_0(\theta)(u,v) &= \left\langle D^{(1)}_{A_0}\theta A_0^{1/2}u, A_0^{1/2}v\right\rangle, \qquad \mathrm{d}\mathfrak{b}_0(\theta)(u,v) = \left\langle D^{(1)}_{B_0}\theta B_0^{1/2}u, B_0^{1/2}v\right\rangle,\\
r_{\mathfrak{a}}(\theta,u,v) &= \left\langle R_{A_0}(\theta)A_0^{1/2}u, A_0^{1/2}v\right\rangle, \qquad r_{\mathfrak{b}}(\theta,u,v) = \left\langle R_{B_0}(\theta)B_0^{1/2}u, B_0^{1/2}v\right\rangle,
\end{aligned} \tag{3.65}$$

where $A_0^{1/2}$ is the positive self-adjoint operator defined on $\mathcal{D}(A_0^{1/2}) = H^1_0(\Omega)$ (the form domain

of A_0) by functional calculus, such that $A_0^{1/2}A_0^{1/2} = A_0$ on $\mathcal{D}(A_0)$, and where the bilinear forms $r_a(\theta,\cdot,\cdot)$, $r_b(\theta,\cdot,\cdot)$ are defined by polarization from the expressions (3.61). Moreover, the operators $D^{(1)}_{A_0}, D^{(1)}_{B_0}$ are clearly linear, and the bounds

$$\begin{aligned} \left\|D^{(1)}_{A_0}\theta\right\|_{\mathcal{B}(L^2(\Omega))} &\leqslant C_{\mathfrak{a},1}(\mathcal{D})\|\theta\|_{\mathcal{W}^{1,\infty}}, \qquad \left\|D^{(1)}_{B_0}\theta\right\|_{\mathcal{B}(L^2(\Omega))} \leqslant C_{\mathfrak{b},1}(\mathcal{D})\|\theta\|_{\mathcal{W}^{1,\infty}}, \\ \|R_{A_0}(\theta)\|_{\mathcal{B}(L^2(\Omega))} &\leqslant C_{\mathfrak{a},2}(\mathcal{D})\|\theta\|^2_{\mathcal{W}^{1,\infty}}, \quad \|R_{B_0}(\theta)\|_{\mathcal{B}(L^2(\Omega))} \leqslant C_{\mathfrak{b},2}(\mathcal{D})\|\theta\|^2_{\mathcal{W}^{1,\infty}} \end{aligned} \tag{3.66}$$

are satisfied uniformly inside $\mathcal{D}$, with the constants appearing in (3.62).

Let $f \in L^2(\Omega)$, and set

$$u := A_0^{-1/2}(\mathrm{Id} + D^{(1)}_{A_0} + R_{A_0}(\theta))^{-1}A_0^{-1/2}f \in \mathcal{D}(A_0^{1/2}),$$

where the inverse is well-defined for $\|\theta\|_{\mathcal{W}^{1,\infty}} < h_0$ sufficiently small, by the estimates (3.66). By the representation result [192, Theorem VI.3.1], it holds for any $v \in \mathcal{D}(A_0^{1/2}) = H^1_0(\Omega)$, that

$$a_\theta(u,v) = \left\langle (\mathrm{Id} + D^{(1)}_{A_0}\theta + R_{A_0}(\theta))A_0^{1/2}u, A_0^{1/2}v\right\rangle_{L^2(\Omega)} = \left\langle A_0^{-1/2}f, A_0^{1/2}v\right\rangle_{L^2(\Omega)} = \langle f, v\rangle_{L^2(\Omega)}\,.$$

By the representation theorem for symmetric positive closed forms [192, Theorem VI.2.1], it holds $u \in \mathcal{D}(A_\theta)$ and $A_\theta u = f$, whence

$$A_\theta^{-1} = A_0^{-1/2}\left(\mathrm{Id} + D^{(1)}_{A_0}\theta + R_{A_0}(\theta)\right)^{-1}A_0^{-1/2},$$

and writing the Neumann series expansion, it then holds that

$$A_\theta^{-1} = A_0^{-1/2}\left(\mathrm{Id} - D^{(1)}_{A_0}\theta\right)A_0{}^{-1/2} + \widetilde{R}_{A_0^{-1}}(\theta),$$

with quadratically bounded remainder: $\|\widetilde{R}_{A_0^{-1}}(\theta)\|_{\mathcal{B}(L^2(\Omega))} \leqslant C_{A_0,2}(\mathcal{D})\|\theta\|^2_{\mathcal{W}^{1,\infty}}$ uniformly inside $\mathcal{D}$ for some constant $C_{A_0,2}(\mathcal{D}) > 0$ and some operator-valued map $\widetilde{R}_{A_0^{-1}} : \mathcal{W}^{1,\infty} \to \mathcal{B}(L^2(\Omega))$. Since $D^{(1)}_{A_0}$ is controlled uniformly inside $\mathcal{D}$ in the $L^2(\Omega)$-operator norm, we only need to check that this is also the case for $A_0^{-1/2}$, but this follows from the lower bound (3.57), which is uniform inside $\mathcal{D}$.

Therefore, $\theta \mapsto A_\theta^{-1}$ is Fréchet-differentiable at $\theta = 0$, with

$$DA_0^{-1}\theta = -A_0^{-1/2}D^{(1)}_{A_0}\theta A_0^{-1/2}.$$

Since $\theta \mapsto B_\theta$ is Fréchet-differentiable at $\theta = 0$ from (3.66), the inverse operator $\theta \mapsto S(\theta)$ is also Fréchet-differentiable at $\theta = 0$, with

$$DS(0)\theta = -A_0^{-1/2}D^{(1)}_{A_0}\theta A_0^{-1/2}B_0 + A_0^{-1}B_0^{1/2}D^{(1)}_{B_0}\theta B_0^{1/2}, \tag{3.67}$$

and with quadratically bounded remainder:

$$S(\theta) = S(0) + DS(0)\theta + R_{S(0)}(\theta), \qquad \|R_{S(0)}(\theta)\|_{\mathcal{B}(L^2(\Omega))} \leqslant C_{S_0,2}(\mathcal{D})\|\theta\|^2_{\mathcal{W}^{1,\infty}} \tag{3.68}$$

uniformly inside $\mathcal{D}$ for some $C_{S_0,2}(\mathcal{D}) > 0$ and some operator-valued map $R_{S(0)} : \mathcal{W}^{1,\infty} \to \mathcal{B}(L^2(\Omega))$.

At this point, we note that, due to the uniformity of the estimates (3.57) and (3.63) inside $\mathcal{D}$, the same analysis shows that, for $\|\theta\|_{\mathcal{W}^{1,\infty}}$ sufficiently small, S is Fréchet differentiable at θ and the expansion

$$S(\theta+\delta\theta) = S(\theta)+DS(\theta)\delta\theta+R_{S(\theta)}(\delta\theta), \qquad \|R_{S(\theta)}(\delta\theta)\|_{\mathcal{B}(L^2(\Omega))} \leqslant C_{S_0,2}(\mathcal{D})\|\delta\theta\|^2_{\mathcal{W}^{1,\infty}}, \tag{3.69}$$

is valid, with crucially the same constant as in (3.68), and some other operator-valued map $R_{S(\theta)} : \mathcal{W}^{1,\infty} \to \mathcal{B}(L^2(\Omega))$.

Indeed, the previous argument applies upon replacing Ω by the bounded Lipschitz domain $\Omega_\theta \subset \mathcal{D}$ as long as $\|\Phi_{\delta\theta} \circ \Phi_\theta - \mathrm{Id}\|_{\mathcal{W}^{1,\infty}} < h_0$. A simple computation shows that $\|\Phi_{\delta\theta} \circ \Phi_\theta - \mathrm{Id}\|_{\mathcal{W}^{1,\infty}} \leqslant \|\theta\|_{\mathcal{W}^{1,\infty}} + \|\delta\theta\|_{\mathcal{W}^{1,\infty}} + \|\theta\|_{\mathcal{W}^{1,\infty}}\|\delta\theta\|_{\mathcal{W}^{1,\infty}}$, so that taking $\|\theta\|_{\mathcal{W}^{1,\infty}}, \|\delta\theta\|_{\mathcal{W}^{1,\infty}} < \sqrt{1+h_0} - 1$ suffices.

Therefore, upon further reducing h_0, we assume from now on that S is Fréchet-differentiable inside $B_{\mathcal{W}^{1,\infty}}(0, h_0)$. In fact, the uniformity with respect to θ of the remainder in (3.69) implies that S is $\mathcal{C}^1$ in a $\mathcal{W}^{1,\infty}$-neighborhood $\mathcal{N}_S$ of $\theta = 0$ for the $L^2(\Omega)$-operator norm, which we now show.

Let $\theta_1, \theta_2 \in \mathcal{W}^{1,\infty}(\mathbb{R}^d)$ be sufficiently small, and write $\theta_2 = \theta_1 + \delta\theta_1$. Additionally, take $w \in \mathcal{W}^{1,\infty}$ with $\|w\|_{\mathcal{W}^{1,\infty}} = 1$, and write $\delta\theta_2 = \|\delta\theta_1\|_{\mathcal{W}^{1,\infty}} w$. By the expansion (3.69), it holds

$$\begin{aligned} S(\theta_2 + \delta\theta_2) &= S(\theta_2) + DS(\theta_2)\delta\theta_2 + R_{S(\theta_2)}(\delta\theta_2), \\ S(\theta_2 + \delta\theta_2) &= S(\theta_1) + DS(\theta_1)(\delta\theta_1 + \delta\theta_2) + R_{S(\theta_1)}(\delta\theta_1 + \delta\theta_2). \end{aligned} \tag{3.70}$$

Substituting the further expansion

$$S(\theta_2) = S(\theta_1) + DS(\theta_1)\delta\theta_1 + R_{S(\theta_1)}(\delta\theta_1)$$

in the first line of (3.70), we find after simplification

$$[DS(\theta_2) - DS(\theta_1)]\,\delta\theta_2 = R_{S(\theta_1)}(\delta\theta_1 + \delta\theta_2) - R_{S(\theta_1)}(\delta\theta_1) - R_{S(\theta_2)}(\delta\theta_2).$$

Estimating the $L^2(\Omega)$-operator norm using (3.69), we find

$$\begin{aligned} \|\,[DS(\theta_2) - DS(\theta_1)]\,w\|_{L^2(\Omega)}\|\delta\theta_1\|_{\mathcal{W}^{1,\infty}} &\leqslant C_{S_0,2}\left(\|\delta\theta_1 + \delta\theta_2\|^2_{\mathcal{W}^{1,\infty}} + \|\delta\theta_1\|^2_{\mathcal{W}^{1,\infty}} + \|\delta\theta_2\|^2_{\mathcal{W}^{1,\infty}}\right) \\ &\leqslant 6C_{S_0,2}\|\delta\theta_1\|^2_{\mathcal{W}^{1,\infty}}, \end{aligned}$$

since $\|\delta\theta_1\|_{\mathcal{W}^{1,\infty}} = \|\delta\theta_2\|_{\mathcal{W}^{1,\infty}}$ and therefore $\|\delta\theta_1 + \delta\theta_2\|_{\mathcal{W}^{1,\infty}} \leqslant 2\|\delta\theta_1\|_{\mathcal{W}^{1,\infty}}$. Therefore,

$$\|[DS(\theta_2) - DS(\theta_1)]w\|_{L^2(\Omega)} \leqslant 6C_{S_0,2}\|\theta_2 - \theta_1\|_{\mathcal{W}^{1,\infty}},$$

which, upon taking the supremum over $\{w \in \mathcal{W}^{1,\infty}, \|w\|_{\mathcal{W}^{1,\infty}} = 1\}$, shows that DS is Lipschitz (and in particular continuous) for the $L^2(\Omega)$-operator norm in a $\mathcal{W}^{1,\infty}$-neighborhood of $\theta = 0$.

We now show the first item in Theorem 3.2. We have already proved that $\theta \mapsto S(\theta)$ and $\theta \mapsto B(\theta)$ are C^1 in a $\mathcal{W}^{1,\infty}$-neighborhood of $\theta = 0$. From the bounds (3.59), the same

regularity holds for $\theta \mapsto B(\theta)^{\pm 1/2}$. Therefore, the map

$$\begin{cases} \mathcal{W}^{1,\infty}(\mathbb{R}^d) \to \mathcal{K}_{\mathrm{sa}}(L^2(\Omega)) \\ \qquad\qquad \theta \mapsto B_\theta^{1/2} S(\theta) B_\theta^{-1/2} \end{cases}$$

is $\mathcal{C}^1$, at $\theta = 0$, hence Lipschitz on some neighborhood $\widetilde{\mathcal{N}_S} \subset \mathcal{W}^{1,\infty}$ of 0, where $\mathcal{K}_{\mathrm{sa}}(L^2(\beta))$ denotes the subspace of compact self-adjoint operators in $\mathcal{B}(L^2(\Omega))$.

A well-known consequence of the Courant–Fischer principle (the so-called Weyl perturbation inequality, see for example [314, Section 1.3.3] for the analogous case of Hermitian matrices) implies that, given a Hilbert space $\mathcal{H}$, for any $j \geqslant 1$, the eigenvalue map

$$\begin{cases} \mathcal{K}_{\mathrm{sa}}(\mathcal{H}) \to \mathbb{R} \\ \qquad A \mapsto \mu_j(A) \end{cases}$$

is 1-Lipschitz in the $\mathcal{H}$-operator norm, where $\mu_k(A)$ denotes the k-th largest eigenvalue of A (counted with multiplicity). By composition, for any $j \geqslant 1$, the map $\theta \mapsto \mu_j(B_\theta^{1/2} S(\theta) B_\theta^{-1/2}) = \mu_j(S(\theta))$ is also Lipschitz on $\widetilde{\mathcal{N}_S}$. The claim then easily follows since $\theta \mapsto (\lambda_{k+\ell}(\Omega_\theta))_{0 \leqslant \ell < m} = (1/\mu_{k+\ell}(S(\theta)))_{0 \leqslant \ell < m}$ with $\mu_{k+\ell}(S(\theta)) > 0$ for any θ, and the map $x \mapsto (1/x_i)_{1 \leqslant i \leqslant m}$ is locally Lipschitz on $(0, +\infty)^m$.

From now on we view $S(\theta)$, for $\theta \in \mathcal{W}^{1,\infty}$ sufficiently small, as an operator on $L^2_\beta(\Omega)$, stressing that, in this setting, $S(0)$ is a compact self-adjoint operator, although for $\theta \neq 0$, these operators are generally non-symmetric, but still compact with real spectrum (since the $S(\theta)$ are conjugate to self-adjoint operators on $L^2(\Omega)$).

Finite-dimensional reduction around eigenvalues clusters. We recall that, by assumption, $\lambda_k(\Omega)$ has multiplicity $m \geqslant 1$. By compactness of the family $S(\theta)$ and the continuity of its eigenvalues, there exists a complex, positively oriented contour $\Gamma : [0,1] \to \mathbb{C}$ separating $1/\lambda_k(\Omega)$ from the eigenvalues of $S(0)$ different from $1/\lambda_k(\Omega)$, and $h_0 > 0$ such that, for any $\theta \in B_{\mathcal{W}^{1,\infty}}(0, h_0)$, $S(\theta)$ has exactly m eigenvalues inside Γ, counted with multiplicity. We denote the Riesz projector by

$$\Pi_\theta = -\frac{1}{2\mathrm{i}\pi} \int_\Gamma \mathcal{R}_\zeta(\theta)\, \mathrm{d}\zeta, \tag{3.71}$$

where we define the resolvent of $S(\theta)$ as

$$\mathcal{R}_\zeta(\theta) = (S(\theta) - \zeta)^{-1} = B_\theta^{-1}(A_\theta^{-1} - \zeta B_\theta^{-1})^{-1}.$$

Note that Π_θ is a projector onto the $S(\theta)$-invariant subspace

$$\mathrm{Span}\left\{u_{k+\ell}(\Omega_\theta), 0 \leqslant \ell < m\right\},$$

and is $L^2_\beta(\Omega)$-orthogonal when $\theta = 0$. We next show that $\theta \mapsto \Pi_\theta$ is $\mathcal{C}^1$ in a $\mathcal{W}^{1,\infty}$-neighborhood of $\theta = 0$ for the $L^2_\beta(\Omega)$-operator norm.

By continuity of the eigenvalues of $S(\theta)$ with respect to θ, we may choose h_0 sufficiently

small and $C(\mathcal{D}) > 0$ so that, uniformly inside $\mathcal{D}$ and for all $\zeta \in \Gamma$, it holds

$$\|\mathcal{R}_\zeta(\theta)\|_{\mathcal{B}(L^2(\Omega))} \leqslant C(\mathcal{D}). \tag{3.72}$$

We furthermore assume h_0 to be sufficiently small so that the expansion (3.69) holds. Let $\theta, \delta\theta \in B_{\mathcal{W}^{1,\infty}}(0, h_0)$. The second resolvent identity states that, for any $\zeta \in \Gamma$,

$$\mathcal{R}_\zeta(\theta + \delta\theta) - \mathcal{R}_\zeta(\theta) = \mathcal{R}_\zeta(\theta + \delta\theta)(S(\theta) - S(\theta + \delta\theta))\mathcal{R}_\zeta(\theta),$$

so that, rearranging, we obtain

$$\mathcal{R}_\zeta(\theta) = \mathcal{R}_\zeta(\theta + \delta\theta)\left(\mathrm{Id} + [S(\theta + \delta\theta) - S(\theta)]\,\mathcal{R}_\zeta(\theta)\right),$$

whence, for $\|S(\theta + \delta\theta) - S(\theta)\|_{\mathcal{B}(L^2(\Omega))} \leqslant \|\mathcal{R}_\zeta(\theta)\|^{-1}_{\mathcal{B}(L^2(\Omega))}$, we have the expression

$$\mathcal{R}_\zeta(\theta + \delta\theta) = \mathcal{R}_\zeta(\theta)\left(\sum_{k=0}^{\infty}(-1)^k\left[(S(\theta + \delta\theta) - S(\theta))\,\mathcal{R}_\zeta(\theta)\right]^k\right).$$

Then, by the expansion (3.69) and the uniform bound (3.72), one can find $h_0, K(\mathcal{D}) > 0$ such that, uniformly inside $\mathcal{D}$, and for any $\zeta \in \Gamma$, $\delta\theta \in \mathcal{W}^{1,\infty}$ with $\|\theta + \delta\theta\|_{\mathcal{W}^{1,\infty}} < h_0$, it holds

$$\mathcal{R}_\zeta(\theta + \delta\theta) = \mathcal{R}_\zeta(\theta) - \mathcal{R}_\zeta(\theta)DS(\theta)\delta\theta\mathcal{R}_\zeta(\theta) + Q(\theta, \delta\theta, \zeta), \quad \|Q(\theta, \delta\theta, \zeta)\| \leqslant K(\mathcal{D})\|\delta\theta\|^2_{\mathcal{W}^{1,\infty}}.$$

Therefore $\mathcal{R}_\zeta$ is Fréchet-differentiable at θ, and its Fréchet derivative is given by $D\mathcal{R}_\zeta(\theta)\delta\theta = -\mathcal{R}_\zeta(\theta)DS(\theta)\delta\theta\mathcal{R}_\zeta(\theta)$, which is continuous in θ in a $\mathcal{W}^{1,\infty}$-neighborhood of $\theta = 0$ for the $L^2_\beta(\Omega)$-operator norm, owing to the $\mathcal{C}^1$-regularity of S and the continuity of $\mathcal{R}_\zeta$. By dominated convergence in (3.71) using the bound (3.72) and the fact that $DS(\theta)$ is bounded in the $L^2_\beta(\Omega)$-operator norm uniformly inside $\mathcal{D}$, it follows that $\theta \mapsto \Pi_\theta$ is also $\mathcal{C}^1$ in the $L^2_\beta(\Omega)$-operator norm in a $\mathcal{W}^{1,\infty}$-neighborhood of $\theta = 0$. We denote its Fréchet derivative by $\delta\theta \mapsto D\Pi_\theta\delta\theta$.

The last key step is to connect the invariant m-dimensional subspaces $\Pi_\theta L^2_\beta(\Omega)$ and $\Pi_0 L^2_\beta(\Omega)$ via a linear isomorphism which is Fréchet differentiable with respect to θ at $\theta = 0$. This will allow to relate eigenvalue variations of $S(\theta)$ to those of a conjugated operator $\widehat{S}(\theta)$ acting on the fixed m-dimensional Hilbert space $\Pi_0 L^2_\beta(\Omega)$ on which perturbation results are readily available. This follows the general construction discussed in [192, Section I.4.6] for continuous families of projectors, to which we refer for additional details. Introduce the bounded operators

$$Q(\theta) = (\Pi_\theta - \Pi_0)^2, \qquad U(\theta) = (\Pi_\theta\Pi_0 + (\mathrm{Id} - \Pi_\theta)(\mathrm{Id} - \Pi_0))\,(\mathrm{Id} - Q(\theta))^{-1/2},$$

where $(\mathrm{Id} - Q(\theta))^{-1/2}$ can be defined via the following expansion for $\|\Pi_\theta - \Pi_0\| < 1$:

$$(\mathrm{Id} - Q(\theta))^{-1/2} = \sum_{k=0}^{\infty}\binom{-1/2}{k}(-Q(\theta))^k.$$

Note that $U(0) = \mathrm{Id}$. The definition of $U(\theta)$ is motivated by the observation

$$C_{\theta,0}D_{0,\theta} = C_{\theta,0}D_{0,\theta} = \mathrm{Id} - Q(\theta),$$

where

$$C_{\theta,0} = \Pi_0\Pi_\theta + (\mathrm{Id} - \Pi_0)(\mathrm{Id} - \Pi_\theta) : \Pi_\theta L^2_\beta(\Omega) \to \Pi_0 L^2_\beta(\Omega),$$

and $D_{0,\theta}$ is the analogous operator obtained by exchanging the roles of θ and 0 in the definition of $C_{\theta,0}$. Simple computations (see also the discussion in [192, Section I.4.6]) then show that $U(\theta) : \Pi_\theta L^2_\beta(\Omega) \to \Pi_0 L^2_\beta(\Omega)$ is an isomorphism, and that Π_θ, Π_0 are conjugated via

$$\Pi_\theta = U(\theta)^{-1}\Pi_0 U(\theta), \qquad \text{where } U(\theta)^{-1} = (\Pi_0\Pi_\theta + (\mathrm{Id} - \Pi_0)(\mathrm{Id} - \Pi_\theta))\,(\mathrm{Id} - Q(\theta))^{-1/2}. \tag{3.73}$$

Setting

$$\widehat{S}(\theta) = U(\theta)S(\theta)U(\theta)^{-1},$$

it holds, since Π_θ commutes with $S(\theta)$ and $U(\theta)$ is bijective, that

$$\widehat{S}(\theta)\Pi_0 L^2_\beta(\Omega) \subset \Pi_0 L^2_\beta(\Omega),$$

so that $\widehat{S}(\theta)|_{\Pi_0 L^2_\beta(\Omega)}$ is a well-defined linear map. The bounded operator $S(\theta)|_{\Pi_\theta L^2_\beta(\Omega)}$ is diagonalizable, as it is conjugate to the operator

$$B_\theta^{1/2} S(\theta) B_\theta^{-1/2}\Big|_{B_\theta^{1/2}\Pi_\theta L^2_\beta(\Omega)},$$

which is self-adjoint for the $L^2(\Omega)$ inner product. Therefore, the conjugate operator $\widehat{S}(\theta)|_{\Pi_0 L^2_\beta(\Omega)}$ is also diagonalizable, and the spectra of these two operators are identical, counting with multiplicity.

Moreover, due to the $\mathcal{C}^1$ regularity of $\theta \mapsto \Pi_\theta$, the map $U(\theta)$ is also $\mathcal{C}^1$ in a $\mathcal{W}^{1,\infty}$-neighborhood of $\theta = 0$, and since $DQ(0) = 0$, it also holds $D(\mathrm{Id} - Q(\theta))^{-1/2}\big|_{\theta=0} = 0$, whence

$$DU(0)\theta = (D\Pi_0\theta)\,\Pi_0 - (D\Pi_0\theta)\,(\mathrm{Id} - \Pi_0) = 2\,(D\Pi_0\theta)\,\Pi_0 - D\Pi_0\theta = 0,$$

since the last expression is the Fréchet differential of $\Pi_\theta^2 - \Pi_\theta = 0$ at $\theta = 0$. Similarly, $DU^{-1}(0)\theta = 0$, so that $\theta \mapsto \widehat{S}(\theta)$ is $\mathcal{C}^1$ as a map $\mathcal{W}^{1,\infty}(\mathbb{R}^d;\mathbb{R}^d) \to \mathcal{B}(\Pi_0 L^2_\beta(\Omega))$ in a $\mathcal{W}^{1,\infty}$-neighborhood of $\theta = 0$, with

$$D\widehat{S}(0)\theta = DS(0)\theta.$$

We stress that $\Pi_0 L^2_\beta(\Omega)$ is a m-dimensional vector space, on which $\widehat{S}(\theta)$ defines a $\mathcal{C}^1$-family of diagonalizable endomorphisms. In particular, for fixed $\theta \in \mathcal{W}^{1,\infty}$, there exists $t_\theta > 0$ such that the map $t \mapsto \widehat{S}(t\theta)|_{\Pi_0 L^2_\beta(\Omega)}$ is differentiable on $(-t_\theta, t_\theta)$, so that from finite-dimensional perturbation theory (see [192, Section II.5.4, Theorem 5.4 and Remark 5.5 and Section II.5.5, Theorem 5.6]), and since $1/\lambda_k(\Omega)$ is semisimple in the sense of [192, Section I.4] (as $\widehat{S}(0)$ is diagonalizable on $\Pi_0 L^2_\beta(\Omega)$), there exist m maps $(\mu_\ell)_{1\leqslant\ell\leqslant m}$, differentiable on $(-t_\theta, t_\theta)$ and satisfying (3.13), such that

$$\forall\, 1 \leqslant \ell \leqslant m, \qquad \mu_\ell'(0) \in \mathrm{Spec}\,(\Pi_0 DS(0)\theta\Pi_0)\,,$$

where $\Pi_0 DS(0)\theta\Pi_0$ is viewed as a linear map on $\Pi_0 L^2_\beta(\Omega)$.

Computation of the Gateaux derivatives. It remains to show the formula (3.14). This reduces to computing the components of the matrix representation of $\Pi_0 DS(0)\theta\Pi_0$ for the $L^2_\beta(\Omega)$ scalar product, in the given $L^2_\beta(\Omega)$-orthonormal basis $\left\{u_k^{(\ell)}(\Omega),\, 1 \leqslant \ell \leqslant m\right\}$. For convenience, we denote by

$$\forall 1 \leqslant \ell \leqslant m, \qquad u_\ell = u_k^{(\ell)}(\Omega), \qquad \text{and} \qquad \lambda = \lambda_k(\Omega).$$

Recall the relation (3.64). Setting

$$M_{ij}(\theta) = -\lambda^2 \left\langle \Pi_0 DS(0)\theta\Pi_0 u_i, u_j \right\rangle_{L^2_\beta(\Omega)},$$

and using (3.67), we find, since Π_0 is $L^2_\beta(\Omega)$-self-adjoint and $\Pi_0 u_i = u_i$ for each $1 \leqslant i \leqslant m$,

$$\begin{aligned}
\left\langle \Pi_0 DS(0)\theta\Pi_0 u_i, u_j \right\rangle_{L^2_\beta(\Omega)} &= \left\langle DS(0)\theta\Pi_0 u_i, \Pi_0 u_j \right\rangle_{L^2_\beta(\Omega)} \\
&= \left\langle B_0 DS(0)\theta u_i, u_j \right\rangle_{L^2(\Omega)} \\
&= \left\langle B_0 \left(-A_0^{-1/2} D^{(1)}_{A_0}\theta A_0^{-1/2} B_0 + A_0^{-1} B_0^{1/2} D^{(1)}_{B_0}\theta B_0^{1/2} \right) u_i, u_j \right\rangle_{L^2(\Omega)} \\
&= \left\langle \left(-A_0^{1/2} D^{(1)}_{A_0}\theta A_0^{1/2} A_0^{-1} B_0 + B_0^{1/2} D^{(1)}_{B_0}\theta B_0^{1/2} \right) u_i, A_0^{-1} B_0 u_j \right\rangle_{L^2(\Omega)} \\
&= -\lambda^{-2} \left\langle A_0^{1/2} D^{(1)}_{A_0}\theta A_0^{1/2} u_i, u_j \right\rangle_{L^2(\Omega)} + \lambda^{-1} \left\langle B_0^{1/2} D^{(1)}_{B_0}\theta B_0^{1/2} u_i, u_j \right\rangle_{L^2(\Omega)},
\end{aligned}$$

taking adjoints of the $L^2(\Omega)$-self-adjoint operators A_0^{-1}, B_0 in the fourth line, and using the eigenrelation $A_0^{-1} B_0 u_i = u_i/\lambda$ for all $1 \leqslant i \leqslant m$ in the last line. It follows that

$$\begin{aligned}
M_{ij}(\theta) &= \left\langle A_0^{1/2} D^{(1)}_{A_0}\theta A_0^{1/2} u_i, u_j \right\rangle_{L^2(\Omega)} - \lambda \left\langle B_0^{1/2} D^{(1)}_{B_0}\theta B_0^{1/2} u_i, u_j \right\rangle_{L^2(\Omega)} \\
&= \mathrm{d}\mathfrak{a}_0(\theta)(u_i, u_j) - \lambda \mathrm{d}\mathfrak{b}_0(\theta)(u_i, u_j),
\end{aligned}$$

where we used the representation formulas (3.65). Substituting in the expressions for the first-order perturbations (3.60) finally yields (3.14).

Fréchet differentiability for simple eigenvalues. We now assume that $\lambda_k(\Omega)$ is a simple eigenvalue. For $\|\theta\|_{\mathcal{W}^{1,\infty}}$ sufficiently small, it holds from the conjugation (3.73) that $\operatorname{rank}\Pi_\theta = 1$, and

$$\frac{1}{\lambda_k(\Omega_\theta)} = \left\langle \widehat{S}(\theta) u_k(\Omega), u_k(\Omega) \right\rangle_{L^2_\beta(\Omega)}.$$

Since $\theta \mapsto \widehat{S}(\theta)$ is $\mathcal{C}^1$ in a $\mathcal{W}^{1,\infty}$-neighborhood of $\theta = 0$ and $\lambda_k(\Omega) > 0$, the map $\theta \mapsto \lambda_k(\Omega_\theta)$ is also $\mathcal{C}^1$ in a $\mathcal{W}^{1,\infty}$-neighborhood of $\theta = 0$ by the chain rule. A closed-form for the Fréchet derivative $D\lambda_k(\Omega_0)\theta$ at $\theta = 0$ is then given by $M_{11}(\theta)$, or by the boundary form

$$D\lambda_k(\Omega_0)\theta = -\frac{1}{\beta} \int_{\partial\Omega} \left(\frac{\partial u_k(\Omega)}{\partial \mathrm{n}} \right)^2 \mathrm{n}^\top a \mathrm{n} \theta^\top \mathrm{n}\, \mathrm{e}^{-\beta V}$$

in the case $\partial\Omega$ is $\mathcal{C}^{1,1}$ or if Ω is convex, as in Corollary 3.4. □

Appendix 3.B: The Parallel Replica algorithm and its efficiency.

In this appendix, we motivate the shape-optimization objective 3.8 by discussing its relevance to a class of accelerated MD methods, the so-called Parallel Replica class of algorithms.

The maximization of (3.7) is motivated by algorithms in accelerated molecular dynamics, where the separation of timescales is key in ensuring the efficiency of the Parallel Replica method (ParRep); see [305, Section 6.2] or [268, Section 2.7], where the authors already discuss the influence of the domain definition on the metric (3.7). In this context, the quantity defined in (3.7) is called the scalability metric, and is directly related to the efficiency of ParRep [334]. While many ParRep-like methods have been proposed (see for instance [325, 42, 12, 266]), we present in this section one of the simplest versions, for which the objective of maximizing (3.7) with respect to Ω is most easily motivated.

At its core, ParRep provides a way, given a metastable domain $\Omega \subset \mathbb{R}^d$, to trade some details of the dynamics inside Ω against a kinetically correct sample of the exit from Ω (in the sense that both the exit time and the exit point are unbiased), coming at a lower cost in wall-clock time, using parallel computing resources. Given a good coverage of the configuration space by a set of good metastable states $(\Omega_\alpha)_{\alpha \in I}$, one can then effectively parallelize in time the sampling of a long, spatially coarse-grained trajectory.

A major advantage of ParRep compared to other accelerated MD methods (see [332, 312]) is that it is largely agnostic to the form of the dynamics and therefore applies to a wide range of Markov processes. The theoretical justification of the method, however, requires proving the existence and uniqueness of the QSD, see [206, 275] for results on the Langevin dynamics in the overdamped and underdamped settings, respectively.

We now describe the Parallel Replica method. While the original formulation [334] of the algorithm used disjoint metastable states, defined as basins of attraction for the steepest descent dynamics on the energy landscape, we formulate a variant which is more general, in the sense that it accommodates metastable states which may overlap, and whose union does not necessarily cover the whole configuration space.

We first introduce a number of hyperparameters.

Parameter	**Description**
$N_{\text{proc}} \in \mathbb{N}^*$	the number of replicas,
$(\Omega_i)_{i \in I}$,	a set of metastable states, and for each $i \in I$:
$\mathcal{C}_i \subset \Omega_i$,	an associated core-set,
$t_{\text{corr}}(\Omega_i) > 0$,	a decorrelation timescale, and
$t_{\text{phase}}(\Omega_i) > 0$	a dephasing timescale.

Input parameters for Algorithm 3.18.

We assume that the core-sets are pairwise disjoint:

$$\forall\, i, j \in I,\ i \neq j, \qquad \mathcal{C}_i \cap \mathcal{C}_j = \varnothing.$$

This condition ensures that there is no ambiguity as to which state is entered in step **A** of the algorithm below.

Algorithm 3.18 (ParRep with rejection and core-sets.)**.** *The algorithm proceeds by iterating the following steps:*

A *Initialization: run the dynamics until it enters a core-set $\mathcal{C}_i$, at time t_0, for some $i \in I$. Denote $\tau = \inf\{t \geqslant t_0 : X_t \notin \Omega_i\}$ the next exit time from the corresponding state Ω_i.*

B1 *Decorrelation (successful case): if the dynamics remains for a time $t_{\mathrm{corr}}(\Omega_i)$ inside Ω_i, it is presumed to be distributed according to the QSD ν^i in Ω_i. This introduces a bias, but which decays quickly with $t_{\mathrm{corr}}(\Omega_i)$ according to (3.6), provided $\lambda_2(\Omega_i) - \lambda_1(\Omega_i)$ is large.*

B2 *Decorrelation (unsuccessful case): if the dynamics exits at $\tau < t_0 + t_{\mathrm{corr}}(\Omega_i)$, record the exit event (τ, X_τ), and proceed from step* **A**.

C *Dephasing: Simulate N_{proc} independent copies $\left(X^{(i)}\right)_{1 \leqslant i \leqslant N_{\mathrm{proc}}}$ of the dynamics starting from $X_0^{(i)} = X_{t_0 + t_{\mathrm{corr}}(\Omega_i)}$, for a time $t_{\mathrm{phase}}(\Omega_i) > 0$.*

D *Conditioning: reject replicas which exited Ω_i during step* **C**. *Denote by $N \leqslant N_{\mathrm{proc}}$ the random variable counting the number of surviving replicas.*
The $(X^{(i)}_{t_{\mathrm{phase}}(\Omega_i)})_{1 \leqslant i \leqslant N}$ are now presumed to be i.i.d. according to ν^i. Again, this is correct up to some bias decaying quickly with $t_{\mathrm{phase}}(\Omega_i)$.

E *Parallel exit: evolve the N replicas independently until the first exits from Ω_i, say $X^{(j)}_{\tau^{(j)}} \notin \Omega_i$, i.e. $\tau^{(j)} = \min\limits_{1 \leqslant i \leqslant N} \tau^{(j)}$. According to the property (3.5), the equality*

$$\left(t_0 + t_{\mathrm{corr}}(\Omega_i) + N\left[\tau^{(j)} - t_{\mathrm{phase}}(\Omega_i)\right], X^{(j)}_{\tau^{(j)}}\right) \overset{\text{law}}{=} (\tau, X_\tau)$$

holds in law.

F *Set $X_{t_0 + t_{\mathrm{corr}}(\Omega_i) + N(\tau^{(j)} - t_{\mathrm{phase}}(\Omega_i))} = X^{(j)}_{\tau^{(j)}}$ and proceed from step* **A**.

Let us make a few remarks about Algorithm 3.18. Steps **C** and **E** can be run on a parallel computer with N_{proc} processors. Assuming synchronized MD engines, these two steps therefore only cost $t_{\mathrm{phase}}(\Omega_i)$ and $\tau^{(j)} - t_{\mathrm{phase}}(\Omega_i)$ respectively in wall-clock time. Since $\tau^{(j)} - t_{\mathrm{phase}}(\Omega_i) \sim \mathcal{E}(N/\lambda_1(\Omega_i))$ conditionally on N, this provides to a large acceleration if N is large, at the cost of an overhead $t_{\mathrm{phase}}(\Omega_i)$ in step **C**, which does not correspond to a physical time evolution.

Because exit events sampled during step **B2** are driven by the original dynamics, they are unbiased. Therefore, ParRep differs from other accelerated MD methods in that it correctly samples the full distribution of exit events, including those corresponding to short, correlated exit times.

Step **B** can also be performed in parallel to step **C**, and this is often done in practice. In this variant of Algorithm 3.18, the replicas are initialized at $X_0^{(i)} = X_{t_0}$ for $1 \leqslant i \leqslant N_{\mathrm{proc}}$, and one usually chooses $t_{\mathrm{corr}}(\Omega_i) = t_{\mathrm{phase}}(\Omega_i)$. Moreover, in the case **B2**, the exit of the reference dynamics Ω_i kills the replicas running in step **C**.

The path obtained by concatenating the segments

$$(X_t)_{t_0 \leqslant t < t_0 + t_{\mathrm{corr}}(\Omega_i)}, \left\{ (X_t^{(i)})_{t \leqslant t_{\mathrm{phase}}(\Omega_i) < \tau^{(j)}},\ 1 \leqslant j \leqslant N \right\} \text{ and } (X_t^{(j)})_{t_{\mathrm{phase}}(\Omega_i) \leqslant t < \tau^{(j)}}$$

has, in law, the same length as the path $(X_t)_{t_0 \leqslant t < \tau}$ under the sequential dynamics (neglecting the bias in steps **B** and **C**). Therefore, Algorithm 3.18 can be understood as sampling a discontinuous modification to the original dynamics, which jumps N times from ν^i to ν^i in the quasi-stationary portion $(X_t)_{t_0 + t_{\mathrm{corr}}(\Omega_i) \leqslant t < \tau}$ of the trajectory.

The core-set $\mathcal{C}_i$ encode how one defines an *entrance* into Ω_i, while the set Ω_i encodes how one defines an *exit* from Ω_i. We argue that the latter is the most important parameter as it impacts all the steps **B**–**E**, with $\mathcal{C}_i$ is only involved in step **A**. The sets $\mathcal{C}_i$ can be defined using physical intuition. In our numerical experiments (see Section 3.5.3 below), we consider two natural definitions of these core-sets, namely small balls around free energy minima, or the intersection of the associated free energy basin with the state Ω_i. An outstanding question, which we leave for future work, is whether one can *optimize* the definition of the core-sets $\mathcal{C}_i$, given definitions for the states Ω_i, to make Algorithm 3.18 efficient. Heuristically, the set $\bigcup_{i \in I} \mathcal{C}_i$ should be visited often by the dynamics, and starting from $\partial \mathcal{C}_i$, convergence to ν^i should be both likely and fast (so as to minimize the time spent in step **B**). This question is related to the minimization of the pre-exponential factor in the error estimate (3.6).

A pathology may occur in the event no replica survives in step **C**. This possibility can be assumed to be rare provided Ω_i is locally metastable and N_{proc} is large, for reasonable choices of $\mathcal{C}_i$. Nevertheless, the rejection sampling performed in step **D** can be replaced by a branching mechanism known as the Fleming–Viot process (see Algorithm 3.16 below), which has the advantage of ensuring $N = N_{\mathrm{proc}}$ replicas survive, at the cost of introducing additional (small) correlations between replicas at the end of step **D**, which therefore induces some bias in step **E**.

Crucial hyperparameters are the decorrelation times $t_{\mathrm{corr}}(\Omega_i)$, and dephasing times $t_{\mathrm{phase}}(\Omega_i)$ for $i \in I$. These should be valid, in the sense that the bias introduced in step **B** and the correlations between replicas in step **C** should be small, but setting $t_{\mathrm{corr}}(\Omega_i)$, $t_{\mathrm{phase}}(\Omega_i)$ to large values will lead to excessive spending of wall-clock time in these two steps, leading to an overall decrease in the achieved speedup. A simple choice is to set

$$t_{\mathrm{corr}}(\Omega_i) = t_{\mathrm{phase}}(\Omega_i) = -\log \varepsilon_{\mathrm{corr}} / (\lambda_2(\Omega_i) - \lambda_1(\Omega_i)) \tag{3.74}$$

where $0 < \varepsilon_{\mathrm{corr}} < 1$ is a small, domain-independent tolerance parameter. This choice, which has already been suggested (see [305, 268]), is motivated by taking logarithms in the estimate (3.6), and neglecting the contribution $|\log C(x)|/(\lambda_2(\Omega_i) - \lambda_1(\Omega_i))$ to the bias coming from the prefactor, which depends on the initial condition x. The choice (3.74) also motivates the need for quantitative estimates of the spectral gap $\lambda_2(\Omega_i) - \lambda_1(\Omega_i)$, for which various strategies have been proposed, see [50, Section 3.3] for recent results in this direction.

Let us fix $i \in I$, and compare the expected wall clock-time to sample a metastable excursion inside Ω_i using Algorithm 3.18 to the expected wall-clock time using a sequential simulation. We assume successful decorrelation in step **B**, rejection sampling in step **C** and the choice (3.74) where $0 < \varepsilon_{\mathrm{corr}} < 1$ is sufficiently small so that the bias and correlations introduced in steps

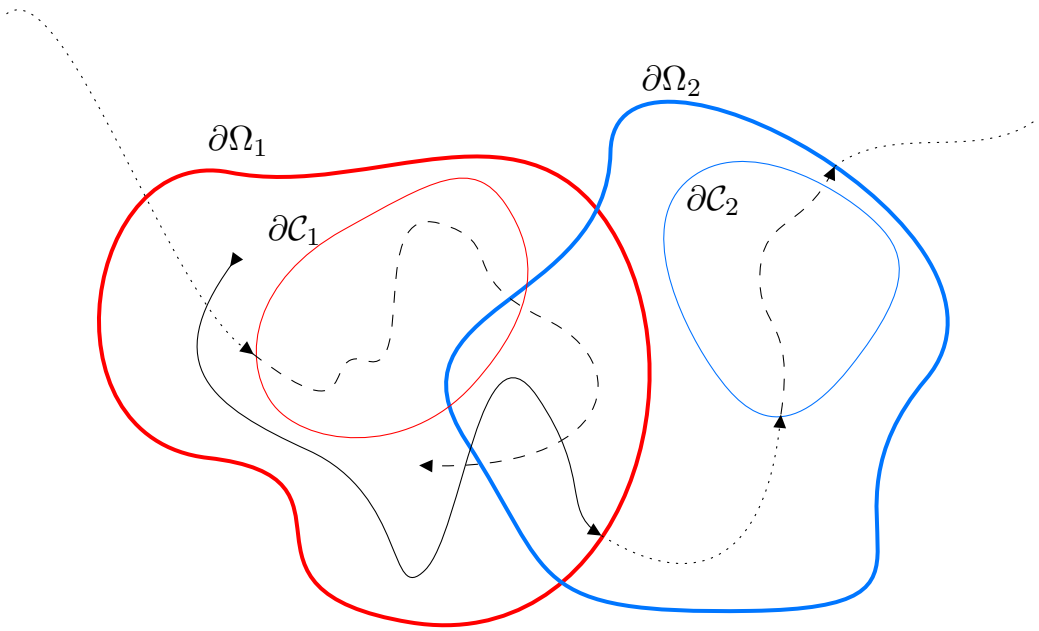

Figure 3.20: A trajectory sampled using Algorithm 3.18. Dotted lines correspond to step **A**, dashed lines to step **B**: a successful decorrelation **B1** in Ω_1, followed by a failed decorrelation **B2** in Ω_2. The solid line corresponds to the trajectory $(X_t^{(j)})_{t_{\mathrm{phase}}(\Omega_1)\leqslant t<\tau^{(j)}}$ in step **E**. The discontinuity hides a (parallel) time evolution of length $(N-1)(\tau^{(j)}-t_{\mathrm{phase}}(\Omega_1))$ in step **D**.

B1 and **C** can be safely neglected. By (3.5), we have $\mathbb{E}_\nu[N]=\mathrm{e}^{-\lambda_1(\Omega_i)t_{\mathrm{phase}}(\Omega_i)}N_{\mathrm{proc}}$ expected replicas at the end of step **C**, i.i.d. according to the QSD. Replacing N by its expected value under ν (and making a so-called annealed approximation in doing so), the expected wall-clock time in step **E** is given by $\mathrm{e}^{\lambda_1(\Omega_i)t_{\mathrm{phase}}(\Omega_i)}/(\lambda_1(\Omega_i)N_{\mathrm{proc}})$, by standard properties of exponential random variables. Therefore, the combined wall-clock time in steps **B1**–**E** is given by

$$t_{\mathrm{PR}}^{\mathbf{B1}\text{–}\mathbf{E}}(\Omega_i)=t_{\mathrm{corr}}(\Omega_i)+t_{\mathrm{phase}}(\Omega_i)+\mathrm{e}^{\lambda_1(\Omega_i)t_{\mathrm{phase}}(\Omega_i)}/(\lambda_1(\Omega_i)N_{\mathrm{proc}}).$$

The second term accounts for the overhead of simulating N trajectories in step B., which can be done in parallel. By contrast, the expected wall-clock time to simulate the same process using direct simulation is given by

$$t_{\mathrm{DNS}}^{\mathbf{B1}\text{–}\mathbf{E}}(\Omega_i)=t_{\mathrm{corr}}(\Omega_i)+1/\lambda_1(\Omega_i).$$

Recalling the definition (3.7) of $N^*(\Omega_i)$, substituting in the definition (3.74) and rearranging, we find

$$\frac{t_{\mathrm{DNS}}^{\mathbf{B1}\text{–}\mathbf{E}}(\Omega)}{t_{\mathrm{PR}}^{\mathbf{B1}\text{–}\mathbf{E}}(\Omega_i)}=\frac{N^*(\Omega_i)-\log\varepsilon_{\mathrm{corr}}}{(N^*(\Omega_i)/N_{\mathrm{proc}})\mathrm{e}^{-(\log\varepsilon_{\mathrm{corr}})/N^*(\Omega_i)}-2\log\varepsilon_{\mathrm{corr}}}. \tag{3.75}$$

One can check that the right-hand side of (3.75) is an increasing function of $N^*(\Omega_i)$ for $N_{\mathrm{proc}}>0$ and $0<\varepsilon_{\mathrm{corr}}<1$. Therefore, $N^*(\Omega_i)$ should be maximized to maximize the effectiveness of the ParRep algorithm. This objective is only reasonable if the bulk of the simulation time is captured by steps of type **B1**, **C**, **D** and **E** in Algorithm 3.18. That is, trajectories drawn from (3.1) should spend most of the time inside metastable states, and not in excursions between them. This constraint is related to the intrinsic metastability of the system as a

whole: in systems for which a significant portion of time is spent in non-metastable regions of phase space, accelerated MD methods are not expected to be efficient, regardless of the choice of states.

We stress that the previous discussion is one of a number of possible ways to present the efficiency of ParRep and its variants, but the conclusion is always the same: one should maximize $N^*(\Omega)$ with respect to Ω to obtain maximal benefits from the algorithm inside the metastable state Ω. The methods described in this work should also allow to directly optimize the ratio (3.75), as well as other objectives whose free parameters are the states defining the Dirichlet eigenvalues $\lambda_1(\Omega)$ and $\lambda_2(\Omega)$ of $-\mathcal{L}_\beta$.

In Figure 3.21, we depict the objective (3.75) as a function of $N^*(\Omega)$ and the number N_{proc} of available processors, as well as the parallel efficiency metric $t_{\mathrm{DNS}}^{\mathbf{B1}\text{–}\mathbf{E}}(\Omega)/\left(N_{\mathrm{proc}} t_{\mathrm{PR}}^{\mathbf{B1}\text{–}\mathbf{E}}(\Omega)\right)$. This metric measures the wall-clock time speedup per number of processors, and therefore how effective Algorithm 3.18 utilizes parallel computing resources for the purpose of acceleration. A simple estimate show that, in the regime $N^*(\Omega) \gg 1$, N_{proc} should be chosen of the order of $\mathcal{O}\left(N^*(\Omega)\right)$ to reach a target parallel efficiency $0 < \alpha < 1$ for Algorithm 3.18 inside Ω. In materials science applications, the separation of timescales (3.7) is often much larger than the number of available processors, and parallel efficiency upwards of $\alpha = 0.95$ are often reported, see [268]. The contour line of parallel efficiency $\alpha = 0.5$ is depicted on the right-hand side of Figure 3.21.

Remark 3.19. It would be somewhat more satisfactory, owing to (3.6), to take the spatially-dependent prefactor $C(x)$ into account in the choice (3.74) of decorrelation time. An unresolved step in this direction is to obtain quantitative estimates of this prefactor, at least in limiting regimes or simple analytic cases. We leave this point for future work. At any rate, we expect the corresponding shape-optimization problem to be substantially more difficult to handle.

Another family of methods (see [156]) attempt to estimate $t_{\mathrm{corr}}(\Omega) + t_{\mathrm{phase}}(\Omega)$ "on the fly" using statistical information generated by a Fleming–Viot process in a combined step (**B**,**C**,**D**). In the work [156], this strategy is implemented using a Gelman–Rubin (non)-convergence diagnostic to estimate the decorrelation time. This opens up the possibility of applying ParRep to situations in which little a priori information is available on the timescales at hand, such as biological systems. However, some questions remain on how to optimally balance reliability and efficiency concerns in this context.

Appendix 3.C: Properties of the coefficients of the effective dynamics

We give sufficient conditions for the regularity assumptions of Proposition 3.9 using the following identities, proven for example in [229, Lemma 3.10] for a $\mathcal{C}^\infty$ function $\varphi : \mathbb{R}^d \to \mathbb{R}$, but which are still valid (with the same proof) under weaker regularity assumptions on φ. Define the partial integration operator with respect to ξ:

$$P_\xi \varphi(z) := \int_{\Sigma_z} \varphi \, \det(G_\xi)^{-1/2} \, \mathrm{d}\mathcal{H}_{\Sigma_z},$$

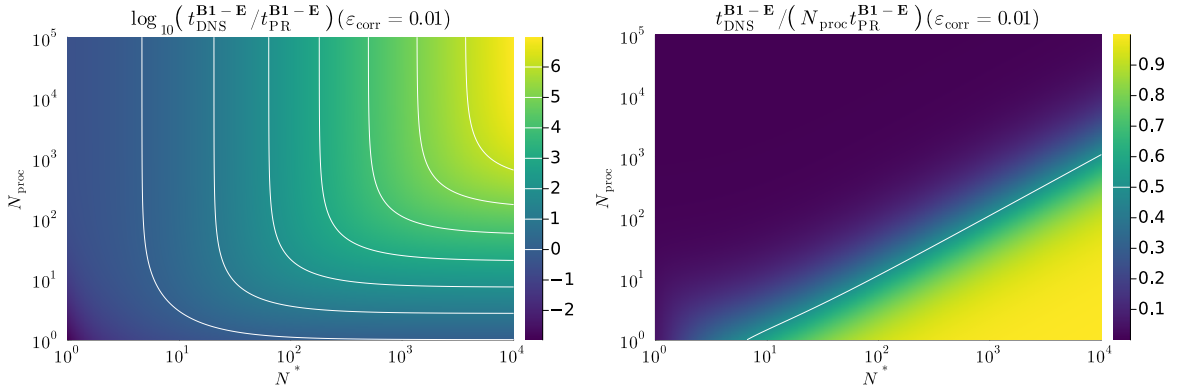

Figure 3.21: Effect of the separation of timescales (3.7) and number N_{proc} of processors on Algorithm 3.18. Left: wall-clock time speedup over direct simulation (Equation (3.75), with values on a $\log_{10}$-scale). Contours corresponding to ten-fold decreases in wall-clock time using ParRep are plotted in white, starting from the break-even contour below which direct simulation is faster. Right: parallel efficiency metric, with contour line $\alpha = 0.5$.

which is continuous, for instance from $L^1(\mathbb{R}^d)$ to $L^1(\mathbb{R}^m)$ by the coarea formula. Then it holds

$$\nabla\left(P_\xi\varphi\right) = P_\xi\left(\nabla_\xi\varphi\right), \qquad \nabla_\xi\varphi := \operatorname{div}\left(\varphi\, G_\xi^{-1}\nabla\xi^\top\right),$$

where in the last line, div denotes the row-wise divergence applied to the $m \times d$ matrix field $\varphi\, G_\xi^{-1}\nabla\xi^\top$. In particular, for $1 \leqslant \alpha, \gamma \leqslant m$, it holds formally that

$$\partial^2_{\alpha\gamma} P_\xi\varphi = P_\xi\left[\left[M_\xi\right]_\gamma^\top \nabla\left(\left[M_\xi\right]_\alpha^\top \nabla\varphi + \varphi \operatorname{div}\left[M_\xi\right]_\alpha\right) + \operatorname{div}\left[M_\xi\right]_\gamma\left(\left[M_\xi\right]_\alpha^\top \nabla\varphi + \varphi \operatorname{div}\left[M_\xi\right]_\alpha\right)\right],$$

where $\left[M_\xi\right]_\alpha$ denotes the α-th row of the matrix $G_\xi^{-1}\nabla\xi^\top$. From this identity, it follows that the mapping $P_\xi : \mathcal{W}^{2,\infty}(\mathbb{R}^d) \to \mathcal{W}^{2,\infty}(\mathbb{R}^m)$ is continuous when $M_\xi \in \mathcal{W}^{2,\infty}(\mathbb{R}^m; \mathbb{R}^{m\times d})$,. In turn, this property is satisfied if $\xi \in \mathcal{W}^{3,\infty}(\mathbb{R}^d; \mathbb{R}^m)$ and if the condition $\inf_{x\in\mathbb{R}^d} G_\xi(x) > 0$ holds in the sense of symmetric matrices.

If this condition on ξ is satisfied, it is then easy to show that the conditions of Proposition 3.9 hold for instance if

$$V \in \mathcal{W}^{2,\infty}(\mathbb{R}^d), \quad a \in \mathcal{W}^{2,\infty}(\mathbb{R}^d; \mathcal{M}_d), \quad \exists\, \varepsilon_a > 0 : u^\top a(x) u \geqslant \varepsilon_a |u|^2 \text{ for almost every } x \in \mathbb{R}^d,$$

which are uniform versions of Assumptions (**Ell**) and (**Reg**), accounting for the fact that Σ_z may not be compact for all $z \in \mathbb{R}^m$.

In practice, it is however often the case that both the dynamics (3.1) and the CV ξ take values in compact manifolds, typically the tori $L(\mathbb{R}/\mathbb{Z})^d$ and $L_\xi(\mathbb{R}/\mathbb{Z})^m$, corresponding respectively to a periodic simulation domain and a set of angular CVs. In this case, the regularity of F_ξ and a_ξ follows immediately from the smoothness of ξ and the condition rank $G_\xi = m$ everywhere.

Data availability. Code and trajectory data used in the production of the numerical results of Section 3.5 are publicly available in the repositories [46] and [47] respectively.

Acknowledgments. We thank Olivier Adjoua, Samuel Amstutz, Benjamin Bogosel, Louis Lagardère, Pierre Monmarché, Feliks Nüske, Danny Perez, Thomas Plé and Julien Reygner for helpful discussions and insightful comments. We are grateful to the OPAL infrastructure from Université Côte d'Azur for providing resources and support. Some of the experiments presented in this paper were carried out using the Grid'5000 testbed, supported by a scientific interest group hosted by Inria and including CNRS, RENATER and several universities as well as other organizations (see https://www.grid5000.fr). This work received funding from the European Research Council (ERC) under the European Union's Horizon 2020 research and innovation program (project EMC2, grant agreement No 810367), and from the Agence Nationale de la Recherche, under grants ANR-19-CE40-0010-01 (QuAMProcs) and ANR-21-CE40-0006 (SINEQ).

Chapter 4

Fixing the flux: a dual approach to computing transport coefficients

Man muss immer umkehren (One must always invert).
Carl Gustav Jacob Jacobi, 1832

Abstract. *We present a method to compute transport coefficients in molecular dynamics. Transport coefficients quantify the linear dependencies of fluxes in non-equilibrium systems subject to small external forcings. Whereas standard non-equilibrium approaches fix the forcing and measure the average flux induced in the system driven out of equilibrium, a dual philosophy consists in fixing the value of the flux, and measuring the average magnitude of the forcing needed to induce it. A deterministic version of this approach, named Norton dynamics, was studied in the 1980s by Evans and Morriss. In this work, we introduce a stochastic version of this method, first developing a general formal theory for a broad class of diffusion processes, and then specializing it to underdamped Langevin dynamics, which are commonly used for molecular dynamics simulations. We provide numerical evidence that the stochastic Norton method provides an equivalent measure of the linear response, and in fact demonstrate that this equivalence extends well beyond the linear response regime. This work raises many intriguing questions, both from the theoretical and the numerical perspectives.*

4.1 Introduction

Molecular dynamics (MD), much like computational statistical physics at large, aims at predicting macroscopic properties of a molecular medium by the use of computer simulations. In order to do so, a classical model of the interactions between atoms is constructed, and

dynamical evolution laws are specified. One can then simulate typical trajectories of the system through phase space, which, provided they are long enough, allows to estimate to a prescribed level of statistical accuracy the quantities of interest. See [20] for a general theoretical account of statistical physics, [324, 7, 133] for an emphasis on numerical methods, and [220, 233] for an overview of the mathematical aspects of molecular simulation. MD simulations may prove useful when the properties of interest are impractical to measure due to physical or cost constraints associated with the experimental setup, or alternatively serve as surrogate tests for theoretical models. At any rate, MD has grown to occupy an important role in many applications ranging from pharmacology and molecular biology to materials science and condensed matter physics, besides having had a significant impact on statistical methodology at large, through the dissemination of tools such as the Metropolis–Hastings algorithm [247]. First applications of MD included the computation of static properties at equilibrium, in particular thermodynamic quantities or free energy differences, which still are of considerable interest today. We refer to [26] for a historical perspective.

Another, more difficult problem is the measurement of dynamical properties, quantities which depend on the trajectory itself, and capture the behavior of systems undergoing a macroscopic time evolution: this is the object of non-equilibrium statistical physics. Of particular interest is the computation of transport coefficients, giving a measure of the sensitivity in the response of a system at equilibrium to the magnitude of perturbations driving it out of equilibrium. See [119, 321] for overviews, and [233, Section 5] for a mathematical presentation. Transport coefficients are of practical importance, since they characterize the diffusion, heat conduction or viscosity properties of a molecular medium, and enter as parameters in macroscopic evolution equations such as the Navier–Stokes equation. One standard approach to compute transport coefficients by molecular dynamics relies on the celebrated Green–Kubo formula [142], which expresses transport coefficients as integrated time-correlations between appropriate fluxes in the system at equilibrium. Another standard approach, see for instance [79], is to directly simulate the non-equilibrium perturbation, and to measure the resulting average response, which is, at the macroscopic level and in the limit of a small perturbation, proportional to the magnitude of this perturbation: this is the so-called non-equilibrium molecular dynamics (NEMD) approach, reviewed in [82]. Estimators deriving from these approaches however suffer from large statistical errors, as quantified in [307, Proposition 2.4] for instance, and convergence requires the simulation of very long trajectories, which comes at a high computational cost. A key metric to measure this cost is, for any given method, the asymptotic variance of estimators of the transport coefficient. Although some variance reduction techniques have been proposed to compute transport coefficients (see [309] for a recent review), efficiently estimating these quantities is still an important area of research.

From a thermodynamic point of view, the NEMD approach can be understood as fixing the magnitude of the non-equilibrium forcing, and measuring the resulting flux in the system driven out of equilibrium, which is conceived as a microscopic state variable. For a small enough magnitude of the forcing, this flux responds approximately linearly to the forcing, and the transport coefficient is precisely the associated proportionality constant. This method also yields a construction of the non-equilibrium ensemble, by defining it as the steady state of the system evolving according to the microscopic dynamics.

However convenient from an implementation standpoint, there is no physical reason to a priori favor an ensemble in which the forcing field is exactly fixed. At the macroscopic level, fluxes and forces play a symmetric role, which opens the possibility for dual approaches in the computation of non-equilibrium responses. Other approaches have been proposed to construct non-equilibrium ensembles in which the forcing does not play such a distinguished role. One can cite McLennan ensembles [77], expressing non-equilibrium steady-states as first-order perturbations of the Boltzmann distribution, where the leading order correction term is the time-integral of some conjugate response; or the dynamical approaches by Komorowski et al [197], whereby an average flux is induced by a time-periodic forcing. When considering a dual perspective, the most radical approach is to fix the flux exactly, and measure the average magnitude of the forcing needed to induce it in the microscopic dynamics. This yields an alternative measure of the transport coefficient. By analogy with Ohm's law, one can think of the NEMD approach as a way to measure a conductance, and the radical dual approach as a way to measure a resistance.

The microscopic implementation of this dual approach is what we will refer to as the Norton method, in accordance with the terminology proposed by Evans and Morriss in [120], by reference to the Norton–Thévenin reciprocity from electrical circuit theory. This approach amounts to considering a constrained dynamics on a submanifold of phase space consisting of a level-set of the flux observable. The idea of using constrained dynamics to simulate non-equilibrium systems already appeared in the 1983 work [117], where it was applied to capture the mobility, and was also explored in [173]. It was further applied to shear viscosity computations in [116], where the consistency of the approach was demonstrated. From a theoretical perspective, formal results under ergodic hypotheses were obtained, including linear response expressions for the transport coefficient in [120], as well as a result on the equivalence of non-equilibrium ensembles in [115].

However, Norton dynamics were only considered in a deterministic setting, and, despite promising results, their potential for practical use was not fully explored. In particular, the numerical performance of estimators of transport coefficients based on time averages of this dynamics has not, to the best of our knowledge, been studied yet. Our aim is to extend the Norton philosophy to the stochastic setting, both for academic motivations (obtaining new results on equivalence of ensembles in non-equilibrium systems), and for numerical reasons, as Norton dynamics potentially allow to more efficiently compute transport coefficients. We will consider both general diffusion processes, and Langevin-type dynamics, which are commonly used in molecular dynamics [262].

Contributions of this work. Let us highlight our main contributions:

- We define a stochastic version of the Norton method, which is convenient from the theoretical point of view as rigorous ergodicity results exist for stochastic dynamics, and are also relevant for simulation since stochastic dynamics are nowadays very commonly used in molecular dynamics.
- We specialize the Norton method to underdamped Langevin dynamics, and apply it to compute the mobility and shear viscosity of a fluid. We demonstrate numerically that the

Norton method gives consistent estimations of the linear response in the thermodynamic limit.

- We observe on the numerical examples we consider that the non-equilibrium responses coincide in fact far outside of the linear regime, raising the question of equivalence between non-equilibrium ensembles.
- We offer numerical evidence that, in some situations, the Norton method is preferable to the standard NEMD approach, in the sense that the Norton estimators for the transport coefficients lead to estimates with a smaller statistical error than their NEMD counterparts.

Many points in the mathematical analysis of the Norton approach are left open at this stage. This should be seen as an invitation to further study the properties of these intriguing dynamics

Outline. This paper is organized as follows. We recall in Section 4.2 a general framework for stochastic dynamics out of equilibrium. In Section 4.3, we introduce the Norton approach, deriving an expression for the diffusion process defining the dynamics, before generalizing the approach to the case of multiple constraints and time-dependent fluxes. In Section 4.4, we specialize the setting to non-equilibrium kinetic Langevin dynamics used for mobility and shear viscosity computations, describing how to apply the Norton philosophy. We also give a physical interpretation of the Norton dynamics, as one satisfying an oblique version of Gauss's principle of least constraint. In Section 4.5, we discuss how to discretize stochastic Norton dynamics, describing in particular a family of schemes obtained by an operator splitting approach. We present the results of our numerical experiments in Section 4.6, demonstrating the consistency with usual NEMD in the thermodynamic limit, and motivating that Norton simulations can be more efficient than NEMD ones. We conclude in Section 4.7 by discussing the many open questions and perspectives raised by the Norton method in the stochastic context.

4.2 Non-equilibrium molecular dynamics

We recall in this section the standard framework of NEMD, first presenting the reference dynamics, before introducing the non-equilibrium dynamics and defining transport coefficients. We finally discuss the statistical properties of NEMD estimators of the transport coefficient. We refer the interested reader to [233, Section 5] and [307] for a more in-depth discussion of the mathematical properties of the NEMD method.

Reference dynamics. We consider a class of non-equilibrium ensembles, obtained as the steady-states of certain stochastic processes corresponding to a perturbation of a reference process (usually a dynamics at equilibrium). We denote by $\mathcal{X}$ the state space of the system. Typically, we consider $\mathcal{X} = \mathbb{R}^d$ or $\mathbb{T}^d$, with $\mathbb{T} = \mathbb{R}/\mathbb{Z}$ the one-dimensional torus, or a product of the two. We introduce a smooth vector field $b : \mathcal{X} \to \mathbb{R}^d$, corresponding to the equilibrium drift, and a matrix valued map $\sigma : \mathcal{X} \to \mathbb{R}^{d\times m}$ corresponding to the diffusion. The reference

dynamics is the following stochastic differential equation (SDE):

$$\mathrm{d}X_t = b(X_t)\,\mathrm{d}t + \sigma(X_t)\,\mathrm{d}W_t,$$

where $(W_t)_{t\geqslant 0}$ a standard m-dimensional Brownian motion. Common choices include the overdamped Langevin dynamics

$$\mathrm{d}X_t = -\nabla V(X_t)\,\mathrm{d}t + \sqrt{\frac{2}{\beta}}\,\mathrm{d}W_t,$$

and the underdamped or kinetic Langevin dynamics (see Equation (4.26) below).

Non-equilibrium perturbations. We consider in this work the case where the perturbation arises from an external non-gradient forcing in the drift of the underlying diffusion process, determined by a smooth vector field $F : \mathcal{X} \to \mathbb{R}^d$. Such dynamics allow the computation of the shear viscosity and mobility of fluids as explained in Section 4.4, as well as the thermal conductivity in atom chains, see [216],[345].

The non-equilibrium dynamics is given by the following SDE:

$$\mathrm{d}X_t^\eta = (b + \eta F)(X_t^\eta)\,\mathrm{d}t + \sigma(X_t^\eta)\,\mathrm{d}W_t. \tag{4.1}$$

The parameter $\eta \in \mathbb{R}$ is a scalar modulating the strength of the perturbation. The equilibrium dynamics is recovered in the absence of a non-equilibrium forcing, i.e. the case $\eta = 0$. The infinitesimal generator of the dynamics (4.1) can be decomposed as the sum

$$\mathcal{L}_\eta = \mathcal{L} + \eta\widetilde{\mathcal{L}}, \qquad \mathcal{L} = b\cdot\nabla + \frac{1}{2}\sigma\sigma^\intercal : \nabla^2, \qquad \widetilde{\mathcal{L}} = F\cdot\nabla, \tag{4.2}$$

where ∇^2 denotes the Hessian matrix and : denotes the Frobenius inner product defined by $A : B = \mathrm{Tr}(A^\intercal B)$. Note that $\mathcal{L}$ is the generator of the reference dynamics, and $\widetilde{\mathcal{L}}$ encodes its perturbation. The invariant probability measure satisfies the stationary Fokker-Planck equation

$$\mathcal{L}_\eta^\dagger \psi_\eta = 0, \tag{4.3}$$

where $\mathcal{L}_\eta^\dagger$ is the flat $L^2(\mathcal{X})$-adjoint of the generator. Existence and regularity results for solutions of (4.3) depend on the particular form of the dynamics, as do properties pertaining to convergence to the steady-state. It is often possible to leverage the standard analytical framework of parabolic and elliptic partial differential equations to prove this convergence, although for degenerate diffusions such as the underdamped Langevin dynamics, one has to resort to more sophisticated tools, such as hypoellipticity [174] to obtain regularity of the steady-state, or hypocoercivity [329] to show exponential decay of the evolution semigroup.

We assume in the remainder of this section that, for $|\eta|$ small enough, the dynamics admits a unique invariant probability measure for which it is ergodic, and denote the corresponding expectation by $\mathbb{E}_\eta$. Given a response observable $R : \mathcal{X} \to \mathbb{R}$ such that

$$\mathbb{E}_0\left[R\right] = 0, \tag{4.4}$$

which we think of as measuring a flux in the system out of equilibrium, we define the associated transport coefficient as the following limit, provided it is well defined:

$$\alpha = \lim_{\eta \to 0} \frac{\mathbb{E}_\eta [R]}{\eta}. \tag{4.5}$$

Rigorous assumptions under which this limit exists are given in [149]. This definition suggests a simple and natural method to estimate these coefficients: one can compute ergodic averages of R over trajectories of the non-equilibrium dynamics (4.1), and estimate the linear relation between η and R for one or several values of η in the linear response regime. The finite-difference estimator for the limit (4.5) is given by the following ergodic average:

$$\widehat{\alpha}_{T,\eta} = \frac{1}{\eta T} \int_0^T R(X_t^\eta) \, \mathrm{d}t. \tag{4.6}$$

The consistency of such estimators is a consequence of the pathwise ergodicity for the process (4.1), which in many cases can be proven using the results of [196]. The latter result also implies the uniqueness of the steady-state. The existence of the steady-state is often obtained by Lyapunov techniques, see for instance [280, Theorem 8.3].

Statistical properties of the estimator $\widehat{\alpha}_{T,\eta}$. A challenge posed by the NEMD method is that the estimator (4.6) is plagued by large statistical errors when $|\eta|$ is small, which is often required to remain in the linear response regime, and avoid biases arising from nonlinear terms in the response. More precisely, one can show that the asymptotic variance of the estimator (4.6) scales as η^{-2} as η approaches 0. Indeed, under technical decay conditions on the evolution semigroup generated by (4.2), one can easily show that the asymptotic variance is given by

$$\sigma_\eta^2 = \lim_{T \to \infty} T \mathrm{Var}_\eta \left(\widehat{\alpha}_{T,\eta} \right) = \frac{2}{\eta^2} \int_0^\infty \mathbb{E}_\eta [\Pi_\eta R(X_t^\eta) \Pi_\eta R(X_0^\eta)] \, \mathrm{d}t,$$

where Var_η denotes the variance with respect to $\mathbb{E}_\eta$, and Π_η is the centering operator $\Pi_\eta \varphi = \varphi - \mathbb{E}_\eta[\varphi]$. Defining the correlation time by

$$\Theta_\eta(R) = \int_0^\infty \frac{\mathbb{E}_\eta [\Pi_\eta R(X_t^\eta) \Pi_\eta R(X_0^\eta)]}{\mathbb{E}_\eta [(\Pi_\eta R)^2]} \, \mathrm{d}t,$$

we further get, using a first-order expansion in powers of η (whose validity has to be verified on a case-by-case basis),

$$\sigma_{\alpha,\eta}^2 = \frac{2}{\eta^2} \mathrm{Var}_\eta(R) \Theta_\eta(R) = \frac{2}{\eta^2} \mathrm{Var}_0(R) \Theta_0(R) + \mathrm{O}\left(\frac{1}{\eta} \right). \tag{4.7}$$

In summary, the asymptotic variance is, at dominant order in $|\eta|$, the asymptotic variance of the time averages of R under the equlibrium dynamics, divided by η^2.

The leading order of the asymptotic variance highlights why it is often computationally expensive to obtain accurate estimates of transport coefficients. Although the computation of such coefficients is recognized as being a difficult problem in practice, only a handful of research works have been proposed to alleviate this issue, including replacing the forcing F by a so-called synthetic forcing devised to induce the same transport coefficient while the range

of the linear response [307], or relying on carefully constructed couplings [88]. We refer the reader to [309, Section 4] for a recent overview of current variance reduction techniques in non-equilibrium molecular dynamics.

4.3 A stochastic Norton method

The Norton approach exploits the macroscopic duality between thermodynamic forces and fluxes: at the macroscopic level, one can equivalently choose to measure the current induced by a constant force, or the resistance opposed to a constant current. The microscopic translation of this duality is the introduction of a new non-equilibrium ensemble in which the flux is held fixed. As in the NEMD case, we define this ensemble as the invariant probability measure for a particular stochastic process, which we refer to as the Norton dynamics.

In Section 4.3.1, we present the Norton pertubation approach for a generic reference dynamics of the form (4.1). We then proceed in Section 4.3.2 to write the dynamics in closed form, by making explicit the constraining force on the flux. In Section 4.3.3, we give the expression of the Norton analogs of the transport coefficient (4.5), and discuss how their statistical properties can be formally analyzed. We finally show in Section 4.3.4 how the Norton approach can be extended to the cases of multiple forcings, or time-dependent flux constraints.

4.3.1 Presentation of the dynamics

At the dynamical level, the Norton ensemble is defined as the invariant probability measure of the following stochastic differential equation:

$$\begin{cases} \mathrm{d}Y_t^r = b(Y_t^r)\,\mathrm{d}t + \sigma(Y_t^r)\,\mathrm{d}W_t + F(Y_t^r)\,\mathrm{d}\Lambda_t^r, \\ R(Y_t^r) = R(Y_0^r) = r. \end{cases} \tag{4.8}$$

Here, the evolution of the state is given by the dynamics of $Y_t^r \in \mathcal{X}$, and $r \in \mathbb{R}$ is the magnitude of the response flux, which is maintained constant. The stochastic dynamics therefore evolves on the submanifold

$$\Sigma_r = \{y \in \mathcal{X},\ R(y) = r\} = R^{-1}\{r\}$$

of the full state space. The dynamics (4.8) can formally still be considered as a perturbation of the equilibrium dynamics, in the same direction as the Thévenin process (4.1), but with a random intensity given by the stochastic process Λ_t^r, acting as the control by which the constant-flux condition is enforced. Provided $\mathbb{E}_0[R] = 0$, we can further interpret the Norton dynamics $Y_t^0 \in \Sigma_0$ as an equilibrium dynamics, constrained to exactly preserve the flux. The relationship between the equilibrium ensemble in which the response fluctuates, and the Norton equilibrium ensemble in which it is exactly fixed at zero, is reminiscent of the relationship between the canonical and microcanonical ensembles when R is a spatial average over local quantities.

We next proceed to show that Λ^r can in fact be defined as an Itô process adapted to the natural filtration of the m-dimensional Brownian motion W. More precisely, we decompose

the intensity of the forcing using the following ansatz:

$$\Lambda_t^r = \Lambda_0^r + \int_0^t \lambda(Y_s^r)\,\mathrm{d}s + \widetilde{\Lambda}_t^r, \qquad \widetilde{\Lambda}_t^r = \int_0^t \widetilde{\lambda}(Y_s^r)\,\mathrm{d}W_s, \tag{4.9}$$

where $\lambda, \widetilde{\lambda}$ are functions defined on $\mathcal{X}$, with λ taking values in $\mathbb{R}$ and $\widetilde{\lambda}$ in $\mathbb{R}^{1\times m}$. This ansatz is natural for constrained dynamics (see for instance [229, Chapter 3]), and will be confirmed a posteriori (see in particular (4.11) and (4.16) in Section 4.3.2 below). The average forcing in the Norton ensemble can then be defined as the expectation of λ under the steady-state probability measure, neglecting the zero-mean contribution of $\widetilde{\lambda}$ (see Section 4.3.3). Numerically, these averages can be computed as ergodic averages over discretized trajectories of the Norton dynamics, as discussed in Section 4.5.3.

4.3.2 A closed form for the forcing process

We make precise here the expressions of the function $\lambda(Y_t^r)$ and the martingale $\widetilde{\Lambda}_t^r$ in (4.9), which allows us to write the Norton dynamics without explicit reference to the forcing. We assume that Λ^r is of the form (4.9), and verify a posteriori that this ansatz is valid. Applying Itô's formula to the constant response condition $R(Y_t^r) = r$ yields

$$\nabla R(Y_t^r)\cdot[b(Y_t^r)\,\mathrm{d}t + \sigma(Y_t^r)\,\mathrm{d}W_t + F(Y_t^r)\,\mathrm{d}\Lambda_t^r] + \frac{1}{2}\nabla^2 R(Y_t^r) : \mathrm{d}\left\langle M^r\right\rangle_t = 0, \tag{4.10}$$

where $\langle M\rangle_t$ denotes the quadratic covariation process for the martingale part in the Itô decomposition of Y^r:

$$\mathrm{d}M_t^r = \sigma(Y_t^r)\,\mathrm{d}W_t + F(Y_t^r)\,\widetilde{\lambda}(Y_t^r)\,\mathrm{d}W_t. \tag{4.11}$$

Using the uniqueness of the Itô decomposition, we can identify the martingale increment in (4.10) as

$$\mathrm{d}\widetilde{\Lambda}_t^r = -\frac{\nabla R(Y_t^r)\cdot\sigma(Y_t^r)\,\mathrm{d}W_t}{\nabla R(Y_t^r)\cdot F(Y_t^r)}, \tag{4.12}$$

provided that $\nabla R\cdot F \neq 0$ almost surely, which we assume here and in the sequel. Plugging this equality in (4.11) in turn gives

$$M_t^r = \int_0^t \left(\mathrm{Id} - \frac{F(Y_s^r)\otimes\nabla R(Y_s^r)}{F(Y_s^r)\cdot\nabla R(Y_s^r)}\right)\sigma(Y_s^r)\,\mathrm{d}W_s = \int_0^t \overline{P}_{F,\nabla R}\sigma(Y_s^r)\,\mathrm{d}W_s,$$

so that the covariation of the martingale increment is

$$d\left\langle M^r\right\rangle_t = \left[\overline{P}_{F,\nabla R}\sigma\sigma^\intercal\overline{P}_{\nabla F,R}^\intercal\right](Y_t^r)\,\mathrm{d}t. \tag{4.13}$$

In the latter two expressions, we make use of the following non-orthogonal projector-valued maps, defined for vector fields A, B such that $A(x)\cdot B(x)\neq 0$:

$$P_{A,B}(x) = \frac{A(x)\otimes B(x)}{A(x)\cdot B(x)}, \qquad \overline{P}_{A,B}(x) = \mathrm{Id} - P_{A,B}(x). \tag{4.14}$$

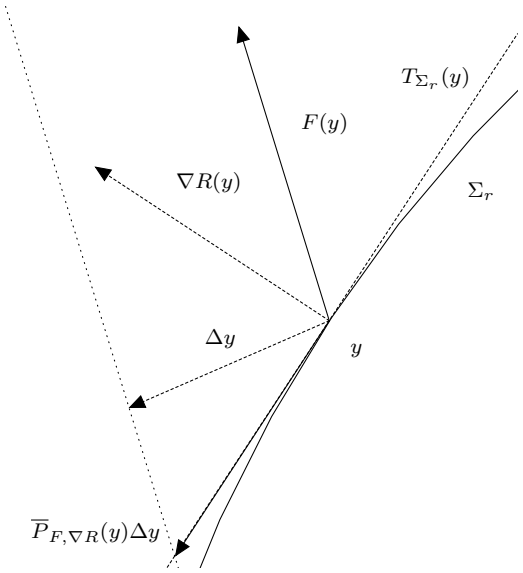

Figure 4.1: Action of the projector $\overline{P}_{F,\nabla R}$: the increment Δy is projected onto the tangent space $T_{\Sigma_r}(y) = \{z \in \mathbb{R}^d \,|\, \nabla R(y) \cdot z = 0\}$ in the direction $F(y)$.

The action of the projector is given, for $\xi \in \mathbb{R}^d$ and $x \in \mathcal{X}$, by

$$P_{A,B}(x)(\xi) = \frac{B(x) \cdot \xi}{A(x) \cdot B(x)} A(x).$$

For notational convenience, we introduce

$$\Pi_{F,\nabla R,\sigma}(y) = \left[\overline{P}_{F,\nabla R} \sigma \sigma^\intercal \overline{P}_{F,\nabla R}^\intercal\right](y). \tag{4.15}$$

We next proceed to identifying the bounded-variation increments on both sides of (4.10). After rearrangement and substitution of (4.13), one obtains the following expression:

$$\lambda_t^r = \lambda(Y_t^r), \qquad \lambda = -\frac{1}{F \cdot \nabla R}\left(b \cdot \nabla R + \frac{1}{2}\nabla^2 R : \Pi_{F,\nabla R,\sigma}\right). \tag{4.16}$$

Substituting the expression for Λ_t^r in (4.8) yields the following expression for the Norton dynamics:

$$\mathrm{d}Y_t^r = \overline{P}_{F,\nabla R}(Y_t^r)\,[b(Y_t^r)\mathrm{d}t + \sigma(Y_t^r)\,\mathrm{d}W_t] - \frac{\left(\nabla^2 R : \Pi_{F,\nabla R,\sigma}\right)(Y_t^r)}{2\nabla R(Y_t^r) \cdot F(Y_t^r)} F(Y_t^r)\,\mathrm{d}t. \tag{4.17}$$

It can now be checked a posteriori, using Itô's formula, that the dynamics (4.17) is such that $R(Y_t^r) = r$ for all $t \geqslant 0$, provided the coefficients are smooth. In Figure 4.1, we illustrate geometrically the action of the projector $\overline{P}_{F,\nabla R}$ at a point y on a vector Δy.

Without further specifying the particular choice for the reference dynamics, the response flux observable R and non-equilibrium forcing F, it is difficult to make general comments about the well-posedness of (4.17). Let us however emphasize that a crucial condition for the dynamics to be well-defined is that the denominator $F(Y_t^r) \cdot \nabla R(Y_t^r)$ in the expression of the projector $P_{F,\nabla R}$ and in the last term of (4.17) (which represents some curvature correction) should not vanish. Thinking of the extreme case where ∇R and F are everywhere orthogonal, we see that this requirement translates into a controllability condition: in this case, any forcing

in the direction F has no effect on the flux, thus there is no way to control the latter using such a perturbation. More generally, starting from a configuration for which $F \cdot \nabla R(q) = 0$, it is not possible to maintain the value of the response function using the forcing F. We therefore assume in the sequel that the condition

$$\forall y \in \Sigma_r, \qquad F(y) \cdot \nabla R(y) \neq 0, \tag{4.18}$$

is satisfied. We discuss the validity of this condition for the numerical examples we consider in Section 4.6.

Remark 4.1. Although the dynamics derived in this section corresponds to a perturbation on the drift of the reference dynamics, it may be of interest to extend the Norton approach to perturbations affecting the diffusion coefficient. In the case of underdamped Langevin dynamics, such methods would for instance allow to study the behavior of nonequilibrium temperature profiles in constant heat flux ensembles, for the computation of thermal conductivity. We leave this point for future work.

4.3.3 Norton analogs of the transport coefficient

We assume the well-posedness of the dynamics (4.8) (or equivalently (4.17)), and also the existence and uniqueness of the invariant steady-state probability measure for this dynamics, whose expectation is denoted by $\mathbb{E}_r^*$. We assume that

$$\mathbb{E}_0^*[\lambda] = 0. \tag{4.19}$$

This condition is the Norton counterpart of the centering condition (4.4) for the observable in usual NEMD simulations. When (4.19) holds, the transport coefficient for the Norton dynamics is defined by analogy with (4.5) as

$$\alpha_{F,R}^* = \lim_{r \to 0} \frac{r}{\mathbb{E}_r^*\left[\lambda\right]}, \tag{4.20}$$

provided the limit exists. In equation (4.20), $\alpha_{F,R}^*$ can be interpreted as the inverse of the resistance to the non-equilibrium forcing. Note that the average forcing in the denominator of the right-hand side of (4.20) only involves the bounded varation part of (4.9), since the expectation of the martingale part vanishes.

Provided the Norton dynamics is ergodic with respect to the steady-state, a natural estimator of the transport coefficient can be constructed by replacing ensemble averages by trajectory averages, similarly to what is done in standard NEMD simulations. More precisely, the estimator is computed using ergodic averages of $\lambda(Y_t^r)$ under $\mathbb{E}_r^*$, that is,

$$\widehat{\alpha}_{T,r}^* = \frac{rT}{\displaystyle\int_0^T \lambda(Y_t^r)\,\mathrm{d}t}. \tag{4.21}$$

The statistical properties of this estimator can be analyzed similarly to what is done for the estimator (4.6), leading to a result similar to (4.7). Assuming that a central limit theorem

holds, and that F, R are such that $\mathbb{E}_0^*[\lambda] = 0$, we can formally write the asymptotic variance associated with the estimator (4.21) as

$$\begin{aligned}\sigma^{2,*}_{\alpha,r} &= \lim_{T\to\infty} T\mathrm{Var}_r^*(\widehat{\alpha}^*_{T,r}) = \frac{r^4}{\mathbb{E}_r^*[\lambda]^4} \lim_{T\to\infty} T\mathrm{Var}_r^*\left(\frac{1}{\widehat{\alpha}^*_{T,r}}\right) \\ &= \frac{r^4}{\mathbb{E}_r^*[\lambda]^4}\frac{2}{r^2}\mathrm{Var}_r^*(\lambda)\Theta_r^*(\lambda),\end{aligned} \tag{4.22}$$

where Var_r^* denotes the variance with respect to $\mathbb{E}_r^*$, and the Norton correlation time is defined similarly to the NEMD case by

$$\Theta_r^*(\lambda) = \int_0^\infty \frac{\mathbb{E}_r^*[\Pi_r^*\lambda(Y_t^r)\Pi_r^*\lambda(Y_0^r)]}{\mathbb{E}_r^*[(\Pi_r^*\lambda)^2]}\,\mathrm{d}t,$$

where Π_r^* is the centering operator with respect to $\mathbb{E}_r^*$. The second equality in (4.22) follows from the Delta method [327, Chapter 3] applied to the reciprocal of $\widehat{\alpha}^*_{T,r}$. Using the first-order expansion given by (4.20), and assumptions similar to the ones leading to (4.7), we may further write, for $|r|$ small:

$$\begin{aligned}\sigma^{2,*}_{\alpha,r} &= \frac{2\left(\alpha^*_{F,R}\right)^4}{r^2}\mathrm{Var}_r^*(\lambda)\Theta_r^*(\lambda) + \mathrm{O}\left(\frac{1}{r}\right) \\ &= \frac{2\left(\alpha^*_{F,R}\right)^4}{r^2}\mathrm{Var}_0^*(\lambda)\Theta_0^*(\lambda) + \mathrm{O}\left(\frac{1}{r}\right),\end{aligned}$$

As in the NEMD setting, one has to verify the validity of each of the expansion in powers of $|r|$ for each of the quantities considered. However, whereas in the NEMD setting this may be done in some cases by using a perturbative expansion of the non-equilibrium measure in powers of η (as done in [307], for instance), there is in the Norton setting an additional technical difficulty in that the invariant measure for the Norton dynamics (4.8) is supported on the $(d-1)$-dimensional manifold Σ_r, which is disjoint from the Norton equilibrium manifold Σ_0, and also of zero Lebesgue measure, so that it is both singular with respect to the invariant measure of the Norton equilibrium dynamics and to that of the reference dynamics (4.1). A dedicated analysis has therefore to be performed to justify these approximations, and rigorously establish the validity of (non-)linear response formulas.

4.3.4 Two straightforward generalizations

For ease of presentation, we restricted ourselves in Sections 4.3.1 to 4.3.3 to the case where only one flux is fixed. However, the derivation of Norton dynamics can be straightforwardly extended to the case where several fluxes are simultaneously constrained. In fact, one can even consider situations where the response depends on time. These two generalizations can of course be combined.

Multiple constraints. We consider in this paragraph the case where $c \geqslant 1$ forces $F_1, \ldots, F_c$ act on the reference system with magnitudes $\Lambda^{\mathbf{r}}_{1,t}, \ldots, \Lambda^{\mathbf{r}}_{c,t}$, chosen to maintain constant the

value of c fluxes $R_1, \dots, R_c$. The dynamics is given by

$$\begin{cases} \mathrm{d}Y_t^{\mathbf{r}} = b(Y_t^{\mathbf{r}})\,\mathrm{d}t + \sigma(Y_t^{\mathbf{r}})\,\mathrm{d}W_t + \displaystyle\sum_{i=1}^{c} F_i(Y_t^{\mathbf{r}})\,\mathrm{d}\Lambda_i^{\mathbf{r}}, \\ R_i(Y_t^{\mathbf{r}}) = r_i, \qquad 1 \leqslant i \leqslant c, \end{cases}$$

where r_i gives the prescribed value of the corresponding flux R_i. By defining the following maps defined on $\mathcal{X}$

$$R = \begin{pmatrix} R_1 \\ \vdots \\ R_c \end{pmatrix} \in \mathbb{R}^c, \qquad F = \begin{pmatrix} | & & | \\ F_1 & \dots & F_c \\ | & & | \end{pmatrix} \in \mathbb{R}^{d\times c},$$

as well as the following vectors,

$$\Lambda_t^{\mathbf{r}} = \begin{pmatrix} \Lambda_{1,t}^{\mathbf{r}} \\ \vdots \\ \Lambda_{c,t}^{\mathbf{r}} \end{pmatrix} \in \mathbb{R}^c, \qquad \mathbf{r} = \begin{pmatrix} r_1 \\ \vdots \\ r_c \end{pmatrix} \in \mathbb{R}^c,$$

the Norton dynamics can be written similarly to (4.8), upon replacing r by $\mathbf{r}$:

$$\begin{cases} \mathrm{d}Y_t^{\mathbf{r}} = b(Y_t^{\mathbf{r}})\,\mathrm{d}t + \sigma(Y_t^{\mathbf{r}})\,\mathrm{d}W_t + F(Y_t^{\mathbf{r}})\,\mathrm{d}\Lambda_t^{\mathbf{r}}, \\ R(Y_t^{\mathbf{r}}) = R(Y_0^{\mathbf{r}}) = \mathbf{r}. \end{cases} \tag{4.23}$$

Computations identical to the ones leading to (4.17) may be performed. As these are verbatim the same, we simply state the result and refer the reader to Appendix 4.A for the complete derivation. The dynamics (4.23) can be written in closed form, using non-orthogonal projectors, as

$$\begin{aligned} \mathrm{d}Y_t^{\mathbf{r}} = {} & \overline{P}_{F,\nabla R}(Y_t^{\mathbf{r}})\,[b(Y_t^{\mathbf{r}})\,\mathrm{d}t + \sigma(Y_t^{\mathbf{r}})\,\mathrm{d}W_t] \\ & - \frac{F(Y_t^{\mathbf{r}})}{2}(\nabla R(Y_t^{\mathbf{r}})^\intercal F(Y_t^{\mathbf{r}}))^{-1}\left(\nabla^2 R(Y_t^{\mathbf{r}})^\intercal : \Pi_{F,\nabla R,\sigma}(Y_t^{\mathbf{r}})\right), \end{aligned} \tag{4.24}$$

where $\nabla R : \mathcal{X} \to \mathbb{R}^{d\times c}$ and $\nabla^2 R : \mathcal{X} \to \mathbb{R}^{d\times d\times c}$ are respectively the Jacobian and Hessian matrices of the fluxes. Here, we define the contraction product by

$$\forall\,(A,B) \in \mathbb{R}^{d\times d\times c} \times \mathbb{R}^{d\times d}, \qquad A : B = \left(\sum_{j,k=1}^{d} A_{kji}B_{kj}\right)_{1\leqslant i\leqslant c} \in \mathbb{R}^c,$$

the projector $\overline{P}_{F,\nabla R}$ is given, for $A, B \in \mathbb{R}^{d\times c}$, by

$$P_{A,B} = A(B^\intercal A)^{-1}B^\intercal, \qquad \overline{P}_{A,B} = \mathrm{Id} - P_{A,B},$$

and $\Pi_{F,\nabla R,\sigma}$ is defined similarly to (4.15) by

$$\Pi_{F,\nabla R,\sigma} = \overline{P}_{F,\nabla R}\sigma\sigma^\intercal\overline{P}_{F,\nabla R}^\intercal.$$

Note that the invariant measure is supported on a codimension c submanifold $\Sigma_{\mathbf{r}}$, and that the controllability condition becomes

$$\forall y \in \Sigma_{\mathbf{r}}, \qquad \det(\nabla R(y)^{\intercal} F(y)) \neq 0.$$

The average value of the forcing can be written as the ergodic average of the following vector-valued observable, which is the analog of (4.16):

$$\boldsymbol{\lambda} = -(\nabla R^{\intercal} F)^{-1} \left[\nabla R^{\intercal} b + \frac{1}{2} \left(\nabla^2 R^{\intercal} : \Pi_{F,\nabla R,\sigma} \right) \right] = \begin{pmatrix} \lambda_1 \\ \vdots \\ \lambda_c \end{pmatrix}.$$

Dynamics such as (4.23) should in particular allow for the numerical computation of Onsager coefficients in the Norton ensemble. By Onsager matrix, we mean the collection of coefficients

$$\boldsymbol{\alpha}_{ij} = \lim_{\eta_j \to 0} \frac{\mathbb{E}_{\boldsymbol{\eta},j}[R_i]}{\eta_j}, \qquad 1 \leqslant i, j \leqslant c,$$

where $\boldsymbol{\eta} = (\eta_j)_{1 \leqslant j \leqslant c}$ and $\mathbb{E}_{\boldsymbol{\eta},j}$ denotes the expectation with respect to the steady-state of the nonequilibrium dynamics (4.1) with F_j taken as the nonequilibrium forcing of magnitude η_j. Using estimators of the form (4.6), each column of the matrix $\boldsymbol{\alpha}$ may be estimated from a single nonequilibrium trajectory. For the same dynamics perturbed in the direction $F\boldsymbol{\eta}$, the average of the vector-valued response R is given asymptotically by $\boldsymbol{\alpha}\boldsymbol{\eta}$ as $\|\boldsymbol{\eta}\| \to 0$.

For Norton dynamics in this context, using a trajectory of the dynamics (4.23) and estimators of the form (4.21), one can estimate a full row of the matrix

$$\boldsymbol{\beta}_{ij} = \lim_{r_i \to 0} \frac{\mathbb{E}^*_{\mathbf{r},i}[\lambda_j]}{r}, \qquad 1 \leqslant i, j \leqslant c,$$

where $\mathbb{E}^*_{\mathbf{r},i}$ denotes expectation with respect to the steady-state of the dynamics (4.23) in which we take $\mathbf{r}$ to be the vector whose components are 0 except the i-th one, which is equal to r. For general $\mathbf{r}$, we expect that the average of the forcing $\boldsymbol{\lambda}$ is given asymptotically by $\boldsymbol{\beta}\mathbf{r}$, as $\|\mathbf{r}\| \to 0$. This suggests that $\boldsymbol{\beta}$ is the Norton analog to the inverse of the Onsager matrix $\boldsymbol{\alpha}^{-1}$, generalizing the definition (4.20).

Time-dependent fluxes. One can also extend the dynamics to the case where we replace the condition $R(Y^r_t) = r$ by $R(Y^{\mathcal{R}}_t) = \mathcal{R}_t$, when $\mathcal{R}_t$ is the Itô process defined by

$$\mathcal{R}_t = R(Y^{\mathcal{R}}_0) + \int_0^t \bar{r}_s \, \mathrm{d}s + \int_0^t \widetilde{r}_s \, \mathrm{d}B_s,$$

with B a one-dimensional Brownian motion independent of W, and $\bar{r}, \widetilde{r}$ stochastic processes adapted to the natural filtration of B. These dynamics in particular cover the deterministic case $\widetilde{r}_t = 0$, so that one can for instance consider time-periodic fluxes

$$\bar{r}_t = \sin(2\pi\omega t), \qquad \widetilde{r}_t = 0,$$

or a stochastic process $\mathcal{R}^r$ whose ergodic properties are well-understood, such as an Ornstein–Uhlenbeck process centered at r:

$$d\mathcal{R}_t^r = \gamma(r - \mathcal{R}_t^r)\,\mathrm{d}t + s\,\mathrm{d}B_t.$$

One expects the resulting steady-state to be non-singular with respect to the invariant measure of the reference dynamics (4.1), which may be of some use from a theoretical perspective. The analog of (4.8) is given by

$$\begin{cases} \mathrm{d}Y_t^{\mathcal{R}} = b(Y_t^{\mathcal{R}})\,\mathrm{d}t + \sigma(Y_t^{\mathcal{R}})\,\mathrm{d}W_t + F(Y_t^{\mathcal{R}})\,\mathrm{d}\Lambda_t^{\mathcal{R}}, \\ R(Y_t^{\mathcal{R}}) = R(Y_0^{\mathcal{R}}) = \mathcal{R}_t^r. \end{cases}$$

Following the same strategy as in the constant response case, one can express the dynamics in closed form as

$$\begin{aligned} \mathrm{d}Y_t^r = \overline{P}_{F,\nabla R}(Y_t^{\mathcal{R}})\left[b(Y_t^{\mathcal{R}})\,\mathrm{d}t + \sigma(Y_t^{\mathcal{R}})\,\mathrm{d}W_t\right] + \frac{\bar{r}_t\,\mathrm{d}t + \widetilde{r}_t\,\mathrm{d}B_t}{\nabla R(Y_t^{\mathcal{R}})\cdot F(Y_t^{\mathcal{R}})}F(Y_t^{\mathcal{R}}) \\ - \frac{1}{2\nabla R(Y_t^{\mathcal{R}})\cdot F(Y_t^{\mathcal{R}})}\left(\nabla^2 R : \left[\frac{F\otimes F}{(\nabla R\cdot F)^2}\widetilde{r}_t^2 + \Pi_{F,\nabla R,\sigma}\right]\right)(Y_t^{\mathcal{R}})F(Y_t^{\mathcal{R}})\,\mathrm{d}t, \end{aligned} \quad (4.25)$$

and the bounded-variation contribution to the forcing as

$$\lambda_t^{\mathcal{R}} = \left[\frac{1}{\nabla R\cdot F}\left(\bar{r}_t - b\cdot\nabla R - \frac{1}{2}\nabla^2 R : \left[\frac{F\otimes F}{(\nabla R\cdot F)^2}\widetilde{r}_t^2 + \Pi_{F,\nabla R,\sigma}\right]\right)\right](Y_t^{\mathcal{R}}),$$

which is still an Itô process adapted to the larger filtration $(\sigma(B_s, W_s : 0 \leqslant s \leqslant t))_{t\geqslant 0}$. We refer to the Appendix 4.B for details of the computations.

4.4 Mobility and shear viscosity computations for Langevin dynamics

So far, we have made very few assumptions about the type of reference dynamics, driving force or flux. We now turn to presenting a framework in which the computation of physically meaningful transport coefficients may be performed, namely that of non-equilibrium (kinetic or underdamped) Langevin dynamics. We first recall the NEMD method for underdamped Langevin dynamics in Section 4.4.1, before specifying the expressions of the non-equilibrium forcings and response observables relevant for mobility and shear viscosity computations in Section 4.4.2. We finally derive the corresponding Norton dynamics in Section 4.4.3, and interpret it in terms of a principle of least constraint.

4.4.1 Standard non-equilibrium Langevin dynamics

The non-equilibrium framework we consider is that of a perturbation of the Langevin dynamics by an external driving force F. The state of the system is described by a vector $q \in \mathcal{D}$, describing the position of atoms, and a vector of corresponding momenta $p \in \mathbb{R}^{dN}$, where d

is the physical dimension and N is the number of atoms. The configurational domain $\mathcal{D}$ is usually considered to be $\mathbb{R}^{dN}$ or $(L\mathbb{T})^{dN}$ for some box length $L > 0$. The evolution of the system is governed by the Hamiltonian

$$H(q,p) = V(q) + \frac{1}{2} p \cdot M^{-1} p,$$

where $V : \mathcal{D} \to \mathbb{R}$ is the potential energy function. In practice, V is determined empirically to give an approximation of the ground-state energy for the Schrödinger Hamiltonian corresponding to the Born–Oppenheimer description of the system. The dynamics is given by the following stochastic differential equation:

$$\begin{cases} \mathrm{d}q_t = M^{-1} p_t \, \mathrm{d}t, \\ \mathrm{d}p_t = [-\nabla V(q_t) + \eta F(q_t)] \, \mathrm{d}t - \gamma M^{-1} p_t \, \mathrm{d}t + \sigma \, \mathrm{d}W_t. \end{cases} \tag{4.26}$$

The parameter $\beta > 0$ is proportional to the inverse temperature, M is a positive-definite symmetric mass matrix (typically a diagonal matrix), and γ and σ are two $dN \times dN$ matrices satisfying the fluctuation-dissipation relation

$$\sigma \sigma^{\mathsf{T}} = \frac{2\gamma}{\beta}.$$

The friction coefficient γ is thus a symmetric positive semi-definite matrix, and W is a standard dN-dimensional Brownian motion. Typically, γ is taken to be either a constant or a positive diagonal matrix, so that one simply writes $\sigma = \sqrt{2\gamma/\beta}$. The parameter η once again governs the magnitude of the non-equilibrium perturbation. One can show that at equilibrium ($\eta = 0$), the Boltzmann–Gibbs distribution

$$\mu(q,p) \, \mathrm{d}q \, \mathrm{d}p = Z^{-1} \mathrm{e}^{-\beta H(q,p)} \, \mathrm{d}q \, \mathrm{d}p \tag{4.27}$$

is an invariant probability measure for (4.26). In view of the separability of the Hamiltonian into a configurational and a kinetic part, the Boltzmann–Gibbs measure can be written in tensor form, as the product of a configurational measure

$$m(q) \, \mathrm{d}q = \frac{1}{Z_m} \mathrm{e}^{-\beta V(q)} \, \mathrm{d}q,$$

and of a Gaussian kinetic measure

$$\kappa(p) \, \mathrm{d}p = \det \left(\frac{2\pi M}{\beta} \right)^{-1/2} \mathrm{e}^{-\frac{\beta}{2} p \cdot M^{-1} p} \, \mathrm{d}p.$$

Momenta and positions are thus uncorrelated at equilibrium. Since the perturbation is generally non-gradient, there is however no way to write out the expression of the invariant probability measure of the non-equilibrium dynamics ($\eta \neq 0$). Momenta and positions typically have a correlation of order η under this measure.

4.4.2 Non-equilibrium forcings and fluxes

In this work, we consider transport coefficients corresponding to fluxes which can be written under the form

$$R(q,p) = G(q)\cdot p, \tag{4.28}$$

where $G : \mathcal{D} \to \mathbb{R}^{dN}$ is a vector field. Such forms of the response can be understood as measuring correlations between the momenta and some possibly non-linear feature of the configurational coordinates. In particular, such responses have zero-mean at equilibrium, owing to the tensor form of the Boltzmann–Gibbs measure and the fact that the average momentum under κ vanishes. The form (4.28) is general enough to capture the cases of mobility and shear viscosity computations for molecular fluids, which we now proceed to present, and which are our numerical test cases.

Mobility computations. We first describe the NEMD method for the computation of diffusion properties. Here, we consider a periodic domain $\mathcal{D} = (L\mathbb{T})^d$. The NEMD method is obtained by taking F as a constant vector field in (4.26), and the velocity in the direction F as the response, which measures the particle flux in the direction F. We assume that F is normalized as $\|F\| = 1$. Thus the perturbation and response observable are defined respectively by

$$F(q) = F \in \mathbb{R}^{3N}, \qquad R(q) = F \cdot M^{-1}p. \tag{4.29}$$

Using the symmetry of M, one may rewrite $R(q,p)$ under the form (4.28). For practical computations, we consider two cases:

- *Single drift*: this corresponds to a perturbation where the force acts on a single component of the momentum, which can be assumed (by indistinguishability of the particles) to be the x component of the first particle:

$$F_{\mathrm{S}} = (1,0,\dots)^{\intercal} \in \mathbb{R}^{dN}. \tag{4.30}$$

- *Color drift* (see [119, Chapter 6]): this corresponds to a perturbation in which the force acts on half of the particles in one direction, and on half of the particles in the opposite direction, which we choose by convention to be the x direction:

$$F_{\mathrm{C}} = \frac{1}{\sqrt{N}}(\underbrace{1,0,\dots,0}_{\in\mathbb{R}^d},-1,0,\dots,1,0\dots)^{\intercal} \in \mathbb{R}^{dN}. \tag{4.31}$$

The corresponding transport coefficients are related to the diffusion properties of the molecular system. More precisely, the transport coefficient $\alpha_{F_{\mathrm{S}}}$ for the single drift forcing can be related to the diffusion coefficient

$$D = \lim_{T\to\infty} \frac{1}{2dNT} \sum_{i=1}^{dN} \mathbb{E}_0\left[\left(\int_0^T M^{-1}p_{s,i}\,\mathrm{d}s\right)^2\right]$$

for an isotropic system via

$$\alpha_{F_{\mathrm{S}}} = \beta D,$$

as shown in [285]. When the potential energy function satisfies

$$\sum_{i=1}^{N} \frac{\partial}{\partial q_{i,x}} V(q) = 0, \tag{4.32}$$

a condition satisfied for instance for pairwise interactions depending only on the relative distances (as for (4.55) below), then the transport coefficient $\alpha_{F_{\mathrm{C}}}$ for the color drift is related to $\alpha_{F_{\mathrm{S}}}$ through

$$\alpha_{F_{\mathrm{C}}} = \alpha_{F_{\mathrm{S}}} - \frac{2\lfloor N/2 \rfloor}{N(N-1)} \left(\frac{1}{\gamma} - \alpha_{F_{\mathrm{S}}} \right). \tag{4.33}$$

See Appendix 4.C for the proof of this relation. In particular $\alpha_{F_{\mathrm{C}}}$ coincides with $\alpha_{F_{\mathrm{S}}}$ in the thermodynamic limit $N \to \infty$.

The interest of considering these two drift perturbations is to assess whether the Norton method requires the forcing to act on the bulk of the sytem (color drift case) to be consistent with the NEMD method. The other extreme is that of a forcing acting on a single particle (single drift case).

Shear viscosity computations. The Norton framework described in this section also allows for the computation of the shear viscosity; see [320] for a review of various approaches to compute this transport coefficient. Instead of considering bulk forcings which require modifying the periodic boundary conditions (as studied in [103] for instance), we consider the method introduced in [141], for which the non-gradient force is periodic. The mathematical properties of this approach in the case of Langevin dynamics are studied in [190]. In this setting, we consider an anisotropic three-dimensional configurational domain of the form

$$\mathcal{D} = (L_x \mathbb{T} \times L_y \mathbb{T} \times L_z \mathbb{T})^N .$$

We further allow for an anisotropic friction coefficient γ which is diagonal and defined by three directional friction coefficients $\gamma_x, \gamma_y, \gamma_z > 0$. A forcing is applied on the momenta in the longitudinal direction x, with an intensity depending on the transverse configurational coordinate y, according to a predefined forcing profile $f : L_y \mathbb{T} \to \mathbb{R}$:

$$\forall\, 1 \leqslant j \leqslant N, \qquad F(q)_{j,x} = f(q_{j,y}), \qquad F(q)_{j,y} = F(q)_{j,z} = 0.$$

In the non-equilibrium steady-state, the system displays an average longitudinal velocity profile depending only the transverse coordinate and the magnitude of the non-equilibrium perturbation. More precisely, given an approximation of the identity $(\psi_\varepsilon)_{\varepsilon>0}$ on $L_y \mathbb{T}$, define

$$u_x(y) = \lim_{\varepsilon \to 0} \lim_{\eta \to 0} \frac{L_y}{\eta N} \mathbb{E}_\eta \left[\sum_{j=1}^{N} \left(M^{-1} p \right)_{j,x} \psi_\varepsilon(q_{j,y} - y) \right]. \tag{4.34}$$

The term L_y in the numerator is motivated by the fact that the average with respect to the y coordinate of the term inside the limits is the velocity, up to a factor $1/\eta$:

$$\frac{1}{L_y}\int_{L_y\mathbb{T}}\left(\frac{L_y}{\eta N}\mathbb{E}_\eta\left[\sum_{j=1}^{N}\left(M^{-1}p\right)_{j,x}\psi_\varepsilon(q_{j,y}-y)\right]\right)\mathrm{d}y = \frac{1}{\eta N}\sum_{j=1}^{N}\mathbb{E}_\eta\left[\left(M^{-1}p\right)_{j,x}\right] = \frac{1}{\eta}\mathbb{E}_\eta\left[\left(M^{-1}p\right)_{1,x}\right],$$

using the indistinguishability of the particles to obtain the last equality. Thus u_x corresponds to a localized linear response of the longitudinal velocity, which can be estimated in practice from trajectory averages using a binning procedure. One can then derive the following differential equation relating u_x to the shear viscosity ν:

$$-\nu u_x''(y) + \gamma_x \rho u_x(y) = \rho f(y),$$

where $\rho = N/(L_xL_yL_z)$ is the particle density of the system. Since this profile is periodic in the transverse coordinate, the shear viscosity can be related to the Fourier coefficients of u_x and f, namely

$$U_1 = \frac{1}{L_y}\int_0^{L_y} u_x(y)\,\mathrm{e}^{\frac{2\mathrm{i}\pi y}{L_y}}\,\mathrm{d}y, \qquad F_1 = \frac{1}{L_y}\int_0^{L_y} f(y)\,\mathrm{e}^{\frac{2\mathrm{i}\pi y}{L_y}}\,\mathrm{d}y,$$

through

$$\nu = \rho\left(\frac{F_1}{U_1} - \gamma_x\right)\left(\frac{L_y}{2\pi}\right)^2.$$

For practical purposes, we choose f such that F_1 is analytically known, which is for instance the case if f is a sinusoidal profile. Taking the limit $\varepsilon \to 0$, in (4.34), the Fourier coefficient U_1 can be rewritten as

$$U_1 = \lim_{\eta\to 0}\frac{1}{\eta N}\mathbb{E}_\eta\left[\sum_{j=1}^{N}\left(M^{-1}p\right)_{j,x}\exp\left(\frac{2\mathrm{i}\pi q_{j,y}}{L_y}\right)\right].$$

This expression is precisely the linear response (4.5) for the following response observable, which is an empirical Fourier coefficient for the longitudinal velocity profile:

$$R(q,p) = \frac{1}{N}\sum_{j=1}^{N}\left(M^{-1}p\right)_{j,x}\exp\left(\frac{2\mathrm{i}\pi q_{j,y}}{L_y}\right). \tag{4.35}$$

This response is also of the form (4.28). One can in turn estimate it using trajectory averages, as in (4.6), yielding the estimator

$$\widehat{U}_{1,\eta,T} = \frac{1}{\eta T N}\sum_{j=1}^{N}\int_0^T\left(M^{-1}p_t\right)_{j,x}\exp\left(\frac{2\mathrm{i}\pi q_{j,y,t}}{L_y}\right)\mathrm{d}t. \tag{4.36}$$

4.4.3 The Norton method for Langevin dynamics

We write more explicitly in this section the Norton dynamics for observables of the form (4.28). The general dynamics (4.8) greatly simplifies in this situation, and also admits a nice physical interpretation.

Closed form of the dynamics. Note first that $\nabla_p^2 R(q,p) = 0$ when R is of the form (4.28), which together with the fact that the noise is degenerate (it acts only on the momenta in (4.26)) implies that the quadratic covariation term in (4.17) vanishes. The forcing F, too, acts only on the momenta, so that computing the projectors (4.14) for the choices

$$A(q,p) = \begin{pmatrix} 0 \\ F(q) \end{pmatrix}, \qquad B(q,p) = \nabla R(q,p) = \begin{pmatrix} \nabla G(q)p \\ G(q) \end{pmatrix},$$

yields the following expression for the projector associated with the Norton dynamics:

$$\mathrm{I}_{2dN} - \frac{A \otimes B}{A \cdot B}(q,p) = \begin{pmatrix} \mathrm{I}_{dN} & 0 \\ -\dfrac{F(q) \otimes \nabla G(q)p}{F(q) \cdot G(q)} & \mathrm{I}_{dN} - \dfrac{F(q) \otimes G(q)}{F(q) \cdot G(q)} \end{pmatrix}.$$

Since

$$\mathrm{I}_{dN} - \frac{F(q) \otimes G(q)}{F(q) \cdot G(q)} = \overline{P}_{F,G}(q),$$

where we slightly abuse the notation (4.14), it follows that the Norton dynamics (4.17) is given by

$$\begin{cases} \mathrm{d}q_t = M^{-1} p_t \, \mathrm{d}t, \\ \mathrm{d}p_t = \overline{P}_{F,G}(q_t) \left(-\nabla V(q_t) \, \mathrm{d}t - \gamma M^{-1} p_t \, \mathrm{d}t + \sqrt{\dfrac{2\gamma}{\beta}} \, \mathrm{d}W_t \right) \\ \qquad\quad - \dfrac{\nabla G(q_t) p_t \cdot M^{-1} p_t}{F(q_t) \cdot G(q_t)} F(q_t) \, \mathrm{d}t. \end{cases} \tag{4.37}$$

Note that the configurational part of the dynamics is unaffected, which is consistent with the choice of a non-equilibrium perturbation acting solely on the momenta. The forcing observable (4.16) is given by

$$\lambda(q,p) = \frac{G(q) \cdot (\nabla V(q) + \gamma M^{-1} p) - \nabla G(q) p \cdot M^{-1} p}{F(q) \cdot G(q)}, \tag{4.38}$$

and the controllability condition is given by

$$(G \cdot F)(q) \neq 0. \tag{4.39}$$

Remark 4.2. We have restricted ourselves to a simple Langevin dynamics where the drift term is the sum of a gradient force and a linear friction term, and the noise is additive. The derivation can however be extended verbatim to a more general dynamics of the form

$$\begin{cases} \mathrm{d}q_t = M^{-1} p_t \, \mathrm{d}t, \\ \mathrm{d}p_t = b(q_t, p_t) \, \mathrm{d}t + \sigma(q_t, p_t) \, \mathrm{d}W_t, \end{cases}$$

for general drift terms b and diffusion matrices σ. For these kinetic dynamics, the associated Norton dynamics is given by

$$\begin{cases} \mathrm{d}q_t = M^{-1} p_t \, \mathrm{d}t, \\ \mathrm{d}p_t = \overline{P}_{F,G}(q_t) \left[b(q_t, p_t) \, \mathrm{d}t + \sigma(q_t, p_t) \, \mathrm{d}W_t \right] - \dfrac{\nabla G(q_t) p_t \cdot M^{-1} p_t}{F(q_t) \cdot G(q_t)} F(q_t) \, \mathrm{d}t. \end{cases}$$

Physical interpretation. In the particular case of Langevin dynamics, the Norton method has the physical interpretation that it obeys a version of Gauss's principle of least constraint. The connection between Gauss's principle and non-equilibrium thermodynamics was already pointed out in [117], see also the discussion in [119, Section 5.2]. The principle of least constraints is a statement of classical dynamics equivalent to D'Alembert's principle, stating that the force applied to a system subject to a set of holonomic or non-holonomic constraints minimizes at every point in time the Euclidean distance to the force of the same system free from any constraints. Although we describe this interpretation in a deterministic setting, we stress that it remains valid, at least on a formal level, upon considering a stochastic version of the dynamics. More precisely, we assume that the dynamics for the unconstrained system can be written under the form

$$\begin{cases} \dot{q} = M^{-1} p, \\ \dot{p} = f_{\mathrm{ref}}(q, p), \end{cases} \tag{4.40}$$

and that the constraint is of the form $R(q) = r$ (holonomic case) or $R(q, p) = r$ (non-holonomic case). We can then write the dynamics of the constrained system as

$$\begin{cases} \dot{q} = M^{-1} p, \\ \dot{p} = f_{\mathrm{cons}}(q, p), \end{cases}$$

where $f_{\mathrm{cons}}(q, p)$ is the force on the constrained system obeying Gauss's principle, which dictates that $f_{\mathrm{cons}}(q, p)$ is the orthogonal projection of $f_{\mathrm{ref}}(q)$ onto the affine hyperplane $\mathcal{H}_{q,p}$ of admissible forces. This hyperplane can be determined by differentiating the constraint in time and setting it to zero. To obtain a constraint on the time derivative of the momenta $\dot{p}$, this differentiation has to be performed once in the non-holonomic case and twice in the holonomic case. A simple computation shows that the hyperplane of admissible forces is thus given in the holonomic case by

$$\mathcal{H}_{q,p} = \left\{ \xi \in \mathbb{R}^{dN} \,\middle|\, \xi \cdot M^{-1} \nabla R(q) + \left(M^{-1} p \right)^{\otimes 2} : \nabla^2 R(q) = 0 \right\},$$

and in the non-holonomic case by

$$\mathcal{H}_{q,p} = \left\{ \xi \in \mathbb{R}^{dN} \,\middle|\, \xi \cdot \nabla_p R(q, p) + \left(M^{-1} p \right) \cdot \nabla_q R(q, p) = 0 \right\}. \tag{4.41}$$

In particular, $f_{\mathrm{cons}}(q, p) - f_{\mathrm{ref}}(q, p)$ is proportional to $\nabla_p R(q, p)$ in the non-holonomic case, and to $M^{-1} \nabla R(q)$ in the holonomic case. The use of holonomic constraints is widespread in MD, where they are used to simulate systems with molecular constraints (such as fixed bond lengths or bond angles). See [220, Chapter 4] for a general introduction, and [230] for a detailed study of the underdamped Langevin case.

The Norton dynamics (4.37) for a response function R of the form (4.28) also satisfies a version of Gauss's principle of least constraint with respect to a non-Euclidean metric for which $F(q)$ is everywhere orthogonal, in the sense of this metric, to $G(q)^\perp$, the Euclidean orthogonal to $G(q)$. More precisely, this metric is induced by the configuration-dependent norm

$$\|\xi\|_q^2 = (\xi \cdot F(q))^2 + \left\| \xi - \frac{\xi \cdot G(q)}{\|G(q)\|^2} G(q) \right\|^2,$$

where $\|\cdot\|$ denotes the usual Euclidean norm. This metric is defined and non-degenerate if F and G are both non-zero, which is implied by the controllability condition (4.18). As we show below, the force on the constrained system is, in this metric, obtained as

$$\operatorname*{argmin}_{\xi \in \mathcal{H}_{q,p}} \|\xi - f_{\mathrm{ref}}(q,p)\|_q = \overline{P}_{F,G}(q) f_{\mathrm{ref}}(q,p) - \frac{\nabla G(q)p \cdot M^{-1}p}{F(q) \cdot G(q)} F(q), \tag{4.42}$$

where $\mathcal{H}_{q,p}$ is the hyperplane defined in (4.41) associated with the non-holonomic constraint $R(q,p) = G(q) \cdot p = r$. This is precisely the Norton force corresponding to the unconstrained system (4.40).

To prove (4.42), we proceed as follows. Note first that $\mathcal{H}_{q,p}$ in (4.41) is an affine translate of $\nabla_p R(q,p)^\perp = G(q)^\perp$, the Euclidean orthogonal to $G(q)$, so that its normal direction with respect to the scalar product induced by $\|\cdot\|_q$ is $F(q)$. Furthermore, the norm $\|\cdot\|_q$ is constructed precisely so that the projector $\overline{P}_{F,G}(q)$, whose action is depicted in Figure 4.1, is an orthogonal projector onto $G(q)^\perp$, for the scalar product associated with $\|\cdot\|_q$. This implies that the minimizer in (4.42) is of the form

$$\xi^*(q,p) = f_{\mathrm{ref}}(q,p) - \alpha F(q) \in \mathcal{H}_{q,p}.$$

The value of α is determined by the condition

$$(f_{\mathrm{ref}}(q,p) - \alpha F(q)) \cdot G(q) + \nabla G(q)p \cdot M^{-1}p = 0,$$

hence

$$\alpha = \frac{f_{\mathrm{ref}}(q) \cdot G(q) + \nabla G(q)p \cdot M^{-1}p}{F(q) \cdot G(q)},$$

and finally

$$\xi^*(q,p) = f_{\mathrm{ref}}(q) - \alpha F(q) = \overline{P}_{F,G}(q) f_{\mathrm{ref}}(q) - \frac{\nabla G(q)p \cdot M^{-1}p}{F(q) \cdot G(q)} F(q).$$

Loosely speaking, the Norton dynamics is the least non-equilibrium like of all dynamics on the constant response manifold, if one measures similarity in terms of the force considered in the $\|\cdot\|_q$ metric.

4.5 Numerical discretizations of Norton dynamics

We describe in this section a discretization of the Norton dynamics, first for the general dynamics (4.8) in Section 4.5.1, before specializing it to the setting of Langevin dynamics. The

numerical schemes are based for Langevin dynamics on splitting schemes, inspired by the ones typically used in the NEMD setting, but have the additional property of exactly preserving the flux throughout the numerical trajectory. For completeness, we describe splitting schemes in the case of standard NEMD Langevin dynamics in Section 4.5.2, and then in the Norton setting in Section 4.5.3. We finally describe in Section 4.5.4 a way to estimate the bounded variation part of the forcing (4.16) from the numerical trajectories, in order to approximate (4.21).

4.5.1 Numerical schemes for general Norton dynamics

We discuss here the simulation of the Norton dynamics (4.8), which requires a discretization in time. Formally, given a time step $\Delta t > 0$, a numerical scheme for the equilibrium dynamics (4.1) is defined by a map $\Phi_{\Delta t} : \mathcal{X} \times \mathbb{R}^m \to \mathcal{X}$ which, iterated with independent and identically distributed (i.i.d.) standard m-dimensional Gaussian variables $(\mathcal{G}_n)_{n \geqslant 0}$ yields a discretization of the dynamics:

$$X^{n+1} = \Phi_{\Delta t}(X^n, \mathcal{G}^n),$$

i.e. X^n is an approximation of $X_{n\Delta t}$. For example, the Euler–Maruyama scheme for the Thévenin dynamics (4.1) corresponds to

$$\Phi^{\mathrm{EM}}_{\Delta t}(x, g) = x + \Delta t \, [b(x) + \eta F(x)] + \sqrt{\Delta t} \, \sigma(x) g.$$

In principle, it would be possible to consider discretizations directly based on the autonomous form of the Norton dynamics (4.17), and average the forcing observable λ along the so-obtained numerical trajectories. However, a key property we require from a numerical scheme is that the constant flux manifold should be preserved under the discrete dynamics. Standard discretizations of (4.17) usually do not satisfy such preservation properties. Moreover, since the autonomous form of the dynamics involves second-order derivatives of the response, which may be cumbersome or expensive to compute, it is typically more convenient numerically to take another approach, obtained by enforcing the constraint via a Lagrange multiplier. Given a stochastic scheme $\Phi_{\Delta t}$ for the reference dynamics, we can consider the following discretization of the Norton dynamics:

$$\begin{cases} \widetilde{X}^{n+1} = \Phi_{\Delta t}(X^n, G^n), \\ X^{n+1} = \widetilde{X}^{n+1} + \Delta t \Lambda^{n,*} F(X^n), \\ R(X^{n+1}) = r. \end{cases} \tag{4.43}$$

Note that we chose here, somewhat arbitrarily, to perform the projection with respect to $F(X^n)$. Other possible choices include $F(\widetilde{X}^{n+1})$ or $F(X^{n+1})$, the latter choice generally yielding an implicit scheme. In any case, finding $\Lambda^{n,*}$ requires solving

$$R\left(\widetilde{X}^{n+1} + \Delta t \Lambda^{n,*} F(X^n)\right) = r,$$

which is typically a non-linear equation, for which the appropriate numerical strategy depends on the situation at hand. A typical choice is to resort to Newton's method or a fixed-point iteration, as done when enforcing holonomic constraints in MD (see [148, Section VII.1] and [222, Chapter 7]), as well as [293, 10] for pioneering works motivated by applications in

MD.

Note that $\Lambda^{n,*}$ approximates the full forcing increment $\Lambda_{(n+1)\Delta t} - \Lambda_{n\Delta t}$, and in particular incorporates the martingale increment. This martingale part should be removed when estimating $\mathbb{E}_r^*[\lambda]$ in order to reduce the variance of the estimator under consideration. This can be done at first order in $\sqrt{\Delta t}$ by using a control variate derived from its analytic expression (4.12), and the following equality in law: $\sqrt{\Delta t}\ G^n \overset{\text{law}}{=} W_{(n+1)\Delta t} - W_{n\Delta t}$. This leads to the following estimator of $\lambda \Delta t$:

$$\Lambda^n = \Lambda^{n,*} + \sqrt{\Delta t} \frac{\nabla R(X^n) \cdot \sigma(X^n) G^n}{\nabla R(X^n) \cdot F(X^n)}. \tag{4.44}$$

The efficiency of such variance reduction methods has already been demonstrated for the estimation of mean Lagrange multipliers associated with holonomic constraints, for example in the context of free energy computations (see [83] and [229, Remark 3.33]). An estimation of the ensemble average $\mathbb{E}_r^*[\lambda]$ can be obtained by considering trajectory averages

$$\widehat{\lambda}_{N_{\text{iter}}} = \frac{1}{N_{\text{iter}}} \sum_{n=1}^{N_{\text{iter}}} \lambda^n, \qquad \lambda^n = \frac{1}{\Delta t} \Lambda^n.$$

As hinted at above, this strategy has the clear advantage that one does not have to compute $\lambda(X^n)$ along the trajectory (which may be tedious to implement in practice), since consistent approximations thereof appear as natural byproducts of the integration procedure.

4.5.2 Splitting schemes for (non-)equilibrium Langevin dynamics

In the particular case where the reference dynamics is the Langevin dynamics (4.26), one can resort to a class of discretization strategies based on operator splittings of the infinitesimal generator, which we briefly recall for completeness in this section (see [219, 221], and [220, Chapter 7] for more details). By carefully choosing the order of the operators appearing in this splitting in the equilibrium setting, one can devise highly stable numerical schemes, which have a lower bias when sampling configurational averages in the overdamped limit $\gamma \to \infty$ compared with other choices of the splitting order (see [219]), while also showing desirable energy-conservation properties in the Hamiltonian limit $\gamma \to 0$. Such schemes have become the standard choice to integrate kinetic Langevin dynamics in MD applications. The general procedure is as follows.

The generator of the (non-)equilibrium Langevin dynamics can be written as the sum of four terms,

$$\mathcal{L}_\eta = \mathcal{L}^{\mathrm{A}} + \mathcal{L}^{\mathrm{B}} + \gamma \mathcal{L}^{\mathrm{O}} + \eta \widetilde{\mathcal{L}},$$

with

$$\begin{cases} \mathcal{L}^{\mathrm{A}} = M^{-1} p \cdot \nabla_q, \\ \mathcal{L}^{\mathrm{B}} = -\nabla V \cdot \nabla_p, \\ \mathcal{L}^{\mathrm{O}} = -M^{-1} p \cdot \nabla_p + \dfrac{1}{\beta} \Delta_p, \\ \widetilde{\mathcal{L}} = F \cdot \nabla_p. \end{cases}$$

The operators $\mathcal{L}^{\mathrm{A}}$, $\mathcal{L}^{\mathrm{B}} + \eta \widetilde{\mathcal{L}}$ and $\gamma \mathcal{L}^{\mathrm{O}}$ can be viewed as infinitesimal generators in their own

right, which correspond respectively to the three following elementary dynamics. The dynamics generated by $\mathcal{L}^{\mathrm{A}}$ is given by

$$\begin{cases} \mathrm{d}q_t = M^{-1} p_t \, \mathrm{d}t, \\ \mathrm{d}p_t = 0, \end{cases} \tag{4.45}$$

while $\mathcal{L}^{\mathrm{B}} + \eta \widetilde{\mathcal{L}}$ gives rise to

$$\begin{cases} \mathrm{d}q_t = 0, \\ \mathrm{d}p_t = \left(-\nabla V(q_t) + \eta F(q_t) \right) \mathrm{d}t. \end{cases} \tag{4.46}$$

Finally, $\mathcal{L}^{\mathrm{O}}$ generates the following Ornstein–Uhlenbeck process on the momenta:

$$\begin{cases} \mathrm{d}q_t = 0, \\ \mathrm{d}p_t = -\gamma M^{-1} p_t \, \mathrm{d}t + \sqrt{\dfrac{2\gamma}{\beta}} \, \mathrm{d}W_t. \end{cases} \tag{4.47}$$

The three elementary dynamics (4.45), (4.46), (4.47) are analytically integrable. Splitting schemes for the Thévenin dynamics are obtained by composing the evolution operators $\mathrm{e}^{\Delta t \mathcal{L}^{\mathrm{A}}}$, $\mathrm{e}^{\Delta t \left(\mathcal{L}^{\mathrm{B}} + \eta \widetilde{\mathcal{L}} \right)}$ and $\mathrm{e}^{\Delta t \mathcal{L}^{\mathrm{O}}}$ corresponding to each of these elementary dynamics. For instance, the evolution operator for the celebrated BAOAB method corresponds to

$$\mathrm{e}^{\frac{\Delta t}{2} \left(\mathcal{L}^{\mathrm{B}} + \eta \widetilde{\mathcal{L}} \right)} \mathrm{e}^{\frac{\Delta t}{2} \mathcal{L}^{\mathrm{A}}} \mathrm{e}^{\Delta t \gamma \mathcal{L}^{\mathrm{O}}} \mathrm{e}^{\frac{\Delta t}{2} \mathcal{L}^{\mathrm{A}}} \mathrm{e}^{\frac{\Delta t}{2} \left(\mathcal{L}^{\mathrm{B}} + \eta \widetilde{\mathcal{L}} \right)}.$$

These schemes can be formally justified, and rigorously analyzed with the Baker–Campbell–Hausdorff formula, yielding error estimates à la Talay–Tubaro on the invariant measure in the linear response regime where $|\eta|$ is small, as well as on estimators of transport coefficients, see [221].

4.5.3 Splitting schemes for Langevin–Norton dynamics

For the Langevin dynamics (4.37) in the Norton setting, a strategy similar to the one in Section 4.5.2 can be used. The generator of the Norton dynamics can be split as the sum of three operators, each of which is the generator of an elementary dynamics, still denoted by A, B and O. In fact, these are the Norton counterparts of the elementary dynamics (4.45), (4.46) and (4.47), which therefore preserve the flux by construction. This splitting strategy is still motivated by the fact that each elementary dynamics individually preserves the flux observable (4.28). However, in contrast to the NEMD case, the flow of the A-dynamics is generally not known in analytical form, and one has to resort to a numerical scheme to approximate it.

In order to make the numerical scheme precise, the first step is to split the generator as

$$\mathfrak{L} = \mathfrak{L}^{\mathrm{A}} + \mathfrak{L}^{\mathrm{B}} + \gamma \mathfrak{L}^{\mathrm{O}}, \tag{4.48}$$

with

$$\begin{cases} \mathfrak{L}^{\mathrm{A}} = M^{-1}p \cdot \nabla_q - \dfrac{(\nabla G)\, p \cdot M^{-1}p}{F \cdot G} F \cdot \nabla_p, \\ \mathfrak{L}^{\mathrm{B}} = -\overline{P}_{F,G} \nabla V \cdot \nabla_p, \\ \mathfrak{L}^{\mathrm{O}} = -\overline{P}_{F,G} M^{-1} p \cdot \nabla_p + \dfrac{1}{\beta} \overline{P}_{F,G} \overline{P}_{F,G}^{\intercal} : \nabla_p^2. \end{cases}$$

This decomposition is motivated by the flux conservation properties $\mathfrak{L}^{\mathrm{B}} R = \mathfrak{L}^{\mathrm{O}} R = 0$, which immediately imply that $\mathfrak{L}^{\mathrm{A}} R = 0$, since the overall dynamics with generator $\mathfrak{L}$ conserves the non-equilibrium response by construction.

Decomposition into elementary dynamics. Analogously to the NEMD case, we interpret the various operators on the right-hand side of (4.48) as the generators of elementary dynamics, and use the same terminology as in Section 4.5.2. In fact, these elementary dynamics are precisely the Norton counterparts (4.17) to each of the NEMD elementary dynamics, so that they indeed individually preserve the response. They read

$$\begin{aligned} &\text{A dynamics:} && \begin{cases} \mathrm{d}q_t = M^{-1} p_t \, \mathrm{d}t, \\ \mathrm{d}p_t = -\dfrac{\nabla G(q_t) p_t \cdot M^{-1} p_t}{F(q_t) \cdot G(q_t)} F(q_t) \, \mathrm{d}t. \end{cases} \\ &\text{B dynamics:} && \begin{cases} \mathrm{d}q_t = 0, \\ \mathrm{d}p_t = -\overline{P}_{F,G}(q_t) \nabla V(q_t) \, \mathrm{d}t. \end{cases} \\ &\text{O dynamics:} && \begin{cases} \mathrm{d}q_t = 0, \\ \mathrm{d}p_t = \overline{P}_{F,G}(q_t) \left(-\gamma M^{-1} p_t \, \mathrm{d}t + \sqrt{\dfrac{2\gamma}{\beta}} \, \mathrm{d}W_t \right). \end{cases} \end{aligned} \tag{4.49}$$

Note that, in contrast to the NEMD setting, the A-dynamics is not analytically solvable, so that one has to resort to a numerical approximation similar to those discussed in Section 4.5.1 to integrate it (see Section 4.5.4). However, the Norton counterparts of the B and O dynamics remain analytically integrable, as we discuss below.

Analytic integration of the B and O dynamics. The B-dynamics is a time-linear evolution in the momenta, whose solution is given by

$$(q_t, p_t) = \left(q_0, p_0 - t \overline{P}_{F,G} \nabla V(q_0) \right) = \left(q_0, P_{F,G}(q_0) p_0 + \overline{P}_{F,G}(q_0) \left[p_0 - t \nabla V(q_0) \right] \right).$$

In view of the equality $G(q) \cdot p = G(q) \cdot P_{F,G}(q) p$, and since $\overline{P}_{F,G}$ is a projector onto $G^{\perp}$, it is immediate that the B-dynamics preserves the response flux. One could also simply notice that it is the Norton counterpart to the NEMD B-dynamics (4.46).

The O-dynamics is a projected Ornstein–Uhlenbeck process. To analytically integrate this dynamics, we assume that $\overline{P}_{F,G}$ and γM^{-1} commute. If this is not the case, the analytical integration below should be replaced by an appropriate numerical scheme, such as a midpoint rule. Using standard arguments of Itô calculus, and the fact that $\overline{P}_{F,G}$ is a projector, it is

straightforward to check that the solution is given for all $t \geqslant 0$ by $q_t = q_0$ and

$$p_t = P_{F,G}(q_0)p_0 + \overline{P}_{F,G}(q_0)\left(\mathrm{e}^{-t\gamma M^{-1}}p_0 + \int_0^t \mathrm{e}^{-\gamma M^{-1}(t-s)}\sqrt{\frac{2\gamma}{\beta}}\,\mathrm{d}W_s\right).$$

This is a Gaussian process, which has the following alternative representation in distribution:

$$p_t = P_{F,G}(q_0)p_0 + \overline{P}_{F,G}(q_0)\left(\mathrm{e}^{-t\gamma M^{-1}}p_0 + \sqrt{\frac{1-\mathrm{e}^{-2t\gamma M^{-1}}}{\beta}}M\mathcal{G}\right),$$

where $\mathcal{G}$ is a standard dN-dimensional Gaussian. By the same arguments as for the B-dynamics, the Norton O-dynamics preserves the response flux, and is likewise the Norton counterpart to the NEMD O-dynamics (4.47).

4.5.4 Estimation of the average forcing

By composing the evolution operators of elementary Norton dynamics, one obtains a natural splitting approximation of the evolution operator for the forcing process of the full Norton dynamics. The numerical translation of this observation is that one can estimate trajectory averages of λ directly from examining individual integration steps of the splitting scheme. We describe in this section the general procedure to this end.

For a fixed time step $\Delta t > 0$ and response magnitude $r \in \mathbb{R}$, we define three discrete flows acting on the augmented state $(q, p, \ell) \in \mathcal{D} \times \mathbb{R}^{dN} \times \mathbb{R}$. The role of the auxiliary variable ℓ is to accumulate the bounded-variation component of Lagrange multipliers enforcing the constant-flux constraint during the integration step. It is thus initialized at 0 at the start of each integration step, accumulating the contributions of each part of the splitting.

Discrete integration of the A dynamics. The discrete flow associated with the A-step is given by

$$\Phi^{\mathrm{A}}_{\Delta t,r}(q,p,\ell) = \left(q + \Delta t M^{-1}p, p + \xi^{\mathrm{A}}_{\Delta t,r}(q,p)F\left(q + \Delta t M^{-1}p\right), \ell + \xi^{\mathrm{A}}_{\Delta t,r}(q,p)\right),$$

where $\xi^{\mathrm{A}}_{\Delta t,r}(q,p)$ is the Lagrange multiplier characterized by the constant-flux condition

$$R\left(\Phi^{\mathrm{A}}_{\Delta t,r}(q,p,\ell)\right) = r,$$

with some abuse of notation in the arguments of R. When the response is of the form $R(q,p) = G(q)\cdot p$, we can explicitly solve for the Lagrange multiplier, as

$$\xi^{\mathrm{A}}_{\Delta t,r}(q,p) = \frac{r - G\left(q + \Delta t M^{-1}p\right)\cdot p}{F\left(q + \Delta t M^{-1}p\right)\cdot G\left(q + \Delta t M^{-1}p\right)}. \tag{4.50}$$

The Norton A-step is therefore equivalent to first evolving the system's coordinate variables according to the corresponding NEMD A-step before correcting the momenta, by applying a constraining force in the direction of $F(q + \Delta t M^{-1}p)$, the forcing evaluated at the updated position. As mentioned after (4.43), there is some freedom in the choice of point at which to

evaluate the forcing when projecting onto the submanifold $\Sigma_r = R^{-1}\{r\}$. The motivation for choosing $F(q + \Delta t M^{-1}p)$ is that the two functions appearing in the scalar product $F \cdot G$ in the denominator of the left-hand side of (4.50) are evaluated at the same point.

Discrete integration of the B dynamics. The discrete flow associated with the Norton B-step is given by

$$\Phi^{\mathrm{B}}_{\Delta t,r}(q,p,\ell) = \left(q, p - \Delta t \nabla V(q) + \xi^{\mathrm{B}}_{\Delta t,r}(q,p)F(q), \ell + \xi^{\mathrm{B}}_{\Delta t,r}(q,p)\right),$$

where $\xi^{\mathrm{B}}_{\Delta t,r}$ is again a Lagrange multiplier enforcing the constraint, given for a response $G(q)\cdot p$ by

$$\xi^{\mathrm{B}}_{\Delta t,r}(q,p) = \frac{r - G(q)\cdot(p - \Delta t \nabla V(q))}{F(q)\cdot G(q)}.$$

This again corresponds to a step of the NEMD B-dynamics, re-projected onto Σ_r in the direction $F(q)$. This coincides in fact with the analytic integration of the elementary B-dynamics (4.49) when $G(q)\cdot p = r$.

Discrete integration of the O dynamics. The flow associated with the Norton O-step is stochastic, hence we formulate it conditionally on a standard dN dimensional Gaussian $\mathcal{G}$ increment. In fact, we show below that, in the case where γ and M are scalar multiples of the identity matrix, a convenient update is

$$\Phi^{\mathrm{O}}_{\Delta t,r}(q,p,\ell|\,\mathcal{G}) = \left(q, \alpha_{\Delta t}p + \sigma_{\Delta t}\sqrt{\Delta t}\,\mathcal{G} + \xi^{\mathrm{O}}_{\Delta t,r}(q,p,\mathcal{G})F(q), \ell + \frac{r(1-\alpha_{\Delta t})}{F(q)\cdot G(q)}\right), \tag{4.51}$$

where $\alpha_{\Delta t}$ and $\sigma_{\Delta t}$ are given by

$$\alpha_{\Delta t} = \mathrm{e}^{-\gamma M^{-1}\Delta t}, \qquad \sigma_{\Delta t} = \sqrt{\frac{1-\alpha^2_{\Delta t}}{\beta \Delta t}M}.$$

To motivate (4.51), we start by deriving the expression of the Lagrange multiplier $\xi^{\mathrm{O}}_{\Delta t,r}$, which can be solved for our particular form of response (4.28) as

$$\xi^{\mathrm{O}}_{\Delta t,r}(q,p,\mathcal{G}) = \frac{r - \alpha_{\Delta t}G(q)\cdot p - \sigma_{\Delta t}\sqrt{\Delta t}\,G(q)\cdot\mathcal{G}}{F(q)\cdot G(q)}.$$

Again, this corresponds to integrating the NEMD O-dynamics over one time step before correcting the momenta in the direction $F(q)$. Since the contribution of $\mathcal{G}$ to this $\xi^{\mathrm{O}}_{\Delta t,r}$ is a centered Gaussian, we can remove it entirely to only accumulate the non-martingale component in ℓ. This is exactly equivalent to the variance reduction technique discussed in (4.44). Using $G(q)\cdot p = r$, one arrives at the expression given in (4.51) for the action of $\Phi^{\mathrm{O}}_{\Delta t,r}$ on ℓ. Once again, $\Phi^{\mathrm{O}}_{\Delta t,r}(q,p,\ell)_{q,p}$ corresponds to the analytic flow of the Norton O-dynamics (4.49) over one time step Δt, with deterministic initial condition (q,p).

If γ and M are genuine matrices, one does not have an exact cancellation of the martingale component of $\xi^{\mathrm{O}}_{\Delta t,r}$, and one has to resort to a variance reduction strategy in the spirit of Equation (4.44).

Construction of the splitting scheme. The steps $\mathrm{A}, \mathrm{B}, \mathrm{O}$ can be composed according to the order of the splitting, and the bounded-variation increment of the constraining process over one time step can be estimated from the final increment in ℓ. For example, conditionally on $\mathcal{G}^{n+1}$, a standard dN dimensional Gaussian, the update rule for the Norton BAOAB scheme is given by

$$(q^{n+1}, p^{n+1}, \ell^{n+1}) = \Phi^{\mathrm{B}}_{\Delta t/2,r} \circ \Phi^{\mathrm{A}}_{\Delta t/2,r} \circ \Phi^{\mathrm{O}}_{\Delta t,r}(\cdot \,|\, \mathcal{G}^{n+1}) \circ \Phi^{\mathrm{A}}_{\Delta t/2,r} \circ \Phi^{\mathrm{B}}_{\Delta t/2,r}(q^n, p^n, 0). \tag{4.52}$$

Note that we start from $\ell^n = 0$, and then accumulate the various increments of the constraining process to obtain ℓ^{n+1}. For concreteness, let us explicitly write the update rules for the numerical scheme (4.52) and a response observable $R(q,p) = G(q) \cdot p$:

$$\begin{cases}
p^{n+\frac{1}{5}} = p^n - \dfrac{\Delta t}{2} \nabla V(q^n) + \xi^{\mathrm{B}}_{\Delta t/2,r}(q^n, p^n) F(q^n), \\
\ell^{n+\frac{1}{5}} = \xi^{\mathrm{B}}_{\Delta t/2,r}(q^n, p^n), \\
q^{n+\frac{2}{5}} = q^n + \dfrac{\Delta t}{2} M^{-1} p^{n+\frac{1}{5}}, \\
p^{n+\frac{2}{5}} = p^{n+\frac{1}{5}} + \xi^{\mathrm{A}}_{\Delta t/2,r}(q^n, p^{n+\frac{1}{5}}) F(q^{n+\frac{2}{5}}), \\
\ell^{n+\frac{2}{5}} = \ell^{n+\frac{1}{5}} + \xi^{\mathrm{A}}_{\Delta t/2,r}(q^n, p^{n+\frac{1}{5}}), \\
p^{n+\frac{3}{5}} = \alpha_{\Delta t} p^{n+\frac{2}{5}} + \sigma_{\Delta t} \mathcal{G}^{n+1} + \xi^{\mathrm{O}}_{\Delta t,r}(q^{n+\frac{2}{5}}, p^{n+\frac{2}{5}}, \mathcal{G}^{n+1}) F(q^{n+\frac{2}{5}}), \\
\ell^{n+\frac{3}{5}} = \ell^{n+\frac{2}{5}} + \dfrac{r(1-\alpha_{\Delta t})}{F(q^{n+\frac{2}{5}}) \cdot G(q^{n+\frac{2}{5}})}, \\
q^{n+1} = q^{n+\frac{2}{5}} + \dfrac{\Delta t}{2} M^{-1} p^{n+\frac{3}{5}}, \\
p^{n+\frac{4}{5}} = p^{n+\frac{3}{5}} + \xi^{\mathrm{A}}_{\Delta t/2,r}(q^{n+\frac{2}{5}}, p^{n+\frac{3}{5}}) F(q^{n+1}), \\
\ell^{n+\frac{4}{5}} = \ell^{n+\frac{3}{5}} + \xi^{\mathrm{A}}_{\Delta t/2,r}(q^{n+\frac{2}{5}}, p^{n+\frac{3}{5}}), \\
p^{n+1} = p^{n+\frac{4}{5}} - \dfrac{\Delta t}{2} \nabla V(q^{n+1}) + \xi^{\mathrm{B}}_{\Delta t/2,r}(q^{n+1}, p^{n+\frac{4}{5}}) F(q^{n+1}), \\
\ell^{n+1} = \ell^{n+\frac{4}{5}} + \xi^{\mathrm{B}}_{\Delta t/2,r}(q^{n+1}, p^{n+\frac{4}{5}}).
\end{cases} \tag{4.53}$$

The average value of λ over the corresponding time step can then be estimated via

$$\lambda^{n+1} = \Delta t^{-1} \ell^{n+1}. \tag{4.54}$$

Since all the substeps are by construction preserving the value of the response function, splitting schemes based on (4.48) define discrete-time Markov chains on Σ_r. Fixing a splitting and a time step Δt, one can hope that the Markov chain admits a unique invariant probability measure $\pi^*_{r,\Delta t}$ close to the invariant measure of the continuous time Norton dynamics for $\Delta t > 0$ sufficiently small. Assessing the quality of these schemes (measured in terms of weak or strong error estimates, or errors on the invariant measure) as a function of the time step Δt, the magnitude of the perturbation r and the ordering of the splitting is an open question.

Remark 4.3. Let us emphasize that, when the form of the response function does not allow for analytical expressions of the Lagrange multipliers, one can still apply a splitting procedure similar to (4.53), upon replacing the explicit expressions of $\xi^X_{\Delta t,r}$ (for $X \in \{\mathrm{A}, \mathrm{B}, \mathrm{O}\}$) by the numerical solution of some nonlinear equation determining these quantities. It is still

possible to cancel at dominant order the martingale increment by subtracting the first order approximation in $\sqrt{\Delta t}$ of the latter quantity.

4.6 Numerical results

We present in this section the results of various numerical simulations for the Lennard–Jones fluid. The numerical experiments we perform have several aims:

- The first one is to verify that, at least in our setting, the Norton dynamics is a viable approach for the computation of transport coefficients, in the sense that Norton estimators of the linear response coincide with those obtained from NEMD computations. Of course, this cannot be expected for low dimensional systems. Consider for example the case of kinetic Langevin dynamics for a single one-dimensional particle on the unit torus $\mathbb{T}$, with $M = F = 1$, and $R(q,p) = p$. The invariant measure for the Norton dynamics is then easily seen to be the product of the uniform measure on $\mathbb{T}$ with the Dirac measure δ_r on momentum space, from which it follows in view of (4.38) that

$$\mathbb{E}_r^*[\lambda] = \int_0^1 V'(q)\,\mathrm{d}q + \gamma r = \gamma r,$$

  since V is periodic, whence the Norton transport coefficient is γ^{-1}, which differs in general from its NEMD counterpart.

- Once the validity of the Norton approach has been established, the second aim is to assess the numerical efficiency of the Norton method, relatively to the standard NEMD method. A crucial point is to determine whether the Norton approach leads to a reduction in the asymptotic variance (4.22) compared to (4.7) for estimators of the transport coefficient, as this quantity determines the magnitude of the statistical error, and therefore the simulation time needed to attain a given level of accuracy.

In Section 4.6.1, we present the system and notation used throughout all numerical experiments. In Section 4.6.2, we show instances of excellent agreement in the linear response between Norton and NEMD dynamics. We also exhibit a case in which the response profiles do not coincide. We further show that the agreement (when it holds) extends far into the non-linear response regime. In Section 4.6.3, we investigate the properties of the Norton and NEMD systems in the thermodynamic limit, showing that the linear responses coincide far before convergence to the thermodynamic limit, and exhibiting an interesting concentration property for the distribution of values of λ, both at equilibrium and in the non-equilibrium regime. Finally, in Section 4.6.4 we assess the efficiency of the Norton approach in terms of asymptotic variance, showing that in some cases the standard NEMD approach is significantly outperformed.

4.6.1 Description of the numerical experiments

Presentation of the system. In all experiments, we consider perturbations of the kinetic Langevin dynamics for a Lennard–Jones fluid. The potential energy function is given by

$$V_{\mathrm{LJ}}(q) = \sum_{1 \leqslant i < j \leqslant N} v\left(\|q_i - q_j\|\right), \tag{4.55}$$

where v is the radial function

$$v(r) = 4\varepsilon \left(\left(\frac{\sigma}{r}\right)^{12} - \left(\frac{\sigma}{r}\right)^{6} \right).$$

Note that $v'(2^{1/6}\sigma) = 0$. The parameters ε and σ modulate respectively the energy and spatial range of the interaction. It is convenient to state results in the system of reduced units in which ε, $2^{1/6}\sigma$, the mass m of each particle and the Boltzmann constant k_{b} are set to 1. In fact, we consider a slightly modified version of the potential (4.55), obtained by truncating the range of v as

$$v_{r_{\mathrm{c}}}(r) = \left[v(r) - v(r_{\mathrm{c}}) - v'(r_{\mathrm{c}})(r - r_{\mathrm{c}})\right] \mathbb{1}_{r \leqslant r_{\mathrm{c}}},$$

where r_{c} is a cutoff radius which prescribes the maximum range of interactions, the added affine term ensuring that $v_{r_{\mathrm{c}}}$ is C^1. We set $r_{\mathrm{c}} = 2.5$ in our simulations, which were performed using the Julia package `Molly` [143]. Both the Norton and NEMD simulations were carried out using a BAOAB numerical splitting scheme.

Discrete estimators of transport coefficients. We compute approximations of the mobility by plotting the average response as a function of the forcing magnitude η, and fitting the slope of the initial linear regime to obtain the transport coefficient. More precisely, continous time estimators for the transport coefficient (4.6) and its Norton analog (4.21) can be obtained by defining appropriate discretizations thereof. These discretizations are given by the following estimators

$$\widehat{\alpha}^{\Delta t}_{N_{\mathrm{iter}},\eta} = \frac{1}{N_{\mathrm{iter}}\eta} \sum_{k=0}^{N_{\mathrm{iter}}-1} R(q^k, p^k), \qquad \widehat{\alpha}^{\Delta t,*}_{N_{\mathrm{iter}},r} = r N_{\mathrm{iter}} \left(\sum_{k=0}^{N_{\mathrm{iter}}-1} \lambda^k \right)^{-1}, \tag{4.56}$$

respectively in the NEMD case and the Norton case, where λ^k is defined in (4.54) for the Norton dynamics preserving some response R. More reliable estimators can further be obtained by fitting the response profile for several small values of η and r.

In the case of mobility computations, the observable $R(q,p) = F \cdot M^{-1}p$ is used, yielding the following NEMD estimator for the mobility:

$$\widehat{\alpha}^{\Delta t}_{N_{\mathrm{iter}},\eta} = \frac{1}{N_{\mathrm{iter}}\eta} \sum_{k=0}^{N_{\mathrm{iter}}-1} F \cdot M^{-1} p^k.$$

For shear viscosity, discretizations of the NEMD estimator (4.36) for the Fourier coefficient U_1

are used, yielding

$$\widehat{U}^{\Delta t}_{1,N_{\mathrm{iter}},\eta} = \frac{1}{NN_{\mathrm{iter}}\eta} \sum_{k=0}^{N_{\mathrm{iter}}} \sum_{j=1}^{N} \left(M^{-1}p^k\right)_{j,x} \exp\left(\frac{2\mathrm{i}\pi q^k_{j,y}}{L_y}\right).$$

Verification of the controllability condition. We conclude this section by discussing the controllability condition (4.39) in the case of mobility and shear viscosity computations.

When computing the mobility using a constant forcing, note that, using the expression for the non-equilibrium response in (4.29), the controllability condition writes

$$(G \cdot F)(q) = F^\intercal M^{-1} F \neq 0,$$

since M^{-1} is a positive definite matrix, so that the controllability condition is trivially satisfied everywhere. Moreover, the existence of strong solutions to (4.37) can be straightforwardly deduced from the existence of strong solutions to (4.26), since in this case $\overline{P}_{F,G} = \overline{P}_{F,M^{-1}F}$ is a constant matrix, which therefore preserves locally Lipschitz maps which grow at most linearly at infinity, see for instance the discussion in [262, Section 3.3].

We examine the controllability condition in the case of a transverse shear forcing profile in the case $M = m\mathrm{Id}$ in order to alleviate the notation (the extension to more general mass matrices being straightforward). Using the expression for the response (4.35), the controllability condition writes

$$(G \cdot F)(q) = \frac{1}{mN} \sum_{j=1}^{N} \exp\left(\frac{2\mathrm{i}\pi q_{j,y}}{L_y}\right) f(q_{j,y}) \neq 0.$$

The quantity $G \cdot F$ could in principle vanish. As the number of particles is increased, this should however be rather unlikely when the first Fourier coefficient of the forcing f is non-zero. Indeed, the marginal distribution of a single particle is uniform over the simulation cell at equilibrium (by translation invariance). Therefore, one expects, for a large number of particles and not too strong a forcing, that $G \cdot F$ is close to

$$\frac{1}{mL_y} \int_0^{L_y} \exp\left(\frac{2\mathrm{i}\pi y}{L_y}\right) f(y)\,\mathrm{d}y,$$

which is exactly the first Fourier coefficient of f, a non-zero quantity.

4.6.2 Equivalence of (non-)equilibrium responses

We begin by checking the consistency between the standard NEMD approach and the Norton approach, by applying these two methods to the cases of mobility and shear viscosity computations discussed in Section 4.4.2.

Mobility computations. We begin by checking the validity of the Norton method on the simple example of mobility. We used identical equilibrium conditions for NEMD and Norton computations, namely a three-dimensional system of $N = 1000$ particles, in a cubic periodic domain of side length L, such that $\rho = N/L^3 = 0.6$, with a temperature $T = 1.25$ and a

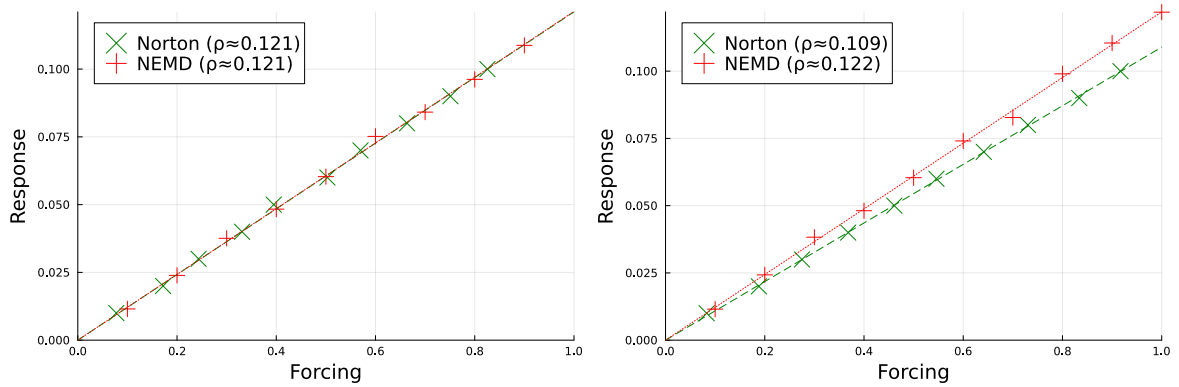

Figure 4.2: Response profiles in the linear regime for the NEMD and Norton mobility dynamics. The slope of the linear regression lines correspond to the estimated transport coefficient. Left: color drift. Right: single drift.

friction coefficient $\gamma = 1.0$. The time step was set to $\Delta t = 10^{-3}$ (this choice ensures that the relative variations of the energy of the system are of the order of 0.6 for Hamiltonian dynamics), and simulations were performed for a minimal physical time of $T_{\text{sim}} = 250,000$ in the linear response regime, and $T_{\text{sim}} = 8,000$ far in the non-linear response regime. Error bars have been omitted for the sake of readability, as they are in all cases smaller than the size of the markers.

In Figure 4.6.2, we plot the response as a function of the forcing magnitude for both the Norton and NEMD dynamics. Thus, the fixed quantity is plotted in the ordinates for the Norton system, and in the abscissas for the NEMD system. Least-squares linear regression lines are plotted, in a dotted red line for the Norton system, and a dashed green line for the NEMD system. The slopes of these lines, indicated in the legend, give the estimated transport coefficient. The left plot corresponds to a color drift perturbation (4.31), while the right plot corresponds to a single drift perturbation (4.30). We observe that, while the agreement is almost perfect in the case of the color-drift forcing, there is a significant discrepancy in the linear responses in the case of a single-drift forcing. In fact, using the relation (4.33), it is readily checked that the Norton estimation of the diffusion coefficient is incorrect. We believe that for the Norton method to be valid, the microscopic perturbation should as a general rule act on the bulk of the system. This condition is not satisfied in the case of a single-drift forcing, which acts on a single particle.

In Figure 4.3, we again look at the color-drift perturbed dynamics, but this time take the system far from equilibrium, so that the response is non-linear. Remarkably, the non-linear responses profiles for the Norton and NEMD systems still coincide for extreme values of the forcing magnitude. This was already formally proven in [115] in a deterministic setting.

Shear viscosity computations In Figures 4.4 to 4.6, we perform an experiment similar to the one done to estimate the mobility, for a system subject to a longitudinal forcing modulated in intensity by a transverse profile as described in Section 4.4.2, for the three forcing profiles considered in [190]. The systems were simulated under the same conditions as for the mobility, except for the temperature and particle density which were respectively chosen to be $T = 0.8$ and $\rho = N/(L_x L_y L_z) = 0.7$.

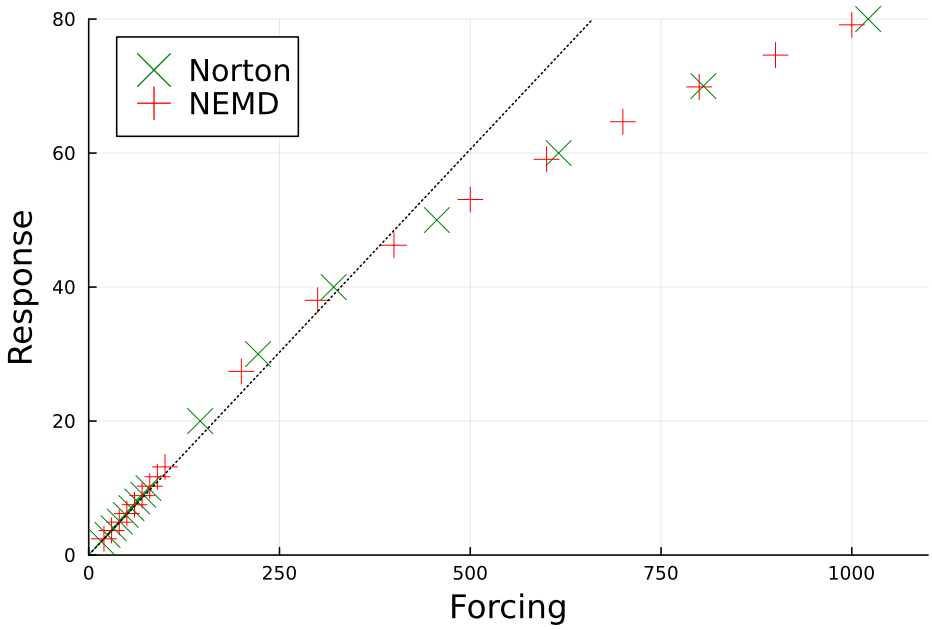

Figure 4.3: Non-linear response profiles for the NEMD and Norton mobility dynamics with color drift. The responses coincide even in the large perturbation regime.

More precisely, Figure 4.4 presents the response obtained for a piecewise linear forcing profile $f(y) = 4\mathbb{1}_{0\leqslant y<L_y/2}(y - L_y/4)/L_y + 4\mathbb{1}_{L_y/2\leqslant y<L_y}(3L_y/4 - y)/L_y)$, Figure 4.5 for a piecewise constant forcing profile $f(y) = 1 - 2\mathbb{1}_{0<y\leqslant L_y/2}$, and Figure 4.6 for a sinusoidal forcing profile $f(y) = \sin(2y\pi/L_y)$. In each case, the linear response regime is plotted on the left-hand side, and the non-linear regime is plotted on the right. Linear regression lines whose slopes are given in the legend are superimposed to the data points. Each time, both the linear and non-linear responses for usual NEMD and Norton dynamics perfectly agree.

Consistency in the thermodynamic limit. We now turn to investigating the behavior of estimators of the shear viscosity in the thermodynamic limit $N \to \infty$. In order for the thermodynamic limit of the viscosity to be well-defined, the quantity $F_1/U_1 - \gamma_x$ must scale asymptotically as $N^{-2/3}$. Indeed, as the system size increases, the length L_y scales as $(N/\rho)^{1/3}$, which, plugged in the expression

$$\nu = \rho \left(\frac{F_1}{U_1} - \gamma_x \right) \left(\frac{L_y}{2\pi} \right)^2$$

implies the claimed scaling for $F_1/U_1 - \gamma_x$. This discussion determines how to fit the asymptotic behavior of F_1/U_1 for increasing system sizes (see Figure 4.7).

In Figure 4.7, we examine the behavior of the response for increasing sizes of the system. Estimations of U_1 were performed at roughly equivalent state points $\eta = 0.3$ and $r = 0.1$ in the linear response regime using estimators of the form (4.56). We find in particular that the scaling law $F_1/U_1 - \gamma_x \sim N^{-2/3}$ is obeyed, and that the estimates of the prefactor C coincide for the NEMD and Norton methods. The agreement between the two methods is excellent for all values of N.

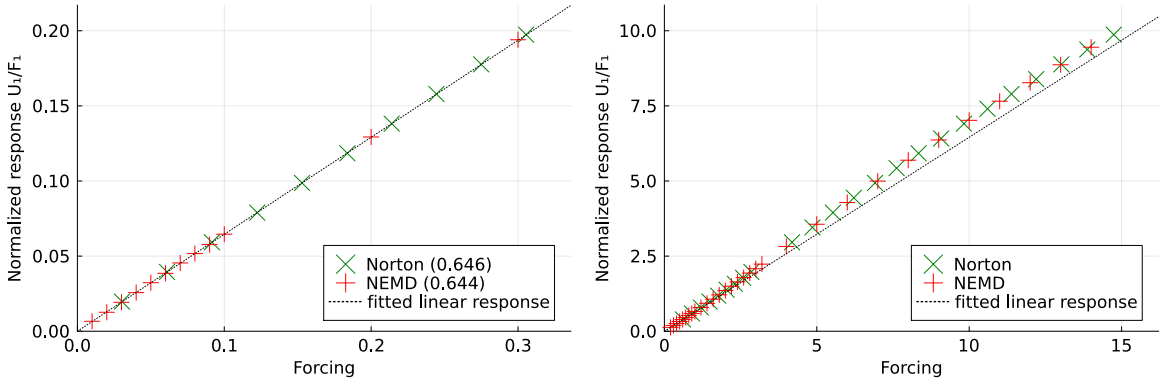

Figure 4.4: Non-equilibrium normalized Fourier response for shear viscosity computations with a piecewise linear forcing profile.

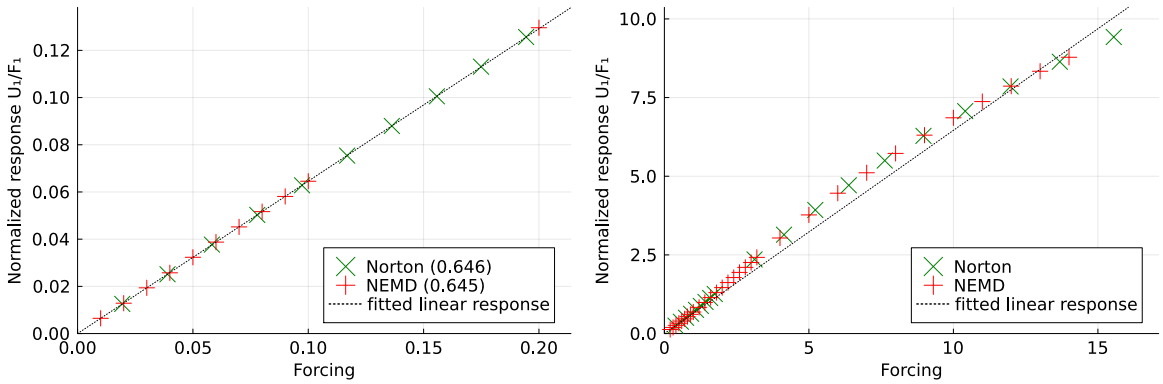

Figure 4.5: Non-equilibrium normalized Fourier response for shear viscosity computations with a piecewise constant forcing profile.

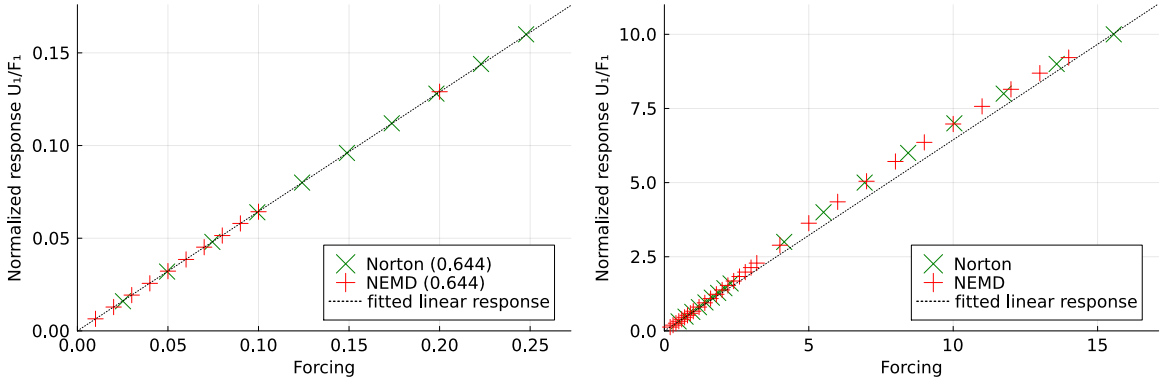

Figure 4.6: Non-equilibrium normalized Fourier response for shear viscosity computations with a sinusoidal forcing profile.

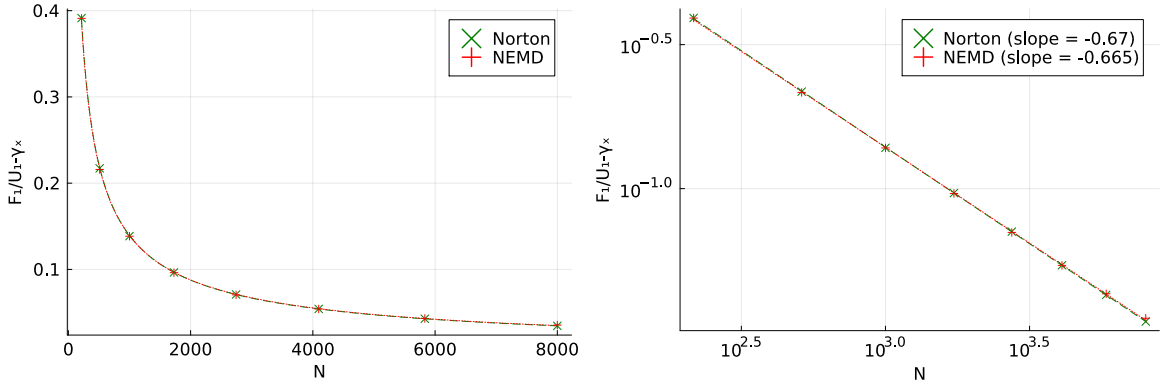

Figure 4.7: Behavior of estimators for $U_1/F_1 - \gamma_x$ in the large N limit. The simulation results, indicated by markers, are fitted by $CN^{-\alpha}$ with $C \approx 14$ and $\alpha \approx 0.66$ with a linear regression of $\log(U_1/F_1 - \gamma_x)$ as a function of $\log N$. The right plot corresponds to the left plot in log-log coordinates.

4.6.3 Concentration properties in the thermodynamic limit

We next investigate the scaling of the variances of the distributions of R and λ as a function of the system size N, respectively in the canonical equilibrium and Norton ensembles, in the case of a sinusoidal shear forcing profile. In Figure 4.8, we show equilibrium distributions of R and λ for increasing values of N. By 'equilibrium', it is meant here that the NEMD dynamics is run for $\eta = 0$ and the Norton dynamics for $r = 0$. Note first that both distributions are centered around 0 and symmetric. Moreover, they concentrate around 0 as the system size N increases. The scaling however differs for the two dynamics. In the canonical ensemble, the usual rate N^{-1} is observed, consistent with some form of spatial averaging of an intensive quantity. Indeed, the rate N^{-1} is the one dictated by a central limit theorem, which makes sense on an intuitive level for a system displaying only short-range interactions, using a decomposition of the full system into weakly correlated subsystems, each of them contributing additively to the total flux.

On the other hand, the scaling of the variance as a function of the system size in the Norton ensemble appears to be quite different, with a variance decreasing much faster than N^{-1}. This is confirmed in Figure 4.9, which shows that the second moment of λ decays as $N^{-5/3}$. The increase in the scaling exponent is presumably due to the coupling introduced by the constant-flux condition, which introduces global correlations in the systems, and hence some form of long range interactions, which are known to lead to significant changes of phenomenology in some situations.

4.6.4 Asymptotic variance

We finally assess the numerical efficiency of the Norton method. NEMD estimators of the form (4.56) are ergodic averages of R for trajectories of the discrete-time Markov chain defined by the numerical scheme, and the central limit theorem for Markov chains implies that the variance is asymptotically $\eta^{-2} N_{\text{iter}}^{-1} \sigma_{\Delta t}^2(R)$, where $\sigma_{\Delta t,\eta}^2(R)$ is the asymptotic variance of R

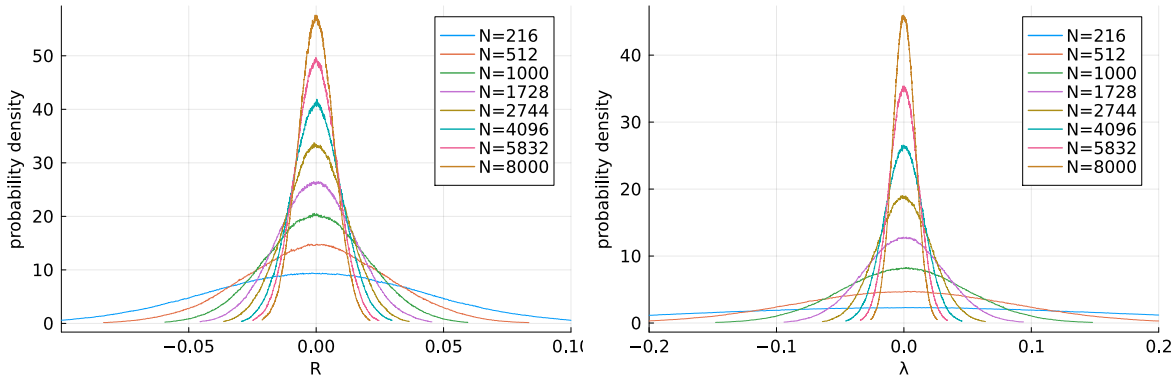

Figure 4.8: Histograms of forcing and response in equilibrium ensembles. Left: standard equilibrium Langevin dynamics ($\eta = 0$). Right: Langevin–Norton dynamics at zero flux ($r = 0$).

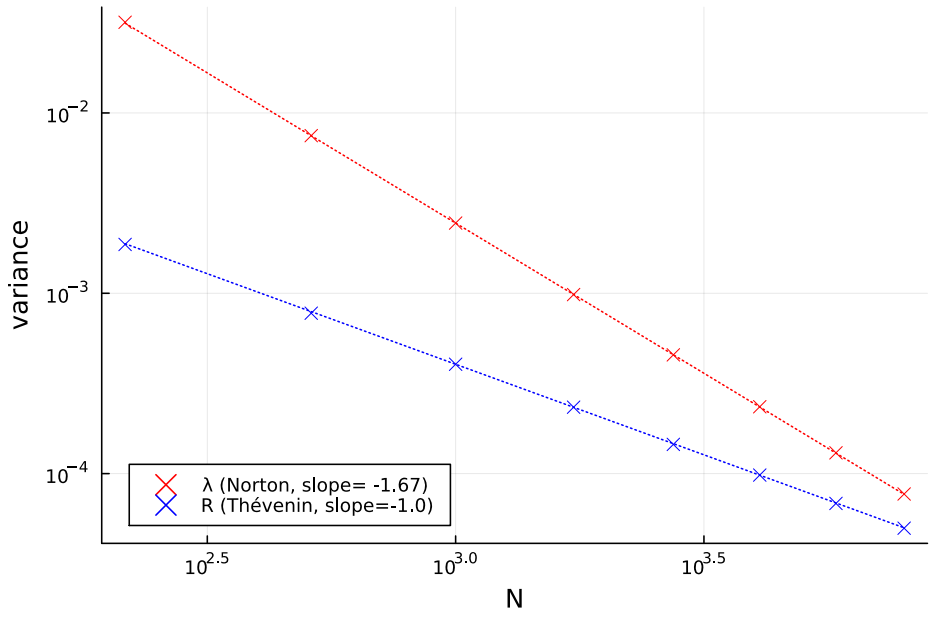

Figure 4.9: Variance of λ and R in the Norton and canonical equilibrium ensembles.

under the scheme's stationary measure $\pi_{\Delta t,\eta}$:

$$\sigma^2_{\Delta t,\eta}(R) = \mathrm{Var}_{\pi_{\Delta t,\eta}}(R) + 2\sum_{k=1}^{\infty} \mathrm{Cov}_{\pi_{\Delta t,\eta}}\left(R(q^k,p^k)R(q^0,p^0)\right) = \mathrm{Var}_{\pi_{\Delta t,\eta}}(R)\Theta_{\pi_{\Delta t,\eta}}(R),$$

where

$$\Theta_{\pi_{\Delta t,\eta}}(R) = \left[1 + 2\sum_{k=1}^{\infty} \frac{\mathrm{Cov}_{\pi_{\Delta t,\eta}}\left(R(q^k,p^k)R(q^0,p^0)\right)}{\mathrm{Var}_{\pi_{\Delta t,\eta}}(R)}\right] \tag{4.57}$$

is the number of correlation steps R for stationary initial distribution, and $\mathrm{Var}_{\pi_{\Delta t,\eta}}(R)$ denotes the centered second moment of R under $\pi_{\Delta t,\eta}$. It can be proved for standard NEMD dynamics [233] that

$$\sigma^2_{\Delta t,\eta}(R) = \sigma^2_{\eta}(R)/\Delta t + \mathrm{O}(1),$$

where $\sigma^2_{\eta}(R)$ is the asymptotic variance (4.7) of the continuous process.

For the Norton estimator in (4.56), it can be shown, using the delta method and a computation similar to (4.22), that the variance of trajectory averages of R is asymptotically $N_{\mathrm{iter}}^{-1} r^4 \mathbb{E}_{\pi^*_{\Delta t,r}}[\lambda]^{-4}\sigma^{2*}_{\Delta t,r}(\lambda)$, where $\pi^*_{\Delta t,r}$ denotes the invariant probability measure of the Markov chain $(\lambda^n)_{n\geqslant 1}$ defined in (4.54), and $\sigma^{2*}_{\Delta t,r}(\lambda)$ is the associated asymptotic variance for λ. Again, we write the asymptotic variance as the product of the centered second moment under the steady-state $\mathrm{Var}_{\pi^*_{\Delta t,r}}(\lambda_0)$ and the number of correlation steps $\Theta_{\pi^*_{\Delta t,r}}(\lambda)$.

As N grows to infinity, and for equivalent state points $r = \eta\alpha$, say in the linear response regime, the numerical results of Section 4.6.3 show that the contribution of the stationary centered second moment will be asymptotically smaller for Norton estimators than for their NEMD counterparts, owing to the fast decay of the variance of λ in the Norton ensemble as $N \to \infty$. This is reason to suspect that Norton estimators of the transport coefficient may have lower asymptotic variance for large enough N, as long as the scaling of correlation times for λ in the Norton ensemble does not cancel this effect. To assess whether this is the case, we plot in Figure 4.10 autocorrelation functions for equilibrium trajectories of λ in the Norton ensemble and R in the canonical ensemble, for several values of the system size N, again in the case of a sinusoidal shear forcing profile. These correspond to the summand in (4.57), plotted as a function of the physical simulation time. We observe that the correlation time is roughly independent of N. In fact, the autocorrelation profile itself barely changes with increasing system sizes.

Furthermore, we observe that the correlation time is much smaller in the Norton ensemble than in the NEMD ensemble. This suggests that even for moderate system sizes, the asymptotic variance for estimators of the linear response should be smaller for Norton systems than for their NEMD counterparts, owing to smaller correlation times. We verify this intuition in Figure 4.11 for a fixed system of $N = 1000$ particles, in the context of shear viscosity computations. The asymptotic variance for estimators of the Fourier linear response U_1 is plotted as a function of the forcing magnitude, for the various forcing profiles considered in Section 4.6.2. Note that the asymptotic variances indeed scale as η^{-2} for NEMD simulations and r^{-2} for Norton dynamics, at least for small values of $|r|$ and $|\eta|$. Interestingly, we find that Norton estimators have lower variance in each situation. We expect that this difference will be more pronounced for larger systems.

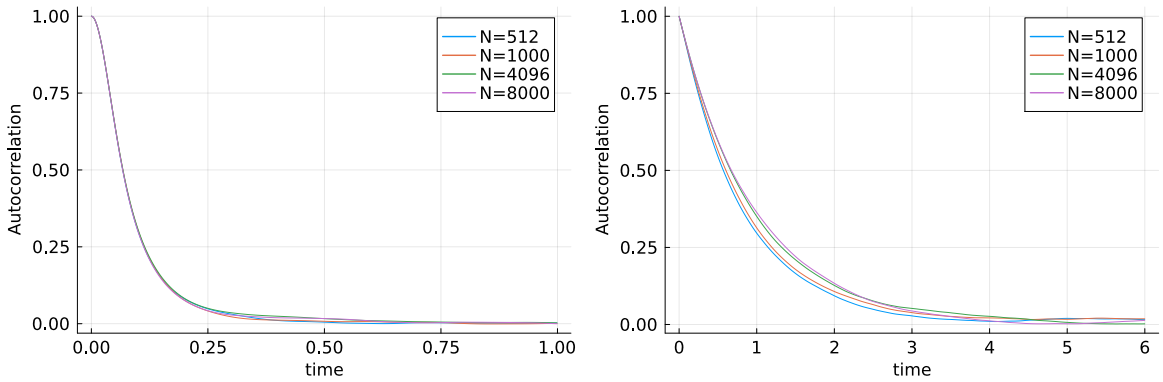

Figure 4.10: Autocorrelation functions at equilibrium for the shear-viscosity Fourier response R (given by (4.35)). Left: autocorrelation function of λ for the Norton dynamics on $R^{-1}\{0\}$. Right: autocorrelation function of R in standard equilibrium simulations.

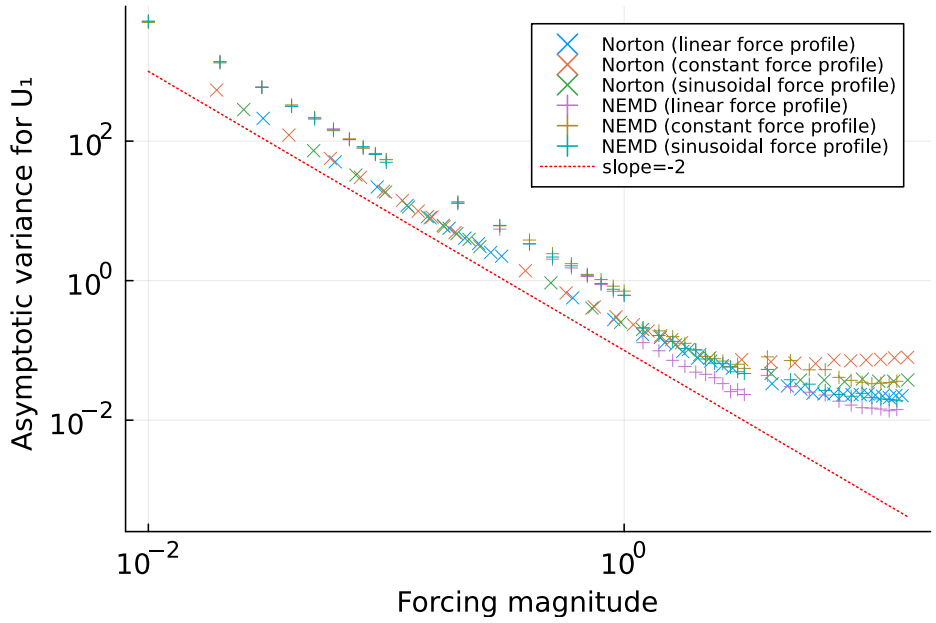

Figure 4.11: Asymptotic variance for estimators of the Fourier response U_1 as a function of the perturbation magnitude, in log-log coordinates. The expected scaling line for small values of the forcing or response is plotted in red.

4.7 Perspectives for future work

We list in this final section some of the many open questions raised by the stochastic Norton approach, both on the theoretical and numerical sides. Certain points are currently being tackled, but a lot remains to be done, and we hope that this work will encourage other researchers to study Norton dynamics. We classify issues to address in three families.

Analysis of the continuous dynamics. A first task is to show that Norton dynamics are well-posed and well-behaved. As such results will undoubtedly constitute necessary tools to investigate the properties of Norton ensembles from a rigorous standpoint, they are of the utmost importance. We identify the following questions:

- Obtain sufficient conditions on the reference dynamics, F and R, for the Norton dynamics to be well-posed on arbitrarily large time horizons.
- Prove the existence and uniqueness of a Norton steady-state.
- Show pathwise ergodicity of the Norton dynamics.
- Obtain bounds on the rate of convergence of arbitrary initial conditions to the Norton steady-state.

In view of conditions such as (4.18), it is clear that not all pairs (F, R) give rise to well-posed Norton dynamics. From a macroscopic point of view, the averages of F and R correspond to conjugate variables, hence we expect any reasonable microscopic realization to appropriately relate the associated observables.

Theoretical questions. We list here various physically motivated questions, which would in particular establish that the Norton method provides a viable way to compute transport coefficients.

- Derive equivalence of ensemble results between the Norton and canonical ensemble at equilibrium (i.e. $r = 0$ and $\eta = 0$, respectively), in the thermodynamic limit.
- Prove the existence of the linear response (4.20) for all systems of finite size, and in fact develop a theory of linear response theory for Norton ensembles. This would include relating the transport coefficient to fluctuations in the Norton equilibrium ensemble, analogously to standard Green–Kubo formulæ in the canonical ensemble. This approach was formally carried out in [120], for the special case of electrical conductivity or mobility, in a deterministic setting. Carrying out this development would in particular require understanding, for small $|r|$, the relation of the Norton equilibrium steady-state to the invariant measure of the reference process (4.1), as well as to the nature of the forcing F and the response R.
- Show the consistency of the Norton approach, by proving that the transport coefficients obtained with NEMD and Norton dynamics have the same thermodynamic limit, for

bulk forcings. This can be considered as some form of equivalence of ensembles in a perturbative nonequilibrium setting.

- Derive a result on the equivalence of ensembles for the Norton and NEMD approaches beyond the linear response regime, for equivalent state points (i.e. the average forcing experienced in Norton dynamics coincides with the fixed forcing in NEMD simulations).
- Develop a theory of the effect of long-range interactions in the Norton dynamics induced by the constant-response constraint.
- Extend the Norton approach to nonequilibrium perturbations of the diffusion matrix, in view of applying it to the study of thermal conductivity.

Numerical analysis of Norton dynamics. A last set of issues to address is related to properties of Norton dynamics which are of practical interest for the efficient and accurate computation of transport coefficient in realistic systems. A crucial point is to derive clear conditions under which one should prefer the Norton approach to the usual NEMD method. Another point concerns the study of the mathematical properties of the discretized dynamics.

- Carry out a rigorous analysis of the scaling of the variance of λ in the thermodynamic limit.
- Explain the shorter correlation times for Norton dynamics compared to the corresponding NEMD dynamics. This and the previous question would ideally yield rigorous asymptotic formulas for both the variance and correlation time in terms of η, r and N.
- Perform the numerical analysis of splitting schemes for Norton dynamics. This analysis is a necessary step to derive error bounds relating quantitative properties of the continuous dynamics with their discrete analogs. Useful results would include error estimates at the level of discrete trajectories, or at the level of the invariant measures of the associated Markov chains.

Acknowledgments. The authors thank Gary Morriss, Julien Roussel and Giovanni Ciccotti for stimulating discussions, and the members of the project ANR SINEQ (in particular Benjamin Jourdain, Tony Lelièvre, Stefano Olla and Mathias Rousset) for valuable feedback on preliminary results presented at the annual meeting of the project. The authors also thank Xiaocheng Shang for bringing several typos to their attention. This work received funding from the European Research Council (ERC) under the European Union's Horizon 2020 research and innovation programme (project EMC2, grant agreement No 810367), and from the Agence Nationale de la Recherche, under grants ANR-19-CE40-0010-01 (QuAMProcs) and ANR-21-CE40-0006 (SINEQ).

Declarations.

Data availability: The code used to perform the simulations reported in this work is available in the repository [45], which also contains processed numerical results and the scripts used to generate the figures.

Conflicts of interest: The authors have no relevant financial or non-financial interests to disclose.

We gather in these appendices the proofs of various technical statements, namely Equation (4.24) in Section 4.A, Equation (4.25) in Section 4.B, and Equation (4.33) in Section 4.C.

Appendix 4.A: Derivation of Norton dynamics in the case of multiple constraints

We write here the proof of (4.24). We proceed as in Section 4.3.2, assuming that the forcing process $\Lambda^{\mathbf{r}}$ may be written as an Itô process before checking a posteriori that this assumption is justified. More precisely, we write

$$\mathrm{d}\Lambda_t^{\mathbf{r}} = \mathrm{d}\widetilde{\Lambda}_t^{\mathbf{r}} + \lambda_t^{\mathbf{r}}\,\mathrm{d}t,$$

where $\widetilde{\Lambda}^{\mathbf{r}}$ is the martingale part of the Itô decomposition of $\Lambda^{\mathbf{r}}$. Applying Itô's formula to the constant-response constraint $R(Y_t^{\mathbf{r}}) = R(Y_0^{\mathbf{r}}) = \mathbf{r}$ yields

$$\nabla R(Y_t^{\mathbf{r}})^\intercal \mathrm{d}Y_t^{\mathbf{r}} + \frac{1}{2}\nabla^2 R(Y_t^{\mathbf{r}}) : \mathrm{d}\langle Y^{\mathbf{r}}\rangle_t = 0. \tag{4.58}$$

Identifying martingale increments, the uniqueness of the Itô decomposition implies

$$\mathrm{d}\widetilde{\Lambda}_t^{\mathbf{r}} = -\left[\nabla R(Y_t^{\mathbf{r}})^\intercal F(Y_t^{\mathbf{r}})\right]^{-1} \nabla R(Y_t^{\mathbf{r}})^\intercal \sigma(Y_t^{\mathbf{r}})\,\mathrm{d}W_t,$$

which in turns allows to compute the quadratic covariation term

$$\mathrm{d}\langle Y^{\mathbf{r}}\rangle_t = \left[\overline{P}_{F,\nabla R}\sigma\sigma^\intercal\overline{P}_{F,\nabla R}^\intercal\right](Y_t^{\mathbf{r}})\,\mathrm{d}t = \Pi_{F,\nabla R,\sigma}(Y_t^{\mathbf{r}})\,\mathrm{d}t.$$

Using this expression in (4.58) and the uniqueness of the Itô decomposition once again to identify bounded-variation parts, we recover

$$\lambda_t^{\mathbf{r}} = -(\nabla R^\intercal F)^{-1}\left[\nabla R^\intercal b + \frac{1}{2}\left(\nabla^2 R^\intercal : \Pi_{F,\nabla R,\sigma}\right)\right](Y_t^{\mathbf{r}}),$$

which yields (4.24) upon substituting the expression for $\mathrm{d}\Lambda_t^{\mathbf{r}}$.

Appendix 4.B: Derivation of the Norton dynamics in the case of time-dependent constraints

To prove (4.25), we once again proceed as in Section 4.3.2, writing the Itô decomposition for the forcing process as

$$\mathrm{d}\Lambda_t^{\mathcal{R}} = \mathrm{d}\widetilde{\Lambda}_t^{\mathcal{R}} + \lambda_t^{\mathcal{R}}\,\mathrm{d}t.$$

Applying Itô's formula to the time-dependent constraint (4.25), we get

$$\nabla R(Y_t^{\mathcal{R}})^{\intercal}\mathrm{d}Y_t^{\mathcal{R}} + \frac{1}{2}\nabla^2 R(Y_t^{\mathcal{R}}) : \mathrm{d}\langle Y^{\mathcal{R}}\rangle_t = \overline{r}_t\,\mathrm{d}t + \widetilde{r}_t\,\mathrm{d}B_t,$$

which, by uniqueness of the Itô decomposition, leads to

$$\mathrm{d}\widetilde{\Lambda}_t^{\mathcal{R}} = \frac{\widetilde{r}_t\,\mathrm{d}B_t - \nabla R(Y_t^{\mathcal{R}})\cdot\sigma(Y_t^{\mathcal{R}})\,\mathrm{d}W_t}{\nabla R(Y_t^{\mathcal{R}})\cdot F(Y_t^{\mathcal{R}})},$$

allowing to compute the covariation bracket as

$$\mathrm{d}\left\langle Y^{\mathcal{R}}\right\rangle_t = \Pi_{F,\nabla R,\sigma}(Y_t^{\mathcal{R}})\,\mathrm{d}t + \frac{F(Y_t^{\mathcal{R}})\otimes F(Y_t^{\mathcal{R}})}{\left(\nabla R(Y_t^{\mathcal{R}})\cdot F(Y_t^{\mathcal{R}})\right)^2}\widetilde{r}_t^2\,\mathrm{d}t.$$

One can then proceed to identify bounded-variation increments, and isolate $\lambda_t^{\mathcal{R}}$:

$$\lambda_t^{\mathcal{R}} = \frac{\overline{r}_t - \frac{1}{2}\nabla^2 R(Y_t^{\mathcal{R}}) : \left[\Pi_{F,\nabla R,\sigma}(Y_t^{\mathcal{R}}) + \frac{F(Y_t^{\mathcal{R}})\otimes F(Y_t^{\mathcal{R}})}{\left(\nabla R(Y_t^{\mathcal{R}})\cdot F(Y_t^{\mathcal{R}})\right)^2}\widetilde{r}_t^2\right] - \nabla R(Y_t^{\mathcal{R}})\cdot b(Y_t^{\mathcal{R}})}{\nabla R(Y_t^{\mathcal{R}})\cdot F(Y_t^{\mathcal{R}})}.$$

Substituting in the expression for the forcing process finally yields (4.25).

Appendix 4.C: Derivation of the relation between color/single drift linear responses

The proof of (4.33) is taken from unpublished notes by Julien Roussel, see the PhD thesis [288]. We assume for the ease of presentation that $M = m\mathrm{Id}$ and $d = 3$, and denote by μ the equilibrium measure (4.27). The dynamics under consideration is the standard Langevin dynamics, namely (4.26) with $\eta = 0$. Let us define, for $1 \leqslant i, j \leqslant N$,

$$c_{ij} = \frac{\beta}{m^2}\int_0^\infty \mathbb{E}_\mu[p_{i,x,t}p_{j,x,0}]\,\mathrm{d}t.$$

In view of (4.32), upon summing over i the longitudinal p-components of the SDE (4.26) and integrating in time,

$$\begin{aligned}\sum_{i=1}^N p_{i,x,t} &= \sum_{i=1}^N\left[p_{i,x,0} + \int_0^t\left(-\frac{\partial}{\partial q_{i,x}}V(q_s) - \frac{\gamma}{m}p_{i,x,s}\,\mathrm{d}s + \sqrt{\frac{2\gamma}{\beta}}\,\mathrm{d}W_{i,x,s}\right)\right]\\ &= \sum_{i=1}^N\left[p_{i,x,0} - \frac{\gamma}{m}\int_0^t p_{i,x,s}\,\mathrm{d}s + \sqrt{\frac{2\gamma}{\beta}}W_{i,x,t}\right].\end{aligned}$$

Multiplying by $p_{1,x,0}$ and taking the expectation over trajectories started from canonical initial conditions (so that the Brownian terms vanishes), it follows that

$$\mathbb{E}_\mu\left[\left(\sum_{i=1}^N p_{i,x,t}\right)p_{1,x,0}\right] = \sum_{i=1}^N\left(\mathbb{E}_\mu\left[p_{i,x,0}p_{1,x,0}\right] - \frac{\gamma}{m}\int_0^t\mathbb{E}_\mu\left[p_{i,x,s}p_{1,x,0}\right]\,\mathrm{d}s\right).$$

By the decay properties of the evolution semigroup (obtained for instance by hypocoercive approaches, see e.g. [329], as well as the introduction of [37] for a review), the left-hand side converges to 0 as $t \to \infty$, while the integral is well-defined. Since p_0 has diagonal covariance with respect to μ, we get

$$\sum_{i=1}^{N} \frac{\gamma}{m} \int_0^\infty \mathbb{E}_\mu \left[p_{i,x,s} p_{1,x,0} \right] \mathrm{d}s = \mathbb{E}_\mu [p_{1,x,0}^2] = \frac{m}{\beta}.$$

Equivalently,

$$\sum_{i=1}^{N} c_{i1} = \frac{1}{\gamma}. \tag{4.59}$$

Using the indistinguishability of the particles,

$$\forall\, 1 \leqslant i, j \leqslant N, \qquad c_{ii} = c_{11}, \qquad c_{ij} = c_{12}. \tag{4.60}$$

We can therefore rewrite (4.59) as

$$c_{12} = \frac{1}{N-1} \left(\frac{1}{\gamma} - c_{11} \right).$$

This equality can be used to relate the linear responses of the single drift and the color drift. By the Green–Kubo formula [142], the transport coefficient for the single drift is given by

$$\alpha_{F_{\mathrm{S}}} = c_{11}.$$

For the color drift, we expand, using the Green–Kubo formula,

$$\alpha_{F_{\mathrm{C}}} = \frac{\beta}{m^2} \int_0^\infty \mathbb{E}_\mu [(F_{\mathrm{C}} \cdot p_t)\,(F_{\mathrm{C}} \cdot p_0)]\, \mathrm{d}t = \frac{1}{N} \left(\sum_{i=1}^{N} c_{ii} + 2 \sum_{1 \leqslant i < j \leqslant N} (-1)^{i+j} c_{ij} \right)$$

In view of (4.60), and using

$$\sum_{1 \leqslant i < j \leqslant N} (-1)^{i+j} = - \left\lfloor \frac{N}{2} \right\rfloor,$$

which is easily seen by induction, we get

$$\alpha_{F_{\mathrm{C}}} = c_{11} - \frac{2\lfloor N/2 \rfloor}{N(N-1)} \left(\frac{1}{\gamma} - c_{11} \right),$$

which is the claimed identity.

Chapter 5

A hypocoercive approach of the overdamped limit for the kinetic Langevin equation with multiplicative noise

Iteration, like friction, is likely to generate heat instead of progress.
— Mary Ann Evans (*a.k.a.* George Eliot), *The Mill on the Floss (Book II)*, 1860

Abstract. *This note provides a simple derivation of the overdamped approximation for kinetic (or underdamped) equilibrium Langevin dynamics, in the case of arbitrary matrix-valued, position-dependent damping parameters. While this problem has previously been addressed using stochastic averaging and PDE homogenization methods, our approach is based on uniform hypocoercive estimates, which may be of interest in their own right. We believe our approach to be of interest since it allows for a very direct proof, providing a transparent explanation for the origin of the "noise-induced drift" term in the limiting equation. Besides, while previous studies of this problem focused on the small-mass limit, our results are given in the large-friction regime. As an application, we compute the overdamped limit of a class of kinetic Langevin dynamics with position-dependent mass matrices, which are for instance used in internal coordinate molecular dynamics.*

5.1 Introduction

We study the overdamped limit of the kinetic Langevin equation, defined by the stochastic differential equation (SDE)

$$\begin{cases} \mathrm{d}q_t^\lambda = \nabla U(p_t^\lambda)\mathrm{d}t, \\ \mathrm{d}p_t^\lambda = -\nabla V(q_t^\lambda)\mathrm{d}t - \lambda D(q_t^\lambda)^{-1}\nabla U(p_t^\lambda)\,\mathrm{d}t + \sqrt{\dfrac{2\lambda}{\beta}} D(q_t^\lambda)^{-1/2}\,\mathrm{d}W_t^\lambda, \end{cases} \tag{5.1}$$

in the high friction regime $\lambda \to +\infty$, where $D : \mathcal{Q} \to \mathcal{S}_d^{++}$ is a symmetric positive-definite matrix field called the friction profile, and W^λ is a standard Brownian motion in $\mathbb{R}^d$. Instead of $D^{-1/2}$ in (5.1), we could take any matrix-field $A : \mathcal{Q} \to \mathbb{R}^{d\times d}$ such that $AA^\top = D^{-1}$, with sufficient regularity (see Assumption 5.1 below). But since any two square roots of D^{-1} are conjugated via an orthogonal transformation, we may assume that $A = D^{-1/2}$ is the positive square root of D^{-1}, up to a change of Brownian motion. In (5.1), the functions U and V correspond respectively to the kinetic and potential energies, which sum to the Hamiltonian

$$H(q,p) = V(q) + U(p).$$

The position variable q evolves in $\mathcal{X}$, where $\mathcal{Q}$ is either the d-dimensional torus $L\mathbb{T}^d$ for some $L > 0$, or $\mathcal{Q} = \mathbb{R}^d$, while the momentum variable $p \in \mathbb{R}^d$ is in all cases unbounded. The typical choice of kinetic energy is given by the physical definition

$$U(p) = \frac{1}{2} p^\top M^{-1} p, \tag{5.2}$$

where M is the mass matrix of the system, although other choices have been considered for sampling, see for instance [310].

For the sake of consistency, we assume that W^λ is given by a diffusive rescaling of some reference Brownian motion W, i.e. $W_t^\lambda = \sqrt{\lambda} W_{t/\lambda}$ for all $\lambda, t > 0$.

We introduce the following family of rescaled-in-time, W-adapted processes:

$$X_t^\lambda := q_{\lambda t}^\lambda, \qquad \forall\, \lambda > 0,\, t \geqslant 0. \tag{5.3}$$

The main result, stated in Proposition 5.6 below, is a pathwise convergence result when $\lambda \to +\infty$ on compact time intervals for the process X^λ defined in (5.3) towards solutions on $\mathcal{Q}$ to the SDE

$$\mathrm{d}X_t = -\left[D(X_t)\nabla V(X_t)\mathrm{d}t - \frac{1}{\beta}\,\mathrm{div} D(X_t)\right]\,\mathrm{d}t + \sqrt{\frac{2}{\beta}} D^{1/2}(X_t)\mathrm{d}W_t, \tag{5.4}$$

with initial data $X_0 \in \mathcal{Q}$, and where div denotes the row-wise (or column-wise) divergence operator, which is well-defined under our regularity assumptions (see Assumption 5.1). The dynamics (5.4) is the so-called Smoluchowski–Kramers dynamics. When $D = \mathrm{Id}$ is the identity matrix, the dynamics (5.4) is the so-called overdamped Langevin equation. The term $\frac{1}{\beta}\,\mathrm{div} D$ is a so-called "noise-induced drift" term, which has gathered attention in the physical literature, see for example [331] and references therein.

In the case where the matrix D is a constant, the convergence of the dynamics (5.1) to the dynamics (5.4) is known since the work of Smoluchowski [306] and Kramers [198]. Moreover, the large friction regime can be mapped to the "small-mass" regime, via an appropriate nondimensionalisation of the dynamics, see for instance [229, Section 2.2.4]. The approximation of the dynamics (5.1) by the dynamics (5.4) in the small-mass regime is known as the Smoluchowski–Kramers approximation. In the case of a state-dependent friction, when the noise in (5.1) and (5.4) is multiplicative, The Smoluchowski–Kramers approximation is more complicated to obtain, but has been studied with a variety of methods (see [130, 131, 177, 339] and references therein), including stochastic averaging and PDE homogenization approaches. The approximation has also been extended to more general settings, including stochastic PDEs [69], kinetic diffusions on manifolds [43] and non-linear SDEs [239].

The purpose of this note is to provide a proof of the overdamped approximation ($\lambda \to +\infty$) by completely different means, using analytical estimates from the theory of hypocoercivity [329], and more precisely the L^2-hypocoercivity approach developed in [105, 106, 37]. Because of the techniques used, our result is limited to equilibrium systems, in which the force in (5.1) is a gradient and the fluctuation-dissipation relation holds between the kinetic damping term and the diffusion coefficient. However, the result is valid and quantitative in λ (in a weak sense, see Proposition 5.6 below) for more general kinetic energies U than the physical kinetic energy (5.2). Moreover, the proof is very simple, and highlights the origin of the noise-induced drift in a straightforward way. We also identify a gap in the proof of [339, Lemma 3.1], and provide a correct argument for a similar step in our setting. Finally, we use our result to derive the overdamped approximation of a more general underdamped Langevin dynamics, in a case where both the mass and the friction are matrix-valued position-dependent functions, computing the limiting dynamics in a one-dimensional system.

In Section 5.2, we introduce the necessary notation and hypotheses, and state the main result. In Section 5.3, we prove the main result, and apply it in Section 5.4 to the more general case of position-dependent masses. We finally prove in Appendix 5.A some key technical results, including the hypocoercive estimates of Lemma 5.7, which may be of independent interest.

5.2 Notation and main result

We introduce the necessary notation, state our hypotheses and our main result (Proposition 5.6).

Notation. Throughout this work, we abuse notation and denote probability measures with the same symbol as their densities whenever they are absolutely continuous with respect to the Lebesgue measure. With this convention, the equilibrium (or Gibbs) measure μ is defined (under Assumption 5.4 below) by the probability measure

$$\mu(\mathrm{d}q\,\mathrm{d}p) = \mu(q,p)\,\mathrm{d}q\,\mathrm{d}p = \exp\left(-\beta H(q,p)\right)/Z_{\mu,\beta}\,\mathrm{d}q\,\mathrm{d}p, \qquad Z_\mu = \int_{\mathcal{Q}\times\mathbb{R}^d} \mathrm{e}^{-\beta H}.$$

The measure (5.5) is a product $\mu(\mathrm{d}q\,\mathrm{d}p) = \kappa(\mathrm{d}p)\otimes\nu(\mathrm{d}q)$, with kinetic and configurational

marginals

$$\kappa(p)\,\mathrm{d}p = \frac{\mathrm{e}^{-\beta U(p)}}{\displaystyle\int_{\mathbb{R}^d} \mathrm{e}^{-\beta U}}\,\mathrm{d}p, \qquad \nu(q)\,\mathrm{d}q = \frac{\mathrm{e}^{-\beta V(q)}}{\displaystyle\int_{\mathcal{Q}} \mathrm{e}^{-\beta V}}\,\mathrm{d}q, \tag{5.5}$$

For any $f \in L^1(\mathcal{Q}\times\mathbb{R}^d,\mu)$, we define the projector

$$\Pi_0 f(q) = \int_{\mathbb{R}^d} f(q,p)\,\kappa(\mathrm{d}p)$$

which sends $f(q,p)$ to its partial average with respect to κ. We make frequent use of the weighted L^2-space

$$L^2(\mu) = \left\{ f \in L^1_{\mathrm{loc}}(\mathcal{Q}\times\mathbb{R}^d) \,:\, \int_{\mathcal{Q}\times\mathbb{R}^d} f^2\,\mathrm{d}\mu < +\infty \right\},$$

and the closed subspace of μ-centered observables

$$L^2_0(\mu) = \left\{ f \in L^2(\mu) : \int_{\mathcal{Q}\times\mathbb{R}^d} f\,\mathrm{d}\mu = 0 \right\}.$$

Note that Π_0 is a $L^2(\mu)$-orthogonal projector, and that $(\mathrm{Id}-\Pi_0)L^2(\mu) \subset L^2_0(\mu)$. We define weighted Sobolev spaces, for $k \geqslant 1$ by

$$H^k(\mu) = \left\{ \varphi \in L^2(\mu) : \forall\, \alpha \in \mathbb{N}^d,\, |\alpha| \leqslant k,\, \partial^\alpha \varphi \in L^2(\mu) \right\},$$

with the usual multi-index notation for $\alpha \in \mathbb{N}^m$ i.e. $|\alpha| = \sum_{j=1}^m \alpha_j$, and $\partial^\alpha f = \partial^{\alpha_1}_{x_1} \dots \partial^{\alpha_m}_{x_m} f$ for $f : \mathbb{R}^m \to \mathbb{R}$. Other weighted L^p-spaces $L^p(\mu)$, $L^p(\nu)$, $L^p(\kappa)$ and the associated Sobolev spaces are defined in a similar fashion.

The generator of the dynamics (5.1) acts on smooth functions as the differential operator

$$\mathcal{L}_\lambda = \mathcal{A} + \lambda \mathcal{S},$$

where $\mathcal{A}$ and $\mathcal{S}$ are Hamiltonian transport and fluctuation-dissipation operators, defined respectively by

$$\mathcal{A} = \nabla U(p)^\top \nabla_q - \nabla V(q)^\top \nabla_p, \qquad \mathcal{S} = -(D^{-1}(q)\nabla U(p))^\top \nabla_p + \frac{1}{\beta} D^{-1}(q) : \nabla_p^2.$$

The $L^2(\mu)$-adjoints of partial derivatives are found by integration by parts to be

$$\partial^*_{q_i} = -\partial_{q_i} + \beta \partial_i V(q), \qquad \partial^*_{p_i} = -\partial_{p_i} + \beta \partial_i U(p), \qquad \forall 1 \leqslant i \leqslant d,$$

from which we find

$$\mathcal{A} = \frac{1}{\beta}\left[\nabla_p^* \nabla_q - \nabla_q^* \nabla_p\right], \qquad \mathcal{S} = -\frac{1}{\beta} \nabla_p^* D^{-1}(q) \nabla_p,$$

so that $\lambda\mathcal{S}$ and $\mathcal{A}$ correspond respectively to the symmetric and antisymmetric parts of $\mathcal{L}_\lambda$ on $L^2(\mu)$.

The generator of the dynamics (5.4), on the other hand, is given by

$$\mathcal{L}_{\mathrm{KS}} = -\nabla V^\top D\nabla + \frac{1}{\beta}\operatorname{div} D^\top \nabla + \frac{1}{\beta} D : \nabla^2 = \frac{1}{\beta} \mathrm{e}^{\beta V} \operatorname{div}\left(\mathrm{e}^{-\beta V} D\nabla\right),$$

which is a symmetric operator on $L^2(\nu)$, a property reflecting the reversibility of the dynamics (5.4) with respect to ν.

On the space $\mathbb{R}^{d\times d}$ of $d \times d$ matrices, we denote by $\|\cdot\|_{\mathrm{HS}}$ the Hilbert–Schmidt (or Frobenius norm), and by $\|\cdot\|_{\mathrm{op}}$ the Euclidean operator norm.

The processes X, X^λ defined respectively in (5.4) and (5.3) are defined on a probability space $(\Omega, \mathcal{F}, \mathbb{P}_{\mu_0})$. Under the probability measure $\mathbb{P}_{\mu_0}$, W is a Brownian motion, which is independent from

$$(q_0^\lambda, p_0^\lambda) = (X_0, p_0) \qquad \forall\, \lambda > 0,$$

which in turn has law $\mu_0 \in \mathcal{P}(\mathcal{Q}\times\mathbb{R}^d)$. As we will consider different choices of μ_0, we emphasize this in the notation $\mathbb{P}_{\mu_0}$, and denote by $\mathbb{E}_{\mu_0}$ the associated expectation. We assume that the SDEs (5.1) and (5.4) have strong solutions on $[0, T]$ for any $T > 0$.

Hypotheses on U, V and D. In this paragraph, we introduce various assumptions which we will use to state and prove our main result.

Assumption 5.1. *The coefficients of (5.1) are smooth*

$$V \in \mathcal{C}^\infty(\mathcal{Q}), \quad U \in \mathcal{C}^\infty(\mathbb{R}^d), \quad D \in \mathcal{C}^\infty(\mathcal{Q}; \mathcal{S}_d^{++}),$$

and ∇V is globally Lipschitz.

Assumption 5.2. *For all $\lambda > 0$, the generator $\mathcal{L}_\lambda$ is hypoelliptic, in the sense that*

$$g = \mathcal{L}_\lambda f,\ g \in \mathcal{C}^\infty(\mathcal{Q}\times\mathbb{R}^d) \implies f \in \mathcal{C}^\infty(\mathcal{Q}\times\mathbb{R}^d). \tag{5.6}$$

Hypoellipticity can often be checked using Hörmander's bracket condition, see [174] or Lemma 5.9 in Appendix 5.A, in which we give simple sufficient conditions on U, V and D for the implication (5.6) to hold.

Assumption 5.3. *The diffusion D is uniformly bounded and elliptic, and has uniformly bounded first derivatives:*

$$\exists\, M_D \geqslant 1 : \forall\, x \in \mathcal{Q}, \frac{1}{M_D}\mathrm{Id} \leqslant D(x) \leqslant M_D \mathrm{Id}, \qquad D' \in L^\infty\left(\mathcal{Q}; \mathbb{R}^d \otimes \mathbb{R}^{d\times d}\right), \tag{5.7}$$

where the inequalities are in the sense of symmetric matrices, and where D', defined by

$$\left(D'(q)\,[u]\right)_{ij} = \sum_{k=1}^d \partial_k D_{ij}(q) u_k, \qquad \forall (q,u) \in \mathcal{Q}\times\mathbb{R}^d,\ \forall 1 \leqslant i,j \leqslant d, \tag{5.8}$$

denotes the Fréchet differential of D.

Note that the conjunction of Assumptions 5.1 and 5.3 implies that the same conditions

on D^{-1} and $D^{\pm 1/2}$.

The next assumption (which contains in particular the conditions [37, Assumptions 3.1 and 3.2]), ensures the validity of some key estimates (Lemma 5.7 below).

Assumption 5.4. *The following conditions on U and V are satisfied.*

- *It holds, for any $\gamma > 0$:*

$$(1+|p|^\gamma)\mathrm{e}^{-\beta U(p)} \in L^1(\mathbb{R}^d), \qquad (1+|q|^\gamma+|\nabla V(q)|^\gamma)\mathrm{e}^{-\beta V(q)} \in L^1(\mathcal{Q}).$$

  In particular, the equilibrium probability measure (5.5) is well-defined.

- *The marginals κ and ν defined in (5.5) satisfy Poincaré inequalities: there exist $K_\kappa, K_\nu > 0$ such that, for any $\varphi \in H^1(\kappa)$ and $\psi \in H^1(\nu)$,*

$$\|\varphi - \kappa(\varphi)\|_{L^2(\kappa)} \leqslant \frac{1}{K_\kappa}\|\nabla_p \varphi\|_{L^2(\kappa)}, \qquad \|\psi - \nu(\psi)\|_{L^2(\nu)} \leqslant \frac{1}{K_\nu}\|\nabla \psi\|_{L^2(\nu)}. \tag{5.9}$$

- *There exist constants $c_1, c_2 > 0$ and $0 \leqslant c_3 \leqslant 1$ such that the following bounds hold pointwise:*

$$\|\nabla^2 V\|_{\mathrm{HS}}^2 \leqslant c_1^2\left(d + |\nabla V|^2\right), \qquad \Delta V \leqslant c_2 d + \frac{c_3\beta}{2}|\nabla V|^2.$$

- *The function U is even, and for all multi-indices $\alpha_1, \alpha_2, \alpha_3 \in \mathbb{N}^d$ such that $|\alpha_i| \leqslant i$ for $1 \leqslant i \leqslant 3$, it holds*

$$\partial^{\alpha_3} U \in L^2(\kappa), \qquad (\partial^{\alpha_2} U)(\partial^{\alpha_1} U) \in L^2(\kappa).$$

A simple case in which all the conditions on V and U imposed by Assumptions 5.1 and 5.4 is the case where these two functions are smooth and grow quadratically at infinity. In particular, the conditions on V are vacuous if $\mathcal{Q}$ is compact.

The final assumption, which will be used to prove the second item in Proposition 5.6, restricts the dynamics (5.1) to the physical setting, in which the kinetic energy is a positive non-degenerate quadratic form.

Assumption 5.5. *The function U in (5.1) is given by*

$$U(p) = \frac{1}{2}p^\top M^{-1} p$$

for some constant matrix $M \in \mathcal{S}_d^{++}$.

Kramers–Smoluchowski approximation. The main result states two convergence results for the time-rescaled position process X^λ, in the limit of a large friction intensity $\lambda \to +\infty$. Recall that $(X_0 = q_0^\lambda, p_0^\lambda) \sim \mu_0$ for all $\lambda > 0$.

Proposition 5.6. *Assume that $\mu_0 \ll \mu$ is such that*

$$(X_0, p_0) \sim \mu_0, \qquad \frac{\mathrm{d}\mu_0}{\mathrm{d}\mu} \in L^p(\mu) \qquad \text{for some } p \in (1, +\infty].$$

Suppose that Assumptions 5.1, 5.2, 5.3 and 5.4 are satisfied, and let $q \in [1, \infty)$ be the conjugate exponent to p, i.e. $q = p/(p-1)$.

- *for any $T > 0$ and $0 < \alpha \leqslant \frac{2}{q}$, there exists $C(T, \alpha, \mu_0) > 0$ such that*

$$\sup_{0 \leqslant t \leqslant T} \mathbb{E}_{\mu_0} \left[|X_t^\lambda - X_t|^\alpha \right] \leqslant \frac{C(T, \alpha, \mu_0)}{\lambda^{\alpha/2}}, \tag{5.10}$$

- *suppose furthermore that Assumption 5.5 is satisfied. Then the following convergence of path distributions holds:*

$$X_*^\lambda \mathbb{P}_{\mu_0} \xrightarrow[\lambda \to +\infty]{\text{weakly}} X_* \mathbb{P}_{\mu_0} \in \mathcal{P}(\mathcal{C}([0,T]; \mathcal{Q})). \tag{5.11}$$

The key technical tool in the proof is the following result.

Lemma 5.7 (Uniform hypocoercivity in $L^2(\mu)$)**.** *Let Assumptions 5.3 to 5.4 be satisfied.*

- *For any $\lambda > 0$, the generator $\mathcal{L}_\lambda$ is invertible on $L_0^2(\mu)$. Namely, for any $\varphi \in L_0^2(\mu)$, the Poisson equation*

$$\mathcal{L}_\lambda f = \varphi$$

has a unique solution $f = \mathcal{L}_\lambda^{-1} \varphi \in L_0^2(\mu)$.

- *If $\varphi \in (\mathrm{Id} - \Pi_0) L_0^2(\mu)$, it furthermore holds that for some constant $C > 0$,*

$$\forall\, \lambda \geqslant 1, \qquad \|\mathcal{L}_\lambda^{-1} \varphi\|_{L^2(\mu)} \leqslant C \|\varphi\|_{L^2(\mu)}, \qquad \|\nabla_p \mathcal{L}_\lambda^{-1} \varphi\|_{L^2(\mu)} \leqslant \frac{C}{\sqrt{\lambda}} \|\varphi\|_{L^2(\mu)}. \tag{5.12}$$

The main interest of this result, beyond providing the L^2-hypocoercivity property for the dynamics (5.1), is the uniformity of the estimates in (5.12). Whereas standard hypocoercive estimates give $\|\mathcal{L}_\lambda^{-1} \varphi\|_{L^2(\mu)} = \mathcal{O}(\max(\lambda, \lambda^{-1})) \|\varphi\|_{L^2(\mu)}$ for general $\varphi \in L_0^2(\mu)$, this bound can be improved when $\varphi \in \ker \Pi_0$. The proof of Lemma 5.7, which uses the L^2-hypocoercivity framework of [37], is given in Section 5.A below.

5.3 Proof of Proposition 5.6

We now prove the main result. For the first item in Proposition 5.6, we first establish the result for $\mu_0 = \mu$ and $p = 2$, and conclude for a more general initial distribution μ_0 via a reweighting argument. This will in particular establish the weak convergence of all finite-dimensional time marginals of X^λ towards those of X. To prove the second point, we exploit the specific form of the dynamics under Assumption (5.5) to obtain the tightness of the family $(X_*^\lambda \mathbb{P})_{\lambda \geqslant 1}$ in $\mathcal{P}(\mathcal{C}([0,T]; \mathcal{Q}))$, which will conclude the argument by a classical corollary of Prokhorov's theorem (see [41, Theorem 8.1]).

The first step is a simple computation with Itô's formula, from which the origin of the noise-induced drift appears clearly.

An Itô computation. For any $\lambda > 0$, since the quadratic covariation $\left\langle q^\lambda \right\rangle$ in the position variable vanishes, it holds

$$\mathrm{d}\left[D(q_t^\lambda)p_t^\lambda\right] = -D(q_t^\lambda)\nabla V(q_t^\lambda)\,\mathrm{d}t - \lambda\,\mathrm{d}q_t^\lambda + \sqrt{\frac{2\lambda}{\beta}}D^{1/2}(q_t^\lambda)\,\mathrm{d}W_t^\lambda + D'(q_t^\lambda)\left[\nabla U(p_t^\lambda)\right]p_t^\lambda \mathrm{d}t,$$

where we recall the definition (5.8) of D'. In particular, for any $1 \leqslant k \leqslant d$,

$$\left(D'(q)\left[\nabla U(p)\right]p\right)_k = \sum_{i,j=1}^d \partial_i D_{kj}(q)\partial_i U(p)p_j.$$

Isolating $\mathrm{d}q_t^\lambda$ and integrating over $[0, \lambda t]$, we get:

$$\begin{aligned} q_{\lambda t}^\lambda - q_0^\lambda = &-\frac{1}{\lambda}\int_0^{\lambda t} D(q_s^\lambda)\nabla V(q_s^\lambda)\,\mathrm{d}s + \sqrt{\frac{2}{\lambda\beta}}\int_0^{\lambda t} D^{1/2}(q_s^\lambda)\,\mathrm{d}W_s^\lambda \\ &+ \frac{1}{\lambda}\int_0^{\lambda t} D'(q_s^\lambda)\left[\nabla U(p_s^\lambda)\right]p_s^\lambda\,\mathrm{d}s + \frac{D(q_0^\lambda)p_0^\lambda - D(q_{\lambda t}^\lambda)p_{\lambda t}^\lambda}{\lambda}. \end{aligned} \tag{5.13}$$

Defining $X_t^\lambda = q_{\lambda t}$, this time-rescaling changes (5.13) into

$$X_t^\lambda = X_0 - \int_0^t \left[D(X_s^\lambda)\nabla V(X_s^\lambda) - \frac{1}{\beta}\mathrm{div}D(X_s^\lambda)\right]\mathrm{d}s + \sqrt{\frac{2}{\beta}}\int_0^t D^{1/2}(X_s^\lambda)\,\mathrm{d}W_s + R(t,\lambda), \tag{5.14}$$

where we introduced the remainder term

$$R(t,\lambda) = \frac{D(q_0^\lambda)p_0^\lambda - D(q_{\lambda t}^\lambda)p_{\lambda t}^\lambda}{\lambda} + \frac{1}{\lambda}\int_0^{\lambda t}\psi(q_s^\lambda, p_s^\lambda)\,\mathrm{d}s, \qquad \psi(q,p) = D'(q)\left[\nabla U(p)\right]p - \frac{1}{\beta}\mathrm{div}D(q), \tag{5.15}$$

and use $X_0^\lambda = q_0^\lambda = X_0$.

Since $p \in L^2(\kappa)$, $U \in H^1(\kappa)$ and $D \in W^{1,\infty}(\kappa)$ (from Assumptions 5.3 and 5.4), an integration by parts shows that component-wise:

$$\Pi_0\left(D'(q)\left[\nabla U(p)\right]p\right) = \frac{1}{\beta}\mathrm{div}D(q),$$

so that $\psi \in \left((\mathrm{Id} - \Pi_0)L^2(\mu)\right)^d \subset L_0^2(\mu)^d$. Indeed, from (5.8) and the form (5.5) for κ, for any $1 \leqslant k \leqslant d$,

$$\begin{aligned} \int_{\mathbb{R}^d}\left(D'(q)\left[\nabla U(p)\right]p\right)_k &= \sum_{i,j=1}^d \int_{R^d}\partial_i D_{kj}(q)(\partial_i U(p))p_j\,\kappa(\mathrm{d}p) \\ &= \frac{1}{\beta}\sum_{i,j=1}^d \partial_i D_{kj}(q)\int_{\mathbb{R}^d}(\partial_i p_j)\,\kappa(\mathrm{d}p) \\ &= \frac{1}{\beta}\sum_{i,j=1}^d \delta_{ij}\partial_i D_{kj}(q) \\ &= \frac{1}{\beta}\left(\mathrm{div}\,D(q)\right)_k. \end{aligned}$$

In view of the form (5.4) of the limiting equation, we interpret $R(\cdot,\lambda)$ as a perturbation term.

Using the first item in Lemma 5.7, we introduce, for each $\lambda \geqslant 1$, the solution $\Phi_\lambda \in L^2(\mu)^d$ to the (component-wise) Poisson equation:

$$\mathcal{L}_\lambda \Phi_\lambda = \psi.$$

Since ψ is smooth and $\mathcal{L}_\lambda$ is hypoelliptic under Assumption (5.2), Φ_λ is smooth, and we may write the integral in (5.15) as

$$\frac{1}{\lambda}\int_0^{\lambda t} \psi(q_s^\lambda, p_s^\lambda)\,\mathrm{d}s = \frac{\Phi_\lambda(X_t^\lambda, p_{\lambda t}^\lambda) - \Phi_\lambda(X_0, p_0^\lambda)}{\lambda} - \sqrt{\frac{2}{\beta}}\int_0^t \nabla_p \Phi_\lambda(X_s^\lambda, p_{\lambda s}^\lambda)^\top D(X_s^\lambda)^{-1/2}\,\mathrm{d}W_s, \tag{5.16}$$

using Itô's formula and making the same rescaling in time as the one leading to (5.14). Using these estimates, the proof of the first item (5.10) in Proposition 5.6 follows from a Grönwall-type argument, which we now detail.

Proof of (5.10). Fix $T > 0$ and assume as a first step that $\mu_0 = \mu$. By Hölder's inequality, it suffices to show the estimate (5.10) for $\alpha = 2$. By stationarity, $X_t, X_t^\lambda \sim \nu$ and $p_{\lambda t}^\lambda \sim \kappa$ for all $0 \leqslant t \leqslant T$ under $\mathbb{P}_\mu$. Note also that, since $\nabla_p \Phi_\lambda$ is in $L^2(\mu)$ component-wise from the second item in Lemma 5.7, the local martingale on the right-hand side of (5.16) is an $L^2(\mathbb{P}_\mu)$ W-martingale.

We denote the difference process by

$$E_t^\lambda := X_t^\lambda - X_t,$$

which has finite second-moments by the first item in Assumption 5.4 under $\mathbb{P}_\mu$, and write, for $0 \leqslant t \leqslant T$,

$$|E_t^\lambda|^2 \leqslant 3\left[\left|\int_0^t \left[b(X_s^\lambda) - b(X_s)\right]\,\mathrm{d}s\right|^2 + \left|\int_0^t \left[\sigma(X_s^\lambda) - \sigma(X_s)\right]\,\mathrm{d}W_s\right|^2 + |R(t,\lambda)|^2\right], \tag{5.17}$$

where $b(x) = -D(x)\nabla V(x) + \frac{1}{\beta}\operatorname{div} D(x)$ and $\sigma(x) = \sqrt{\frac{2}{\beta}} D(x)^{1/2}$. We estimate each of these terms separately. Let $L_b, L_\sigma > 0$ be Lipschitz constants for b and σ (in the norm $\|\cdot\|_{\mathrm{HS}}$ for σ), which exist by Assumptions 5.1 and 5.3. Then the first two terms inside the bracket on the right side of (5.17) are bounded in expectation by

$$(L_b^2 + L_\sigma^2)\int_0^t \mathbb{E}_\mu\left[|E_s^\lambda|^2\right]\,\mathrm{d}s, \tag{5.18}$$

using Itô's isometry to bound the second term. To control the remainder, we write, using (5.15) and (5.16)

$$\begin{aligned}\mathbb{E}_\mu\left[|R(t,\lambda)|^2\right] &\leqslant 5\left(\frac{2}{\lambda^2}\left[\|Dp\|_{L^2(\mu)}^2 + \|\Phi_\lambda\|_{L^2(\mu)}^2\right] + \frac{2}{\beta}\mathbb{E}_\mu\left[\left|\int_0^t \nabla_p \Phi_\lambda(X_s^\lambda, p_{\lambda s}^\lambda)^\top D(X_s^\lambda)^{-1/2}\,\mathrm{d}W_s\right|^2\right]\right) \\ &\leqslant 5\left(\frac{2}{\lambda^2}\left[\|Dp\|_{L^2(\mu)}^2 + \|\Phi_\lambda\|_{L^2(\mu)}^2\right] + \frac{2T}{\beta}\|D\|_{L^\infty(\mathcal{Q};\mathcal{S}_d^{++})}\|\nabla_p \Phi\|_{L^2(\mu),\mathrm{HS}}^2\right),\end{aligned}$$

using once again Itô's isometry in the second line. We may now use the two estimates of Lemma 5.7 to obtain

$$\mathbb{E}_\mu\left[|R(\lambda,t)|^2\right] \leqslant \frac{C_T}{\lambda} \tag{5.19}$$

for some constant $C_T > 0$ independent of λ. Collecting the estimates (5.17), (5.18) and (5.19), we get, taking expectations,

$$\mathbb{E}_\mu\left[|E_t^\lambda|^2\right] \leqslant 3\left(L_b^2 + L_\sigma^2\right)\int_0^t \mathbb{E}_\mu\left[|E_s^\lambda|^2\right]\,\mathrm{d}s + \frac{3C_T}{\lambda},$$

from which Grönwall's lemma gives

$$\sup_{0\leqslant t\leqslant T}\mathbb{E}_\mu\left[|E_t^\lambda|^2\right] \leqslant \frac{3C_T}{\lambda}\mathrm{e}^{3T(L_b^2+L_\sigma^2)},$$

which concludes the proof of (5.10) for $\mu_0 = \mu$ and $\alpha = 2$.

To extend the argument to μ_0, we simply reweight the initial condition. Let $0 < \alpha \leqslant 2/q$. We write, by Hölder's inequality,

$$\mathbb{E}_{\mu_0}\left[|E_t^\lambda|^\alpha\right] = \mathbb{E}_\mu\left[|E_t^\lambda|^\alpha \frac{\mathrm{d}\mu_0}{\mathrm{d}\mu}(X_0,p_0)\right] \leqslant \mathbb{E}_\mu\left[|E_t^\lambda|^{q\alpha}\right]^{1/q}\left\|\frac{\mathrm{d}\mu_0}{\mathrm{d}\mu}\right\|_{L^p(\mu)} \leqslant \mathbb{E}_\mu\left[|E_t^\lambda|^2\right]^{\alpha/2}\left\|\frac{\mathrm{d}\mu_0}{\mathrm{d}\mu}\right\|_{L^p(\mu)}, \tag{5.20}$$

from which the proof of (5.10) follows from the case $(\mu_0,\alpha) = (\mu,2)$.

Tightness. We now prove (5.11). Since all finite-dimensional marginals of X^λ converge to those of X by (5.10), it is sufficient, in order to conclude to the result of Proposition 5.6, to prove tightness for the family of pushforward measures $(X_*^\lambda\mathbb{P}_{\mu_0})_{\lambda\geqslant 1}$ on $\mathcal{C}([0,T];\mathcal{Q})$. We use the following criterion, which is an immediate corollary of [41, Theorem 12.3]. If the family of initial laws $\left(\left[X_0^\lambda\right]_*\mathbb{P}_{\mu_0}\right)_{\lambda\geqslant 1}$ is tight in $\mathcal{P}(\mathcal{Q})$, and there exist real numbers $a,b,C>0$ such that

$$\forall\,\lambda>0,\ 0\leqslant s<t\leqslant T, \qquad \mathbb{E}_{\mu_0}\left[\left|X_s^\lambda - X_t^\lambda\right|^a\right] \leqslant C(t-s)^{1+b}, \tag{5.21}$$

then $(X_*^\lambda\mathbb{P}_{\mu_0})_{\lambda\geqslant 1}$ is tight in $\mathcal{P}(\mathcal{C}([0,T];\mathcal{Q}))$. Since $\left[X_0^\lambda\right]_*\mathbb{P}_{\mu_0} = \mu_0$ for all λ, it is sufficient to control moments of the form (5.21).

Fix $0\leqslant s<t\leqslant T$. The first step is to write the velocity $M^{-1}p_t^\lambda$ in a more explicit form. We recall that under Assumption 5.5, $U(p) = \frac{1}{2}p^\top M^{-1}p$ for some constant $M\in\mathcal{S}_d^{++}$. We view the equation

$$\begin{aligned}\mathrm{d}(M^{-1/2}p^\lambda)_t =& -M^{-1/2}\nabla V(q_t^\lambda)\,\mathrm{d}t - \lambda\left(M^{-1/2}D(q_t^\lambda)^{-1}M^{-1/2}\right)M^{-1/2}p_t^\lambda\,\mathrm{d}t\\ &+\sqrt{\frac{2\lambda}{\beta}}M^{-1/2}D(q_t^\lambda)^{-1/2}\,\mathrm{d}W_t\end{aligned}$$

as a time-dependent linear ODE with a source term. To solve this equation, we introduce the matrix of fundamental solutions to the associated homogeneous problem, namely the $\mathcal{S}_d^{++}$-valued process defined pathwise by the ODE:

$$\mathrm{d}\mathcal{R}_t^\lambda = -\lambda M^{-1/2}D(q_t^\lambda)^{-1}M^{-1/2}\mathcal{R}_t^\lambda\,\mathrm{d}t, \qquad \mathcal{R}_0^\lambda = \mathrm{Id}. \tag{5.22}$$

We will use the shorthand D_M for the matrix field appearing in (5.22), i.e.

$$D_M(q) = M^{-1/2} D(q)^{-1} M^{-1/2}.$$

Note that D_M also satisfies Assumption (5.3), so that the existence, uniqueness and W-adaptiveness of $\mathcal{R}_\lambda$ on $[0, \lambda T]$ all follow from the general theory of linear ODEs with continuous coefficients, see for instance [317, Section 3.4].

Using Duhamel's principle, we can write

$$\begin{aligned} M^{-1/2} p_t^\lambda =& \mathcal{R}_t^\lambda M^{-1/2} p_0^\lambda - \mathcal{R}_t^\lambda \int_0^t (\mathcal{R}_s^\lambda)^{-1} M^{-1/2} \nabla V(q_s^\lambda)\, \mathrm{d}s \\ &+ \sqrt{\frac{2\lambda}{\beta}} \mathcal{R}_t^\lambda \int_0^t (\mathcal{R}_s^\lambda)^{-1} M^{-1/2} D(q_s^\lambda)^{-1/2}\, \mathrm{d}W_s^\lambda. \end{aligned}$$

The validity of this expression may be checked a posteriori by applying Itô's product rule to $(\mathcal{R}_t^\lambda)^{-1} M^{-1/2} p_t^\lambda$, and using the expression

$$\mathrm{d}\left(\mathcal{R}_t^\lambda\right)^{-1} = \lambda \left(\mathcal{R}_t^\lambda\right)^{-1} D_M(q_t^\lambda)\, \mathrm{d}t,$$

which itself is a consequence the well-known matrix identity $\partial_t (A(t)^{-1}) = -A(t)^{-1} \partial_t A(t) A(t)^{-1}$.

Left-multiplying $M^{-1/2} p_t$ by $M^{-1/2}$ and integrating over $[\lambda s, \lambda t]$, it follows, according to the SDE (5.1), that the time-rescaled position increments can be written as

$$\begin{aligned} X_t^\lambda - X_s^\lambda = \int_{\lambda s}^{\lambda t} M^{-1} p_r^\lambda\, \mathrm{d}r = M^{-1/2} \Bigg[\int_{\lambda s}^{\lambda t} \Bigg(& \mathcal{R}_r^\lambda M^{-1/2} p_0 - \mathcal{R}_r \int_0^r (\mathcal{R}_u^\lambda)^{-1} M^{-1/2} \nabla V(q_u^\lambda)\, \mathrm{d}u \\ & + \sqrt{\frac{2\lambda}{\beta}} \mathcal{R}_r^\lambda \int_0^r \left(\mathcal{R}_u^\lambda\right)^{-1} M^{-1/2} D(q_u^\lambda)^{-1/2}\, \mathrm{d}W_u^\lambda \Bigg)\, \mathrm{d}r \Bigg], \end{aligned}$$

which we split into three summands as $M^{-1/2}\left[I_1(s,t) + I_2(s,t) + I_3(s,t)\right]$.

Take $\gamma > 1$. Using the bound $|X_t^\lambda - X_s^\lambda|^\gamma \leqslant \|M^{-1/2}\|_{\mathrm{op}}^\gamma 3^{\gamma-1} (|I_1(s,t)|^\gamma + |I_2(s,t)|^\gamma + |I_3(s,t)|^\gamma)$, it remains to control the three integral terms separately, seeking uniform-in-λ estimates for their $\mathbb{P}_{\mu_0}$-expectation. We use the inequality:

$$\forall\, 0 \leqslant s \leqslant t \leqslant T, \qquad \left\| \mathcal{R}_t^\lambda \left(\mathcal{R}_s^\lambda\right)^{-1} \right\| \leqslant \mathrm{e}^{-\lambda \varepsilon_{D,M}(t-s)} \qquad \mathbb{P}_{\mu_0}\text{-almost surely,} \tag{5.23}$$

where $\|\cdot\|$ is the standard Euclidean operator norm on $\mathbb{R}^d$, for some $\varepsilon_{D,M} > 0$ independent of λ. This identity follows from the uniform bound (5.3), upon applying Grönwall's inequality pathwise, to $|v(t)|^2 = \left|\mathcal{R}_t^\lambda (\mathcal{R}_s^\lambda)^{-1} v_0\right|^2$, where v solves the ODE:

$$\frac{\mathrm{d}}{\mathrm{d}t} v(t) = -\lambda D_M(q_t^\lambda)^{-1} v(t), \qquad v(s) = v_0,$$

for any $v_0 \in \mathbb{R}^d$ (see also [317, Problem 3.31]).

Applying (5.23) to I_1, we get the following almost-sure inequality:

$$|I_1(s,t)|^\gamma \leqslant |M^{-1/2}p_0|^\gamma \left(\int_{\lambda s}^{\lambda t} \mathrm{e}^{-\lambda \varepsilon_{D,M} r}\,\mathrm{d}r\right)^\gamma,$$

which gives, upon taking the expectation with respect to μ_0,

$$\mathbb{E}_{\mu_0}\left[|I_1(s,t)|^\gamma\right] \leqslant \frac{\mu_0(|M^{-1/2}p_0|^\gamma)}{\lambda^\gamma \varepsilon_{D,M}^\gamma}[\mathrm{e}^{-\lambda^2\varepsilon_{D,M}s} - \mathrm{e}^{-\lambda^2\varepsilon_{D,M}t}]^\gamma \leqslant \frac{\mu(|M^{-1/2}p_0|^{\gamma q})^{1/q}}{\lambda^\gamma \varepsilon_{D,M}^\gamma} C_p(\mu_0). \tag{5.24}$$

using the reweighting argument of (5.20) in the last inequality. Since p_0 is Gaussian under μ, the γq-th moment $\mu(|M^{-1/2}p_0|^{\gamma q})$ is finite, and the estimate (5.24) controls the contribution of $I_1(s,t)$ to $\mathbb{E}_{\mu_0}[|X_s^\lambda - X_t^\lambda|^\gamma]$ uniformly with respect to λ.

Next, we treat the second term, writing:

$$\begin{aligned}
|I_2(s,t)|^\gamma &\leqslant \left(\int_{\lambda s}^{\lambda t}\int_0^r \left|\mathcal{R}_r^\lambda (\mathcal{R}_u^\lambda)^{-1} M^{-1/2}\nabla V(q_u^\lambda)\right| \mathrm{d}u\,\mathrm{d}r\right)^\gamma \\
&\leqslant (\lambda(t-s))^{\gamma-1}\int_{\lambda s}^{\lambda t}\left(\int_0^r \mathrm{e}^{-\lambda\varepsilon_{D,M}(r-u)}|M^{-1/2}\nabla V(q_u^\lambda)|\,\mathrm{d}u\right)^\gamma \mathrm{d}r \\
&\leqslant (\lambda(t-s))^{\gamma-1}\int_{\lambda s}^{\lambda t}\left(\int_0^r \mathrm{e}^{-\lambda\varepsilon_{D,M}(r-u)}\,\mathrm{d}u\right)^{\gamma-1}\left(\int_0^r \mathrm{e}^{-\lambda\varepsilon(r-u)}|M^{-1/2}\nabla V(q_u^\lambda)|^\gamma\,\mathrm{d}u\right)\mathrm{d}r \\
&\leqslant \frac{(t-s)^{\gamma-1}}{\varepsilon_{D,M}^{\gamma-1}}\int_{\lambda s}^{\lambda t}\int_0^r \mathrm{e}^{-\lambda\varepsilon_{D,M}(r-u)}|M^{-1/2}\nabla V(q_u^\lambda)|^\gamma\,\mathrm{d}u\,\mathrm{d}r,
\end{aligned}$$

where we used Hölder's inequality twice: once in r in the second line for the Lebesgue measure, and once in u in the third line for the exponentially-weighted measure $\mathrm{e}^{-\lambda\varepsilon_{D,M}(r-u)}\,\mathrm{d}u$. Taking the expectation with respect to $\mathbb{P}_{\mu_0}$, we get, with the same reweighting argument as in previous estimates:

$$\begin{aligned}
\mathbb{E}_{\mu_0}\left[|I_2(s,t)|^\gamma\right] &\leqslant \sup_{0\leqslant u\leqslant t}\mathbb{E}_{\mu_0}[|M^{-1/2}\nabla V(q_u^\lambda)|^\gamma]\frac{(t-s)^{\gamma-1}}{\varepsilon_{D,M}^{\gamma-1}}\int_{\lambda s}^{\lambda t}\int_0^r \mathrm{e}^{-\lambda\varepsilon_{D,M}(r-u)}\,\mathrm{d}u\,\mathrm{d}r \\
&\leqslant C_p(\mu_0)\|M^{-1/2}\|_{\mathrm{op}}^\gamma \mu\left(|\nabla V|^{\gamma q}\right)^{1/q}\frac{(t-s)^{\gamma-1}}{\varepsilon_{D,M}^{\gamma-1}}\frac{\lambda t-\lambda s}{\lambda\varepsilon_{D,M}} \\
&= C_p(\mu_0)\|M^{-1/2}\|_{\mathrm{op}}^\gamma \mu\left(|\nabla V|^{\gamma q}\right)^{1/q}\frac{(t-s)^\gamma}{\varepsilon_{D,M}^\gamma}.
\end{aligned} \tag{5.25}$$

We finally treat the last term $I_3(s,t)$, which requires some care. In the proof of [339, Lemma 3.1], the authors suggest controlling similar double integrals by a (stochastic) Fubini theorem followed by Doob's maximal inequality. This argument, while giving sufficient control formally, seems incorrect, as the resulting time-swapped integrands are not W-adapted, nor in general (sub)martingales. A similar mistake can be found in the proof of [176, Section 3.4.2, Lemma 10]. To avoid this difficulty, we write instead

$$I_3(s,t) = \int_{\lambda s}^{\lambda t} Z_r^\lambda\,\mathrm{d}r, \qquad Z_t^\lambda := \sqrt{\frac{2\lambda}{\beta}}\mathcal{R}_t^\lambda \int_0^t \left(\mathcal{R}_s^\lambda\right)^{-1} M^{-1/2}D(q_s^\lambda)^{-1/2}\,\mathrm{d}W_s^\lambda,$$

from which we get, using (5.22),

$$\mathrm{d}Z_t^\lambda = -\lambda D_M(q_t^\lambda) Z_t^\lambda \mathrm{d}t + \sqrt{\frac{2\lambda}{\beta}} M^{-1/2} D(q_t^\lambda)^{-1/2}\, \mathrm{d}W_t^\lambda, \tag{5.26}$$

which we integrate against $-\lambda^{-1} D_M(q^\lambda)^{-1}$ over $[\lambda s, \lambda t]$ to obtain

$$I_3(s,t) = \sqrt{\frac{2}{\lambda\beta}} \int_{\lambda s}^{\lambda t} \left[D_M^{-1} M^{-1/2} D^{-1/2}\right](q_r^\lambda)\, \mathrm{d}W_r^\lambda - \lambda^{-1} \int_{\lambda s}^{\lambda t} D_M(q_r^\lambda)^{-1} \mathrm{d}Z_r^\lambda. \tag{5.27}$$

To treat the first term, we use the Burkholder–Davis–Gundy inequality to obtain the existence of $C_{\gamma,\beta} > 0$ such that

$$\begin{aligned}\mathbb{E}_{\mu_0}\left[\left|\sqrt{\frac{2}{\lambda\beta}} \int_{\lambda s}^{\lambda t} \left[D_M^{-1} D^{-1/2}\right](q_r^\lambda)\, \mathrm{d}W_r^\lambda\right|^\gamma\right] &\leqslant C_{\gamma,\beta} \lambda^{-\gamma/2} \mathbb{E}_{\mu_0}\left[\left(\int_{\lambda s}^{\lambda t} \left\|\left[D_M^{-1} M^{-1/2} D^{-1/2}\right](q_r^\lambda)\right\|_{\mathrm{HS}}^2 \mathrm{d}r\right)^{\gamma/2}\right] \\ &\leqslant C_{\gamma,\beta} \|D_M^{-1} M^{-1/2} D^{-1/2}\|_{L^\infty_{\mathrm{HS}}}^\gamma (t-s)^{\gamma/2}.\end{aligned} \tag{5.28}$$

We rewrite the second term in (5.27), using Itô's product rule, which gives

$$\int_{\lambda s}^{\lambda t} D_M(q_r^\lambda)^{-1}\, \mathrm{d}Z_r^\lambda = D_M(q_{\lambda t}^\lambda)^{-1} Z_{\lambda t}^\lambda - D_M(q_{\lambda s}^\lambda)^{-1} Z_{\lambda s}^\lambda - \int_{\lambda s}^{\lambda t} \left(D_M^{-1}\right)'(q_r^\lambda)[M^{-1} p_r^\lambda] Z_r^\lambda\, \mathrm{d}r.$$

Controlling these three terms requires some moment bounds on Z^λ. The idea is to apply Itô's formula to Z^λ with $f(z) = |z|^\gamma$. In view of the SDE (5.26) satisfied by Z^λ, it holds for $\gamma > 2$:

$$\begin{aligned}\frac{\mathrm{d}}{\mathrm{d}r}\mathbb{E}_{\mu_0}\left[|Z_r^\lambda|^\gamma\right] &= -\lambda\gamma \mathbb{E}_{\mu_0}\left[|Z_r^\lambda|^{\gamma-2} \left(Z_r^\lambda\right)^\top D_M(q_r^\lambda) Z_r^\lambda\right] \\ &\quad + \lambda \frac{\gamma(\gamma-2)}{\beta} \mathbb{E}_{\mu_0}\left[|Z_r^\lambda|^{\gamma-4} M^{-1/2} D(q_r^\lambda)^{-1} M^{-1/2} : Z_r^\lambda \otimes Z_r^\lambda\right] \\ &\quad + \lambda \frac{\gamma}{\beta} \mathbb{E}_{\mu_0}\left[|Z_r^\lambda|^{\gamma-2} \mathrm{Tr}\left(M^{-1/2} D(q_r^\lambda)^{-1} M^{-1/2}\right)\right] \\ &\leqslant -\lambda C_\gamma^{(1)} \mathbb{E}_{\mu_0}\left[|Z_r^\lambda|^\gamma\right] + \lambda C_\gamma^{(2)} \mathbb{E}_{\mu_0}\left[|Z_r^\lambda|^{\gamma-2}\right] \\ &\leqslant -\lambda C_\gamma^{(3)} \mathbb{E}_{\mu_0}\left[|Z_r^\lambda|^\gamma\right] + \lambda C_\gamma^{(4)},\end{aligned} \tag{5.29}$$

where the constants $C_\gamma^{(i)} > 0$, $1 \leqslant i \leqslant 4$ depend on D, β and M, but may be chosen uniformly in λ. Indeed, by optimizing $\theta^{\gamma-2} - \alpha t^\gamma$ with respect to θ, we get the inequality

$$\forall\, \theta \geqslant 0, \alpha > 0, \gamma > 2 \qquad \theta^{\gamma-2} \leqslant \alpha\theta^\gamma + \alpha^{-\frac{\gamma-2}{2}} \frac{2}{\gamma} \left(\frac{\gamma-2}{\gamma}\right)^{\frac{\gamma-2}{2}},$$

which we use in the last line of (5.29) with $\alpha < C_\gamma^{(1)}/C_\gamma^{(2)}$ to absorb $\mathbb{E}_{\mu_0}\left[|Z_r^\lambda|^{\gamma-2}\right]$ into the dissipative term.

Solving the differential inequality with $Z_0^\lambda = 0$, we get:

$$\mathbb{E}_{\mu_0}\left[|Z_r^\lambda|^\gamma\right] \leqslant \lambda C_\gamma^{(4)} \frac{1 - \mathrm{e}^{-r\lambda C_\gamma^{(3)}}}{\lambda C_\gamma^{(3)}} \leqslant \frac{C_\gamma^{(4)}}{C_\gamma^{(3)}} \tag{5.30}$$

for all $r \geqslant 0$. To make this argument rigorous, one should really apply Itô's formula to the stopped process $Z^\lambda_{t\wedge\tau^\lambda_K}$ with $\tau^\lambda_K = \inf\{t \geqslant 0 : |Z^\lambda_t| \geqslant K\}$ and f_K a bounded $\mathcal{C}^2$ function satisfying $f_K(z)\mathbb{1}_{\{|z|\leqslant K\}} = |z|^\gamma$. One can then obtain $\mathbb{E}_{\mu_0}\left[|Z^\lambda_{r\wedge\tau^\lambda_K}|^\gamma\right] \leqslant C$ by the computation (5.29) (for some C not depending on K or λ), and pass to the limit $K \to +\infty$.

From the bound (5.30), it follows that

$$\mathbb{E}_{\mu_0}\left[\left|\lambda^{-1}D_M^{-1}(q^\lambda_{\lambda s})Z^\lambda_{\lambda s}\right|^\gamma\right], \mathbb{E}_{\mu_0}\left[\left|\lambda^{-1}D_M^{-1}(q^\lambda_{\lambda t})Z^\lambda_{\lambda t}\right|^\gamma\right] \leqslant \lambda^{-\gamma}\left\|D_M^{-1}\right\|^\gamma_{L^\infty_{\mathrm{op}}}\frac{C^{(4)}_\gamma}{C^{(3)}_\gamma}, \tag{5.31}$$

and by Hölder's inequality we finally get

$$\begin{aligned}\mathbb{E}_{\mu_0}\left[\left|\lambda^{-1}\int_{\lambda s}^{\lambda t}\left(D_M^{-1}\right)'(q^\lambda_r)\left[M^{-1}p^\lambda_t\right]Z^\lambda_r\,\mathrm{d}r\right|^\gamma\right] &\leqslant C_{M,D,\gamma}\lambda^{-1}(t-s)^{\gamma-1}\int_{\lambda s}^{\lambda t}\mathbb{E}_{\mu_0}\left[\left|M^{-1}p^\lambda_r\right|^\gamma\left|Z^\lambda_r\right|^\gamma\right]\mathrm{d}r \\ &\leqslant C_{M,D,\gamma}(t-s)^\gamma\left(\frac{C^{(4)}_{2\gamma}}{C^{(3)}_{2\gamma}}\right)^{1/2}\mu\left(\left|M^{-1}p\right|^{2\gamma q}\right)^{1/q}C_p(\mu_0)\end{aligned} \tag{5.32}$$

where $C_{M,D,\gamma} = \left\|\left(D_M^{-1}\right)'\right\|^\gamma_{L^\infty(\mathcal{Q};\mathcal{L}(\mathbb{R}^d;\mathbb{R}^{d\times d}))}$ is finite by Assumptions 5.1 and 5.3, where we used Hölder's inequality in the first line and a Cauchy–Schwarz inequality with the same reweighting argument as before in the last line.

Collecting the estimates (5.24) (5.25), (5.28), (5.31) and (5.32), we find that there exists $\gamma > 2$ and $C > 0$ such that, for all $\lambda \geqslant 1$ and all $0 \leqslant s < t \leqslant T$, it holds

$$\mathbb{E}_{\mu_0}\left[\left|X^\lambda_t - X^\lambda_s\right|^\gamma\right] \leqslant C(t-s)^{\gamma/2}.$$

By the criterion (5.21), the family of path laws $\left(X^\lambda_*\mathbb{P}_{\mu_0}\right)_{\lambda\geqslant 1}$ is tight, which concludes the proof of (5.11).

5.4 Overdamped limit for a class of variable-mass matrices

In this section, we derive the overdamped limit for the underdamped Langevin dynamics, in a simple setting where the mass matrix itself depends on the position variable. In contrast to the dynamics (5.1) in Section 5.1, the Hamiltonian is no longer separable into a sum of kinetic and potential terms. More precisely, we consider dynamics of the form

$$\begin{cases}\mathrm{d}q^\lambda_t = \nabla_p H_M(q^\lambda_t, p^\lambda_t)\,\mathrm{d}t, \\ \mathrm{d}p^\lambda_t = -\nabla_q H_M(q^\lambda_t, p^\lambda_t)\,\mathrm{d}t - \lambda\Sigma(q^\lambda_t)\nabla_p H_M(q^\lambda_t, p^\lambda_t)\,\mathrm{d}t + \sqrt{\dfrac{2\lambda}{\beta}}\Sigma(q^\lambda_t)^{1/2}\,\mathrm{d}W^\lambda_t,\end{cases} \tag{5.33}$$

on $\mathcal{Q}\times\mathbb{R}^d$, where H_M is given by the Hamiltonian

$$H_M(q,p) := \frac{1}{2}p^\top M^{-1}(q)p + E(q), \qquad E(q) = V(q) + \frac{1}{2\beta}\log\det M(q), \tag{5.34}$$

with $M, \Sigma : \mathcal{Q} \to \mathcal{S}_d^{++}$ are smooth, symmetric positive-definite matrix fields. Physically, the variables (q, p) correspond respectively to the positions and momenta, and the matrix M to a position-dependent "mass" parameter. Note that the corresponding Boltzmann–Gibbs measure

$$\mu_M(q,p)\,\mathrm{d}q\,\mathrm{d}p = \frac{1}{Z}\mathrm{e}^{-\beta H_M(q,p)}\,\mathrm{d}q\,\mathrm{d}p, \qquad Z = (2\pi/\beta)^{d/2}\int_{\mathcal{Q}} \mathrm{e}^{-\beta V(q)}\,\mathrm{d}q \tag{5.35}$$

is such that, conditionally on q, the momentum p is again Gaussian, with a covariance matrix $\frac{1}{\beta}M(q)$. The normalization constant in (5.35) is independent of M, thanks to the term $\frac{1}{2\beta}\log\det M(q)$ appearing in the potential E. Since H_M is non-separable, the Boltzmann–Gibbs measure can no longer be written as a product measure. However, the marginal in q is again the Gibbs measure (5.5), i.e.

$$\int_{\mathbb{R}^d} \mu_M(q,p)\,\mathrm{d}p = \nu(q).$$

For this reason, the dynamics (5.33) can be used to sample canonical configurations. It is a natural alternative to (5.1) if one views M as a preconditionner, adapting the covariance in the momentum variable to anisotropic features of the target distribution. In the case of a scalar friction $\Sigma = \gamma > 0$, these dynamics have been linked to the generalized Hamiltonian Monte Carlo family of sampling algorithm, see [231, Section 3.2]. Position-dependent mass matrices also appear naturally when considering internal-coordinate molecular dynamics, see [326], in which the state of the system is parametrized by "internal" degrees of freedom, such as nuclear bond lengths and torsion angles. In this setting, the dynamics (5.33) is the natural counterpart to the Cartesian equation (5.1).

A canonical transformation. We consider the class of dynamics which can be transformed into one of the form (5.1) via a smooth diffeomorphism

$$\Gamma(q,p) = (x,v) = (x(q,p), v(q,p)) \tag{5.36}$$

satisfying the following three conditions.

- To come back to the original coordinates from the limiting equation in x, the coordinate $x \in \mathcal{Q}$ from (5.36) should depend solely on q, i.e.

$$\nabla_p x = 0. \tag{5.37}$$

- In order to preserve the Hamiltonian nature of the dynamics in the case $\lambda = 0$, the change of variables should be a canonical transformation, meaning that it should satisfy locally the symplecticity condition

$$\nabla\Gamma^\top J \nabla\Gamma = J, \qquad J = \begin{pmatrix} 0 & \mathrm{Id}_{\mathbb{R}^d} \\ -\mathrm{Id}_{\mathbb{R}^d} & 0 \end{pmatrix}. \tag{5.38}$$

- Finally, to apply the pathwise convergence result of Proposition 5.6, the Hamiltonian

should become separable, with the kinetic energy given by a quadratic form

$$H_M(q,p) = \frac{1}{2} v^\top G_M v + V_M \circ x \tag{5.39}$$

for some constant matrix $G_M \in \mathcal{S}_d^{++}$ and $V_M : \mathcal{Q} \to \mathbb{R}$.

Writing the symplecticity condition, we find

$$\begin{pmatrix} \nabla_q x & 0 \\ \nabla_q v & \nabla_p v \end{pmatrix}^\top J \begin{pmatrix} \nabla_q x & 0 \\ \nabla_q v & \nabla_p v \end{pmatrix} = \begin{pmatrix} \nabla_q x^\top \nabla_q v - \nabla_q v^\top \nabla_q x & \nabla_q x^\top \nabla_p v \\ -\nabla_p v^\top \nabla_q x & 0 \end{pmatrix},$$

which imposes (since $\nabla_q x$ must be invertible for Γ to be a diffeomorphism) that $\nabla_q x = (\nabla_p v)^{-\top}$, and that the matrix $\left[\nabla_q x^\top \nabla_q v\right](q,p)$ is symmetric. The first condition and (5.37) impose $\nabla_p^2 v = 0$, so that $v(q,p) = A(q)p + b(q)$ is affine in p. Substituting this ansatz into (5.39), equating linear and quadratic parts in p, we find

$$v(q,p) = A(q)p, \qquad \forall\, q \in \mathcal{Q}, \qquad A(q)^{-\top} M^{-1}(q) A(q)^{-1} = G_M, \qquad b(q) = 0. \tag{5.40}$$

Then, $\nabla_q x = A(q)^{-\top}$, so that the rows of $A(q)^{-\top}$ must be gradients of smooth functions on $\mathcal{Q}$. Therefore, x can be defined by

$$x(q) = q_0 + \int_0^1 A^{-\top}(\gamma(t))\gamma'(t)\,\mathrm{d}t, \qquad \forall\, \gamma \in \{f \in \mathcal{C}^\infty([0,1];\mathcal{Q}) :\ f(0) = q_0, f(1) = q\}, \tag{5.41}$$

for any choice of base point $q_0 = x(q_0)$ and path γ. One can check with some index computation (see Lemma 5.10) that this condition in turn implies the local symmetry property

$$\nabla_q x^\top \nabla_q v = A^{-1}(q)\nabla_q v = \nabla_q v^\top \nabla_q x = \nabla_q v^\top A^{-\top}, \tag{5.42}$$

so that the symplecticity condition (5.38) is indeed verified for this choice of (x,v).

Various classes of mass matrices ensure that the factorization (5.40) holds, with $A^{-\top}$ having gradient rows. When $\mathcal{Q} = \mathbb{R}^d$, one can simply choose $M = (\nabla^2\Phi)^2$ for some smooth potential $\Phi : \mathbb{R}^d \to \mathbb{R}$ with non-degenerate Hessian, in which case $A = (\nabla^2\Phi)^{-1}$ and $G_M = \mathrm{Id}$, or $M = (\mathrm{Id} + \nabla\theta)(\mathrm{Id} + \nabla\theta)^\top$ for some sufficiently small vector field θ, in which case $A = (\mathrm{Id} + \nabla\theta)^{-1}$ and again $G_M = \mathrm{Id}$. More generally, this construction is valid when M factors as $M = \nabla\Psi\nabla\Psi^\top$ for some smooth diffeomorphism $\Psi : \mathcal{Q} \to \mathcal{Q}$.

An Itô computation. We assume in this paragraph that the transformation Γ defined in (5.36) by (5.40) by (5.41) is valid and smooth.

Denote by $(x_t^\lambda, v_t^\lambda) := \Gamma(q_t^\lambda, p_t^\lambda)$. We apply Itô's lemma to (5.33) in order to derive an SDE in these new variables. The first simplification follows from noting that, since $\Gamma(q,p)$ is linear with respect to p, the partial Hessian of each component of Γ with respect to p vanishes – this will simplify the computation by dropping the quadratic covariation terms.

We first write, using $\nabla_q x = A^{-\top}(q)$,

$$\mathrm{d}x_t^\lambda = \nabla_q x(q_t^\lambda)\nabla_p H_M(q_t^\lambda, p_t^\lambda)\,\mathrm{d}t = A^{-\top}(q_t^\lambda) M^{-1}(q_t^\lambda) p_t^\lambda\,\mathrm{d}t = G_M v_t^\lambda\,\mathrm{d}t,$$

using (5.40) and the form (5.34) of the Hamiltonian in the third equality. Next,

$$\begin{aligned}\mathrm{d}v_t^\lambda &= \nabla_q v(q_t^\lambda, p_t^\lambda)\,\mathrm{d}q_t^\lambda + \nabla_p v(q_t^\lambda, p_t^\lambda)\,\mathrm{d}p_t^\lambda \\ &= \nabla_q v(q_t^\lambda, p_t^\lambda) M^{-1}(q_t^\lambda) p_t^\lambda\,\mathrm{d}t \\ &+ A(q_t^\lambda)\left(-\nabla_q H_M(q_t^\lambda, p_t^\lambda)\,\mathrm{d}t - \lambda\Sigma(q_t^\lambda)\nabla_p H_M(q_t^\lambda, p_t^\lambda)\,\mathrm{d}t + \sqrt{\frac{2\lambda}{\beta}}\Sigma(q_t^\lambda)^{1/2}\,\mathrm{d}W_t^\lambda\right)\end{aligned}$$

The fluctuation-dissipation term writes

$$-\lambda A(q_t^\lambda)\Sigma(q_t^\lambda)M^{-1}(q_t^\lambda)p_t^\lambda\,\mathrm{d}t + \sqrt{\frac{2\lambda}{\beta}}A(q_t^\lambda)\Sigma(q_t^\lambda)^{1/2}\,\mathrm{d}W_t^\lambda = -\lambda\widetilde{\Sigma}(q_t^\lambda)G_M v_t^\lambda\,\mathrm{d}t + \sqrt{\frac{2\lambda}{\beta}}\widetilde{\Sigma}(q_t^\lambda)^{1/2}\,\mathrm{d}W_t^\lambda,$$

where $\widetilde{\Sigma}(q) = A(q)\Sigma(q)A(q)^\top$, and $\widetilde{\Sigma}(q)^{1/2} := A(q)\Sigma(q)^{1/2}$ is clearly a square root for $\widetilde{\Sigma}(q)$.

For the contribution of the force term, we write $\nabla_q H_M(q,p) = \frac{1}{2}\nabla_q\left(p^\top M^{-1}(q)p\right) + \nabla E(q)$. Note that

$$-A(q_t^\lambda)\nabla E(q_t^\lambda)\,\mathrm{d}t = -\left[\nabla_q x\right]^{-\top}\nabla_q E(q_t^\lambda)\,\mathrm{d}t = -\nabla_x\left(E\circ q\right)(x_t^\lambda)\,\mathrm{d}t,$$

using $A(q)^\top = \left[\nabla_q x\right]^{-1}(q)$, leaving a final term

$$\nabla_q v(q_t^\lambda, p_t^\lambda)M^{-1}(q_t^\lambda)p_t^\lambda\,\mathrm{d}t - \frac{1}{2}A(q_t^\lambda)\nabla_q\left(p_t^{\lambda\top}M^{-1}(q_t^\lambda)p_t^\lambda\right)\,\mathrm{d}t.$$

We write

$$\begin{aligned}\frac{1}{2}A(q)\nabla_q\left(p^\top M^{-1}(q)p\right) &= \frac{1}{2}A(q)\nabla_q\left(v^\top G_M v\right) \\ &= A(q)\nabla_q v^\top G_M v,\end{aligned}$$

as well as

$$\begin{aligned}\nabla_q v M^{-1}(q)p &= \nabla_q v A(q)^\top A(q)^{-\top}M^{-1}(q)A^{-1}(q)A(q)p \\ &= \nabla_q v A(q)^\top G_M v.\end{aligned}$$

Multiplying the symmetry condition (5.42) on the left by $A(q)$ and on the right by $A(q)^\top$, we see that $\nabla_q v A(q)^\top = A(q)\nabla_q v^\top$, which shows the remaining term is zero.

Collecting terms, $(x_t^\lambda, v_t^\lambda)$ satisfies the following Langevin equation

$$\begin{cases}\mathrm{d}x_t^\lambda = G_M v_t^\lambda\,\mathrm{d}t, \\ \mathrm{d}v_t^\lambda = -\nabla V_M(q_t^\lambda)\,\mathrm{d}t - \lambda\Sigma_M(q_t^\lambda)G_M v_t^\lambda\,\mathrm{d}t + \sqrt{\frac{2\lambda}{\beta}}\Sigma_M(q_t^\lambda)^{1/2}\,\mathrm{d}W_t^\lambda,\end{cases} \tag{5.43}$$

which is Equation (5.1) for the modified potential $V = V_M$, kinetic energy $U(v) = \frac{1}{2}v^\top G_M v$, and friction matrix $D = \Sigma_M$ defined by

$$V_M(x) = \left[E\circ q\right](x), \qquad \Sigma_M(x) = \left[A\Sigma A^\top\circ q\right](x), \qquad \Sigma_M(x)^{1/2} = \left[A\Sigma^{1/2}\circ q\right](x). \tag{5.44}$$

Overdamped limit and application to the case $\mathcal{Q} = \mathbb{R}$. We apply Proposition 5.6 to the transformed equation (5.43).

Corollary 5.8. *Assume that $V : \mathcal{Q} \to \mathbb{R}$ satisfies Assumptions 5.1 and 5.4, and that the transformation Γ defined in (5.36) is a smooth symplectic transformation, where M satisfies a factorization of the form (5.40). Assume moreover that M, A, Σ are smooth and $\mathcal{W}^{2,\infty}$, and that Assumption 5.3 is satisfied for $D = M$ (and therefore also for $D = AA^\top$) and $D = \Sigma^{-1}$. Suppose that, for each $\lambda > 0$, $(q_0^\lambda, p_0^\lambda) = (q_0, p_0)$, with $(q_0, p_0) \sim \mu_0 \in \mathcal{P}(\mathcal{Q} \times \mathbb{R}^d)$, such that $\mu_0 \ll \mu_M$, and $\frac{\mathrm{d}\mu_0}{\mathrm{d}\mu_M} \in L^p(\mu_M)$ for some $p > 1$. For any $\lambda > 0$, let $(q_t^\lambda, p_t^\lambda)_{t\geqslant 0}$ be a solution to (5.33).*

Then, denoting $(Q_t^\lambda)_{t\geqslant 0} = (q_{\lambda t}^\lambda)_{t\geqslant 0}$, it holds

$$Q_*^\lambda \mathbb{P}_{\mu_0} \xrightarrow[\lambda\to+\infty]{\text{weakly}} Q_*^M \mathbb{P}_{\mu_0} \quad \text{in } \mathcal{P}(\mathcal{C}([0,T],\mathcal{Q})),$$

where $Q_t^M = q(Z_t^M)$ and Z^M solves the SDE

$$\mathrm{d}Z_t^M = -\Sigma_M^{-1}(Z_t^M)\nabla V_M(Z_t^M)\,\mathrm{d}t + \frac{1}{\beta}\operatorname{div}\Sigma_M^{-1}(Z_t^M)\,\mathrm{d}t + \sqrt{\frac{2}{\beta}}\Sigma_M^{-1/2}(Z_t^M)\,\mathrm{d}W_t, \tag{5.45}$$

and $Z_0^M \sim \nu$ is independent from W.

Proof. Denote $Z_t^{M,\lambda} = x_{\lambda t}^\lambda$, where (x^λ, v^λ) solves the SDE (5.43). By the previous computation, $q \circ Z^{M,\lambda} = Q^\lambda$.

Since M and $\log\det M$ are uniformly bounded on $\mathcal{Q}$, is straightforward to check that the coefficients V_M and Σ_M in Equation (5.43) and the kinetic energy $U_M(v) = \frac{1}{2}v^\top G_M v$ satisfy Assumptions 5.1, 5.3 and 5.4 of Theorem 5.6. Furthermore, Assumption (5.5) is obviously satisfied, as well as Assumption 5.2 using Lemma 5.9.

The fact that the distribution of $(x_0^\lambda, v_0^\lambda)$, given by $\Gamma_*\mu_0 \ll \mu$, satisfies $\frac{\mathrm{d}(\Gamma_*\mu_0)}{\mathrm{d}\mu} \in L^p(\mu)$ follows from a change of variables, since $\Gamma_*\mu_M = \mu$ and Γ is a symplectic transformation, with Jacobian determinant $|\det \nabla\Gamma|^2 = |\det J| = 1$.

Moreover $(q \circ Z^{M,\lambda})_*\mathbb{P}_{\mu_0} = Q_*^\lambda \mathbb{P}_{\mu_0}$ for all $\lambda \geqslant 0$, from the previous computation. Since the mapping $f \mapsto q \circ f$ is continuous on $\mathcal{C}([0,T];\mathcal{Q})$, taking the weak limit of this identity as $\lambda \to +\infty$ using the second item in Proposition 5.6 shows that $Q_*^\lambda \mathbb{P}_{\mu_0} \to (q \circ Z^M)_*\mathbb{P}_{\mu_0}$ weakly in $\mathcal{P}(\mathcal{C}([0,T];\mathcal{Q}))$, where Z^M satisfies the SDE (5.45). □

The limiting dynamics from Corollary 5.8 is not fully explicit, but in view of the specific form of the coefficients (5.44), it is in fact closed with respect to Q_t^M. We make this observation precise in the one-dimensional case $\mathcal{Q} = \mathbb{R}$, keeping in mind that similar computations can be performed in the higher-dimensional case.

The dynamics (5.33) writes

$$\begin{cases} \mathrm{d}q_t^\lambda = \dfrac{p_t^\lambda}{m(q_t^\lambda)}\,\mathrm{d}t, \\ \mathrm{d}p_t^\lambda = -e'(q_t^\lambda)\,\mathrm{d}t - \dfrac{1}{2\beta}\dfrac{m'(q_t^\lambda)}{m(q_t^\lambda)}\,\mathrm{d}t - \lambda\dfrac{\sigma(q_t^\lambda)}{m(q_t^\lambda)}p_t^\lambda\,\mathrm{d}t + \sqrt{\dfrac{2\lambda\sigma(q_t^\lambda)}{\beta}}\,\mathrm{d}B_t, \end{cases}$$

where m, σ, e' are smooth and globally Lipschitz, $\varepsilon \leqslant m, \sigma \leqslant \varepsilon^{-1}$ for some $\varepsilon > 0$, and B is a Wiener process. The condition (5.40) is verified vacuously for $a(q) = m(q)^{-1/2}$, with

$$\Gamma(q,p) = (x,v) = \left(\int_0^q \sqrt{m(t)}\,\mathrm{d}t, p/\sqrt{m(q)} \right).$$

From Corollary 5.8, the overdamped limit of $x(q^\lambda_{\lambda t})$ in the limit $\lambda \to +\infty$ satisfies the one-dimensional SDE

$$\begin{aligned}
\mathrm{d}Z_t &= -q'(Z_t)\frac{v'}{a^2\sigma}(q(Z_t))\,\mathrm{d}t - q'(Z_t)\frac{m'}{2\beta m a^2 \sigma}(q(Z_t))\,\mathrm{d}t + \frac{1}{\beta}\left(\frac{1}{a^2\sigma}\circ q\right)'(Z_t)\,\mathrm{d}t + \sqrt{\frac{2}{\beta}}\frac{1}{a\sqrt{\sigma}}(q(Z_t))\,\mathrm{d}B_t \\
&= -\frac{e'\sqrt{m}}{\sigma}(q(Z_t))\,\mathrm{d}t - \frac{m'}{2\beta\sigma\sqrt{m}}(q(Z_t))\,\mathrm{d}t + \frac{1}{\beta}\left(\frac{m}{\sigma}\circ q\right)'(Z_t)\,\mathrm{d}t + \sqrt{\frac{2m}{\beta\sigma}}(q(Z_t))\,\mathrm{d}B_t \\
&= -\frac{e'\sqrt{m}}{\sigma}(q(Z_t))\,\mathrm{d}t - \frac{m'}{2\beta\sigma\sqrt{m}}(q(Z_t))\,\mathrm{d}t + \frac{1}{\beta}\left[\frac{m'}{\sqrt{m}\sigma} - \frac{\sigma'\sqrt{m}}{\sigma^2}\right](q(Z_t))\,\mathrm{d}t + \sqrt{\frac{2m}{\beta\sigma}}(q(Z_t))\,\mathrm{d}B_t,
\end{aligned} \tag{5.46}$$

using $q' = \frac{1}{\sqrt{m}} \circ q$ in the last two lines. We now apply Itô's formula with $f(z) = q(z)$. Denoting $Q_t = q(z_t)$, $\mathrm{d}Q_t = q'(z_t)\mathrm{d}z_t + \frac{m}{\sigma\beta}(q(z_t))q''(z_t)\,\mathrm{d}t$, substituting (5.46), and using $q'' = -\frac{m'}{2m^2} \circ q$, we find, after a simple computation, that

$$\mathrm{d}Q_t = -\frac{e'}{\sigma}(Q_t)\,\mathrm{d}t - \frac{1}{\beta}\frac{\sigma'}{\sigma^2}(Q_t)\,\mathrm{d}t + \sqrt{\frac{2}{\beta\sigma}}(Q_t)\,\mathrm{d}B_t,$$

which corresponds to the dynamics (5.4) with the choice $D = \sigma^{-1}$, and is interestingly independent from the choice of m.

Appendix 5.A: Proofs of technical results

In this appendix, we gather the proofs of some useful technical lemmas.

Lemma 5.9 (Sufficient condition for hypoellipticity)**.** *Suppose Assumptions 5.1 and 5.3 are satisfied, and furthermore that $\nabla^2 U$ is everywhere non-degenerate. Then Assumption 5.2 is satisfied.*

Proof. We write

$$\mathcal{L}_\lambda = \mathcal{A}_{0,\lambda} + \sum_{j=1}^d \mathcal{A}_{j,\lambda}^\dagger \mathcal{A}_{j,\lambda}, \quad \forall\, 1 \leqslant j \leqslant d, \quad \mathcal{A}_{j,\lambda} = \sqrt{\frac{\lambda}{\beta}}\left(D^{-1/2}(q)\nabla_p\right)_j,$$

where "†" denotes the $L^2(\mathcal{Q}\times\mathbb{R}^d)$ formal adjoint, and

$$\mathcal{A}_{0,\lambda} = \mathcal{A} - \lambda \nabla U^\top D^{-1}(q)\nabla_p.$$

We check that the vector fields $(\mathcal{A}_{j,\lambda})_{0\leqslant j\leqslant d}$ satisfy Hörmander's bracket condition (see [174]), namely that their Lie algebra has full rank $2d$ everywhere.

Computing, for $1 \leqslant \alpha \leqslant d$, the commutator

$$\begin{aligned}
[\mathcal{A}_{0,\lambda}, \mathcal{A}_{\alpha,\lambda}] &= \sqrt{\frac{\lambda}{\beta}} \sum_{i,j,k} \left[(\partial_i U)\partial_{q_i} - (\partial_i V)\,\partial_{p_i} - \lambda\,(\partial_i U)\,D^{-1}_{ij}\partial_{p_j}, D^{-1/2}_{\alpha k}\partial_{p_k} \right] \\
&= \sqrt{\frac{\lambda}{\beta}} \sum_{i,j,k} \left[(\partial_i U)\partial_{q_i} - \lambda\,(\partial_i U)\,D^{-1}_{ij}\partial_{p_j}, D^{-1/2}_{\alpha k}\partial_{p_k} \right] \\
&= -\sum_{i,k} \sqrt{\frac{\lambda}{\beta}} (\partial^2_{ki} U) D^{-1/2}_{\alpha k}\partial_{q_i} + \mathfrak{X}_{\alpha,\lambda} \\
&= -\sqrt{\frac{\lambda}{\beta}} \left(D^{-1/2}\nabla^2 U \nabla_q \right)_\alpha + \mathfrak{X}_{\alpha,\lambda}
\end{aligned}$$

for some $\mathfrak{X}_{\alpha,\lambda} \in \mathrm{Span}(\partial_{p_i}, 1 \leqslant i \leqslant d)$. Since $D^{-1/2}$ has full rank everywhere by Assumption 5.3, it follows that $\mathrm{Span}(\partial_{q_i}, \partial_{p_i}, 1 \leqslant i \leqslant d) = \mathrm{Span}(\mathcal{A}_{i,\lambda}, [\mathcal{A}_{0,\lambda}, \mathcal{A}_{i,\lambda}], 1 \leqslant i \leqslant d)$ whenever $\nabla^2 U$ has full rank. □

Even if $\nabla^2 U$ is degenerate at some points, one may still be able to show the hypoellipticity of the generator by considering higher-order brackets, which leads to sufficient conditions involving higher derivatives of U, see the discussion in [62, Appendix A].

Proof of Lemma 5.7. We prove the uniform-in-λ $L^2_0(\mu)$-hypocoercivity estimates used in the proof of Proposition 5.6.

Proof. We adapt the proof of [37, Theorem 3.3], and refer to it for more details. It suffices to replace $\mathcal{L}_{\mathrm{FD}} = -\frac{1}{\beta}\nabla_p^*\nabla_p$ by $\mathcal{S} = -\frac{1}{\beta}\nabla_p^* D^{-1}\nabla_p$ whenever this operator appears, and use the uniform bound (5.7) to carry through the estimates. Note that since $\mathcal{A}^*\mathbb{1} = \mathcal{S}^*\mathbb{1} = 0$, both $\mathcal{A}$ and $\mathcal{S}$ preserve $L^2_0(\mu)$. As in [37], we write $\Pi_+ = \mathrm{Id} - \Pi_0$, and $A_{\alpha\alpha'} = \Pi_\alpha A \Pi_{\alpha'}$ for any operator A on $L^2_0(\mu)$ and $\alpha, \alpha' \in \{0, +\}$.

To check that [37, Assumption 2.2] holds, we make the choice

$$s = \lambda \frac{K_\kappa^2}{M_D \beta}, \tag{5.47}$$

whose validity follows from Assumptions 5.3 and the Poincaré inequality (5.9) for κ. The verification of [37, Assumption 2.3] is unchanged, since the antisymmetric part $\mathcal{A}$ does not involve D. We now check [37, Assumption 2.6]. This involves showing the $L^2_0(\mu)$-boundedness of two operators, defined by

$$A_\lambda = \lambda \Pi_1 \mathcal{S} \Pi_1, \qquad B_\lambda = \lambda \Pi_2 \mathcal{S}\mathcal{A}\Pi_0 \left(\mathcal{A}_{+0}^*\mathcal{A}_{+0}\right)^{-1} + \Pi_2 \mathcal{A}^2 \Pi_0 \left(\mathcal{A}_{+0}^*\mathcal{A}_{+0}\right)^{-1},$$

where Π_1 is the orthogonal projector onto $\mathrm{Ran}\mathcal{A}_{+0} \subset \Pi_+ L^2_0(\mu)$ and Π_2 is the projector onto its orthogonal complement in $\Pi_+ L^2_0(\mu)$.

To show that A_λ is bounded, we compute (as in [37])

$$-\mathcal{A}_{+0}^*\mathcal{S}\mathcal{A}_{+0} = \frac{1}{\beta}\nabla_q^* \mathcal{N} \nabla_q \Pi_0, \qquad \mathcal{N}(q) = \int_{\mathbb{R}^d} \nabla^2 U D^{-1}(q) \nabla^2 U \,\mathrm{d}\kappa,$$

and the entries of this matrix $\mathcal{N}$ are bounded as multiplication operators on $L^2(\nu)$ from Assumption 5.3. Therefore, the same factorization argument as in [37, Theorem 3.3] shows that A_λ is bounded, with a bound

$$\|A_\lambda\| = \lambda \|A_1\| < +\infty, \tag{5.48}$$

where $\|\cdot\|$ denotes the $L^2_0(\mu)$-operator norm.

To show the boundeness of B_λ, we only need to check that

$$G = \Pi_2 \mathcal{S} \mathcal{A} \Pi_0 \left(\mathcal{A}_{+0}^* \mathcal{A}_{+0}\right)^{-1}$$

is a bounded operator, since

$$H = \Pi_2 \mathcal{A}^2 \Pi_0 \left(\mathcal{A}_{+0}^* \mathcal{A}_{+0}\right)^{-1}$$

is a bounded operator which does not involve D, following the same arguments as in the proof of [37, Theorem 3.3].

To show that G is a bounded operator, we compute

$$\lambda \mathcal{S} \mathcal{A} \Pi_0 = \lambda \mathscr{T} \nabla_q, \qquad \mathscr{T}(q) = -\frac{1}{\beta^2} \nabla_p^* D^{-1}(q) \nabla_p \nabla_p^* \Pi_0,$$

and the entries of the row-vector $\mathscr{T}$ are bounded operators on $L^2_0(\mu)$, since $D^{-1}(q)$ is a matrix of bounded operators on $L^2(\nu)$, whose entries commute with any of the ∂_{p_i}, $\partial_{p_i}^*$. From here, the boundedness of G and therefore of B_λ follows using Assumption 5.4, with the same factorizations and commutation relations as in the proof of [37, Theorem 3.3]. In particular we get the following bound:

$$\|B_\lambda\| \leqslant \lambda \|G\| + \|H\| < +\infty. \tag{5.49}$$

We now show the uniform-in-λ estimates (5.12). In [37, Equation 2.3], the authors compute the block decomposition of $\mathcal{L}_\lambda^{-1}$ on $L^2_0(\mu) = \Pi_0 L^2_0(\mu) \oplus \Pi_+ L^2_0(\mu)$, which is given by

$$\mathcal{L}_\lambda^{-1} = \left(\begin{array}{c|c} \mathfrak{S}_{0,\lambda}^{-1} & -\mathfrak{S}_{0,\lambda}^{-1} \mathcal{A}_{0+} \left[\mathcal{L}_\lambda^{-1}\right]_{++} \\ \hline -\left[\mathcal{L}_\lambda^{-1}\right]_{++} \mathcal{A}_{+0} \mathfrak{S}_{0,\lambda}^{-1} & \left[\mathcal{L}_\lambda^{-1}\right]_{++} + \left[\mathcal{L}_\lambda^{-1}\right]_{++} \mathcal{A}_{+0} \mathfrak{S}_{0,\lambda}^{-1} \mathcal{A}_{0+} \left[\mathcal{L}_\lambda^{-1}\right]_{++} \end{array}\right), \tag{5.50}$$

where $\mathfrak{S}_{0,\lambda} = \mathcal{A}_{+0}^* \left[\mathcal{L}_\lambda^{-1}\right]_{++} \mathcal{A}_{+0}$ is the Schur complement associated with this decomposition, acting on $\Pi_0 L^2_0(\mu)$. The proof of [37, Theorem 2.7] shows that all these blocks are bounded operators from $L^2_0(\mu)$ to $L^2(\mu)$. The top-left block $\mathfrak{S}_{0,\lambda}^{-1}$ can be shown to be of order λ in operator norm, while the bottom-right block is of order λ^{-1}, and the off-diagonal blocks are of order 1. Therefore, general hypocoercive estimates only provide a bound on the operator norm $\left\|\mathcal{L}_\lambda^{-1}\right\|_{L^2_0(\mu) \to L^2(\mu)} = \mathcal{O}(\max(\lambda, \lambda^{-1}))$.

However, in the specific case $\varphi \in \Pi_+ L^2_0(\mu)$, some terms (namely those corresponding to the left-column of the decomposition (5.50)) will be dropped from the final estimate for $\|\mathcal{L}_\lambda^{-1}\varphi\|_{L^2(\mu)}$, which leads to an estimate $\left\|\mathcal{L}_\lambda^{-1}\right\|_{\Pi_+ L^2_0(\mu) \to L^2(\mu)} = \mathcal{O}(1)$ in the limit $\lambda \to +\infty$. More precisely,

in this case,

$$\mathcal{L}_\lambda^{-1}\varphi = \left(-\mathfrak{S}_{0,\lambda}^{-1}\mathcal{A}_{0+}\left[\mathcal{L}_\lambda^{-1}\right]_{++} + \left[\mathcal{L}_\lambda^{-1}\right]_{++} + \left[\mathcal{L}_\lambda^{-1}\right]_{++}\mathcal{A}_{+0}\mathfrak{S}_{0,\lambda}^{-1}\mathcal{A}_{0+}\left[\mathcal{L}_\lambda^{-1}\right]_{++}\right)\varphi,$$

where the proof of [37, Theorem 2.7] shows that

$$\left\|\left[\mathcal{L}_\lambda^{-1}\right]_{++} + \left[\mathcal{L}_\lambda^{-1}\right]_{++}\mathcal{A}_{+0}\mathfrak{S}_{0,\lambda}^{-1}\mathcal{A}_{0+}\left[\mathcal{L}_\lambda^{-1}\right]_{++}\right\| \leqslant \frac{2}{s} \tag{5.51}$$

in operator norm on $L^2_0(\mu)$, with s is defined in (5.47). The remaining term is bounded by

$$\left\|\mathfrak{S}_{0,\lambda}^{-1}\mathcal{A}_{0+}\left[\mathcal{L}_\lambda^{-1}\right]_{++}\right\| \leqslant \sqrt{\frac{\left\|\mathfrak{S}_{0,\lambda}^{-1}\right\|}{s}} \leqslant s^{-1/2}\sqrt{\frac{\|A_\lambda\|}{a^2} + b\frac{\|B_\lambda\|}{s}}, \tag{5.52}$$

where the constants a, b are independent from λ. From the bounds (5.51) and (5.52), the first estimate in (5.12) follows from the linear scaling in λ of each of s, $\|A_\lambda\|$ and $\|B_\lambda\|$ as $\lambda \to +\infty$, which follows from (5.47), (5.48) and (5.49).

To estimate $\nabla_p \mathcal{L}_\lambda^{-1}\varphi$, we have from an integration by parts that

$$\begin{aligned}
\left\langle \varphi, \mathcal{L}_\lambda^{-1}\varphi\right\rangle_{L^2(\mu)} &= \lambda\left\langle \mathcal{S}\mathcal{L}_\lambda^{-1}\varphi, \mathcal{L}_\lambda^{-1}\varphi\right\rangle_{L^2(\mu)} \\
&= -\frac{\lambda}{\beta}\mu\left(\left[\nabla_p\mathcal{L}_\lambda^{-1}\varphi\right]^\top D^{-1}\left[\nabla_p\mathcal{L}_\lambda^{-1}\varphi\right]\right) \\
&\leqslant -\frac{\lambda}{\beta M_D}\|\nabla_p\mathcal{L}_\lambda^{-1}\varphi\|^2_{L^2(\mu)},
\end{aligned}$$

using Assumption 5.3 in the last line. From this bound, a Cauchy–Schwarz inequality gives

$$\left\|\nabla_p\mathcal{L}_\lambda^{-1}\varphi\right\|^2_{L^2(\mu)} \leqslant \frac{\beta M_D}{\lambda}\|\varphi\|_{L^2(\mu)}\|\mathcal{L}_\lambda^{-1}\varphi\|_{L^2(\mu)} \leqslant \frac{C_1\beta M_D}{\lambda}\|\varphi\|^2_{L^2(\mu)},$$

using the previous bound on $\|\mathcal{L}_\lambda^{-1}\varphi\|_{L^2(\mu)}$. □

Lemma 5.10 (Index computation). *Let $A : \mathcal{Q} \to \mathbb{R}^{d\times d}$ be a smooth matrix field such that $A^{-\top}$ has gradient rows, and $v(q,p) = A(q)p$. Then the relation (5.42) holds.*

Proof. Since A^{-1} has gradient columns, we may write locally $(A^{-1})_{ij} = \partial_i\phi_j$ for some $(\phi_j)_{1\leqslant j\leqslant d} \in \mathcal{C}^\infty(\mathcal{Q})^d$. We compute, with derivatives taken with respect to the q-variable:

$$\begin{aligned}
(A^{-1}\nabla_q v)_{ij} &= \sum_{\alpha,\beta}(A^{-1})_{i\alpha}\partial_j(A_{\alpha\beta})p_\beta \\
&= -\sum_{\alpha,\beta}(A^{-1})_{i\alpha}\left[A\partial_j(A^{-1})A\right]_{\alpha\beta}p_\beta \\
&= -\sum_{\gamma,\beta}\partial_j(A^{-1})_{i\gamma}A_{\gamma\beta}p_\beta \\
&= -\sum_{\gamma}\partial^2_{ji}\phi_\gamma v_\gamma,
\end{aligned}$$

using the matrix identity $\partial_j A = -A\partial_j(A^{-1})A$. This shows that $A^{-1}\nabla_q v$ is symmetric, and therefore that (5.42) holds. □

Bibliography

[1] F. Abraham, R. Walkup, H. Gao, M. Duchaineau, T. Diaz De La Rubia, and M. Seager, *Simulating materials failure by using up to one billion atoms and the world's fastest computer: Work-hardening*, Proceedings of the National Academy of Sciences, 99 (2002), pp. 5783–5787.

[2] A. Agarwal, S. Gnanakaran, N. Hengartner, A. Voter, and D. Perez, *Arbitrarily accurate representation of atomistic dynamics via Markov renewal processes*, preprint arXiv:2008.11623, (2020).

[3] B. Alder, D. Gass, and T. Wainwright, *Studies in molecular dynamics. VIII. The transport coefficients for a hard-sphere fluid*, The Journal of Chemical Physics, 53 (1970), pp. 3813–3826.

[4] B. Alder and T. Wainwright, *Phase transition for a hard sphere system*, The Journal of Chemical Physics, 27 (1957), pp. 1208–1209.

[5] A. Aleksian, P. Del Moral, A. Kurtzmann, and J. Tugaut, *Self-interacting diffusions: Long-time behaviour and exit-problem in the uniformly convex case*, ESAIM: Probability and Statistics, 28 (2024), pp. 46–61.

[6] G. Allaire and M. Schoenauer, *Conception optimale de structures*, vol. 58 of SMAI Mathématiques et Applications, Springer, 2007.

[7] M. Allen and D. Tildesley, *Computer Simulation of Liquids*, Oxford University Press, 2017.

[8] R. Allen, C. Valeriani, and P. Ten Wolde, *Forward flux sampling for rare event simulations*, Journal of Physics: Condensed Matter, 21 (2009), pp. 463102:1–21.

[9] H. Ammari, K. Kalimeris, H. Kang, and H. Lee, *Layer potential techniques for the narrow escape problem*, Journal de mathématiques pures et appliquées, 97 (2012), pp. 66–84.

[10] H. Andersen, *RATTLE: A "velocity" version of the SHAKE algorithm for molecular dynamics calculations*, Journal of Computational Physics, 52 (1983), pp. 24–34.

[11] S. Andradóttir, D. Heyman, and T. Ott, *Variance reduction through smoothing and control variates for Markov chain simulations*, ACM Transactions on Modeling and Computer Simulation (TOMACS), 3 (1993), pp. 167–189.

[12] D. Aristoff, *Generalizing parallel replica dynamics: trajectory fragments, asynchronous computing, and PDMPs*, SIAM/ASA Journal on Uncertainty Quantification, 7 (2019), pp. 685–719.

[13] D. Aristoff, M. Johnson, and D. Perez, *Arbitrarily accurate, nonparametric coarse graining with Markov renewal processes and the Mori–Zwanzig formulation*, AIP Advances, 13 (2023), p. 095131.

[14] D. Aristoff and T. Leli'evre, *Mathematical analysis of temperature accelerated dynamics*, Multiscale Modeling & Simulation, 12 (2014), pp. 290–317.

[15] D. Aristoff, T. Lelièvre, and G. Simpson, *The parallel replica method for simulating long trajectories of Markov chains*, Applied Mathematics Research eXpress, 2014 (2014), pp. 332–352.

[16] S. Arrhenius, *On the reaction velocity of the inversion of cane sugar by acids*, in Selected Readings in Chemical Kinetics, Elsevier, 1967, pp. 31–35.

[17] G. Arya, E. J. Maginn, and H.-C. Chang, *Efficient viscosity estimation from molecular dynamics simulation via momentum impulse relaxation*, The Journal of Chemical Physics, 113 (2000), pp. 2079–2087.

[18] M. Ashbaugh and R. Benguria, *A sharp bound for the ratio of the first two eigenvalues of Dirichlet Laplacians and extensions*, Annals of Mathematics, 135 (1992), pp. 601–628.

[19] R. Azencott, Y. Guivarc'h, and R. F. Gundy, *Ecole d'Eté de Probabilités de Saint-Flour VIII-1978*, vol. 774 of Lecture Notes in Mathematics, Springer, 1980.

[20] R. Balian, *From Microphysics to Macrophysics*, vol. 3 of Theoretical and Mathematical Physics, Springer, 1991.

[21] G. Barrera and M. Jara, *Thermalisation for small random perturbations of dynamical systems*, The Annals of Applied Probability, 30 (2020), pp. 1164–1208.

[22] E. Barth, K. Kuczera, B. Leimkuhler, and R. Skeel, *Algorithms for constrained molecular dynamics*, Journal of Computational Chemistry, 16 (1995), pp. 1192–1209.

[23] A. Bartók, R. Kondor, and G. Csányi, *On representing chemical environments*, Physical Review B—Condensed Matter and Materials Physics, 87 (2013), p. 184115.

[24] A. Bartók, M. Payne, R. Kondor, and G. Csányi, *Gaussian approximation potentials: The accuracy of quantum mechanics, without the electrons*, Physical Review Letters, 104 (2010), p. 136403.

[25] M. Baskes, J. Nelson, and A. Wright, *Semiempirical modified embedded-atom potentials for silicon and germanium*, Physical Review B, 40 (1989), p. 6085.

[26] G. Battimelli, G. Ciccotti, and P. Greco, *Computer Meets Theoretical Physics*, vol. 85 of The Frontiers Collection, Springer, 2020.

[27] A. Baydin, B. Pearlmutter, A. Radul, and J. Siskind, *Automatic differentiation in machine learning: a survey*, Journal of Machine Learning Research, 18 (2018), pp. 1–43.

[28] J. Behler, *Four generations of high-dimensional neural network potentials*, Chemical Reviews, 121 (2021), pp. 10037–10072.

[29] J. Behler and M. Parrinello, *Generalized neural-network representation of high-dimensional potential-energy surfaces*, Physical Review Letters, 98 (2007), p. 146401.

[30] M. Benaïm, N. Champagnat, W. Oçafrain, and D. Villemonais, *Degenerate processes killed at the boundary of a domain*, The Annals of Probability, 53 (2025), pp. 720–752.

[31] M. Benaim, B. Cloez, and F. Panloup, *Stochastic approximation of quasi-stationary distributions on compact spaces and applications*, The Annals of Applied Probability, 28 (2018), pp. 2370–2416.

[32] F. Berezin and M. Shubin, *The Schrödinger Equation*, vol. 66, Springer Science & Business Media, 2012.

[33] N. Berglund, *Kramers' law: Validity, derivations and generalisations*, Markov Processes And Related Fields, 19 (2013), pp. 459–490.

[34] N. Berglund, G. Di Gesù, and H. Weber, *An Eyring–Kramers law for the stochastic Allen–Cahn equation in dimension two*, Electronic Journal of Probability, 22 (2017), pp. 1–27.

[35] N. Berglund and B. Gentz, *The Eyring–Kramers law for potentials with nonquadratic saddles*, Markov Processes And Related Fields, 16 (2010), pp. 549–598.

[36] ——, *The Eyring–Kramers law for potentials with nonquadratic saddles*, Markov Processes and Related Fields, 16 (2010), pp. 549–598.

[37] E. Bernard, M. Fathi, A. Levitt, and G. Stoltz, *Hypocoercivity with Schur complements*, Annales Henri Lebesgue, 5 (2022), pp. 523–557.

[38] R. Bhattacharya, *On the functional central limit theorem and the law of the iterated logarithm for Markov processes*, Zeitschrift für Wahrscheinlichkeitstheorie und Verwandte Gebiete, 60 (1982), pp. 185–201.

[39] A. Bianchi and A. Gaudilliere, *Metastable states, quasi-stationary distributions and soft measures*, Stochastic Processes and their Applications, 126 (2016), pp. 1622–1680.

[40] A. Bianchi, A. Gaudillière, and P. Milanesi, *On soft capacities, quasi-stationary distributions and the pathwise approach to metastability*, Journal of Statistical Physics, 181 (2020), pp. 1052–1086.

[41] P. Billingsley, *Convergence of Probability Measures*, Wiley Series in Probability and Statistics, John Wiley & Sons, 1968.

[42] A. Binder, T. Lelièvre, and G. Simpson, *A generalized parallel replica dynamics*, Journal of Computational Physics, 284 (2015), pp. 595–616.

[43] J. Birrell, S. Hottovy, G. Volpe, and J. Wehr, *Small mass limit of a langevin equation on a manifold*, Annales Henri Poincaré, 18 (2017), pp. 707–755.

[44] N. Biswas, P. Jacob, and P. Vanetti, *Estimating convergence of Markov chains with L-lag couplings*, Advances in neural information processing systems, 32 (2019).

[45] N. Blassel, *Code and data repository for chapter 4:* https://github.com/noeblassel/NortonMethod, 2023.

[46] ——, *Code repository for chapter 3:* https://github.com/noeblassel/sosad, 2025.

[47] ——, *Data repository for chapter 3:* https://zenodo.org/records/15727493, 2025.

[48] ——, *A hypocoercive approach of the overdamped limit for the kinetic Langevin equation with multiplicative noise*, In preparation, (2025).

[49] N. Blassel, L. Carillo, S. Darshan, R. Gastaldello, A. Iacobucci, E. Marini, R. Santet, X. Shang, G. Stoltz, and U. Vaes, *Mathematical analysis and numerical methods for the computation of transport coefficients in molecular dynamics*, In preparation, (2025).

[50] N. Blassel, T. Lelièvre, and G. Stoltz, *Quantitative low-temperature asymptotics for reversible diffusions in temperature-dependent domains*, preprint arXiv:2501.16082, (2025).

[51] ——, *Shape optimization of metastable states*, preprint arXiv:2507.12575, (2025).

[52] N. Blassel and G. Stoltz, *Fixing the flux: A dual approach to computing transport coefficients*, Journal of Statistical Physics, 191 (2024).

[53] M. Blazhynska, J. Gumbart, H. Chen, E. Tajkhorshid, B. Roux, and C. Chipot, *A rigorous framework for calculating protein–protein binding affinities in membranes*, Journal of Chemical Theory and Computation, 19 (2023), pp. 9077–9092.

[54] P. Bolhuis, C. Dellago, and D. Chandler, *Reaction coordinates of biomolecular isomerization*, Proceedings of the National Academy of Sciences, 97 (2000), pp. 5877–5882.

[55] J. Bony, D. Le Peutrec, and L. Michel, *Eyring–Kramers law for Fokker–Planck type differential operators*, Journal of the European Mathematical Society, Online First (2024).

[56] M. Born and R. Oppenheimer, *Zur Quantentheorie der Molekeln*, Annalen der Physik, 84 (1927), pp. 457–484.

[57] F. Bouchet and J. Reygner, *Generalisation of the Eyring–Kramers transition rate formula to irreversible diffusion processes*, Annales Henri Poincaré, 17 (2016), pp. 3499–3532.

[58] A. Bovier and F. Den Hollander, *Metastability: A Potential-Theoretic Approach*, vol. 351 of A Series of Comprehensive Studies in Mathematics, Springer, 2016.

[59] A. Bovier, M. Eckhoff, V. Gayrard, and M. Klein, *Metastability and low lying spectra in reversible Markov chains*, Communications in Mathematical Physics, 228 (2002), pp. 219–255.

[60] ——, *Metastability in reversible diffusion processes. I: Sharp asymptotics for capacities and exit times*, Journal of the European Mathematical Society, 6 (2004), pp. 399–424.

[61] A. Bovier, V. Gayrard, and M. Klein, *Metastability in reversible diffusion processes. II: Precise asymptotics for small eigenvalues*, Journal of the European Mathematical Society, 7 (2005), pp. 69–99.

[62] G. Brigati and G. Stoltz, *How to construct explicit decay rates for kinetic Fokker–Planck equations?*, SIAM Journal on Mathematical Analysis, 57 (2025), pp. 3587–3622.

[63] B. Brooks, R. Bruccoleri, B. Olafson, D. States, S. Swaminathan, and M. Karplus, *CHARMM: a program for macromolecular energy, minimization, and dynamics calculations*, Journal of Computational Chemistry, 4 (1983), pp. 187–217.

[64] K. Burdzy, R. Hołyst, and P. March, *A Fleming–Viot particle representation of the Dirichlet Laplacian*, Communications in Mathematical Physics, 214 (2000), pp. 679–703.

[65] E. Cancès, C. Le Bris, and Y. Maday, *Méthodes Mathématiques en Chimie Quantique*, vol. 53 of Mathématiques & Applications, Springer, 2006.

[66] N. Cancrini and S. Olla, *Ensemble dependence of fluctuations: Canonical/microcanonical equivalence of ensembles*, Journal of Statistical Physics, 168 (2017), pp. 707–730.

[67] R. Carmona, *Pointwise bounds for Schrödinger eigenstates*, Communications in Mathematical Physics, 62 (1978), pp. 97–106.

[68] F. Cérou, A. Guyader, and M. Rousset, *Adaptive multilevel splitting: Historical perspective and recent results*, Chaos: An Interdisciplinary Journal of Nonlinear Science, 29 (2019), pp. 043108:1–12.

[69] S. Cerrai and M. Freidlin, *Smoluchowski-Kramers approximation for a general class of SPDEs*, Journal of Evolution Equations, 6 (2006), pp. 657–689.

[70] M. Chak, N. Kantas, T. Lelièvre, and G. Pavliotis, *Optimal friction matrix for underdamped Langevin sampling*, ESAIM: Mathematical Modelling and Numerical Analysis, 57 (2023), pp. 3335–3371.

[71] N. Champagnat, K. Coulibaly-Pasquier, and D. Villemonais, *Criteria for exponential convergence to quasi-stationary distributions and applications to multidimensional diffusions*, in Séminaire de Probabilités XLIX, vol. 2215 of Lecture Notes in Mathematics, Springer, 2018, pp. 165–182.

[72] N. Champagnat and D. Villemonais, *Exponential convergence to quasi-stationary distribution and Q-process*, Probability Theory and Related Fields, 164 (2016), pp. 243–283.

[73] ——, *General criteria for the study of quasi-stationarity*, Electronic Journal of Probability, 28 (2023), pp. 1–84.

[74] M. Chen, *Collective variable-based enhanced sampling and machine learning*, The European Physical Journal B, 94 (2021), pp. 1–17.

[75] D. Chenais, *On the existence of a solution in a domain identification problem*, Journal of Mathematical Analysis and Applications, 52 (1975), pp. 189–219.

[76] R. Chetrite and H. Touchette, *Nonequilibrium microcanonical and canonical ensembles and their equivalence*, Physical Review Letters, 111 (2013), pp. 120601:1–5.

[77] M. Christian and N. Karel, *Rigorous meaning of McLennan ensembles*, Journal of Mathematical Physics, 51 (2010), p. 015219.

[78] G. Ciccotti and M. Ferrario, *Non-equilibrium by molecular dynamics: A dynamical approach*, Molecular Simulation, 42 (2016), pp. 1385–1400.

[79] G. Ciccotti and G. Jacucci, *Direct computation of dynamical response by molecular dynamics: The mobility of a charged Lennard–Jones particle*, Physical Review Letters, 35 (1975), pp. 789–792.

[80] G. Ciccotti, G. Jacucci, and I. McDonald, *Transport properties of molten alkali halides*, Physical Review A, 13 (1976), pp. 426–436.

[81] G. Ciccotti, G. Jacucci, and I. R. McDonald, *"Thought-experiments" by molecular dynamics*, Journal of Statistical Physics, 21 (1979), pp. 1–22.

[82] G. Ciccotti, R. Kapral, and A. Sergi, *Non-Equilibrium Molecular Dynamics*, in Handbook of Materials Modeling: Methods, S. Yip, ed., Springer, 2005, pp. 745–761.

[83] G. Ciccotti, T. Lelièvre, and E. Vanden-Eijnden, *Projection of diffusions on submanifolds: Application to mean force computation*, Communications on Pure and Applied Mathematics, 61 (2008), pp. 371–408.

[84] P. Collet, S. Martínez, and J. San Martín, *Quasi-Stationary Distributions*, Probability and its Applications, Springer, 2013.

[85] J. Comer, J. Gumbart, J. Hénin, T. Lelièvre, A. Pohorille, and C. Chipot, *The adaptive biasing force method: everything you always wanted to know but were afraid to ask*, The Journal of Physical Chemistry B, 119 (2015), pp. 1129–1151.

[86] T. Cui, X. Tong, and O. Zahm, *Optimal Riemannian metric for Poincaré inequalities and how to ideally precondition Langevin dynamics*, preprint arXiv:2404.02554, (2024).

[87] C. Dapogny, P. Frey, F. Omnès, and Y. Privat, *Geometrical shape optimization in fluid mechanics using FreeFem++*, Structural and Multidisciplinary Optimization, 58 (2018), pp. 2761–2788.

[88] S. Darshan, A. Eberle, and G. Stoltz, *Sticky coupling as a control variate for sensitivity analysis*, preprint arXiv:2409.15500, (2024).

[89] S. Darshan and G. Stoltz, *Equivalence of Norton and Thévenin ensembles for mean-field interacting particle systems*, In preparation, (2025).

[90] E. Davies, *Metastable states of symmetric Markov semigroups I*, Proceedings of the London Mathematical Society, 3 (1982), pp. 133–150.

[91] E. B. Davies, *Metastable states of symmetric Markov semigroups II*, Journal of the London Mathematical Society, 2 (1982), pp. 541–556.

[92] M. Daw and M. Baskes, *Embedded-atom method: Derivation and application to impurities, surfaces, and other defects in metals*, Physical review B, 29 (1984), pp. 6443–6453.

[93] M. Day, *On the exponential exit law in the small parameter exit problem*, Stochastics: An International Journal of Probability and Stochastic Processes, 8 (1983), pp. 297–323.

[94] F. De Gournay, *Velocity extension for the level-set method and multiple eigenvalues in shape optimization*, SIAM Journal on Control and Optimization, 45 (2006), pp. 343–367.

[95] P. Del Moral and L. Miclo, *A Moran particle system approximation of Feynman–Kac formulae*, Stochastic processes and their applications, 86 (2000), pp. 193–216.

[96] J. Delhommelle and P. Cummings, *Simulation of friction in nanoconfined fluids for an arbitrarily low shear rate*, Physical Review B, 72 (2005), pp. 172201:1–4.

[97] C. Dellago, P. Bolhuis, and P. Geissler, *Transition path sampling*, Advances in Chemical Physics, 123 (2002), pp. 1–78.

[98] A. Dembo and O. Zeitouni, *Large Deviations Techniques and Applications*, vol. 38 of Applications of Mathematics, Springer, 2009.

[99] G. Di Gesù, T. Lelièvre, D. Le Peutrec, and B. Nectoux, *Jump Markov models and transition state theory: the quasi-stationary distribution approach*, Faraday discussions, 195 (2016), pp. 469–495.

[100] ——, *Sharp asymptotics of the first exit point density*, Annals of PDE, 5 (2019).

[101] ——, *The exit from a metastable state: Concentration of the exit point distribution on the low energy saddle points, part 1*, Journal de Mathématiques Pures et Appliquées, 138 (2020), pp. 242–306.

[102] M. Dimassi and J. Sjostrand, *Spectral Asymptotics in the Semi-Classical Limit*, no. 268 in London Mathematical Society Lecture Note Series, Cambridge University Press, 1999.

[103] M. Dobson, *Periodic boundary conditions for long-time nonequilibrium molecular dynamics simulations of incompressible flows*, The Journal of Chemical Physics, 141 (2014), p. 184103.

[104] M. Dobson, F. Legoll, T. Lelièvre, and G. Stoltz, *Derivation of langevin dynamics in a nonzero background flowfield*, ESAIM: Mathematical Modelling and Numerical Analysis, 47 (2013), pp. 1583–1626.

[105] J. Dolbeault, A. Klar, C. Mouhot, and C. Schmeiser, *Exponential rate of convergence to equilibrium for a model describing fiber lay-down processes*, Applied Mathematics Research eXpress, 2013 (2013), pp. 165–175.

[106] J. Dolbeault, C. Mouhot, and C. Schmeiser, *Hypocoercivity for linear kinetic equations conserving mass*, Transactions of the American Mathematical Society, 367 (2015), pp. 3807–3828.

[107] R. Douc, E. Moulines, P. Priouret, and P. Soulier, *Markov Chains*, vol. 4, Springer, 2018.

[108] R. Drautz, *Atomic cluster expansion for accurate and transferable interatomic potentials*, Physical Review B, 99 (2019), p. 014104.

[109] Y. Duan and P. Kollman, *Pathways to a protein folding intermediate observed in a 1-microsecond simulation in aqueous solution*, Science, 282 (1998), pp. 740–744.

[110] S. Duane, A. Kennedy, B. Pendleton, and D. Roweth, *Hybrid Monte Carlo*, Physics letters B, 195 (1987), pp. 216–222.

[111] D. Dürr, S. Goldstein, and J. Lebowitz, *A mechanical model of brownian motion*, Communications in Mathematical Physics, 78 (1981), pp. 507–530.

[112] J. Eckmann and M. Hairer, *Spectral properties of hypoelliptic operators*, Communications in Mathematical Physics, 235 (2003), pp. 233–253.

[113] S. Edwards and P. Anderson, *Theory of spin glasses*, Journal of Physics F: Metal Physics, 5 (1975), pp. 965–974.

[114] A. Einstein, *Über die von der molekularkinetischen Theorie der Wärme geforderte Bewegung von in ruhenden Flüssigkeiten suspendierten Teilchen*, Annalen der Physik, 4 (1905), pp. 549–560.

[115] D. Evans, *The equivalence of Norton and Thévenin ensembles*, Molecular Physics, 80 (1993), pp. 221–224.

[116] D. Evans and J. Ely, *Viscous flow in the stress ensemble*, Molecular Physics, 59 (1986), pp. 1043–1048.

[117] D. Evans, W. Hoover, B. Failor, B. Moran, and A. Ladd, *Nonequilibrium molecular dynamics via Gauss's principle of least constraint*, Physical Review A, 28 (1983), pp. 1016–1021.

[118] D. Evans and G. Morriss, *The isothermal/isobaric molecular dynamics ensemble*, Physics Letters A, 98 (1983), pp. 433–436.

[119] D. Evans and G. Morriss, *Statistical Mechanics of Nonequilibrium Liquids*, Cambridge University Press, 2008.

[120] D. Evans and G. P. Morriss, *Equilibrium-fluctuation expression for the resistance of a Norton circuit*, Physical Review A, 31 (1985), pp. 3817–3819.

[121] L. Evans, *Partial Differential Equations*, vol. 19 of Graduate Studies in Mathematics, American Mathematical Society, 2022.

[122] H. Eyring, *The activated complex in chemical reactions*, The Journal of Chemical Physics, 3 (1935), pp. 107–115.

[123] P. Fearnhead, J. Bierkens, M. Pollock, and G. Roberts, *Piecewise deterministic Markov processes for continuous-time Monte Carlo*, Statistical Science, 33 (2018), pp. 386–412.

[124] V. Felli, B. Noris, and R. Ognibene, *Eigenvalues of the Laplacian with moving mixed boundary conditions: the case of disappearing Dirichlet region*, Calculus of Variations and Partial Differential Equations, 60 (2021).

[125] A. Ferguson, *Machine learning and data science in soft materials engineering*, Journal of Physics: Condensed Matter, 30 (2018), p. 043002.

[126] R. Feynman, *Statistical Mechanics: A Set of Lectures*, W.A. Benjamin, 1972.

[127] G. Fiorin, M. Klein, and J. Hénin, *Using collective variables to drive molecular dynamics simulations*, Molecular Physics, 111 (2013), pp. 3345–3362.

[128] H. Flyvbjerg and H. Petersen, *Error estimates on averages of correlated data*, The Journal of Chemical Physics, 91 (1989), pp. 461–466.

[129] G. Ford, M. Kac, and P. Mazur, *Statistical mechanics of assemblies of coupled oscillators*, Journal of Mathematical Physics, 6 (1965), pp. 504–515.

[130] M. Freidlin, *Some remarks on the Smoluchowski–Kramers approximation*, Journal of Statistical Physics, 117 (2004), pp. 617–634.

[131] M. Freidlin and W. Hu, *Smoluchowski–Kramers approximation in the case of variable friction*, preprint arXiv:1203.0603, (2012).

[132] M. Freidlin and A. Wentzell, *Random Perturbations of Dynamical Systems*, vol. 260 of A Series of Comprehensive Studies in Mathematics, Springer, 2012.

[133] D. Frenkel and B. Smit, *Understanding Molecular Simulation*, vol. 1 of Computational Science Series, Academic Press, 2001.

[134] M. Gabrié, G. Rotskoff, and E. Vanden-Eijnden, *Adaptive Monte Carlo augmented with normalizing flows*, Proceedings of the National Academy of Sciences, 119 (2022), pp. e2109420119:1–9.

[135] T. Germann and K. Kadau, *Trillion-atom molecular dynamics becomes a reality*, International Journal of Modern Physics C, 19 (2008), pp. 1315–1319.

[136] J. Gibbs, *Elementary Principles in Statistical Mechanics*, Charles Scribner's Sons, 1902.

[137] D. Gilbarg and N. Trudinger, *Elliptic Partial Differential Equations of Second Order*, vol. 224, Springer, 2001.

[138] P. Gkeka, G. Stoltz, A. Fariman, Z. Belkacemi, M. Ceriotti, J. Chodera, A. Dinner, A. Ferguson, J.-B. Maillet, H. Minoux, C. Peter, F. Pietrucci, A. Silveira, A. Tkatchenko, Z. Trstanova, R. Wiewiora, and T. Lelièvre, *Machine learning force fields and coarse-grained variables in molecular dynamics: application to materials and biological systems*, Journal of Chemical Theory and Computation, 16 (2020), pp. 4757–4775.

[139] A. Glielmo, B. Husic, A. Rodriguez, C. Clementi, F. Noé, and A. Laio, *Unsupervised learning methods for molecular simulation data*, Chemical Reviews, 121 (2021), pp. 9722–9758.

[140] A. González, *Measurement of areas on a sphere using Fibonacci and latitude–longitude lattices*, Mathematical Geosciences, 42 (2010), pp. 49–64.

[141] E. Gosling, I. McDonald, and K. Singer, *On the calculation by molecular dynamics of the shear viscosity of a simple fluid*, Molecular Physics, 26 (1973), pp. 1475–1484.

[142] M. Green, *Markoff random processes and the statistical mechanics of time-dependent phenomena. II. Irreversible processes in fluids*, The Journal of Chemical Physics, 22 (1954), pp. 1281–1295.

[143] J. Greener, *Differentiable simulation to develop molecular dynamics force fields for disordered proteins*, Chemical Science, 15 (2024), pp. 4897–4909.

[144] P. Grisvard, *Elliptic Problems in Nonsmooth Domains*, vol. 69 of Classics in Applied Mathematics, SIAM, 2011.

[145] A. Guillin, B. Nectoux, and W. L., *Quasi-stationary distribution for strongly Feller Markov processes by Lyapunov functions and applications to hypoelliptic Hamiltonian systems.*, Journal of the European Mathematical Society (EMS Publishing), 26 (2024), pp. 3047–3090.

[146] J. Hadamard, *Mémoire sur le problème d'analyse relatif à l'équilibre des plaques élastiques encastrées*, vol. 33 of Mémoires présentés par divers savants à l'Académie des sciences de l'Institut de France., Imprimerie nationale, 1908.

[147] E. Hairer, C. Lubich, and G. Wanner, *Geometric numerical integration illustrated by the Störmer–Verlet method*, Acta numerica, 12 (2003), pp. 399–450.

[148] E. Hairer, G. Wanner, and C. Lubich, *Geometric Numerical Integration*, vol. 31 of Springer Series in Computational Mathematics, Springer, 2006.

[149] M. Hairer and A. Majda, *A simple framework to justify linear response theory*, Nonlinearity, 23 (2010), pp. 909–922.

[150] M. Hairer and J. Mattingly, *Yet another look at Harris' ergodic theorem for Markov chains*, in Seminar on Stochastic Analysis, Random Fields and Applications VI, vol. 63 of Progress in Probability, Springer, 2011, pp. 109–117.

[151] W. K. Hastings, *Monte Carlo sampling methods using Markov chains and their applications*, Biometrika, 57 (1970), pp. 97–109.

[152] E. Haug and B. Rousselet, *Design sensitivity analysis in structural mechanics. I. Static response variations*, Journal of Structural Mechanics, 8 (1980), pp. 17–41.

[153] ——, *Design sensitivity analysis in structural mechanics. II. Eigenvalue variations*, Journal of Structural Mechanics, 8 (1980), pp. 161–186.

[154] ——, *Design sensitivity analysis in structural mechanics. III. Effects of shape variation*, Journal of Structural Mechanics, 10 (1982), pp. 273–310.

[155] F. Hecht, O. Pironneau, A. Le Hyaric, and K. Ohtsuka, *FreeFem++ Manual*, Laboratoire Jacques Louis Lions, (2005), pp. 1–188.

[156] F. Hédin and T. Lelièvre, *Gen. parRep: A first implementation of the generalized parallel replica dynamics for the long time simulation of metastable biochemical systems*, Computer Physics Communications, 239 (2019), pp. 311–324.

[157] B. Helffer, M. Klein, and F. M.Nier, *Quantitative analysis of metastability in reversible diffusion processes via a Witten complex approach.*, Matemática contemporânea, 26 (2004), pp. 41–85.

[158] B. Helffer and F. Nier, *Quantitative analysis of metastability in reversible diffusion processes via a Witten complex approach: The case with boundary*, Matemática contemporânea, 26 (2004), pp. 41–85.

[159] ——, *Quantitative analysis of metastability in reversible diffusion processes via a Witten complex approach: the case with boundary*, no. 105 in Mémoires de la Société Mathématique de France, Mémoires de la Société Mathématique de France and Centre Nationale de la Recherche Scientifique, 2006.

[160] B. Helffer and J. Sjöstrand, *Puits multiples en mécanique semi-classique. IV: Étude du complexe de Witten*, Communications in Partial Differential Equations, 10 (1985), pp. 245–340.

[161] S. Henderson and P. Glynn, *Approximating martingales for variance reduction in Markov process simulation*, Mathematics of Operations Research, 27 (2002), pp. 253–271.

[162] J. Hénin, T. Lelièvre, M. Shirts, O. Valsson, and L. Delemotte, *Enhanced sampling methods for molecular dynamics simulations*, Living Journal of Computational Molecular Science, 4 (2022), pp. 1583:1–60.

[163] A. Henrot, *Extremum Problems for Eigenvalues of Elliptic Operators*, Frontiers in Mathematics, Birkhäuser Basel, 2006.

[164] A. Henrot and M. Pierre, *Variation et optimisation de formes : une analyse géométrique*, vol. 48 of Mathématiques et applications, Springer, 2005.

[165] D. Henry, *Perturbation of the Boundary in Boundary-Value Problems of Partial Differential Equations*, no. 318 in London Mathematical Society Lecture Note Series, Cambridge University Press, 2005.

[166] F. Hérau, M. Hitrik, and J. Sjöstrand, *Tunnel effect for Kramers–Fokker–Planck type operators*, Annales Henri Poincaré, 9 (2008), pp. 209–274.

[167] ——, *Tunnel effect for Kramers–Fokker–Planck type operators: return to equilibrium and applications*, International Mathematics Research Notices, 2008 (2008), pp. rnn057:1–48.

[168] F. Hérau, M. Hitrik, and J. Sjöstrand, *Tunnel effect and symmetries for Kramers–Fokker–Planck type operators*, Journal of the Institute of Mathematics of Jussieu, 10 (2011), pp. 567–634.

[169] F. Hérau and F. Nier, *Isotropic hypoellipticity and trend to equilibrium for the Fokker–Planck equation with a high-degree potential*, Archive for Rational Mechanics and Analysis, 171 (2004), pp. 151–218.

[170] S. Hollingsworth and R. Dror, *Molecular dynamics simulation for all*, Neuron, 99 (2018), pp. 1129–1143.

[171] W. Hoover, *Molecular Dynamics*, vol. 258 of Lecture Notes in Physics, Springer, 1986.

[172] ——, *Nonequilibrium molecular dynamics: The first 25 years*, Physica A: Statistical Mechanics and its Applications, 194 (1993), pp. 450–461.

[173] W. Hoover, H. Posch, and L. Campbell, *Thermal heat reservoirs via Gauss' principle of least constraint: Dissipation, chaos, and phase-space dimensionality loss in one-dimensional chains*, Chaos, 3 (1993), pp. 325–332.

[174] L. Hörmander, *Hypoelliptic second order differential equations*, Acta Mathematica, 119 (1967), pp. 147–171.

[175] A. Horowitz, *A generalized guided Monte Carlo algorithm*, Physics Letters B, 268 (1991), pp. 247–252.

[176] S. Hottovy, *The Smoluchowski–Kramers approximation for stochastic differential equations with arbitrary state dependent friction*, Ph.D. thesis, The University of Arizona, 2013.

[177] S. Hottovy, A. McDaniel, G. Volpe, and J. Wehr, *The Smoluchowski-Kramers limit of stochastic differential equations with arbitrary state-dependent friction*, Communications in Mathematical Physics, 336 (2015), pp. 1259–1283.

[178] W. Huisinga and B. Schmidt, *Metastability and dominant eigenvalues of transfer operators*, in New Algorithms for Macromolecular Simulation, vol. 49 of Lecture Notes in Computational Science and Engineering, Springer, 2006, pp. 167–182.

[179] N. Hunt-Smith, W. Melnitchouk, F. Ringer, N. Sato, A. Thomas, and M. White, *Accelerating Markov chain Monte Carlo sampling with diffusion models*, Computer Physics Communications, 296 (2024), pp. 109059:1–9.

[180] W. Hurewicz and H. Wallman, *Dimension Theory*, vol. 4 of Princeton Legacy Library, Princeton University Press, 2015.

[181] B. Husic and V. Pande, *Markov state models: From an art to a science*, Journal of the American Chemical Society, 140 (2018), pp. 2386–2396.

[182] A. Iacobucci, S. Olla, and G. Stoltz, *Convergence rates for nonequilibrium Langevin dynamics*, Annales mathématiques du Québec, 43 (2019), pp. 73–98.

[183] J. H. Irving and J. G. Kirkwood, *The statistical mechanical theory of transport processes. IV. The equations of hydrodynamics*, The Journal of Chemical Physics, 18 (1950), pp. 817–829.

[184] R. Jacobs, D. Morgan, S. Attarian, J. Meng, C. Shen, Z. Wu, C. Y. Xie, J. H. Yang, N. Artrith, B. Blaiszik, G. Ceder, K. Choudhary, G. Csanyi, E. D. Cubuk, B. Deng, R. Drautz, X. Fu, J. Godwin, V. Honavar, O. Isayev, A. Johansson, B. Kozinsky, S. Martiniani, S. P. Ong, I. Poltavsky, K. J. Schmidt, S. Takamoto, A. P. Thompson, J. Westermayr, and B. M. Wood, *A practical guide to machine learning interatomic potentials–Status and future*, Current Opinion in Solid State and Materials Science, 35 (2025), pp. 101214:1–28.

[185] E. Jaynes, *Information theory and statistical mechanics*, Physical Review, 106 (1957), pp. 620–630.

[186] ——, *Information theory and statistical mechanics. II*, Physical Review, 108 (1957), pp. 171–190.

[187] ——, *The minimum entropy production principle*, Annual Review of Physical Chemistry, 31 (1980), pp. 579–601.

[188] F. Jensen, *Introduction to Computational Chemistry*, John Wiley & sons, 1999.

[189] H. Jónsson, G. Mills, and K. Jacobsen, *Nudged elastic band method for finding minimum energy paths of transitions*, in Classical and quantum dynamics in condensed phase simulations, World Scientific, 1998, pp. 385–404.

[190] R. Joubaud and G. Stoltz, *Nonequilibrium shear viscosity computations with Langevin dynamics*, Multiscale Modeling & Simulation, 10 (2012), pp. 191–216.

[191] L. Journel and P. Monmarché, *Uniform convergence of the Fleming–Viot process in a hard killing metastable case*, The Annals of Applied Probability, 35 (2025), pp. 1019–1048.

[192] T. Kato, *Perturbation Theory for Linear Operators*, vol. 132 of Classics in Mathematics, Springer, 1995.

[193] R. Khasminskii, *Stochastic Stability of Differential Equations*, vol. 66 of Stochastic Modelling and Applied Probability, Springer, 2012.

[194] S. Kim, D. Perez, and A. Voter, *Local hyperdynamics*, The Journal of Chemical Physics, 139 (2013).

[195] W. Kirsch, H. Cycon, R. Froese, and B. Simon, *Schrödinger Operators*, Theoretical and Mathematical Physics, Springer, 1987.

[196] W. Kliemann, *Recurrence and invariant measures for degenerate diffusions*, The Annals of Probability, 15 (1987), pp. 690–107.

[197] T. Komorowski, J. Lebowitz, S. Olla, and M. Simon, *On the conversion of work into heat: microscopic models and macroscopic equations*, Ensaios Matemaáticos, 38 (2023), pp. 325–341.

[198] H. Kramers, *Brownian motion in a field of force and the diffusion model of chemical reactions*, Physica, 7 (1940), pp. 284–304.

[199] S. Krantz and H. Parks, *Geometric Integration Theory*, Cornerstones, Birkhäuser Boston, 2008.

[200] S. Krumscheid, M. Pradas, G. Pavliotis, and S. Kalliadasis, *Data-driven coarse graining in action: Modeling and prediction of complex systems*, Physical Review E, 92 (2015), p. 042139.

[201] R. Kubo, *Statistical-mechanical theory of irreversible processes. I. General theory and simple applications to magnetic and conduction problems*, Journal of the Physical Society of Japan, 12 (1957), pp. 570–586.

[202] R. Kubo, M. Yokota, and S. Nakajima, *Statistical-mechanical theory of irreversible processes. II. Response to thermal disturbance*, Journal of the Physical Society of Japan, 12 (1957), pp. 1203–1211.

[203] L. Lagardère, L. Jolly, F. Lipparini, F. Aviat, B. Stamm, Z. Jing, M. Harger, H. Torabifard, G. Cisneros, and M. Schnieders, *Tinker-HP: A massively parallel molecular dynamics package for multiscale simulations of large complex systems with advanced point dipole polarizable force fields*, Chemical Science, 9 (2018), pp. 956–972.

[204] E. Lampin, P. Palla, P.-A. Francioso, and F. Cleri, *Thermal conductivity from approach-to-equilibrium molecular dynamics*, Journal of Applied Physics, 114 (2013), pp. 033525:1–6.

[205] C. Landim, M. Mariani, and I. Seo, *Dirichlet's and Thomson's principles for non-selfadjoint elliptic operators with application to non-reversible metastable diffusion processes*, Archive for Rational Mechanics and Analysis, 231 (2019), pp. 887–938.

[206] C. Le Bris, T. Lelièvre, M. Luskin, and D. Perez, *A mathematical formalization of the parallel replica dynamics*, Monte–Carlo Methods and Applications, 18 (2012), pp. 119–146.

[207] D. Le Peutrec, *Small eigenvalues of the Neumann realization of the semiclassical Witten Laplacian*, Annales de la Faculté des sciences de Toulouse: Mathématiques, Series 6, 9 (2010), pp. 735–809.

[208] D. Le Peutrec and L. Michel, *Sharp spectral asymptotics for nonreversible metastable diffusion processes*, Probability and Mathematical Physics, 1 (2020), pp. 3–53.

[209] D. Le Peutrec and B. Nectoux, *Small eigenvalues of the Witten Laplacian with Dirichlet boundary conditions: the case with critical points on the boundary*, Analysis & PDE, 14 (2021), pp. 2595–2651.

[210] D. L. Le Peutrec, L. Michel, and B. Nectoux, *Eyring–Kramers formula for the mean exit time of non-Gibbsian elliptic processes: the non characteristic boundary case*, preprint: arXiv 2509.17678, (2025).

[211] J. L. Lebowitz, J. K. Percus, and L. Verlet, *Ensemble dependence of fluctuations with application to machine computations*, Physical Review, 153 (1967), pp. 250–254.

[212] J. Lee and I. Seo, *Non-reversible metastable diffusions with Gibbs invariant measure I: Eyring–Kramers formula*, Probability Theory And Related Fields, 182 (2022), pp. 849–903.

[213] S. Lee, M. Ramil, and I. Seo, *Asymptotic stability and cut-off phenomenon for the underdamped Langevin dynamics*, preprint arXiv:2311.18263, (2023).

[214] ——, *Eyring–Kramers law for the underdamped Langevin process*, preprint arXiv:2503.12610, (2025).

[215] A. W. Lees and S. F. Edwards, *The computer study of transport processes under extreme conditions*, Journal of Physics C: Solid State Physics, 5 (1972), pp. 1921–1929.

[216] R. Lefevere, *On the local space–time structure of non-equilibrium steady states*, Journal of Statistical Mechanics: Theory and Experiment, (2007), p. P01004.

[217] F. Legoll and T. Lelièvre, *Effective dynamics using conditional expectations*, Nonlinearity, 23 (2010), pp. 21–31.

[218] R. Lehoucq, D. Sorensen, and C. Yang, *ARPACK users' guide: Solution of large-scale eigenvalue problems with implicitly restarted Arnoldi methods*, Software, Environments, and Tools, SIAM, 1998.

[219] B. Leimkuhler and C. Matthews, *Rational construction of stochastic numerical methods for molecular sampling*, Applied Mathematics Research eXpress, 2013 (2013), pp. 34–56.

[220] ——, *Molecular Dynamics*, vol. 39 of Interdisciplinary Applied Mathematics, Springer, 2015.

[221] B. Leimkuhler, C. Matthews, and G. Stoltz, *The computation of averages from equilibrium and nonequilibrium Langevin molecular dynamics*, IMA Journal of Numerical Analysis, 36 (2016), pp. 13–79.

[222] B. Leimkuhler and S. Reich, *Simulating Hamiltonian Dynamics*, vol. 14 of Cambridge Monographs on Applied and Computational Mathematics, Cambridge University Press, 2004.

[223] T. Lelièvre, D. Le Peutrec, and B. Nectoux, *Exit event from a metastable state and Eyring-Kramers law for the overdamped Langevin dynamics*, in Stochastic Dynamics Out of Equilibrium, Springer Proceedings in Mathematics & Statistics, Springer, 2019, pp. 331–363.

[224] ——, *Eyring-Kramers exit rates for the overdamped Langevin dynamics: the case with saddle points on the boundary*, Journal de l'École Polytechnique – Mathématiques, 12 (2025), pp. 881–982.

[225] T. Lelièvre and F. Nier, *Low temperature asymptotics for quasistationary distributions in a bounded domain*, Analysis & PDE, 8 (2015), pp. 561–628.

[226] T. Lelièvre, G. Pavliotis, G. Robin, R. Santet, and G. Stoltz, *Optimizing the diffusion coefficient of overdamped Langevin dynamics*, Mathematics of Computation, (2025).

[227] T. Lelièvre, M. Rachid, and G. Stoltz, *A spectral approach to the narrow escape problem in the disk*, preprint arXiv:2401.06903, (2024).

[228] T. Lelièvre, M. Ramil, and J. Reygner, *Quasi-stationary distribution for the Langevin process in cylindrical domains, part I: existence, uniqueness and long-time convergence*, Stochastic Processes and their Applications, 144 (2022), pp. 173–201.

[229] T. Lelièvre, M. Rousset, and G. Stoltz, *Free Energy Computations - A Mathematical Perspective*, Imperial College Press, 2010.

[230] ——, *Langevin dynamics with constraints and computation of free energy differences*, Mathematics of Computation, 81 (2012), pp. 2071–2125.

[231] T. Lelièvre, R. Santet, and G. Stoltz, *Unbiasing Hamiltonian Monte Carlo algorithms for a general Hamiltonian function*, Foundations of Computational Mathematics, (2024), pp. 1–74.

[232] ——, *Improving sampling by modifying the effective diffusion*, Journal of Computational Physics, (2025), p. 114313.

[233] T. Lelièvre and G. Stoltz, *Partial differential equations and stochastic methods in molecular dynamics*, Acta Numerica, 25 (2016), pp. 681–880.

[234] D. Levesque and L. Verlet, *Computer "experiments" on classical fluids. III. Time-dependent self-correlation functions*, Physical Review A, 2 (1970), pp. 2514–2528.

[235] D. Levesque, L. Verlet, and J. Kürkijarvi, *Computer "experiments" on classical fluids. IV. Transport properties and time-correlation functions of the Lennard–Jones liquid near its triple point*, Physical Review A, 7 (1973), pp. 1690–1700.

[236] M. Levitt and R. Sharon, *Accurate simulation of protein dynamics in solution.*, Proceedings of the National Academy of Sciences, 85 (1988), pp. 7557–7561.

[237] M. Levitt and A. Warshel, *Computer simulation of protein folding*, Nature, 253 (1975), pp. 694–698.

[238] J. S. Liu and J. S. Liu, *Monte Carlo Strategies in Scientific Computing*, vol. 10 of Springer Series in Statistics, Springer, 2001.

[239] X. Liu, Q. Jiang, and W. Wang, *The Smoluchowski–Kramers approximation for a system with arbitrary friction depending on both state and distribution*, preprint arXiv:2406.18056, (2024).

[240] L. Lorenzi and M. Bertoldi, *Analytical Methods for Markov Semigroups*, Pure and applied mathematics, Chapman and Hall/CRC, 2006.

[241] L. Maffioli, E. Smith, J. Ewen, P. Daivis, D. Dini, and B. Todd, *Slip and stress from low shear rate nonequilibrium molecular dynamics: The transient-time correlation function technique*, The Journal of Chemical Physics, 156 (2022).

[242] A. Martini, Y. Dong, D. Perez, and A. Voter, *Low-speed atomistic simulation of stick–slip friction using parallel replica dynamics*, Tribology letters, 36 (2009), pp. 63–68.

[243] J. C. Mattingly, A. M. Stuart, and D. J. Higham, *Ergodicity for SDEs and approximations: locally Lipschitz vector fields and degenerate noise*, Stochastic Procosses and their Applications, 101 (2002), pp. 185–232.

[244] J. Maxwell, *On the dynamical evidence of the molecular constitution of bodies*, Journal of the Chemical Society, 28 (1875), pp. 493–508.

[245] S. Méléard and D. Villemonais, *Quasi-stationary distributions and population processes*, Probability Surveys, 9 (2012), pp. 340–410.

[246] G. Menz and A. Schlichting, *Poincaré and logarithmic Sobolev inequalities by decomposition of the energy landscape*, The Annals of Probability, 42 (2014), pp. 1809 – 1884.

[247] N. Metropolis, A. W. Rosenbluth, M. Rosenbluth, A. Teller, and E. Teller, *Equation of state calculations by fast computing machines*, The Journal of Chemical Physics, 21 (1953), pp. 1087–1092.

[248] S. Meyn and R. Tweedie, *Markov Chains and Stochastic Stability*, Springer, 2012.

[249] R. Miron and K. Fichthorn, *Accelerated molecular dynamics with the bond-boost method*, The Journal of Chemical Physics, 119 (2003), pp. 6210–6216.

[250] G. Morriss and D. Evans, *Application of transient correlation functions to shear flow far from equilibrium*, Physical Review A, 35 (1987), pp. 792–797.

[251] V. Nateghi and F. Nüske, *Kinetically consistent coarse graining using kernel-based extended dynamic mode decomposition*, Journal of Chemical Theory and Computation, 21 (2025), pp. 7236–7248.

[252] B. Nectoux, *Sharp estimate of the mean exit time of a bounded domain in the zero white noise limit*, Markov Processes And Related Fields, 26 (2020), pp. 403–422.

[253] F. Nier, *Boundary conditions and subelliptic estimates for geometric Kramers-Fokker-Planck operators on manifolds with boundaries*, Memoirs of the American Mathematical Society, 252 (2018).

[254] F. Nier and B. Helffer, *Hypoelliptic Estimates and Spectral Theory for Fokker–Planck Operators and Witten Laplacians*, vol. 1862 of Lecture Notes in Mathematics, Springer, 2005.

[255] J. Nocedal and S. Wright, *Numerical Optimization*, vol. 2 of Springer Series in Operations Research and Financial Engineering, Springer, 1999.

[256] F. Noé and F. Nüske, *A variational approach to modeling slow processes in stochastic dynamical systems*, Multiscale Modeling & Simulation, 11 (2013), pp. 635–655.

[257] F. Noé, S. Olsson, J. Köhler, and H. Wu, *Boltzmann generators: Sampling equilibrium states of many-body systems with deep learning*, Science, 365 (2019), p. eaaw1147.

[258] F. Nüske, P. Koltai, L. Boninsegna, and C. Clementi, *Spectral properties of effective dynamics from conditional expectations*, Entropy, 23 (2021), p. 134.

[259] B. Øksendal, *Stochastic Differential Equations*, Universitext, Springer, 2013.

[260] E. Olivieri and M. Vares, *Large deviations and metastability*, Encyclopedia of Mathematics and its Applications, Cambridge University Press, 2005.

[261] E. Oudet, *Numerical minimization of eigenmodes of a membrane with respect to the domain*, ESAIM: Control, Optimisation and Calculus of Variations, 10 (2004), pp. 315–330.

[262] G. A. Pavliotis, *Stochastic Processes and Applications*, vol. 60 of Texts in Applied Mathematics, Springer, 2014.

[263] L. Payne, G. Pólya, and H. Weinberger, *On the ratio of consecutive eigenvalues*, Journal of Mathematical Physics, 35 (1956), pp. 289–298.

[264] D. Pearlman, D. Case, J. Caldwell, W. Ross, T. Cheatham, S. DeBolt, D. Ferguson, G. Seibel, and P. Kollman, *AMBER, a package of computer programs for applying molecular mechanics, normal mode analysis, molecular dynamics and free energy calculations to simulate the structural and energetic properties of molecules*, Computer Physics Communications, 91 (1995), pp. 1–41.

[265] P. Peretto, *Collective properties of neural networks: a statistical physics approach*, Biological Cybernetics, 50 (1984), pp. 51–62.

[266] D. Perez, E. Cubuk, A. Waterland, E. Kaxiras, and A. Voter, *Long-time dynamics through parallel trajectory splicing*, Journal of Chemical Theory and Computation, 12 (2016), pp. 18–28.

[267] D. Perez, B. Uberuaga, Y. Shim, J. Amar, and A. Voter, *Accelerated molecular dynamics methods: introduction and recent developments*, Annual Reports in Computational Chemistry, 5 (2009), pp. 79–98.

[268] D. Perez, B. Uberuaga, and A. Voter, *The parallel replica dynamics method – Coming of age*, Computational Materials Science, 100 (2015), pp. 90–103.

[269] J. Perilla and K. Schulten, *Physical properties of the HIV-1 capsid from all-atom molecular dynamics simulations*, Nature Communications, 8 (2017), pp. 15959:1–10.

[270] R. Pinsky, *On the convergence of diffusion processes conditioned to remain in a bounded region for large time to limiting positive recurrent diffusion processes*, The Annals of Probability, 13 (1985), pp. 363–378.

[271] ——, *Positive Harmonic Functions and Diffusion*, vol. 45 of Cambridge Studies in Advanced Mathematics, Cambridge University Press, 1995.

[272] J. Prinz, H. Wu, M. Sarich, B. Keller, M. Senne, M. Held, J. Chodera, C. Schütte, and F. Noé, *Markov models of molecular kinetics: Generation and validation*, The Journal of Chemical Physics, 134 (2011), pp. 174105:1–24.

[273] A. Rahman, *Correlations in the motion of atoms in liquid Argon*, Physical Review, 136 (1964), pp. 405–411.

[274] A. Rahman and F. Stillinger, *Molecular dynamics study of liquid water*, The Journal of Chemical Physics, 55 (1971), pp. 3336–3359.

[275] M. Ramil, T. Lelièvre, and J. Reygner, *Mathematical foundations for the Parallel Replica algorithm applied to the underdamped Langevin dynamics*, MRS Communications, 12 (2022), pp. 454–459.

[276] M. Reed and B. Simon, *II: Self-adjointness*, vol. 2 of Methods of Modern Mathematical Physics, Elsevier Science, 1975.

[277] ——, *IV: Analysis of Operators*, vol. 4 of Methods of Modern Mathematical Physics, Elsevier Science, 1978.

[278] D. Reinsel, J. Gantz, and J. Rydning, *Data age 2025: the digitization of the world from edge to core*, IDC white paper, (2018).

[279] D. Revuz and M. Yor, *Continuous Martingales and Brownian motion*, vol. 293 of A Series of Comprehensive Studies in Mathematics, Springer, 2013.

[280] L. Rey-Bellet, *Ergodic properties of Markov processes*, in Open Quantum Systems II: The Markovian Approach, vol. 1881 of Lecture Notes in Mathematics, Springer, 2006, pp. 1–39.

[281] L. Richardson, *The approximate arithmetical solution by finite differences of physical problems involving differential equations, with an application to the stresses in a masonry dam*, Philosophical Transactions of the Royal Society of London. Series A, containing papers of a mathematical or physical character, 210 (1911), pp. 307–357.

[282] H. Rieger and A. Young, *Quantum spin glasses*, in Complex Behaviour of Glassy Systems, Springer, 1996, pp. 256–265.

[283] C. Robert and G. Casella, *Monte Carlo Statistical Methods*, vol. 2 of Springer Texts in Statistics, Springer, 1999.

[284] G. Roberts and J. Rosenthal, *Optimal scaling of discrete approximations to Langevin diffusions*, Journal of the Royal Statistical Society: Series B (Statistical Methodology), 60 (1998), pp. 255–268.

[285] H. Rodenhausen, *Einstein's relation between diffusion constant and mobility for a diffusion model*, Journal of Statistical Physics, 55 (1989), pp. 1065–1088.

[286] P. Rossky, J. Doll, and H. Friedman, *Brownian dynamics as smart Monte Carlo simulation*, The Journal of Chemical Physics, 69 (1978), pp. 4628–4633.

[287] P. Rotondo, M. Marcuzzi, J. Garrahan, I. Lesanovsky, and M. Müller, *Open quantum generalisation of Hopfield neural networks*, Journal of Physics A: Mathematical and Theoretical, 51 (2018), p. 115301.

[288] J. Roussel, *Theoretical and Numerical Analysis of Non-Reversible Dynamics in Computational Statistical Physics*, PhD thesis, Université Paris-Est, 2018.

[289] J. Roussel and G. Stoltz, *A perturbative approach to control variates in molecular dynamics*, Multiscale Modeling & Simulation, 17 (2019), pp. 552–591.

[290] B. Rousselet, *Shape design sensitivity of a membrane*, Journal of Optimization Theory and Applications, 40 (1983), pp. 595–623.

[291] M. Rousset, *On the control of an interacting particle estimation of Schrödinger ground states*, SIAM journal on mathematical analysis, 38 (2006), pp. 824–844.

[292] V. Roy, *Convergence diagnostics for Markov chain Monte Carlo*, Annual Review of Statistics and Its Application, 7 (2020), pp. 387–412.

[293] J. Ryckaert, G. Ciccotti, and H. Berendsen, *Numerical integration of the Cartesian equations of motion of a system with constraints: molecular dynamics of n-alkanes*, Journal of Computational Physics, 23 (1977), pp. 327–341.

[294] L. Sandoval, D. Perez, B. Uberuaga, and A. Voter, *Competing kinetics and he bubble morphology in w*, Physical review letters, 114 (2015), pp. 105502:1–5.

[295] A. Sard, *The measure of the critical values of differentiable maps*, Bulletin of the American Mathematical Society, 48 (1942), pp. 883–990.

[296] R. Sasaki, Y. Tateyama, and D. Searles, *Constant-current nonequilibrium molecular dynamics approach for accelerated computation of ionic conductivity including ion-ion correlation*, PRX Energy, 4 (2025), pp. 013005:1–16.

[297] D. Schneider, *The exascale era is upon us: The Frontier supercomputer may be the first to reach 1,000,000,000,000,000,000 operations per second*, IEEE spectrum, 59 (2022), pp. 34–35.

[298] C. Schütte, S. Klus, and C. Hartmann, *Overcoming the timescale barrier in molecular dynamics: Transfer operators, variational principles and machine learning*, Acta Numerica, 32 (2023), pp. 517–673.

[299] W. Scott, P. Hünenberger, I. Tironi, A. Mark, S. Billeter, J. Fennen, A. Torda, T. Huber, P. Krüger, and W. Van Gunsteren, *The GROMOS biomolecular simulation program package*, The Journal of Physical Chemistry A, 103 (1999), pp. 3596–3607.

[300] D. Shaw, M. Deneroff, R. Dror, J. Kuskin, R. Larson, J. Salmon, C. Young, B. Batson, K. Bowers, J. Chao, et al., *Anton, a special-purpose machine for molecular dynamics simulation*, Communications of the ACM, 51 (2008), pp. 91–97.

[301] D. Shaw, P. Maragakis, K. Lindorff-Larsen, S. Piana, R. Dror, M. Eastwood, J. Bank, J. Jumper, J. Salmon, Y. Shan, and W. Wriggers, *Atomic-level characterization of the structural dynamics of proteins*, Science, 330 (2010), pp. 341–346.

[302] M. Shirts and J. Chodera, *Statistically optimal analysis of samples from multiple equilibrium states*, The Journal of Chemical Physics, 129 (2008), pp. 124105:1–11.

[303] B. Simon, *Semiclassical analysis of low lying eigenvalues. I. Non-degenerate minima: asymptotic expansions*, Annales de l'Institut Henri Poincaré: Physique Théorique, 38 (1983), pp. 295–308.

[304] B. Simon, *Semiclassical analysis of low lying eigenvalues, II. Tunneling*, Annals of Mathematics, (1984), pp. 89–118.

[305] G. Simpson and M. Luskin, *Numerical analysis of parallel replica dynamics*, ESAIM: Mathematical Modelling and Numerical Analysis, 47 (2013), pp. 1287–1314.

[306] M. Smoluchowski, *Drei Vorträge über Diffusion, Brownsche Molekularbewegung und Koagulation von Kolloidteilchen*, Zeitschrift fur Physik, 17 (1916), pp. 557–571.

[307] R. Spacek and G. Stoltz, *Extending the regime of linear response with synthetic forcings*, Multiscale Modeling & Simulation, 21 (2023), pp. 1602–1643.

[308] M. Sprik and G. Ciccotti, *Free energy from constrained molecular dynamics*, The Journal of Chemical Physics, 109 (1998), pp. 7737–7744.

[309] G. Stoltz, *Error estimates and variance reduction for nonequilibrium stochastic dynamics*, in Monte Carlo and Quasi-Monte Carlo Methods (MCQMC 2022), A. Hinrichs, P. Kritzer, and F. Pillichshammer, eds., vol. 460 of Springer Proceedings in Mathematics & Statistics, 2024, pp. 163–187.

[310] G. Stoltz and Z. Trstanova, *Langevin dynamics with general kinetic energies*, Multiscale Modeling & Simulation, 16 (2018), pp. 777–806.

[311] G. Szegö, *Orthogonal Polynomials*, vol. 23 of Colloqium Publications, American Mathematical Society, 1939.

[312] M. Sørensen and A. Voter, *Temperature-accelerated dynamics for simulation of infrequent events*, The Journal of Chemical Physics, 112 (2000), pp. 9599–9606.

[313] D. Talay and L. Tubaro, *Expansion of the global error for numerical schemes solving stochastic differential equations*, Stochastic Analysis and Applications, 8 (1990), pp. 483–509.

[314] T. Tao, *Topics in Random Matrix Theory*, vol. 132 of Graduate Studies in Mathematics, American Mathematical Society, 2012.

[315] S. R. Tee and D. J. Searles, *Constant potential and constrained charge ensembles for simulations of conductive electrodes*, Journal of Chemical Theory and Computation, 19 (2023), pp. 2758–2768.

[316] J. Tersoff, *Modeling solid-state chemistry: Interatomic potentials for multicomponent systems*, Physical review B, 39 (1989), pp. 5566–5568.

[317] G. Teschl, *Ordinary Differential Equations and Dynamical Systems*, vol. 140 of Graduate Studies in Mathematics, American Mathematical Society, 2000.

[318] ——, *Mathematical Methods in Quantum Mechanics*, vol. 157 of Graduate Studies in Mathematics, American Mathematical Society, 2014.

[319] A. Thompson, L. Swiler, C. Trott, S. Foiles, and G. Tucker, *Spectral neighbor analysis method for automated generation of quantum-accurate interatomic potentials*, Journal of Computational Physics, 285 (2015), pp. 316–330.

[320] B. D. Todd and P. J. Daivis, *Homogeneous non-equilibrium molecular dynamics simulations of viscous flow: Techniques and applications*, Molecular Simulation, 33 (2007), pp. 189–229.

[321] ——, *Nonequilibrium Molecular Dynamics*, Cambridge University Press, 2017.

[322] S. T. Tokdar and R. E. Kass, *Importance sampling: A review*, WIREs Computational Statistics, 2 (2010), pp. 54–60.

[323] H. Touchette, *Equivalence and nonequivalence of ensembles: thermodynamic, macrostate, and measure levels*, Journal of Statistical Physics, 159 (2015), pp. 987–1016.

[324] M. Tuckerman, *Statistical Mechanics: Theory and Molecular Simulation*, Oxford Graduate Texts, Oxford University Press, 2010.

[325] B. Uberuaga, S. Stuart, and A. Voter, *Parallel replica dynamics for driven systems: derivation and application to strained nanotubes*, Physical Review B—Condensed Matter and Materials Physics, 75 (2007), p. 014301.

[326] N. Vaidehi and A. Jain, *Internal coordinate molecular dynamics: A foundation for multiscale dynamics*, The Journal of Physical Chemistry B, 119 (2015), pp. 1233–1242.

[327] A. Van der Vaart, *Asymptotic Statistics*, vol. 3 of Cambridge Series in Statistical and Probabilistic Mathematics, Cambridge University Press, 2000.

[328] L. Verlet, *Computer "experiments" on classical fluids. I. Thermodynamical properties of Lennard–Jones molecules*, Physical Review, 159 (1967), pp. 98–103.

[329] C. Villani, *Hypocoercivity*, Memoirs of the American Mathematical Society, 202 (2009).

[330] D. Villemonais, *General approximation method for the distribution of Markov processes conditioned not to be killed*, ESAIM: Probability and Statistics, 18 (2014), pp. 441–467.

[331] G. Volpe, L. Helden, T. Brettschneider, J. Wehr, and C. Bechinger, *Influence of noise on force measurements*, Physical Review Letters, 104 (2010), p. 170602.

[332] A. Voter, *Hyperdynamics: accelerated molecular dynamics of infrequent events*, Physical Review Letters, 78 (1997), p. 3908.

[333] ——, *A method for accelerating the molecular dynamics simulation of infrequent events*, The Journal of Chemical Physics, 106 (1997), pp. 4665–4677.

[334] ——, *Parallel replica method for dynamics of infrequent events*, Physical Review B, 57 (1998), pp. 9599–9606.

[335] ——, *Introduction to the kinetic Monte Carlo method*, in Radiation effects in solids, Springer, 2007, pp. 1–23.

[336] A. Voter and T. Germann, *Accelerating the dynamics of infrequent events: combining hyperdynamics and parallel replica dynamics to treat epitaxial layer growth*, MRS Online Proceedings Library, 528 (1998), pp. 221–236.

[337] A. Voter, F. Montalenti, and T. Germann, *Extending the time scale in atomistic simulation of materials*, Annual review of materials research, 32 (2002), pp. 321–346.

[338] A. Wang, G. Roberts, and D. Steinsaltz, *An approximation scheme for quasi-stationary distributions of killed diffusions*, Stochastic Processes and their Applications, 130 (2020), pp. 3193–3219.

[339] M. Wang, D. Su, and W. Wang, *Averaging on macroscopic scales with application to Smoluchowski–Kramers approximation*, Journal of Statistical Physics, 191 (2024), p. 22.

[340] E. Witten, *Supersymmetry and Morse theory*, Journal of Differential Geometry, 17 (1982), pp. 661–692.

[341] H. Wu and F. Noé, *Variational approach for learning Markov processes from time series data*, Journal of Nonlinear Science, 30 (2020), pp. 23–66.

[342] X. Wu and X. Shang, *Stochastic Norton dynamics: An alternative approach for the computation of transport coefficients in Dissipative Particle Dynamics*, Journal of Computational Physics, 541 (2025), pp. 114316:1–19.

[343] A. Yaglom, *Some limit theorems in the theory of branching random processes*, Doklady Akademii Nauk SSSR (in Russian), 56 (1947), pp. 795–798.

[344] R. Zamora, B. Uberuaga, D. Perez, and A. Voter, *The modern temperature-accelerated dynamics approach*, Annual review of chemical and biomolecular engineering, 7 (2016), pp. 87–110.

[345] F. Zhang, D. Isbister, and D. Evans, *Nonequilibrium molecular dynamics simulations of heat flow in one-dimensional lattices*, Physical Review E, 61 (2000), pp. 3541–3546.

[346] W. Zhang, C. Hartmann, and C. Schütte, *Effective dynamics along given reaction coordinates, and reaction rate theory*, Faraday Discussions, 195 (2016), pp. 365–394.